PRINCIPLES OF ECE THEORY

VOLUME II: CLOSING THE GAP BETWEEN EXPERIMENT AND THEORY

Myron W. Evans, Horst Eckardt, Douglas W. Lindstrom,
Stephen J. Crothers, Ulrich E. Bruchholz

Edited and collated by Horst Eckardt

August 20, 2017

ISBN X-X-X-X

Print: epubli, a service of neopubli GmbH, Berlin, Germany

The scientific mind is the same
as the poetic mind and musical mind.

Preface

The vast impact of this monograph among the best in the world of the physical sciences and engineering shows that one cannot stop the march of ideas, in the words of Victor Hugo, nothing stands between science and the freedom of thought, blind censorship always fails in a dismal way. Intolerance and scorn always gives way to enlightenment and acceptance of a new truth. The scientific imagination is no different from poetic or musical imagination. The paper UFT 313 on `www.aias.us` and `www.upitec.org` is the theme for many variations, producing an objectively powerful post Einsteinian paradigm shift, in the words of Alwyn van der Merwe. The theme is geometry, the closest thing to eternity that the human intellect has devised. Geometry is unchanging, a kind of objective perfection upon which to build variations with hypotheses of physics. The variations are rigorously tested at every stage, with the use of computer algebra whenever possible.

History always repeats itself as generation after generation finds its own voice. For example on July 3rd 1822 Schubert produced a short prose piece called "Mein Traum", or "My Dream", a kind of prelude to the songs in Winterreise, Winter's Journey: "I wandered away to a far, far land ..... through the long, long years I sang my songs ..... and before I knew it I was in that circle from which the loveliest melody sounded. I felt the whole measure of eternal bliss compressed, as it were, into a moment's space." He died just short of his thirty second birthday on 19th November 1828, having produced over a thousand works, many of them unparalleled masterpieces. Earlier, in the seventeenth century, Henry Vaughan produced the lines: "I saw eternity the other night, / Like a great ring of pure and endless light, / All calm as it was bright." Both the musical and poetic mind record discoveries made in an instant which last for centuries, a flash of light can last an eternity, a melody can be composed in an instant and last forever.

We know that ECE theory will last indefinitely, because the scientometrics show that the interest has reached a high, constant plateau, and in some ways the interest is still increasing after fifteen years (March 2003 to present). So the theory has passed one test of history very quickly, the acid test of permanence. Schubert was less lucky, apart from his small intellectual circle of good friends he was unknown in his lifetime until Schumann started to play his music and publish his work. For more than a century he was still regarded as a songwriter, until his true place in history emerged. One has to wander into a far, far land to rid the mind of bad ideas, received ideas, then one finds one's own voice in

science, music or poetry, or any area of the human intellect as it strives ever onward, generation after generation.

Schubert and Brahms always asked who dare follow Beethoven or Mozart or Haydn. The answer though was always there. Beethoven changed music after Mozart had achieved a perfection of a kind. Then Schubert changed music after Beethoven had achieved a perfection of another kind, and so it goes on. Who dares challenge the dogma of standard physics? The answer is already here. All humanity can share in the song, millions already do.

In writing my part of this book, all acknowledgment is due to the colleagues, who are like Schubert's group of friends. In particular Dr. Horst Eckardt, who has developed the use of computer algebra and graphics literally to a fine art, checked everything for over a decade, and added works of his own with Dr. Douglas Lindstrom. The other main co author is the eminent scholar and critic Stephen Crothers, so we make a harmonious string quartet. The orchestra consists of Fellows and staff of AIAS / UPITEC, particular thanks are due to Dave Burleigh, Gareth Evans, Alex Hill, Robert Cheshire, Steve Bannister, Kerry Pendergast, Alwyn van der Merwe, Jose Croca, Bo Lehnert, Simon Clifford, Norman Page, Bob Fritzius, Franklin Amador, Russ Davis and Axel Westrenius, amid many others. Special thanks to Manfred Feiger for the artistic design of the book cover and Jakob Jungmaier for precise typesetting.

Craig Cefn Parc, 2017 *Myron W. Evans*

Contents

1 Introduction **3**

2 The Effect of Torsion on Geometry **13**
2.1 The ECE 2 Theory 13
2.2 Totally Antisymmetric Torsion Tensor 20
2.3 Diagonal Metric 24

3 The Field Equations of ECE 2 **25**
3.1 General Theory 25
3.2 Numerical Analysis and Graphics 49
3.2.1 Plots of Photon Mass from ECE 2 Theory 49

4 Orbital Theory **51**
4.1 General Theory 51
4.2 Numerical Analysis and Graphics 81
4.2.1 Examples of a Gravitomagnetic Field 81
4.2.2 Relativistic Lagrange Theory and x Theory 84
4.2.3 Relativistic Orbit Properties 88
4.2.4 Correct Solution of the Einstein Integral 98
4.2.5 Quantization of the Free Particle 100

5 New Spectroscopies **105**
5.1 General Theory 105
5.2 Numerical Analysis and Graphics 134
5.2.1 ECE 2 Energy Levels of Spin-Orbit Coupling 134
5.2.2 Hyperfine Spin Orbit ESR 137
5.2.3 Energy Level Diagrams of Relativistic Zeeman Spectroscopy 138
5.2.4 Energy Level Diagrams of Anomalous Zeeman Hyperfine Shifts 147
5.2.5 Relativistic Correction of Energy Levels 151

6 The ECE 2 Vacuum **153**
6.1 General Theory 153
6.2 Numerical Analysis and Graphics 169
6.2.1 Graphical Demonstration of Vector Potential Properties 169

7 Precessional Theory **173**
7.1 General Theory 173
7.2 Numerical Analysis and Graphics 199
7.2.1 Vector Potential and Torque of a Dipole Field 199
7.2.2 The Gravitomagnetic Field in Spherical Symmetry . . . 202
7.2.3 Orbits of Thomas and de Sitter Precession 205
7.2.4 Lense Thirring and Geodetic Precession 208
7.2.5 Precession from Orbital Lorentz Force 211

8 Triple Unification: Fluid Electrodynamics **217**
8.1 General Theory 217
8.2 Technical Appendix: Scheme for Computation and Animation . 242
8.3 Numerical Analysis and Graphics 243
8.3.1 Examples of Kambe Fields 243
8.3.2 Solutions of Fluid Dynamics Equations 252
8.3.3 Wave Equations of Fluid Electrodynamics 256
8.3.4 Examples for Applications of Fluid Electrodynamics . . 263

9 Triple Unification: Fluid Gravitation **273**
9.1 General Theory 273
9.2 Numerical Analysis and Graphics 295
9.2.1 Examples for Fluid Spacetime Fields 295
9.2.2 Non-classical Acceleration 302
9.2.3 New Force Law and Precession 307

10 Unified Field Theory of the Rainich Space: Determining Properties of Elementary Particles **311**
10.1 Introduction 311
10.2 The Equations 312
10.3 Explanation of the Numerical Method 313
10.4 Determination of the Parameters 314
10.5 The Singularity Problem and its Solution 314
10.6 Numerical Simulations 315
10.7 Computational Results 318
10.7.1 Spins, Electric Charges, Magnetic Moments 318
10.7.2 Masses 319
10.8 Conclusion 320

11 Kirchhoff's Law of Thermal Emission and its Consequences for Astronomy, Astrophysics and Cosmology **327**
11.1 Introduction 327
11.2 Kirchhoff's Law of Thermal Emission (Blackbody Radiation) . 329
11.3 The 'Cosmic Microwave Background' 336
11.4 The Cosmic Background Explorer satellite 340
11.5 The Wilkinson Microwave Anisotropy Probe satellite 347
11.6 The *Planck* Satellite 356

Chapter 1

Introduction

The first volume of this book [1] (see also [2] - [24]), is entitled "Principles of ECE Theory: A New Paradigm Shift of Physics", (PECE), a paradigm shift based on geometry. "Ubi materia ibi geometria", "where there is matter there is geometry" was a saying coined by Johannes Kepler several hundred years ago. The teaching of ECE on `www.aias.us` and `www.upitec.org` has made a tremendous impact on physics and the great paradigm shift has developed rapidly. PECE covered the development up to early 2014. Since then a hundred further papers have appeared so it is timely and important to review the major advances contained in them, beginning with UFT 313. This paper developed the rigorous second Bianchi identity using the Jacobi and Ricci identities. This was the method used by Bianchi and earlier by Ricci, However, spacetime torsion was unknown in their time so they proceeded with a curvature based theory. UFT 313 rigorously corrects their work for the presence of torsion, first inferred by Cartan and others in the early twenties. By basing the correction in the fundamental Jacobi identity, a rigorous new identity emerges, named the Jacobi Cartan Evans (JCE) identity purely in order to distinguish it from other identities in the literature.

The first and by now famous development of the second Bianchi identity in UFT 88 has made its way around the best universities in the world because it is the first paper to realize that the structure of the Einsteinian general relativity is changed completely and fundamentally by torsion. The ECE theory is based on torsion, and from the outset re-established the correct geometry. UFT 88 was followed by UFT 99, which uses the commutator method to show that if torsion is zero then curvature is zero. So neglect of torsion means that the Einstein theory is fundamentally erroneous. The Einsteinian curvature is zero, so its gravitational field is zero, reductio ad absurdum. About a dozen definitive proofs were spun off from UFT 99 and all have been read avidly for nearly a decade, without any objection. Nothing could be a clearer demonstration of the complete failure of the Einstein theory. It was an influential theory in its time, but progress means that it is now obsolete. The UFT papers now show many faults in the Einstein theory, which is greatly improved by ECE 2.

It was decided to base ECE 2 on the JCE identity because it in turn is

based on the rigorous Jacobi identity. This required the use of the Evans torsion identity of UFT 109, and of the Ricci identity generalized for torsion. The tensor algebra of UFT 313 must be translated to vector algebra in order to define the geometry of the ECE 2 field equations. These are field equations of gravitation, electrodynamics, fluid dynamics and indeed any area of physics, a demonstration of the fundamental meaning of a generally covariant unified field theory. This translation was carried out in UFT 314 and forms part of chapter two on geometry. Chapter two is a synopsis of UFT 313, UFT 314 and UFT 354. The latter shows that correct consideration of torsion in the fundamental theorem of metric compatibility completely changes the relation between connection and metric used by Ricci, Bianchi, and later Einstein. UFT 354 concludes that the torsion tensor must be completely antisymmetric, in all three indices, a new discovery in fundamental geometry that goes beyond Cartan's work. This means that Einstein's field equation is completely incorrect. The field equation of Einstein was abandoned after the realizations and implications of UFT 88 were accepted worldwide.

The ECE 2 vector geometry of UFT 314 produces a structure which is superficially similar to the electromagnetic field equations of special relativity, which are Lorentz covariant in a Minkowski spacetime as is well known. In Minkowski spacetime however, both torsion and curvature are zero. The ECE 2 field equations are generally covariant in a mathematical space in which both torsion and curvature must be non zero. This is a fundamental requirement of any geometry in any mathematical space of any dimension. As shown in UFT 99, the requirement follows from the action of the commutator of covariant derivatives on any tensor, for example a vector. The result of the operation of the commutator on the vector is to define the curvature and torsion simultaneously. This is demonstrated in full detail in UFT 99 and in the definitive proofs. The latter are simplifications of UFT 99. The obsolete physics removed the torsion tensor arbitrarily by use of a symmetric connection and continued to neglect torsion incorrectly. The symmetric connection implies a symmetric commutator, which vanishes, so the curvature vanishes if torsion is arbitrarily neglected. ECE does not use an arbitrary "censorship" of torsion.

UFT 315 introduced a new fundamental axiom, which showed that the field equations could be based on curvature as well as torsion. This realization greatly extends the scope of the original ECE field equations. The curvature based equations were based on the JCE identity. This new axiom is the basis of ECE 2 and is developed in chapter three, on electrodynamics and gravitation, and following chapters. The field equations were simplified by removal of internal Cartan indices so their mathematical structure is also simplified. It looks identical to the Maxwell Heaviside (MH) field equations but with big differences and advantages. The key difference is that the field equations of ECE 2 are generally covariant in a space with non zero torsion and curvature. The general covariance of ECE 2 reduces to Lorentz covariance, but the underlying mathematical space is one in which the torsion and curvature are both zero. This was given the name "ECE 2 covariance".

The ECE 2 field equations of electrodynamics, gravitation, fluid dynamics, and any subject area of physics are all Lorentz covariant in a space with

finite torsion and curvature. The property of Lorentz covariance has the great advantage of allowing the use of properties which up to the emergence of ECE 2 were associated with special relativity in Minkowski spacetime. For example the hamiltonian and lagrangian, and the Lorentz force equation. However, ECE 2 has a considerably richer structure than special relativity, and ECE 2 has the overwhelming advantage of being able to unify what are thought to be the fundamental force fields of nature: gravitation, electromagnetism, weak and strong nuclear fields. Unification takes place with ECE 2 covariance.

ECE 2 offers a much greater flexibility in the definitions of fields and potentials than ECE, so there is considerable scope for development. Chapter three of this book exemplifies this development with UFT 315 to UFT 319, which define the ECE 2 field equations of gravitation and electromagnetism and draw several completely original inferences. In UFT 316 the earlier, torsion based, axioms of ECE theory were augmented by curvature based axioms, and this is the key advance given the appellation ECE 2 theory. For example the magnetic flux density can be defined in ECE 2 as being proportional to spin torsion and also as being proportional to spin curvature. In the first case the proportionality is the scalar magnitude of vector potential, in the second case it has the units of magnetic flux, which is weber. Similarly the electric field strength is defined in ECE 2 as being proportional to the orbital torsion, and also as being proportional to the orbital curvature. Another key insight of UFT 316 is that internal Cartan indices can be removed, resulting in field equations that look identical to the Maxwell Heaviside equations (MH), but these are field equations defined in a space with finite torsion and curvature. This is the essence of ECE 2 theory.

In UFT 317 the complete set of equations of ECE 2 electrodynamics is given without internal Cartan indices. In general the magnetic charge current density is non zero, and vanishes if and only if a choice of spin connection is made. The set of equations is based directly on Cartan geometry and has the same format as the MH equations in a mathematical space with non zero torsion and curvature. This poperty defines ECE 2 covariance and also defines special relativity in a space with non zero torsion and curvature. In ECE 2, both torsion and curvature are always non zero as required by fundamental considerations of the commutator described already. This is true of any geometry in any dimension in any mathematical space. The space of ECE 2 is four dimensional - spacetime. The spin connection enters directly in to these equations. In UFT 317 the continuity equation of ECE 2 is derived from geometry and a new set of field potential relations is defined.

In UFT 318 the ECE 2 field equations of gravitation are derived from the same Cartan geometry as the field equations of electromagnetism, so a generally covariant unified field theory is derived. The gravitational field equations are also ECE 2 covariant, and have the same overall properties as electromagnetism. Example properties are given in UFT 318: antisymmetry, equivalence principle, counter gravitation and Aharonov Bohm effects. Newtonian gravitation is a small part of ECE 2 gravitational field theory.

This fact is emphasized in UFT 319, which develops Newtonian and non Newtonian gravitation. The Newtonian limit of ECE 2 gravitational theory

is defined, and the ECE 2 antisymmetry law used to derive the equivalence principle between gravitational and inertial mass. Non Newtonian effects in ECE 2 are exemplified by light deflection due to gravitation, simple estimates of photon mass are made. These major advances have made UFT 319 a popular paper, currently being read about one thousand two hundred times a year from combined sites `www.aias.us` and `www.upitec.org`. The combined ECE 2 papers used as the basis of this book are currently being read about forty one thousand times a year.

The advances made in UFT 313 to UFT 319 form the basis for chapters two and three of this book. Chapters Five and Six develop the ECE 2 covariance principle from relevant source papers. In UFT 320 the gravitomagnetic Lorentz transform is developed on the basis of ECE 2 covariance, which is defined as Lorentz covariance in a space with finite torsion and curvature. Applying the ECE 2 transform to the field tensor of gravitation produces the Lorentz force equation, which is in general relativistic. The gravitomagnetic Biot Savart and Ampère laws are developed for comparison. The laws are applied to planar orbits to find the gravitomagnetic field of the orbit and the current of mass density of the planar orbit. The method is generally valid and can be used on all scales.

In UFT 322, perihelion precession and light deflection due to gravitation are developed with the gravitomagnetic Ampère law of ECE 2. The ECE 2 gravitomagnetic field is developed for dynamics in general and for an orbit in three dimensions. For two dimensional orbits the perihelion precession and light deflection due to gravitation are expressed in terms of the gravitomagnetic field of the relevant mass. In UFT 323 orbital theory in general is developed in terms of the Lorentz transform of the field tensor of ECE 2 gravitomagnetic and dynamic theories. The concept of Lorentz transform is extended to the Lorentz transform of frames. In ECE 2 the Lorentz transform becomes a concept of general rather than special relativity. The theory is applied to an a priori calculation of the perihelion precession in terms of the gravitomagnetic field.

In UFT 324 the relativistic Binet equation (RBE) is inferred and used to solve the Lorntz force equation of ECE 2. The RBE is inferred from the Sommerfeld hamiltonian and relativistic orbital velocity calculated straightforwardly. The orbital velocity equation is used to derive the velocity curve of a whirlpool galaxy and also to give a precise explanation of the deflection of light and electromagnetic radiation due to gravity. These major advances are collected in Chapter Seven and overthrow the obsolete Einstein theory. In UFT 325 the solution of the ECE gravitomagnetic Lorentz force equation is expressed in terms of the ECE 2 covariant hamiltonian and lagrangian. The lagrangian is the classical Sommerfeld lagrangian and is solved by computer algebra and relativistic methods. A scatter plot method is used to infer the true precessing orbit. It is shown that this is not the result of the Einstein theory, which develops severe difficulties. Therefore ECE 2 gives the exactly correct result both for perihelion precession and light deflection due to gravitation.

Chapter Five deals with quantization of ECE 2 and applications to spectroscopy. Several new types of spectroscopy are inferred. Quantization is based on ECE 2 covariance, so the quantization of special relativity can be

applied but in a space with finite torsion and curvature. Various schemes of quantization are developed in UFT 327, resulting in new types of shifts that can be tested experimentally. A new axiom of ECE 2 relativity is introduced, that the laboratory frame velocity of the ECE transform is bounded above by $c/\sqrt{2}$, where c is the universal constant of standards laboratories known as the vacuum speed of light. This axiom allows a particle of mass m (notably the photon) to move at c, thus removing many obscurities of standard special relativity. The axiom results immediately in the experimentally observed light deflection due to gravitation, the "twice Newton" result.

In UFT 327 the ECE 2 metric is used to produce an orbital equation which can be interpreted as a precessing ellipse. This result confirms the demonstration that the lagrangian and hamiltonian of ECE 2 relativity produce a precessing ellipse without any further assumption. None of the assumptions used in the obsolete Einstein theory are needed. This is a healthy development because the Einstein theory is riddled with errors, being fundamentally incorrect due to neglect of torsion. UFT 327 provides an important demonstration of the failings of the Einstein theory. Its claims to produce a precessing ellipse fail qualitatively (i.e. completely) due to poor methods of approximation.

In UFT 328 the existence of precessing orbits from ECE 2 relativity is confirmed using both numerical and theoretical methods. These are used to find the true precessing orbit using ECE 2 covariance. The true orbit is given by simultaneous solution of the ECE 2 lagrangian and hamiltonian using numerical methods. The only concepts used are the infinitesimal line element, lagrangian and hamiltonian of ECE 2 relativity. The analytical problem is in general intractable, but the numerical solution is precise. The elaborate and incorrect methods of Einsteinian relativity are clearly obsolete.

In UFT 329 new types of electron spin resonance (ESR) and nuclear magnetic resonance (NMR) spectroscopy are developed. These are of general utility in atoms and molecules, and in all materials. The novel resonance terms are expressed in terms of the W potential of ECE 2, which has the same units as the A potential of the obsolete Maxwell Heaviside (MH) theory. UFT 330 develops hyperfine spin orbit coupling theory by replacing the restrictive Dirac approximation. This method reveals the presence of several novel spectroscopies of great potential utility. New schemes of quantization are proposed and order of magnitude estimates made of the hyperfine splitting.

UFT 331 develops a new type of relativistic Zeeman splitting by discarding the Dirac approximation. The Zeeman effect develops an intricate new structure, which is illustrated graphically and illustrated with the 2p to 3d (visible) transitions, and 4p to 5d (infra red) transitions. The former splits into nine lines, the latter into forty five lines. These can be resolved to produce an entirely new spectroscopy. This is a popular paper, heavily studied. It challenges the traditional approach in many ways. UFT 332 follows with the ECE 2 theory of the anomalous Zeeman effect, producing novel spectroscopic structure that can be tested experimentally. This paper shows that the ninety year old Dirac approximation implies that the classical hamiltonian vanishes. This unphysical result means that a lot of hyperfine structure has been missed. If this structure exists, it is of great use in the laboratory, if it does not exist

there is a crisis in relativistic quantum mechanics. It is become clear that Dirac carefully chose approximations in a subjective manner in order to give the experimental results. Einstein also used this subjective approach in an incorrect manner.

UFT 333 develops new and rigorous schemes of quantization of ECE 2 relativity. Each scheme leads to different spectral results. The method used by Dirac in the twenties used a subjective choice of approximation, which is taken literally means that the classical hamiltonian always vanishes, an absurd result. Dirac avoided the problem by subjective laundering of the approximations. UFT 333 reveals the fragility of this method because it shows that different rigorous schemes of approximation give different spectra. This means that relativistic quantum mechanics is not rigorous, it is a transitional theory to an as yet unknown theory. Einstein regarded quantum mechanics in much the same way, and rejected the Copenhagen interpretation out of hand, with de Broglie, Schroedinger and others.

UFT 334 develops a rigorous test of relativistic quantum mechanics with ESR. Two example set ups are used: an electron beam and the anomalous Zeeman effect in atoms and molecules. UFT 335 follows up by considering the effect on NMR of discarding the Dirac approximation, and replacing it with rigorous ECE 2 quantization. There are measurable effects on the chemical shift, spin orbit and spin spin interaction.

UFT 336 begins a new phase of development of vacuum ECE 2 theory by considering the ECE 2 vacuum needed for the Aharonov Bohm (AB) effect. This vacuum is traditionally defined as regions where potentials are non zero but in which fields are zero. It is shown that the AB vacuum contains an ECE 2 vector potential which can cause ESR and NMR in the absence of a magnetic field. It should be possible to test these effects experimentally by using a variation of the Chambers experiments. UFT 337 follows up by showing that the ECE 2 theory is richly structured AB type vacuum and can be defined entirely by the spin connection. The ECE 2 vacuum can be used to explain the radiative corrections, so the theory can be tested experimentally. The minimal prescription is defined by the W potential of the ECE 2 vacuum, which is developed in terms of a Tesla vacuum and a relativistic particle flux.

UFT 338 introduces the ECE 2 vacuum particle and defines its mass by using experimental data on the anomalous g factor of the electron. The vacuum particle mass can be used to define the g factor to any precision. The severe limitations of the Dirac theory of the electron are discussed. These limitations are due to the fact that the Dirac approximation, applied directly and literally, means that the classical hamiltonian always vanishes. The theory of UFT 338 replaces quantum electrodynamics, which is riddled with subjectivity and which cannot be tested experimentally without the arbitrary adjustment of variables and the arbitrary removal of infinities known as renormalization.

UFT 339 follows up by developing the dynamics of the ECE 2 vacuum particle. The relativistic hamiltonian of the ECE 2 vacuum is inferred, and the Hilbert constant is reinterpreted as the velocity of the vacuum particle multiplied by the universal power absorption coefficient of UFT 49 on `www.aias.us`. It is argued that the universe is an equilibrium between elementary and vac-

uum particles. This process has no beginning and no end. The mass of the universe is made up of the combined mas of elementary and vacuum particles and there is no "missing mass" as in the obsolete physics. Some examples are given of Compton type scattering processes which could be used for experimental testing. UFT 340 follows up by developing the ECE 2 theory of the Lamb shift from the ECE 2 vacuum, an AB vacuum made up of wave-particles which can transfer energy and momentum to elementary particles. A survey on the vacuum papers is given in chapter Six.

UFT 341 is a paper that deals with gravitational amplification by stimulated emission of radiation (GASER). This apparatus design is based on that of the LASER, and stems from the ECE 2 gravitational field equations, whose structure is the same as the ECE electromagnetic field equations. The gravitational Rayleigh Jeans and Stefan Boltzmann laws are inferred. The energy density of gravitational radiation, if observed without controversy, is proportional to the fourth power of temperature. It is reasonable to assume that gravitons are absorbed and emitted by atoms and molecules. It may become possible to amplify gravitational radiation to the point where it becomes observable in the laboratory.

UFT 342 begins a series of papers on cosmology and develops an exact and simple description of light deflection due to gravitation and perihelion precession from ECE 2 relativity. Therefore ECE 2 unifies the now obsolete special and general relativity. UFT 343 develops Thomas and de Sitter precession from the concepts introduced in UFT 342 and using the foundational definition of relativistic momentum. UFT 344 develops the theory of planetary precession as a Larmor precession produced by the torque between the ECE 2 gravitomagnetic field of the sun and the gravitomagnetic dipole moment of the Earth or any planet. In general, any observable precession can be explained with the ECE 2 field equations. UFT 345 follows up by applying the method geodetic and Lense Thirring precessions using ECE 2 gravitomagnetostatics in an ECE 2 covariant theory. The Lense Thirring calculation is in exact agreement with Gravity Probe B and the geodetic precessional calculation in good agreement. UFT 346 is a heavily studied paper and gives a general theory of any precession in terms of the vorticity. The result is given in terms of the tetrad and spin connection of Cartan geometry. The theory is applied to the planetary, geodetic and Lense Thirring precessions, giving an exact agreement in each case in terms of the vorticity of the mathematical space of the ECE 2 field equations.

In UFT 347 the precession of an elliptical orbit is considered in terms of the ECE 2 Lorentz force equation. The method is to use ECE 2 relativity and the minimal prescription. The hamiltonian is defined of a particle in the presence of a gravitomagnetic vector potential with the units of velocity. The lagrangian is calculated from the hamiltonian using the canonical momentum and the Euler Lagrange equation used to derive the Lorentz force equation. In the absence of gravitomagnetism this equation reduces to the Newton equation. Any precessional frequency of any kind can be described by the precession of the Lorentz force equation. UFT 348 follows up by considering the minimal prescription introduced in UFT 347 in order to show that precession emerges

directly from the relevant hamiltonian. This is the simplest way to describe precession. The Leibnitz force equation is augmented by terms which include the observed precession frequency, and becomes a Lorentz force equation. For a uniform gravitomagnetic field the force equation can be derived from a simple lagrangian, and the former can be expressed as a Binet equation. UFT 348 is a heavily studied paper.

UFT 349 begins the development of the ECE 2 theory of fluid dynamics and shows that they have the same ECE 2 covariant structure as the ECE 2 equations of gravitation and electromagnetism, thus achieving triple unification in terms of ECE 2 relativity described in Chapter Eight. The series UFT 349 to UFT 360 is very heavily studied. UFT 349 shows that spacetime turbulence can be detected by its effect on a circuit such as that in UFT 311 on `www.aias.us`. It is shown that Ohm's Law and the Lorentz force equation are intrinsic to the ECE 2 field equations, and emerge from their geometry. They therefore have equivalents in gravitation and fluid dynamics.

UFT 350 is a posting of "Principles of ECE Theory". UFT 351 develops the new subject of fluid electrodynamics. The Reynolds number is incorporated into the calculations, producing the transition to turbulence. Electric power form spacetime is a direct consequence of fluid electrodynamics. It is shown that the Stokes and convective derivatives are examples of the Cartan covariant derivative. The spin connection for the convective derivative is the Jacobian and is a fundamental concept of fluid dynamics and fluid electrodynamics. Numerical solutions illustrate flows. UFT 352 develops a scheme of computation and animation to calculate the electric field strength (E) and magnetic flux density (B) imparted to a circuit from the vacuum, or spacetime. All relevant quantities are calculated from the velocity field, which becomes turbulent at a given Reynolds number. It is a heavily studied paper.

UFT 353 generalizes ECE 2 fluid dynamics by introducing viscous effects using the most general format of the Navier Stokes and vorticity equations. The resulting structure is that of ECE 2 relativity, and it is shown that the whole of fluid dynamics can be reduced ot one wave equation. UFT 354 is on connections of the anti symmetric and totally antisymmetric torsion tensor and is incorporated in Chapter Two on fundamental geometry.

UFT 355 is the most heavily studied paper of the ECE 2 series at present and introduces simple field and wave equations of fluid electrodynamics. These describe the transfer of energy and power from a fluid spacetime, aether or vacuum to a circuit, notably that of UFT 311. It is shown that the process conserves total energy/momentum and total charge/current density, which are transferred from fluid spacetime to the circuit. It is followed up by UFT 356, another very heavily studied paper that considers the induction of spacetime properties by material fields and potentials. It shows that spacetime is a richly structured fluid described by fluid electrodynamics. The spacetime in turn induces properties in a circuit. UFT 357 verifies fluid electrodynamics experimentally by using the well known radiative corrections, known to high precision experimentally. These include the g factors of elementary particles such as the electron, and the Lamb shift in atomic hydrogen. The anomalous g of the electron is explained to any precision with spacetime vorticity and the

Lamb shift to any precision with the spacetime potential. All this is subject of chapter Eight.

UFT 358 introduces the subject area of fluid gravitation, which is ECE 2 unification of gravitation with fluid dynamics. In fluid dynamics, the acceleration due to gravity, mass density and other fundamental concepts originate in spacetime considered as a fluid. Ultimately, all concepts are derived from a moving frame of reference. It is shown that the main features of a whirlpool galaxy can be described with fluid dynamics without the use of dark matter or black holes. UFT 359 describes spacetime structure generated by Newtonian gravitation, which is illustrated with the velocity field, vorticity, the charge defined by the divergence of the velocity field, the vorticity (the curl of the velocity field, the current and so on). These are illustrated with Gnuplot graphics. This is followed up by UFT 360 which gives the generally covariant inverse square law of all orbits, in which the acceleration due to gravity is defined as the Lagrange or convective derivative of the orbital velocity. This is the derivative in a moving frame of reference and is an example of the covariant derivative of Cartan. These results on unification of gravitation with fluid dynamics are presented in chapter Nine.

Chapter Ten, contributed by Ulrich E. Bruchholz, presents an alternative method of unifying Riemann geometry with electromagnetism. As a stunning result, properties of elementary particles are obtained. Standard modellers haven even given up to try this. Chapter Eleven was written by Stephen J. Crothers and reviews the invalidity of Kirchhoff's Law of thermal emission and the non-universality thereby of Planck's equation for thermal spectra, and the implications for the "CMB" and Big Bang cosmology.

Chapter 2

The Effect of Torsion on Geometry

2.1 The ECE 2 Theory

The effect of torsion on Riemannian geometry is profound and far reaching. This was not fully realized until 2003, when the Einstein Cartan Evans (ECE) unified field theory was inferred. It gradually became clear as the ECE series of papers progressed that the entire edifice of the Riemennian geometry collapses if torsion is forced to vanish through use of a symmetric Christoffel symbol. This means that Einsteinian general relativity becomes meaningless, because the Einstein field equation is based on torsionless Riemannian geometry. Most of the obsolete textbooks of the twentieth century do not even mention torsion, and if they do it is regarded as a removable nuisance. These textbooks are based on the arbitrary and unprovable assertion that torsion does not exist because the Christoffel connection is by definition symmetric in its lower two indices.

This meaningless dogma is based on an astonishing inflexibility of thought. A casual glance at the mathematics of the connection shows that it is in general asymmetric in its lower two indices. It consists of a symmetric part and an antisymmetric part. The latter defines the torsion tensor or its equivalent in Cartan's differential geometry, the torsion form, a vector valued two form antisymmetric in its lower two indices. The torsion form is defined by one of the Maurer Cartan structure equations, and the curvature form by the other structure equation. The torsion form is the covariant derivative of the tetrad, and the curvature form is the covariant derivative of the Cartan spin connection. The torsion and curvature are related by the Cartan identity [2]- [13], and by the Evans identity, inferred in the early UFT papers. The Evans identity is the Cartan identity for Hodge duals. The Cartan and Evans identities are the geometrical basis of the field equations of ECE. This is a paradigm shift which led to the first successful unified theory of physics. It has been described by Alwyn van der Merwe as the post Einsteinian paradigm shift, and has made an enormous impact on physics, measured accurately by

the scientometrics of www.aias.us.

The second major paradigm shift occurred in UFT 313 onwards on www.aias.us and www.upitec.org. It simplified the ECE equations and introduced equations based both on torsion and curvature. The ECE 2 field equations of electrodynamics look like the obsolete Maxwell Heaviside (MH) field equations but are written in a mathematical space in which both torsion and curvature are non zero. This is summarized in chapter one. The second paradigm shift is called the ECE 2 theory, which has advantages of simplicity and greater scope. The obsolete Einstein field equation is replaced by a set of field equations in ECE 2 theory which look like the MH field equations of electrodynamics, but which are written in a space with finite torsion and curvature. The MH theory is written in the Minkowski spacetime, which has no torsion and no curvature and which is therefore known as the mathematical space of special relativity, which is Lorentz covariant but not generally covariant. In the most recent advances of ECE 2, made in the latter half of 2016, the equations of fluid dynamics have also been developed as field equations which look like the MH equations, but which are again written in a space with finite torsion and curvature. So a triple unification has been achieved; that of gravitation, electrodynamics and fluid dynamics, allowing the possibility of major advances.

The groundwork for the second paradigm shift was laid down in the classic UFT 88, which has been read several tens of thousands of times since it was inferred in 2007. It has been read in several hundred of the world's best universities and is an accepted classic. The quality of universities can be ranked by webometrics, Times, Shanghai and QS world rankings for example. The readership of ECE and ECE 2 has always been in the world's best universities, often in the world's top twenty. UFT 88 was the first attempt to incorporate torsion into the second Bianchi identity, upon which the Einstein field equation is based directly. UFT 88 shows that the incorporation of torsion changes the identity completely, so the Einstein field equation was discarded as being incorrect and obsolete in 2007. The scientometrics of www.aias.us (its filtered statistics section and UFT 307 for example), show that the Einstein field equation has been discarded completely by a large percentage of the colleagues internationally. This is in itself an important paradigm shift of the history of science, because a major theory of physics has been discarded by means of the knowledge revolution brought about by the world wide net. Knowledge is no longer confined within Plato's dogmatic cave, and once it is out in the open, a freedom to think follows and the light of reason prevails.

In UFT 99 it was shown that the well known commutator method of simultaneously generating the curvature and torsion tensors also proves that if torsion vanishes, curvature vanishes. So the arbitrary removal of torsion by the obsolete physics also removed curvature, leaving no geometry, reductio ad absurdum, Any valid geometry must be developed in a space where torsion and curvature are both identically non-zero. UFT 99 was supplemented by well known definitive proofs, which simplified UFT 99 to its essence: the commutator is antisymmetric by definition. The indices of the commutator of covariant derivative are the indices of torsion, so if torsion is forcibly removed by using

equal indices, the commutator vanishes. In consequence the curvature also vanishes. Removing torsion removes curvature. If curvature is removed the entire Einsteinian theory collapses.

In UFT 109 a new identity of the torsion tensor was inferred and was named the Evans torsion identity to distinguish it from the Evans identity of Hodge duals that is a variation on the Cartan identity. These papers are essential background reading for UFT 313, in which the Jacobi Cartan Evans (JCE) identity is inferred. This is the final form of UFT 88, and fully incorporates torsion into the second Bianchi identity using the methods used by Ricci and Bianchi, but developing them for torsion.

Ricci and Bianchi were students and friends in the Scuola Normale Superiore in Pisa. It is thought that Ricci was the first to infer the second Bianchi identity, as a follow up to his inference of the Ricci identity. The latter must be used to prove the second Bianchi identity. Ricci seems to have lost or discarded his notes, so it was left to Bianchi to prove the identity in about 1902. The starting point of Bianchi's proof was the Jacobi identity of covariant derivatives, a very fundamental theorem which is also true in the presence of torsion. In 1902 it was an identity of the then new group theory. It can be written as:

$$([D_\rho,[D_\mu,D_\nu]]+[D_\nu,[D_\rho,D_\mu]]+[D_\mu,[D_\nu,D_\rho]])\,V^\kappa := 0 \tag{2.1}$$

where V^κ is a vector in any space of any dimension, and where D_μ denotes the covariant derivative. Consider the first term and use the Leibnitz theorem to find that:

$$[D_\rho,[D_\mu,D_\nu]]V^\kappa = D_\rho\left([D_\mu,D_\nu]V^\kappa\right) - [D_\mu,D_\nu]D_\rho V^\kappa. \tag{2.2}$$

From UFT 99:

$$[D_\mu,D_\nu]V^\kappa = R^\kappa{}_{\lambda\mu\nu}V^\lambda - T^\lambda{}_{\mu\nu}\,D_\lambda V^\kappa \tag{2.3}$$

where $R^\kappa{}_{\lambda\mu\nu}$ is the curvature tensor and $T^\lambda{}_{\mu\nu}$ the torsion tensor, defined as:

$$T^\lambda{}_{\mu\nu} = \Gamma^\lambda{}_{\mu\nu} - \Gamma^\lambda{}_{\nu\mu}. \tag{2.4}$$

The torsion tensor has the same indices as the commutator so if the torsion vanishes, the commutator vanishes and in consequence the curvature vanishes, reduction ad absurdum. The commutator is antisymmetric in its indices by definition, and it follows that the connection is antisymmetric:

$$\Gamma^\lambda{}_{\mu\nu} = -\Gamma^\lambda{}_{\nu\mu}. \tag{2.5}$$

The Ricci identity must also be corrected for torsion, and becomes:

$$[D_\mu,D_\nu]D_\rho V^\kappa = R^\kappa{}_{\lambda\mu\nu}D_\rho V^\lambda - R^\lambda{}_{\rho\mu\nu}D_\lambda V^\kappa - T^\lambda{}_{\mu\nu}\,D_\lambda D_\rho V^\kappa \tag{2.6}$$

in which the commutator acts on a rank two tensor $D_\rho V^\kappa$. Therefore as shown in UFT 313 the first term of the Jacobi identity is:

$$\begin{aligned}[D_\rho,[D_\mu,D_\nu]]V^\kappa =& D_\rho R^\kappa{}_{\lambda\mu\nu}V^\lambda - D_\rho T^\lambda{}_{\mu\nu}\,D_\lambda V^\kappa \\ &+ R^\lambda{}_{\rho\mu\nu}D_\lambda V^\kappa - T^\lambda{}_{\mu\nu}\,[D_\rho,D_\lambda]V^\kappa.\end{aligned} \tag{2.7}$$

Adding the other two terms of the Jacobi identity and using the Cartan identity:

$$D_\rho T^\lambda{}_{\mu\nu} + D_\nu T^\lambda{}_{\rho\mu} + D_\mu T^\lambda{}_{\nu\rho} := R^\lambda{}_{\rho\mu\nu} + R^\lambda{}_{\nu\rho\mu} + R^\lambda{}_{\mu\nu\rho} \tag{2.8}$$

gives the Jacobi Cartan Evans (JCE) identity, an exact identity in any mathematical space of any dimension:

$$\begin{aligned}([D_\rho,&[D_\mu, D_\nu]] + [D_\nu, [D_\rho, D_\mu]] + [D_\mu, [D_\nu, D_\rho]])V^\kappa \\ &= \left(D_\rho R^\kappa{}_{\lambda\mu\nu} + D_\nu R^\kappa{}_{\lambda\rho\mu} + D_\mu R^\kappa{}_{\lambda\nu\rho}\right) V^\lambda \\ &\quad - \left(T^\lambda{}_{\mu\nu}\left[D_\rho, D_\lambda\right] + T^\lambda{}_{\rho\mu}\left[D_\nu, D_\lambda\right] + T^\lambda{}_{\nu\rho}\left[D_\mu, D_\lambda\right]\right) V^\kappa.\end{aligned} \tag{2.9}$$

In this identity:

$$\begin{aligned}(T^\lambda{}_{\mu\nu}&\left[D_\rho, D_\lambda\right] + T^\lambda{}_{\rho\mu}\left[D_\nu, D_\lambda\right] + T^\lambda{}_{\nu\rho}\left[D_\mu, D_\lambda\right])V^\kappa \\ &= \left(T^\lambda{}_{\mu\nu} R^\kappa{}_{\alpha\rho\lambda} + T^\lambda{}_{\rho\mu} R^\kappa{}_{\alpha\nu\lambda} + T^\lambda{}_{\nu\rho} R^\kappa{}_{\alpha\mu\lambda}\right) V^\alpha \\ &\quad - \left(T^\lambda{}_{\mu\nu} T^\alpha{}_{\rho\lambda} + T^\lambda{}_{\rho\mu} T^\alpha{}_{\nu\lambda} + T^\lambda{}_{\nu\rho} T^\alpha{}_{\mu\nu}\right) D_\alpha V^\kappa.\end{aligned} \tag{2.10}$$

Now use the Evans torsion identity of UFT 109:

$$T^\lambda{}_{\mu\nu} T^\alpha{}_{\rho\lambda} + T^\lambda{}_{\rho\mu} T^\alpha{}_{\nu\lambda} + T^\lambda{}_{\nu\rho} T^\alpha{}_{\mu\lambda} := 0 \tag{2.11}$$

to reduce the JCE identity to:

$$D_\rho R^\kappa{}_{\lambda\mu\nu} + D_\nu R^\kappa{}_{\lambda\rho\mu} + D_\mu R^\kappa{}_{\lambda\nu\rho} := T^\alpha{}_{\mu\nu} R^\kappa{}_{\lambda\rho\alpha} + T^\alpha{}_{\rho\mu} R^\kappa{}_{\lambda\nu\alpha} + T^\alpha{}_{\nu\rho} R^\kappa{}_{\lambda\mu\alpha}. \tag{2.12}$$

This equation means that:

$$D_\rho R^\kappa{}_{\lambda\mu\nu} + D_\nu R^\kappa{}_{\lambda\rho\mu} + D_\mu R^\kappa{}_{\lambda\nu\rho} \neq 0. \tag{2.13}$$

Q. E. D.

The original 1902 second Bianchi identity is

$$D_\rho R^\kappa{}_{\lambda\mu\nu} + D_\nu R^\kappa{}_{\lambda\rho\mu} + D_\mu R^\kappa{}_{\lambda\nu\rho} =? \ 0 \tag{2.14}$$

and was apparently first inferred by Ricci in 1880. Eq. (2.14) is completely incorrect because it relies on zero torsion, which means zero curvature, reductio ad absurdum.

Unfortunately Eq. (2.14) was used uncritically by Einstein and all his contemporaries, because torsion was unknown until Cartan and his co workers inferred it in the early twenties.

In UFT 313 the Bianchi Cartan Evans (BCE) identity was also proven:

$$D_\mu D_\lambda T^\kappa{}_{\nu\rho} + D_\rho D_\lambda T^\kappa{}_{\mu\nu} + D_\nu D_\lambda T^\kappa{}_{\rho\mu} := D_\mu R^\kappa{}_{\lambda\nu\rho} + D_\rho R^\kappa{}_{\lambda\mu\nu} + D_\nu R^\kappa{}_{\lambda\rho\mu}. \tag{2.15}$$

This was first inferred in UFT 255. It is a development of the Cartan identity, Eq. (2.8). If torsion is neglected the BCE identity becomes the original second

Bianchi identity of 1902, and the Cartan identity becomes the first Bianchi identity:

$$R^{\lambda}{}_{\rho\mu\nu} + R^{\lambda}{}_{\nu\rho\mu} + R^{\lambda}{}_{\mu\nu\rho} =? \ 0 \tag{2.16}$$

Torsion was inferred in the early twenties by Cartan, who communicated his discovery to Einstein. There ensued the well known Einstein Cartan correspondence, but Einstein made no attempt to incorporate torsion into his field equation. The first attempt to do so was made in the classic UFT 88, culminating in UFT 313 summarized in this chapter. The Einstein field equation, being geometrically incorrect, cannot have inferred any correct physics. It has been replaced by ECE, and by ECE 2 using the second paradigm shift described in this book.

These are described as the post Einsteinian paradigm shifts by van der Merwe. They change the entire face of physics, so the latter is currently split into two schools of thought, the ECE 2 theory and the dogmatic and obsolete standard model.

It is useful to develop these new tensor identities into vector identities, because this leads to the ECE 2 field equations. Consider firstly the Evans torsion identity of UFT 109 in Riemannian format:

$$T^{\lambda}{}_{\mu\nu} T^{\alpha}{}_{\rho\lambda} + T^{\lambda}{}_{\rho\mu} T^{\alpha}{}_{\nu\lambda} + T^{\lambda}{}_{\nu\rho} T^{\alpha}{}_{\mu\lambda} := 0. \tag{2.17}$$

Replace the λ indices by a indices of Cartan geometry:

$$T^{a}{}_{\mu\nu} T^{\alpha}{}_{\rho a} + T^{a}{}_{\rho\mu} T^{\alpha}{}_{\nu a} + T^{a}{}_{\nu\rho} T^{\alpha}{}_{\mu a} := 0 \tag{2.18}$$

and use:

$$T^{\alpha}{}_{\rho\lambda} = T^{a}{}_{\rho\lambda} q^{\alpha}{}_{a} \tag{2.19}$$

where $q^{\alpha}{}_{a}$ is the inverse tetrad. It follows that:

$$(T^{a}{}_{\mu\nu} T^{b}{}_{\rho a} + T^{a}{}_{\rho\mu} T^{b}{}_{\nu a} + T^{a}{}_{\nu\rho} T^{b}{}_{\mu a}) q^{\alpha}{}_{b} := 0 \tag{2.20}$$

a possible solution of which is:

$$T^{a}{}_{\mu\nu} T^{b}{}_{\rho a} + T^{a}{}_{\rho\mu} T^{b}{}_{\nu a} + T^{a}{}_{\nu\rho} T^{b}{}_{\mu a} = 0. \tag{2.21}$$

In the notation of differential geometry Eq. (2.21) is a wedge product

$$T^{b}{}_{\rho a} \wedge T^{a}{}_{\mu\nu} = 0 \tag{2.22}$$

between a tensor valued one form $T^{b}{}_{\rho a}$ and a vector valued two form $T^{a}{}_{\mu\nu}$.

In order to transform this geometry to electrodynamics the original ECE hypotheses are used:

$$F^{b}{}_{\rho a} = A^{(0)} T^{b}{}_{\rho a} ; \ F^{a}{}_{\mu\nu} = A^{(0)} T^{a}{}_{\mu\nu} \tag{2.23}$$

in order to obtain a new identity of electrodynamics:

$$F^{b}{}_{\rho a} \wedge F^{a}{}_{\mu\nu} = 0. \tag{2.24}$$

Similar equations can be obtained for gravitation and mixed gravitation and electrodynamics. Now express Eq. (2.24) as:

$$F^{b}_{\ \mu a}\,\widetilde{F}^{a\mu\nu} = 0. \tag{2.25}$$

where the tilde denotes Hodge dual. The free space field tensors are defined as:

$$\begin{aligned}
\widetilde{F}^{a\mu\nu} &= \begin{bmatrix} 0 & -cB^a_X & -cB^a_Y & -cB^a_Z \\ cB^a_X & 0 & E^a_Z & -E^a_Y \\ cB^a_Y & -E^a_Z & 0 & E^a_X \\ cB^a_Z & E^a_Y & -E^a_X & 0 \end{bmatrix}; \\
F^{b\mu\nu} &= \begin{bmatrix} 0 & E^b_X & E^b_Y & E^b_Z \\ -E^b_X & 0 & -cB^b_Z & cB^b_Y \\ -E^b_Y & cB^b_Z & 0 & -cB^b_X \\ -E^b_Z & -cB^b_Y & cB^b_X & 0 \end{bmatrix}
\end{aligned} \tag{2.26}$$

where **E** is the electric field strength in volts per metre and where **B** is the magnetic flux density in tesla. Here c is the universal constant known as the vacuum speed of light.

The tensor $F^{b}_{\ \mu a}$ is a tensor valued one form:

$$F^{b}_{\ \mu a} = (F^{b}_{\ 0a}, -\mathbf{F}^{b}_{\ a}) \tag{2.27}$$

and the tensor equation (2.25) splits into two vector equations of electrodynamics:

$$\mathbf{F}^{b}_{\ a} \cdot \mathbf{B}^{a} = 0, \tag{2.28}$$

$$cF^{b}_{\ 0a}\,\mathbf{B}^{a} = \mathbf{F}^{b}_{\ a} \times \mathbf{E}^{b}. \tag{2.29}$$

There are also equivalent equations of gravitation. Now use:

$$F^{b}_{\ \mu a} = F^{b}_{\ \mu\nu}\,q^{\nu}_{\ a} \tag{2.30}$$

in Eq. (2.25) to obtain:

$$q^{\nu}_{\ a} F^{b}_{\ \mu\nu}\,\widetilde{F}^{a\mu\nu} = 0 \tag{2.31}$$

a possible solution of which is:

$$F^{b}_{\ \mu\nu}\,\widetilde{F}^{a\mu\nu} = 0. \tag{2.32}$$

This is the second format of the Evans torsion identity. Using the field tensors (2.26) gives the result:

$$\mathbf{E}^{b} \cdot \mathbf{B}^{a} + \mathbf{B}^{b} \cdot \mathbf{E}^{a} = 0, \tag{2.33}$$

which is a new fundamental equation of electrodynamics. Using the equation:

$$F^{b}_{\ \mu\nu} = q^{a}_{\ \nu} F^{b}_{\ \mu a} \tag{2.34}$$

it follows that:

$$F^{b}{}_{\mu\nu} = A^{a}{}_{\nu} T^{b}{}_{\mu a} \tag{2.35}$$

and this is a new relation between field and potential in electrodynamics.

It also follows that the Evans torsion identity gives a new structure equation of differential geometry:

$$T^{b}{}_{\mu\nu} = q^{a}{}_{\nu} T^{b}{}_{\mu a} \,. \tag{2.36}$$

Note 314(3) systematically develops the properties of the field tensor $F^{a}{}_{\mu b}$ and shows that one possible solution is:

$$\mathbf{F}^{b}{}_{a} \times \mathbf{E}^{a} = \mathbf{0}. \tag{2.37}$$

The Evans torsion identity applied to Hodge duals gives the second Evans torsion identity:

$$\widetilde{T}^{\lambda}{}_{\mu\nu} \widetilde{T}^{\alpha}{}_{\rho\lambda} + \widetilde{T}^{\lambda}{}_{\rho\mu} \widetilde{T}^{\alpha}{}_{\nu\lambda} + \widetilde{T}^{\lambda}{}_{\nu\rho} \widetilde{T}^{\alpha}{}_{\mu\lambda} := 0 \tag{2.38}$$

which is valid only in four dimensions because of the way in which its Hodge duals are defined. The Evans torsion identity itself is valid in any space of any dimension. Eq. (2.38) may be written as:

$$\widetilde{T}^{b}{}_{\mu\nu} T^{a\mu\nu} = 0 \tag{2.39}$$

and using the field tensors:

$$\begin{aligned} F^{\mu\nu a} &= \begin{bmatrix} 0 & -E^{a}_{X} & -E^{a}_{Y} & -E^{a}_{Z} \\ E^{a}_{X} & 0 & -cB^{s}_{Z} & cB^{a}_{Y} \\ E^{a}_{Y} & cB^{a}_{Z} & 0 & -cB^{a}_{X} \\ E^{a}_{Z} & -cB^{a}_{Y} & cB^{a}_{X} & 0 \end{bmatrix}; \\ \widetilde{F}^{b}{}_{\mu\nu} &= \begin{bmatrix} 0 & cB^{b}_{X} & cB^{b}_{Y} & cB^{b}_{Z} \\ -cB^{b}_{X} & 0 & E^{b}_{Z} & -E^{b}_{Y} \\ -cB^{b}_{Y} & -E^{b}_{Z} & 0 & E^{b}_{X} \\ -cB^{b}_{Z} & E^{b}_{Y} & -E^{b}_{X} & 0 \end{bmatrix} \end{aligned} \tag{2.40}$$

two equations of electrodynamics are obtained:

$$\widetilde{\mathbf{F}}^{a}{}_{b} \cdot \mathbf{E}^{b} = 0 \tag{2.41}$$

and

$$c\widetilde{\mathbf{F}}^{a}{}_{b} \times \mathbf{B}^{b} + \widetilde{F}^{a}{}_{0b} \mathbf{E}^{b} = \mathbf{0}. \tag{2.42}$$

Eq. (2.39) also gives:

$$\mathbf{E}^{b} \cdot \mathbf{B}^{a} + \mathbf{B}^{b} \cdot \mathbf{E}^{a} = 0. \tag{2.43}$$

Therefore the complete set of equations is

$$\mathbf{F}^{b}{}_{a} \cdot \mathbf{B}^{a} = 0 \tag{2.44}$$

$$cF^{b}{}_{0a}\,\mathbf{B}^{a} = \mathbf{F}^{b}{}_{a} \times \mathbf{E}^{a} \tag{2.45}$$

$$\widetilde{\mathbf{F}}^{a}{}_{b} \cdot \mathbf{E}^{a} = 0 \tag{2.46}$$

$$\widetilde{F}^{a}{}_{0b}\,\mathbf{E}^{b} + c\widetilde{\mathbf{F}}^{a}{}_{b} \times \mathbf{B}^{b} = \mathbf{0} \tag{2.47}$$

and from both identities:

$$\mathbf{E}^{b} \cdot \mathbf{B}^{a} + \mathbf{B}^{b} \cdot \mathbf{E}^{a} = 0. \tag{2.48}$$

Eqs. (2.44) to (2.47) are identical in structure to the ECE free space equations given in the Engineering Model (UFT 303):

$$\boldsymbol{\omega}^{a}{}_{b} \cdot \mathbf{B}^{b} = 0 \tag{2.49}$$

$$c\omega^{a}{}_{0b}\mathbf{B}^{b} = \boldsymbol{\omega}^{a}{}_{b} \times \mathbf{E}^{b} \tag{2.50}$$

$$\boldsymbol{\omega}^{a}{}_{b} \cdot \mathbf{E}^{b} = 0 \tag{2.51}$$

$$c\boldsymbol{\omega}^{a}{}_{b} \times \mathbf{B}^{b} + \omega^{a}{}_{0b}\mathbf{E}^{b} = \mathbf{0} \tag{2.52}$$

where the spin connection is defined as:

$$\omega^{a}{}_{\mu b} = (\omega^{a}{}_{0b}, -\boldsymbol{\omega}^{a}{}_{b}). \tag{2.53}$$

2.2 Totally Antisymmetric Torsion Tensor

Let us consider, as discussed in UFT 354, the case where the torsion tensor is totally antisymmetric, as would be expected for an isotropic spacetime:

$$T^{\rho}{}_{\mu\nu} = -T^{\rho}{}_{\nu\mu};\; T^{\rho}{}_{\mu\nu} = -T^{\mu}{}_{\rho\nu};\; T^{\rho}{}_{\mu\nu} = -T^{\nu}{}_{\mu\rho}. \tag{2.54}$$

Any two of the above anti-symmetries imply the third so that there is equality of the torsion tensor elements under counterclockwise cyclic permutation of the indices, and the negative equality under a clockwise cyclic permutation.

There is a well known relation between the symmetric Christoffel symbols and the metric [25]:

$$\Gamma^{\sigma}{}_{\mu\nu} = \frac{1}{2} g^{\rho\sigma} \left(\frac{\partial g_{\nu\rho}}{\partial x^{\mu}} + \frac{\partial g_{\rho\mu}}{\partial x^{\nu}} - \frac{\partial g_{\mu\nu}}{\partial x^{\rho}} \right). \tag{2.55}$$

This however, is not valid for a generally asymmetric or antisymmetric connection, generally being restricted to the case of zero torsion. When this is not true, a more general approach is required.

We can derive an equation similar to equation (2.55) for a connection of arbitrary symmetry if we start with the equations of metric compatibility as given for example in [14]:

$$\frac{\partial g_{\mu\nu}}{\partial x^{\rho}} - \Gamma^{\lambda}{}_{\rho\mu} g_{\lambda\nu} - \Gamma^{\lambda}{}_{\rho\nu} g_{\mu\lambda} = 0, \tag{2.56}$$

$$\frac{\partial g_{\nu\rho}}{\partial x^{\mu}} - \Gamma^{\lambda}{}_{\mu\nu} g_{\lambda\rho} - \Gamma^{\lambda}{}_{\mu\rho} g_{\nu\lambda} = 0, \tag{2.57}$$

$$\frac{\partial g_{\rho\mu}}{\partial x^{\nu}} - \Gamma^{\lambda}{}_{\nu\rho} g_{\lambda\mu} - \Gamma^{\lambda}{}_{\nu\mu} g_{\rho\lambda} = 0. \tag{2.58}$$

Straightforward manipulation of these three equations, as shown in UFT 354, gives equation (2.55) corrected for the presence of torsion:

$$\Gamma^{\sigma}{}_{\mu\nu} = \frac{1}{2} g^{\rho\sigma} \left(\frac{\partial g_{\nu\rho}}{\partial x^{\mu}} + \frac{\partial g_{\rho\mu}}{\partial x^{\nu}} - \frac{\partial g_{\mu\nu}}{\partial x^{\rho}} - T_{\nu\mu\rho} - T_{\mu\nu\rho} + T_{\sigma\mu\nu} \right). \tag{2.59}$$

This has been reported elsewhere [25].

Using equations (2.55) through (2.59) we can write:

$$\begin{aligned} &\Gamma^{\rho}{}_{\mu\nu} + \Gamma^{\rho}{}_{\nu\mu} \\ &\quad = \frac{1}{2} g^{\rho\sigma} \left(\frac{\partial \left(g_{\nu\sigma} + g_{\sigma\nu} \right)}{\partial x^{\mu}} + \frac{\partial \left(g_{\sigma\mu} + g_{\mu\sigma} \right)}{\partial x^{\nu}} - \frac{\partial \left(g_{\mu\nu} + g_{\nu\mu} \right)}{\partial x^{\sigma}} \right. \\ &\quad \left. -2T_{\nu\mu\sigma} - 2T_{\mu\nu\sigma} + T_{\sigma\mu\nu} + T_{\sigma\nu\mu} \right) \end{aligned} \tag{2.60}$$

and:

$$\begin{aligned} &\Gamma^{\rho}{}_{\mu\nu} - \Gamma^{\rho}{}_{\nu\mu} \\ &\quad = \frac{1}{2} g^{\rho\sigma} \left(\frac{\partial \left(g_{\nu\sigma} - g_{\sigma\nu} \right)}{\partial x^{\mu}} + \frac{\partial \left(g_{\sigma\mu} + g_{\mu\sigma} \right)}{\partial x^{\nu}} - \frac{\partial \left(g_{\mu\nu} - g_{\nu\mu} \right)}{\partial x^{\sigma}} \right. \\ &\quad \left. +T_{\sigma\mu\nu} - T_{\sigma\nu\mu} \right) \end{aligned} \tag{2.61}$$

With total antisymmetry of the torsion tensor equation (2.61) simplifies to:

$$\Gamma^{\rho}{}_{\mu\nu} - \Gamma^{\rho}{}_{\nu\mu} = \frac{1}{2} g^{\rho\sigma} \left(\frac{\partial \left(g_{\nu\sigma} - g_{\sigma\nu} \right)}{\partial x^{\mu}} + \frac{\partial \left(g_{\sigma\mu} - g_{\mu\sigma} \right)}{\partial x^{\nu}} - \frac{\partial \left(g_{\mu\nu} - g_{\nu\mu} \right)}{\partial x^{\sigma}} + 2T_{\sigma\mu\nu} \right) \tag{2.62}$$

which reduces to the standard definition of torsion equation (2.4) for a symmetric metric. Note that:

$$T_{\mu\nu\sigma} = \left(\Gamma^{\lambda}{}_{\nu\sigma} - \Gamma^{\lambda}{}_{\sigma\nu} \right) g_{\lambda\mu} = \Gamma_{\mu\nu\sigma} - \Gamma_{\mu\sigma\nu}. \tag{2.63}$$

For antisymmetry of the torsion tensor in the μ, ν indices, equation (2.60) simplifies to:

$$\begin{aligned} S^{\rho}{}_{\mu\nu} &= \Gamma^{\rho}{}_{\mu\nu} + \Gamma^{\rho}{}_{\nu\mu} \\ &= \frac{1}{2} g^{\rho\sigma} \left(\frac{\partial \left(g_{\nu\sigma} + g_{\sigma\nu} \right)}{\partial x^{\mu}} + \frac{\partial \left(g_{\sigma\mu} + g_{\mu\sigma} \right)}{\partial x^{\nu}} - \frac{\partial \left(g_{\mu\nu} + g_{\nu\mu} \right)}{\partial x^{\sigma}} \right. \\ &\quad \left. -2T_{\nu\mu\sigma} - 2T_{\mu\nu\sigma} \right) \end{aligned} \tag{2.64}$$

where we introduce a tensor $S^{\rho}{}_{\mu\nu}$ which we will call the shear of the spacetime.

It it straightforward, albeit a bit tedious to show equality of the the shear elements under clockwise and counterclockwise cyclic permutation of the indices. Noting that we can write:

$$S_{\mu\nu\sigma} = \left(\Gamma^{\lambda}{}_{\nu\sigma} + \Gamma^{\lambda}{}_{\sigma\nu}\right) g_{\lambda\mu} = \Gamma_{\mu\nu\sigma} + \Gamma_{\mu\sigma\nu} \tag{2.65}$$

which allows us to write:

$$S_{\nu\sigma\mu} = \Gamma_{\nu\sigma\mu} + \Gamma_{\nu\mu\sigma} \tag{2.66}$$

so that:

$$S_{\nu\sigma\mu} - S_{\mu\nu\sigma} = (\Gamma_{\nu\sigma\mu} - \Gamma_{\mu\sigma\nu}) + (\Gamma_{\nu\mu\sigma} - \Gamma_{\mu\nu\sigma}) = T_{\nu\sigma\mu} + T_{\nu\mu\sigma} \tag{2.67}$$

which from (2.54) becomes:

$$S_{\nu\sigma\mu} - S_{\mu\nu\sigma} = 0. \tag{2.68}$$

This can be repeated for all of the cyclic permutations for the shear as asserted above to give:

$$S_{\nu\mu\sigma} = S_{\mu\nu\sigma} = S_{\nu\sigma\mu} = S_{\mu\sigma\nu} = S_{\sigma\nu\mu} = S_{\sigma\mu\nu}. \tag{2.69}$$

Q.E.D.

In a similar manner, the symmetry of the shear and the antisymmetry of the torsion demonstrate antisymmetry in the connection. Compare, for example, from equation (2.69):

$$S_{\sigma\mu\nu} - S_{\mu\nu\sigma} = 0 \tag{2.70}$$

with, from equation (2.54), using two cyclic permutations:

$$T_{\sigma\mu\nu} - T_{\mu\nu\sigma} = 0. \tag{2.71}$$

Expanding these equations with their definitions in terms of the connection gives:

$$\left(\Gamma_{\sigma\mu\nu} + \Gamma_{\sigma\nu\mu}\right) - \left(\Gamma_{\mu\nu\sigma} + \Gamma_{\mu\sigma\nu}\right) = 0 \tag{2.72}$$

$$\left(\Gamma_{\sigma\mu\nu} - \Gamma_{\sigma\nu\mu}\right) - \left(\Gamma_{\mu\nu\sigma} - \Gamma_{\mu\sigma\nu}\right) = 0. \tag{2.73}$$

Adding these gives:

$$\Gamma_{\sigma\mu\nu} = \Gamma_{\mu\nu\sigma} \ . \tag{2.74}$$

Subtracting gives:

$$\Gamma_{\sigma\nu\mu} = \Gamma_{\mu\sigma\nu} \ . \tag{2.75}$$

Notice that this equation requires two permutations of indices, implying that three solutions exist:

$$\Gamma_{\sigma\mu\nu} + \Gamma_{\sigma\nu\mu} = 0 \tag{2.76}$$

or:

$$\Gamma_{\sigma\mu\nu} - \Gamma_{\sigma\nu\mu} = 0. \tag{2.77}$$

or:

$$\Gamma_{\sigma\mu\nu} = \Gamma_{\sigma\nu\mu} = 0. \tag{2.78}$$

Thus the connection is either fully symmetric, or anti-symmetric, or zero not considering the diagonals. If we allow for a non-zero torsion, then the shear must be zero, and the connection antisymmetric.
Q.E.D.

Total antisymmetry of a non-zero torsion, therefore antisymmetry of the connection, implies total antisymmetry of the connection as can be seen from the following arguments.

Equations (2.70) and (2.71) are parts of the larger symmetry equations given by (2.54) and (2.69). Equation (2.54) can be rewritten as

$$T_{\sigma\mu\nu} = T_{\nu\sigma\mu} = T_{\mu\nu\sigma} \ . \tag{2.79}$$

Substituting the connections into this equation and the corresponding parts of (2.69) results in two equations;

$$\Gamma_{\sigma\mu\nu} - \Gamma_{\sigma\mu\nu} = \Gamma_{\mu\nu\sigma} - \Gamma_{\mu\sigma\nu} = \Gamma_{\nu\sigma\mu} - \Gamma_{\nu\mu\sigma} \ . \tag{2.80}$$

Applying the same procedure to equation (2.70) and applying antisymmetry to:

$$\Gamma_{\sigma\mu\nu} + \Gamma_{\sigma\mu\nu} = \Gamma_{\mu\nu\sigma} + \Gamma_{\mu\sigma\nu} = \Gamma_{\nu\sigma\mu} + \Gamma_{\nu\mu\sigma} = 0. \tag{2.81}$$

Adding and subtracting these equations gives:

$$a = \Gamma_{\sigma\mu\nu} = \Gamma_{\mu\nu\sigma} = \Gamma_{\nu\sigma\mu} \tag{2.82}$$

$$b = \Gamma_{\sigma\mu\nu} = \Gamma_{\mu\sigma\nu} = \Gamma_{\nu\mu\sigma} \tag{2.83}$$

with :

$$a + b = 0 \ . \tag{2.84}$$

This represents a totally antisymmetric connection, non considering the diagonal elements.
Q.E.D.

2.3 Diagonal Metric

In this section, we restrict ourselves to the case where the metric has only diagonal elements, the most common form of metric. The diagonal elements of the connection are shown to be directly calculable from the diagonal metric elements.

For a totally antisymmetric torsion as defined by equation (2.54), equation (2.64) becomes:

$$S^{\rho}_{\ \mu\nu} = \Gamma^{\rho}_{\ \mu\nu} + \Gamma^{\rho}_{\ \nu\mu} = \frac{1}{2} g^{\rho\sigma} \left(\frac{\partial \left(g_{\nu\sigma} + g_{\sigma\nu} \right)}{\partial x^{\mu}} + \frac{\partial \left(g_{\sigma\mu} + g_{\mu\sigma} \right)}{\partial x^{\nu}} - \frac{\partial \left(g_{\mu\nu} + g_{\nu\mu} \right)}{\partial x^{\sigma}} \right) \tag{2.85}$$

which for a symmetric metric is:

$$S^{\rho}_{\ \mu\nu} = \Gamma^{\rho}_{\ \mu\nu} + \Gamma^{\rho}_{\ \nu\mu} = g^{\rho\sigma} \left(\frac{\partial g_{\sigma\nu}}{\partial x^{\mu}} + \frac{\partial g_{\mu\sigma}}{\partial x^{\nu}} - \frac{\partial g_{\mu\nu}}{\partial x^{\sigma}} \right). \tag{2.86}$$

If we restrict ourselves to the case where the metric is diagonal, then equation (2.78) reduces to:

$$\Gamma^{\rho}_{\ \mu\nu} + \Gamma^{\rho}_{\ \nu\mu} = \begin{cases} g^{\rho\rho} \left(\frac{\partial g_{\rho\nu}}{\partial x^{\mu}} + \frac{\partial g_{\mu\rho)}}{\partial x^{\nu}} - \frac{\partial g_{\mu\nu}}{\partial x^{\rho}} \right) & \text{if } \rho = \nu, \text{ or } \rho = \mu, \text{ or } \mu = \nu \\ 0 & \text{otherwise.} \end{cases} \tag{2.87}$$

(Note that in the preceding and remaining equations of this section, no summation is implied over repeated indices.) That is, on the basis of the compatibility of the metric alone, for a metric that is diagonal and torsion that is totally antisymmetric, $\Gamma^{\rho}_{\ \mu\nu}$ is either "antisymmetric" in the lower two indices or zero, with the exception of the diagonals. The diagonal elements of $\Gamma^{\rho}_{\ \mu\nu}$ are given by:

$$\Gamma^{\rho}_{\ \mu\mu} = -\frac{1}{2} g^{\rho\rho} \frac{\partial g_{\mu\mu}}{\partial x^{\rho}} \text{ if } \rho \neq \nu, \rho \neq \mu, \mu = \nu \tag{2.88}$$

$$\Gamma^{\nu}_{\ \mu\nu} + \Gamma^{\nu}_{\ \nu\mu} = g^{\nu\nu} \frac{\partial g_{\nu\nu}}{\partial x^{\mu}} \text{ if } \rho = \nu, \rho \neq \mu, \mu \neq \nu \tag{2.89}$$

$$\Gamma^{\mu}_{\ \mu\mu} = \frac{1}{2} g^{\mu\mu} \frac{\partial g_{\mu\mu}}{\partial x^{\mu}} \text{ if } \rho = \nu, \ \rho = \mu, \mu = \nu. \tag{2.90}$$

Given the above, symmetry of the connection is impossible unless it is identically zero. Earlier arguments have shown, using that antisymmetry of the commutator, that antisymmetry of $\Gamma^{\rho}_{\ \mu\nu}$ given by equation (2.5) is valid for the non-diagonal terms of any connection, requiring that the Christoffel connection be written as the sum of a diagonal tensor plus an antisymmetric tensor in the lower two indices.

Chapter 3

The Field Equations of ECE 2

3.1 General Theory

The field equations of ECE 2 unify gravitation, electromagnetism and fluid dynamics based on the Jacobi Cartan Evans (JCE) identity of UFT 313 on www.aias.us and www.upitec.org. They have the same basic mathematical structure as the obsolete Maxwell Heaviside (MH) field equations of nineteenth century electrodynamics, but are written in a mathematical space in which curvature and torsion are identically non-zero. They are equations of a generally covariant unified field theory. The MH equations are Lorentz covariant and are not equations of a unified field theory, being equations of Minkowski or flat spacetime in which both torsion and curvature vanish identically. The JCE identity of geometry is transformed into field equations using a new hypothesis which distinguishes ECE 2 theory from the earlier ECE theory. This is the second post Einsteinian paradigm shift developed in this book.

The JCE identity corrects the original 1902 identity of Bianchi, probably first derived by Ricci, for torsion. The development of UFT 313 started with the classic UFT 88, published in 2007, which has been read in several hundred of the world's best universities, institutes and similar and which has been accepted as refuting Einsteinian relativity. The new hypothesis is based on curvature, and exists in addition to the original ECE hypothesis based on torsion. The JCE identity gives unified field equations for what are thought to be the fundamental force fields: gravitation, electromagnetism and the weak and strong nuclear fields. The field equations of fluid dynamics can be unified with those of gravitation and electrodynamics using the geometrical structure of the JCE identity, This process eventually leads to the unification of classical dynamics and fluid dynamics.

In ECE 2 theory the original ECE equations are simplified by a well defined and rigorous removal of the internal Cartan indices. This can be achieved without loss of generality, and when more detail is required (such as in the process that leads to the B(3) field), the indices can be reinstated. The removal

of indices results in field equations of electrodynamics for example which are Lorentz covariant in a space with finite torsion and curvature. This is given the appellation "ECE 2 covariance". One of the major advantages of ECE 2 over MH is that in the former theory the magnetic and electric charge current densities are defined geometrically. In ECE 2, the field equations of gravitation, fluid dynamics and the weak and strong nuclear forces have the same format precisely as the field equations of electrodynamics, so it is clear that unification of the four fundamental fields, and also of fluid dynamics, has been achieved for the first time in the history of physics.

Attempts at unification using the standard model are well known to be riddled with unknowns and unobservables, a theory that Pauli would have described as "not even wrong", meaning that it cannot be tested experimentally and is non Baconian.

Consider the JCE identity in a space of any dimensionality and identically non-zero torsion and curvature:

$$D_\rho R^a{}_{\lambda\mu\nu} + D_\nu R^a{}_{\lambda\rho\mu} + D_\mu R^a{}_{\lambda\nu\rho} := R^a{}_{\lambda\rho\alpha} T^\alpha{}_{\mu\nu} + R^a{}_{\lambda\nu\alpha} T^\alpha{}_{\rho\mu} + R^a{}_{\lambda\mu\alpha} T^\alpha{}_{\nu\rho} \quad (3.1)$$

in the notation of chapter two the identity is a cyclic sum of covariant derivatives of curvature tensors. In Eq. (3.1) the index a of the Cartan space [2]- [13] has been used. In the famous 1902 second Bianchi identity, on which the Einstein field equation is based directly, this cyclic sum is incorrectly zero. So the JCE identity, part of the second post Einsteinian paradigm shift thus named by Alwyn van der Merwe, immediately signals the fact that the Einstein field equation is incorrect and should be discarded as obsolete. The `www.aias.us` scientometrics show clearly that this is a mainstream point of view. So there are two main schools of thought, ECE and ECE 2, and the obsolete standard model.

Clearly, the rigorously correct JCE identity contains torsion tensors. In a four dimensional space, the Hodge dual of an antisymmetric tensor or tensor valued two form of differential geometry is another antisymmetric tensor or vector valued two form. The Hodge dual is denoted by a tilde. So in four dimensions the second JCE identity is:

$$D_\rho \widetilde{R}^a{}_{\lambda\mu\nu} + D_\nu \widetilde{R}^a{}_{\lambda\rho\mu} + D_\mu \widetilde{R}^a{}_{\lambda\nu\rho} := R^a{}_{\lambda\rho\alpha} \widetilde{T}^\alpha{}_{\mu\nu} + R^a{}_{\lambda\nu\alpha} \widetilde{T}^\alpha{}_{\rho\mu} + R^a{}_{\lambda\mu\alpha} \widetilde{T}^\alpha{}_{\nu\rho} . \quad (3.2)$$

Eqs. (3.1) and (3.2) can be rewritten as:

$$D_\mu \widetilde{R}^a{}_\lambda{}^{\mu\nu} := R^a{}_{\lambda\mu\alpha} \widetilde{T}^{\alpha\mu\nu} \quad (3.3)$$

and

$$D_\mu R^a{}_\lambda{}^{\mu\nu} := R^a{}_{\lambda\mu\alpha} T^{\alpha\mu\nu} \quad (3.4)$$

respectively.

Now define a new curvature tensor as follows:

$$R^{\mu\nu} := q^\lambda{}_a R^a{}_\lambda{}^{\mu\nu} . \quad (3.5)$$

Its Hodge dual is:

$$\widetilde{R}^{\mu\nu} := q^{\lambda}{}_{a}\widetilde{R}^{a}{}_{\lambda}{}^{\mu\nu}. \tag{3.6}$$

The new curvature $R^{\mu\nu}$ and its Hodge dual lead to the new field equations of ECE 2 theory, and are part of the second paradigm shift. They lead to vector field equations which have the same fundamental structure as the MH equations but which contain much more information. Using the tetard postulate as describe in Note 315(7) on `www.aias.us` leads to

$$D_{\mu}\widetilde{R}^{\mu\nu} = R_{\mu\alpha}\widetilde{T}^{\alpha\mu\nu};\ D_{\mu}R^{\mu\nu} = R_{\mu\alpha}T^{\alpha\mu\nu} \tag{3.7}$$

Now use the Ricci identity, which is the same thing as the covariant derivative of a rank two tensor:

$$D_{\sigma}T^{\mu_1\mu_2} = \partial_{\sigma}T^{\mu_1\mu_2} + \Gamma^{\mu_1}{}_{\sigma\lambda}T^{\lambda\mu_2} + \Gamma^{\mu_2}{}_{\sigma\lambda}T^{\mu_1\lambda} \tag{3.8}$$

to find that:

$$D_{\mu}\widetilde{R}^{\mu\nu} = \partial_{\mu}\widetilde{R}^{\mu\nu} + \Gamma^{\mu}{}_{\mu\lambda}\widetilde{R}^{\lambda\nu} + \Gamma^{\nu}{}_{\mu\lambda}\widetilde{R}^{\mu\lambda} \tag{3.9}$$

and

$$D_{\mu}R^{\mu\nu} = \partial_{\mu}R^{\mu\nu} + \Gamma^{\mu}{}_{\mu\lambda}R^{\lambda\nu} + \Gamma^{\nu}{}_{\mu\lambda}R^{\mu\lambda}. \tag{3.10}$$

It follows that:

$$\partial_{\mu}\widetilde{R}^{\mu\nu} = j^{\nu} \tag{3.11}$$

and

$$\partial_{\mu}R^{\mu\nu} = J^{\nu} \tag{3.12}$$

where:

$$j^{\nu} = R_{\mu\alpha}\widetilde{T}^{\alpha\mu\nu} - \Gamma^{\mu}{}_{\mu\lambda}\widetilde{R}^{\lambda\nu} - \Gamma^{\nu}{}_{\mu\lambda}\widetilde{R}^{\mu\lambda} \tag{3.13}$$

and

$$J^{\nu} = R_{\mu\alpha}T^{\alpha\mu\nu} - \Gamma^{\mu}{}_{\mu\lambda}R^{\lambda\nu} - \Gamma^{\nu}{}_{\mu\lambda}R^{\mu\lambda}. \tag{3.14}$$

This geometry is transformed into electrodynamics using the ECE 2 hypothesis:

$$F^{\mu\nu} = W^{(0)}R^{\mu\nu} \tag{3.15}$$

where $W^{(0)}$ is a scalar with the units of magnetic flux (weber or tesla metres squared). It follows that the tensorial equations of electrodynamics in ECE 2 theory are:

$$\partial_{\mu}\widetilde{F}^{\mu\nu} = W^{(0)}j^{\nu} = j^{\nu}_{M} \tag{3.16}$$

and

$$\partial_\mu F^{\mu\nu} = W^{(0)} J^\nu = J_E^\nu \tag{3.17}$$

where j_M^ν and J_E^ν are magnetic and electric charge / current densities. To translate the tensor field equations into vector field equations define:

$$F^{\mu\nu} := \begin{bmatrix} 0 & -E_X/c & -E_Y/c & -E_Z/c \\ E_X/c & 0 & -B_Z & B_Y \\ E_Y/c & B_Z & 0 & -B_X \\ E_Z/c & -B_Y & B_X & 0 \end{bmatrix} \tag{3.18}$$

and

$$\widetilde{F}^{\mu\nu} := \begin{bmatrix} 0 & -B_X & -B_Y & -B_Z \\ B_X & 0 & E_Z/c & -E_Y/c \\ B_Y & -E_Z/c & 0 & E_X/c \\ B_Z & E_Y/c & -E_X/c & 0 \end{bmatrix} \tag{3.19}$$

In the notation of chapter two. It follows that the ECE 2 field equations of electrodynamics are the following four equations

$$\boldsymbol{\nabla} \cdot \mathbf{B} = W^{(0)} j_0 \tag{3.20}$$

$$\boldsymbol{\nabla} \times \mathbf{E} + \frac{\partial \mathbf{B}}{\partial t} = c W^{(0)} \mathbf{j} \tag{3.21}$$

$$\boldsymbol{\nabla} \cdot \mathbf{E} = c W^{(0)} J_0 \tag{3.22}$$

$$\boldsymbol{\nabla} \times \mathbf{B} - \frac{1}{c^2} \frac{\partial \mathbf{E}}{\partial t} = W^{(0)} \mathbf{J}. \tag{3.23}$$

In these equations:

$$\boldsymbol{j} = j^1 \mathbf{i} + j^2 \mathbf{j} + j^3 \mathbf{k} = j_X \mathbf{i} + j_Y \mathbf{j} + j_Z \mathbf{k} \tag{3.24}$$

and

$$\boldsymbol{J} = J^1 \mathbf{i} + J^2 \mathbf{j} + J^3 \mathbf{k} = J_X \mathbf{i} + J_Y \mathbf{j} + J_Z \mathbf{k}. \tag{3.25}$$

In Eqs. (3.20) to (3.25) the internal indices are implied (UFT 315 on `www.aias.us`). As described in this chapter, they can be removed without loss of generality.

Eqs. (3.20) to (3.23) have the same overall structure as the MH equations but contain much more information. This book begins their development.

The ECE 2 field equations (3.20) to (3.23) allow for the existence of the magnetic charge, or magnetic monopole:

$$j_M^0 = W^{(0)} j^0 \tag{3.26}$$

where

$$j^0 = R_{\mu\alpha} \widetilde{T}^{\alpha\mu 0} - \Gamma^\mu{}_{\mu\lambda} \widetilde{R}^{\lambda 0} - \Gamma^0{}_{\mu\lambda} \widetilde{R}^{\mu\lambda}. \tag{3.27}$$

The magnetic current density is:

$$\mathbf{j}_M = cW^{(0)}\mathbf{j} \tag{3.28}$$

where

$$j^\nu = R_{\mu\alpha}\widetilde{T}^{\alpha\mu\nu} - \Gamma^\mu{}_{\mu\lambda}\widetilde{R}^{\lambda\nu} - \Gamma^\nu{}_{\mu\lambda}\widetilde{R}^{\mu\lambda} \tag{3.29}$$

for the three indices

$$\nu = 1, 2, 3. \tag{3.30}$$

The electric charge density is defined by:

$$J^0_E = cW^{(0)}J^0 \tag{3.31}$$

where

$$J^0 = R_{\mu\alpha}T^{\alpha\mu 0} - \Gamma^\mu{}_{\mu\lambda}R^{\lambda 0} - \Gamma^0{}_{\mu\lambda}R^{\mu\lambda} \tag{3.32}$$

and the electric current density is:

$$\mathbf{J}_E = W^{(0)}\mathbf{J} \tag{3.33}$$

where

$$\mathbf{J} = J^1\mathbf{i} + J^2\mathbf{j} + J^3\mathbf{k}. \tag{3.34}$$

For the three indices:

$$\nu = 1, 2, 3 \tag{3.35}$$

then:

$$J^\mu = R_{\mu\alpha}T^{\alpha\mu\nu} - \Gamma^\mu{}_{\mu\lambda}R^{\lambda\nu} - \Gamma^\nu{}_{\mu\lambda}R^{\mu\lambda}. \tag{3.36}$$

Eqs. (3.20) to (3.23) are the curvature based Gauss, Faraday, Coulomb and Ampère Maxwell laws.

In the second ECE 2 hypothesis introduced in UFT 315, the electromagnetic field is defined as:

$$F^a{}_{\lambda\mu\nu} := W^{(0)}R^a{}_{\lambda\mu\nu} \tag{3.37}$$

which compares with the original ECE hypothesis of 2003:

$$F^a{}_{\mu\nu} := A^{(0)}T^a{}_{\mu\nu}\,. \tag{3.38}$$

Using the Cartan identity:

$$D_\mu T^a{}_{\nu\rho} + D_\rho T^a{}_{\mu\nu} + D_\nu T^a{}_{\rho\mu} := R^a{}_{\mu\nu\rho} + R^a{}_{\rho\mu\nu} + R^a{}_{\nu\rho\mu} \tag{3.39}$$

it follows that:

$$D_\mu F^a{}_{\nu\rho} + D_\rho F^a{}_{\mu\nu} + D_\nu F^a{}_{\rho\mu} := \frac{A^{(0)}}{W^{(0)}}\left(F^a{}_{\mu\nu\rho} + F^a{}_{\rho\mu\nu} + F^a{}_{\nu\rho\mu}\right). \tag{3.40}$$

The Cartan tangent indices can be removed without loss of generality as described in UFT 316. In the vector notation introduced in UFT 254 and UFT 255, the Cartan identity splits into two vector equations, the first of which is:

$$\boldsymbol{\nabla} \cdot \mathbf{T}^a(\text{spin}) + \boldsymbol{\omega}^a{}_b \cdot \mathbf{T}^b(\text{spin}) = \mathbf{q}^b \cdot \mathbf{R}^a{}_b(\text{spin}) \tag{3.41}$$

where $\mathbf{T}^a(\text{spin})$ is the spin torsion vector, $\boldsymbol{\omega}^a{}_b$ is the spin connection vector, $\mathbf{q}^b$ the tetrad vector and $\mathbf{R}^a{}_b(\text{spin})$ the spin curvature vector. In the original ECE theory the magnetic flux density is defined as:

$$\mathbf{B}^a = A^{(0)}\mathbf{T}^a(\text{spin}) \tag{3.42}$$

where the scalar $A^{(0)}$ has the units of flux density (tesla or weber per square metre). This definition is used also in ECE 2 and is supplemented by the new hypothesis:

$$\mathbf{B}^a{}_b = W^{(0)}\mathbf{R}^a{}_b(\text{spin}) \tag{3.43}$$

where $W^{(0)}$ has the units of weber and where the units of spin curvature are inverse square metres.

Therefore Eq. (3.41) of geometry becomes:

$$\boldsymbol{\nabla} \cdot \mathbf{B}^a + \boldsymbol{\omega}^a{}_b \cdot \mathbf{B}^b = \left(\frac{A^{(0)}}{W^{(0)}}\right)\mathbf{A}^b \cdot \mathbf{B}^a{}_b = \frac{1}{r^{(0)}}\mathbf{q}^b \cdot \mathbf{B}^a{}_b \tag{3.44}$$

of electrodynamics, where the characteristic length $r^{(0)}$ has the units of metres. The electromagnetic potential $\mathbf{A}^b$ is defined in the original ECE theory:

$$\mathbf{A}^b = A^{(0)}\mathbf{q}^b \tag{3.45}$$

so Eq. (3.44) becomes the Gauss law of magnetism, Q. E. D.:

$$\boldsymbol{\nabla} \cdot \mathbf{B}^a = \frac{1}{W^{(0)}}\mathbf{A}^b \cdot \mathbf{B}^a{}_b - \boldsymbol{\omega}^a{}_b \cdot \mathbf{B}^b \tag{3.46}$$

The magnetic charge or monopole is defined by:

$$J_m^{(0)} = \frac{1}{W^{(0)}}\mathbf{A}^b \cdot \mathbf{B}^a{}_b - \boldsymbol{\omega}^a{}_b \cdot \mathbf{B}^b. \tag{3.47}$$

The tangent indices can be removed without loss of generality using a procedure introduced in UFT 316:

$$\mathbf{B} := -e_a\mathbf{B}^a \tag{3.48}$$

where e_a is the unit vector in the tangent space. In the Cartesian basis:

$$e_a = (1, -1, -1, -1) \tag{3.49}$$

and in the complex circular basis:

$$e_a = \left(1, -\frac{1}{\sqrt{2}}(1+i), -\frac{1}{\sqrt{2}}(1-i), -1\right). \tag{3.50}$$

So in the complex circular basis:

$$\mathbf{B} = e_{(0)}\mathbf{B}^{(0)} - e_{(1)}\mathbf{B}^{(1)} - e_{(2)}\mathbf{B}^{(2)} - e_{(3)}\mathbf{B}^{(3)}. \tag{3.51}$$

By definition:

$$\mathbf{B}^{(0)} = \mathbf{0} \tag{3.52}$$

because the spacelike vector $\mathbf{B}$ has no timelike component. In general:

$$\mathbf{B}^{(1)} = \frac{1}{\sqrt{2}}\left(B_X\mathbf{i} - iB_Y\mathbf{j}\right) \tag{3.53}$$

and:

$$\mathbf{B}^{(2)} = \frac{1}{\sqrt{2}}\left(B_X\mathbf{i} + iB_Y\mathbf{j}\right). \tag{3.54}$$

So in Eq. (3.51):

$$\begin{aligned}\mathbf{B} &= \frac{1}{\sqrt{2}}(1+i)\frac{1}{\sqrt{2}}\left(B_X\mathbf{i} - iB_Y\mathbf{j}\right) + \frac{1}{\sqrt{2}}(1-i)\frac{1}{\sqrt{2}}\left(B_X\mathbf{i} + iB_Y\mathbf{j}\right) + B_Z\mathbf{k} \\ &= B_X\mathbf{i} + B_Y\mathbf{j} + B_Z\mathbf{k}\end{aligned} \tag{3.55}$$

where we have used:

$$\mathbf{B}^{(3)} = B_Z\mathbf{k}. \tag{3.56}$$

Now multiply both sides of Eq. (3.46) by $-e_a$ to obtain:

$$\boldsymbol{\nabla}\cdot\mathbf{B} = \frac{1}{W^{(0)}}\mathbf{A}^b\cdot\mathbf{B}_b - \boldsymbol{\omega}_b\cdot\mathbf{B}^b \tag{3.57}$$

in which:

$$\mathbf{A}^b\cdot\mathbf{B}_b = e^b e_b\mathbf{A}\cdot\mathbf{B} \tag{3.58}$$

$$\boldsymbol{\omega}_b\cdot\mathbf{B}^b = e_b e^b\boldsymbol{\omega}\cdot\mathbf{B}. \tag{3.59}$$

In the Cartesian basis:

$$e_b e^b = e^b e_b = -2 \tag{3.60}$$

and

$$e_b e^{b*} = e^b e_b{}^* = -2 \tag{3.61}$$

where $*$ denotes complex conjugate. So:

$$\boldsymbol{\nabla}\cdot\mathbf{B} = 2\mathbf{B}\cdot\left(\boldsymbol{\omega} - \frac{1}{W^{(0)}}\mathbf{A}\right) \tag{3.62}$$

and the magnetic monopole can be defined as:

$$J_m^0 = 2\mathbf{B} \cdot \left(\boldsymbol{\omega} - \frac{1}{W^{(0)}} \mathbf{A} \right) \tag{3.63}$$

and vanishes if and only if:

$$\mathbf{A} = W^{(0)} \boldsymbol{\omega}. \tag{3.64}$$

The spin torsion and spin curvature are defined in vector notation as:

$$\mathbf{T}^b(\text{spin}) = \boldsymbol{\nabla} \times \mathbf{q}^b - \boldsymbol{\omega}^b{}_c \times \mathbf{q}^c \tag{3.65}$$

and

$$\mathbf{R}^a{}_b(\text{spin}) = \boldsymbol{\nabla} \times \boldsymbol{\omega}^a{}_b - \boldsymbol{\omega}^a{}_c \times \boldsymbol{\omega}^c{}_b \tag{3.66}$$

from which it follows after some algebra that:

$$\boldsymbol{\nabla} \cdot \mathbf{q}^b \times \boldsymbol{\omega}^a{}_b = 0. \tag{3.67}$$

This is the most succinct format of the vector equation (3.41).

In ECE 2, the magnetic flux potential is defined by:

$$\mathbf{W}^a{}_b = W^{(0)} \boldsymbol{\omega}^a{}_b. \tag{3.68}$$

in units of tesla metres. The ECE 2 hypothesis (3.68) augments the original ECE hypothesis:

$$\mathbf{A}^a = A^{(0)} \mathbf{q}^a. \tag{3.69}$$

It follows from the geometrical equation (3.67) that:

$$\boldsymbol{\nabla} \cdot \mathbf{A}^b \times \mathbf{W}^a{}_b = 0 \tag{3.70}$$

and after removal of indices:

$$\boldsymbol{\nabla} \cdot \mathbf{A} \times \mathbf{W} = 0 \tag{3.71}$$

giving a fundamental relation between $\mathbf{A}$ and $\mathbf{W}$.

The Faraday law of induction is derived from the second vector format of the Cartan identity:

$$\begin{aligned} \frac{1}{c} \frac{\partial \mathbf{T}^a(\text{spin})}{\partial t} + \boldsymbol{\nabla} \times \mathbf{T}^a(\text{orb}) = q^b{}_0 \mathbf{R}^a{}_b(\text{spin}) + \mathbf{q}^b \times \mathbf{R}^a{}_b(\text{orb}) \\ - \left(\omega^a{}_{0b} \mathbf{T}^b(\text{spin}) + \boldsymbol{\omega}^a{}_b \times \mathbf{T}^b(\text{orb}) \right) \end{aligned} \tag{3.72}$$

in which:

$$\mathbf{T}^a(\text{orb}) = -\boldsymbol{\nabla} q^a{}_0 - \frac{1}{c} \frac{\partial \mathbf{q}^a}{\partial t} - \boldsymbol{\omega}^a{}_{0b} \mathbf{q}^b + q^b{}_0 \boldsymbol{\omega}^a{}_b \tag{3.73}$$

is the orbital torsion and

$$\mathbf{R}^a{}_b(\text{orb}) = -\boldsymbol{\nabla}\boldsymbol{\omega}^a{}_{0b} - \frac{1}{c}\frac{\partial \boldsymbol{\omega}^a{}_b}{\partial t} - \omega^a{}_{0c}\boldsymbol{\omega}^c{}_b + \omega^c{}_{0b}\boldsymbol{\omega}^a{}_c \tag{3.74}$$

is the orbital curvature. Notes 316(6) and 316(7) on `www.aias.us` translate these into equations of electromagnetism using:

$$\begin{aligned} &\mathbf{B}^a = A^{(0)}\mathbf{T}^a(\text{spin});\ \mathbf{B}^a{}_b = W^{(0)}\mathbf{R}^a{}_b(\text{spin}); \\ &\mathbf{E}^a = cA^{(0)}\mathbf{T}^a(\text{orb});\ \mathbf{E}^a{}_b = cW^{(0)}\mathbf{R}^a{}_b(\text{orb}). \end{aligned} \tag{3.75}$$

After some vector algebra written out in full in Note 316(7), the Faraday law of induction is deduced:

$$\frac{\partial \mathbf{B}}{\partial t} + \boldsymbol{\nabla} \times \mathbf{E} = \mathbf{J}_m \tag{3.76}$$

where the magnetic current density is:

$$\mathbf{J}_m = 2\left(c\left(\omega_0 - \frac{q_0}{r^{(0)}}\right)\mathbf{B} + \left(\boldsymbol{\omega} - \frac{1}{r^{(0)}}\mathbf{q}\right) \times \mathbf{E}\right). \tag{3.77}$$

This is zero if and only if

$$q_0 = r^{(0)}\omega_0 \tag{3.78}$$

and

$$\mathbf{q} = r^{(0)}\boldsymbol{\omega}. \tag{3.79}$$

The complete set of ECE 2 field and potential equations can also be derived from the Cartan and Cartan Evans identities with two fundamental hypotheses. The tangent indices can be removed and the equations of electrodynamics derived exactly, together with the conservation laws. The ECE 2 field potential relations are derived from the Maurer Cartan structure equations. The resulting field equations as derived in UFT 317 are as follows:

$$\boldsymbol{\nabla} \cdot \mathbf{B} = \boldsymbol{\kappa} \cdot \mathbf{B} \tag{3.80}$$

$$\boldsymbol{\nabla} \cdot \mathbf{E} = \boldsymbol{\kappa} \cdot \mathbf{E} \tag{3.81}$$

$$\frac{\partial \mathbf{B}}{\partial t} + \boldsymbol{\nabla} \times \mathbf{E} = -\left(\kappa_0 c\mathbf{B} + \boldsymbol{\kappa} \times \mathbf{E}\right) \tag{3.82}$$

$$\boldsymbol{\nabla} \times \mathbf{B} - \frac{1}{c^2}\frac{\partial \mathbf{E}}{\partial t} = \frac{\kappa_0}{c}\mathbf{E} + \boldsymbol{\kappa} \times \mathbf{B} \tag{3.83}$$

where:

$$\kappa_0 = 2\left(\frac{q_0}{r^{(0)}} - \omega_0\right) \tag{3.84}$$

$$\boldsymbol{\kappa} = 2\left(\frac{1}{r^0}\mathbf{q} - \boldsymbol{\omega}\right) \tag{3.85}$$

and where the tetrad four vector is:

$$q_\mu = (q_0, -\mathbf{q})\,. \tag{3.86}$$

The spin connection four vector is:

$$\omega_\mu = (\omega_0, -\boldsymbol{\omega})\,. \tag{3.87}$$

Here $\boldsymbol{\kappa}$ is the wave vector of spacetime, and $c\kappa_0$ has the units of frequency. The tetrad and spin connection are incorporated into the wave four vector of spacetime itself:

$$\kappa^\mu = \left(\kappa^0, \boldsymbol{\kappa}\right), \tag{3.88}$$

$$\kappa_\mu = (\kappa_0, -\boldsymbol{\kappa})\,. \tag{3.89}$$

In the absence of a magnetic charge / current density:

$$\boldsymbol{\nabla} \cdot \mathbf{B} = 0 \tag{3.90}$$

$$\boldsymbol{\nabla} \times \mathbf{E} + \frac{\partial \mathbf{B}}{\partial t} = \mathbf{0} \tag{3.91}$$

$$\boldsymbol{\nabla} \cdot \mathbf{E} = \boldsymbol{\kappa} \cdot \mathbf{E} = \frac{\rho}{\epsilon_0} \tag{3.92}$$

$$\boldsymbol{\nabla} \times \mathbf{B} - \frac{1}{c^2}\frac{\partial \mathbf{E}}{\partial t} = \mu_0 \mathbf{J} = \boldsymbol{\kappa} \times \mathbf{B}. \tag{3.93}$$

This is precisely the structure of MH theory but written in a space in which both curvature and torsion are identically non-zero. In the absence of a magnetic charge current density

$$\kappa_0 = 2\left(\frac{q_0}{r^{(0)}} - \omega_0\right) = 0 \tag{3.94}$$

and

$$\mathbf{B} \perp \boldsymbol{\kappa};\ \mathbf{E} \parallel \boldsymbol{\kappa}. \tag{3.95}$$

It follows that:

$$\mathbf{E} \perp \mathbf{B}, \tag{3.96}$$

a result that is self consistently derivable from the JCE identity of UFT 313 in UFT 314 ff. and summarized in this chapter.

The electric charge density is:

$$\rho = \epsilon_0 \boldsymbol{\kappa} \cdot \mathbf{E} \tag{3.97}$$

and the electric current density is:

$$\mathbf{J} = \frac{1}{\mu_0}\boldsymbol{\kappa} \times \mathbf{B} \tag{3.98}$$

where

$$\epsilon_0 \mu_0 = \frac{1}{c^2}. \tag{3.99}$$

The electric charge current density is therefore:

$$J^\mu = (c\rho, \mathbf{J}) = \frac{1}{\mu_0}\left(\frac{1}{c}\boldsymbol{\kappa}\cdot\mathbf{E}, \boldsymbol{\kappa}\times\mathbf{B}\right) \tag{3.100}$$

in the absence of a magnetic monopole. The conservation of charge current density is a fundamental law of physics which is given immediately by ECE 2 as follows. From Eq. (3.93)

$$\mu_0 \boldsymbol{\nabla}\cdot\mathbf{J} = \boldsymbol{\nabla}\cdot\boldsymbol{\nabla}\times\mathbf{B} - \frac{1}{c^2}\boldsymbol{\nabla}\cdot\frac{\partial\mathbf{E}}{\partial t} = -\frac{1}{c^2}\frac{\partial}{\partial t}\left(\boldsymbol{\nabla}\cdot\mathbf{E}\right) = -\mu_0\frac{\partial\rho}{\partial t} \tag{3.101}$$

using Eq. (3.91). Therefore:

$$\frac{\partial\rho}{\partial t} + \boldsymbol{\nabla}\cdot\mathbf{J} = 0 \tag{3.102}$$

i. e.

$$\partial\mu J^\mu = 0. \tag{3.103}$$

This means that:

$$\frac{\partial}{\partial t}\left(\boldsymbol{\kappa}\cdot\mathbf{E}\right) + c^2\boldsymbol{\nabla}\cdot\left(\boldsymbol{\kappa}\times\mathbf{B}\right) = 0 \tag{3.104}$$

in the absence of magnetic charge / current density. Therefore if $\mathbf{E}$ and $\mathbf{B}$ are known, $\boldsymbol{\kappa}$ can be found from Eq. (3.104). The free space equations are defined by Eq. (3.94) together with

$$\mathbf{q} = r^{(0)}\boldsymbol{\omega} \tag{3.105}$$

and so in free space:

$$\boldsymbol{\nabla}\cdot\mathbf{B} = 0 \tag{3.106}$$

$$\boldsymbol{\nabla}\cdot\mathbf{E} = 0 \tag{3.107}$$

$$\boldsymbol{\nabla}\times\mathbf{E} + \frac{\partial B}{\partial t} = \mathbf{0} \tag{3.108}$$

$$\boldsymbol{\nabla}\times\mathbf{B} - \frac{1}{c^2}\frac{\partial\mathbf{E}}{\partial t} = \mathbf{0}. \tag{3.109}$$

So classical electrodynamics can be inferred from the Cartan and Evans identities together with the hypotheses (3.75).

ECE 2 gives all the information in ECE in a much simpler format that is easily used by scientists and engineers.

The key difference between ECE 2 and MH is that in MH:

$$A^\mu = (\phi, c\mathbf{A})\,;\ \mathbf{B} = \boldsymbol{\nabla}\times\mathbf{A} \tag{3.110}$$

and in ECE 2:

$$\mathbf{B} = \boldsymbol{\nabla} \times \mathbf{A} + 2\boldsymbol{\omega} \times \mathbf{A} \tag{3.111}$$

where the spin connection four vector is defined by:

$$\omega_\mu = (\omega_0, -\boldsymbol{\omega}) . \tag{3.112}$$

Similarly, in MH:

$$\mathbf{E} = -\boldsymbol{\nabla}\phi - \frac{\partial \mathbf{A}}{\partial t} \tag{3.113}$$

and in ECE 2:

$$\mathbf{E} = -\boldsymbol{\nabla}\phi - \frac{\partial \mathbf{A}}{\partial t} + 2\left(c\omega_0 \mathbf{A} - \phi\boldsymbol{\omega}\right). \tag{3.114}$$

The existence of the spin connection was proven recently in UFT 311, a paper in which precise agreement was reached with experimental data by use of the spin connection. So ECE 2 is based firmly on experimental data and is a Baconian theory.

In ECE 2 there are new relations between the fields and spin connections based on the vector formats of the second Maurer Cartan structure equations:

$$\mathbf{R}^a{}_b(\text{spin}) = \boldsymbol{\nabla} \times \boldsymbol{\omega}^a{}_b - \boldsymbol{\omega}^a{}_c \times \boldsymbol{\omega}^c{}_b \tag{3.115}$$

and:

$$\mathbf{R}^a{}_b(\text{orb}) = -\boldsymbol{\nabla}\omega^a{}_{0b} - \frac{1}{c}\frac{\partial \boldsymbol{\omega}^a{}_b}{\partial t} - \omega^a{}_{0c}\boldsymbol{\omega}^c{}_b + \boldsymbol{\omega}^c{}_{0b}\boldsymbol{\omega}^a{}_c. \tag{3.116}$$

Tangent indices are removed using:

$$\mathbf{R}(\text{spin}) = e^b e_a \mathbf{R}^a{}_b(\text{spin}) \tag{3.117}$$

and:

$$\mathbf{R}(\text{orb}) = e^b e_a \mathbf{R}^a{}_b(\text{orb}). \tag{3.118}$$

Therefore:

$$\mathbf{R}(\text{spin}) = \boldsymbol{\nabla} \times \boldsymbol{\omega} - \boldsymbol{\omega}_c \times \boldsymbol{\omega}^c = \boldsymbol{\nabla} \times \boldsymbol{\omega} \tag{3.119}$$

and:

$$\mathbf{R}(\text{orb}) = -\boldsymbol{\nabla}\omega_0 - \frac{1}{c}\frac{\partial \boldsymbol{\omega}}{\partial t} - \omega_{0c}\boldsymbol{\omega}^c + \omega^c{}_0\boldsymbol{\omega}_c = -\boldsymbol{\nabla}\omega_0 - \frac{1}{c}\frac{\partial \boldsymbol{\omega}}{\partial t}. \tag{3.120}$$

The geometry is converted into electrodynamics using:

$$\mathbf{B} = W^{(0)}\mathbf{R}(\text{spin}) \tag{3.121}$$

$$\mathbf{E} = cW^{(0)}\mathbf{R}(\text{orb}) \tag{3.122}$$

and:

$$W^{\mu} = W^{(0)}\omega^{\mu} \tag{3.123}$$

and the new potential four vector:

$$W^{\mu} = (\phi_w, c\mathbf{W}) \tag{3.124}$$

which has the same units as A^{μ}. Here $W^{(0)}$ has the units of magnetic flux (weber). Therefore:

$$\mathbf{B} = \boldsymbol{\nabla} \times \mathbf{W} \tag{3.125}$$

and:

$$\mathbf{E} = -c\boldsymbol{\nabla}W_0 - \frac{\partial \mathbf{W}}{\partial t} = -\boldsymbol{\nabla}\phi_w - \frac{\partial \mathbf{W}}{\partial t} \tag{3.126}$$

where:

$$\phi_w = c\mathbf{W}_0. \tag{3.127}$$

The overall result is:

$$\boldsymbol{B} = \boldsymbol{\nabla} \times \mathbf{W} = \boldsymbol{\nabla} \times \mathbf{A} + 2\boldsymbol{\omega} \times \mathbf{A} \tag{3.128}$$

and

$$\boldsymbol{E} = -\boldsymbol{\nabla}\phi_w - \frac{\partial \mathbf{W}}{\partial t} = -\boldsymbol{\nabla}\phi - \frac{\partial \mathbf{A}}{\partial t} + 2\left(c\omega_0\mathbf{A} - \phi\boldsymbol{\omega}\right). \tag{3.129}$$

The ECE 2 gravitational field equations are derived from the same geometry as the electrodynamical field equations. One of the major discoveries of this method is that the gravitational field can vanish under well defined conditions, and can become positive, so an object of mass m can be repelled by an object of mass M. The antisymmetry laws of ECE 2 are derived in the following development and are used to derive the Newtonian equivalence principle from geometry. The theory of spin connection resonance can be developed to result in zero gravitation. The Aharonov Bohm effects of vacuum ECE 2 theory are analyzed.

The gravitational field equations of ECE 2 are as follows (UFT 317 and accompanying notes):

$$\boldsymbol{\nabla} \cdot \mathbf{g} = \boldsymbol{\kappa} \cdot \mathbf{g} = 4\pi G\rho_m \tag{3.130}$$

$$\boldsymbol{\nabla} \times \mathbf{g} + \frac{\partial \boldsymbol{\Omega}}{\partial t} = -\left(c\kappa_0\boldsymbol{\Omega} + \boldsymbol{\kappa} \times \mathbf{g}\right) = \frac{4\pi G}{c}\mathbf{J}_{\Omega} \tag{3.131}$$

$$\boldsymbol{\nabla} \cdot \boldsymbol{\Omega} = \boldsymbol{\kappa} \cdot \boldsymbol{\Omega} = \frac{4\pi G}{c}\rho_{\Omega} \tag{3.132}$$

$$\boldsymbol{\nabla} \times \boldsymbol{\Omega} - \frac{1}{c^2}\frac{\partial \mathbf{g}}{\partial t} = \frac{\kappa_0}{c}\mathbf{g} + \boldsymbol{\kappa} \times \boldsymbol{\Omega} = \frac{4\pi G}{c^2}\mathbf{J}_m \tag{3.133}$$

Here $\mathbf{g}$ is the gravitational field, G is Newton's constant, ρ_m is the mass density, $\mathbf{J}_m$ is the current of mass density, $\boldsymbol{\Omega}$ is the gravitomagnetic field, ρ_{Ω}

is the gravitomagnetic mass density, and $\mathbf{J}_\Omega$ is the current of gravitomagnetic mass density. In these equations, κ_0 and $\boldsymbol{\kappa}$ are defined in the same way as for electrodynamics and the tetrad and spin connection vectors, being quantities of geometry, are defined in the same way. The field potential relations are derived in the same way as those of electrodynamics, from the Cartan and Evans identities. They are:

$$\mathbf{g} = -\boldsymbol{\nabla}\Phi - \frac{\partial \mathbf{Q}}{\partial t} + 2\left(c\omega_0 \mathbf{Q} - \Phi\boldsymbol{\omega}\right) \tag{3.134}$$

and

$$\boldsymbol{\Omega} = \boldsymbol{\nabla} \times \mathbf{Q} + 2\boldsymbol{\omega} \times \mathbf{Q} \tag{3.135}$$

where the mass / current density four vector is:

$$J_m^\mu = (c\rho_m, \mathbf{J}_m) \tag{3.136}$$

and where the gravitational vector four potential is:

$$Q^\mu = (\Phi, c\mathbf{Q})\,. \tag{3.137}$$

In electrodynamics it is always assumed that the magnetic charge / current density is zero. The parallel assumption in gravitational theory leads to the gravitational field equations:

$$\boldsymbol{\nabla} \cdot \boldsymbol{\Omega} = 0 \tag{3.138}$$

$$\boldsymbol{\nabla} \times \mathbf{g} + \frac{\partial \boldsymbol{\Omega}}{\partial t} = \mathbf{0} \tag{3.139}$$

$$\boldsymbol{\nabla} \cdot \mathbf{g} = \boldsymbol{\kappa} \cdot \mathbf{g} = 4\pi G \rho_m \tag{3.140}$$

$$\boldsymbol{\nabla} \times \boldsymbol{\Omega} - \frac{1}{c^2}\frac{\partial \mathbf{g}}{\partial t} = \boldsymbol{\kappa} \times \boldsymbol{\Omega} = \frac{4\pi G}{c^2}\mathbf{J}_m \tag{3.141}$$

whose overall structure is the same as the ECE 2 electrodynamical equations and both sets of field equations are ECE 2 covariant. From Eqs. (3.140) and (3.141):

$$\frac{4\pi G}{c^2}\boldsymbol{\nabla} \cdot \mathbf{J}_m = -\frac{1}{c^2}\frac{\partial}{\partial t}\left(\boldsymbol{\nabla} \cdot \mathbf{g}\right) = -\frac{4\pi G}{c^2}\frac{\partial \rho_m}{\partial t} \tag{3.142}$$

and it follows that:

$$\frac{\partial \rho_m}{\partial t} + \boldsymbol{\nabla} \cdot \mathbf{J}_m = 0 \tag{3.143}$$

i. e.

$$\partial_\mu J_m^\mu = 0 \tag{3.144}$$

which is the ECE 2 equation of conservation of mass current density.

In Newtonian gravitation, it is known by experiment that:

$$\mathbf{g} = g_r \mathbf{e}_r = -\frac{MG}{r^2}\mathbf{e}_r \tag{3.145}$$

to an excellent approximation, although the law (3.145) does not account for precession of the perihelion and similar, and it does not account for the Coriolis accelerations without the use of a rotating frame such as the plane polar coordinates. It follows that:

$$\frac{\partial g_r}{\partial_r} = \frac{2MG}{r^3} = 2g_r\left(\frac{1}{r^{(0)}}q_r - \omega_r\right) = -\frac{2MG}{r^2}\left(\frac{1}{r^{(0)}}q_r - \omega_r\right) \tag{3.146}$$

and that:

$$\kappa_r = -\frac{2}{r}. \tag{3.147}$$

This equation reduces ECE 2 gravitation to Newtonian gravitation, whose only field equations are:

$$\mathbf{g} = -\boldsymbol{\nabla}\Phi \tag{3.148}$$

and

$$\boldsymbol{\nabla}\cdot\mathbf{g} = 4\pi G\rho_m \tag{3.149}$$

together with the Newtonian equivalence principle:

$$\mathbf{F} = m\mathbf{g} = -\frac{mMG}{r^2}\mathbf{e}_r \tag{3.150}$$

In the Newtonian theory Eq. (3.150) is theoretically unproven but in ECE 2 gravitation it can be derived from geometry and asymmetry as follows.

Consider the ECE 2 generalizations of the Coulomb and Newton laws:

$$\boldsymbol{\nabla}\cdot\mathbf{E} = \boldsymbol{\kappa}\cdot\mathbf{E} = \rho_e/\epsilon_0 \tag{3.151}$$

and

$$\boldsymbol{\nabla}\cdot\mathbf{g} = \boldsymbol{\kappa}\cdot\mathbf{g} = 4\pi G\rho_m \tag{3.152}$$

The electric field strength is defined by:

$$\mathbf{E} = -\boldsymbol{\nabla}\phi_e - \frac{\partial\mathbf{A}}{\partial t} + 2\left(c\omega_0\mathbf{A} - \phi_e\boldsymbol{\omega}\right) \tag{3.153}$$

and the electromagnetic four potential is:

$$\mathbf{A}^\mu = (c\rho_e, \mathbf{J}_e) \tag{3.154}$$

The antisymmetry laws of ECE 2 [1]- [12] are therefore:

$$-\boldsymbol{\nabla}\phi_e + 2c\omega_0\mathbf{A} = -\frac{\partial\mathbf{A}}{\partial t} - 2\phi_e\boldsymbol{\omega} \tag{3.155}$$

and

$$-\boldsymbol{\nabla}\Phi_m + 2c\omega_0 Q = -\frac{\partial\mathbf{Q}}{\partial t} - 2\Phi_m\boldsymbol{\omega}. \tag{3.156}$$

In the absence of a vector potential $\mathbf{A}$ and vector gravitomagnetic potential $\mathbf{Q}$:

$$\mathbf{E} = -\boldsymbol{\nabla}\phi_e = -2\phi_e\boldsymbol{\omega} \tag{3.157}$$

and

$$\mathbf{g} = -\boldsymbol{\nabla}\Phi_m = -2\Phi_m\boldsymbol{\omega}. \tag{3.158}$$

The Newtonian equivalence principle follows immediately from Eq. (3.158):

$$\mathbf{F} = m\mathbf{g} = -m\boldsymbol{\nabla}\Phi = -2m\Phi\boldsymbol{\omega} \tag{3.159}$$

where the scalar gravitational potential of Newtonian universal gravitation is:

$$\Phi = -\frac{MG}{r}. \tag{3.160}$$

So:

$$\mathbf{F} = m\mathbf{g} = -\frac{mM}{r^2}\mathbf{e}_r = -\frac{2mMG}{r}\boldsymbol{\omega}. \tag{3.161}$$

It follows that the spin connection vector is:

$$\boldsymbol{\omega} = \frac{1}{2r}\mathbf{e}_r \tag{3.162}$$

Similarly in electrostatics:

$$\mathbf{F} = e\mathbf{E} = -e\boldsymbol{\nabla}\phi_e = -2m\phi_e\boldsymbol{\omega} \tag{3.163}$$

where the scalar potential is:

$$\phi_e = -\frac{e_1}{4\pi\epsilon_0 r}. \tag{3.164}$$

So

$$\mathbf{F} = e\mathbf{E} = -\frac{ee_1}{4\pi\epsilon_0 r^2}\mathbf{e}_r = -\frac{2e_1}{4\pi\epsilon_0 r}\boldsymbol{\omega} \tag{3.165}$$

and the spin connection vector is again:

$$\boldsymbol{\omega} = \frac{1}{2r}\mathbf{e}_r. \tag{3.166}$$

In the absence of a vector potential:

$$\mathbf{E} = -\boldsymbol{\nabla}\phi_e - 2\phi_e\boldsymbol{\omega} \tag{3.167}$$

and:

$$\boldsymbol{\nabla}\cdot\mathbf{E} = \frac{\rho_e}{\epsilon_0} \tag{3.168}$$

or:

$$\left(\nabla^2 + k_0^2\right)\phi_e = -\frac{\rho_e}{\epsilon_0} \tag{3.169}$$

where k_0^2 is defined by:

$$k_0^2 = 2\boldsymbol{\nabla}\cdot\boldsymbol{\omega}. \tag{3.170}$$

Eq. (3.169) becomes an undamped Euler Bernoulli equation with the following choice of electric charge density:

$$\rho_e = -\epsilon_0 A\cos(kZ) \tag{3.171}$$

so the Euler Bernoulli equation is:

$$\frac{\partial^2\phi_e}{\partial Z^2} + k_0^2\phi_e = A\cos(kZ) \tag{3.172}$$

whose solution is:

$$\phi_e = A\frac{\cos(kZ)}{k_0^2 - k^2}. \tag{3.173}$$

Similarly, in gravitational theory:

$$\left(\nabla^2 + k_0^2\right)\Phi_m = -4\pi G\rho_m. \tag{3.174}$$

This equation becomes an Euler Bernoulli equation if:

$$4\pi G\rho_m = -A\cos(kZ) \tag{3.175}$$

giving the solution:

$$\Phi_m = A\frac{\cos(kZ)}{k_0^2 - k^2}. \tag{3.176}$$

Eq. (3.174) reduces to the Poisson equation of Newtonian dynamics:

$$\nabla^2\Phi_m = -4\pi G\rho_m \tag{3.177}$$

when:

$$k_0^2 = 2\boldsymbol{\nabla}\cdot\boldsymbol{\omega} = 0. \tag{3.178}$$

The acceleration due to gravity of the laboratory mass m in ECE 2 theory is:

$$\mathbf{g}_m = -\nabla\Phi_m - 2\boldsymbol{\omega}\Phi_m \tag{3.179}$$

and the gravitational force between a test mass m and a mass M such as that of the earth is:

$$\mathbf{F} = M\mathbf{g}_m. \tag{3.180}$$

In the Z axis:

$$\Phi_m = A\frac{\cos(k_Z Z)}{k_0^2 - k_Z^2} \tag{3.181}$$

and:

$$-\boldsymbol{\nabla}\Phi_m = -\frac{\partial \Phi_m}{\partial Z} = Ak_Z \frac{\sin(k_Z Z)}{k_0^2 - k_Z^2} \tag{3.182}$$

so

$$g_Z = \frac{A}{k_0^2 - k_Z^2}\left(k_Z \sin(\kappa_Z Z) - 2\omega_Z \cos(k_Z Z)\right). \tag{3.183}$$

Under the condition:

$$\tan(k_Z Z) = 2\frac{\omega_Z}{\kappa_Z} \tag{3.184}$$

it follows that:

$$g_Z = 0 \tag{3.185}$$

and

$$\mathbf{F} = Mg_Z = 0. \tag{3.186}$$

Therefore in ECE 2 theory it is possible for gravitation to vanish.

The gravitational potential energy in joules of the mass m is:

$$U_m = m\Phi_m \tag{3.187}$$

and the electrostatic potential energy in joules of a charge e is:

$$U_e = e\phi_e. \tag{3.188}$$

Therefore:

$$\left(\nabla^2 + k_0^2\right) U_m = -4\pi m G \rho_m \tag{3.189}$$

and:

$$\left(\nabla^2 + k_0^2\right) U_e = -\frac{e\rho_e}{\epsilon_0}. \tag{3.190}$$

All forms of energy are interconvertible so:

$$\left(\nabla^2 + k_0^2\right)(U_m + U_e) = -\left(4\pi m G \rho_m + \frac{e\rho_e}{\epsilon_0}\right). \tag{3.191}$$

For a mass m of one kilogram and a charge e of one coulomb in a volume of one cubic metre

$$\frac{e\rho_e}{\epsilon_0} \gg 4\pi m G \rho_m \tag{3.192}$$

so to an excellent approximation:

$$\left(\nabla^2 + k_0^2\right)\left(m\Phi_m + e\phi_e\right) = -\frac{e}{\epsilon_0}\rho_e. \tag{3.193}$$

This equation shows that gravitation can be engineered by an on board device that is designed to produce the driving force:

$$A\cos(k_Z Z) = -\frac{e\rho_e}{\epsilon_0} \tag{3.194}$$

giving the Euler Bernoulli equation:

$$\left(\nabla^2 + k_0^2\right)\left(m\Phi_m + e\phi_e\right) = A\cos\left(\mathbf{k}\cdot\mathbf{r}\right) \tag{3.195}$$

whose solution is:

$$m\Phi_m + e\phi_e = \frac{A\cos(k_Z Z)}{k_0^2 - k_Z^2}. \tag{3.196}$$

In the Z axis:

$$\Phi_{mZ} = \frac{1}{m}\left(\frac{A\cos(k_Z Z)}{k_0^2 - k_Z^2} - e\phi_e\right) \tag{3.197}$$

and so:

$$-\frac{\partial\Phi_{mZ}}{\partial Z} = \frac{1}{m}\left(\frac{A\kappa_Z\sin(k_Z Z)}{k_0^2 - k_Z^2} - e\frac{\partial\phi_e}{\partial Z}\right) \tag{3.198}$$

giving the acceleration due to gravity:

$$g_Z = \frac{1}{m}\left[\left(\frac{Ak_Z\sin(k_Z Z)}{k_0^2 - k_Z^2} - 2\omega_Z\cos(k_Z Z)\right) + e\left(\frac{\partial\phi_e}{\partial Z} + 2\omega_Z\phi_e\right)\right]. \tag{3.199}$$

There is no gravitational force between m and M under the condition:

$$\tan(k_Z Z) = 2\frac{\omega_Z}{k_Z} \tag{3.200}$$

and:

$$\frac{\partial\phi_e}{\partial Z} = -2\omega_Z\phi_e. \tag{3.201}$$

From Eqs. (3.197) and (3.194) the gravitational potential is:

$$\Phi_m = \frac{e}{m}\left(\frac{\rho_e}{\epsilon_0(k_Z^2 - k_0^2)} - \phi_e\right) \tag{3.202}$$

and there is no gravitational force between m and M if Φ_m is zero, so in this case:

$$\phi_e = \frac{\rho_e}{\epsilon_0(k_Z^2 - k_0^2)} \tag{3.203}$$

and the electric field strength needed for the condition (3.203) is:

$$\mathbf{E} = -\boldsymbol{\nabla}\phi_e - 2\phi_e\boldsymbol{\omega}. \tag{3.204}$$

When the electric field strength of an on board device contained within a vehicle of mass m is tuned to condition (3.203), the $\mathbf{g}$ forces between m and M vanish. The vehicle is no longer attracted to the earth's mass M.

The condition for counter gravitation (positive $\mathbf{g}$) is a negative spin connection so using:

$$\mathbf{g} = -\boldsymbol{\nabla}\Phi_m + 2\Phi_m\boldsymbol{\omega} \tag{3.205}$$

$\mathbf{g}$ becomes positive, or repulsive, when

$$2\boldsymbol{\omega}\Phi_0 > \boldsymbol{\nabla}\Phi_m \tag{3.206}$$

and a mass m is lifted off the ground, i. e. is repelled by the earth's mass M. This process can be amplified by spin connection resonance as described already.

The ECE 2 vacuum is defined in several ways in this book. It is convenient to begin the development of vacuum theory using the equations:

$$\mathbf{E} = -\boldsymbol{\nabla}\phi - \frac{\partial \mathbf{A}}{\partial t} + 2\left(c\omega_0\mathbf{A} - \phi\boldsymbol{\omega}\right) = \mathbf{0} \tag{3.207}$$

and

$$\mathbf{B} = \boldsymbol{\nabla} \times \mathbf{A} + 2\boldsymbol{\omega} \times \mathbf{A} = \mathbf{0} \tag{3.208}$$

which show that ϕ and $\mathbf{A}$ can be non zero when $\mathbf{E}$ and $\mathbf{B}$ are zero. These are the well known conditions for the Aharonov Bohm (AB) effects, potentials are observed experimentally to exist in the absence of fields.

Under the AB condition, the ECE 2 potentials describe the electromagnetic energy present in spacetime (or vacuum or aether).

By antisymmetry:

$$-\boldsymbol{\nabla}\phi + 2c\omega_0\mathbf{A} = -\frac{\partial \mathbf{A}}{\partial t} - 2\phi\boldsymbol{\omega} \tag{3.209}$$

and it follows that the vacuum potentials are defined by:

$$-\boldsymbol{\nabla}\phi + 2c\omega_0\mathbf{A} = \mathbf{0}, \tag{3.210}$$

$$-\frac{\partial \mathbf{A}}{\partial t} = 2\phi\boldsymbol{\omega}, \tag{3.211}$$

$$\boldsymbol{\nabla} \times \mathbf{A} + 2\boldsymbol{\omega} \times \mathbf{A} = \mathbf{0}. \tag{3.212}$$

If it is assumed for the sake of simplicity that:

$$\omega_0 = 0 \tag{3.213}$$

then there are three equations in three unknowns:

$$-\boldsymbol{\nabla}\phi + 2c\omega_0\mathbf{A} = \mathbf{0} \tag{3.214}$$

$$-\frac{\partial \mathbf{A}}{\partial t} = 2\phi\boldsymbol{\omega};\ \boldsymbol{\nabla}\times\mathbf{A} + 2\boldsymbol{\omega}\times\mathbf{A} = \mathbf{0}. \tag{3.215}$$

These can be solved for ϕ, $\mathbf{A}$ and $\boldsymbol{\omega}$ of the vacuum.

Using the minimal prescription the energy momentum contained in the vacuum is:

$$E^{\mu} = \left(\frac{E}{c}, \mathbf{p}\right) = eA^{\mu} = e\left(\frac{\phi}{c}, \mathbf{A}\right). \tag{3.216}$$

Therefore the ECE 2 vacuum is made up of photons with mass with energy momentum:

$$E^{\mu} = eA^{\mu} = \hbar\kappa^{\mu} = \hbar\left(\frac{\omega}{c}, \boldsymbol{\kappa}\right) \tag{3.217}$$

obeying the vacuum Einstein/de Broglie equations:

$$E = e\phi = \hbar\omega = \gamma mc^2 \tag{3.218}$$

and

$$\mathbf{p} = e\mathbf{A} = \hbar\boldsymbol{\kappa} = \gamma m\mathbf{v} \tag{3.219}$$

where m is the mass of the photon and where the Lorentz factor is

$$\gamma = \left(1 - \frac{v^2}{c^2}\right)^{-1/2}. \tag{3.220}$$

In UFT 311 on `www.aias.us` and `www.upitec.org`, the circuit design needed to take energy from the vacuum is described in all detail, and excellent agreement is reported with the earlier ECE theory, developed into ECE 2 theory in this book.

ECE 2 provides a new and simple explanation for light deflection due to gravitation, and in so doing gives new estimates of photon mass using ECE 2 covariance. In ECE 2 the force due to gravity is

$$\mathbf{F} = m\mathbf{g} = -\boldsymbol{\nabla}U - \frac{\partial \mathbf{p}}{\partial t} - 2U\boldsymbol{\omega} + 2c\omega_0\mathbf{p} \tag{3.221}$$

where the potential energy in joules is:

$$U = m\Phi. \tag{3.222}$$

The spin connection four vector is:

$$\omega^{\mu} = (\omega_0, \boldsymbol{\omega}) \tag{3.223}$$

and from the minimal prescription the linear momentum $\mathbf{p}$ is:

$$\mathbf{p} = m\mathbf{Q} \tag{3.224}$$

where the gravitational four potential is:

$$\Phi^{\mu} = \left(\frac{\Phi}{c}, \mathbf{Q}\right). \tag{3.225}$$

By antisymmetry:

$$-\boldsymbol{\nabla}U - \frac{\partial \mathbf{p}}{\partial t} = -2U\boldsymbol{\omega} + 2c\omega_0\mathbf{p} \tag{3.226}$$

so the gravitational force is:

$$\mathbf{F} = m\mathbf{g} = 2\left(-\boldsymbol{\nabla}U - \frac{\partial \mathbf{p}}{\partial t}\right) = 4\left(c\omega_0\mathbf{p} - U\boldsymbol{\omega}\right). \tag{3.227}$$

It is well known [2]- [13] that there are severe limitations to the Newtonian theory, it does not give perihelion precession, and cannot explain light deflection due to gravity or the velocity curve of a whirlpool galaxy. It is also known that the Einstein theory is riddled with errors and omissions, and cannot describe the velocity curve of a whirlpool galaxy [2]- [13]. It has already been shown in this chapter how ECE 2 theory reduces to Newtonian theory, but the former theory has several major advantages. For example it gives a reason for gravitation, the latter is geometry with non zero torsion and curvature. Newton did not give a reason for gravitation.

The ECE 2 theory can be reduced to its Newtonian limit by using:

$$\boldsymbol{\nabla}U = \frac{\partial \mathbf{p}}{\partial t} \tag{3.228}$$

and

$$c\omega_0\mathbf{p} = -U\boldsymbol{\omega} \tag{3.229}$$

which are expressions of the equivalence principle as argued in UFT 319 and its accompanying notes on `www.aias.us`. Using Eqs. (3.228) and (3.229) in Eq. (3.226):

$$\mathbf{F} = m\mathbf{g} = -4\boldsymbol{\nabla}U = -8U\boldsymbol{\omega} = -\frac{mMG}{r^2}\mathbf{e}_r \tag{3.230}$$

so:

$$U = -\frac{mMG}{4r} \tag{3.231}$$

and it follows that the spin connection vector is:

$$\boldsymbol{\omega} = \frac{1}{2r}\mathbf{e}_r. \tag{3.232}$$

From Eqs. (3.147) and (3.232):

$$\kappa_r = \frac{1}{r^{(0)}}q_r - \omega_r = -\frac{2}{r} \tag{3.233}$$

so the tetrad vector is:

$$\boldsymbol{\kappa} = \kappa_r\mathbf{e}_r; \quad \mathbf{q} = -\frac{3}{2}\frac{r^{(0)}}{r}\mathbf{e}_r. \tag{3.234}$$

Using:

$$\omega_0 c\mathbf{p} = -U\boldsymbol{\omega} = \frac{mMG}{8r^2}\mathbf{e}_r \tag{3.235}$$

it follows that the momentum vector is:

$$\mathbf{p} = p_r\mathbf{e}_r = -\int_0^\tau \frac{mMG}{8r^2}\mathbf{e}_r dt \tag{3.236}$$

so the scalar part of the spin connection is defined in the Newtonian limit by:

$$\omega_0 = -\frac{1}{cr^2}\left(\int_0^\tau \frac{1}{r^2}dt\right)^{-1}. \tag{3.237}$$

The Newtonian potential ϕ and the ECE 2 potential Φ are related by

$$\phi = 4\Phi. \tag{3.238}$$

The force is therefore defined in the Newtonian limit of ECE 2 as:

$$\mathbf{F} = m\mathbf{g} = -4\boldsymbol{\nabla}U = -8U\boldsymbol{\omega} = 4\frac{\partial \mathbf{p}}{\partial t} = 8c\omega_0\mathbf{p} \tag{3.239}$$

and in the absence of gravitomagnetic charge current density:

$$q_0 = r^{(0)}\omega_0. \tag{3.240}$$

More generally the usual definition of force:

$$\mathbf{F} = m\mathbf{g} \tag{3.241}$$

should be replaced by the gravitational Lorentz force, a concept that does not exist in standard physics. Note 319(2) on `www.aias.us` shows that a possible operator solution of the Newtonian limit of ECE theory is:

$$(\omega_0, \boldsymbol{\omega}) = \frac{1}{2}\left(\frac{1}{c}\frac{\partial}{\partial t}, -\boldsymbol{\nabla}\right) \tag{3.242}$$

or

$$\omega^\mu = \frac{1}{2}\partial^\mu. \tag{3.243}$$

Using the Schrödinger quantum condition:

$$p^\mu = i\hbar\partial^\mu = 2i\hbar\omega^\mu \tag{3.244}$$

the Newtonian condition (3.228) becomes:

$$\boldsymbol{\nabla}\frac{\partial}{\partial t} + \frac{\partial}{\partial t}\boldsymbol{\nabla} = \mathbf{0} \tag{3.245}$$

giving a new anticommutator equation of quantum gravity:

$$\left\{\boldsymbol{\nabla}, \frac{1}{c}\frac{\partial}{\partial t}\right\}\psi = 0. \tag{3.246}$$

Non Newtonian effects can be explained by deviations from the above set of equations. For example in Note 319(3) it is shown that the condition for zero gravity is:

$$\omega^{\mu} = -\frac{1}{2}\partial^{\mu} \tag{3.247}$$

which is the opposite of Eq. (3.243). In Note 319(4) it is shown that ECE 2 gives a simple and original explanation for light deflection due to gravitation.

ECE 2 covariance means that the infinitesimal line element of the theory leads to:

$$c^2 d\tau^2 = \left(c^2 - v^2\right) dt^2 \tag{3.248}$$

where the orbital velocity in plane polar coordinates is:

$$v^2 = \left(\frac{dr}{dt}\right)^2 + r^2 \left(\frac{d\theta}{dt}\right)^2 . \tag{3.249}$$

Here τ is the proper time. For light deflection by the sun, the orbit to an excellent approximation is the hyperbola:

$$r = \frac{\alpha}{1 + \epsilon \cos\theta} \tag{3.250}$$

with very large eccentricity ϵ, so the orbit is almost a straight line and the light from a star grazing the sun is only very slightly deflected. Here α is the half right latitude. As shown in Note 319(4), the velocity from Eqs. (3.249) and (3.250) is

$$v^2 = \frac{mG}{R_0}\left(1 + \epsilon\right) \tag{3.251}$$

where R_0 is the distance of closest approach, equal to the half right latitude:

$$R_0 = \alpha. \tag{3.252}$$

The angle of deflection is:

$$\zeta = 2\psi = \frac{2}{\epsilon} \sim \frac{2MG}{R_0 v^2} \tag{3.253}$$

to an excellent approximation. The experimentally observed result is:

$$\zeta = \frac{4MG}{R_0 c^2} \tag{3.254}$$

so it follows that:

$$v^2 = \frac{1}{2}c^2 \tag{3.255}$$

which is equivalent to a Lorentz factor:

$$\gamma = \frac{dt}{d\tau} = \left(1 - \frac{v^2}{c^2}\right)^{-1/2} = 0.707. \tag{3.256}$$

Therefore ECE 2 covariance gives a simple and straightforward explanation of the experimental result (3.254). The result (3.255) is further interpreted in UFT 324. It means that there is an upper bound to the non relativistic velocity used in the Lorentz transform. The existence of this upper bound immediately explains the observed deflection of light and electromagnetic radiation due to gravitation in terms of ECE 2 covariance.

The photon mass can be calculated from

$$\hbar\omega = \gamma m c^2 \tag{3.257}$$

and is graphed in the subsequent section.

3.2 Numerical Analysis and Graphics

3.2.1 Plots of Photon Mass from ECE 2 Theory

The photon mass from the de Broglie-Einstein equation (3.257) is

$$m = \frac{\hbar\omega}{\gamma c^2} \tag{3.258}$$

where γ was shown to be

$$\gamma = \frac{1}{\sqrt{2}}. \tag{3.259}$$

If photons are considered as oscillators with statistical energy distribution, the average energy is given by

$$\langle\hbar\omega\rangle = \frac{\hbar\omega}{\exp(\frac{\hbar\omega}{kT}) - 1} \tag{3.260}$$

from which follows for the photon mass:

$$m = \frac{\hbar\omega}{\gamma c^2} \cdot \frac{1}{\exp(\frac{\hbar\omega}{kT}) - 1}. \tag{3.261}$$

Here k is the Boltzmann constant and T the temperature of the environment. Since the temperature near to the surface of the sun is of some thousand Kelvin, we used corresponding values for the numerical evaluation of Eq. (3.260). The results for both equations (with and without statistics) are graphed in Fig. 3.1. The photon mass of a single photon grows linearly on a double-logarithmic scale while it drops to zero for finite temperatures. There is a plateau (constant limit) in the infrared.

In a second plot (Fig. 3.2), the ratio v/c in the gamma factor has been varied for T=293 K. Obviously the results are not very sensitive to γ. Only in the ultra-relativistic limit the photon mass drops significantly.

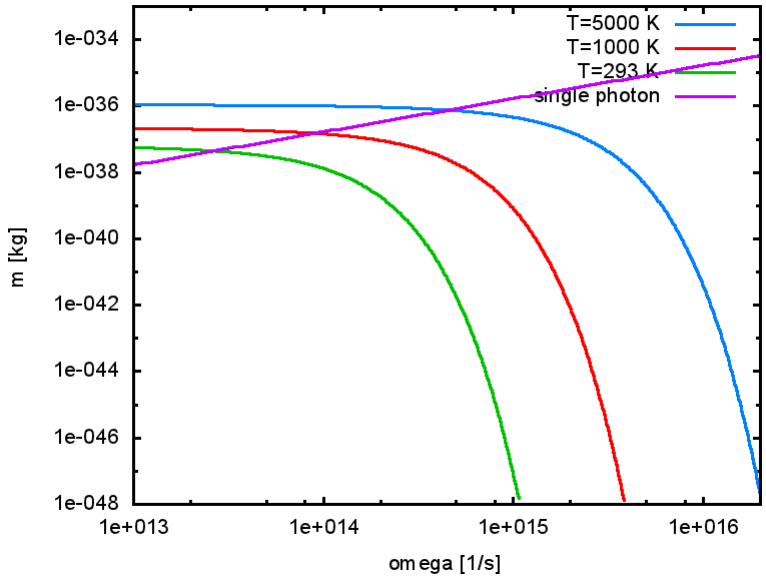

Figure 3.1: Photon mass in dependence of light frequency for various temperatures and the single-photon case.

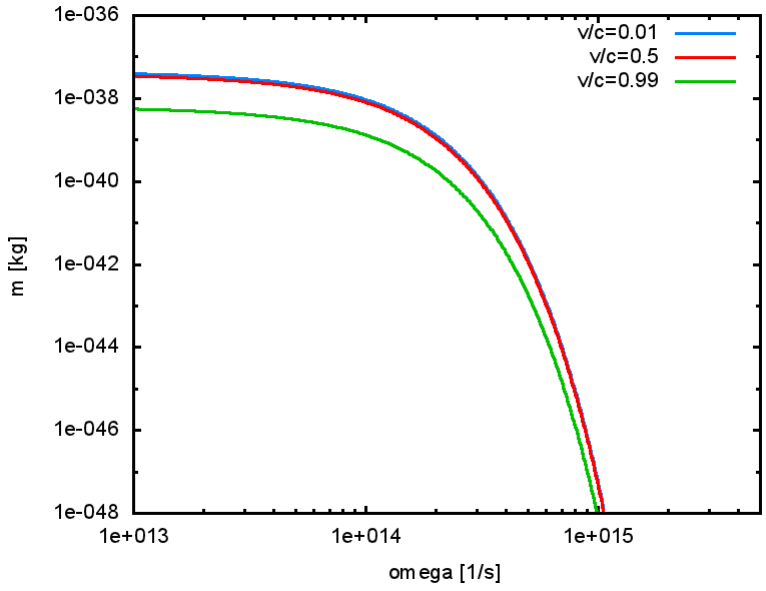

Figure 3.2: Photon mass for T=293K and different ratios v/c.

Chapter 4

Orbital Theory

4.1 General Theory

In this chapter ECE 2 covariance is developed to produce the Lorentz force equation, and to develop quantization and orbital theory. In the opening section the gravitomagnetic Biot Savart and Ampère laws are developed and these laws are applied to planar orbits and the current of mass density of the planar orbit. The method is generally valid and can be used on all scales. The gravitomagnetic field responsible for the centrifugal force of planar orbits can be calculated. Following sections of this chapter develop ECE 2 quantization and precessional theory, together with other aspects of orbital theory. From chapter three, the ECE 2 equations of gravitomagnetism are

$$\partial_\mu \widetilde{G}^{\mu\nu} = 0 \tag{4.1}$$

and

$$\partial_\mu G^{\mu\nu} = J^\nu \tag{4.2}$$

where the field tensors are defined as:

$$\widetilde{G}^{\mu\nu} = \begin{bmatrix} 0 & -c\Omega^1 & -c\Omega^2 & -c\Omega^3 \\ c\Omega^1 & 0 & g^3 & -g^2 \\ c\Omega^2 & -g^3 & 0 & g^1 \\ c\Omega^3 & g^2 & -g^1 & 0 \end{bmatrix} \tag{4.3}$$

and

$$G^{\mu\nu} = \begin{bmatrix} 0 & -g^1 & -g^2 & -g^3 \\ g^1 & 0 & -c\Omega^3 & c\Omega^2 \\ g^2 & c\Omega^3 & 0 & -c\Omega^1 \\ g^3 & -c\Omega^2 & c\Omega^1 & 0 \end{bmatrix}. \tag{4.4}$$

In these equations $\mathbf{g}$ denotes the gravitational field and $\mathbf{\Omega}$ the gravitomagnetic field. It is assumed that the gravitomagnetic charge/current density vanishes.

The contravariant index notation means that:

$$\begin{aligned} &g^1 = g_X,\ g^2 = g_Y,\ g^3 = g_Z, \\ &\Omega^1 = \Omega_X,\ \Omega^2 = \Omega_Y,\ \Omega^3 = \Omega_Z. \end{aligned} \tag{4.5}$$

Lorentz transformation [2]- [13] of the field tensors gives the result:

$$\mathbf{g}' = \gamma\left(\mathbf{g} + \mathbf{v} \times \mathbf{\Omega}\right) - \frac{\gamma^2}{1+\gamma}\frac{\mathbf{v}}{c}\left(\frac{\mathbf{v}}{c} \cdot \mathbf{g}\right) \tag{4.6}$$

$$\mathbf{\Omega}' = \gamma\left(\mathbf{\Omega} - \frac{1}{c^2}\mathbf{v} \times \mathbf{g}\right) - \frac{\gamma^2}{1+\gamma}\frac{\mathbf{v}}{c}\left(\frac{\mathbf{v}}{c} \cdot \mathbf{\Omega}\right) \tag{4.7}$$

where γ is the Lorentz factor:

$$\gamma = \left(1 - \frac{v^2}{c^2}\right)^{-1/2} \tag{4.8}$$

in which $\mathbf{v}$ is the non relativistic velocity. In the rest frame:

$$\mathbf{v} = \mathbf{0}. \tag{4.9}$$

Eqs. (4.6) and (4.7) exactly parallel electrodynamics [2]- [13]:

$$\mathbf{E}' = \gamma\left(\mathbf{E} + \mathbf{v} \times \mathbf{B}\right) - \frac{\gamma^2}{1+\gamma}\frac{\mathbf{v}}{c}\left(\frac{\mathbf{v}}{c} \cdot \mathbf{E}\right) \tag{4.10}$$

and

$$\mathbf{B}' = \gamma\left(\mathbf{B} - \frac{1}{c^2}\mathbf{v} \times \mathbf{E}\right) - \frac{\gamma^2}{1+\gamma}\frac{\mathbf{v}}{c}\left(\frac{\mathbf{v}}{c} \cdot \mathbf{B}\right) \tag{4.11}$$

where $\mathbf{E}$ is the electric field strength in volts per metre and $\mathbf{B}$ is the magnetic flux density. In the non relativistic limit:

$$v \ll c,\ \gamma \to 1 \tag{4.12}$$

the gravitomagnetic Lorentz force is

$$\mathbf{F} = m\left(\mathbf{g} + \mathbf{v} \times \mathbf{\Omega}\right). \tag{4.13}$$

In plane polar coordinates the orbital velocity of a mass m attracted to a mass M is, in general:

$$\mathbf{v} = \dot{r}\mathbf{e}_r + \boldsymbol{\omega} \times \mathbf{r} = \dot{r}\mathbf{e}_r + \omega r \mathbf{e}_\theta \tag{4.14}$$

where the unit vectors of the cylindrical polar system are cyclically related as follows

$$\begin{aligned} &\mathbf{e}_r = \mathbf{e}_\theta \times \mathbf{k} \\ &\mathbf{e}_\theta = \mathbf{k} \times \mathbf{e}_r \\ &\mathbf{k} = \mathbf{e}_r \times \mathbf{e}_\theta. \end{aligned} \tag{4.15}$$

For a planar orbit, the acceleration in general is:

$$\mathbf{a} = \left(\ddot{r} - \omega^2 r\right)\mathbf{e}_r = \ddot{r}\mathbf{e}_r - \boldsymbol{\omega} \times (\boldsymbol{\omega} \times \mathbf{r}) \tag{4.16}$$

where $\mathbf{r}$ is the radial vector defined by:

$$\mathbf{r} = r\mathbf{e}_r \tag{4.17}$$

and where the angular velocity vector is:

$$\boldsymbol{\omega} = \omega\mathbf{k}. \tag{4.18}$$

The planar orbital force is therefore:

$$\mathbf{F} = m\mathbf{g} - \boldsymbol{\omega} \times (\boldsymbol{\omega} \times \mathbf{r}) = -\frac{mMG}{r^2}\mathbf{e}_r \tag{4.19}$$

where G is Newton's constant. Eq. (4.19) is the 1689 Leibniz equation of orbits. The orbital force equation can be written as:

$$\mathbf{F} = m\mathbf{g} + \mathbf{v}_{\text{rot}} \times \boldsymbol{\omega} \tag{4.20}$$

where

$$\mathbf{v}_{\text{rot}} = \boldsymbol{\omega} \times \mathbf{r} \tag{4.21}$$

is the velocity due to a rotating frame first inferred by Coriolis in 1835. The orbital force equation is the Lorentz force equation if:

$$\boldsymbol{\Omega} = \boldsymbol{\omega} = \frac{d\theta}{dt}\mathbf{k} \tag{4.22}$$

and

$$\mathbf{v} = \mathbf{v}_{\text{rot}} = \boldsymbol{\omega} \times \mathbf{r}. \tag{4.23}$$

Therefore $\boldsymbol{\Omega}$ is the gravitomagnetic field responsible for the centrifugal force of any planar orbit. The velocity due to the rotating frame of the plane polar coordinates is:

$$\mathbf{v}_{\text{rot}} = \boldsymbol{\omega} \times \mathbf{r}. \tag{4.24}$$

In the non-relativistic limit the electromagnetic Lorentz transforms are:

$$\mathbf{E}' = \mathbf{E} + \mathbf{v} \times \mathbf{B} \tag{4.25}$$

$$\mathbf{B}' = \mathbf{B} - \frac{1}{c^2}\mathbf{v} \times \mathbf{E} \tag{4.26}$$

and the gravitomagnetic Lorentz transforms are:

$$\mathbf{g}' = \mathbf{g} + \mathbf{v} \times \boldsymbol{\Omega} \tag{4.27}$$

$$\mathbf{\Omega}' = \mathbf{\Omega} - \frac{1}{c^2}\mathbf{v} \times \mathbf{g}. \tag{4.28}$$

The primes indicate the field in the observer frame in which the velocity of a charge or mass is non zero. The Biot Savart law of magnetism is obtained from Eq. (4.26) with:

$$\mathbf{B} = \mathbf{0} \tag{4.29}$$

which means that there is no magnetic field in the rest frame, the frame in which the electric charge does not move. The electromagnetic Biot Savart law is therefore:

$$\mathbf{B}' = -\frac{1}{c^2}\mathbf{v} \times \mathbf{E} \tag{4.30}$$

in S. I. Units. The prime in Eq. (4.30) means that the law is written in the observer frame, the frame in which the velocity $\mathbf{v}$ of the electric charge is non-zero. In the usual electrodynamics textbooks the prime is omitted by convention and the law becomes:

$$\mathbf{B} = -\frac{1}{c^2}\mathbf{v} \times \mathbf{E}. \tag{4.31}$$

The Biot Savart law can be written [2]- [13] as:

$$\boldsymbol{\nabla} \times \mathbf{B} = \mu_0 \mathbf{J} \tag{4.32}$$

which is the Ampère law of magnetostatics, describing the magnetic flux density generated by a current loop of any shape. It follows in ECE 2 theory that:

$$\boldsymbol{\nabla} \times \mathbf{B} = -\frac{1}{c^2}\boldsymbol{\nabla} \times (\mathbf{v} \times \mathbf{E}) = \mu_0 \mathbf{J} \tag{4.33}$$

so the current density of electrodynamics is:

$$\mathbf{J} = -\frac{1}{\mu_0 c^2}\boldsymbol{\nabla} \times (\mathbf{v} \times \mathbf{E}) = -\epsilon_0 \boldsymbol{\nabla} \times (\mathbf{v} \times \mathbf{E}) \,. \tag{4.34}$$

Here:

$$\boldsymbol{\nabla} \times (\mathbf{v} \times \mathbf{E}) = \mathbf{v} \left(\boldsymbol{\nabla} \cdot \mathbf{E}\right) - \left(\boldsymbol{\nabla} \cdot \mathbf{v}\right) \mathbf{E} + \left(\mathbf{E} \cdot \boldsymbol{\nabla}\right) \mathbf{v} - \left(\mathbf{v} \cdot \boldsymbol{\nabla}\right) \mathbf{E}. \tag{4.35}$$

The electromagnetic charge current density is:

$$J^{\mu} = \left(c\rho, \mathbf{J}\right). \tag{4.36}$$

In exact analogy, the ECE 2 gravitomagnetic mass/current density is:

$$J_m^{\mu} = \left(c\rho_m, \mathbf{J}_m\right). \tag{4.37}$$

Therefore:

$$\boldsymbol{\nabla} \times \mathbf{\Omega} = -\frac{1}{c^2}\boldsymbol{\nabla} \times (\mathbf{v} \times \mathbf{g}) = \frac{4\pi G}{c^2}\mathbf{J}_m \tag{4.38}$$

and the current of mass density is:

$$\mathbf{J}_m = -\frac{1}{4\pi G}\boldsymbol{\nabla} \times (\mathbf{v} \times \mathbf{g}) \,. \tag{4.39}$$

Now use:

$$\Omega^2 = \frac{1}{c^4}(\mathbf{v} \times \mathbf{g}) \cdot (\mathbf{v} \times \mathbf{g}) = \frac{1}{c^4}\left(v^2 g^2 - (\mathbf{v} \cdot \mathbf{g})^2\right). \tag{4.40}$$

Eqs. (4.38) and (4.40) are general to any orbit.

For the Hooke/Newton inverse square law:

$$\mathbf{F} = -\frac{mMG}{r^2}\mathbf{e}_r \tag{4.41}$$

the orbit in plane polar coordinates is the conic section [2]- [13]:

$$r = \frac{\alpha}{1 + \epsilon \cos\theta} \tag{4.42}$$

and the orbital linear velocity is:

$$v^2 = \left(\frac{dr}{dt}\right)^2 + r^2\left(\frac{d\theta}{dt}\right)^2 = MG\left(\frac{2}{r} - \frac{1}{a}\right) \tag{4.43}$$

where the semi major axis of an ellipse, for example, is:

$$a = \frac{\alpha}{1 - \epsilon^2}. \tag{4.44}$$

Here α is the half right latitude and ϵ is the eccentricity. Some examples of the gravitomagnetic field are developed and graphed later on in this chapter.

The ECE 2 gravitomagnetic field can be calculated for dynamics in general and for a three dimensional orbit. For the planar part of this orbit the gravitomagnetic Ampère law can be used to calculate the light deflection due to gravitation and the precession of the perihelion from the ECE 2 field equations.

In planar orbital theory it is well known [2]- [13] that the angular velocity is defined from a Lagrangian analysis in terms of the angular momentum of the system comprised of a mass m orbiting a mass M:

$$\frac{d\theta}{dt}\mathbf{k} = \boldsymbol{\omega} = \frac{L}{mr^2}\mathbf{k}. \tag{4.45}$$

In this case the gravitomagnetic field is:

$$\boldsymbol{\Omega} = -\left(\frac{MG}{mc^2}\right)\frac{L}{r^3}\mathbf{k} \tag{4.46}$$

and the current of mass density is:

$$\mathbf{J}_m = -\frac{3ML}{4\pi m r^4}\mathbf{e}_\theta \tag{4.47}$$

where the unit vectors are defined as:

$$\mathbf{e}_\theta = -\mathbf{i}\sin\theta + \mathbf{j}\cos\theta \tag{4.48}$$

$$\mathbf{e}_r = \mathbf{i}\cos\theta + \mathbf{j}\sin\theta \tag{4.49}$$

in terms of the Cartesian unit vectors $\mathbf{i}$ and $\mathbf{j}$. From a a hamiltonian analysis for a force law:

$$\mathbf{F} = -\frac{mMG}{r^2}\mathbf{e}_r \tag{4.50}$$

it follows that:

$$L^2 = m^2 MG\alpha \tag{4.51}$$

in order that the orbit be the conic section (4.42). For an ellipse:

$$\alpha = \left(1 - \epsilon^2\right) a \tag{4.52}$$

and for a hyperbola:

$$\alpha = \left(\epsilon^2 - 1\right) a \tag{4.53}$$

where a is the semi major axis for the ellipse.

The ECE 2 gravitomagnetic Ampère law (4.38) was first developed in UFT 117 and UFT 119, and orbital theory can be described by this law.

In cylindrical polar coordinates the position vector is:

$$\mathbf{r} = r\mathbf{e}_r + Z\mathbf{k}, \tag{4.54}$$

the velocity vector is:

$$\mathbf{v} = \dot{r}\mathbf{e}_r + \omega r\mathbf{e}_\theta + \dot{Z}\mathbf{k} \tag{4.55}$$

and the acceleration vector is:

$$\mathbf{a} = \left(\ddot{r} - r\dot{\theta}^2\right)\mathbf{e}_r + \left(r\ddot{\theta} + 2\dot{r}\dot{\theta}\right)\mathbf{e}_\theta + \ddot{Z}\mathbf{k}. \tag{4.56}$$

In dynamics in general the gravitomagnetic field is:

$$\mathbf{\Omega} = -\frac{1}{c^2}\mathbf{v}\times\mathbf{a}. \tag{4.57}$$

If the gravitational potential energy is defined as:

$$U = -\frac{mMG}{r} \tag{4.58}$$

the lagrangian is:

$$\mathscr{L} = T - U \tag{4.59}$$

where the kinetic energy is:

$$T = \frac{1}{2}mv^2 = \frac{1}{2}m\left(\dot{r}^2 + \dot{\theta}^2 r^2 + \dot{Z}^2\right). \tag{4.60}$$

There are three Euler Lagrange equations:

$$\frac{\partial \mathscr{L}}{\partial \theta} = \frac{d}{dt}\frac{\partial \mathscr{L}}{\partial \dot{\theta}} \tag{4.61}$$

$$\frac{\partial \mathscr{L}}{\partial r} = \frac{d}{dt}\frac{\partial \mathscr{L}}{\partial \dot{r}} \tag{4.62}$$

$$\frac{\partial \mathscr{L}}{\partial Z} = \frac{d}{dt}\frac{\partial \mathscr{L}}{\partial Z}. \tag{4.63}$$

Eq. (4.62) gives the Leibniz equation:

$$F(r) = -\frac{\partial U}{\partial r} = m\left(\ddot{r} - r\dot{\theta}^2\right). \tag{4.64}$$

Eq. (4.63) gives:

$$\ddot{Z} = \frac{d^2 Z}{dt^2} = 0 \tag{4.65}$$

and Eq. (4.61) gives the conserved angular momentum

$$L = \frac{\partial \mathscr{L}}{\partial \dot{\theta}}. \tag{4.66}$$

In cylindrical polar coordinates:

$$\mathbf{L} = m\mathbf{r} \times \mathbf{v} = m\left(\omega r Z \mathbf{e}_r + \dot{r} Z \mathbf{e}_\theta + \omega r^2 \mathbf{k}\right) \tag{4.67}$$

so for a three dimensional orbit $\mathbf{L}$ is not perpendicular to the orbital plane. It follows from Eq. (4.67) that the Z component of angular momentum is:

$$L_Z = mr^2\omega \tag{4.68}$$

and is a conserved constant of motion:

$$\frac{dL_Z}{dt} = 0 \tag{4.69}$$

if the angular velocity is defined as in Eq. (4.45). The total angular momentum is defined by:

$$L^2 = L_r^2 + L_\theta^2 + L_Z^2 \tag{4.70}$$

and is not conserved, i. e.:

$$\frac{dL}{dt} \neq 0. \tag{4.71}$$

The Binet equation [2]- [13] of orbits is defined by Eqs. (4.64) and (4.68) and is:

$$F(r) = -\frac{L_Z^2}{mr^2}\left(\frac{d^2}{d\theta^2}\left(\frac{1}{r}\right) + \frac{1}{r}\right). \tag{4.72}$$

It gives the force law for any orbit, not only the conic section orbits.

For planar orbits it can be shown [2]- [13] that:

$$r\ddot{\theta} + 2\dot{r}\dot{\theta} = 0 \tag{4.73}$$

so the velocity is:

$$\mathbf{v} = \dot{r}\mathbf{e}_r + \omega r\mathbf{e}_\theta \tag{4.74}$$

and the acceleration is:

$$\mathbf{a} = \left(\ddot{r} - r\dot{\theta}^2\right)\mathbf{e}_r. \tag{4.75}$$

In three dimensions the position vector is:

$$\mathbf{r} = r\mathbf{e}_r + Z\mathbf{k} \tag{4.76}$$

and the angular momentum vector is:

$$\mathbf{L} = m\left(Z\left(\omega r\mathbf{e}_r + \dot{r}\mathbf{e}_\theta\right) + \omega r^2\mathbf{k}\right) \tag{4.77}$$

so a planar orbit of any kind is embedded in the three dimensions defined by r, θ, and Z. In the usual planar orbit theory it is assumed that

$$Z = 0 \tag{4.77a}$$

in Eq. (4.77).

Eq. (4.76) can be defined as:

$$\mathbf{r}_{\text{total}} = r\mathbf{e}_r + Z\mathbf{k} \tag{4.78}$$

so:

$$\mathbf{r}_{\text{total}}^2 = r^2 + Z^2 \tag{4.79}$$

so a conic section orbit in cylindrical coordinates is defined in general by:

$$\mathbf{r}_{\text{total}}^2 = \left(\frac{\alpha}{1 + \epsilon\cos\theta}\right)^2 + Z^2. \tag{4.80}$$

In general the lagrangian is:

$$\mathscr{L} = \frac{1}{2}m\left(\dot{r}^2 + \dot{\theta}^2 r^2 + \dot{Z}^2\right) - U\left(r, \theta, Z\right) \tag{4.81}$$

and the potential energy and force depend on Z as well as on r. Most generally, the velocity in the observer frame is:

$$\mathbf{v} = \dot{r}\mathbf{e}_r + \boldsymbol{\omega} \times \mathbf{r} \tag{4.82}$$

and the acceleration in the observer frame is:

$$\mathbf{a} = \ddot{r}\mathbf{e}_r - \boldsymbol{\omega} \times (\boldsymbol{\omega} \times \mathbf{r}) + \frac{d\boldsymbol{\omega}}{dt} \times \mathbf{r} + 2\boldsymbol{\omega} \times \frac{dr}{dt}\mathbf{e}_r. \tag{4.83}$$

The vector definitions (4.82) and (4.83) are equivalent to:

$$\mathbf{v} = \dot{r}\mathbf{e}_r + r\dot{\theta}\mathbf{e}_\theta \tag{4.84}$$

and

$$\mathbf{a} = \left(\ddot{r} - \omega^2 r\right)\mathbf{e}_r + \left(2\dot{r}\dot{\theta} + r\ddot{\theta}\right)\mathbf{e}_\theta. \tag{4.85}$$

The gravitomagnetic field is proportional to the vector product of $\mathbf{v}$ from Eq. (4.82) and $\mathbf{a}$ from Eq. (4.83).

Using these concepts, the phenomena of light deflection due to gravitation and perihelion precession can be described straightforwardly by ECE 2 theory as follows.

A precessing orbit can be modelled by:

$$r = \frac{\alpha}{1 + \epsilon\cos(x\theta)} \tag{4.86}$$

and advances by:

$$\Delta\theta = (x - 1)\,\theta \tag{4.87}$$

In the solar system, x is very close to unity. Later on in this chapter an exact ECE 2 theory of the perihelion precession is developed by simultaneous solution of the ECE 2 lagrangian and hamiltonian. However Eq. (4.86) is accurate in the solar system to a very good approximation. Since x is very close to unity:

$$L^2 = m^2 MG\alpha \tag{4.88}$$

to an excellent approximation. From Eqs. (4.72) and (4.86) the force necessary for the precessing orbital model (4.86) is:

$$\mathbf{F} = mMG\left(-\frac{x^2}{r^2} + \frac{\left(x^2 - 1\right)\alpha}{r^3}\right)\mathbf{e}_r. \tag{4.89}$$

Note carefully that this is not the force law of the incorrect Einstein theory, whose claims to accuracy are nullified because its underlying geometry is incorrect [2]- [13]. For light grazing the sun, the orbit is a hyperbola with a very large eccentricity, so the path of the light grazing the sun is almost a straight line. At the distance of closest approach (R_0):

$$a = R_0. \tag{4.90}$$

The angle of deflection of the light is defined by:

$$\Delta\zeta = \frac{2}{\epsilon} \tag{4.91}$$

and the gravitomagnetic field is:

$$\mathbf{\Omega} = \frac{MGL}{mc^2}\left(-\frac{x^2}{r^3} + \frac{\left(x^2-1\right)\alpha}{r^4}\right)\mathbf{k}. \tag{4.92}$$

To an excellent approximation:

$$x \sim 1 \tag{4.93}$$

and the gravitomagnetic field at closest approach is:

$$\Omega_Z^2 = \frac{\left(MG\right)^3}{c^4 r^6} a\left(\epsilon^2 - 1\right). \tag{4.94}$$

Now use:

$$r = a = R_0 \tag{4.95}$$

to find that:

$$\Omega_Z^2 = \frac{\left(MG\right)^3}{c^4 R_0^5}\left(\epsilon^2 - 1\right). \tag{4.96}$$

The angle of deflection is therefore:

$$\Delta\zeta = \frac{2}{\epsilon} = \frac{2}{\Omega_Z c^2}\left(\frac{\left(MG\right)^3}{R_0^5}\right)^{1/2}. \tag{4.97}$$

For light deflection by the sun:

$$\Delta\zeta = 8.4848 \times 10^{-6}\,\text{radians} \tag{4.98}$$

so the gravitomagnetic field for light deflection by the sun is:

$$\Omega_Z = 0.000314 \text{ radians per second.} \tag{4.99}$$

The precession of the perihelion of a planet such as Mercury is defined by the Z component of the gravitomagnetic field as follows:

$$\Omega_Z = \frac{MGL}{mc^2}\left(-\frac{x^2}{r^3} + \frac{\left(x^2-1\right)\alpha}{r^4}\right) \tag{4.100}$$

where

$$\alpha = b\left(1-\epsilon^2\right)^{1/2}. \tag{4.101}$$

Here b is the perihelion. Therefore at the perihelion:

$$\Omega_Z = \frac{-\left(MG\right)^{3/2}\left(1-\epsilon^2\right)^{1/4} x^2}{c^2 b^{5/2}} \tag{4.102}$$

and

$$\Delta\theta = (x-1)\,\frac{\pi}{2}. \tag{4.103}$$

The observed precession of the perihelion of Mercury is

$$\Delta\theta = 7.9673 \times 10^{-7} \text{ radians per year} \tag{4.104}$$

and at the perihelion:

$$\theta = \frac{\pi}{2} \tag{4.105}$$

so

$$x = 1 + 1.268 \times 10^{-7} \tag{4.106}$$

and to an excellent approximation:

$$x \sim 1 \tag{4.107}$$

thus justifying Eq. (4.93). The required experimental data are:

$$\begin{aligned} M &= 3.285 \times 10^{23}\,\mathrm{kg} \\ b &= 4.60012 \times 10^{10}\,\mathrm{m} \\ \epsilon &= 0.205630 \end{aligned} \tag{4.108}$$

so the gravitomagnetic field responsible for the precession of the perihelion of Mercury is:

$$\Omega_Z = -2.489 \times 10^{-24}\,\mathrm{rad\,s^{-1}}. \tag{4.109}$$

As in UFT 323 the concept of Lorentz transform can be extended to the Lorentz transform of frames, so in ECE 2 the transform becomes one of a generally covariant unified field theory. The primed frame is the Newtonian or inertial frame whose axes are at rest. The notes accompanying UFT 323 give clarifying examples. In contrast to the usual concept of the Lorentz transform in special relativity a particle may move in the primed Newtonian frame. In the original theory by Lorentz, the particle is at rest in its own frame of reference, known as the "rest frame". The unprimed frame in this theory can move in any way with respect to the Newtonian or primed frame, so the 1835 theory by Coriolis is developed into a generally covariant unified field theory.

This theory produces the following force equation for orbits:

$$\mathbf{F} = m\left(\gamma\left(\mathbf{g} + \mathbf{v}\times\boldsymbol{\Omega}\right) - \frac{\gamma^2}{1+\gamma}\frac{\mathbf{v}}{c}\left(\frac{\mathbf{v}}{c}\cdot\mathbf{g}\right)\right) = -\frac{mMG}{r^2}\mathbf{e}_r \tag{4.110}$$

and is therefore the generally covariant Leibniz force equation. It is shown as follows that this equation can describe precessional effects in orbits. The 1835 Coriolis theory is recovered in the limit:

$$\gamma \to 1,\ v \ll c \tag{4.111}$$

from which:

$$\mathbf{F} = m\left(\mathbf{g} + \mathbf{v} \times \mathbf{\Omega}\right) = -\frac{mMG}{r^2}\mathbf{e}_r. \tag{4.112}$$

In conventional notation the well known Coriolis theory is:

$$\mathbf{F} = m\left(\left(\ddot{r} - r\dot{\theta}^2\right)\mathbf{e}_r + \left(r\ddot{\theta} + 2\dot{r}\dot{\theta}\right)\mathbf{e}_\theta\right) = -\frac{mMG}{r^2}\mathbf{e}_r \tag{4.113}$$

in which:

$$r\ddot{\theta} + 2\dot{r}\dot{\theta} = 0 \tag{4.114}$$

for all planar orbits [2]- [13]. So for planar orbits:

$$\mathbf{F} = m\left(\ddot{r} - r\dot{\theta}^2\right)\mathbf{e}_r = -\frac{mMG}{r^2}\mathbf{e}_r. \tag{4.115}$$

The 1689 Leibniz equation is:

$$m\ddot{r} = r\dot{\theta}^2 - \frac{mMG}{r^2} \tag{4.116}$$

which is recovered from the general theory using:

$$\mathbf{v} = \boldsymbol{\omega} \times \mathbf{r},\ \mathbf{\Omega} = -\boldsymbol{\omega}. \tag{4.117}$$

Therefore in the Leibniz equation one frame moves with respect to another with the circular part of the orbital velocity

$$\mathbf{v} = \boldsymbol{\omega} \times \mathbf{r}. \tag{4.118}$$

This is the angular part of the total orbital velocity:

$$\mathbf{v} = \dot{r}\mathbf{e}_r + \boldsymbol{\omega} \times \mathbf{r}. \tag{4.119}$$

The Leibniz orbital equation produces the conic section:

$$r = \frac{\alpha}{1 + \epsilon\cos\theta} \tag{4.120}$$

whereas the observed orbit is accurately modelled by:

$$r = \frac{\alpha}{1 + \epsilon\cos(x\theta)} \tag{4.121}$$

so the precession is due to the generalization of Eq. (4.115) to Eq. (4.110). In the Coriolis limit the gravitomagnetic field is given by Eq. (4.117), so Eq. (4.110) becomes

$$\mathbf{F} = m\gamma\left(\frac{d^2r}{dt^2} - \Omega^2 r\right)\mathbf{e}_r. \tag{4.122}$$

Using:

$$\mathbf{v} = \omega r \mathbf{e}_\theta = \boldsymbol{\omega} \times \mathbf{r} \tag{4.123}$$

and:

$$\mathbf{a} = -\frac{MG}{r^2}\mathbf{e}_r \tag{4.124}$$

Eq. (4.110) reduces to:

$$\mathbf{F} = m\gamma \left(\frac{d^2 r}{dt^2} + |\mathbf{v} \times \boldsymbol{\Omega}| \right) \mathbf{e}_r. \tag{4.125}$$

The relativistic correction is due to an effective potential V defined by:

$$V = U(r) \tag{4.126}$$

used with the lagrangian:

$$\mathscr{L} = \frac{1}{2}mv^2 - U(r) \tag{4.127}$$

and the Euler Lagrange equation:

$$\frac{\partial \mathscr{L}}{\partial r} = \frac{d}{dt}\frac{\partial \mathscr{L}}{\partial \dot{r}}. \tag{4.128}$$

From Eqs. (4.121) and (4.72) the orbit due to Eq. (4.125) is:

$$\frac{d^2}{d\theta^2}\left(\frac{1}{r}\right) + \frac{1}{r} = \frac{1}{\gamma\alpha} \tag{4.129}$$

in which the Lorentz factor is defined by:

$$\gamma = \left(1 - \frac{v^2}{c^2}\right)^{-1/2}. \tag{4.130}$$

The force given by the Binet Eq. (4.72) must be the same as the force given by Eq. (4.125) so:

$$x^2 + \left(x^2 - 1\right)\frac{\alpha}{r} = \frac{1}{\gamma}. \tag{4.131}$$

At the perihelion:

$$r = \frac{\alpha}{1 + \epsilon} \tag{4.132}$$

so:

$$x^2 + \left(x^2 - 1\right)(1 + \epsilon) = \frac{1}{\gamma} \tag{4.133}$$

so x can be found in terms of γ. The velocity of the Lorentz transform is defined by:

$$v_\Omega = \Omega r \tag{4.134}$$

so:

$$x^2 + \left(x^2 - 1\right)(1 + \epsilon) = \left(1 - \frac{v_\Omega^2}{c^2}\right)^{1/2}. \tag{4.135}$$

The precession can be worked out in terms of v_Ω for the orbit of the earth about the sun, and this is done later on in this chapter.

The Lorentz force equation of ECE 2 theory can be solved by using the relativistic Binet equation for force, and its integral form for the hamiltonian. The relativistic Binet equation is derived from the Sommerfeld hamiltonian and the relativistic orbital velocity can be calculated straightforwardly and used to derive the observed velocity curve of a whirlpool galaxy and the precisely observed deflection of light due to gravity. These are major advances in understanding that overthrow the obsolete Einstein theory.

The property of ECE 2 covariance means that the well known equations and ideas of special relativity can be used in orbital theory. The Lorentz transform is sufficient to produce the velocity curve of a whirlpool galaxy and the famous result of light deflection due to gravitation. Therefore these phenomena are explained by ECE 2 theory straightforwardly. The relativistic Binet force equation is equivalent to the ECE 2 Lorentz force equation derived earlier in this chapter. The former can be derived from the well known lagrangian of special relativity. The integral form of the Binet equation allows the evaluation of the hamiltonian for any orbit and the Binet force equation allows the evaluation of the central force and gravitational potential for any orbit. The methods can be exemplified with use of the plane polar coordinates and a precessing planar orbit. However it can be applied to three dimensional orbits.

It is shown as follows that the solution of the ECE 2 Lorentz force equation for a planar orbit is:

$$\begin{aligned}\mathbf{F} &= m\left(\gamma\left(\ddot{\mathbf{r}} + \mathbf{v}_\Omega \times \boldsymbol{\Omega}\right) - \frac{\gamma^2}{1+\gamma}\frac{\mathbf{v}_\Omega}{c}\left(\frac{\mathbf{v}_\Omega}{c}\cdot\mathbf{g}\right)\right) \\ &= \frac{\partial}{\partial r}\left(\left(\gamma - 1\right)mc^2\right)\mathbf{e}_r.\end{aligned} \tag{4.136}$$

The relativistic Binet equation for a planar orbit is:

$$\mathbf{F} = \frac{\partial}{\partial r}\left(\left(\gamma - 1\right)mc^2\right)\mathbf{e}_r \tag{4.137}$$

in which the Lorentz factor is:

$$\gamma = \left(1 - \frac{v^2}{c^2}\right)^{-1/2} \tag{4.138}$$

and in which the velocity used in the Lorentz factor is:

$$v^2 = \dot{r}^2 + \dot{\theta}^2 r^2. \tag{4.139}$$

In the Lorentz force equation $\mathbf{v}_\Omega$ is the velocity of one frame with respect to another.

The relativistic Binet equation is derived from the lagrangian of special relativity:

$$\mathscr{L} = -\frac{mc^2}{\gamma} - U(r) \tag{4.140}$$

where $U(r)$ is a central potential. The hamiltonian of special relativity can be derived from the lagrangian [2]- [13] and is:

$$H = E + U(r) \tag{4.141}$$

where the total relativistic energy is:

$$E = \gamma mc^2. \tag{4.142}$$

The hamiltonian (4.142) can be written as the Sommerfeld hamiltonian:

$$H(\text{Sommerfeld}) = H - mc^2 = (\gamma - 1)\, mc^2 + U(r) \tag{4.143}$$

where:

$$T = (\gamma - 1)\, mc^2 \tag{4.144}$$

is the relativistic kinetic energy. In the non relativistic limit:

$$T \to \left(1 + \frac{v^2}{2c^2} - 1\right) mc^2 = \frac{1}{2}mv^2 = \frac{p^2}{2m}. \tag{4.145}$$

The Euler Lagrange equations of the system are:

$$\frac{\partial \mathscr{L}}{\partial \theta} = \frac{d}{dt}\frac{\partial \mathscr{L}}{\partial \dot{\theta}} \tag{4.146}$$

$$\frac{\partial \mathscr{L}}{\partial r} = \frac{d}{dt}\frac{\partial \mathscr{L}}{\partial \dot{r}}. \tag{4.147}$$

For a central potential that depends on r but not θ they produce the results

$$\frac{\partial \mathscr{L}}{\partial \theta} = \gamma m r^2 \dot{\theta} \tag{4.148}$$

and:

$$\frac{d}{dt}\left(\gamma m \dot{r}\right) - \gamma m r \dot{\theta}^2 = -\frac{\partial U}{\partial r} = F(r). \tag{4.149}$$

Eq. (4.148) defines the relativistic angular momentum:

$$L = \gamma m r^2 \dot{\theta} \tag{4.150}$$

which is a constant of motion:

$$\frac{dL}{dt} = 0. \tag{4.151}$$

Eq. (4.149) defines the relativistic force equation of the orbit:

$$F(r) = \frac{d}{dt}\left(\gamma m \dot{r}\right) - \gamma m r \dot{\theta}^2 \tag{4.152}$$

in which:

$$m\frac{d}{dt}\left(\gamma \dot{r}\right) = m\left(\dot{r}\frac{d\gamma}{dt} + \gamma \ddot{r}\right). \tag{4.153}$$

Here:

$$\frac{d\gamma}{dt} = \frac{d\gamma}{dv}\frac{dv}{dt} \tag{4.154}$$

so:

$$\frac{d}{dt}\left(\gamma m \dot{r}\right) = m\left(\frac{\dot{r}\gamma^3 v}{c^2}\frac{dv}{dt} + \gamma \ddot{r}\right) \tag{4.155}$$

where

$$v = \left(\dot{r}^2 + \dot{\theta}^2 r^2\right)^{1/2}. \tag{4.156}$$

In general this is a complicated expression that must be developed with computer algebra.

The Binet equation is defined by making a change of variable:

$$\frac{d}{d\theta}\left(\frac{1}{r}\right) = -\frac{1}{r^2}\frac{dr}{d\theta} = -\frac{1}{r^2}\frac{dr}{dt}\frac{dt}{d\theta} \tag{4.157}$$

where:

$$\frac{dt}{d\theta} = \frac{\gamma m r^2}{L}. \tag{4.158}$$

From Eq. (4.150) it follows that:

$$\dot{\theta} = \frac{L}{\gamma m r^2} \tag{4.159}$$

and

$$\dot{r} = -\frac{L}{\gamma m}\frac{d}{d\theta}\left(\frac{1}{r}\right). \tag{4.160}$$

The orbital velocity is therefore:

$$v_N^2 = \dot{r}^2 + \dot{\theta}^2 r^2 = \frac{L^2}{\gamma^2 m^2}\left(\left(\frac{d}{d\theta}\left(\frac{1}{r}\right)\right)^2 + \frac{1}{r^2}\right) \tag{4.161}$$

and the integral form of the relativistic Binet equation is found directly from the Sommerfeld hamiltonian:

$$H - mc^2 = \left(\gamma - 1\right)mc^2 - \frac{mMG}{r} \tag{4.162}$$

in which:

$$L = \gamma m r^2 \dot{\theta} = \gamma L_0. \tag{4.163}$$

So the relativistic orbital velocity is:

$$v_N^2 = \frac{L^2}{m^2}\left(\left(\frac{d}{d\theta}\left(\frac{1}{r}\right)\right)^2 + \frac{1}{r^2}\right)\left(1 + \frac{L^2}{m^2 c^2}\left(\left(\frac{d}{d\theta}\left(\frac{1}{r}\right)\right)^2 + \frac{1}{r^2}\right)\right)^{-1}. \tag{4.164}$$

Note carefully that

$$H - mc^2 = H(\text{Sommerfeld}) \tag{4.165}$$

is a constant of motion, so the relativistic Binet force equation is:

$$F = \frac{\partial}{\partial r}\left(\left(\gamma - 1\right) mc^2\right) \tag{4.166}$$

which is the required solution of the ECE 2 Lorentz force equation (4.136), Q. E. D.

In the non relativistic limit the integral form of the Binet equation is:

$$U = H - \frac{L^2}{2m}\left(\left(\frac{d}{d\theta}\left(\frac{1}{r}\right)\right)^2 + \frac{1}{r^2}\right) \tag{4.167}$$

and the Binet force equation in the non relativistic limit is the well known [2]-[13]:

$$F(r) = -\frac{L^2}{mr^2}\left(\frac{d^2}{d\theta^2}\left(\frac{1}{r}\right) + \frac{1}{r}\right). \tag{4.168}$$

For the precessing conic section (4.121) for example, the central force is:

$$F = -\frac{\partial U}{\partial r} = -\frac{x^2 L^2}{mr^2 \alpha} + \frac{\left(x^2 - 1\right) L^2}{mr^3} \tag{4.169}$$

and the gravitational potential is:

$$U = -\frac{mMG}{r}. \tag{4.170}$$

The hamiltonian is:

$$H = \frac{x^2 L^2}{2m}\left(\frac{\epsilon^2 - 1}{\alpha^2}\right). \tag{4.171}$$

In the Newtonian limit:

$$F = -\frac{mMG}{r^2},\ U = -\frac{mMG}{r},\ |E| = \frac{mMG}{2a}, \tag{4.172}$$

and the following well known results are recovered:

$$x \rightarrow 1,\ r \rightarrow \frac{\alpha}{1 + \epsilon \cos\theta}. \tag{4.173}$$

It follows that the Einstein theory is not needed to describe a precessing elliptical orbit. It can be derived classically as above. The Einstein theory gives an incorrect force law [2]- [13] that is the sum of terms that are inverse squared in r and inverse fourth power in r. The correct expression is given in Eq. (4.169).

The relativistic orbital velocity (4.161) gives the correct experimental result for the velocity curve of a whirlpool galaxy using the hyperbolic spiral orbit of a star moving outwards from the galactic centre:

$$\frac{1}{r} = \frac{\theta}{r_0}. \tag{4.174}$$

From Eqs. (4.161) and (4.174) the velocity curve of the spiral galaxy is:

$$v_N^2 = \frac{L_0^2}{m^2}\left(\frac{1}{r_0^2} + \frac{1}{r^2}\right)\left(1 - \frac{L_0^2}{m^2c^2}\left(\frac{1}{r_0^2} + \frac{1}{r^2}\right)\right)^{-1} \tag{4.175}$$

and goes to the observed constant plateau:

$$v_N \xrightarrow[r\rightarrow\infty]{} \frac{L_0}{mr_0}\left(1 - \frac{L_0^2}{m^2c^2r_0^2}\right)^{-1/2}. \tag{4.176}$$

These results amount to a strong indication that ECE 2 is preferred by Ockham's Razor, and by observation, to the Einstein theory, because the latter fails completely to produce the velocity curve of a whirlpool galaxy [2]- [13]. The non relativistic Newtonian orbital velocity is:

$$v^2(\text{Newton}) = MG\left(\frac{2}{r} - \frac{1}{a}\right) \tag{4.177}$$

so:

$$v^2(\text{Newton}) = \frac{MG}{r}\left(2 + \frac{\left(\epsilon^2 - 1\right)}{1 + \epsilon\cos\theta}\right) \xrightarrow[r\rightarrow\infty]{} 0 \tag{4.178}$$

and the Newton theory fails completely in a whirlpool galaxy. The Einsteinian orbit is claimed to be able to reproduce the precessing ellipse (4.121), so:

$$v^2(\text{Einstein}) = \frac{MG}{r}\left(2 + \frac{\left(\epsilon^2 - 1\right)}{1 + \epsilon\cos(x\theta)}\right) \xrightarrow[r\rightarrow\infty]{} 0 \tag{4.179}$$

and the Einsteinian general relativity also fails completely in a whirlpool galaxy.

The relativistic orbital velocity from Eq. (4.164) is:

$$v_N^2 = v^2\left(1 + \frac{v^2}{c^2}\right)^{-1} \tag{4.180}$$

where v_N is the non relativistic orbital velocity:

$$v_N^2 = \dot{r}^2 + \dot{\theta}^2 r^2 \tag{4.181}$$

in plane polar coordinates. In light deflection by gravitation:

$$v \sim c. \tag{4.182}$$

It follows from Eqs. (4.180) and (4.182) that:

$$v_N^2 \rightarrow \frac{c^2}{2} \tag{4.183}$$

and that there is an upper bound to the non relativistic velocity. This simple inference of ECE 2 theory exactly explains light deflection by gravitation as follows.

The non relativistic orbital velocity is:

$$v_N^2 = MG\left(\frac{2}{r} - \frac{1}{a}\right) \tag{4.184}$$

where the semi major axis is:

$$a = \frac{\alpha}{1-\epsilon^2}. \tag{4.185}$$

The distance of closest approach is:

$$R_0 = \frac{\alpha}{1+\epsilon}. \tag{4.186}$$

It follows that:

$$v_N^2 = \frac{MG}{R_0}\left(2 + \frac{\epsilon^2 - 1}{\epsilon + 1}\right) = \frac{MG}{R_0}\left(1 + \epsilon\right). \tag{4.187}$$

Light grazing the sum follows a hyperbolic trajectory with a very large eccentricity:

$$\epsilon \gg 1 \tag{4.188}$$

so the orbit is almost a straight line. From Eqs. (4.187) and (4.188):

$$\epsilon \sim \frac{R_0 v_N^2}{MG} \tag{4.189}$$

and the angle of deflection is:

$$\Delta\zeta = \frac{2}{\epsilon} = \frac{2MG}{R_0 v_N^2}. \tag{4.190}$$

This is often known as the Newtonian result. However, the non relativistic velocity from Eq. (4.180) is:

$$v_N^2 = \frac{c^2}{2} \tag{4.191}$$

so the angle of deflection is:

$$\Delta\zeta = \frac{4MG}{R_0 c^2} \tag{4.192}$$

which is exactly the precisely measured experimental result, Q. E. D. The Einstein theory is not needed to produce this result.

The lagrangian and hamiltonian of ECE 2 (those of special relativity) can be solved simultaneously using numerical scatter plot methods as in UFT 325 on www.aias.us. The result is the precise orbit, the precisely defined precessing ellipse without any further assumption or theory. Note carefully that this is not the Einsteinian result, which is based on an incorrect geometry without torsion. As shown in several UFT papers, the Einstein result produces a mirage of precision when the precession is tiny as in the solar system, over the full range of angle it gives a wildly incorrect orbit [2]- [13] and is known to be incorrect in many other ways. ECE 2 is a great improvement because it gives a precessing ellipse directly from the simultaneous solution of the ECE 2 lagrangian and hamiltonian – a precise, correct and general result. ECE 2 gives the precessing orbit without any empiricism. The true precessing orbit is not that of Einstein, and is not the model (4.121). The non relativistic Newton theory gives no precession at all.

The hamiltonian and lagrangian of ECE 2 are given by Eqs. (4.141) and (4.140) respectively. It is assumed that the gravitational potential is:

$$U = -\frac{mMG}{r}. \tag{4.193}$$

The orbital velocity is defined by the infinitesimal line element of special relativity [2]- [13]:

$$c^2 d\tau^2 = \left(c^2 - v_N^2\right) dt^2 \tag{4.194}$$

where $d\tau$ is the infinitesimal of proper time, the time in the frame moving with the object m orbiting an object M. It follows that the non relativistic velocity is:

$$v_N^2 = \dot{r}^2 + r^2\dot{\theta}^2. \tag{4.195}$$

The Euler Lagrange equations for this system produce Eq. (4.164) as shown already.

As shown in Note 325(9) and by computer algebra, the Einstein theory gives an exceedingly complicated orbit and diverges, so the Einstein theory when correctly tested over its complete range gives un unphysical result, in fact it gives complete nonsense. UFT 325 on www.aias.us was the first paper to point this out in irrefutable detail using computer algebra to eliminate human error. The Einstein theory is therefore obsolete. The basic incorrectness of the Einstein theory can be demonstrated easily as follows. The Einsteinian hamiltonian and lagrangian are well known to be:

$$H(\text{Einstein}) = \frac{1}{2}m\left(\dot{r}^2 + r^2\dot{\theta}^2\left(1 + \frac{r_0}{r}\right)\right) + U \tag{4.196}$$

and

$$\mathscr{L}(\text{Einstein}) = \frac{1}{2}m\left(\dot{r}^2 + r^2\dot{\theta}^2\left(1 + \frac{r_0}{r}\right)\right) - U \tag{4.197}$$

where:

$$U = -\frac{mMG}{r} \tag{4.198}$$

and where

$$r_0 = \frac{2MG}{c^2} \tag{4.199}$$

is known in the obsolete physics as the Schwarzschild radius. The conserved angular momentum of the Einstein theory is:

$$L = \frac{\partial \mathscr{L}}{\partial \dot{\theta}} = \left(1 + \frac{r_0}{r}\right) mr^2\dot{\theta} \tag{4.200}$$

and it follows that:

$$\dot{\theta} = \frac{L}{mr^2} = \left(1 + \frac{r_0}{r}\right)^{-1} \tag{4.201}$$

and

$$\dot{r} = -\frac{L}{m}\left(1 + \frac{r_0}{r}\right)^{-1}\frac{d}{d\theta}\left(\frac{1}{r}\right). \tag{4.202}$$

Therefore the Einsteinian orbital velocity can be worked out from:

$$v^2 = \dot{r}^2 + r^2\dot{\theta}^2 \tag{4.203}$$

using Eqs. (4.201) and (4.202), giving the result:

$$v^2(\text{Einstein}) = v_N^2\left(1 + \frac{r_0}{r}\right)^{-2}. \tag{4.204}$$

As:

$$v_N \to c \tag{4.205}$$

and at the distance of closest approach:

$$r = R_0 \tag{4.206}$$

the Newtonian angle of deflection is changed to:

$$\Delta\zeta = \frac{2MG}{R_0c^2}\left(1 + \frac{r_0}{r}\right)^2 \tag{4.207}$$

and this is not the experimental result, Q. E. D. As shown in detail in papers such as UFT 150 and UFT 155 on `www.aias.us`, by now classic papers, Einstein obtained the twice Newton result by a series of invalid approximations.

The Euler Lagrange equation (4.147) gives the relativistic Leibniz orbital equation of ECE 2:

$$\frac{d}{dt}\left(\gamma m\dot{r}\right) - \gamma m r\dot{\theta}^2 = -\frac{\partial U}{\partial r} = F(r). \tag{4.208}$$

In the limit:

$$\gamma \rightarrow 1 \tag{4.209}$$

Eq. (4.208) becomes the 1689 Leibniz equation:

$$m\ddot{r} = mr\dot{\theta}^2 - \frac{mMG}{r^2} \tag{4.210}$$

which gives a non precessing orbit. The Newtonian or non relativistic orbital velocity is:

$$v_N^2 = \frac{L^2}{m^2}\left(\left(\frac{d}{d\theta}\left(\frac{1}{r}\right)\right)^2 + \frac{1}{r^2}\right) = MG\left(\frac{2}{r} - \frac{1}{a}\right). \tag{4.211}$$

From Eqs. (4.164) and (4.211) it can be shown that:

$$v^2 = MG\left(\frac{2}{r} - \frac{1}{a}\right)\left(1 - \frac{MG}{c^2}\left(\frac{2}{r} - \frac{1}{a}\right)\right)^{-1}. \tag{4.212}$$

This result is graphed later in this chapter, in which a synopsis of UFT 325 Section 3 is also given, a Section in which computer algebra is used to show that simultaneous solution of the lagrangian and hamiltonian of ECE 2 theory gives the true precessing elliptical orbit for the first time in scientific history. The solution is a stable orbit and not an unstable, unphysical orbit as in the Einstein theory.

The property of ECE 2 covariance means that quantization of ECE 2 theory can be developed straightforwardly, as in UFT 326, which is reviewed briefly as follows. These quantization schemes accompany a new axiom introduced logically by ECE 2 theory, that the maximum value of the non relativistic velocity v_N is:

$$v_N^2 = \frac{c^2}{2}. \tag{4.213}$$

As shown already, this axiom immediately results in the precisely observed light deflection due to gravity, now known with claimed high precision. This axiom allows a particle with mass to travel at c. This fact is observed experimentally when electrons are accelerated to very close to c. The usual dogma of the obsolete physics claimed that only "massless particles" such as the photon can travel at c. ECE 2 allows the photon with mass to travel at c.

The fundamental equations for the quantization schemes are the Einstein/de Broglie equations:

$$E = \gamma mc^2 = \hbar\omega \tag{4.214}$$

and

$$\mathbf{p} = \gamma m \mathbf{v}_N = \hbar \boldsymbol{\kappa}. \tag{4.215}$$

The hamiltonian and lagrangian are defined as in Eqs. (4.141) and (4.140). The relativistic total energy is given by the well known Einstein equation:

$$E^2 = p^2 c^2 + m^2 c^4. \tag{4.216}$$

This can be factorized in two ways:

$$E - mc^2 = \frac{p^2 c^2}{E + mc^2} \tag{4.217}$$

and

$$E - pc = \frac{m^2 c^4}{E + pc} \tag{4.218}$$

each of which may be quantized using:

$$p^\mu = \left(\frac{E}{c}, \mathbf{p} \right) = i\hbar \partial^\mu = i\hbar \left(\frac{1}{c} \frac{\partial}{\partial t}, -\boldsymbol{\nabla} \right) \tag{4.219}$$

for the relativistic energy E and relativistic momentum $\mathbf{p}$ used in Eqs. (4.214) and (4.215).

The relativistic Schrödinger equation is obtained from Eqs. (4.217) and (4.219)

$$\frac{p^2}{2m} \psi = \frac{mc^2}{2} \left(\gamma^2 - 1 \right) \psi \tag{4.220}$$

and can be developed using various types of quantization as described in the notes of UFT 326 on `www.aias.us`. In the non relativistic limit:

$$v_N \ll c \tag{4.221}$$

the following result is obtained:

$$\frac{p^2}{2m} \rightarrow mc^2 \left(\left(1 - \frac{v_N^2}{c^2} \right)^{-1} - 1 \right) \xrightarrow[v_N \ll c]{} \frac{1}{2} m v_N^2. \tag{4.222}$$

The relativistic Schrödinger equation of ECE 2 may also be expressed as:

$$\left(\frac{p^2}{(1+\gamma)\, m} + U \right) \psi = \left(H - mc^2 \right) \psi \tag{4.223}$$

as explained in Note 326(8). The equation is therefore developed from the familiar Schrödinger equation using:

$$\frac{p^2}{2m} \rightarrow \frac{p^2}{(1+\gamma)\, m}, \tag{4.224}$$

the non relativistic Schrödinger equation being defined by:

$$\left(\frac{p^2}{2m}+U\right)\psi=\left(H-mc^2\right)\psi:=E_{\rm tot}\psi. \tag{4.225}$$

The relativistic Schrödinger equation may be developed as:

$$\left(\frac{p^2}{2m}+U\right)\psi=E_{\rm tot}\psi+\frac{1}{2}\left(\gamma-1\right)\left(E_{\rm tot}-U\right)\psi \tag{4.226}$$

where:

$$E_{\rm tot}=H-mc^2 \tag{4.227}$$

and where the Coulomb potential is:

$$U=-\frac{e^2}{4\pi\epsilon_0 r}. \tag{4.228}$$

So the energy levels of the H atom are shifted by:

$$E_{\rm tot}\rightarrow E_{\rm tot}+\frac{m^2v_N^2}{4}\left(\left(1-\frac{v_N^2}{c^2}\right)^{-1/2}-1\right) \tag{4.229}$$

and this allows v_N to be found from the spectrum of the H atom. In the usual Dirac quantization scheme:

$$H-U-mc^2=\frac{p^2c^2}{H-U+mc^2} \tag{4.230}$$

the rough approximation:

$$H=\gamma mc^2+U\rightarrow mc^2 \tag{4.231}$$

is used, implying:

$$\gamma\rightarrow 1,\ U\ll E. \tag{4.232}$$

Using these approximations in Eq. (4.226) leads to:

$$\left(-\frac{\hbar^2\nabla^2}{2m}+U\right)\psi=E_{\rm tot}\psi+\frac{\hbar^2}{4m^2c^2}\nabla^2\left(U\psi\right) \tag{4.233}$$

where:

$$\nabla^2\left(U\psi\right)=U\nabla^2\psi+2\boldsymbol{\nabla}U\cdot\boldsymbol{\nabla}\psi+\psi\nabla^2U. \tag{4.234}$$

The energy levels of the H atom are shifted in the Dirac approximation to:

$$\begin{aligned}\langle\Delta E_{\rm tot}\rangle=-\frac{\hbar^2}{4m^2c^2}\Bigg(&\int\psi^*U\nabla^2\psi\,d\tau+\int\psi^*\left(\nabla^2U\right)\psi\,d\tau\\&+2\int\psi^*\boldsymbol{\nabla}U\cdot\boldsymbol{\nabla}\psi\,d\tau\Bigg)\end{aligned} \tag{4.235}$$

and this can be evaluated in the approximation of hydrogenic wave functions.

In the usual interpretation of special relativity the non relativistic velocity v_N of the Lorentz transform is allowed to reach c, the universal constant known as the vacuum speed of light. The experimentally untestable assumption:

$$v_N \rightarrow ?\ c \tag{4.236}$$

results however in an unphysical infinity:

$$\gamma \rightarrow \infty \tag{4.237}$$

obscurely known in the obsolete physics as the hyper relativistic limit. The obsolete physics dealt with this unphysical infinity by inventing the massless particle. The relativistic momentum became indeterminate, zero multiplied by infinity, for this massless particle. A photon without mass became a dogmatic feature of the obsolete physics but at the same time introduced many severe difficulties [2]- [13] and obscurities which were acknowledged by the dogmatists themselves. The ECE 2 axiom (4.213) removes all these difficulties straightforwardly. Under condition (4.213) the relativistic velocity v reaches c and the Lorentz factor remains finite:

$$\gamma \rightarrow \sqrt{2}. \tag{4.238}$$

As shown already, the ECE 2 axiom (4.213) immediately gives the observed light deflection due to gravitation. It also gives the correct O(3) little group of the Poincaré group for a particle with mass, allows canonical quantization without problems, produces the Proca equation, and is also compatible with the B(3) field [2]- [13]. The ECE 2 axiom (4.213) introduces photon mass theory which refutes the Higgs boson and the entire structure of the obsolete physics. It removes the Gupta Bleuler condition, which was very obscure, and allows canonical quantization to take place self consistently. Some methods of measuring v_N have been suggested already in order to test the axiom (4.213) experimentally.

As described in notes such as 326(6) on `www.aias.us` the relativistic Schrödinger equation may also be written as:

$$-\frac{\hbar^2}{2m}\nabla^2\psi = \frac{1}{2}\left(\gamma^2 - 1\right)mc^2\psi := E_{\text{rel}}\psi \tag{4.239}$$

whose solution is:

$$\psi = A\exp\left(i\kappa Z\right) + B\exp\left(-i\kappa Z\right) \tag{4.240}$$

where:

$$\kappa^2 = \frac{2mE_{\text{rel}}}{\hbar^2}. \tag{4.241}$$

This leads to relativistic quantum theory and also an expression for v_N:

$$\left(\frac{v_N}{c}\right)^2 = 1 - \left(1 + \left(\frac{\hbar\kappa}{mc}\right)^2\right)^{-1} \tag{4.242}$$

which may be used with Eq. (4.215) to measure v_N and m experimentally.

Further details and numerical development are given in UFT 326 and in numerical methods in UFT 326 Section 3 summarized later in this chapter.

The Minkowski metric of ECE 2 relativity produces a precessing elliptical orbit, confirming the demonstration earlier in this chapter that the precessing elliptical orbit is produced by simultaneous solution of the lagrangian and hamiltonian of ECE 2 relativity. The details for the use of the Minkowski metric to produce precession are given in the background notes accompanying UFT 327 on `www.aias.us`. The notes for UFT 327 also refute the Einstein theory in several ways. For example notes 327(2) and 327(3) use computer algebra to show that the integral approximations used by Einstein in his paper of Nov. 1915 are incorrect. This paper was heavily criticizsed by Schwarzschild in Dec. 1915. The computational methods now available remove the need for the approximations used by Einstein. In UFT 150 and UFT 155 several other approximations used by Einstein are shown to be incorrect and meaningless. The scientometrics show that these are heavily studied and accepted papers. The omission of torsion means that the geometry used by Einstein is fundamentally incorrect as already discussed in chapter two of this book.

It is therefore accepted by leading scholars that Einsteinian general relativity is meaningless. In Note 327(6) for example an accurate computational method is developed which proves in another way that the claim by Einstein to have produced orbital precession is fundamentally incorrect. The results of this numerical method are given later on in this chapter, together with graphics.

Consider the ECE 2 infinitesimal line element:

$$c^2 d\tau^2 = \left(c^2 - v_N^2\right) dt^2. \tag{4.243}$$

This has the same mathematical format as the well known Minkowski metric of special relativity. Here $d\tau$ is the infinitesimal of proper time (the time in the moving frame) and v_N is the Newtonian velocity of the observer frame, defined in plane polar coordinates by:

$$v_N^2 = \left(\frac{dr}{dt}\right)^2 + r^2 \left(\frac{d\theta}{dt}\right)^2. \tag{4.244}$$

The rest energy is therefore:

$$mc^2 = mc^2 \left(\frac{dt}{d\tau}\right)^2 - m\left(\frac{dr}{d\tau}\right)^2 - mr^2 \left(\frac{d\theta}{d\tau}\right)^2 \tag{4.245}$$

where the Lorentz factor is defined by:

$$\gamma = \frac{dt}{d\tau} = \left(1 - \frac{v_N^2}{c^2}\right)^{-1/2}. \tag{4.246}$$

There are two constants of motion, the relativistic total energy:

$$E = \gamma mc^2 \tag{4.247}$$

and the relativistic angular momentum:

$$L = \gamma m r^2 \frac{d\theta}{dt} := \gamma L_0. \tag{4.248}$$

The relativistic linear momentum is defined by:

$$\mathbf{p} = \gamma m \mathbf{v}_N = \gamma \mathbf{p}_N \tag{4.249}$$

so it follows that:

$$p^2 = \gamma^2 m^2 v_N^2 \tag{4.250}$$

and Eq. (4.245) becomes the Einstein energy equation:

$$E^2 = p^2 c^2 + m^2 c^4. \tag{4.251}$$

As shown in Note 327(1) and in several UFT papers on `www.aias.us`, the orbit of ECE 2 relativity is:

$$\left(\frac{dr}{d\theta}\right)^2 = r^4 \left(\frac{E^2 - m^2 c^4}{c^2 L^2} - \frac{1}{r^2}\right) = r^4 \left(\left(\frac{p}{L}\right)^2 - \frac{1}{r^2}\right). \tag{4.252}$$

The ratio p/L is defined by:

$$\frac{p}{L} = \frac{\gamma p_N}{\gamma L_N} = \frac{p_N}{L_N} \tag{4.253}$$

Therefore in the Newtonian limit the orbit becomes:

$$\left(\frac{dr}{d\theta}\right)^2 = r^4 \left(\left(\frac{p_N}{L_N}\right)^2 - \frac{1}{r^2}\right) \tag{4.254}$$

in which the non relativistic momentum $\mathbf{p}_N$ is defined by the classical hamiltonian:

$$H_0 = \frac{p_N^2}{2m} + U \tag{4.255}$$

From Eqs. (4.254) and (4.255):

$$\left(\frac{dr}{d\theta}\right)^2 = \frac{r^4}{L_N^2} \left(2m \left((H_0 - U) - \frac{L_N^2}{2mr^2}\right)\right) \tag{4.256}$$

an equation which is well known to give the conic section orbits:

$$r = \frac{\alpha}{1 + \epsilon \cos\theta} \tag{4.257}$$

which do not precess.

The infinitesimal (4.243) of ECE 2 relativity is derived from the Lorentz invariance:

$$x^\mu x_\mu = x^{\mu'} x_{\mu'} \tag{4.258}$$

of the position four vector. In ECE 2 relativity, Lorentz invariance is defined in a space with finite torsion and curvature. In the original special relativity, the torsion and curvature are both zero. In ECE 2 relativity the orbit is described by the underlying Cartan and Evans identities of geometry.

In the fully relativistic version of Eq. (4.252) the relativistic angular momentum L is the constant of motion:

$$\frac{d\mathbf{L}}{dt} = \mathbf{0} \tag{4.259}$$

and not the classical angular momentum $\mathbf{L}_N$ defined by:

$$\mathbf{L}_N = mr^2 \frac{d\theta}{dt}\mathbf{k}. \tag{4.260}$$

The relativistic orbit is:

$$\left(\frac{dr}{d\theta}\right)^2 = r^4\left(\frac{\gamma^2 p_N^2}{L^2} - \frac{1}{r^2}\right) \tag{4.261}$$

where the square of the Lorentz factor is:

$$\gamma^2 = \left(1 - \frac{p_N^2}{m^2c^2}\right)^{-1}. \tag{4.262}$$

Earlier in this chapter (and in UFT 324 and UFT 325) it was shown that simultaneous numerical solution of the relativistic hamiltonian of ECE 2:

$$H = \gamma mc^2 + U \tag{4.263}$$

and the relativistic lagrangian of ECE 2:

$$\mathscr{L} = -\frac{mc^2}{\gamma} - U \tag{4.264}$$

gives a precessing orbit from the relevant Euler Lagrange equations. The infinitesimal line element corresponding to Eqs. (4.263) and (4.264) is Eq. (4.243), whose orbit is defined by Eq. (4.252). Therefore Eq. (4.252) must also give a precessing orbit for self consistency. The relativistic hamiltonian can be defined as:

$$H = \left(c^2p^2 + m^2c^4\right)^{1/2} + U \tag{4.265}$$

so the relativistic momentum:

$$\mathbf{p} = \gamma\mathbf{p}_N = \gamma m\mathbf{v}_N \tag{4.266}$$

can be defined as:

$$c^2p^2 + m^2c^4 = (H - U)^2. \tag{4.267}$$

As shown earlier in this chapter (and also in UFT 326), Eq. (4.267) can be expressed as:

$$H - U - mc^2 = \frac{c^2 p^2}{H - U + mc^2} \tag{4.268}$$

which reduces to the classical hamiltonian (4.255) in the limit:

$$v_N \ll c. \tag{4.269}$$

In the well known Dirac approximation:

$$U \ll H \sim mc^2 \tag{4.270}$$

the classical hamiltonian is defined by:

$$H_0 = H - mc^2 \tag{4.271}$$

and from Eqs. (4.270) and (4.271):

$$H_0 = \frac{p^2}{2m}\left(1 - \frac{U}{2mc^2}\right)^{-1} + U, \tag{4.272}$$

and since:

$$U \ll 2mc^2 \tag{4.273}$$

the classical hamiltonian becomes:

$$H_0 \sim \frac{p^2}{2m}\left(1 + \frac{U}{2mc^2}\right) + U. \tag{4.274}$$

The factor two in the brackets on the right hand side is the Thomas factor observable in spin orbit interaction in spectra. In the Dirac approximation the relativistic momentum is given by:

$$p^2 = \left(1 - \frac{U}{2mc^2}\right) p_N^2 \tag{4.275}$$

and the orbit from Eqs. (4.252) and (4.275) is

$$\left(\frac{dr}{d\theta}\right)^2 = r^4\left(\frac{1}{L^2}\left(1 + \frac{MG}{2c^2 r}\right) p_N^2 + \frac{1}{r^2}\right). \tag{4.276}$$

This is the ECE 2 correction of the Newtonian theory of orbits.

The rigorously correct precession is obtained by simultaneous numerical solution of Eqs. (4.263) and (4.264) as shown in UFT 324 and UFT 325. However, for small precessions of arc seconds a year, such as those in the solar system, the precessing orbit can be modelled by:

$$r = \frac{\alpha}{1 + \epsilon\cos(x\theta)} \tag{4.277}$$

in which x is observed by high precision astronomy to be:

$$x = 1 + \frac{3MG}{\alpha c^2}. \tag{4.278}$$

It follows from Eqs. (4.276) and (4.277) that:

$$\left(\frac{dr}{d\theta}\right)^2 = \frac{x^2\epsilon^2 r^4}{\alpha^2}\sin^2(x\theta) = r^4\left(\left(\frac{p_N^2}{L^2} + \frac{1}{r^2}\right) + \left(\frac{MG}{2c^2 r}\right)\frac{p_N^2}{L^2}\right) \tag{4.279}$$

so it has been proven that ECE 2 relativity gives the experimentally observed precessing orbit provided that Eq. (4.279) is true. So ECE 2 replaces the obsolete and incorrect Einstein theory.

Additional analysis and graphics are given later on this chapter.

As shown analytically and numerically in UFT 328 the true precessing orbit must be found by simultaneous solution of the ECE 2 hamiltonian and lagrangian. The true orbit is not the one modelled in Eq. (4.277), and is certainly not the orbit asserted in the early work of Einstein, work which is riddled with errors. The true precession is given by simultaneous solution of Eqs. (4.263) and (4.264), in which the gravitational potential is assumed to be:

$$U = -\frac{mMG}{r} \tag{4.280}$$

of the Hooke/Newton inverse square law. The orbit is considered to be planar. As shown in UFT 324 and UFT 325 an analysis based on the Euler Lagrange equations for r and θ leads to:

$$\ddot{r} = \frac{\left(-\gamma^2 v_N^2 + \gamma^2\dot{r}^2 - c^2\right)MG + r\left(\gamma^3 r^4 + \gamma c^2 v_N^2\right) + r\dot{r}\left(-\gamma^3 v_N^2 - \gamma c^2\right)}{r^2\left(\gamma^3 v_N^2 + \gamma c^2\right)} \tag{4.281}$$

and:

$$\ddot{\theta} = \frac{\gamma\dot{r}\dot{\theta}MG + r\dot{r}\dot{\theta}\left(-2\gamma^2 v_N^2 - 2c^2\right)}{r^2\left(\gamma^2 v_N^2 + c^2\right)}. \tag{4.282}$$

In the classical limit these equations reduce to the Leibniz equation:

$$\ddot{r} = r\dot{\theta}^2 - \frac{MG}{r^2} \tag{4.283}$$

and to:

$$\ddot{\theta} = -\frac{2\dot{r}\dot{\theta}}{r} \tag{4.284}$$

respectively.

In order to compute the relativistic orbit use:

$$\dot{r} = \int \ddot{r}\, dt \tag{4.285}$$

and:

$$\dot{\theta} = \int \ddot{\theta}\, dt \tag{4.286}$$

to give various results graphed later in this chapter. As discussed in UFT 328 and its background notes, the ECE 2 version of the Leibniz equation is:

$$F(r) = -\frac{\partial U}{\partial r} = \frac{d}{dt}\left(\gamma m \dot{r}\right) - \gamma m r \dot{\theta}^2 \tag{4.287}$$

with the constant of motion:

$$L = \gamma m r^2 \dot{\theta}. \tag{4.288}$$

From Eq. (4.263), the transition from classical to ECE 2 dynamics can be described as:

$$p_N^2 \rightarrow 2\left(\frac{E^2}{mc^2\left(E + mc^2\right)}\right) p_N^2. \tag{4.289}$$

The method of solution and precessing graphics are given later in this section. It follows that the most general and rigorously correct method of describing orbital precession is to solve the ECE 2 hamiltonian and lagrangian simultaneously. The resulting graphics show clearly the presence of the true orbital precession. This method is valid for true precessions of any magnitude. The Einstein theory becomes wildly incorrect for large precessions, and the model (4.277) gives fractal conic sections.

4.2 Numerical Analysis and Graphics

4.2.1 Examples of a Gravitomagnetic Field

The gravitomagnetic field in dipole approximation has been analysed numerically and graphically in three dimensions. In ECE 2 theory the gravitomagnetic field is defined by

$$\mathbf{\Omega}_g = \boldsymbol{\nabla} \times \mathbf{W}_g \tag{4.290}$$

where $\mathbf{W}_g$ is the gravitomagnetic vector potential. This is – in analogy to electromagnetism – given by

$$\mathbf{W}_g = \frac{G}{c^2 r^3} \mathbf{m}_g \times \mathbf{r} \tag{4.291}$$

where $\mathbf{m}_g$ is a gravitational dipole moment. For a given $\mathbf{m}_g$ the vector potential and gravitomagnetic field can be computed in three dimensions by computer algebra. (The equations are quite complicated and not shown.) It would be desirable to draw equipotential lines because these are perpendicular to the field lines and demonstrate the curving of the field clearly. As the name says,

these are results of a scalar potential which is not available in the gravitomagnetic case. However, it is known from electrodynamics that dipole fields can be defined by a magnetic scalar potential Φ in analogy to the electric case:

$$\boldsymbol{\Omega}_g = -\boldsymbol{\nabla}\Phi. \tag{4.292}$$

Therefore we defined a dipole by two distinct charges $\pm q$ and a potential

$$\Phi(\mathbf{r}) = C\left(\frac{q}{|\mathbf{r}-\mathbf{r}_1|} - \frac{q}{|\mathbf{r}-\mathbf{r}_2|}\right) \tag{4.293}$$

with the "charges" at positions $\mathbf{r}_1$ and $\mathbf{r}_2$, here placed on the Z axis. The corresponding field $\boldsymbol{\Omega}_g$ is rotationally symmetric around this axis and is shown in Fig. 4.1, together with the equipotential lines of Φ.

It may be interesting how the field looks like if two dipoles are positioned upon one another. This is a linear arrangement without a quadrupole moment which would occur in other cases. The results are graphed in Fig. 4.2. There is a recess in the XY plane which is shown in more detail in Fig. 4.3. Field lines do not go straight from pole to pole in this region, contrary to the single dipole. It has been reported by Johnson in the seventies that such a behaviour has been found for certain magnets.

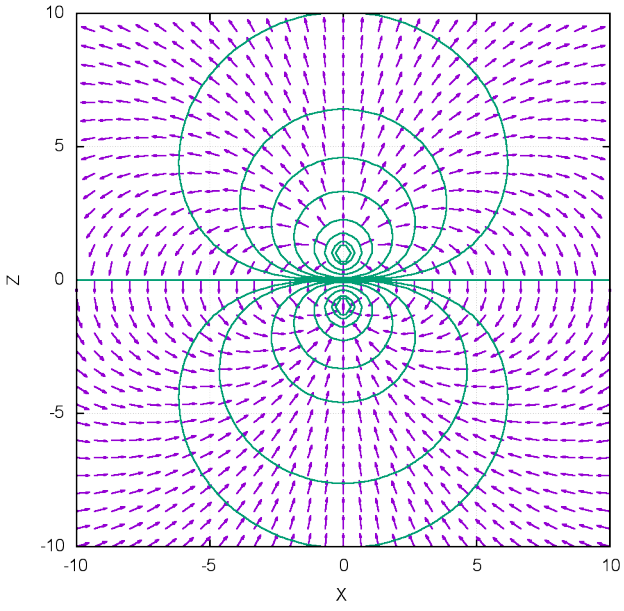

Figure 4.1: Dipole vector field $\boldsymbol{\Omega}_g$ (directional vectors only) in XZ plane and equipotential lines.

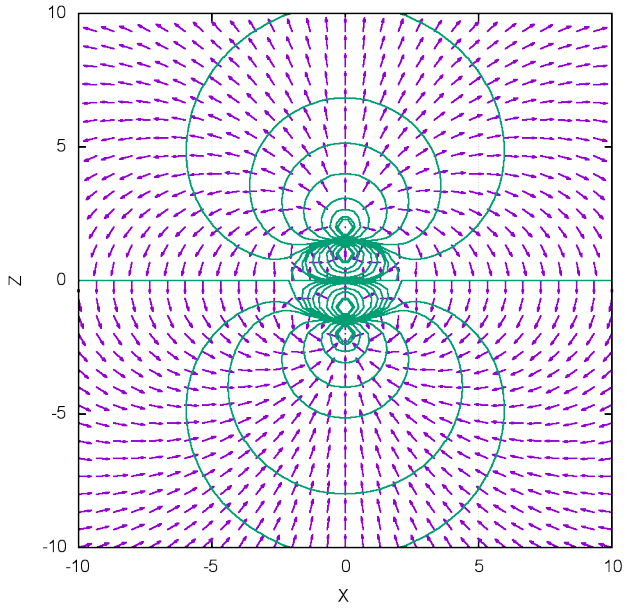

Figure 4.2: Double-dipole vector field in XZ plane and equipotential lines.

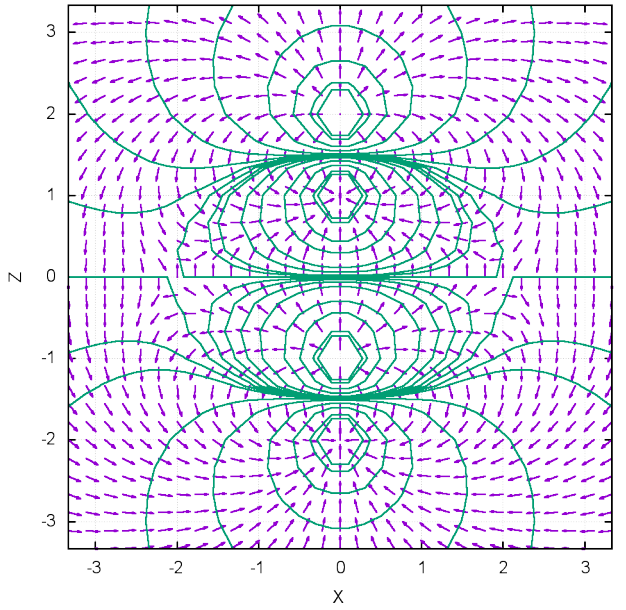

Figure 4.3: Double-dipole vector field and equipotential lines, enlarged view.

4.2.2 Relativistic Lagrange Theory and x Theory

The Lagrangian from special relativity, or Sommerfeld Lagrangian (Eq. (4.140)), is

$$\mathscr{L} = -\frac{m\,c^2}{\gamma} - U \tag{4.294}$$

with potential energy, γ factor and velocity

$$U = -\frac{m\,M\,G}{r}, \tag{4.295}$$

$$\gamma = \frac{1}{\sqrt{1-\frac{v^2}{c^2}}}, \tag{4.296}$$

$$v^2 = \dot{r}^2 + r^2\,\dot{\theta}^2. \tag{4.297}$$

The evaluation of Lagrange equations

$$\frac{\partial \mathscr{L}}{\partial r} = \frac{d}{dt}\frac{\partial \mathscr{L}}{\partial \dot{r}}, \tag{4.298}$$

$$\frac{\partial \mathscr{L}}{\partial \theta} = \frac{d}{dt}\frac{\partial \mathscr{L}}{\partial \dot{\theta}} \tag{4.299}$$

gives from the Sommerfeld Lagrangian (4.294):

$$\ddot{r} = -\frac{c^2\,G\,M + \gamma^3\,r^4\,\dot{r}\,\dot{\theta}\,\ddot{\theta} + \left(\gamma^3\,r^3\,\dot{r}^2 - \gamma\,c^2\,r^3\right)\,\dot{\theta}^2}{\gamma^3\,r^2\,\dot{r}^2 + \gamma\,c^2\,r^2}. \tag{4.300}$$

and

$$\ddot{\theta} = -\frac{\gamma^2\,r^2\,\dot{r}\,\dot{\theta}^3 + \left(\gamma^2\,r\,\dot{r}\,\ddot{r} + 2\,c^2\,\dot{r}\right)\,\dot{\theta}}{\gamma^2\,r^3\,\dot{\theta}^2 + c^2\,r}. \tag{4.301}$$

Both equations contain the second derivatives of r and θ in linear form. To obtain an equation set useable for numerical integration, both $\ddot{\theta}$ and $\ddot{r}$ have to be separated first. From the two equations with two unknowns (4.300,4.301) the solutions are

$$\ddot{r} = \frac{\left(-\gamma^2\,v^2 + \gamma^2\,\dot{r}^2 - c^2\right)\,G\,M + r\,\gamma\left(\gamma^2\,v^4 + c^2\,v^2\right) - r\,\dot{r}^2\,\gamma\left(\gamma^2\,v^2 + c^2\right)}{r^2\,\gamma\left(\gamma^2\,v^2 + c^2\right)}, \tag{4.302}$$

$$\ddot{\theta} = \frac{\gamma\,\dot{r}\,\dot{\theta}\,G\,M + r\,\dot{r}\,\dot{\theta}\,\left(-2\,\gamma^2\,v^2 - 2\,c^2\right)}{r^2\,\left(\gamma^2\,v^2 + c^2\right)}. \tag{4.303}$$

These are the relativistic Lagrange equations for central motion in a two-dimensional polar coordinate system. The non-relativistic form of them is obtained by assuming $\gamma \approx 1$ and making the transition $c \to \infty$ which leads to

$$\ddot{r} = r\,\dot{\theta}^2 - \frac{G\,M}{r^2}, \tag{4.304}$$

$$\ddot{\theta} = -\frac{2\,\dot{r}\,\dot{\theta}}{r}. \tag{4.305}$$

These are exactly the non-relativistic equations of Newton theory.

For comparison we also investigate the equations of motion from x theory. The x potential is given by

$$U = \frac{L^2\,\left(x^2-1\right)}{2\,m\,r^2} - \frac{L^2\,x^2}{\alpha\,m\,r}. \tag{4.306}$$

With the half latus rectum

$$\alpha = \frac{L^2}{m^2\,M\,G}, \tag{4.307}$$

the non-relativistic Lagrangian

$$\mathscr{L} = \frac{1}{2}mv^2 - U \tag{4.308}$$

is

$$\mathscr{L} = \frac{m\,x^2\,G\,M}{r} - \frac{L^2\,\left(x^2-1\right)}{2\,m\,r^2} + \frac{m\,\left(r^2\,\dot{\theta}^2+\dot{r}^2\right)}{2} \tag{4.309}$$

which leads to the non-relativistic Lagrange equations with x correction:

$$\ddot{r} = -\frac{x^2\,G\,M}{r^2} + \frac{Lm^2\,\left(x^2-1\right)}{m^2\,r^3} + r\,\dot{\theta}^2, \tag{4.310}$$

$$\ddot{\theta} = -\frac{2\,\dot{r}\,\dot{\theta}}{r}. \tag{4.311}$$

The equation for $\ddot{\theta}$ is unchanged. For $x = 1$ the non-relativistic equations are obtained. For $x < 1$ a negative contribution of $1/r^3$ is added to the radial force component, leading to a precession of the ellipse in the direction of the orbital motion which is observed for the planet Mercury.

Velocity Comparison

For a graphical examination of the results, we first will examine the graphs of the velocities. As was shown by Eq.(4.180), the non-relativistic velocity is given by

$$v_N^2 = \frac{v^2}{1+v^2/c^2} \tag{4.312}$$

where v_N for an ellipse is given according to Eq.(4.184) by

$$v_N^2 = M\,G\left(\frac{2}{r}-\frac{1}{a}\right) \tag{4.313}$$

with $a = \alpha/(1-\epsilon^2)$ being the major axis. Solving Eq.(4.312) for v gives

$$v^2 = \frac{v_N^2}{1-v_N^2/c^2}. \tag{4.314}$$

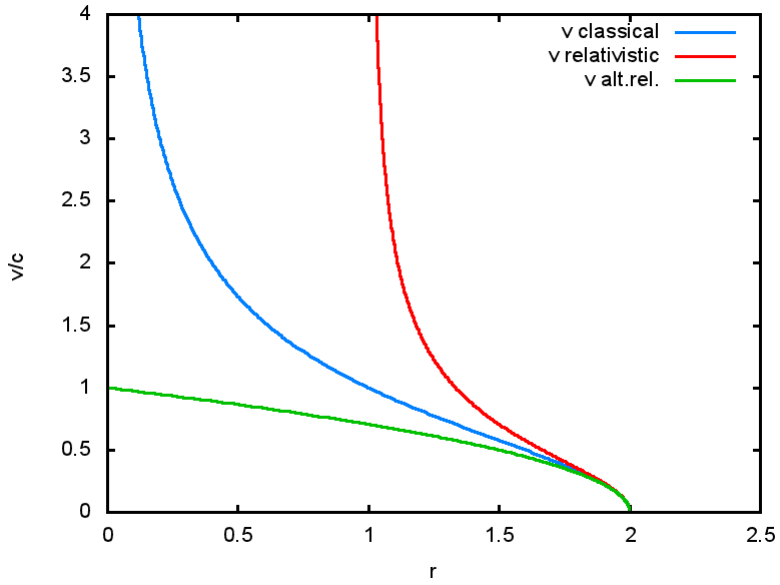

Figure 4.4: Newtonian and relativistic velocity ratio v/c.

By inserting (4.313) into (4.314), v and v_N can be compared in their radial dependence. The ratios v/c and v_N/c are graphed in Fig. 4.4. All parameters were set to unity. For $r \to 0$, the classical velocity diverges to an infinite value. For the relativistic velocity, this happens for $v_N = c$ where we have $v_N = 1$ in the actual scaling. This behaviour motivates an alternative definition for v' and v'_N with reversed signs in the denominator:

$$v_N'^2 = \frac{v'^2}{1 - v'^2/c^2}, \tag{4.315}$$

$$v'^2 = \frac{v_N'^2}{1 + v_N'^2/c^2}. \tag{4.316}$$

This effectively leads to an alternative relativistic velocity curve v/c which approaches unity for $r \to 0$ as expected (green curve in Fig. 4.4). Otherwise the case $v = c$ is reached at a much higher r value. However the non-relativistic formula of the orbit has been used in (4.313) which may be a source of an error, and the elliptic orbit is defined only in a restricted range of r.

It was shown in UFT 325 that the classical velocity in case of x theory correction is

$$v_x^2 = \frac{L^2}{\alpha^2\, m^2} \left(\frac{\alpha\, \left(x^2 + 1\right)}{r} + \left(\epsilon^2 - 1\right)\, x^2 \right). \tag{4.317}$$

To make this comparable with Eq.(4.313), we replace L^2 by

$$L^2 = m^2\, M\, G\, \alpha \tag{4.318}$$

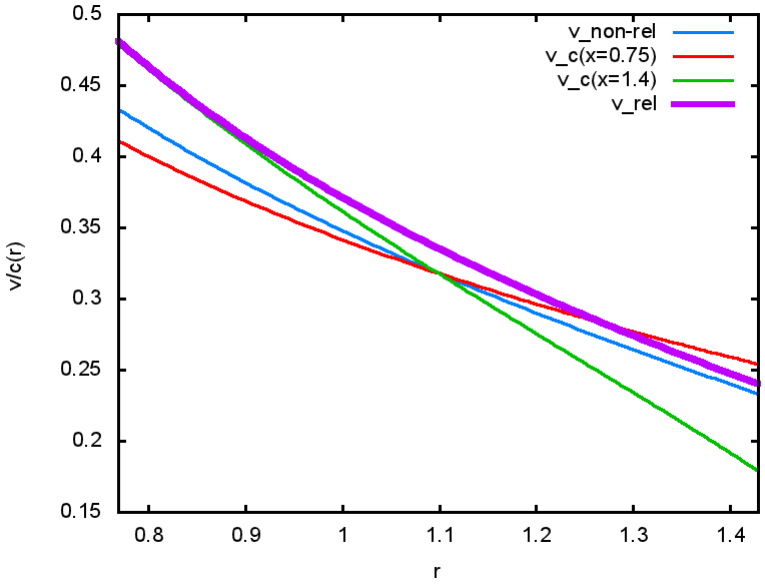

Figure 4.5: velocity ratio v/c for non-relativistic (Newtonian) and relativistic case, and for two values of x theory.

and obtain

$$v_x^2 = \frac{\left(\left(\left(\epsilon^2 - 1\right)\, r + \alpha\right)\, x^2 + \alpha\right)\, G\, M}{\alpha\, r}. \tag{4.319}$$

From (4.313) and (4.314) then follows

$$v_N^2 = \frac{\left(\left(\epsilon^2 - 1\right)\, r + 2\,\alpha\right)\, G\, M}{\alpha\, r}, \tag{4.320}$$

$$v^2 = \frac{\left(\left(\epsilon^2 - 1\right)\, r + 2\,\alpha\right)\, G\, M\, c^2}{\left(\left(\epsilon^2 - 1\right)\, r + 2\,\alpha\right)\, G\, M + \alpha\, c^2\, r}. \tag{4.321}$$

With parameters set to $\epsilon = 0.3$, $c = 3$, all other parameters unity, we can compare all three velocity expressions. The results are graphed in Fig. 4.5 for two values of $x = 0.75$ and $x = 1.4$. These are the velocities for a precessing or non-precessing ellipse in the high-relativistic case up to $v/c = 0.5$. The curves $v(r)/c$ are plotted in the range [rmin, rmax] of an ellipse with $\alpha = 1$. It can be noticed that the relativistic curve (thick line) is not covered exactly neither by x theory nor by Newton theory. The latter underestimates velocity at perihelion. Using $x = 0.75$ (red line) fits the velocity of x theory near to the aphelion but underestimates it at perihelion. Values for $x > 1$ cannot remedy this because the slope becomes too large. The true theoretical orbit is that from the Lagrangian of special relativity, which is also the Lagrangian of ECE 2 theory.

Numerical Solution of Relativistic Orbits and Control Parameters

The equations (4.302-4.303) have been solved numerically as for example in UFT paper 239 (but we used θ as the integration variable therein, while we use the time in this work). The results $r(t)$ and $\theta(t)$ can be combined in a so-called scatter-plot in a polar coordinate system to obtain the orbit $r(\theta)$. So the orbit is not given by an analytical formula in this case but numerically by "points". The result is graphed in Fig. 4.6, showing directly the precession of the ellipse. Orbital motion is in positive mathematical angular direction as is the rotation of the elliptic orbit. This is in coincidence with astronomical findings.

There is additional information that can be obtained from the solutions $r(t)$ and $\theta(t)$ and their derivatives. Important checks are the constants of motion: relativistic angular momentum and energy. We validated that the relativistic momentum is conserved as well as the relativistic energy (Hamiltonian). Fig. 4.7 shows the ratio v/c which is minimal in aphelion as expected. The same holds for the difference of the r component of force and the angular momentum between relativistic and non-relativistic calculation (Fig. 4.8). The total energy is identical to the non-relativistic case at aphelion (Fig. 4.9).

We did the same numerical calculation for the potential of x theory. In the Newtonian case ($x = 1$) the well known ellipses follow, for the x theory the precessing ellipses, all numerically, and can be compared with the relativistic solution. It is a bit difficult to define comparable x factors for the relativistic case because there is no analytically given orbit and both theories show quantitatively different behaviour, see discussion of Fig. 4.5 above. The initial conditions do not reflect expressions like ϵ and α, one has to use r, θ, $\dot{r}$ and $\dot{\theta}$ primarily, where we pre-computed $\dot{\theta}$ from the same value of given non-relativistic angular momentum in all cases. Fig. 4.10 shows the precessing orbit for $x = 0.98$. The v/c ratio (Fig. 4.11) looks similar as for the relativistic theory, The force difference changes signs in the orbit and the angular momentum is the same as in the non-relativistic case, i.e. $\Delta L = 0$. The difference of total energy (Fig. 4.13) shows more variation than in the relativistic case.

The numerical calculations have shown that the solution of relativistic Lagrange equations is a parameter-free, first-principles method of solving the relativistic Kepler problem. It will be difficult however to obtain orbital precession values for real planets because these effects are very small and require very high numerical accuracy.

4.2.3 Relativistic Orbit Properties

We investigate some further parameters derived from the numerical solution of the relativistic Lagrange equations (4.302, 4.303) and compare them with the Newtonian solution from (4.304, 4.305). The orbital derivative is given by (setting $\dot{\theta} = \omega$):

$$\frac{dr}{d\theta} = \frac{dr}{d\tau}\frac{d\tau}{d\theta} = \frac{dr}{dt}\frac{dt}{d\theta} = \frac{\dot{r}}{\omega}. \tag{4.322}$$

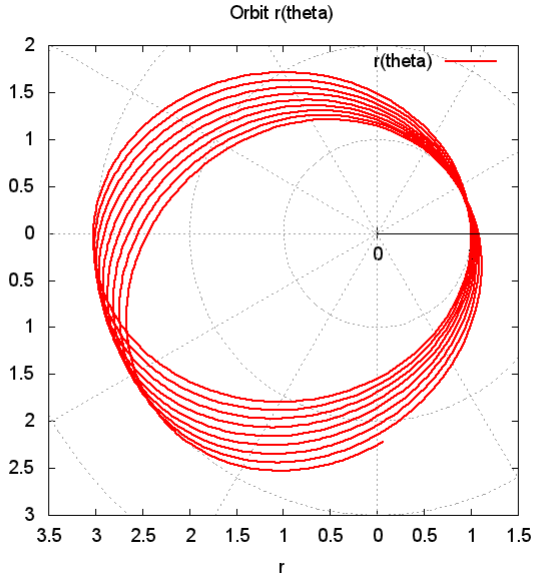

Figure 4.6: Orbit from relativistic theory.

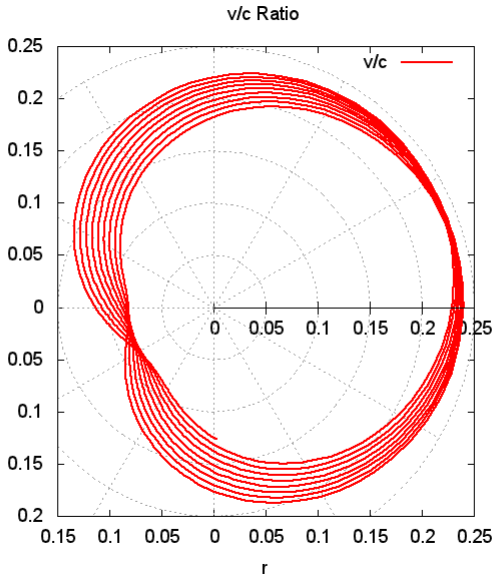

Figure 4.7: Ratio v/c from relativistic theory.

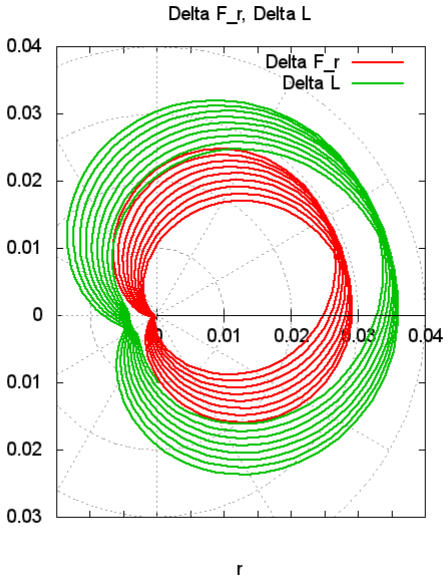

Figure 4.8: Difference of force component F_r and angular momentum L between relativistic and Newton theory.

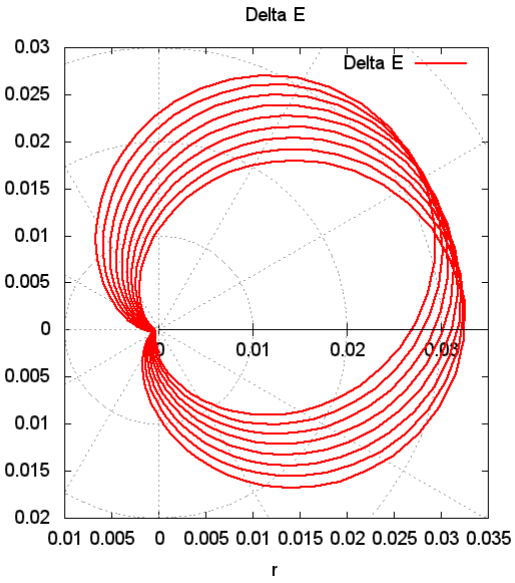

Figure 4.9: Difference of total energy E between relativistic and Newton theory.

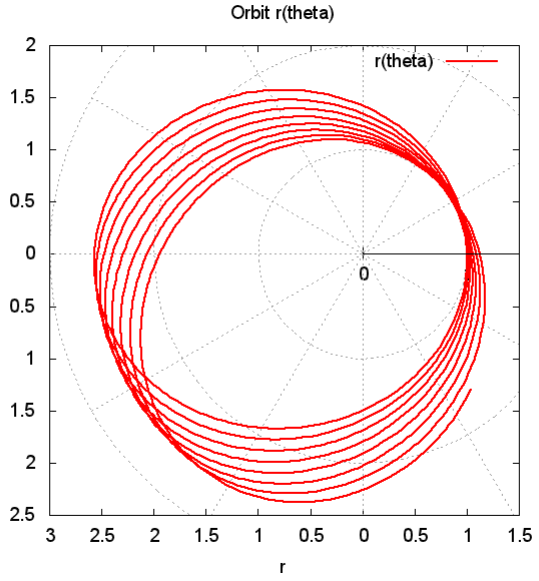

Figure 4.10: Orbit from non-relativistic x theory, $x = 0.98$.

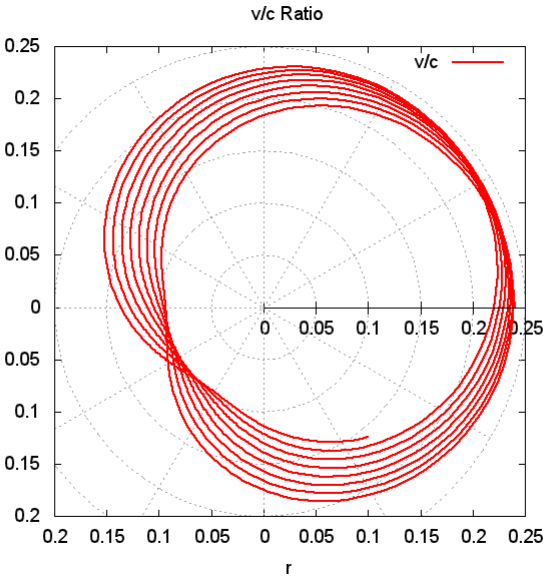

Figure 4.11: Ratio v/c from non-relativistic x theory.

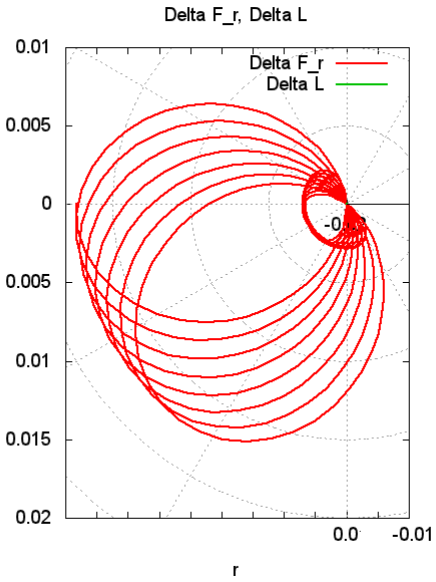

Figure 4.12: Difference of force component F_r and angular momentum L between x theory and Newton theory.

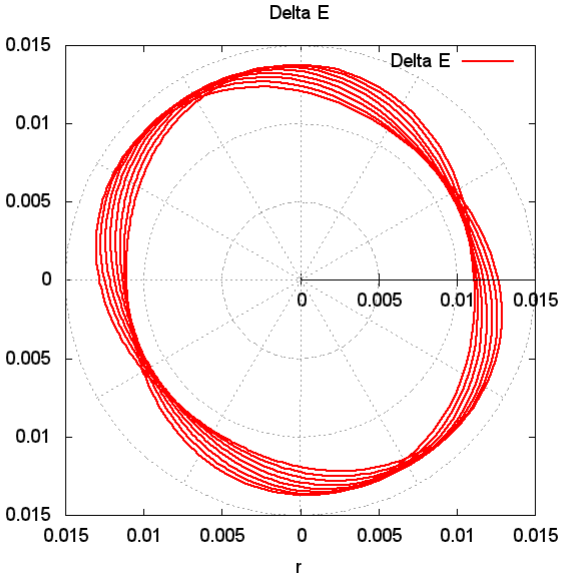

Figure 4.13: Difference of total energy E between x theory and Newton theory.

We obtain for the relativistic ratio of p/L:

$$\frac{p}{L} = \frac{\gamma m v_0}{\gamma m r^2 \omega} = \frac{v_0}{\omega r^2} \tag{4.323}$$

with constituting equations

$$v_0 = \sqrt{\dot{r}^2 + r^2\omega^2}, \tag{4.324}$$

$$v = \gamma v_0, \tag{4.325}$$

$$\gamma = \frac{1}{\sqrt{1 - v_0^2/c^2}}. \tag{4.326}$$

The numerical results are compared with the corresponding results of the non-relativistic, Newtonian Lagrangian (4.307).

The relativistic and non-relativistic calculations started at $\theta = 0$ with the same radius and initial angular velocity. Therefore the angular momenta were not the same at the starting point. It is however not possible to use the non-relativistic L_0 in the relativistic equation because this is not a constant of motion there. From Fig. 4.14 (orbits) it can be seen that the relativistic orbit is significantly larger for identical initial conditions. This is a hint that it makes no sense to use an equation for the non-relativistic orbit in a relativistic context. The orbital derivative $\frac{dr}{d\theta}$ is graphed in Fig. 4.15. Since the derivative takes both signs, there are two overlapping elliptic curves in the polar plot (negative values are represented by an angular shift of π).

The graph of $\dot{r}$ (Fig. 4.16) is a circle in the non-relativistic case which is run through twice because of the symmetry with sign change for a full ellipse. In the relativistic case the precession leads to a splitting of the circle which can well be observed in the figure. The angular velocity (Fig. 4.17) remains positive and shows the relativistic precessing behaviour as do nearly all other curves.

Fig. 4.18 shows $\gamma(\theta)$, this varies only between 1.00 and 1.03 for this particular orbit although the orbital precession (graphed in Fig. 4.14) is significant. The ratio v/c (Fig. 4.19) is dominated by the angular velocity component of v and therefore resembles ω (Fig. 4.17). The ratio p/L (Fig. 4.20) looks also very similar due to its dependence on v. There is always a bend in the curves at the aphelion. The differences between Newtonian and relativistic results for linear momentum, angular momentum and force have already been shown in the preceding subsection.

It is of some interest to inspect the angular dependence of the orbital precession described by Newtonian and relativistic theory. In Newtonian and x theory, the orbit is

$$r_1(\theta) = \frac{\alpha}{1 + \epsilon\cos(x\theta)} \tag{4.327}$$

(with $x = 1$ for the Newtonian case), while from the relativistic theory the precession of θ is not constant but a general function $\theta_1(\theta)$:

$$r_2(\theta) = \frac{\alpha}{1 + \epsilon\cos(\theta_1(\theta))}. \tag{4.328}$$

The first problem is to find a meaningful method for comparing the Newtonian and relativistic case since the maximum radius (as well as the effective ϵ and time dependence) are different. Therefore we used the orbital derivatives

$$\frac{dr_1}{d\theta} = \frac{\dot{r_1}}{\omega_1} \tag{4.329}$$

and

$$\frac{dr_2}{d\theta} = \frac{\dot{r_2}}{\omega_2} \tag{4.330}$$

for the Newtonian (r_1) and relativistic case (r_2). Both curves are crossing zero at perihelion and aphelion and have been normalized so that they look identical except their dependence on angle θ, see Fig. 4.21. The horizontal difference between both for a given ordinate value is a measure of the progression of angular precession, see Fig. 4.21. The difference

$$\Delta\theta = \theta_2 - \theta_1 \quad \text{for} \quad \frac{dr_1}{d\theta_1} = \frac{dr_2}{d\theta_2} \tag{4.331}$$

has also been plotted in Fig. 4.21. It can be seen that there is no linearly growing $\Delta\theta$ as assumed in x theory. Within the first orbit round (0-2π) the difference becomes even negative just before θ approaches 2π. This is the most realistic calculation of precession we have done in all papers so far.

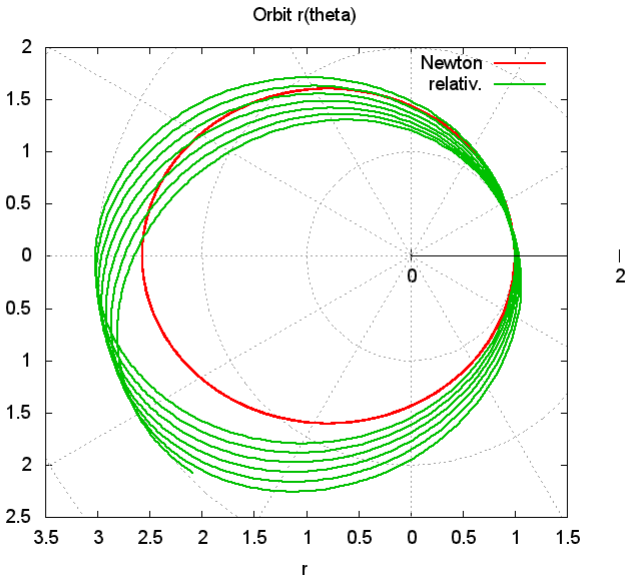

Figure 4.14: Orbit $r(\theta)$.

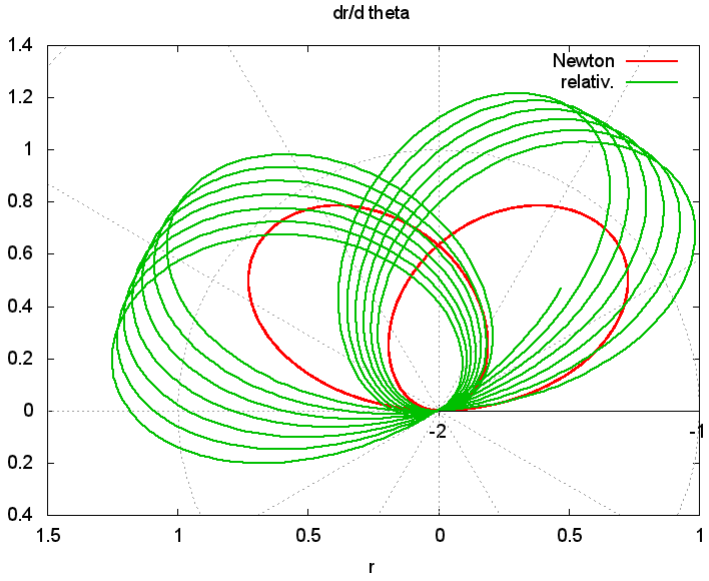

Figure 4.15: Orbit derivative $dr/d\theta$.

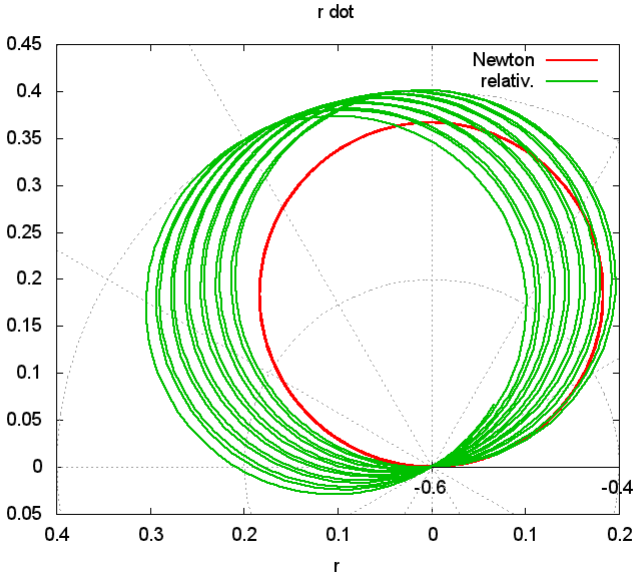

Figure 4.16: Radial derivative $\dot{r}$.

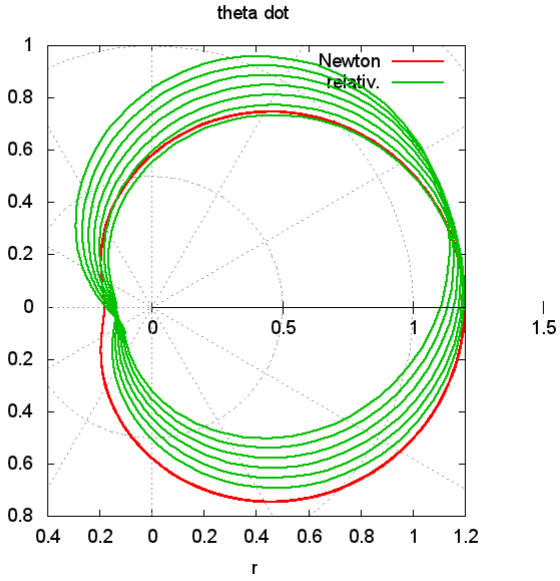

Figure 4.17: Angular velocity $\dot{\theta} = \omega$.

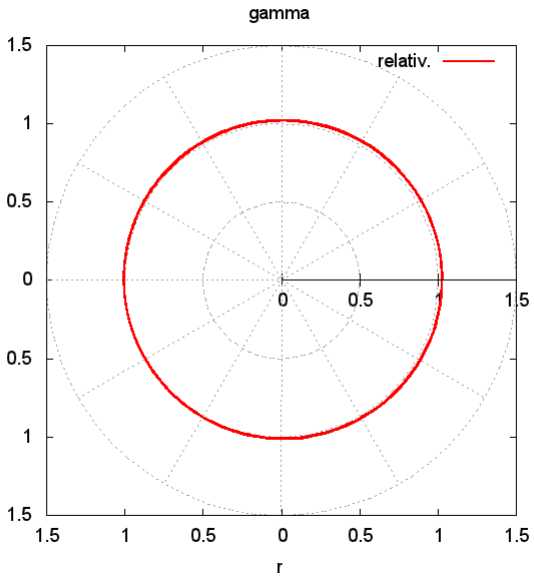

Figure 4.18: Relativistic γ factor.

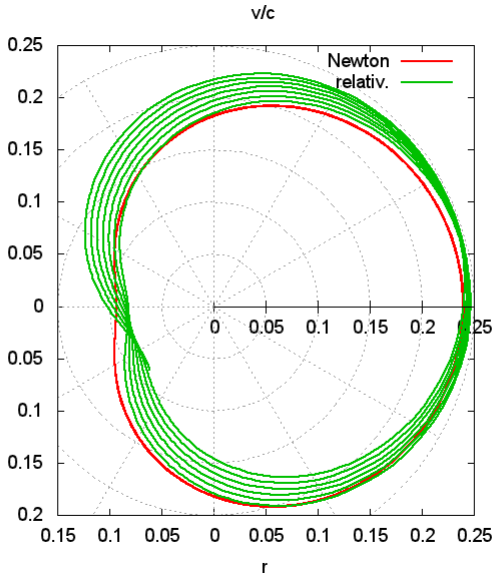

Figure 4.19: Ratio v/c.

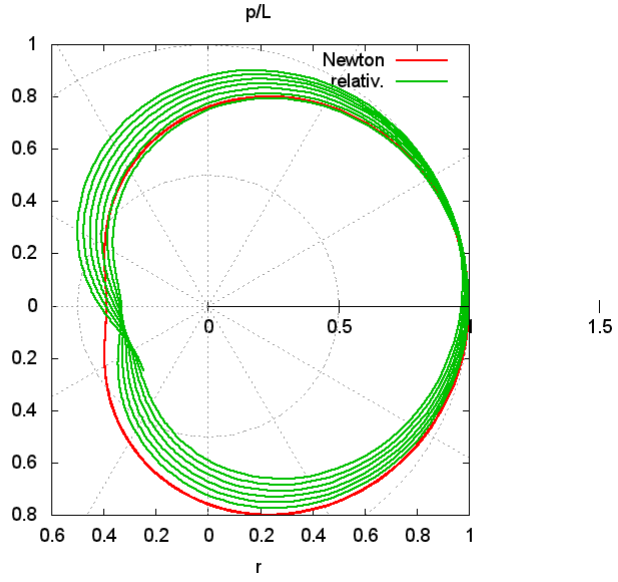

Figure 4.20: Ratio p/L.

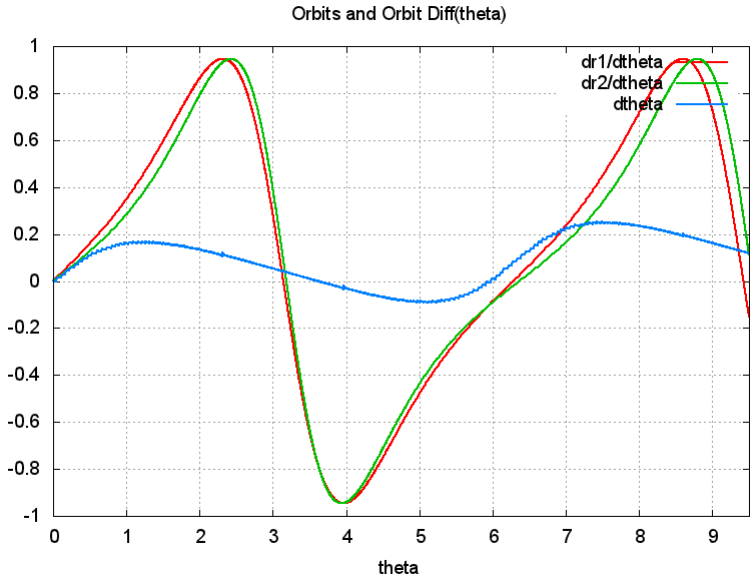

Figure 4.21: Normalized $dr/d\theta$ for Newtonian and relativistic calculation, and difference $\Delta\theta(\theta)$.

4.2.4 Correct Solution of the Einstein Integral

We investigate the counterpart of the orbital equation (4.276) in Einstein's obsolete theory. In Einsteinian theory (see UFT 327) the orbit $\theta(u)$ with $u = 1/r$ has to be computed from solving the integral

$$\theta(u) = \int \frac{L_0\, du}{\sqrt{2m(H + ku - \frac{L_0^2}{2m}u^2 + \frac{L_0^2}{2m}r_0 u^3)}} \tag{4.332}$$

with non-relativistic angular momentum L_0, total energy H, $k = mMG$ and "Schwarzschild radius" r_0. The term in the square root is a polynomial of third order in u and can be written as

$$\frac{1}{\alpha}(u - u_1)(u - u_2)(u - u_3) \tag{4.333}$$

where $u_1 = 1/r_1$ etc. are characteristic inverse radii. The constants u_1, u_2, u_3 are defined by Eq.(4.332), and

$$\frac{1}{\alpha} = u_1 + u_2 + u_3. \tag{4.334}$$

Einstein argued by the roots of Eq.(4.333). The physical range of u is between two values of u where the denominator vanishes, i.e. one has to find the roots of (4.333) to find the integration interval. In his terminology Einstein wrote

the terms in the denominator in form of

$$\frac{2A}{B^2} + \frac{\alpha}{B^2}u - u^2 + \alpha u^3 \tag{4.335}$$

and additionally omitted the cubic term. This seems to be arbitrary but guarantees that only two roots exist which then are

$$u^{(1,2)} = \frac{\pm\sqrt{8\,A\,B^2 + \alpha^2} + \alpha}{2\,B^2}. \tag{4.336}$$

The correct method, however, would be finding the roots of the cubic equation (4.333). By computer algebra this is possible. Quite complicated solutions follow from which two are complex-valued. This problem of the "true" solution of (4.333) has never been addressed in literature.

With modern computer algebra, it is possible to solve Eq.(4.332) analytically. Writing it in the form

$$\theta(u) = \int \frac{du}{\sqrt{\alpha(u-u_1)(u-u_2)(u-u_3)}} \tag{4.337}$$

leads to a solution which, after some simplifications, reads

$$\theta(u) = \frac{2}{\sqrt{\alpha(u_2-u_1)}}\,\mathrm{F}\left(\mathrm{asin}\left(\sqrt{\frac{u_1-u_2}{u_1-u}}\right),\ \frac{u_3-u_1}{u_2-u_1}\right) \tag{4.338}$$

with the elliptic integral of first kind $\mathrm{F}(x,y)$. It has to be noted that this integral is complex-valued. The real value has to be taken as physical value.

Having found this solution, the result can be plotted and computer graphics gives an impression of the solution immediately. First we have graphed the integrand of (4.337) as a function $f(u)$ with parameters $u_1 = 3,\ u_2 = 2,\ \alpha = 0.1$ from which follows $u_3 = 5$. Fig. 4.22 shows that the integrand has strong infinite asymptotes as was already known from corresponding plots in UFT papers 150 and 155. u_1 and u_2 are the physical inverse radii, above u_3 an unlimited unphysical range appears. The real part of solution (4.338) (Fig. 4.23) is dominated by the inverse sine function which is defined between u_1 and u_2 correctly. The imaginary part pertains to an unphysical range. Choosing parameters differently with $u_1 < u_2$ (not shown) gives similar results with positive $\theta(u)$. We conclude that there is no multiplicity of solution for θ, i.e. there is no room for any precession effects from this Einsteinian solution which probably was analysed in these details for the first time.

The last example is an assessment of relativistic effects for a non-relativistic elliptic orbit. The latter is given by

$$r = \frac{\alpha}{1 + \epsilon\cos(\theta)}. \tag{4.339}$$

We assume that the half-right latitude α is affected by relativistic effects:

$$\alpha = \gamma\ \alpha_0 = \frac{1}{1 - v_0^2/c^2}\,\alpha_0 \tag{4.340}$$

for a non-relativistic α_0. Using the well-known solution

$$v_0^2 = \left(\frac{2}{r} - \frac{1}{a}\right) MG \tag{4.341}$$

and inserting this into (4.339), we obtain an equation for the orbit $r(\theta)$ with relativistic correction:

$$r = \frac{(2\,a\,\epsilon\cos(\theta) + 2\,a)\;M\,G + a\,\alpha_0\,c^2}{(\epsilon\cos(\theta) + 1)\;M\,G + a\,c^2\,\epsilon\cos(\theta) + a\,c^2}. \tag{4.342}$$

The graph (Fig. 4.24) shows what is to be expected from (4.340): the effective alpha is enlarged by relativistic effects (here obtained by varying c and keeping all other parameters to unity). The enlargement is not constant, but there is no crossing of the curves, that means that the constants of motion are different. This is plausible because the angular momentum L_0 is increased by the gamma factor. A smaller c here means stronger relativistic effects.

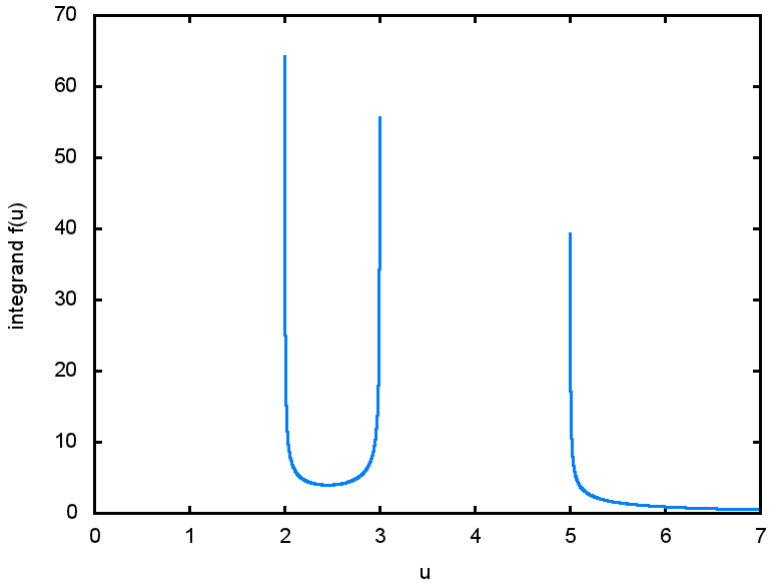

Figure 4.22: Integrand of Einstein integral in form of Eq. (4.337).

4.2.5 Quantization of the Free Particle

The relativistic Schroedinger equation for a free particle is according to UFT 326 (note 4):

$$H_1 = H - m\,c^2 = \frac{p^2}{m(1+\gamma)} \tag{4.343}$$

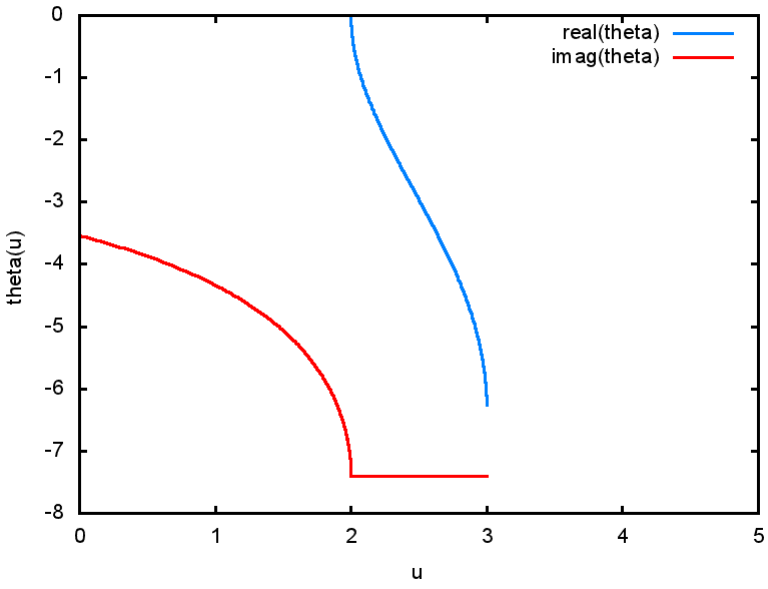

Figure 4.23: Analytical solution (4.338) of the Einstein integral.

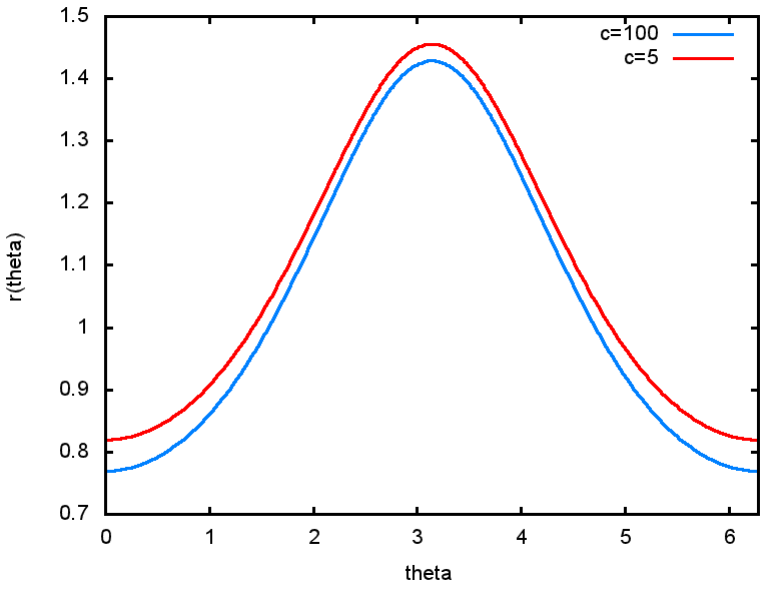

Figure 4.24: Radius function $r(\theta)$ for different cases of relativistic effects, characterized by c.

with relativistic momentum

$$p = \gamma\, p_0 = \gamma\, m\, v_0 \tag{4.344}$$

and γ factor

$$\gamma = \frac{1}{\sqrt{1 - \frac{p_0^2}{m^2 c^2}}}. \tag{4.345}$$

Inserting p and γ into (4.343) gives a relation between H_1, p_0 and v_0, i.e. the relativistic energy can be set in relation with the non-relativistic momentum and the frame velocity. From (4.343) follows

$$\frac{{p_0}^2}{m\left(1 - \frac{{p_0}^2}{m^2\, c^2}\right)} = \left(\frac{1}{\sqrt{1 - \frac{{p_0}^2}{m^2\, c^2}}} + 1\right) H_1. \tag{4.346}$$

This equation can be resolved for p_0 by computer algebra, giving intermediately an equation of eighth order for p_0 with three solutions for p_0^2:

$$p_0^2 = 0, \tag{4.347}$$

$$p_0^2 = \frac{m^2 c^2\, H_1\, \left(H_1 - 2\, m\, c^2\right)}{\left(H_1 - m\, c^2\right)^2}, \tag{4.348}$$

$$p_0^2 = \frac{m^2 c^2\, H_1\, \left(H_1 + 2\, m\, c^2\right)}{\left(H_1 + m\, c^2\right)^2}. \tag{4.349}$$

It can be seen that in the approximation $H_1 \ll m\, c^2$ the third solution approaches the non-relativistic case

$$\frac{p_0^2}{2m} = H_1. \tag{4.350}$$

Alternatively, the two non-trivial equations (4.348, 4.349) can be resolved for H_1, resulting in two solutions

$$H_1 = \frac{-m\, c^2\, p_0^2 \pm m^2 c^3 \sqrt{m^2 c^2 - p_0^2} + m^3 c^4}{p_0^2 - m^2 c^2}. \tag{4.351}$$

This is the relativistic free particle energy, written in terms of p_0.

The relativistic de Broglie wave number was derived in UFT 326, note 6:

$$\kappa^2 = \left(\frac{m\, c}{\hbar}\right)^2 \left(\frac{1}{1 - \left(\frac{p_0}{m\, c}\right)^2} - 1\right). \tag{4.352}$$

With $p_0 = m\, v_0$ the dependence of κ on v_0 can be graphed and compared with the non-relativistic

$$\kappa^2 = \left(\frac{m\, v_0}{\hbar}\right)^2. \tag{4.353}$$

In Fig. 4.25 both curves are presented with all constants set to unity. It can well be seen that the relativistic κ approaches the non-relativistic, linear curve for low velocities but diverges for $v_0 \to c$.

The de Broglie frequency for free particles was given by Eq. (30) of UFT 326:

$$\omega = \kappa c + \frac{1}{\hbar}\frac{m\,c^3}{\gamma(c+v_0)}. \tag{4.354}$$

Inverting this equation for v_0 gives the result:

$$v_0 = \frac{c\,\left(\hbar\,\omega - m\,c^2 - \hbar\,c\,\kappa\right)\,\left(\hbar\,\omega + m\,c^2 - \hbar\,c\,\kappa\right)}{\hbar^2\,\left(\omega^2 - 2\,c\,\kappa\,\omega + c^2\,\kappa^2\right) + m^2\,c^4}. \tag{4.355}$$

Its dependence on κ and ω has been graphed in a 3D plot (Fig. 4.26). There is a range of negative velocities at the borders which is unphysical. The range is further confined by Eq. (4.352).

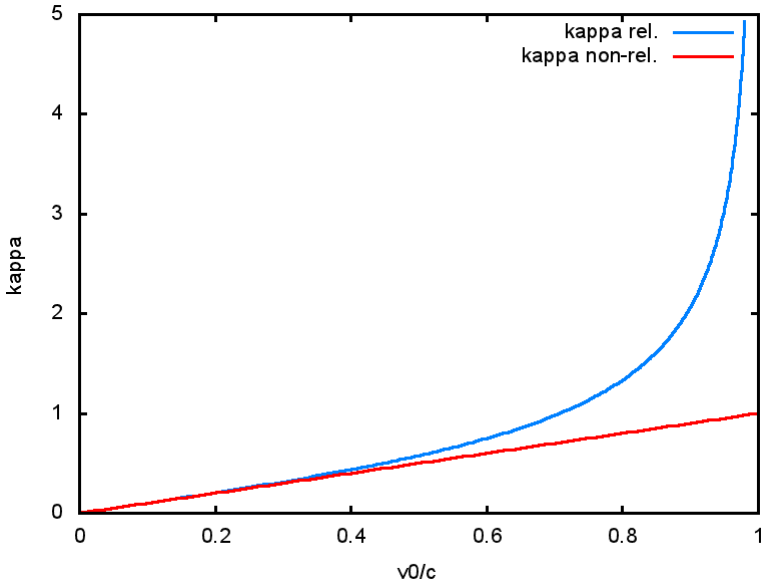

Figure 4.25: Free particle de Broglie wave number κ in dependence of v_0/c.

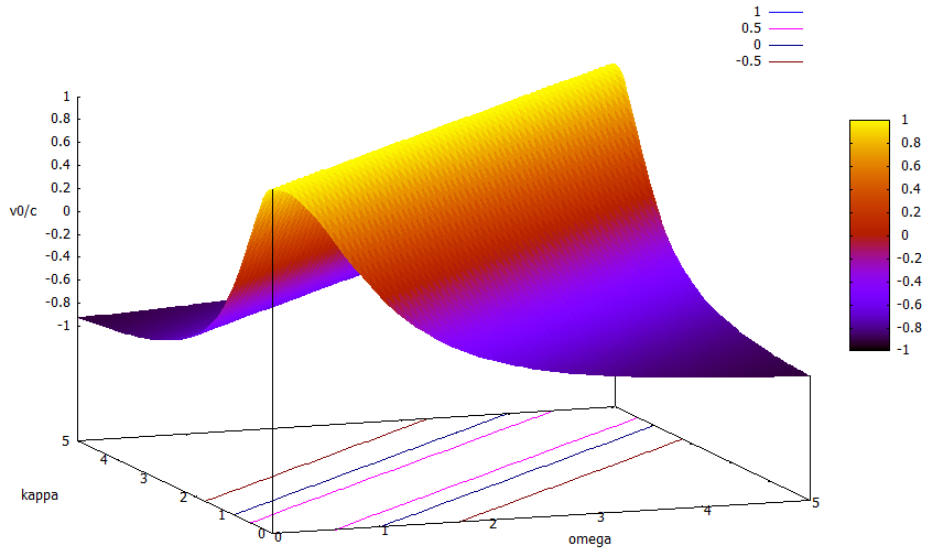

Figure 4.26: Free particle velocity v_0 in dependence of κ and ω.

Chapter 5

New Spectroscopies

5.1 General Theory

The ECE 2 unified field theory can be used to develop new types of spectroscopy of general utility, for example electron spin resonance (ESR) and nuclear magnetic resonance (NMR). Novel resonance terms can be developed and expressed in terms of the **W** potential of ECE 2 theory. This has the same units as the **A** potential of the standard model. The new types of ESR and NMR emerge from the hamiltonian of ECE 2, which can be deduced using its covariance properties explained in previous chapters:

$$H = \left(p^2c^2 + m^2c^4\right)^{1/2} + U. \tag{5.1}$$

Here U is the potential energy, $\mathbf{p}$ the relativistic momentum, m the particle mass, and c the vacuum speed of light regarded as a universal constant. In the H atom, the potential energy between the electron and proton is the Coulomb potential:

$$U = -\frac{e^2}{4\pi\epsilon_0 r} \tag{5.2}$$

where e is the charge on the proton and ϵ_0 is the vacuum permittivity in S. I. Units. Here $\mathbf{r}$ is the distance between the electron and proton in the H atom. The hamiltonian (5.1) can be rewritten as:

$$H_0 := H - mc^2 = \frac{p^2}{m\left(1+\gamma\right)} + U \tag{5.3}$$

in which the Lorentz factor is:

$$\gamma = \left(1 - \frac{p_0^2}{m^2c^2}\right)^{-1/2} \tag{5.4}$$

where p_0 is the non relativistic momentum defined by:

$$p_0^2 = 2m\left(H_0 - U\right). \tag{5.5}$$

The relativistic momentum is defined by:

$$\mathbf{p} = \gamma \mathbf{p}_0 \tag{5.6}$$

and quantization takes place through the relativistic momentum:

$$-i\hbar \boldsymbol{\nabla} \psi = \mathbf{p}\psi \tag{5.7}$$

where ψ is the relevant wave function of the hydrogen atom. Therefore the relativistic quantum mechanical wave equation is constructed from Eq. (5.3), in which either the operator or classical function can always be used. Using the operator in the numerator and the classical function in the denominator produces the following relativistic quantum mechanical equation:

$$\langle H_0 \rangle = -\hbar^2 c^2 \int \frac{\psi^* \nabla^2 \psi \, d\tau}{m\,(1+\gamma)} + \int \psi^* U \psi \, d\tau \tag{5.8}$$

in which:

$$\mathbf{p}_0 = m\mathbf{v}_0. \tag{5.9}$$

In a first approximation:

$$\left(1 - \frac{p_0^2}{m^2 c^2}\right)^{-1/2} \sim 1 + \frac{1}{2}\frac{p_0^2}{m^2 c^2} \tag{5.10}$$

so the energy levels from Eq. (5.8) become:

$$\langle H_0 \rangle = -\hbar^2 c^2 \int \frac{\psi^* \nabla^2 \psi \, d\tau}{\left(2 + \frac{p_0^2}{2m^2 c^2}\right) mc^2} + \int \psi^* U \psi \, d\tau. \tag{5.11}$$

In the limit:

$$H_0 - U \ll mc^2 \tag{5.12}$$

Eq. (5.11) reduces to the well known hydrogen atom energy levels of the Schrödinger equation:

$$\langle H_0 \rangle = -\frac{\hbar^2}{2m} \int \psi^* \nabla^2 \psi \, d\tau + \int \psi^* U \psi \, d\tau = \frac{-me^4}{32\pi^2 \epsilon_0^2 \hbar^2 n^2}. \tag{5.13}$$

Using:

$$\left(2 + \frac{H_0 - U}{mc^2}\right)^{-1} = \frac{1}{2}\left(1 + \frac{H_0 - U}{2mc^2}\right)^{-1} \sim \frac{1}{2}\left(1 - \frac{H_0 - U}{2mc^2}\right) \tag{5.14}$$

and for:

$$H_0 - U \ll 2mc^2 \tag{5.15}$$

Eq. (5.11) reduces to:

$$\langle H_0 \rangle = \frac{-me^4}{32\pi^2\epsilon_0^2\hbar^2 n^2} + \frac{\hbar^2}{4m^2c^2}\int \psi^* \nabla^2 \left((H_0 - U)\,\psi \right) d\tau. \tag{5.16}$$

There is a novel shift in the energy levels of the H atom which is different for each principal quantum number n.

Now use the fact that the classical hamiltonian defined by:

$$H_0 = \frac{-me^4}{32\pi^2\epsilon_0^2\hbar^2 n^2} \tag{5.17}$$

is a constant of motion. Therefore:

$$\langle H_0 \rangle = \frac{-me^4}{32\pi^2\epsilon_0^2\hbar^2 n^2} - \frac{\hbar^2}{4m^2c^2}\int \psi^* \nabla^2 \left(U\psi \right) d\tau + \frac{\hbar^2 H_0}{4m^2c^2}\int \psi^* \nabla^2 \psi \, d\tau. \tag{5.18}$$

In the first approximation, Eq. (5.17) can be used for H_0 on the right hand side, so

$$\begin{aligned} \langle H_0 \rangle = \frac{-me^4}{32\pi^2\epsilon_0^2\hbar^2 n^2} \left(1 + \frac{\hbar^2}{4m^2c^2}\int \psi^* \nabla^2 \psi \, d\tau \right) \\ - \frac{\hbar^2}{4m^2c^2}\int \psi^* \nabla^2 \left(U\psi \right) d\tau \end{aligned} \tag{5.19}$$

and details of this calculation are given in Note 329(3) on `www.aias.us`. The usual Dirac approximation:

$$H \sim E \sim mc^2, \tag{5.20}$$

$$U \ll E \sim mc^2 \tag{5.21}$$

leads to:

$$\langle H_0 \rangle = \frac{-me^4}{32\pi^2\epsilon_0^2\hbar^2 n^2} - \frac{\hbar^2}{4m^2c^2}\int \psi^* \nabla^2 \left(U\psi \right) \tag{5.22}$$

and misses the following term:

$$\langle H_0 \rangle_1 = \frac{-me^4}{32\pi^2\epsilon_0^2\hbar^2 n^2} \left(\frac{\hbar^2}{4m^2c^2}\int \psi^* \nabla^2 \psi \, d\tau \right). \tag{5.23}$$

The energy levels in this term can be evaluated by assuming in the first approximation that wave functions are those from the Schrödinger equation. Code libraries can be used to develop a more accurate approximation.

As shown in detail in Note 329(4) the new hamiltonian in the SU(2) basis is:

$$H_{01} = -\frac{1}{4m^2c^2}\boldsymbol{\sigma} \cdot \mathbf{p}\, H_0\, \boldsymbol{\sigma} \cdot \mathbf{p} \tag{5.24}$$

and leads to the energy level shifts:

$$H_{01} = \frac{\hbar^2 H_0}{4m^2c^2}\nabla^2 \psi. \tag{5.25}$$

The effect of an external magnetic field can be described by the minimal prescription, using the **W** potential of ECE 2 theory introduced in chapter three. The hamiltonian (5.24) in the presence of a magnetic field becomes:

$$H_{01} = -\frac{H_0}{4m^2c^2}\boldsymbol{\sigma}\cdot(\mathbf{p}-e\mathbf{W})\,\boldsymbol{\sigma}\cdot(\mathbf{p}-e\mathbf{W}) \tag{5.26}$$

which quantizes to:

$$H_{01}\psi = \frac{H_0}{4m^2c^2}\left(-\hbar^2\nabla^2 + e^2W^2 + i\hbar e\left(\boldsymbol{\nabla}\cdot\mathbf{W}+\mathbf{W}\cdot\boldsymbol{\nabla}\right)\right)\psi \tag{5.27}$$

giving many effects as described in UFT 250 and UFT 252 and their background notes. As shown in detail in Note 329(5) on `www.aias.us` the quantization scheme that leads to new types of ESR and NMR is:

$$H_{01}\psi = -\frac{H_0}{4m^2c^2}\boldsymbol{\sigma}\cdot(-i\hbar\boldsymbol{\nabla}-e\mathbf{W})\,\boldsymbol{\sigma}\cdot(\mathbf{p}-e\mathbf{W})\,\psi \tag{5.28}$$

where **p** is the relativistic momentum. As shown in Note 329(6) the hamiltonian of relevance is:

$$H_{\mathrm{ESR}}\psi = -\frac{ie\hbar H_0}{4m^2c^2}\boldsymbol{\sigma}\cdot\boldsymbol{\nabla}\,\boldsymbol{\sigma}\cdot\mathbf{W}\psi. \tag{5.29}$$

Using the Pauli algebra:

$$\boldsymbol{\sigma}\cdot\boldsymbol{\nabla}\,\boldsymbol{\sigma}\cdot\mathbf{W} = \boldsymbol{\nabla}\cdot\mathbf{W} + i\boldsymbol{\sigma}\cdot\boldsymbol{\nabla}\times\mathbf{W} \tag{5.30}$$

its real and physical part is:

$$Re\left(H_{\mathrm{ESR}}\psi\right) = \frac{e\hbar H_0}{4m^2c^2}\boldsymbol{\sigma}\cdot\mathbf{B}\psi \tag{5.31}$$

where:

$$\mathbf{B} = \boldsymbol{\nabla}\times\mathbf{W} \tag{5.32}$$

is the magnetic flux density. Using Eq. (5.17) in the first approximation the new ESR aand NMR hamiltonian is:

$$\langle Re\left(H_{\mathrm{ESR}}\right)\rangle = \frac{-e^5}{128\pi^2\epsilon_0^2\hbar mc^2n^2}\boldsymbol{\sigma}\cdot\mathbf{B}. \tag{5.33}$$

The minimal prescription for the energy momentum four vector is defined by:

$$p^\mu \rightarrow p^\mu - eW^\mu \tag{5.34}$$

where:

$$W^\mu = (\phi_W, c\mathbf{W}) \tag{5.35}$$

and the magnetic flux density is defined by the spin curvature vector as in UFT 317. Therefore as shown in detail in Note 329(7) the new hamiltonian is defined by:

$$Re\left(H_{\mathrm{ESR}}\right)\psi = \frac{e\hbar H_0 W^{(0)}}{4m^2c^2}\boldsymbol{\sigma}\cdot\mathbf{R}(\mathrm{spin})\psi. \tag{5.36}$$

The energy levels of the new ESR terms are computed and graphed later in this chapter.

New types of hyperfine spin orbit interaction can also be inferred by removing the restrictive Dirac approximation (5.20). These new methods result in a severe test of the basics of relativistic, because they lead to a new type of hyperfine splitting superimposed on the fine structure of spin orbit spectroscopy. If these new details are not observed, then the foundations of relativistic quantum mechanics are challenged.

The new hamiltonian term obtained by lifting the restrictive Dirac approximation is:

$$H_{01} = -\boldsymbol{\sigma}\cdot\mathbf{p}\frac{H_0}{4m^2c^2}\boldsymbol{\sigma}\cdot\mathbf{p} \tag{5.37}$$

in the SU(2) basis, where $\mathbf{p}$ is the relativistic momentum. In the presence of a magnetic field:

$$H_{01} = -\boldsymbol{\sigma}\cdot\left(\mathbf{p}-e\mathbf{W}\right)\frac{H_0}{4m^2c^2}\boldsymbol{\sigma}\cdot\left(\mathbf{p}-e\mathbf{W}\right) \tag{5.38}$$

where the hamiltonian H_0 is quantized with the ususal Schrödinger equation:

$$H_0\psi = \left(-\frac{\hbar^2}{2m}\nabla^2 + U\right)\psi. \tag{5.39}$$

In the H atom the hydrogenic wavefunctions of Eq. (5.39) are well known analytically.

For comparison the usual Dirac approximation leads to the well known spin orbit term:

$$H_{02} = \boldsymbol{\sigma}\cdot\left(\mathbf{p}-e\mathbf{W}\right)\frac{U}{4m^2c^2}\boldsymbol{\sigma}\cdot\left(\mathbf{p}-e\mathbf{W}\right) \tag{5.40}$$

in which the following relativistic quantization is used, the subscript r denoting this fact:

$$p^\mu\psi_r = i\hbar\partial^\mu\psi_r. \tag{5.41}$$

The relativistic four momentum is:

$$p^\mu = \left(\frac{E}{c},\mathbf{p}\right) \tag{5.42}$$

and by definition the four derivative is:

$$\partial^\mu = \left(\frac{1}{c}\frac{\partial}{\partial t},-\boldsymbol{\nabla}\right) \tag{5.43}$$

The energy momentum four vector (5.42) is defined by the relativistic energy and momentum:

$$E = \gamma mc^2, \tag{5.44}$$

$$\mathbf{p} = \gamma \mathbf{p}_0 = \gamma m \mathbf{v}_0. \tag{5.45}$$

Eq. (5.37) can therefore be quantized to:

$$H_{01}\psi_r = i\hbar \boldsymbol{\sigma} \cdot \boldsymbol{\nabla} \frac{H_0}{4m^2c^2} \boldsymbol{\sigma} \cdot \mathbf{p}\, \psi_r \tag{5.46}$$

in which the Dirac approximation (5.20) is no longer used. In ECE theory [2]- [13] the Dirac equation was developed into the fermion equation, which removes negative energy levels and the need for the unobservable and non Baconian Dirac sea. In Eq. (5.46), the true relativistic wave functions can be approximated by the non relativistic Schrödinger wave functions in the first approximation, justified by the fact that spin orbit splitting in the H atom is a small effect. There are two types of hamiltonian possible:

$$H_{011}\psi = \frac{i\hbar}{4m^2c^2} H_0 \psi\, \boldsymbol{\sigma} \cdot \boldsymbol{\nabla}\, \boldsymbol{\sigma} \cdot \mathbf{p} \tag{5.47}$$

and

$$H_{012}\psi = \frac{i\hbar H_0}{4m^2c^2} \boldsymbol{\sigma} \cdot \mathbf{p}\, \boldsymbol{\sigma} \cdot \boldsymbol{\nabla} \psi \tag{5.48}$$

because H_0 is a constant of motion. Using Pauli algebra produces:

$$\boldsymbol{\sigma} \cdot \mathbf{p}\, \boldsymbol{\sigma} \cdot \boldsymbol{\nabla} \psi = \mathbf{p} \cdot \boldsymbol{\nabla} \psi + i\, \boldsymbol{\sigma} \cdot \mathbf{p} \times \boldsymbol{\nabla} \psi. \tag{5.49}$$

Therefore the real and physical parts are:

$$Re\,(H_{011}\psi) = -\frac{\hbar}{4m^2c^2} H_0 \psi\, \boldsymbol{\sigma} \cdot \boldsymbol{\nabla} \times \mathbf{p} \tag{5.50}$$

and

$$Re\,(H_{012}\psi) = -\frac{\hbar H_0}{4m^2c^2} \boldsymbol{\sigma} \cdot \mathbf{p} \times \boldsymbol{\nabla} \psi. \tag{5.51}$$

Using the minimal prescription with the $\mathbf{W}$ potential of ECE 2 theory produces:

$$\mathbf{p} \rightarrow \mathbf{p} - e\mathbf{W} \tag{5.52}$$

giving rise to new spectral structure in the presence of a magnetic flux density $\mathbf{B}$:

$$H_{\mathrm{ESR}}\psi = \frac{e\hbar H_0}{4m^2c^2} \boldsymbol{\sigma} \cdot \boldsymbol{\nabla} \times \mathbf{W} = \frac{e\hbar H_0}{4m^2c^2} \psi\, \boldsymbol{\sigma} \cdot \mathbf{B} \tag{5.53}$$

whose energy levels are:

$$\langle H_{\mathrm{ESR}} \rangle = \frac{e\hbar}{4m^2c^2} \langle H_0 \rangle\, \boldsymbol{\sigma} \cdot \mathbf{B} \tag{5.54}$$

where for the H atom:

$$\langle H_0 \rangle = -\frac{e^4 m}{32\pi^2 \epsilon_0^2 \hbar^2 n^2}. \tag{5.55}$$

This is the same result as Eq. (8) of Note 329(6) on `www.aias.us` producing a rigorous check for self consistency. The expectation value of Eq. (5.55) can be expressed as:

$$\langle H_0 \rangle = -\frac{\hbar c}{2}\left(\frac{\alpha}{r_B}\right)\frac{1}{n^2} \tag{5.56}$$

where r_B is the Bohr radius and α is the fine structure constant. The conventional ESR hamiltonian is:

$$\langle H_{\mathrm{ESR0}} \rangle = -\frac{e\hbar}{2m}\boldsymbol{\sigma}\cdot\mathbf{B} \tag{5.57}$$

so the magnitude of this new type of fine structure is:

$$\begin{aligned}\langle H_{\mathrm{ESR}} \rangle =& \frac{1}{4}\left(\frac{\hbar}{mc}\right)\left(\frac{\alpha}{r_B}\right)\frac{1}{n^2}\langle H_{\mathrm{ESR0}} \rangle \\ =& \frac{1.33128\times 10^{-5}}{n^2}\langle H_{\mathrm{ESR0}} \rangle\end{aligned} \tag{5.58}$$

in the H atom. This is within range of ESR and NMR spectrometers, and if found would be very useful in analytical laboratories. In the H atom it depends on the principal quantum number n, but in general in atoms and molecules it would produce a rich and new spectral structure. If this structure is not found, a fundamental challenge to relativistic quantum mechanics will have been discovered.

Two more new types of spectra can be inferred using:

$$H_0\psi = \left(-\frac{\hbar^2\nabla^2}{2m} - \frac{e^2}{4\pi\epsilon_0 r^2}\right)\psi \tag{5.59}$$

and:

$$H_{012}\psi = \frac{i\hbar}{4m^2c^2}\boldsymbol{\sigma}\cdot\boldsymbol{\nabla}\left(H_0\psi\right)\boldsymbol{\sigma}\cdot\mathbf{p} \tag{5.60}$$

to give:

$$H_{012}\psi = \frac{ie^2\hbar}{16\pi\epsilon_0 r^3}\boldsymbol{\sigma}\cdot\mathbf{r}\,\boldsymbol{\sigma}\cdot\mathbf{p}\,\psi - \frac{i\hbar^3}{8m^3c^2}\boldsymbol{\sigma}\cdot\boldsymbol{\nabla}\left(\nabla^2\psi\right)\boldsymbol{\sigma}\cdot\mathbf{p}. \tag{5.61}$$

The first part of this expression gives the conventional spin orbit term:

$$ReH_{\mathrm{so}}\psi = \frac{e^2\hbar}{16\pi\epsilon_0 m^2c^2r^3}\boldsymbol{\sigma}\cdot\mathbf{L}\,\psi \tag{5.62}$$

where the relativistic orbital angular momentum is:

$$\mathbf{L} = \mathbf{r}\times\mathbf{p}. \tag{5.63}$$

This is related to the non relativistic angular momentum L_0 by:

$$\mathbf{L} = \gamma \mathbf{L}_0. \tag{5.64}$$

Additional and new types of fine structure appear from Eq. (5.62). These should be looked for experimentally. If found, they give new types of spectroscopy, if not found, this new theory challenges relativistic quantum theory, because the latter would have been shown to be restrictive and empirical rather than a true theory.

In addition there is a second new term from Eq. (5.61):

$$ReH_2\psi = -\frac{e\hbar^3}{8m^3c^2}\boldsymbol{\sigma}\cdot\boldsymbol{\nabla}\left(\nabla^2\psi\right)\times\mathbf{p}. \tag{5.65}$$

In the presence of a magnetic field this term gives:

$$ReH_3\psi = -\frac{e\hbar^3}{8m^3c^2}\boldsymbol{\sigma}\cdot\boldsymbol{\nabla}\left(\nabla^2\psi\right)\times\mathbf{W} \tag{5.66}$$

whose energy levels are:

$$\langle H_3\rangle = -\frac{e\hbar^3}{8m^3c^2}\boldsymbol{\sigma}\cdot\int\psi^*\boldsymbol{\nabla}\left(\nabla^2\psi\right)d\tau\times\mathbf{W}. \tag{5.67}$$

These levels should also be looked for spectroscopically, and if found they would provide useful new structure. If not found, relativistic quantum theory is challenged in another way.

As shown in Note 330(7) on `www.aias.us` the Dirac approximation (5.20) gives:

$$\langle ReH_{\mathrm{so1}}\rangle = \frac{e\hbar}{8\pi\epsilon_0 mc^2}\left\langle\frac{1}{r^3}\right\rangle\boldsymbol{\sigma}\cdot\mathbf{m}_{\mathrm{ind}} \tag{5.68}$$

where $\mathbf{m}_{\mathrm{ind}}$ is the induced magnetic dipole moment proportional to the $\mathbf{B}$ Field [2]- [13]. In the H atom it is well known that:

$$\left\langle\frac{1}{r^3}\right\rangle = \frac{1}{r_B^3 L\left(L+\frac{1}{2}\right)(L+1)\,n^3} \tag{5.69}$$

where L is the angular momentum quantum number, and n the principal quantum number. In more complex atoms and molecules the expectation value has a much richer structure. This should also be present in ESR, NMR and MRI. As in Note 330(7) there is also a conventional type two hamiltonian:

$$\langle H_{\mathrm{so2}}\rangle = \frac{e^3\hbar}{16\pi\epsilon_0 m^2c^2}\left\langle\frac{1}{r}\right\rangle\boldsymbol{\sigma}\cdot\mathbf{B}. \tag{5.70}$$

In H:

$$\langle U\rangle = \int\psi^* U\psi\,d\tau = -\frac{e^4 m}{16\pi^2\epsilon_0^2\hbar^2 n^2} \tag{5.71}$$

so the energy levels are:

$$\langle H_{\mathrm{so2}} \rangle = \frac{e^5}{4mc^2\left(16\pi^2\epsilon_0^2\hbar c^2\right)}\frac{\boldsymbol{\sigma}\cdot\mathbf{B}}{n^2} \tag{5.72}$$

and should also be observable. If not, then the basics of the standard model relativistic quantum theory are challenged in yet another way.

The various energy levels from these calculations are computed and tabulated later in this chapter.

As described in UFT 331 a new type of Zeeman spectroscopy can be inferred by using the correctly relativistic momentum in the kinetic energy term of the ECE fermion equation. The Lorentz factor is calculated without using the Dirac approximation, which effectively reduces the relativistic momentum to the classical momentum. Quantization shows that the Zeeman effect develops an intricate new structure if correctly calculated in this way. This structure is exemplified with the visible 2d to 3p line of the H atom, and the infra red 4p to 5d line. The former is split into nine lines, and the latter into forty five lines, all of which should be looked for spectroscopically. If they exist, a very useful new structure would have been found, if not, relativistic quantum theory is essentially refuted, despite its apparent successes.

The usual theory of the Zeeman effect [2]- [13] is based on the classical hamiltonian:

$$H_0 = T + U \tag{5.73}$$

in which the classical kinetic energy is:

$$T = \frac{p_0^2}{2m}. \tag{5.74}$$

The influence of an external magnetic flux density $\mathbf{B}$ can be calculated using the ECE 2 $\mathbf{W}$ potential in the minimal prescription:

$$\mathbf{p}_0 \rightarrow \mathbf{p}_0 - e\mathbf{W}. \tag{5.75}$$

Non relativistic quantization produces Schrödinger's rule:

$$\mathbf{p}_0\psi = -i\hbar\boldsymbol{\nabla}\psi \tag{5.76}$$

where ψ is the non relativistic wave function. As shown in detail in Note 331(1) on `www.aias.us` the non relativistic theory contains a term:

$$H_1 = -\frac{e}{m}\mathbf{W}\cdot\mathbf{p}_0 \tag{5.77}$$

in which the vector potential of a static magnetic field is defined as:

$$\mathbf{W} = \frac{1}{2}\mathbf{B}\times\mathbf{r} \tag{5.78}$$

so the term (5.77) becomes:

$$H_1 = -\frac{e}{2m}\mathbf{B}\times\mathbf{r}\cdot\mathbf{p}_0 = -\frac{e}{2m}\mathbf{B}\cdot\mathbf{r}\times\mathbf{p}_0 = -\frac{e}{2m}\mathbf{B}\cdot\mathbf{L}_0 \tag{5.79}$$

where the non relativistic angular momentum is:

$$\mathbf{L}_0 = \mathbf{r} \times \mathbf{p}_0. \tag{5.80}$$

As shown already in this chapter, the classical hamiltonian (5.73) is the limit of the relativistic hamiltonian:

$$H_0 = H - mc^2 = \frac{p^2}{(1+\gamma)\, m} + U \sim \frac{p^2}{2m}\left(1 - \left(\frac{\left\langle \hat{H}_0 \right\rangle - U}{2mc^2}\right)\right) + U \tag{5.81}$$

so the non relativistic hamiltonian may be written as

$$H_0 = H - mc^2 \sim \frac{p^2}{2m} + U - \cdots \tag{5.82}$$

in which $\mathbf{p}$ is the relativistic momentum and in which the Lorentz factor is defined by the non relativistic momentum:

$$\gamma = \left(1 - \frac{p_0^2}{m^2c^2}\right)^{-1/2}. \tag{5.83}$$

The relativistic hamiltonian governing the Zeeman effect is defined and developed in Note 331(5) on `www.aias.us` and is:

$$H_1 = -\frac{e}{2m}\left(1 - \frac{p_0^2}{m^2c^2}\right)^{-1/2} \mathbf{L}_0 \cdot \mathbf{B} \sim -\frac{e}{2m}\left(1 + \frac{1}{2}\frac{p_0^2}{m^2c^2}\right) \mathbf{L}_0 \cdot \mathbf{B} \tag{5.84}$$

when:

$$p_0 \ll mc. \tag{5.85}$$

The relativistic hamiltonian may be quantized using:

$$\hat{H}_1 \psi = -\frac{e}{2m}\left(1 + \frac{1}{2}\frac{p_0^2}{m^2c^2}\right) \mathbf{B} \cdot \hat{\mathbf{L}}_0 \psi \tag{5.86}$$

in which $\hat{L}_0$ is an operator and p_0^2 is a function. Now align the magnetic field in Z to produce:

$$\hat{H}_1 \psi = -\frac{e}{2m}\left(1 + \frac{1}{2}\frac{p_0^2}{m^2c^2}\right) B_Z \hat{L}_{0Z} \psi \tag{5.87}$$

where:

$$\hat{L}_{0Z} = \hbar m_L \psi \tag{5.88}$$

with:

$$m_L = -L, \ldots, L. \tag{5.89}$$

Here, $\hbar$ is the reduced Planck constant, L is the orbital angular momentum quantum number, and m_L is the azimuthal quantum number. The observable energy levels are given by the expectation value:

$$H_1 = \left\langle \hat{H}_1 \right\rangle = -\frac{e\hbar}{2m}\left(1 + \frac{1}{2}\frac{p_0^2}{m^2c^2}\right) m_L \tag{5.90}$$

in which:

$$\frac{p_0^2}{2m} = \left\langle \frac{\hat{p}_0^2}{2m} \right\rangle. \tag{5.91}$$

Therefore the energy levels are:

$$\begin{aligned} H_1 &= -\frac{e\hbar}{2m} m_L \left(1 + \frac{1}{mc^2}\left\langle \frac{\hat{p}_0^2}{2m} \right\rangle\right) \\ &= -\frac{e\hbar}{2m} m_L \left(1 - \frac{\hbar^2}{4m^2c^2}\int \psi^* \nabla^2 \psi \, d\tau\right). \end{aligned} \tag{5.92}$$

In a more rigorous development ψ must be the relativistic wave function.

To illustrate the new Zeeman spectroscopy consider atomic H, and in an approximation use the non realtivistic hydrogenic wavefunctions. In this approximation:

$$\left\langle \frac{p_0^2}{2m} \right\rangle = \frac{me^4}{32\pi^2\epsilon_0^2\hbar^2 n^2} \tag{5.93}$$

so the hamiltonian of the relativistic Zeeman effect is:

$$H_1 = \frac{e\hbar}{2m} m_L \left(1 + \frac{e^4}{32\pi^2\epsilon_0^2\hbar^2c^2n^2}\right). \tag{5.94}$$

Here ϵ_0 is the S. I. vacuum permittivity, c is the vacuum speed of light, and n is the principal quantum number. The result (5.94) can be expressed as:

$$H_1 = -\frac{e\hbar}{2m} m_L \left(1 + \frac{1}{2}\left(\frac{\lambda c}{r_B}\right)\frac{\alpha}{n^2}\right) \tag{5.95}$$

in which the Compton wavelength is:

$$\lambda c = \frac{\hbar}{mc} = 3.861591 \times 10^{-13}\,\mathrm{m} \tag{5.96}$$

the Bohr radius is:

$$r_B = \frac{4\pi\epsilon_0\hbar^2}{me^2} = 5.29177 \times 10^{-11}\,\mathrm{m} \tag{5.97}$$

and the fine structure constant is:

$$\alpha = \frac{e^2}{4\pi\hbar c\epsilon_0} = 0.007297351. \tag{5.98}$$

So the relativistic Zeeman effect hamiltonian is:

$$H_1 = \langle H_1 \rangle = -\frac{e\hbar}{2m} m_L B_Z \left(1 + \frac{2.662567 \times 10^{-5}}{n^2}\right) \tag{5.99}$$

and is added to the energy levels of the H atom.

In the first approximation use the non relativistic hydrogenic energy levels:

$$E_0 = -\frac{me^4}{32\pi^2 \epsilon_0^2 \hbar^2 n^2}. \tag{5.100}$$

The usual non relativistic Zeeman effect is therefore:

$$E_1 = E_0 - \frac{e\hbar}{2m} m_L B_Z \tag{5.101}$$

and the new and correctly relativistic Zeeman effect is:

$$E_2 = E_0 - \frac{e\hbar}{2m} m_L B_Z \left(1 + \frac{2.662567 \times 10^{-5}}{n^2}\right). \tag{5.102}$$

The selection rules are:

$$\Delta L = \pm 1 \tag{5.103}$$

and:

$$\Delta m_L = 0, \pm 1. \tag{5.104}$$

For an absorption:

$$\Delta L = 1. \tag{5.105}$$

The selection rule (5.104) means that Δm_L is zero for linear polarization [2]-[13], 1 for left circularly polarized radiation, and -1 for right circularly polarized radiation.

Now consider the H alpha line of H in the Balmer series. This is the 2p to 3d transition and occurs at $15,241.4\,\mathrm{cm}^{-1}$ in the red part of the visible. The Grotian diagram of possible transitions is defined as follows. For left circular polarization ($\Delta m_L = 1$):

$$\begin{aligned} &2p\,(n=2,\, L=1,\, m_L=0) \to 3d\,(n=3,\, L=2,\, m_L=1) \\ &2p\,(n=2,\, L=1,\, m_L=1) \to 3d\,(n=3,\, L=2,\, m_L=2) \\ &2p\,(n=2,\, L=1,\, m_L=-1) \to 3d\,(n=3,\, L=2,\, m_L=0)\,. \end{aligned} \tag{5.106}$$

For linear polarization ($\Delta m_L = 0$):

$$\begin{aligned} &2p\,(n=2,\, L=1,\, m_L=0) \to 3d\,(n=3,\, L=2,\, m_L=0) \\ &2p\,(n=2,\, L=1,\, m_L=1) \to 3d\,(n=3,\, L=2,\, m_L=1) \\ &2p\,(n=2,\, L=1,\, m_L=-1) \to 3d\,(n=3,\, L=2,\, m_L=-1)\,. \end{aligned} \tag{5.107}$$

For right circular polarization ($\Delta m_L = -1$):

$$\begin{aligned} &2p\,(n=2,\,L=1,\,m_L=0) \to 3d\,(n=3,\,L=2,\,m_L=-1) \\ &2p\,(n=2,\,L=1,\,m_L=1) \to 3d\,(n=3,\,L=2,\,m_L=0) \\ &2p\,(n=2,\,L=1,\,m_L=-1) \to 3d\,(n=3,\,L=2,\,m_L=-2)\,. \end{aligned} \tag{5.108}$$

Using these rules in the usual non relativistic Zeeman hamiltonian (5.101) produces three absorption lines:

$$\Delta m_L = -1, 0, 1 \tag{5.109}$$

illustrated later in this chapter. Each of these lines are made up of triply degenerate transitions occurring with the same energy. So the usual non relativistic Zeeeman spectrum consists of three lines, one at the original frequency, one at a higher and one at a lower frequency, symmetrically arranged.

This is the well known Zeeman effect.

However the new and correctly relativistic hamiltonian (5.102) produces a hitherto unknown spectrum of nine lines illustrated later in this chapter, because relativistic effects lift the triple degeneracy of the non relativistic theory. In the relativistic theory there is a symmetric central grouping and two asymmetric groupings which are mirror images of each other. The relativistic effects are small, but within range of contemporary high resolution spectroscopy and should be looked for experimentally.

Note 331(7) illustrates the relativistic splittings in the $n = 4$ to $n = 5$ transition of atomic hydrogen at $2,469.1\,\mathrm{cm}^{-1}$ in the infra red. There are seventeen degenerate transitions as follows for $\Delta m_L = 1$:

$$\begin{aligned} 1)\quad & 4s \to 5p\,(n=4,\,L=0,\,m_L=0 \to n=5,\,L=1,\,m_L=1) \\ 2)\quad & 4p \to 5s\,(n=4,\,L=1,\,m_L=-1 \to n=5,\,L=0,\,m_L=0) \\ *3)\quad & 4p \to 5d\,(n=4,\,L=1,\,m_L=-1 \to n=5,\,L=2,\,m_L=0) \\ *4)\quad & 4p \to 5d\,(n=4,\,L=1,\,m_L=0 \to n=5,\,L=2,\,m_L=1) \\ *5)\quad & 4p \to 5d\,(n=4,\,L=1,\,m_L=1 \to n=5,\,L=2,\,m_L=2) \\ *6)\quad & 4d \to 5f\,(n=4,\,L=2,\,m_L=-2 \to n=5,\,L=3,\,m_L=-1) \\ *7)\quad & 4d \to 5f\,(n=4,\,L=2,\,m_L=-1 \to n=5,\,L=3,\,m_L=0) \\ *8)\quad & 4d \to 5f\,(n=4,\,L=2,\,m_L=0 \to n=5,\,L=3,\,m_L=1) \\ *9)\quad & 4d \to 5g\,(n=4,\,L=2,\,m_L=1 \to n=5,\,L=3,\,m_L=2) \\ *10)\quad & 4d \to 5g\,(n=4,\,L=2,\,m_L=2 \to n=5,\,L=3,\,m_L=3) \\ *11)\quad & 4f \to 5g\,(n=4,\,L=3,\,m_L=-3 \to n=5,\,L=4,\,m_L=-2) \\ *12)\quad & 4f \to 5g\,(n=4,\,L=3,\,m_L=-2 \to n=5,\,L=4,\,m_L=-1) \\ *13)\quad & 4f \to 5g\,(n=4,\,L=3,\,m_L=-1 \to n=5,\,L=4,\,m_L=0) \\ *14)\quad & 4f \to 5g\,(n=4,\,L=3,\,m_L=0 \to n=5,\,L=4,\,m_L=1) \\ *15)\quad & 4f \to 5g\,(n=4,\,L=3,\,m_L=1 \to n=5,\,L=4,\,m_L=2) \\ *16)\quad & 4f \to 5g\,(n=4,\,L=3,\,m_L=2 \to n=5,\,L=4,\,m_L=3) \\ *17)\quad & 4f \to 5g\,(n=4,\,L=3,\,m_L=3 \to n=5,\,L=4,\,m_L=4)\,. \end{aligned} \tag{5.110}$$

For absorption ($\Delta L = 1$) there are fifteen degenerate transitions marked with an asterisk. Therefore the non relativistic hamiltonian (5.101) produces three Zeeman lines, each of which are fifteen fold degenerate. The correctly relativistic hamiltonian (5.111) produces forty five lines in three groupings of fifteen lines as illustrated later in this chapter. These should be looked for with high resolution spectroscopy.

In general for an n to $n+1$ absorption of atomic H there are $3n^2 - 1$ absorption lines in the new relativistic Zeeman effect. So for example, for the $n = 13$ to $n = 14$ transition that occurs at $81.52\,\mathrm{cm}^{-1}$ in the far infra red, there are 804 lines in three groupings of 268 lines each. For atoms and molecules more complicated than atomic H, a very rich new spectroscopy emerges from the relativistic Zeeman effect.

In many cases what is observed experimentally is the anomalous Zeeman effect [2]- [13] and well known Landé factor. A correctly relativistic treatment of the anomalous Zeeman effect again produces rich spectral detail which can be looked for experimentally. All of this detail is the result of using ECE 2 covariance and the $\mathbf{W}$ potential, so in ECE 2 relativity it is due to the spin curvature of spacetime. Consider the relativistic ECE 2 hamiltonian:

$$E^2 = p^2c^2 + m^2c^4 \tag{5.111}$$

from which the following hamiltonian may be defined for convenience:

$$H = E + U, \tag{5.112}$$

$$H_0 = H - mc^2. \tag{5.113}$$

As shown in detail in Note 332(1), Eq. (5.112) may be written as:

$$H_0 = \frac{p^2}{m\left(1+\gamma\right)} + U \tag{5.114}$$

where the Lorentz factor is defined in Eq. (5.83). In the usual Dirac approximation:

$$H_0 = \frac{p^2c^2}{H - U + mc^2} + U \sim \frac{p^2c^2}{mc^2 - U + mc^2} + U \tag{5.115}$$

so:

$$H_0 \sim \frac{p^2c^2}{2mc^2 - U} + U \sim \frac{p^2}{2m}\left(1 + \frac{U}{2m^2c^2}\right) + U. \tag{5.116}$$

Therefore Dirac assumed that:

$$E = \gamma mc^2 = H - U \sim mc^2 - U \tag{5.117}$$

i. e. that the Lorentz factor can be approximated by:

$$\gamma \sim 1 - \frac{U}{mc^2}. \tag{5.118}$$

However, the correct Lorentz factor is Eq. (5.83). In the limit:

$$v_0 \ll c \tag{5.119}$$

the correct Lorentz factor can be approximated by:

$$\gamma \sim 1 + \frac{1}{2}\frac{p_0^2}{m^2c^2}. \tag{5.120}$$

Comparing Eqs. (5.118) and (5.120):

$$\frac{p_0^2}{2m} = -U \tag{5.121}$$

which means that the classical hamiltonian vanishes in the Dirac approximation.

Despite its uncritical use for almost ninety years, the Dirac approximation is therefore highly restrictive, and as shown already in this chapter loses a great deal of hyperfine structure of great potential utility. The usual Dirac approximation leads to:

$$H_0 = H - mc^2 = \frac{p^2}{2m} + \frac{U}{4m^2c^2}p^2 + U \tag{5.122}$$

and produces the well known spin orbit hamiltonian:

$$ReH_{\rm so}\psi = -\frac{\hbar e^2}{16\pi\epsilon_0 m^2c^2r^3}\boldsymbol{\sigma}\cdot\mathbf{L}\,\psi \tag{5.123}$$

in which $\mathbf{L}$ is the relativistic angular momentum:

$$\mathbf{L} = \gamma\mathbf{L}_0 \tag{5.124}$$

as mentioned already in this chapter. Now use the well known spin angular momentum operator:

$$\hat{\mathbf{S}} = \frac{\hbar}{2}\hat{\boldsymbol{\sigma}} \tag{5.125}$$

where $\hat{\boldsymbol{\sigma}}$ is the Pauli matrix operator.

As in note 332(1) the expectation value of the relativistic hamiltonian (5.114) is

$$\langle ReH_{\rm so}\rangle = \frac{-e^2}{16\pi\epsilon_0 m^2c^2}\left(\frac{J\left(J+1\right)-L\left(L+1\right)-S\left(S+1\right)}{r_B^3n^3L\left(L+\frac{1}{2}\right)\left(L+1\right)}\right)\left(1+\frac{1}{mc^2}\left\langle\frac{p_0^2}{2m}\right\rangle\right) \tag{5.126}$$

in which:

$$\frac{1}{mc^2}\left\langle\frac{p_0^2}{2m}\right\rangle = \frac{1}{2}\left(\frac{\lambda c}{r_B}\right)\frac{\alpha}{n^2} = \frac{2.662567\times10^{-5}}{n^2}. \tag{5.127}$$

The new hyperfine structure depends on the way in which the rigorous hamiltonian (5.114) is developed. This is a new inference that affects the whole of relativistic quantum theory because it means that the latter is not rigorously logical and objective. Different choices for operators and functions produce different spectra. Using:

$$p^2 = \gamma^2 p_0^2 \tag{5.128}$$

the hamiltonian (5.114) can be written as:

$$H_0 = \left(\frac{\gamma^2}{1+\gamma}\right)\frac{p_0^2}{2m} + U. \tag{5.129}$$

In the SU(2) basis, as detailed in Note 332(2) on `www.aias.us`, it can be written in three ways:

$$H_0 = \frac{1}{m}\boldsymbol{\sigma}\cdot\mathbf{p}_0\frac{\gamma^2}{1+\gamma}\boldsymbol{\sigma}\cdot\mathbf{p}_0 + U \tag{5.130}$$

$$H_0 = \frac{\gamma}{m}\boldsymbol{\sigma}\cdot\mathbf{p}_0\frac{\gamma}{1+\gamma}\boldsymbol{\sigma}\cdot\mathbf{p}_0 + U \tag{5.131}$$

$$H_0 = \frac{1}{m}\left(\frac{\gamma^2}{1+\gamma}\right)\boldsymbol{\sigma}\cdot\mathbf{p}_0\,\boldsymbol{\sigma}\cdot p_0 + U \tag{5.132}$$

which give rise to three different patterns of hyperfine structure. This means that the foundations of relativistic quantum mechanics are incompletely defined. This was noted by Einstein for example, who thought that quantum mechanics is a transition to a more complete theory.

As shown in Note 332(2) on `www.aias.us`:

$$\frac{\gamma^2}{1+\gamma} \doteqdot \frac{1}{2}\left(1 - \frac{U}{2mc^2} + \frac{1}{mc^2}\left(\frac{H_0}{2} + \frac{p_0^2}{2m}\right)\right) \tag{5.133}$$

where

$$\left\langle \frac{p_0^2}{2m^2c^2} \right\rangle = \frac{1}{2}\left(\frac{\lambda c}{r_B}\right)\frac{\alpha}{n^2} \tag{5.134}$$

and:

$$\left\langle \frac{H_0}{2mc^2} \right\rangle = -\frac{1}{4}\left(\frac{\lambda c}{a_0}\right)\frac{\alpha}{n^2} \tag{5.135}$$

so if the relativistic quantized hamiltonian is chosen to be:

$$H_0\psi = \left(\frac{1}{m}\boldsymbol{\sigma}\cdot\mathbf{p}_0\frac{\gamma^2}{1+\gamma}\boldsymbol{\sigma}\cdot\mathbf{p}_0 + U\right)\psi \tag{5.136}$$

it can be developed as in Note 332(2) as:

$$H_0\psi = \frac{p_0^2}{2m}\left(1 + \frac{1}{mc^2}\left(\frac{H_0}{2} + \frac{p_0^2}{2m}\right)\right)\psi - \frac{1}{4m^2c^2}\boldsymbol{\sigma}\cdot\mathbf{p}_0\,U\,\boldsymbol{\sigma}\cdot p_0\,\psi. \tag{5.137}$$

The second term on the right hand side of this equation gives the usual spin orbit fine structure of the Dirac approximation, and the first term gives a hitherto unknown hyperfine structure.

Note 332(3) gives the transition rules needed and later on this chapter a table of shifts is given. These can be looked for experimentally. The transition rules for spin orbit fine structure are:

$$\Delta J = 0, \pm 1, \;\; J = 0 \nrightarrow J = 0 \tag{5.138}$$

with:

$$m_J = -J, \ldots, J \tag{5.139}$$

and:

$$\Delta m_J = 0, \pm 1. \tag{5.140}$$

The usual spin orbit energy levels are:

$$E_{\text{so}} = \frac{-e^2}{16\pi\epsilon_0 m^2 c^2} \left(\frac{J\left(J+1\right) - L\left(L+1\right) - S\left(S+1\right)}{r_B^3 n^3 L\left(L+\frac{1}{2}\right)\left(L+1\right)} \right) \tag{5.141}$$

but the correct levels according to the choice (5.130) are:

$$E_{\text{so1}} = E_{\text{so}} \left(1 + \frac{2.662567 \times 10^{-5}}{n^2} \right). \tag{5.142}$$

A table of shifts due to this correction is given later on in this chapter. In the presence of a magnetic field a very richly structured hyperfine spectrum is obtained as follows:

$$E_{\text{so2}} = E_{\text{so1}} - \frac{e\hbar}{2m} g_J m_J B_Z \tag{5.143}$$

where g_J is the well known [2]- [13] Landé factor:

$$g_J = 1 + \frac{J\left(J+1\right) + S\left(S+1\right) - L\left(L+1\right)}{2J\left(J+1\right)}. \tag{5.144}$$

Note 332(4) gives further details of the evaluation of the hamiltonian (5.137) and Note 332(5) develops the hamiltonian in the presence of a magnetic field, giving details of how the Landé factor is derived. It is shown in Note 332(5) that the correct hamiltonian of the anomalous Zeeman effects is:

$$\langle H_{AZE} \rangle = -\frac{mc^2\alpha}{n^2} \left(1 - \frac{1}{4} \frac{\lambda c}{r_B} \frac{\alpha}{n^2} \right) - \frac{e\hbar}{2m} g_J m_J B_Z. \tag{5.145}$$

The H alpha line of atomic hydrogen for example is split into six lines by the anomalous Zeeman effect, the three lines of the normal Zeeman effect being further split into three pairs. The rigorously correct hamiltonian (5.145) produces hitherto unknown hyperfine shifts of the anomalous Zeeman effect as discussed later in this chapter.

In UFT 333 it is shown that the ECE 2 hamiltonian can be quantized using at least four different classification schemes, each leading to different spectral results. The method used by Dirac is a subjective choice of approximation. The schemes in UFT 333 are illustrated with rigorous quantization of the class one hamiltonian. If the spectral detail predicted by the class one hamiltonian is not observed, there would be a major crisis in physics, because the philosophy of the Dirac equation would have been refuted. The ECE 2 hamiltonian is mathematically the same as the one used to produce relativistic quantum mechanics in the SU(2) basis. For over ninety years it has been thought that the procedure used by Dirac is rigorous and foundational, because it appeared to produce so many well known data, but in this chapter it is shown that it depends on a subjective choice of approximation and choice of quantization procedure. In the following it is shown that different spectral detail emerges from a given choice of quantization.

Classification schemes can be constructed and exemplified by the following four types of SU(2) hamiltonian:

$$H_0 = \frac{1}{m}\boldsymbol{\sigma}\cdot\mathbf{p}_0\frac{\gamma^2}{1+\gamma}\boldsymbol{\sigma}\cdot\mathbf{p}_0 + U \tag{5.146}$$

$$H_0 = \frac{\gamma}{m}\boldsymbol{\sigma}\cdot\mathbf{p}_0\frac{\gamma}{1+\gamma}\boldsymbol{\sigma}\cdot\mathbf{p}_0 + U \tag{5.147}$$

$$H_0 = \frac{\gamma^2}{m}\boldsymbol{\sigma}\cdot\mathbf{p}_0\frac{1}{1+\gamma}\boldsymbol{\sigma}\cdot\mathbf{p}_0 + U \tag{5.148}$$

$$H_0 = \frac{1}{m}\frac{\gamma^2}{1+\gamma}\boldsymbol{\sigma}\cdot\mathbf{p}_0\,\boldsymbol{\sigma}\cdot\mathbf{p}_0 + U. \tag{5.149}$$

For all four schemes the classical relativistic hamiltonian is:

$$H = E + U \tag{5.150}$$

where E is the relativistic total energy:

$$E = \gamma mc^2 = \left(c^2p^2 + m^2c^4\right)^{1/2}. \tag{5.151}$$

It follows that:

$$H_0 = H - mc^2 = \frac{c^2p^2}{E+mc^2} + U. \tag{5.152}$$

The Dirac approximation is discussed earlier in this chapter, and is:

$$H = mc^2 \tag{5.153}$$

which gives the unphysical result:

$$H_0 = 0. \tag{5.154}$$

The result (5.154) does not seem to have been realized clearly but it leads to the famous result:

$$H_0 = \frac{c^2p^2}{2mc^2 - U} + U \tag{5.155}$$

which describes spectral fine structure, the Thomas factor, and the Landé factor, and which inferred ESR, and later NMR and MRI.

Using:

$$p_0^2 = 2m\left(H_0 - U\right) \tag{5.156}$$

it follows that:

$$\frac{\gamma^2}{1+\gamma} = \left(\left(1 - \frac{2\left(H_0 - U\right)}{mc^2}\right) + \left(1 - \frac{2\left(H_0 - U\right)}{mc^2}\right)^{1/2}\right)^{-1}. \tag{5.157}$$

In the H atom, using the non relativistic, hydrogenic, wave functions in the first approximation:

$$\langle U \rangle = -2\langle H_0 \rangle = -mc^2\left(\frac{\alpha}{n}\right)^2 \tag{5.158}$$

as described in detail in Note 333(4). Quantization takes place by using:

$$-i\hbar\boldsymbol{\nabla}\psi = \mathbf{p}_0\psi \tag{5.159}$$

for the first $\mathbf{p}_0$ in Eq. (5.146) and by using the function for the second $\mathbf{p}_0$. This procedure has no theoretical justification, it is a subjective choice made in order to produce experimental data. In this sense, the theory is empiricism, despite its scientific fame. The procedure gives:

$$\begin{aligned} H_0\psi = -\frac{i\hbar}{m}\boldsymbol{\sigma}\cdot\boldsymbol{\nabla}\Bigg(\Bigg(1 - \frac{2\left(H_0 - U\right)}{mc^2} \\ + \left(1 - \frac{2\left(H_0 - U\right)}{mc^2}\right)^{1/2}\Bigg)^{-1}\boldsymbol{\sigma}\cdot\mathbf{p}_0\,\psi\Bigg) + U\psi. \end{aligned} \tag{5.160}$$

Using computer algebra it is found that:

$$\boldsymbol{\nabla}\left(\frac{\gamma^2}{1+\gamma}\right) = -\left(\frac{2 + \left(1 - \frac{p_0^2}{m^2c^2}\right)^{-1/2}}{\left(1 - \frac{p_0^2}{m^2c^2} + \left(1 - \frac{p_0^2}{m^2c^2}\right)^{1/2}\right)^2}\right)\frac{e^2}{4\pi\epsilon_0 m^2c^2}\frac{\mathbf{r}}{r^3} \tag{5.161}$$

using the Coulomb potential between the electron and proton of the H atom:

$$U = -\frac{e^2}{4\pi\epsilon_0 r}. \tag{5.162}$$

Defining:

$$A := \frac{2 + \left(1 - \frac{p_0^2}{m^2c^2}\right)^{-1/2}}{\left(\left(1 - \frac{p_0^2}{m^2c^2}\right)^{1/2} + 1 - \frac{p_0^2}{m^2c^2}\right)^2} \tag{5.163}$$

it is found that:

$$H_0\psi = -\frac{ie^2\hbar A}{4\pi\epsilon_0 m^2c^2r^3}\boldsymbol{\sigma}\cdot\mathbf{r}\,\boldsymbol{\sigma}\cdot\mathbf{p}_0\,\psi + U\psi. \tag{5.164}$$

Using the Pauli algebra:

$$\boldsymbol{\sigma}\cdot\mathbf{r}\,\boldsymbol{\sigma}\cdot\mathbf{p}_0 = \mathbf{r}\cdot\mathbf{p}_0 + i\,\mathbf{r}\times\mathbf{p}_0 \tag{5.165}$$

and the non relativistic angular momentum:

$$\mathbf{L} = \mathbf{r}\times\mathbf{p}_0 \tag{5.166}$$

it is found that

$$E = \langle H_{\rm so}\rangle = \frac{e^2\hbar A}{4\pi\epsilon_0 m^2c^2}\left\langle\frac{\boldsymbol{\sigma}\cdot\mathbf{L}}{r^3}\right\rangle. \tag{5.167}$$

This result is described as having been obtained from the class one hamiltonian.

Eq. (5.167) reduces to the result obtained by Dirac in the limit:

$$\gamma \to 1. \tag{5.168}$$

If $\mathbf{p}_0$ and $\mathbf{A}$ are regarded as functions in Eq. (5.164), the fine structure obtained by Dirac is shifted as described later in this chapter. If $\mathbf{p}_0$ is very large, the shift becomes very large and should be experimentally observable. If it is not observed the foundations of relativistic quantum mechanics are challenged.

If the expectation value

$$\left\langle\frac{p_0^2}{m^2c^2}\right\rangle = \frac{1}{2}\left(\frac{\alpha}{n}\right)^2 = \frac{2.662567\times10^{-5}}{n^2} \tag{5.169}$$

is used an entirely different spectrum emerges from the same starting equation (5.146). The energy levels of this spectrum are:

$$\begin{aligned} E = \langle H_{\rm so}\rangle &= \frac{e^2\hbar A}{4\pi\epsilon_0 m^2c^2}\left\langle\frac{\boldsymbol{\sigma}\cdot\mathbf{L}}{r^3}\right\rangle \\ &= \frac{e^2A}{16\pi\epsilon_0 m^2c^2}\left(\frac{J\,(J+1) - L\,(L+1) - S\,(S+1)}{r_B^3 n^3 L\left(L+\frac{1}{2}\right)(L+1)}\right) \end{aligned} \tag{5.170}$$

in which the total angular momentum quantum number is defined by the Clebsch Gordan series:

$$J = L+S, L+S-1, \ldots, |L-S| \tag{5.171}$$

where L is the orbital angular momentum quantum number and in which S is the spin angular momentum quantum number. In Eq. (5.170), A is defined by the expectation values:

$$A = \frac{2 + \left(1 - \left\langle\frac{p_0^2}{m^2c^2}\right\rangle\right)^{-1/2}}{\left(\left(1 - \left\langle\frac{p_0^2}{m^2c^2}\right\rangle\right)^{1/2} + 1 - \left\langle\frac{p_0^2}{m^2c^2}\right\rangle\right)^2}. \tag{5.172}$$

The selection rules for such a spectrum are:

$$\Delta J = 0, \pm 1, \tag{5.173}$$

$$\Delta m_J = 0, \pm 1. \tag{5.174}$$

Recall that Eq. (5.170) is the rigorous consequence of:

$$H_0 = \frac{1}{m}\boldsymbol{\sigma} \cdot \mathbf{p}_0 \frac{\gamma^2}{1+\gamma}\boldsymbol{\sigma} \cdot \mathbf{p}_0 + U \tag{5.175}$$

which reduces to the classical hamiltonian:

$$H_0 = \frac{\mathbf{p}_0^2}{2m} + U \tag{5.176}$$

in the limit

$$\gamma \to 1. \tag{5.177}$$

The energy levels from Eq. (5.170) are graphed later on in this chapter. If these are not observed experimentally the ninety year old Dirac equation fails completely.

Electron spin resonance (ESR) and relativistic electron beams can be used to test the above theory. Consider for example the class one hamiltonian:

$$H = \frac{1}{m}\boldsymbol{\sigma} \cdot \mathbf{p}_0 \frac{\gamma^2}{1+\gamma}\boldsymbol{\sigma} \cdot \mathbf{p}_0 \tag{5.178}$$

in the presence of a magnetic field, so that:

$$\mathbf{p}_0 \to \mathbf{p}_0 - e\mathbf{W},\ r = \left(1 - \frac{p_0^2}{m^2c^2}\right)^{-1/2}. \tag{5.179}$$

In the O(3) basis the hamiltonian (5.178) becomes:

$$H = \frac{1}{m}\left(\frac{\gamma^2}{1+\gamma}\right)(\mathbf{p}_0 - e\mathbf{W}) \cdot (\mathbf{p}_0 - e\mathbf{W}). \tag{5.180}$$

The $\mathbf{W}$ potential of ECE 2 theory can be written as:

$$\mathbf{W} = \frac{1}{2}\mathbf{B} \times \mathbf{r} \tag{5.181}$$

for a uniform external magnetic flux density $\mathbf{B}$ and position vector $\mathbf{r}$. By vector algebra:

$$\mathbf{B} \times \mathbf{r} \cdot \mathbf{p}_0 = \mathbf{r} \times \mathbf{p}_0 \cdot \mathbf{B} = \mathbf{L}_0 \cdot \mathbf{B} \tag{5.182}$$

where the classical orbital angular momentum is:

$$\mathbf{L}_0 = \mathbf{r} \times \mathbf{p}_0. \tag{5.183}$$

The orbital angular momentum term of the class one hamiltonian is therefore:

$$H = -\frac{e}{m}\left(\frac{\gamma^2}{1+\gamma}\right)\mathbf{L}_0 \cdot \mathbf{B} \tag{5.184}$$

and for a Z axis magnetic field $\mathbf{B}$ the Zeeman effect is modified to:

$$H\psi = -\frac{e}{m}\left(\frac{\gamma^2}{1+\gamma}\right)L_Z B_Z \psi. \tag{5.185}$$

As described in Note 334(1) the energy levels of the H atom are modified in this rigorous theory to:

$$E_{\mathrm{H}} = -\frac{1}{2}mc^2\left(\frac{\alpha}{m}\right)^2 - \left(\frac{\gamma^2}{1+\gamma}\right)\frac{e\hbar}{m}m_L B_Z \tag{5.186}$$

where α is the fine structure constant and where n is the principal quantum number. In this equation:

$$m_L = -L, \ldots, L \tag{5.187}$$

and $\hbar$ is the reduced Planck constant. The usual Zeeman effect is recovered in the non relativistic limit:

$$\frac{\gamma^2}{1+\gamma} \to \frac{1}{2}. \tag{5.188}$$

The selection rules in Eq. (5.186) are:

$$\text{any } \Delta n,\ \Delta L = 1,\ \Delta m_L = 0, \pm 1 \tag{5.189}$$

and in Eq (5.186):

$$\frac{\gamma^2}{1+\gamma} = \left(1 - \frac{p_0^2}{m^2c^2} + \left(1 - \frac{p_0^2}{m^2c^2}\right)^{-1/2}\right)^{-1}. \tag{5.190}$$

If p_0^2 is regarded as function then the usual Zeeman effect is shifted. If expectation values in the H atom are used:

$$E_{\mathrm{H}} = -\frac{1}{2}mc^2\left(\frac{\alpha}{n}\right)^2 - \left(1 - \left(\frac{\alpha}{n}\right)^2 + \left(1 - \left(\frac{\alpha}{n}\right)^2\right)^{1/2}\right)^{-1}\frac{e\hbar}{m}m_L B_Z \tag{5.191}$$

the energy levels from Eq. (5.191) become:

$$\frac{p_0^2}{m^2c^2} = \left\langle \frac{p_0^2}{m^2c^2} \right\rangle = \left(\frac{\alpha}{n}\right)^2 = \frac{5.3144 \times 10^{-5}}{n} \tag{5.192}$$

and the Zeeman effect is split into hyperfine structure. There is no theoretical way of knowing which is the correct choice, Eq. (5.190) or Eq. (5.191), but an experimental method can be developed based on ESR.

First quantize the hamiltonian (5.180) as follows as in Note 334(2):

$$H\psi = \frac{ie\hbar}{m}\left(\frac{\gamma^2}{1+\gamma}\right)\boldsymbol{\sigma}\cdot\boldsymbol{\nabla}\,\boldsymbol{\sigma}\cdot\mathbf{W}\,\psi + \cdots \tag{5.193}$$

so:

$$Re\,(H\psi) = -\frac{e\hbar}{m}\left(\frac{\gamma^2}{1+\gamma}\right)\boldsymbol{\sigma}\cdot\mathbf{B} + \cdots \tag{5.194}$$

where in ECE 2 theory (see chapter three):

$$\mathbf{B} = \boldsymbol{\nabla}\times\mathbf{W}. \tag{5.195}$$

Using the spin angular momentum:

$$\mathbf{S} = \frac{\hbar}{2}\boldsymbol{\sigma} \tag{5.196}$$

the rigorous hamiltonian of the anomalous Zeeman effect is obtained:

$$H = -\frac{e}{m}\left(\frac{\gamma^2}{1+\gamma}\right)(\mathbf{L}+2\mathbf{S})\cdot\mathbf{B} \tag{5.197}$$

and reduces to the usual anomalous Zeeman effect hamiltonian

$$H = -\frac{e}{2m}(\mathbf{L}+2\mathbf{S})\cdot\mathbf{B} \tag{5.198}$$

in the limit:

$$\frac{\gamma^2}{1+\gamma}\rightarrow\frac{1}{2}. \tag{5.199}$$

Eq. (5.197) can be expressed [2]- [13] as:

$$H = -\frac{e}{m}\left(\frac{\gamma^2}{1+\gamma}\right)g_J\,\mathbf{J}\cdot\mathbf{B} \tag{5.200}$$

where the well known Landé factor is:

$$g_J = 1+\frac{J\,(J+1)+S\,(S+1)-L\,(L+1)}{2J\,(J+1)}. \tag{5.201}$$

In this definition of the Landé factor, Sommerfeld's J quantum number is:

$$J = L+S,\ldots,|L-S| \tag{5.202}$$

with:

$$J_Z\psi = \hbar m_J\psi, \tag{5.203}$$

$$J^2\psi = \hbar^2 J\,(J+1)\,\psi \tag{5.203a}$$

and:

$$m_J = -J, \ldots, J. \tag{5.204}$$

Therefore the energy levels of the H atom are:

$$E_{\mathrm{H}} = -\frac{1}{2}mc^2\left(\frac{\alpha}{n}\right)^2 - \frac{e\hbar}{m}\left(\frac{\gamma^2}{1+\gamma}\right)g_J m_J B_Z \tag{5.205}$$

with selection rules:

$$\Delta J = 0, \pm 1, \ J = 0 \nrightarrow J = 0, \ \Delta m_J = 0, \pm 1, \text{ any } \Delta n. \tag{5.206}$$

Again, there is no way of knowing if the relativistic factor $\gamma^2/(1+\gamma)$ should be a function or an expectation value. This question can be answered experimentally with ESR of sufficiently high resolution.

Consider a relativistic electron beam in which electrons can be accelerated to essentially the speed of light, and apply a magnetic field in the Z axis. In the non relativistic limit of slow moving electrons:

$$ReH_{\mathrm{ESR}}\psi = -\frac{e}{m}S_Z B_Z \psi \tag{5.207}$$

where:

$$S_Z\psi = m_S\hbar\psi \tag{5.208}$$

and:

$$m_S = -S, \ldots, S = -\frac{1}{2}, \frac{1}{2} \tag{5.209}$$

with selection rule:

$$\Delta m_S = 1 \tag{5.210}$$

for absorption of radiation at the well known ESR frequency [2]- [13]:

$$\omega_{\mathrm{ESR}} = \frac{e}{m}B_Z. \tag{5.211}$$

For relativistic electrons however:

$$ReH_{\mathrm{ESR}}\psi = -\frac{e\hbar}{m}\left(\frac{\gamma^2}{1+\gamma}\right)\boldsymbol{\sigma}\cdot\mathbf{B}\,\psi = -\frac{2e}{m}\left(\frac{\gamma^2}{1+\gamma}\right)\mathbf{S}\cdot\mathbf{B}\,\psi \tag{5.212}$$

and the ESR frequency (5.211) is shifted to:

$$\omega_{\mathrm{ESR}} = 2\left(\frac{\gamma^2}{1+\gamma}\right)\frac{e}{m}B_Z \tag{5.213}$$

and is directly measurable. In this case the relativistic factor is always:

$$\frac{\gamma^2}{1+\gamma} = \left(1 - \frac{p_0^2}{m^2c^2} + \left(1 - \frac{p_0^2}{m^2c^2}\right)^{1/2}\right)^{-1}. \tag{5.214}$$

As discussed in chapter four, the experimentally measurable momentum of the electron in the beam is always the relativistic momentum:

$$\mathbf{p} = \gamma \mathbf{p}_0. \tag{5.215}$$

The Lorentz factor on the other hand is always defined by the non relativistic momentum as follows:

$$\gamma^2 = \left(1 - \frac{p_0^2}{m^2 c^2}\right)^{-1} \tag{5.216}$$

so:

$$p_0^2 = p^2 \left(1 + \frac{p^2}{m^2 c^2}\right)^{-1} \tag{5.217}$$

The experiment consists of measuring the ESR frequency of a relativistic electron beam, and measuring the relativistic momentum of the beam. This gives a simple and direct test of the foundations of relativistic quantum mechanics.

ESR can also be used to test the rigorously relativistic version of Eq. (5.198), in which:

$$H = -\frac{e}{2m} (\mathbf{L} + 2\mathbf{S}) \cdot \mathbf{B} = -\frac{e}{2m} g_J \, \mathbf{J} \cdot \mathbf{B}. \tag{5.218}$$

The spin part of the hamiltonian (5.198) is:

$$H_{\text{ESR}} = -\frac{e}{2m} g_J \, \mathbf{S} \cdot \mathbf{B}. \tag{5.219}$$

If the magnetic field is aligned in the Z axis:

$$H_{\text{ESR}} = -\frac{e}{2m} g_J S_Z B_Z \tag{5.220}$$

where:

$$S_Z \psi = m_S \hbar \psi \tag{5.221}$$

and:

$$m_S = \pm \frac{1}{2} \tag{5.222}$$

so the ESR resonance frequency of the anomalous Zeeman effect is:

$$\omega_{\text{ESR}} = \frac{1}{2} g_J \frac{e B_Z}{m} \tag{5.223}$$

where:

$$J = L + S, L + S - 1, \ldots, |L - S|. \tag{5.224}$$

The anomalous Zeeman effect in the ESR spectrum of one electron is split by the Landé factor g_J. This is the most useful feature of ESR in analytical chemistry.

For a free electron in a beam:

$$J = S,\ L = 0 \tag{5.225}$$

so the Landé factor is:

$$g_J = 1 + \frac{2S\left(S+1\right)}{2S\left(S+1\right)} = 2. \tag{5.226}$$

This is known as the g factor of the electron. This factor is obtained from the Dirac equation if and only if the Dirac approximation is used:

$$H = H_0 + mc^2 \sim mc^2, H_0 \sim 0, \tag{5.227}$$

as explained earlier in this chapter.

In the rigorously correct theory of this chapter the ESR frequency in the H atom becomes:

$$\omega_{\mathrm{ESR}} = \left(\frac{\gamma^2}{1+\gamma}\right)\left(1 + \frac{J\left(J+1\right) + S\left(S+1\right) - L\left(L+1\right)}{2J\left(J+1\right)}\right)\frac{eB_Z}{m}. \tag{5.228}$$

If we use the expectation values:

$$\frac{\gamma^2}{1+\gamma} = \left(1 - \left(\frac{\alpha}{n}\right)^2 + \left(1 - \left(\frac{\alpha}{n}\right)^2\right)^{1/2}\right)^{-1} \tag{5.229}$$

the expected ESR splittings can be observed directly.

The above development can also be applied to nuclear magnetic resonance (NMR) in which the magnetic dipole moment of the nucleus of an atom or molecule is:

$$\mathbf{m}_N = g_N \frac{e}{2m_p}\mathbf{I} \tag{5.230}$$

where g_N is the nuclear g factor, m_p is the mass of the proton, e the modulus of the charge on the electron and $\mathbf{I}$ the nuclear spin angular momentum. The interaction hamiltonian between an external magnetic flux density $\mathbf{B}$ and the nuclear magnetic dipole moment is:

$$H_{\mathrm{int,N}} = -\mathbf{m}_N \cdot \mathbf{B}. \tag{5.231}$$

The interaction between $\mathbf{B}$ and the spin angular momentum $\mathbf{S}$ of the electron is as discussed earlier in this chapter:

$$H_{\mathrm{int,e}} = -2\frac{e}{m_e}\left(\frac{\gamma^2}{1+\gamma}\right)\mathbf{S} \cdot \mathbf{B}. \tag{5.232}$$

Therefore the complete interaction hamiltonian in atomic H (one electron and one proton) is:

$$H_{\mathrm{int}} = -2\frac{e}{m_e}\left(\frac{\gamma^2}{1+\gamma}\right)\mathbf{S} \cdot \mathbf{B} - g_N \frac{e}{2m_p}\mathbf{I} \cdot \mathbf{B}. \tag{5.233}$$

This type of hamiltonian is discussed in detail in Note 335(1) on www.aias.us. In Note 335(2) it is developed with the Landé method [2]- [13], so Eq. (5.233) becomes:

$$H_{\text{int}} = -eg_M \mathbf{I} \cdot \mathbf{B} \tag{5.234}$$

where:

$$g_M = \frac{1}{2}\left(\frac{1}{m_e}\left(\frac{\gamma^2}{1+\gamma}\right)\left(1+\frac{S(S+1)-I(I+1)}{M(M+1)}\right) + \frac{g_N}{m_p}\left(1+\frac{I(I+1)-S(S+1)}{M(M+1)}\right)\right) \tag{5.235}$$

The magnetic quantum number is defined by:

$$M = I+S, \ldots, |I-S| \tag{5.236}$$

and the total angular momentum is

$$\mathbf{M} = \mathbf{I} + \mathbf{S}. \tag{5.237}$$

Therefore ESR in this system is described by:

$$H_{\text{ESR}} = -eg_M \mathbf{S} \cdot \mathbf{B} \tag{5.238}$$

and NMR by:

$$H_{\text{NMR}} = -eg_M \mathbf{I} \cdot \mathbf{B}. \tag{5.239}$$

The ESR and NMR resonance frequencies are the same:

$$\omega_{\text{res}} = eg_M B_Z \tag{5.240}$$

and both are changed by discarding the Dirac approximation.

The most important feature of NMR and magnetic resonance imaging (MRI) is the chemical shift due to the magnetic flux density induced by a nuclear magnetic dipole moment:

$$\mathbf{B}(\mathbf{m}_N) = -\frac{\mu_0}{4\pi r^3}(\mathbf{m}_N - 3\hat{\mathbf{r}}\hat{\mathbf{r}} \cdot \mathbf{m}_N) \tag{5.241}$$

where μ_0 is the vacuum permeability. The induced magnetic flux density is equivalent to the nuclear $\mathbf{W}$ potential of ECE 2:

$$\mathbf{W}_N = \frac{\mu_0}{4\pi r^3}\mathbf{m}_N \times \mathbf{r} \tag{5.242}$$

and the non relativistic linear momentum of the electron is changed in the minimal prescription to:

$$\mathbf{p}_0 \rightarrow \mathbf{p}_0 - e\mathbf{W}_N. \tag{5.243}$$

The classical hamiltonian is changed to:

$$H = \frac{1}{2m}\left(\mathbf{p}_0 - e\mathbf{W}_N\right)\cdot\left(\mathbf{p}_0 - e\mathbf{W}_N\right) + U \tag{5.244}$$

and as shown in detail in note 335(3) the interaction hamiltonian:

$$H_{\text{int}} = -\frac{e}{m_e}\mathbf{p}_0\cdot\mathbf{W}_N + \cdots \tag{5.245}$$

gives the energy of interaction:

$$E = -\int \mathbf{W}_N\cdot\mathbf{j}\,d\tau \tag{5.246}$$

where the current density is:

$$\mathbf{j} = \frac{e}{2me}\left(\psi^*\mathbf{p}_0\psi + \psi\mathbf{p}_0^*\psi^*\right). \tag{5.247}$$

Using Eq. (5.231) the interaction energy is:

$$E = -\mathbf{m}_N\cdot\mathbf{B}_N = -\int \mathbf{W}_N\cdot\mathbf{j}\,d\tau \tag{5.248}$$

and is responsible for the chemical shift because $\mathbf{B}_N$ is present as well as the applied magnetic flux density $\mathbf{B}$ of the spectrometer.

The chemical shift is affected by the removal of the Dirac approximation. In the class one hamiltonian this means:

$$\frac{p_0^2}{2m_e} \rightarrow \left(\frac{\gamma^2}{1+\gamma}\right)\frac{p_0^2}{m_e}. \tag{5.249}$$

This type of theory is developed in detail in Notes 335(4) and 335(5) on `www.aias.us`. In the presence of a nuclear magnetic potential the hamiltonian (5.146) is changed as in Note 335(4) to give the interaction hamiltonian:

$$H_{\text{int}} = -2\frac{e}{m_e}\mathbf{p}_1\cdot\mathbf{p}_N \tag{5.250}$$

where

$$\mathbf{p}_1 = \left(\frac{\gamma^2}{1+\gamma}\right)^{1/2}\mathbf{p}_0 \tag{5.251}$$

and

$$\mathbf{p}_N = e\mathbf{W}_N. \tag{5.252}$$

The nuclear magnetic flux density can be defined as:

$$\mathbf{B}_N = \frac{\mu_0 e}{2\pi m_e r^3}\mathbf{L}_1 \tag{5.253}$$

where $\mathbf{L}_1$ is an orbital angular momentum of the electron. In the presence of an external magnetic flux density $\mathbf{B}$ the complete hamiltonian is:

$$H_{\text{int}} = -\mathbf{m}_N \cdot (\mathbf{B} + \mathbf{B}_N) \tag{5.254}$$

and in spin orbit format (Note 335(4)) this becomes:

$$H_{\text{int}} = -\frac{g_N \mu_0 e^2}{4\pi m_e m_p r^3} \left(\frac{\gamma^2}{1+\gamma} \right)^{1/2} \mathbf{I} \cdot \mathbf{L} \tag{5.255}$$

where $\mathbf{I}$ is the spin angular momentum of the nucleus and $\mathbf{L}$ is the orbital angular momentum of the electron.

In direct analogy with the ususal spin orbit theory of electrons, the energy levels from the hamiltonian (5.255) are given by the following expectation values:

$$E_{\text{int}} = -\frac{g_N \mu_0 e^2}{4\pi m_e m_p} \left\langle \left(\frac{\gamma^2}{1+\gamma} \right)^{1/2} \frac{\mathbf{I} \cdot \mathbf{L}}{r^3} \right\rangle. \tag{5.256}$$

Assume that this can be written as:

$$E_{\text{int}} = -\frac{g_N \mu_0 e^2}{4\pi m_e m_p} \left(\frac{\gamma^2}{1+\gamma} \right)^{1/2} \left\langle \frac{\mathbf{I} \cdot \mathbf{L}}{r^3} \right\rangle \tag{5.257}$$

using:

$$A = \frac{\gamma^2}{1+\gamma} = \left(1 - \left(\frac{\alpha}{n} \right)^2 + \left(1 - \left(\frac{\alpha}{n} \right)^2 \right)^{1/2} \right)^{-1}. \tag{5.258}$$

In analogy with the spin orbit theory of electrons:

$$\left\langle \frac{\mathbf{I} \cdot \mathbf{L}}{r^3} \right\rangle = \hbar^2 \left(\frac{J(J+1) - L(L+1) - I(I+1)}{2 r_B^3 n^3 L \left(L + \frac{1}{2} \right) (L+1)} \right) \tag{5.259}$$

where:

$$J = L + I, \ldots, |L - I|. \tag{5.260}$$

For the proton:

$$I = \frac{1}{2}, -\frac{1}{2}. \tag{5.261}$$

In the presence of an external magnetic field the complete hamiltonian is:

$$H = -\mathbf{m}_N \cdot \mathbf{B} + E_{\text{int}} = \frac{-g_N e \hbar m_I}{2 m_p} B_Z + E_{\text{int}} \tag{5.262}$$

where the interaction energy is:

$$E_{\text{int}} = \frac{-g_N \mu_0 e^2 A^{1/2} \hbar^2}{4\pi m_e m_p} \left(\frac{J(J+1) - L(L+1) - I(I+1)}{2 r_B^3 n^3 L \left(L + \frac{1}{2} \right) (L+1)} \right). \tag{5.263}$$

The NMR resonance condition is:

$$\hbar\omega = E\left(m_I - 1\right) - E\left(m_I\right) \tag{5.264}$$

and it is clear that the entire spectrum is affected by the factor:

$$A = \frac{\gamma^2}{1+\gamma} \tag{5.265}$$

and the effect is within range of a high resolution FT NMR spectrometer. If it is not found the Dirac theory is challenged in another way.

The well known theory of hyperfine interaction in NMR is also changed on a foundational level by removing the Dirac approximation. Hyperfine structure in NMR is one of its most useful analytical features, and is generated by the interaction of the magnetic spin dipole moment of the electron with the nuclear magnetic field due to the spin angular momentum I of the nucleus. In the Dirac approximation the magnetic spin dipole moment of the electron is:

$$\mathbf{m}_S = \frac{e}{m_e}\mathbf{S} \tag{5.266}$$

but the rigorous definition is:

$$\mathbf{m}_S = 2\left(\frac{\gamma^2}{1+\gamma}\right)\frac{e}{m_e}\mathbf{S}. \tag{5.267}$$

The nuclear magnetic spin dipole moment is:

$$\mathbf{m}_N = g_N\frac{e}{2m_p}\mathbf{I} \tag{5.268}$$

where g_N is the nuclear g factor and in atomic H, m_p is the proton mass because the nucleus consists of one proton. The nuclear magnetic flux density is:

$$\mathbf{B}\left(\mathbf{I}\right) = -\frac{\mu_0}{4\pi r^3}\left(\mathbf{m}_N - 3\hat{\mathbf{r}}\hat{\mathbf{r}}\cdot\mathbf{m}_N\right) \tag{5.269}$$

so the interaction hamiltonian is:

$$H_{\text{int}} = \left(\frac{\gamma^2}{1+\gamma}\right)\frac{\mu_0 e^2 g_N}{4\pi m_e m_p r^3}\left(\mathbf{S}\cdot\mathbf{I} - 3\mathbf{S}\cdot\hat{\mathbf{r}}\hat{\mathbf{r}}\cdot\mathbf{I}\right) \tag{5.270}$$

and it is clear that the hyperfine structure of NMR is affected by the factor A, i. e. is affected by the removal of the Dirac approximation as shown later in this chapter.

5.2 Numerical Analysis and Graphics

5.2.1 ECE 2 Energy Levels of Spin-Orbit Coupling

According to Eq. (5.18), the relativistic expectation value of the Hamiltonian can be approximated by

$$\langle H_0\rangle = E_0 + \langle H_0\rangle_{s-o} + \langle H_0\rangle_1 \tag{5.271}$$

where the three parts are the non-relativistic energy eigenvalues

$$E_0 = -\frac{e^4}{32\ \pi^2\ \epsilon_0^2\ n^2\ m\ c^2}, \tag{5.272}$$

the spin-orbit contribution of Dirac theory

$$\langle H_0 \rangle_{s-o} = f \int \psi^* \nabla^2 (U\psi)\ d\tau, \tag{5.273}$$

and the new additional part

$$\langle H_0 \rangle_1 = -f E_0 \int \psi^* \nabla^2 \psi\ d\tau, \tag{5.274}$$

both with the factor

$$f = -\frac{\hbar^2}{4m^2c^2}. \tag{5.275}$$

The integrals are evaluated for the Hydrogen wave functions in three dimensions, for details see UFT papers 250 and 308. The Laplace operator in three dimensions with spherical coordinates (r, θ, ϕ) is

$$\nabla^2 \psi = \frac{1}{r^2}\ \frac{\partial}{\partial r}\left(r^2 \frac{\partial \psi}{\partial r}\right) + \frac{1}{r^2 \sin(\theta)} \frac{\partial}{\partial \theta}\left(\sin(\theta) \frac{\partial \psi}{\partial \theta}\right) + \frac{1}{r^2 \sin^2(\theta)} \frac{\partial^2 \psi}{\partial \phi^2}. \tag{5.276}$$

Additional parameters appearing in the wave functions are the atomic number Z and the Bohr radius a_0. The Coulomb energy has been assumed as

$$U = -\frac{Ze^2}{4\pi\epsilon_0 r}. \tag{5.277}$$

For Hydrogen we have $Z = 1$, for higher Z values these are very crude approximations.

The integral values appearing in Eqs. (5.273, 5.274) have been computed analytically and are listed in Table 5.1. The ordinary spin-orbit terms depend on the n and l quantum numbers, not on m_l. Surprisingly, the additional term $\langle H_0 \rangle_1$ does not depend on the angular quantum number l, only on the main quantum number n. Obviously a factor of $1/n^2$ is contained in the result. It should be noticed that this factor also appears in E_0 but has not been multiplied here for the integral values. Test runs with a Laplace operator (5.276) without angular parts showed that $\langle H_0 \rangle_1$ becomes dependent on the l quantum number then. In spectroscopy which is angle-sensitive, we expect that the new term will show an l dependence.

The numerical values of energy shifts in eV are shown in Table 5.2. The corrections $\langle H_0 \rangle_1$ are smaller than those of the Dirac term of spin-orbit coupling. Nonetheless the $1s$ state is shifted significantly by the new term. This is in the order of magnitude of 10^{-4} eV and should be observable by spectroscopy. From Table 5.1 it is seen that the new effects grow with atomic number Z^2 while the ordinary spin-orbit terms grow with Z^4. Therefore these corrections will be less significant for heavier elements.

n	l	Integral $\langle H_0 \rangle_{s-o}$	Integral $\langle H_0 \rangle_1$
1	0	$-\frac{Z^4}{a_0^3}$	$-\frac{Z^2}{a_0^2}$
2	0	$-\frac{Z^4}{16\,a_0^3}$	$-\frac{Z^2}{4a_0^2}$
2	1	$\frac{5Z^4}{48\,a_0^3}$	$-\frac{Z^2}{4a_0^2}$
3	0	$-\frac{Z^4}{81\,a_0^3}$	$-\frac{Z^2}{9a_0^2}$
3	1	$\frac{Z^4}{27\,a_0^3}$	$-\frac{Z^2}{9a_0^2}$
3	2	$\frac{7Z^4}{405\,a_0^3}$	$-\frac{Z^2}{9a_0^2}$

Table 5.1: Energy shifts of Integrals (5.273) and (5.274).

n	l	E_0	$\langle H_0 \rangle_{s-o}$	$\langle H_0 \rangle_1$	$\langle H_0 \rangle$
1	0	-13.6056919	0.0003623	0.0001811	-13.6051485
2	0	-3.4014230	0.0000226	0.0000113	-3.4013890
2	1	-3.4014230	-0.0000075	0.0000038	-3.4014268
3	0	-1.5117435	0.0000045	0.0000022	-1.5117368
3	1	-1.5117435	-0.0000045	0.0000012	-1.5117468
3	2	-1.5117435	-0.0000009	0.0000004	-1.5117440

Table 5.2: Energy shifts of Eqs. (5.273, 5.274) and total energies in eV.

5.2.2 Hyperfine Spin Orbit ESR

Further relevant terms for Hydrogen ESR are the expectation values of $1/r^3$ and $1/r^4$. The former is given by Eq. (5.69), the latter has been computed by evaluating the integral

$$\left\langle \frac{1}{r^4} \right\rangle = \int \psi^* \frac{1}{r^4} \psi \, d\tau. \tag{5.278}$$

In Table 5.3 the expectation values of $1/r^3$ and $1/r^4$ and their ratio are compiled. We used again the non-relativistic wave functions of Hydrogen as an approximation as described earlier. For quantum number $l = 0$, the expectation values do not exist, which can be seen from the denominator of Eq.(5.69) for $\langle 1/r^3 \rangle$. The ratio is a multiple of Z/a_0 where a_0 is the Bohr radius. This means that spectroscopic terms of $\langle 1/r^4 \rangle$ are smaller but relevant.

Another expectation value appearing in the new spectroscopy is according to Eq.(5.67):

$$\langle \mathbf{I}_2 \rangle = \int \psi^* \boldsymbol{\nabla} (\nabla^2 \psi) \, d\tau. \tag{5.279}$$

We present the radial component of this term in Table 5.4, together with the kinetic energy

$$\langle E_{\text{kin}} \rangle = -\hbar \int \psi^* (\nabla^2 \psi) \, d\tau. \tag{5.280}$$

The kinetic energy is positive and only depends on the main quantum number. The integral itself is negative. The radial component of the term (5.279) exists only for s states and is proportional to $(Z/a_0)^3$.

n	l	$\langle 1/r^3 \rangle$	$\langle 1/r^4 \rangle$	$\frac{\langle 1/r^4 \rangle}{\langle 1/r^3 \rangle}$
1	0	–	–	–
2	0	–	–	–
2	1	$\frac{Z^3}{24\, a_0^3}$	$\frac{Z^4}{24\, a_0^4}$	$\frac{Z}{a_0}$
3	0	–	–	–
3	1	$\frac{Z^3}{81\, a_0^3}$	$\frac{10\ Z^4}{729\ a_0^4}$	$\frac{10\ Z}{9\ a_0}$
3	2	$\frac{Z^3}{405\, a_0^3}$	$\frac{2\ Z^4}{3645\ a_0^4}$	$\frac{2\ Z}{9\ a_0}$

Table 5.3: Expectation values $\langle 1/r^3 \rangle$, $\langle 1/r^4 \rangle$ and their ratio.

n	l	$\langle E_{\text{kin}} \rangle$	$\langle I_2 \rangle_r$
1	0	$\frac{\hbar Z^2}{a_0^2}$	$\frac{10\sqrt{\pi}\, Z^3}{a_0^3}$
2	0	$\frac{\hbar Z^2}{4\, a_0^2}$	$\frac{11\sqrt{\pi}\, Z^3}{8\, a_0^3}$
2	1	$\frac{\hbar Z^2}{4\, a_0^2}$	0
3	0	$\frac{\hbar Z^2}{9\, a_0^2}$	$\frac{4\sqrt{\pi}\, Z^3}{3^{\frac{5}{2}}\sqrt{6}\, a_0^3}$
3	1	$\frac{\hbar Z^2}{9\, a_0^2}$	0
3	2	$\frac{\hbar Z^2}{9\, a_0^2}$	0

Table 5.4: Expectation values of kinetic energy and special term Eq. (5.279).

5.2.3 Energy Level Diagrams of Relativistic Zeeman Spectroscopy

The energies of the transitions described in Eqs. (5.106 - 5.110) have been calculated for atomic Hydrogen. The non-realtivistic energies E_1 and new relativistic energies E_2 of the Zeeman effect were defined in Eqs. (5.101, 5.102). The new splitting depends on the magnetic quantum number m_L as usual and, in addition, on the principal quantum number n. There is no dependence on the angular quantum number l. It is therefore sufficient to to consider the transitions with highest possible l for given main quantum numbers n_1 and n_2. For example the splittings of the transition

$$3p \to 4d$$

are contained in

$$3d \to 4f$$

for all possible m_L values and selection rules $\Delta m_L = 0, \pm 1$. For comparability of the results we plottet the relative energy differences related to the non-relativistic case. For an initial state i and final state f the spectroscopically observable energy difference is

$$\Delta E = E_f - E_i. \tag{5.281}$$

This difference, giving the new Zeeman splitting, is first related to the non-relativistic case. Then the splitting is normalized by dividing by $e\hbar/(2m)$ so that a dimensionless number for the splitting is obtained:

$$\Delta E_{relative} = \frac{2m}{e\hbar}\ \left(E_f - E_i - (E_{f,non-rel} - E_{i,non-rel})\right). \tag{5.282}$$

Figs. 5.1 - 5.12 show all possible splittings with $\Delta l = 1$ (absorption) and $\Delta m_L = 0, \pm 1$ for neighboring principal quantum numbers, i.e. $n_1 = 1 \to n_2 = 2$, $n_1 = 2 \to n_2 = 3$, etc. The diagrams are separate for each of the three selection rules $\Delta m_L = 0, \pm 1$ which correspond to linear and circularly polarized light. For comparability, the scale of the Y axis has been chosen equal for all diagrams. For the transition $1s \to 2p$ there is only a shift for $\Delta m_L = \pm 1$ and no splitting because there is only one possible transition. The transition for $\Delta m_L = 0$ is unchanged because of $m_L = 0$. In general the splitting is $2l-1$ fold where l is the angular quantum number of the final state. The terms are graphed in Figs. 5.3 - 5.12. It can be seen that the splitting becomes smaller for higher n values. This is a consequence of the factor $1/n^2$ in Eq.(5.102).

In addition to the transitions between neighbouring principal quantum numbers, we have also investigated two cases with larger differences:

$$2p \to 4d$$

and

$$2p \to 5d,$$

see Figs. 5.13 and 5.14, plotted only for the selection rule $\Delta m_L = -1$. These diagrams should be compared with Fig. 5.4 which describes the corresponding splitting for $2p \to 3d$. The width of the splitting is somewhat enlarged and the splitting is shifted to the middle for transitions to higher n. Another general result is that the splitting is always equidistant.

The calculations have been done by a Maxima program which computes transitions between any energy levels of Hydrogen with automatic plot. The program can be obtained from the authors on request.

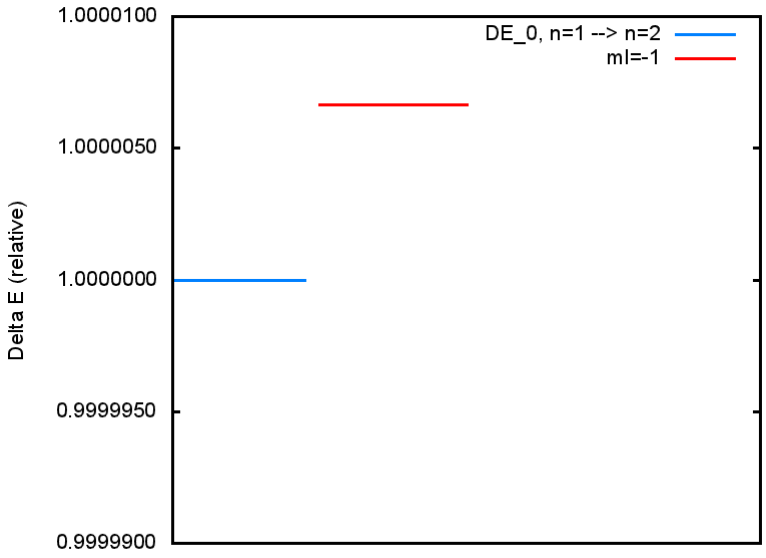

Figure 5.1: Term schema for $n = 1 \to 2$, $\Delta m_L = -1$.

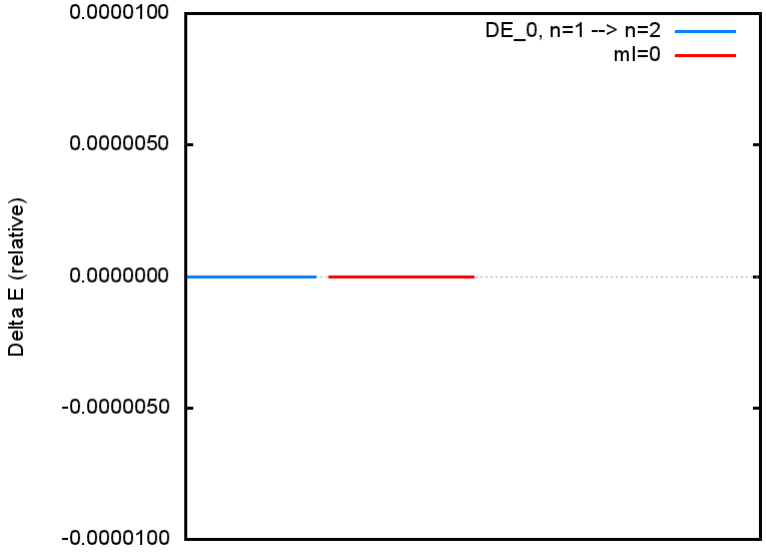

Figure 5.2: Term schema for $n = 1 \to 2$, $\Delta m_L = 0$.

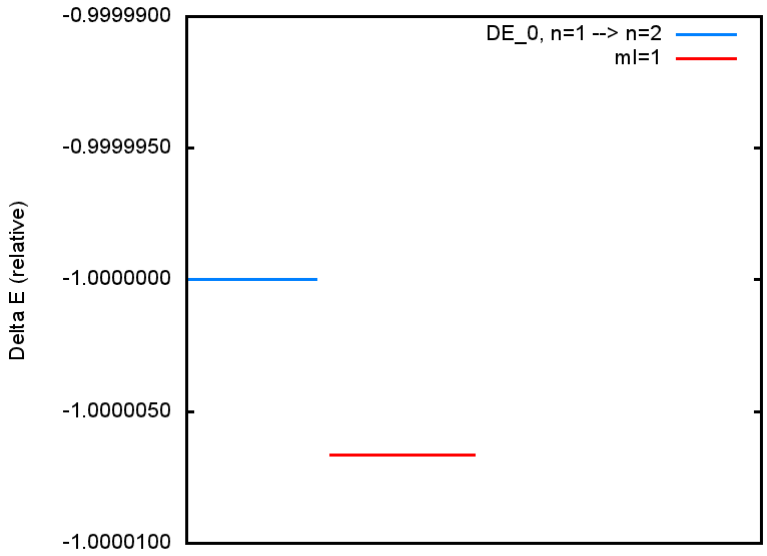

Figure 5.3: Term schema for $n = 1 \to 2$, $\Delta m_L = 1$.

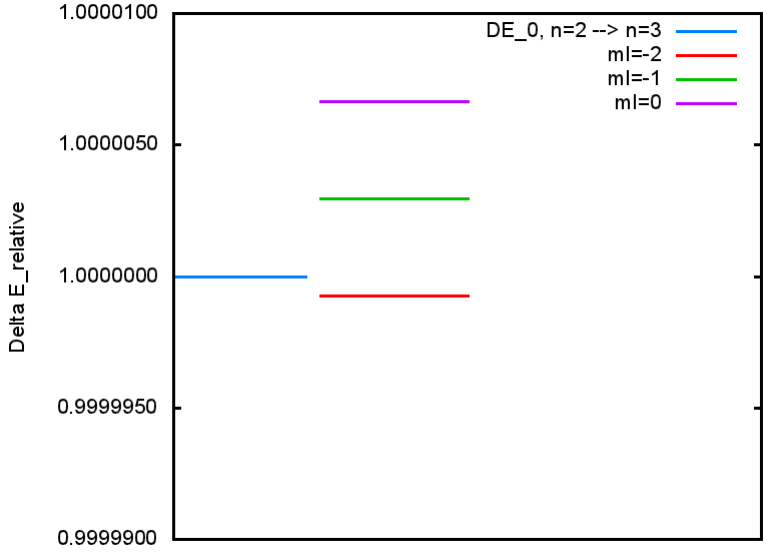

Figure 5.4: Term schema for $n = 2 \to 3$, $\Delta m_L = -1$.

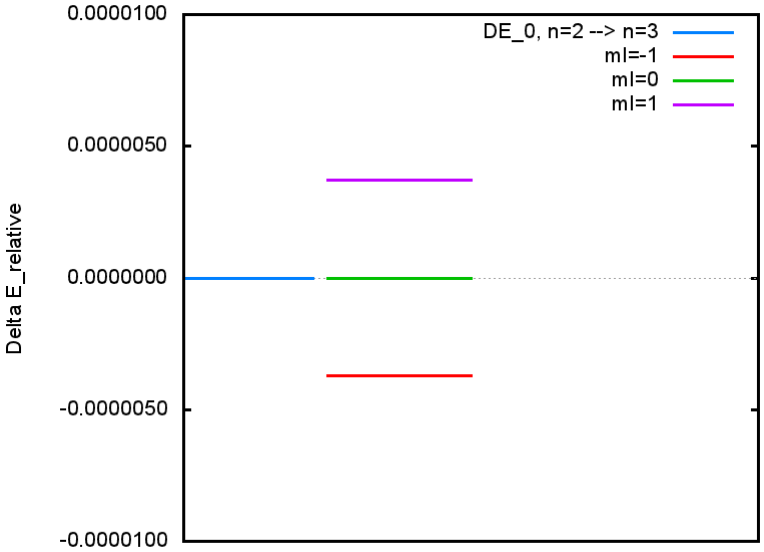

Figure 5.5: Term schema for $n = 2 \to 3$, $\Delta m_L = 0$.

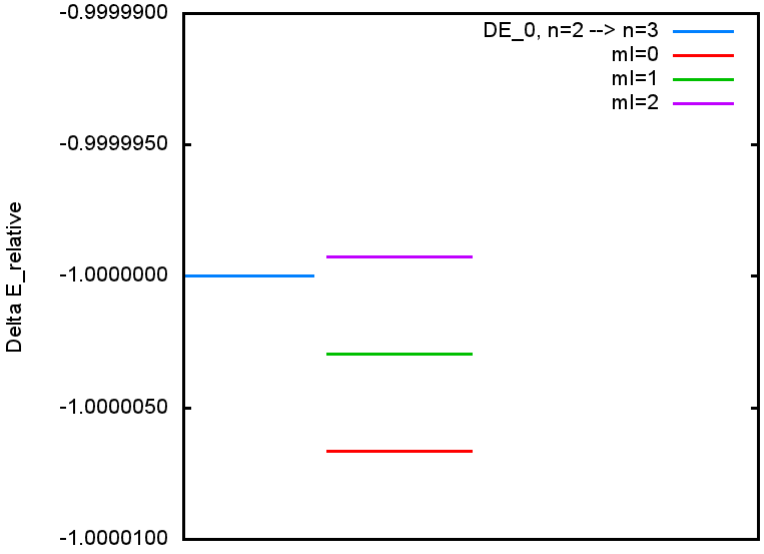

Figure 5.6: Term schema for $n = 2 \to 3$, $\Delta m_L = 1$.

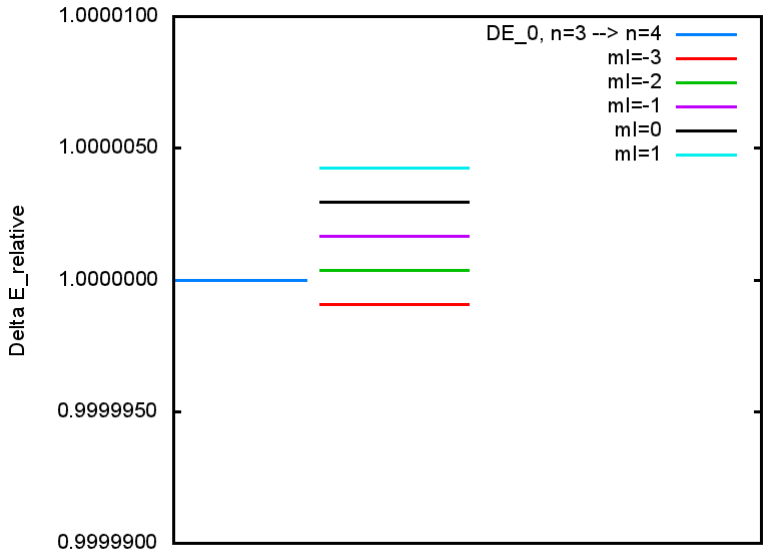

Figure 5.7: Term schema for $n = 3 \to 4$, $\Delta m_L = -1$.

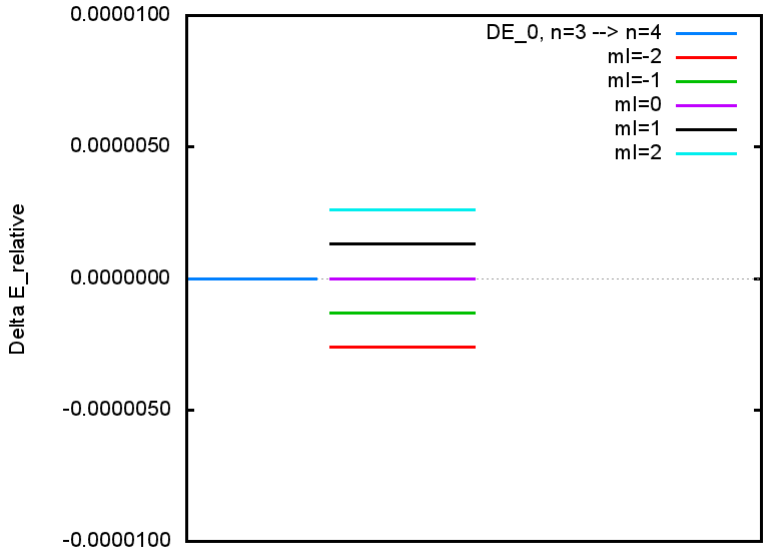

Figure 5.8: Term schema for $n = 3 \to 4$, $\Delta m_L = 0$.

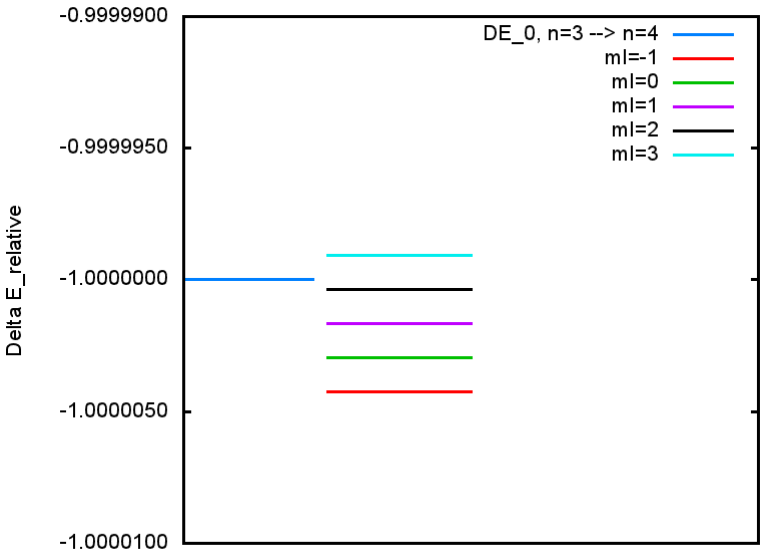

Figure 5.9: Term schema for $n = 3 \to 4$, $\Delta m_L = 1$.

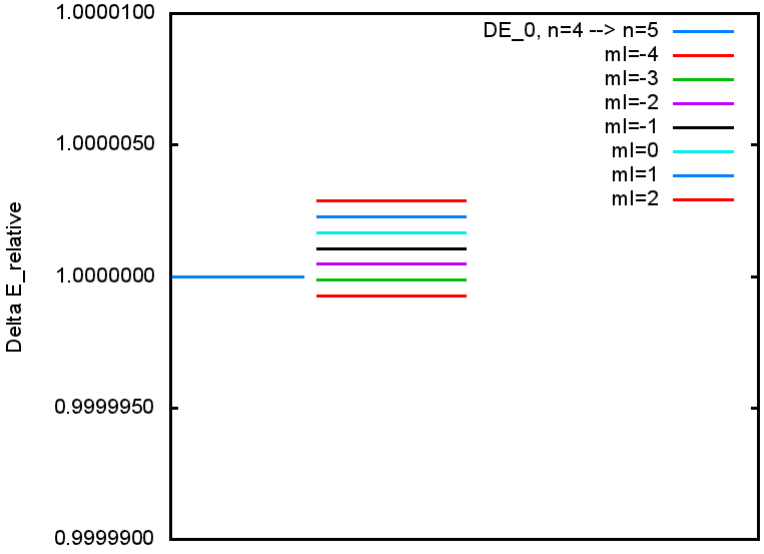

Figure 5.10: Term schema for $n = 4 \to 5$, $\Delta m_L = -1$.

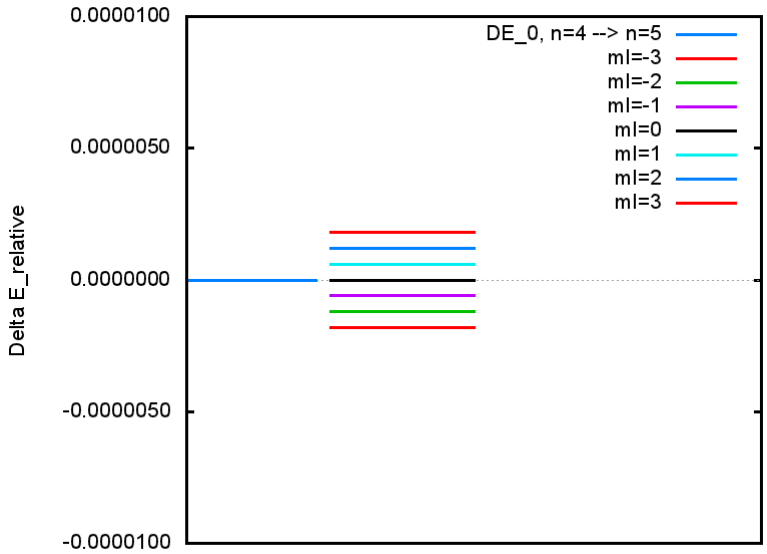

Figure 5.11: Term schema for $n = 4 \to 5$, $\Delta m_L = 0$.

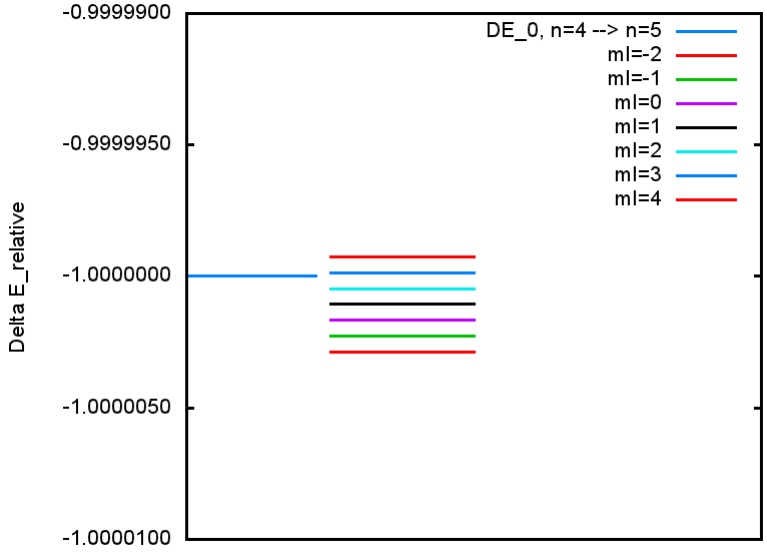

Figure 5.12: Term schema for $n = 4 \to 5$, $\Delta m_L = 1$.

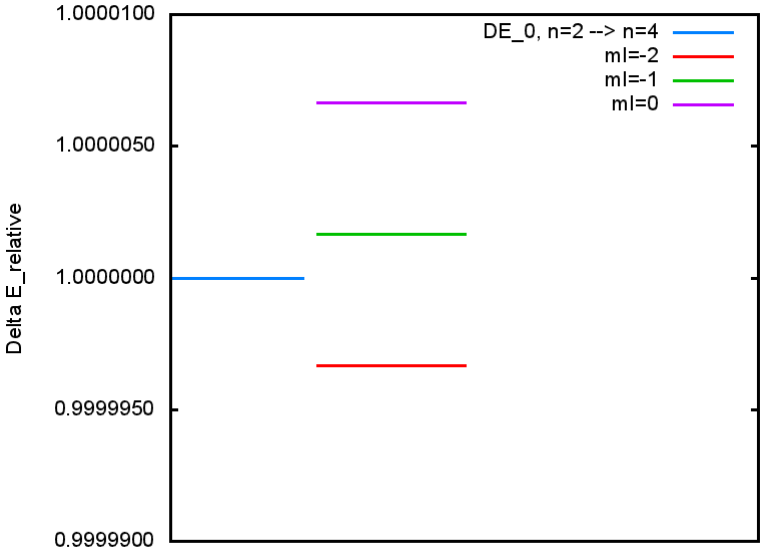

Figure 5.13: Term schema for $n = 2 \to 4$, $\Delta m_L = -1$.

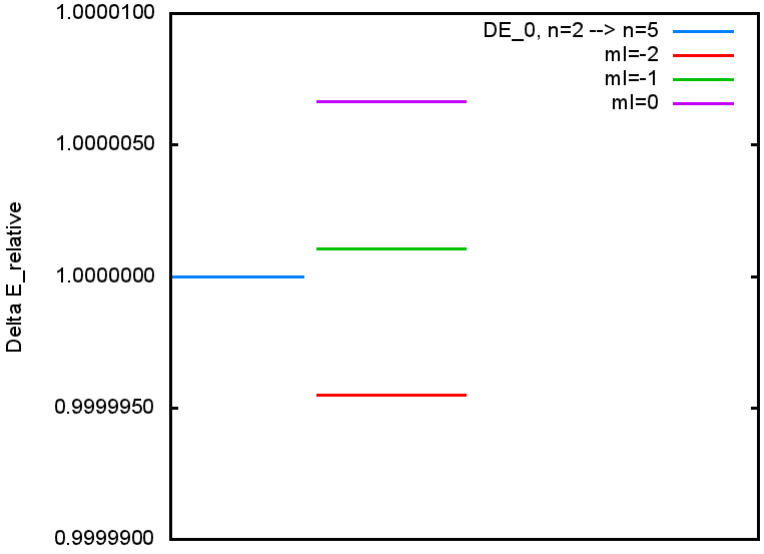

Figure 5.14: Term schema for $n = 2 \to 5$, $\Delta m_L = -1$.

5.2.4 Energy Level Diagrams of Anomalous Zeeman Hyperfine Shifts

The expectation value of the potential energy can be calculated from the relation

$$\langle U \rangle = -2 \langle T \rangle \tag{5.283}$$

with the non-relativistic kinetic energy

$$\langle T \rangle = \left\langle -\frac{\hbar \nabla^2}{2m} \right\rangle = \left\langle \frac{p_0^2}{2m} \right\rangle = m\,c^2\,\frac{\alpha^2}{2\,n^2} \tag{5.284}$$

as was derived in UFT 332. The relativistic energy levels of Dirac theory (without an external magnetic field) are given by

$$E_D = \langle U \rangle + \frac{m\ c^2\,\alpha^2}{2\,n^2} + \frac{\alpha^2}{4\,m\,a_0\,n^3}\ \frac{J(J+1) - L(L+1) - S((S+1)}{L(L+1/2)(L+1)} \tag{5.285}$$

while the new hyperfine structure leads to the result:

$$\begin{aligned} E =& \langle U \rangle + \frac{m\,c^2\,\alpha^2}{2\,n^2}\left(1 + \frac{\alpha^2}{4\,n^2}\right) \\ &+ \frac{\alpha^2}{4\,m\,a_0\,n^3}\left(1 + \frac{\alpha^2}{2\,n^2}\right)\ \frac{J(J+1) - L(L+1) - S((S+1)}{L(L+1/2)(L+1)}. \end{aligned} \tag{5.286}$$

The term schema of transitions will not change since the new hyperfine structure does not depend on the m_J quantum numbers. Therefore there are no additional splittings for the Zeeman effect, only a small shift. The energies of both cases are compared for the first levels of atomic Hydrogen in Table 5.5. There is always a lifting of energies due to the correct solution of the fermion/Dirac equation presented in this work. In addition, the energies are shown as term schemas in Figs. 5.15 - 5.20.

Term	Non-rel.	Dirac	ECE2 theory	Diff. ECE2-Dirac
1 $s_{1/2}$	-0.5	-0.5	-0.4999933435807	$6.656 \cdot 10^{-6}$
2 $s_{1/2}$	-0.125	-0.125	-0.1249995839738	$4.160 \cdot 10^{-7}$
2 $p_{1/2}$	-0.125	-0.1250001386754	-0.1249997226492	$4.160 \cdot 10^{-7}$
2 $p_{3/2}$	-0.125	-0.1250001386754	-0.1249997226492	$4.160 \cdot 10^{-7}$
3 $s_{1/2}$	-0.05555555555555	-0.0555555555556	-0.0555554733775	$8.218 \cdot 10^{-8}$
3 $p_{1/2}$	-0.05555555555555	-0.0555555677301	-0.0555554855521	$8.218 \cdot 10^{-8}$
3 $p_{3/2}$	-0.05555555555555	-0.0555555494683	-0.0555554672903	$8.218 \cdot 10^{-8}$
3 $d_{3/2}$	-0.05555555555555	-0.0555555592079	-0.0555554770299	$8.218 \cdot 10^{-8}$
3 $d_{5/2}$	-0.05555555555555	-0.0555555531207	-0.0555554709426	$8.218 \cdot 10^{-8}$

Table 5.5: Energies (in Hartree units) of atomic Hydrogen with spin-orbit splitting (Dirac theory and this work).

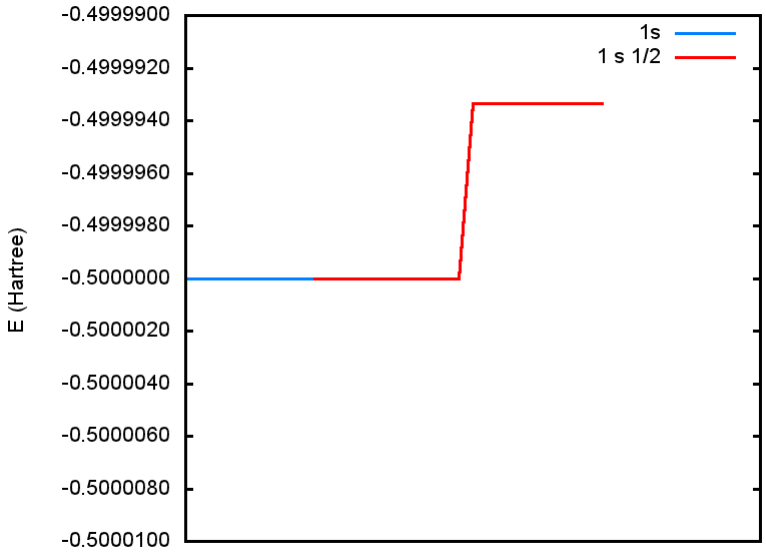

Figure 5.15: Energy schema for 1s states (non-rel., Dirac theory, ECE2 theory).

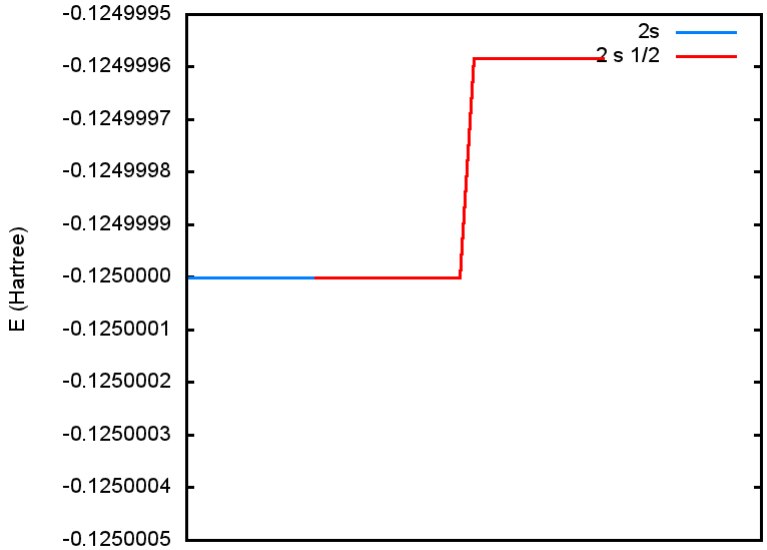

Figure 5.16: Energy schema for $2s$ states (non-rel., Dirac theory, ECE2 theory).

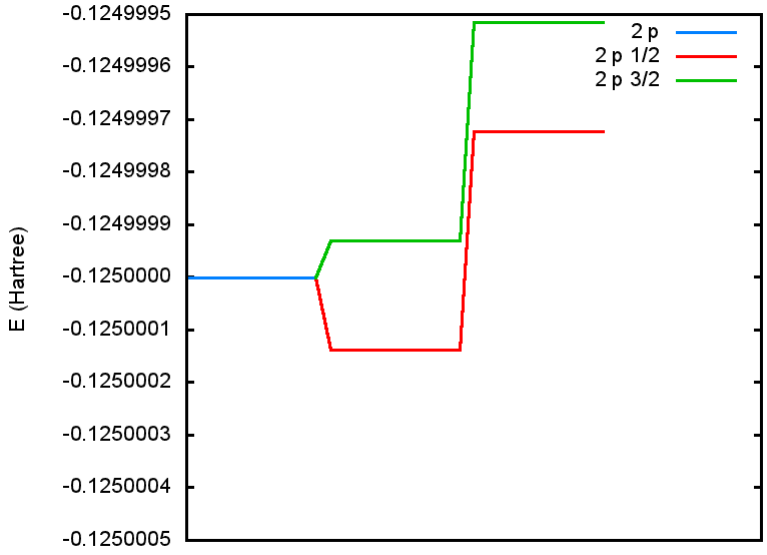

Figure 5.17: Energy schema for $2p$ states (non-rel., Dirac theory, ECE2 theory).

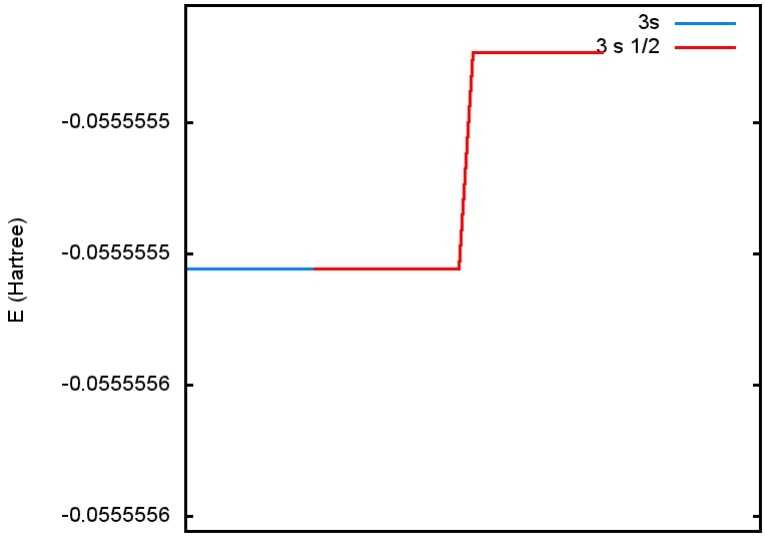

Figure 5.18: Energy schema for $3s$ states (non-rel., Dirac theory, ECE2 theory).

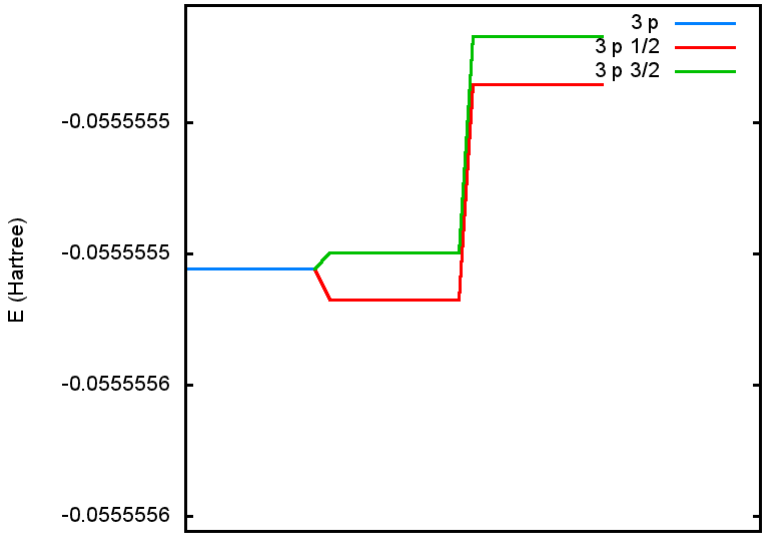

Figure 5.19: Energy schema for $3p$ states (non-rel., Dirac theory, ECE2 theory).

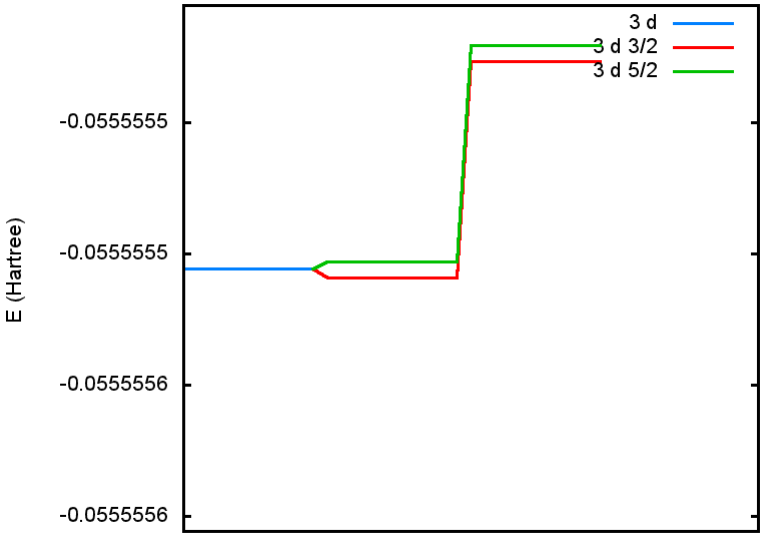

Figure 5.20: Energy schema for $3d$ states (non-rel., Dirac theory, ECE2 theory).

5.2.5 Relativistic Correction of Energy Levels

As described from Eq. (5.232) onwards in this chapter, the electronic interaction energy for ESR etc. is modified by the relativistic factor

$$A = \frac{\gamma^2}{1+\gamma} \tag{5.287}$$

where γ is defined by Eq. (5.216). The electronic momentum is modified by the square root of this factor, see Eq. (5.251), and the magnetic spin dipole moment of the electron depends on $2A$ according to Eq. (5.267):

$$\mathbf{m}_S = 2\left(\frac{\gamma^2}{1+\gamma}\right)\frac{e}{m_e}\mathbf{S}. \tag{5.288}$$

For spin-orbit splitting, the gradient of A in (5.167) appears as an additional factor, whose radial part is given by (5.161) and (5.163).

To demonstrate the effects, the appearances of A have been graphed in Fig. 5.21. We plotted the A factor in dependence of a normalized momentum p_0, i.e. a variable

$$\bar{p}^2 = \frac{p_0^2}{2m}. \tag{5.289}$$

For comparison, the gamma factor $\gamma(\bar{p})$ has been graphed too. A, $2A$, $\sqrt{A}$ and grad(A) go to infinity for $\bar{p}$ reaching unity which corresponds to velocity $v_0 = c$.

In Hydrogen the spin-orbit splitting is small ($\approx 10^{-5}$ eV). In heavy atoms the splitting becomes high and the linear momentum is significantly larger than in Hydrogen. Therefore the gradient of the A factor grows remarkably, giving additional enlargement of splittings. It is seen that the gradient of A rises much faster than the relativistic gamma factor. An effect should be detectable in spectra of heavy elements.

The magnetic spin dipole moment (5.288) depends on $2A$, which grows faster than γ in the relativistic range. This gives a change in the magnetic moment being also larger than the γ enhancement. Only the A and $\sqrt{A}$ behaviour is less pronounced than γ.

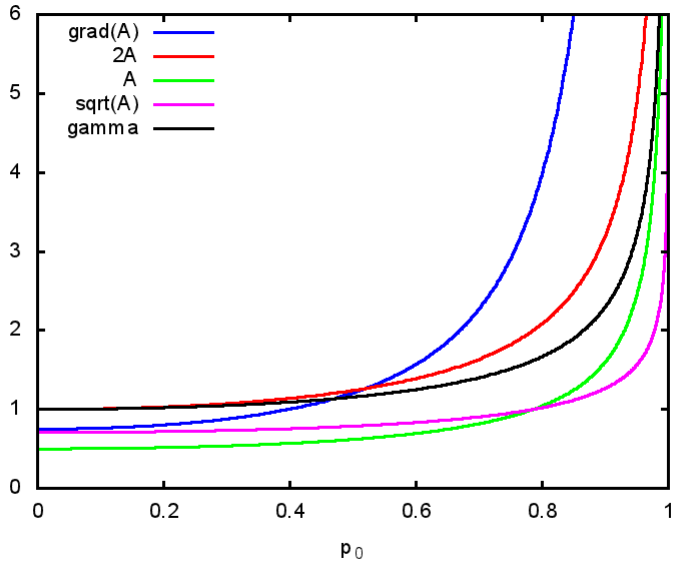

Figure 5.21: Diverse functions depending on $A(\bar{p})$ and $\gamma(\bar{p})$.

Chapter 6

The ECE 2 Vacuum

6.1 General Theory

In ECE 2 theory the vacuum is considered as the geometry of spacetime, so is richly structured and has physical effects such as the radiative corrections and the Aharonov Bohm (AB) effects (the subject of UFT 336). The AB vacuum is defined as regions in which electric and magnetic fields are zero but in which the ECE 2 vacuum four-potential is non zero and may cause observable effects. The opening of this chapter summarizes UFT 336, in which it is shown that the vacuum potential causes effects in electron spin resonance in the absence of a magnetic field. The well known Chambers experiment can be adopted for experiments designed to look for this effect.

The AB effects are well known [2]- [13] to be due to potentials in the absence of fields. Consider the ECE 2 definition of magnetic flux density used in previous chapters:

$$\mathbf{B} = \boldsymbol{\nabla} \times \mathbf{W} = \boldsymbol{\nabla} \times \mathbf{A} + 2\boldsymbol{\omega} \times \mathbf{A} \tag{6.1}$$

where

$$\mathbf{W} = W^{(0)}\boldsymbol{\omega},\ \mathbf{A} = A^{(0)}\mathbf{q}. \tag{6.2}$$

Here $\boldsymbol{\omega}$ and $\mathbf{q}$ are respectively the spin connection and tetrad vectors. Therefore the AB vacuum is defined by the geometry:

$$\boldsymbol{\nabla} \times \boldsymbol{\omega} = \mathbf{0} \tag{6.3}$$

and

$$\boldsymbol{\nabla} \times \mathbf{q} = 2\mathbf{q} \times \boldsymbol{\omega}. \tag{6.4}$$

Using the identity:

$$\boldsymbol{\nabla} \cdot \boldsymbol{\nabla} \times \mathbf{q} = 0 \tag{6.5}$$

the AB vacuum geometry becomes:

$$\boldsymbol{\omega} \cdot \boldsymbol{\nabla} \times \mathbf{q} = 0 \tag{6.6}$$

i. e.

$$\mathbf{W} \cdot \boldsymbol{\nabla} \times \mathbf{A} = 0. \tag{6.7}$$

Now consider the electric field strength $\mathbf{E}$ and magnetic flux density of ECE 2 theory as defined by the spin and orbital curvature vectors as in previous chapters:

$$\mathbf{E} = cW^{(0)}\mathbf{R}(\text{orb}) \tag{6.8}$$

and

$$\mathbf{B} = W^{(0)}\mathbf{R}(\text{spin}). \tag{6.9}$$

So the AB effects in this type of theory are defined by a Cartan geometry in which torsion and curvature vanish but in which the tetrad and spin connection are finite. In minimal notation [2]- [13]:

$$T = d \wedge q + \omega \wedge q, \tag{6.10}$$

$$R = d \wedge \omega + \omega \wedge \omega, \tag{6.11}$$

so the AB vacuum geometry is:

$$d \wedge q + \omega \wedge q = 0, \tag{6.12}$$

$$d \wedge \omega + \omega \wedge \omega = 0, \tag{6.13}$$

with:

$$T = R = 0. \tag{6.14}$$

The well known Chambers experiment [2]- [13] shows that the AB vacuum is a physical vacuum because the Young diffraction of electron matter waves is affected by potentials in the absence of fields. The AB vacuum is defined in a different way from the traditional definition in electromagnetic theory, one based on the absence of charge current density. In this case the ECE 2 electrodynamical field equations are:

$$\boldsymbol{\nabla} \cdot \mathbf{B} = 0 \tag{6.15}$$

$$\boldsymbol{\nabla} \cdot \mathbf{E} = 0 \tag{6.16}$$

$$\frac{\partial \mathbf{B}}{\partial t} + \boldsymbol{\nabla} \times \mathbf{E} = \mathbf{0} \tag{6.17}$$

$$\boldsymbol{\nabla} \times \mathbf{B} - \frac{1}{c^2}\frac{\partial \mathbf{E}}{\partial t} = \mathbf{0} \tag{6.18}$$

with:

$$\boldsymbol{\kappa} \cdot \mathbf{B} = \boldsymbol{\kappa} \cdot \mathbf{E} = 0, \tag{6.19}$$

$$\kappa_0 c\mathbf{B} + \boldsymbol{\kappa} \times \mathbf{E} = \mathbf{0},\ \kappa_0 \frac{\mathbf{E}}{c} + \boldsymbol{\kappa} \times \mathbf{B} = \mathbf{0} \tag{6.20}$$

where:

$$\kappa_0 = 2\left(\frac{q_0}{r^{(0)}} - \omega_0\right), \tag{6.21}$$

$$\boldsymbol{\kappa} = 2\left(\frac{\mathbf{q}}{r^{(0)}} - \boldsymbol{\omega}\right). \tag{6.22}$$

Note 336(4) on `www.aias.us` shows that the solution:

$$\kappa_0 = 0,\ \boldsymbol{\kappa} = \mathbf{0} \tag{6.23}$$

means that $\mathbf{E}$ and $\mathbf{B}$ vanish. The simplest solution of Eqs. (6.15) to (6.22) is:

$$\mathbf{E} = \mathbf{B} = \mathbf{0},\ \kappa_0 = 0,\ \boldsymbol{\kappa} = \mathbf{0} \tag{6.24}$$

in which case the traditional vacuum, in which the charge current four density vanishes, reduces to the AB vacuum.

Note 336(4) shows that if the traditional vacuum is accepted, and plane wave solutions used for Eqs. (6.15–6.18), the result is:

$$\boldsymbol{\kappa} = \left(\frac{\kappa^2 + \kappa_0^2}{\kappa_x + \kappa_y}\right)(\mathbf{i} + \mathbf{j}). \tag{6.25}$$

Under condition (6.25), ECE 2 theory allows vacuum electric and magnetic fields to exist in the absence of charge current density – the traditional vacuum of electrodynamics. The AB vacuum on the other hand is is defined by Eq. (6.24). The interaction of the AB vacuum with one electron leads to the possibility of NMR and ESR (Chapter five) in the absence of a magnetic field. This type of interaction is considered in Note 336(5) and is based on the minimal prescription:

$$p^\mu \rightarrow p^\mu - eA^\mu \tag{6.26}$$

where the relevant four potential is defined in previous chapters:

$$A^\mu = \left(\frac{\phi}{c}, \mathbf{A}\right). \tag{6.27}$$

Therefore the Einstein energy equation becomes:

$$(E - e\phi)^2 = c^2 (\mathbf{p} - e\mathbf{A}) \cdot (\mathbf{p} - e\mathbf{A}) + m^2 c^4. \tag{6.28}$$

The total relativistic energy E and the relativistic momentum $\mathbf{p}$ are defined by the Einstein/de Broglie equations as in previous chapters:

$$E = \gamma m c^2 = \hbar\omega \tag{6.29}$$

and

$$\mathbf{p} = \gamma \mathbf{p}_0 = \hbar\boldsymbol{\kappa}. \tag{6.30}$$

The Lorentz factor is therefore:

$$\gamma = \frac{\hbar\omega}{mc^2} = \left(1 - \frac{p_0^2}{m^2c^2}\right)^{-1/2} \tag{6.31}$$

and it follows that:

$$E - mc^2 = \frac{1}{(1+\gamma)\,m}\boldsymbol{\sigma}\cdot(\mathbf{p} - e\mathbf{A})\left(1 - \frac{e\phi}{(1+\gamma)\,mc^2}\right)^{-1}\boldsymbol{\sigma}\cdot(\mathbf{p} - e\mathbf{A}) + e\phi. \tag{6.32}$$

As in chapter five this reduces to the Dirac theory if

$$\gamma \to 1 \tag{6.33}$$

i. e. by the de Broglie equation:

$$\hbar\omega_0 = mc^2 \tag{6.34}$$

where ω_0 is the rest angular frequency. The Dirac theory is therefore self contradictory because the electron is not moving:

$$H_0 = H - mc^2 =? \; 0. \tag{6.35}$$

In the approximation:

$$e\phi \ll (1+\gamma)\,mc^2 \tag{6.36}$$

Eq. (6.32) becomes:

$$\begin{aligned} E - mc^2 \sim \frac{1}{(1+\gamma)\,m}\boldsymbol{\sigma}\cdot(\mathbf{p} - e\mathbf{A})\,\boldsymbol{\sigma}\cdot(\mathbf{p} - e\mathbf{A}) + \frac{1}{(1+\gamma)\,m} \\ \boldsymbol{\sigma}\cdot(\mathbf{p} - e\mathbf{A})\left(\frac{e\phi}{(1+\gamma)\,mc^2}\right)\boldsymbol{\sigma}\cdot(\mathbf{p} - e\mathbf{A}) + e\phi. \end{aligned} \tag{6.37}$$

The ESR term is contained in the first term on the right hand side, and spin orbit effects in the second term. Relativistic quantization is defined by:

$$p^\mu\psi = i\hbar\partial^\mu\psi \tag{6.38}$$

i. e.:

$$E\psi = i\hbar\frac{\partial\psi}{\partial t} \tag{6.39}$$

and

$$\mathbf{p}\psi = -i\hbar\boldsymbol{\nabla}\psi. \tag{6.40}$$

This procedure cannot be proven ab initio, it is an empirical rule. The required ESR term is given by:

$$\begin{aligned} \left(E - mc^2\right)\psi &= \frac{1}{m\,(1+\gamma)}\left(\boldsymbol{\sigma}\cdot(-i\hbar\boldsymbol{\nabla} - e\mathbf{A})\cdot((\boldsymbol{\sigma}\cdot\mathbf{p} - e\mathbf{A})\,\psi)\right) \\ &= \frac{ie\hbar}{m\,(1+\gamma)}\boldsymbol{\sigma}\cdot\boldsymbol{\nabla}\,\boldsymbol{\sigma}\cdot\mathbf{A}\,\psi + \cdots \end{aligned} \tag{6.41}$$

Using the Pauli algebra:

$$\boldsymbol{\sigma} \cdot \boldsymbol{\nabla}\, \boldsymbol{\sigma} \cdot \mathbf{A} = \boldsymbol{\nabla} \cdot \mathbf{A} + i\, \boldsymbol{\sigma} \cdot \boldsymbol{\nabla} \times \mathbf{A} \tag{6.42}$$

so the real and physical part of Eq. (6.41) is:

$$\left(E - mc^2\right) \psi = -\frac{e\hbar}{m\,(1+\gamma)} \boldsymbol{\sigma} \cdot \boldsymbol{\nabla} \times \mathbf{A}\, \psi + \cdots \tag{6.43}$$

The spin angular momentum of the electron is:

$$\mathbf{S} = \frac{\hbar}{2} \boldsymbol{\sigma} \tag{6.44}$$

so:

$$\left(E - mc^2\right) \psi = -2 \frac{e}{m\,(1+\gamma)} \mathbf{S} \cdot \boldsymbol{\nabla} \times \mathbf{A}\, \psi + \cdots \tag{6.44a}$$

in which:

$$S_Z \psi = \hbar m_S \psi \tag{6.45}$$

where:

$$m_S = -S, \ldots, S = -\frac{1}{2}, \frac{1}{2}. \tag{6.46}$$

Therefore:

$$\left(E - mc^2\right) \psi = -2 \frac{e\hbar}{m\,(1+\gamma)} m_S \left(\boldsymbol{\nabla} \times \mathbf{A}\right)_Z \tag{6.47}$$

in which electron spin resonance is defined by:

$$\hbar \omega_{\text{res}} = 2 \frac{e\hbar}{m\,(1+\gamma)} \left(\frac{1}{2} - (-\frac{1}{2})\right) \left(\boldsymbol{\nabla} \times \mathbf{A}\right)_Z \tag{6.48}$$

with resonance frequency:

$$\omega_{\text{res}} = 2 \frac{e}{m\,(1+\gamma)} \left(\boldsymbol{\nabla} \times \mathbf{A}\right)_Z . \tag{6.49}$$

In the AB effects $\mathbf{A}$ is non zero when $\mathbf{B}$ is zero, so from Eq. (6.1) the AB vacuum is defined by:

$$\boldsymbol{\nabla} \times \mathbf{A} = -2 \boldsymbol{\omega} \times \mathbf{A} \tag{6.50}$$

and under this condition the AB vacuum causes the resonance defined by Eq. (6.49).

A computational and graphical analysis of this theory is given later on in this chapter.

As in UFT 337 the ECE 2 theory that describes the AB vacuum can be used to describe the radiative corrections, notably the Lamb shift. In order to do this, the minimal prescription used earlier in this chapter for ESR effects

of the vacuum is replaced by a new type of minimal prescription using the **W** potential. This can be developed in terms of a relativistic particle flux and the Tesla vacuum. The theory of UFT 337 defines the ECE 2 vacuum particles, which are identified as particles of the Tesla vacuum. Therefore there is particulate energy momentum in the ECE 2 vacuum that can be transferred to matter using well known theoretical methods.

Consider the ECE 2 minimal prescription:

$$p^\mu \rightarrow p^\mu + eW^\mu \tag{6.51}$$

where:

$$p^\mu = \left(\frac{E}{c}, \mathbf{p} \right), \tag{6.52}$$

$$W^\mu = \left(\frac{\phi_W}{c}, \mathbf{W} \right). \tag{6.53}$$

In ECE 2 theory:

$$W^\mu = W^{(0)} \left(\Omega^{(0)}, \mathbf{\Omega} \right) \tag{6.54}$$

where the spin connection four vector is:

$$\Omega^\mu = \left(\Omega^{(0)}, \mathbf{\Omega} \right). \tag{6.55}$$

It follows that:

$$\phi_W = cW^{(0)}\Omega^{(0)} \tag{6.56}$$

and:

$$\mathbf{W} = W^{(0)}\boldsymbol{\omega}. \tag{6.57}$$

The units of $W^{(0)}$ are those of magnetic flux:

$$[W^{(0)}] = \text{weber} = \text{volt sec} = \text{JC}^{-1}\text{s}. \tag{6.58}$$

A summary of S. I. Units is given as follows:

$$[\phi_W] = \text{volt} = \text{JC}^{-1} \tag{6.59a}$$

$$[W] = \text{tesla metres} = \text{JC}^{-1}\text{sm}^{-1} \tag{6.60a}$$

$$[\Omega^{(0)}] = \mathbf{\Omega} = \text{m}^{-1} \tag{6.59b}$$

$$[W^{(0)}] = \text{JC}^{-1}\text{s}. \tag{6.60b}$$

The ECE 2 magnetic flux density **B** (in units of tesla) is defined by Eq. (6.1), and the ECE 2 electric field strength **E** in volts per metre is:

$$\mathbf{E} = -\boldsymbol{\nabla}\phi_W - \frac{\partial \mathbf{W}}{\partial t} = -\boldsymbol{\nabla}\phi - \frac{\partial \mathbf{A}}{\partial t} + 2\left(c\Omega^{(0)}\mathbf{A} - \phi\mathbf{\Omega} \right). \tag{6.61}$$

The elementary quantum of magnetic flux is [2]- [13]:

$$W^{(0)} = \frac{\hbar}{e} \tag{6.62}$$

where $\hbar$ is the reduced Planck constant, the quantum of angular momentum in Js. Therefore:

$$\phi_W = \left(\frac{\hbar c}{e}\right)\Omega^{(0)}. \tag{6.63}$$

The AB spacetime can therefore be defined in terms of the vacuum potential:

$$W^{\mu}(\text{vac}) = \left(\frac{\phi_W(\text{vac})}{c}, \mathbf{W}(\text{vac})\right) \tag{6.64}$$

and on the most fundamental level:

$$W^{\mu}(\text{vac}) = \frac{\hbar}{e}\Omega^{\mu}(\text{vac}). \tag{6.65}$$

So the AB spacetime is defined by the spin connection vector within the fluxon $\hbar/e$. The latter is negative under charge conjugation symmetry. In the absence of electric and magnetic fields the AB spacetime (or vacuum or aether) is defined by Eq. (6.65). The fields $\mathbf{E}$ and $\mathbf{B}$ on the other hand are defined by curvature as in Eqs. (6.8) and (6.9). The latter is zero in the AB vacuum, and so is the torsion:

$$R = d \wedge \Omega + \Omega \wedge \Omega = 0, \tag{6.66}$$

$$T = d \wedge q + \Omega \wedge q = 0. \tag{6.67}$$

Consider now the Einstein energy equation:

$$p^{\mu}p_{\mu} = m^2c^2. \tag{6.68}$$

Using the minimal prescription (6.51) the effect of the AB spacetime on material matter such as an electron is:

$$\left(p^{\mu} + eW^{\mu}\right)\left(p_{\mu} + eW_{\mu}\right) = m^2c^2. \tag{6.69}$$

If the electron is at rest:

$$p^{\mu} = \left(\frac{E_0}{c}, \mathbf{0}\right),\ W^{\mu} = \frac{\hbar}{e}\left(\Omega^{(0)}, \mathbf{0}\right) \tag{6.70}$$

so:

$$\left(E_0 + \hbar\Omega^{(0)}c\right)\left(E_0 + \hbar\Omega^{(0)}c\right) = m^2c^4. \tag{6.71}$$

The AB spacetime contains an angular frequency:

$$\omega(\text{vac}) = c\Omega^{(0)} \tag{6.72}$$

so Eq. (6.71) becomes:

$$E_0 + \hbar\omega(\text{vac}) = mc^2 \tag{6.73}$$

from which it is clear that the rest frequency of a particle of material matter is increased by:

$$\omega_0 \rightarrow \omega_0 + \omega(\text{vac}) \tag{6.74}$$

due to the presence of the AB vacuum. So the mechanism of energy from spacetime becomes clear.

The AB spacetime imparts energy momentum to material matter as follows:

$$p^\mu \rightarrow p^\mu + p^\mu(\text{vac}) \tag{6.75}$$

where:

$$p^\mu(\text{vac}) = eW^\mu = \hbar\Omega^\mu. \tag{6.76}$$

The angular frequency of the AB spacetime is:

$$\omega(\text{vac}) = c\Omega^{(0)} \tag{6.77}$$

and the wave vector of the AB spacetime is:

$$\boldsymbol{\kappa}(\text{vac}) = \boldsymbol{\Omega}. \tag{6.78}$$

The Einstein/de Broglie equations of the AB spacetime (or vacuum) are:

$$E(\text{vac}) = \hbar\omega(\text{vac}) = \gamma m(\text{vac})\, c^2, \tag{6.79}$$

$$\mathbf{p}(\text{vac}) = \hbar\boldsymbol{\kappa}(\text{vac}) = \gamma m(\text{vac})\, \mathbf{v}_0(\text{vac}), \tag{6.80}$$

where the vacuum Lorentz factor is:

$$\gamma(\text{vac}) = \left(1 - \frac{v_0^2(\text{vac})}{c^2}\right)^{-1/2}. \tag{6.81}$$

Therefore the existence of a vacuum particle of mass $m(\text{vac})$ has been inferred via the Einstein/de Broglie equations. There is a statistical ensemble of such particles. The AB vacuum is quantized using:

$$E(\text{vac})\, \psi(\text{vac}) = i\hbar \frac{\partial \psi(\text{vac})}{\partial t} \tag{6.82}$$

and:

$$\mathbf{p}(\text{vac})\, \psi(\text{vac}) = -i\hbar \boldsymbol{\nabla} \psi(\text{vac}) \tag{6.83}$$

where $\psi(\text{vac})$ is the wavefunction of the vacuum wave/particle. The wavefunction obeys the ECE wave equation [2]- [13] in the limit:

$$\left(\Box + \kappa^2(\text{vac})\right) \psi(\text{vac}) = 0 \tag{6.84}$$

where:

$$\kappa(\text{vac}) = \frac{m(\text{vac})\, c}{\hbar}. \tag{6.85}$$

The vacuum wavefunction is therefore:

$$\psi(\text{vac}) = \exp\left(-i\left(\omega(\text{vac})\, t - \boldsymbol{\kappa}(\text{vac}) \cdot \mathbf{r}\right)\right) \tag{6.86}$$

and the ECE wave equation of the vacuum is:

$$\left(\square + R(\text{vac})\right)\psi(\text{vac}) = 0. \tag{6.87}$$

Eq. (6.87) is the quantized version of the Einstein energy equation of the vacuum:

$$E^2(\text{vac}) = c^2 p^2(\text{vac}) + m^2(\text{vac})\, c^4. \tag{6.88}$$

The process of taking energy from the vacuum becomes simple to understand:

$$E \rightarrow E + E(\text{vac}) \tag{6.89}$$

$$\mathbf{p} \rightarrow \mathbf{p} + \mathbf{p}(\text{vac}) \tag{6.90}$$

and is observed as an energy shift in spectra, notably the Lamb shift of atomic hydrogen, and also in the anomalous g of the electron.

It appears that such a particle vacuum was proposed but not proven by Tesla.

The Lamb shift and anomalous g factor can be defined in terms of emergy/momentum transfer. The conventional theory of the Lamb shift assumes that the electron in the H atom fluctuates in the presence of the vacuum – this phenomenon is known as jitterbugging. It can be shown as follows that this is due to vacuum energy of ECE 2 theory, and the observed Lamb shift can be used to calculate a mean vacuum angular frequency. The AB vacuum and the B(3) field [2]- [13] can be defined in terms of ECE 2 theory.

By considerations of the Einstein energy equation in ECE 2 theory, and by use of the minimal prescription, it can be shown as in Notes 340(1) and 340(2) that the anomalous g factor of the electron is defined by:

$$g = 1 + \frac{H}{mc^2} \tag{6.91}$$

where H is the hamiltonian of ECE 2 relativity:

$$H = \gamma mc^2 + U = \left(p^2c^2 + m^2c^4\right)^{1/2} + U. \tag{6.92}$$

For a static electron for which the de Broglie equation (6.34) holds:

$$g = 2 + \frac{\hbar\omega(\text{vac})}{mc^2}. \tag{6.93}$$

In general, the anomalous g factor of the electron is:

$$g = 1 + \frac{\hbar}{mc^2}\left(\omega + \omega(\text{vac})\right) \tag{6.94}$$

where ω is the angular frequency of the electron wave, and $\omega(\text{vac})$ is the angular frequency of the ECE 2 vacuum wave particle. In Note 340(2) on `www.aias.us` it is shown in complete detail that the process of momentum transfer from the vacuum wave particle results in the observable energy shift:

$$\Delta E = -\frac{e^2}{4\pi\epsilon_0 g m^2 c^2}\left\langle \frac{\mathbf{S}\cdot\mathbf{L}(\text{vac})}{r^3}\right\rangle . \tag{6.95}$$

Various methods of calculating this shift are described in Note 340(3). Therefore momentum as well as energy can be transferred from the ECE 2 vacuum.

In Note 340(4) the ECE 2 vacuum potential is defined as:

$$U(\text{vac}) = e\phi_W(\text{vac}) = \hbar c\Omega^{(0)}(\text{vac}) = \hbar\omega(\text{vac}). \tag{6.96}$$

It follows that the Coulomb potential U_C between an electron and a proton in the H atom is augmented by:

$$U_C \rightarrow U_C + U(\text{vac}) = -\frac{e^2}{4\pi\epsilon_0 r} + \hbar\omega(\text{vac}). \tag{6.97}$$

In the well known Bethe theory [2]- [13] of the Lamb shift, it is assumed that U_C jitterbugs as described in Note 340(3):

$$U_C = U\left(\mathbf{r} - \delta\mathbf{r}\right) - U\left(\mathbf{r}\right) \tag{6.98}$$

in which $\partial\mathbf{r}$ denotes the fluctuation in position of the electron due to the vacuum, in this case the ECE 2 vacuum. This idea implies that the vacuum potential is:

$$U(\text{vac}) = \hbar\omega(\text{vac}) = -\frac{e^2}{4\pi\epsilon_0}\left(\frac{1}{r-\delta r} - \frac{1}{r}\right) = \frac{e^2\delta r}{4\pi\epsilon_0\left(r-\delta r\right)r} \tag{6.99}$$

in which the change in potential energy due to the ECE vacuum is, self consistently:

$$\Delta U = U(\text{vac}) = U\left(\mathbf{r} - \delta\mathbf{r}\right) - U\left(\mathbf{r}\right). \tag{6.100}$$

If it is assumed that:

$$\delta r \ll \mathbf{r} \tag{6.101}$$

Eq (6.99) can be written as:

$$U(\text{vac}) = \hbar\omega(\text{vac}) = \frac{e^2}{4\pi\epsilon_0}\left(\frac{\delta r}{r^2} + \frac{\left(\delta r\right)^2}{r^3}\right) \tag{6.102}$$

and averaging over the ensemble of vacuum particles:

$$\left\langle U(\text{vac})\right\rangle = \hbar\left\langle\omega(\text{vac})\right\rangle = \frac{e^2}{4\pi\epsilon_0}\left(\frac{\left\langle\delta r\right\rangle}{r^2} + \frac{\left\langle\left(\delta r\right)^2\right\rangle}{r^3}\right). \tag{6.103}$$

Using the Bethe assumption:

$$\langle \delta \mathbf{r} \rangle = \mathbf{0} \tag{6.104}$$

it follows that:

$$\langle \omega(\text{vac}) \rangle = \frac{e^2}{4\pi\epsilon_0 \hbar r^3} \left\langle (\delta r)^2 \right\rangle = \frac{c\alpha}{r^3} \left\langle (\delta r)^2 \right\rangle \tag{6.105}$$

where α is the fine structure constant. So the mean square fluctuations result in a mean vacuum angular frequency.

By using a Maclaurin series expansion of the equation:

$$\Delta U = U(\mathbf{r} - \delta \mathbf{r}) - U(\mathbf{r}) \tag{6.106}$$

it can be shown that

$$\langle \Delta U \rangle = \frac{1}{6} \left\langle (\delta r)^2 \right\rangle \nabla^2 U_C. \tag{6.107}$$

For the ${}^2S_{1/2}$ orbital of the H atom [2]- [13]:

$$\left\langle \nabla^2 U_0 \right\rangle = \left\langle \nabla^2 \left(\frac{-e^2}{4\pi\epsilon_0 r} \right) \right\rangle = \frac{e^2}{\epsilon_0} |\psi(0)|^2 \tag{6.108}$$

where $\psi(0)$ is the value of the ${}^2S_{1/2}$ wavefunction of H at the origin:

$$\left| \psi_{^2S_{1/2}}(0) \right|^2 = \frac{1}{8\pi r_B^3} \tag{6.109}$$

where r_B is the Bohr radius. From Eqs. (6.107) and (6.105) the Lamb shift in the ${}^2S_{1/2}$ energy level of the H atom is:

$$\langle \Delta U \rangle = \frac{e^2 r^3}{48\epsilon_0 r_B^3 \alpha c} \langle \omega(\text{vac}) \rangle . \tag{6.110}$$

The measured Lamb shift is:

$$\Delta f = 1.058 \times 10^9 \,\text{Hz} \sim 0.04 \,\text{cm}^{-1} \tag{6.111}$$

where:

$$\langle \Delta U \rangle = 2\pi\hbar \langle \Delta f \rangle . \tag{6.112}$$

Computing expectation values from the hydrogenic wavefunctions it is found that:

$$\frac{\langle r \rangle}{r_B}(1S) = \frac{3}{2}, \ \frac{\langle r \rangle}{r_B}(2S) = 6, \ \frac{\langle r \rangle}{r_B}(3S) = \frac{27}{2}. \tag{6.113}$$

The relevant value for ${}^2S_{1/2}$ is:

$$\langle r \rangle \left(2S_{1/2} \right) = 6 r_B. \tag{6.114}$$

This gives the mean vacuum angular frequency of an ensemble of vacuum wave particles:

$$\langle\omega(\text{vac})\rangle = \frac{96\pi\epsilon_0\alpha\hbar c r_B^3}{e^2 r^3}\Delta f = 3.96750 \times 10^8\,\text{rad}\,\text{s}^{-1}. \tag{6.115}$$

The de Broglie frequency of one vacuum particle is:

$$\omega(\text{vac}) = 1.80058 \times 10^{18}\,\text{rad}\,\text{s}^{-1}. \tag{6.116}$$

The ensemble averaged frequency is much lower than the de Broglie frequency, and the former is responsible for the Lamb shift in H. This means that there is a tiny universal anisotropy in the vacuum, and this is a tiny anisotropy of the universe itself, for example in the microwave background radiation. The ${}^2P_{1/2}$ wavefunction of atomic H vanishes at the origin and so there is no Lamb shift in this case.

The mass of the fundamental vacuum particle can be calculated from the experimentally observed anomalous g factor of the electron. The relativistic quantum theory of this chapter defines the interaction of the electron with the ECE 2 vacuum as follows:

$$\left(H - e\phi_W - mc^2\right)\psi = ie\hbar\,\boldsymbol{\sigma}\cdot\boldsymbol{\nabla}\left(\left(\frac{c^2\,\boldsymbol{\sigma}\cdot\mathbf{W}}{H - e\phi_W + mc^2}\right)\psi\right) + \cdots \tag{6.117}$$

where:

$$\Omega^\mu = \left(\Omega^{(0)}, \boldsymbol{\Omega}\right) = \frac{e}{\hbar}W^\mu. \tag{6.118}$$

Here ψ is the wave function and H is the hamiltonian of ECE 2 relativity:

$$H = \gamma mc^2 + U. \tag{6.119}$$

The potential energy in joules is defined as:

$$U = e\phi_W. \tag{6.120}$$

In the denominator on the right hand side of Eq (6.117):

$$H - e\phi_W = \gamma mc^2 \tag{6.121}$$

in which the Lorentz factor is defined by:

$$\gamma = \frac{\hbar\omega}{mc^2}. \tag{6.122}$$

It follows that:

$$\left(H - e\phi_W - mc^2\right)\psi = \frac{ie\hbar}{(1+\gamma)\,m}\boldsymbol{\sigma}\cdot\boldsymbol{\nabla}\,\boldsymbol{\sigma}\cdot\mathbf{W}\,\psi \tag{6.123}$$

whose real part (note 338(4) on `www.aias.us`) is:

$$\text{Real}\left(H - e\phi_W - mc^2\right)\psi = \frac{-e\hbar}{(1+\gamma)\,m}\boldsymbol{\sigma}\cdot\boldsymbol{\nabla}\times\mathbf{W}\,\psi. \tag{6.124}$$

Therefore the anomalous g factor of the electron is:

$$g = 1 + \gamma = 1 + \frac{\hbar\omega}{mc^2}. \tag{6.125}$$

For an electron at rest:

$$g = 1 + \frac{\hbar\omega_0}{mc^2} = 2 \tag{6.126}$$

because of the de Broglie equation for a rest particle:

$$\hbar\omega_0 = mc^2. \tag{6.127}$$

Notes 338(1) to 338(3) show that the frequency of an electron wave in contact with the ECE 2 vacuum is:

$$\omega_0 \rightarrow \omega_0 + \omega(\text{vac}) \tag{6.128}$$

so the anomalous g factor of the rest electron is:

$$g = 2 + \frac{\hbar\omega(\text{vac})}{mc^2} = 2.002319314 \tag{6.129}$$

to nine decimal places. Therefore

$$\hbar\omega(\text{vac}) = 0.002319314\ m(\text{vac})\, c^2. \tag{6.130}$$

It follows that the mass of the vacuum particle is given by the de Broglie Einstein equation:

$$m(\text{vac}) = \frac{\hbar\omega(\text{vac})}{c^2} = \frac{\hbar\Omega^{(0)}}{c} = 2.1127 \times 10^{-33}\,\text{kg}. \tag{6.131}$$

This calculation infers the existence of a new elementary particle whose mass is known with precision, and which is given the appellation "vacuum particle".

It follows from Ockham's Razor that hugely more complicated theories such as quantum electrodynamics are not needed to calculate the g factor of elementary particles. It is well known that QED is made up of adjustables and artificial procedures, so it is not a Baconian theory. It has problems of renormalization, dimensional regularization, summation of series with numerous terms, series whose convergence is dubious. It has virtual particles that can never be observed. QED is not an exact theory because of these adjustables and procedures, unknowables and unobservables – Pauli's "not even wrong" type of theory. Pauli meant that such a theory cannot be tested experimentally. Feynman himself described QED as dippy hocus pocus, and Dirac described it as an ugly theory. QCD has yet more difficulties.

The above calculation is a great improvement, it does not use the Dirac approximation, criticised earlier in this book, and is the first Baconian explanation of the anomalous g factor of the electron. It can be repeated for other elementary particles.

The effect of the vacuum wave/particle of angular frequency ω_1 on an electron wave/particle of angular frequency ω is:

$$\omega \rightarrow \omega + \omega_1. \tag{6.132}$$

The electron's wave vector is changed analogously:

$$\boldsymbol{\kappa} \rightarrow \boldsymbol{\kappa} + \boldsymbol{\kappa}_1. \tag{6.133}$$

The Einstein/de Broglie equations become:

$$E = \hbar\left(\omega + \omega_1\right) = \gamma mc^2 \tag{6.134}$$

$$\mathbf{p} = \hbar\left(\boldsymbol{\kappa} + \boldsymbol{\kappa}_1\right) = \gamma m\mathbf{v}_0 \tag{6.135}$$

and the Lorentz factor is changed to:

$$\gamma = \frac{\hbar}{mc^2}\left(\omega + \omega_1\right). \tag{6.136}$$

For the rest electron:

$$\gamma = \frac{\hbar}{mc^2}\left(\omega_0 + \omega_1\right) = 1 + \frac{\hbar\omega_1}{mc^2} \tag{6.137}$$

and as in Eq. (6.125) the anomalous g factor of the electron is:

$$g = 1 + \gamma. \tag{6.138}$$

The de Broglie / Einstein equation:

$$\hbar\omega_1 = \gamma m_1 c^2 \tag{6.139}$$

gives the mass of the vacuum particle.

In UFT 49 on `www.aias.us` the Hubble constant is defined to be:

$$H = \alpha c \tag{6.140}$$

where α is the power absorption coefficient thought to be responsible for the cosmological red shift. Eq. (6.140) rejects "big bang", which is refuted in ECE and ECE 2 theory [2]- [13]. Big bang has also been refuted experimentally. Now introduce the new equation:

$$H = v(\text{vac})\,\alpha_1 \tag{6.141}$$

where v(vac) is the velocity of the vacuum frame with respect to a static elementary particle and in which α_1 is a universal power absorption coefficient. These ideas are derivable from ECE 2 relativity. The Hubble constant in S. I. units is:

$$H = 2.333 \times 10^{-16}\text{s}^{-1} \tag{6.142}$$

and the velocity of the vacuum particle can be identified with that of the aether frame:

$$v(\text{vac}) = 0.068\, c. \tag{6.143}$$

Therefore the Hubble constant is:

$$H = 0.068\, c\alpha(\text{universal}). \tag{6.144}$$

It is proposed that α is a universal constant with S. I. Units of:

$$\alpha(\text{universal}) = 1.1444 \times 10^{-23}\, \text{m}^{-1} \tag{6.145}$$

and the conventional spectroscopic units of:

$$\alpha(\text{universal}) = 1.144 \times 10^{-25}\, \text{neper}\, \text{cm}^{-1}. \tag{6.146}$$

The Hubble constant no longer indicates that distant objects recede in an expanding universe. It means that light from distant objects is absorbed to a greater extent in an universe in equilibrium, an equilibrium between elementary and vacuum particles. The anthropomorphic concepts of beginning and end of the universe become irrelevant.

Compton scattering theory has been developed in the classic UFT 158 to UFT 248 and can be applied in the present context as described in notes 339(5) to 339(7). The original theory of Compton scattering has been greatly developed in UFT 158 to UFT 248, and relied on the scattering of an assumed massless photon from a massive electron. It was shown in these UFT papers that the original theory collapses completely when attempts are made to modify it for two particles with mass. The reason is that Compton scattering is elastic scattering, whereas particle collisions in general are inelastic and endoergic. In general there is transmutation, so the particle collision process is:

$$A + B \rightarrow C + D + E \tag{6.147}$$

where E is the energy released in the collision. It follows that the collision of the massive vacuum particle with a massive elementary particle produces energy from the ECE 2 vacuum. Crossover symmetry in particle physics implies that:

$$A + \bar{C} \rightarrow \bar{B} + D + E \tag{6.148}$$

where the bar denotes antiparticle.

In elastic collisions:

$$E = 0 \tag{6.149}$$

and elastic Compton scattering is denoted as:

$$\gamma + e^- \rightarrow \gamma + e^-. \tag{6.150}$$

By crossover symmetry:

$$\gamma \rightarrow e^+ \left(B \rightarrow \bar{C}\right) \tag{6.151}$$

and

$$e^- \rightarrow \gamma \left(C \rightarrow \bar{B} \right) \tag{6.152}$$

giving the annihilation of a positron and electron to give two photons:

$$e^- + e^+ \rightarrow 2\gamma. \tag{6.153}$$

In UFT 171 it was shown that an elastic, Compton type, theory cannot be applied to equal mass scattering, such a procedure produces nonsense. The correct theory must be inelastic with release of energy E:

$$e^- + e^+ \rightarrow 2\gamma + E. \tag{6.154}$$

Electron positron annihilation is well known ot be the basis of experiments for example at CERN. These produce many types of elementary particle as is well known. Similarly the scattering of a photon with mass from an electron makes sense if and only if:

$$\gamma + e^- \rightarrow \gamma + e^- + E. \tag{6.155}$$

Similarly the collision of two massive vacuum particles (denoted "vac") may lead to transmutation as follows:

$$\text{vac} + \text{vac} \rightarrow A + B + E \tag{6.156}$$

where A and B are elementary particles and E is energy from the ECE 2 vacuum. It is known experimentally that electron positron pairs emerge from the vacuum:

$$\text{vac} + \text{vac} \rightarrow e^- + e^+ + E. \tag{6.157}$$

The conservation of parity inversion symmetry requires that:

$$\text{vac} + \overline{\text{vac}} \rightarrow e^- + e^+ + E \tag{6.158}$$

because a vacuum particle has finite mass. A particle is its own antiparticle only if it is massless, and in ECE 2 there are no massless particles. This means that there exists a vacuum antiparticle. Synthesis of matter in the universe therefore occurs by:

$$\text{vac} + \overline{\text{vac}} \rightarrow A + \bar{A} + E. \tag{6.159}$$

where A and $\bar{A}$ denote any particle and antiparticle from which evolve stars, planets, galaxies and so on using well known processes. If m_1 denotes the mass of the vacuum particle, its collision with a static elementary particle of mass m_2 is governed by the law of conservation of energy:

$$\gamma m_1 c^2 + m_2 c^2 = \gamma' m_3 c^2 + \gamma'' m_4 c^2 + E \tag{6.160}$$

in which new particles of mass m_3 and m_4 appear. This process is detailed in Note 339(7).

6.2 Numerical Analysis and Graphics

6.2.1 Graphical Demonstration of Vector Potential Properties

We demonstrate some properties of the vector potential in order to explain that it is difficult to assess the type of vector potential from its appearance. First we consider a dipole vector field in two dimensions:

$$\mathbf{A}(X,Y) = q_1 \begin{pmatrix} \frac{X-X_0}{((X-X_0)^2+Y^2)^{3/2}} \\ \frac{Y}{((X-X_0)^2+Y^2)^{3/2}} \end{pmatrix} + q_2 \begin{pmatrix} \frac{X+X_0}{((X+X_0)^2+Y^2)^{3/2}} \\ \frac{Y}{((X+X_0)^2+Y^2)^{3/2}} \end{pmatrix}. \tag{6.161}$$

The direction vectors of this field have been graphed in Fig. 6.1, together with the equipotential lines following from the Coulomb-type potential

$$V(X,Y) = \frac{q_1}{((X-X_0)^2+Y^2)^{1/2}} + \frac{q_2}{((X-X_0)^2+Y^2)^{1/2}}. \tag{6.162}$$

The two values of charges were chosen different from each other: $q_1 = 1,\ q_2 = -1.6$. As a result, the potential and dipole field at the right hand side is much more contracted than at the left, and a rotational structure of directional vectors can be seen at the right hand side. Nevertheless, the curl of a dipole field vanishes as can be calculated from Eq. (6.161):

$$\boldsymbol{\nabla} \times \mathbf{A}(X,Y) = \mathbf{0}. \tag{6.163}$$

This seems not to be as expected at a first glance.

As a second example we consider the vector potential of an infinitely extended solenoid in cylindrical coordinates $(r,\ \theta,\ Z)$. From electrodynamics is known that the corresponding vector potential has only a θ component. It rises linearly within the solenoid (until radius a) and drops hyperbolically outside:

$$A_\theta = \begin{cases} fr & \text{for } r \le a \\ f\frac{a^2}{r} & \text{for } r > a \end{cases} \tag{6.164}$$

where f is a factor. The Z component of the curl of this vector potential is

$$(\boldsymbol{\nabla} \times \mathbf{A})_Z = \begin{cases} 2f & \text{for } r \le a \\ 0 & \text{for } r > a \end{cases}, \tag{6.165}$$

the other components are zero. This describes the fact that an idealized infinite solenoid contains a homogeneous magnetic field inside, and the magnetic field vanishes outside as is the case for the Aharonov Bohm effect. The vector potential is graphed in Fig. 6.2 with some circles describing isolines of the magnitude of $\mathbf{A}$. Although the structure of this potential is very regular compared to Fig. 6.1, the curl does not vanish in the inner part. The curl follows from the coordinate dependence of the $\mathbf{A}$ components in a quite intricate way.

Fig. 6.2 may serve as a demonstration of the potential for the Aharonov Bohm effect where the solenoid normally has a torus-like, closed form. Interpreting $\mathbf{A}$ as a vacuum potential, it may even be permitted that the curl does

not vanish outside. According to newest experimental results there may fluctuating electric and magnetic fields be present in the vacuum on a very short time scale. This justifies the approach for electron spin resonance (Eq. (6.49)) in this paper.

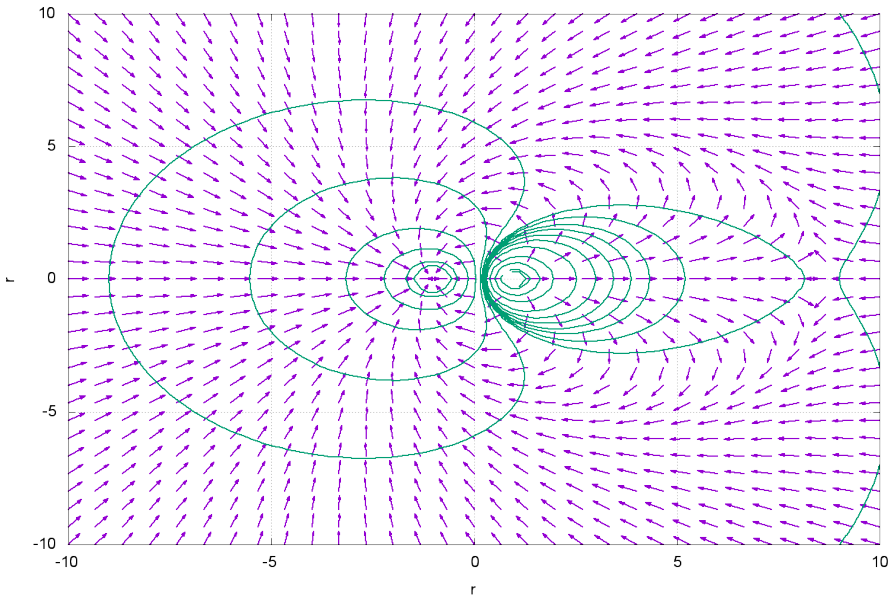

Figure 6.1: Equipotential lines and direction vectors of a dipole field.

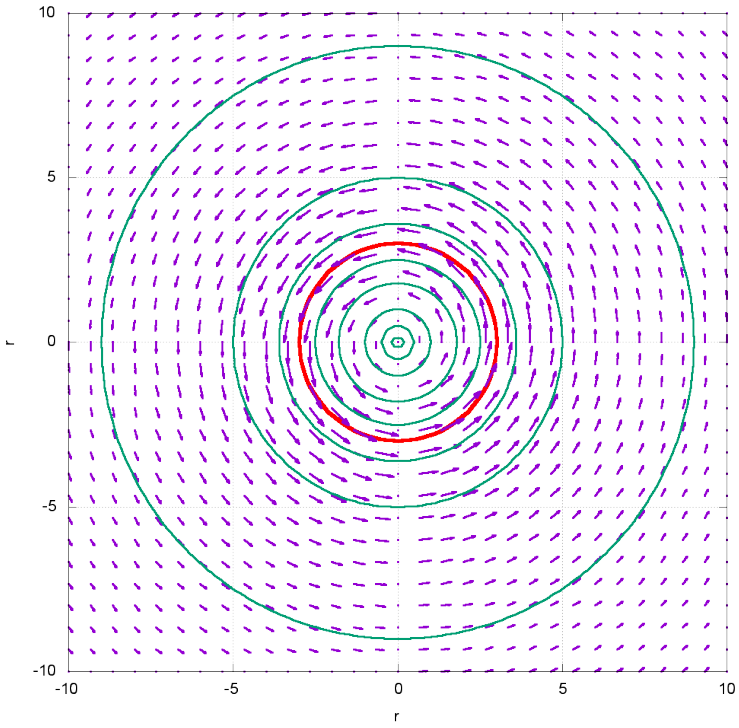

Figure 6.2: Vector potential and lines of equal magnitude for an infinite solenoid (cross section). The red circle indicates the radius of the solenoid.

Chapter 7

Precessional Theory

7.1 General Theory

ECE 2 theory gives an exact description of light deflection due to gravity and also of planar orbital precession, as described in UFT 342 and UFT 325, where a fundamental new hypothesis was introduced, one that imposed an upper bound on the Lorentz factor. It was shown in UFT 325 that massive particles such as electrons can travel at the speed of light without violating fundamental laws. This fact is well known experimentally at accelerators such as SLAC and CERN, which routinely accelerate electrons to c. The new hypothesis of UFT 325 also means that photons with mass can travel at c. In UFT 328 planar orbital precession was described without additional hypothesis simply by simultaneously solving the hamiltonian and lagrangian of ECE 2 theory. None of these methods use the incorrect and obsolete Einstein theory.

The planetary precession of the perihelion is known experimentally with claimed accuracy, although there have been severe criticisms by Myles Mathis and others, developed in the UFT papers on `www.aias.us` [2]- [13]. Accepting the experimental claims for the sake of argument, the experimental data are summarized empirically as follows:

$$r = \frac{\alpha}{1 + \epsilon \cos(x\theta)} \tag{7.1}$$

$$x = 1 - \frac{3MG}{c^2 \alpha} \tag{7.2}$$

in plane polar coordinates (r, θ). Here M is the mass of an object around which an object m orbits. G is Newton's constant, c is the universal constant known as the vacuum speed of light and α is the half right latitude of the orbit, for example a precessing ellipse and ϵ is the eccentricity. Both α and ϵ are observable with precision. In the solar system x is very close to unity.

As in previous chapters the ECE 2 lagrangian is:

$$\mathscr{L} = -\frac{mc^2}{\gamma} - U \tag{7.3}$$

and the ECE 2 hamiltonian is:

$$H = \gamma mc^2 + U \tag{7.4}$$

in which the Lorentz factor is:

$$\gamma = \left(1 - \frac{v_N^2}{c^2}\right)^{-1/2}. \tag{7.5}$$

Note carefully that $\mathbf{v}_N$ is the Newtonian velocity. The experimentally observable velocity is always the relativistic velocity:

$$\mathbf{v} = \gamma \mathbf{v}_N. \tag{7.6}$$

In these equations U is the potential energy of attraction between m and M. The Euler Lagrange analysis of UFT 325 and UFT 328 defines the relativistic angular momentum:

$$L = \gamma m r^2 \dot{\theta} \tag{7.7}$$

which is a constant of motion:

$$\frac{dL}{dt} = 0. \tag{7.8}$$

The Newtonian and non precessing planar orbit is:

$$r = \frac{\alpha}{1 + \epsilon \cos\theta} \tag{7.9}$$

and is described by the non relativistic hamiltonian:

$$H = \frac{1}{2} m v_N^2 + U \tag{7.10}$$

and non relativistic lagrangian:

$$\mathscr{L} = \frac{1}{2} m v_N^2 - U. \tag{7.11}$$

In this case the non relativistic angular momentum:

$$L_0 = m r^2 \dot{\theta}_0 \tag{7.12}$$

is the constant of motion:

$$\frac{dL_0}{dt} = 0. \tag{7.13}$$

The relativistic angular velocity is

$$\omega = \frac{d\theta}{dt} \tag{7.14}$$

and the non relativistic angular velocity is:

$$\omega_0 = \frac{d\theta_0}{dt}. \tag{7.15}$$

The relativistic orbital velocity is defined as follows in terms of the relativistic angular momentum:

$$v^2 = \frac{L^2}{m^2 r^4}\left(r^2 + \left(\frac{dr}{d\theta}\right)^2\right). \tag{7.16}$$

From Eqs. (7.1) and (7.16):

$$v^2 = \frac{L^2}{m^2}\left(\frac{1}{r^2} + \frac{x^2\epsilon^2}{\alpha^2}\sin^2(x\theta)\right). \tag{7.17}$$

Eq. (7.6) means that:

$$v^2 = \frac{v_N^2}{1 - \frac{v_N^2}{c^2}}. \tag{7.18}$$

From Eq. (7.9):

$$v_N^2 = \frac{L_0^2}{m^2}\left(\frac{1}{r^2} + \frac{\epsilon^2}{\alpha^2}\sin^2\theta\right). \tag{7.19}$$

It follows from Eqs. (7.18), (7.17) and (7.19) that:

$$L^2\left(\frac{1}{r^2} + \frac{x^2\epsilon^2}{\alpha^2}\sin^2(x\theta)\right) = \frac{L_0^2\left(\frac{1}{r^2} + \frac{\epsilon^2}{\alpha^2}\sin^2\theta\right)}{1 - \left(\frac{L_0}{mrc}\right)^2\left(\frac{1}{r^2} + \frac{\epsilon^2}{\alpha^2}\sin^2\theta\right)} \tag{7.20}$$

an equation which is analyzed numerically and graphically later in this chapter. It is demonstrated that $r(\theta)$ from Eq. (7.20) is a precessing ellipse. This confirms the results of UFT 328 and shows that ECE 2 relativity produces a precessing ellipse directly from the lagrangian and hamiltonian, without any additional assumption. This theory is Lorentz covariant in a space of finite torsion and curvature and is part of the ECE 2 generally covariant unified field theory.

In UFT 343 the Thomas and de Sitter precessions are developed with ECE 2 relativity. In the standard physics, Thomas precession is the rotation of the Minkowski line element and de Sitter precession is the rotation of the Schwarzschild line element. In previous UFT papers [2]- [13] it has been shown that the derivation of the Schwarzschild line element is riddled with errors, notably it is based on an incorrect geometry without torsion. The Thomas frame rotation in the Newtonian limit is:

$$\theta_1 = \theta + \omega_\theta t \tag{7.21}$$

where ω_θ is the constant angular velocity of frame rotation. The angle θ_1 is that of a rotating plane polar coordinate system denoted (r, θ_1). The total angular velocity is defined by:

$$\omega_1 = \frac{d\theta_1}{dt} = \frac{d\theta}{dt} + \omega_\theta \tag{7.22}$$

and the classical lagrangian is:

$$\mathscr{L}_1 = \frac{1}{2}mv_1^2 - U \tag{7.23}$$

where:

$$v_1^2 = \left(\frac{dr}{dt}\right)^2 + r^2\left(\frac{d\theta_1}{dt}\right)^2. \tag{7.24}$$

The Euler Lagrange equations are:

$$\frac{\partial \mathscr{L}_1}{\partial \theta_1} = \frac{d}{dt}\frac{\partial \mathscr{L}_1}{\partial \dot{\theta}_1} \tag{7.25}$$

and

$$\frac{\partial \mathscr{L}_1}{\partial r} = \frac{d}{dt}\frac{\partial \mathscr{L}_1}{\partial \dot{r}} \tag{7.26}$$

from which the conserved angular momentum in the rotating frame is:

$$L_1 = mr^2\frac{d\theta_1}{dt} = L + \omega_\theta m r^2 \tag{7.27}$$

where:

$$L = mr^2\frac{d\theta}{dt} \tag{7.28}$$

is the conserved angular momentum of the static frame (r, θ). Both L_1 and L are constants of motion.

The hamiltonian in the rotating frame is:

$$H_1 = \frac{1}{2}m\left(\frac{dr}{dt}\right)^2 + \frac{1}{2}\frac{L_1^2}{mr^2} + U(r) \tag{7.29}$$

where:

$$U(r) = -\frac{mMG}{r} \tag{7.30}$$

is the gravitational potential. As shown in Note 343(2) the hamiltonian produces the rotating conic section:

$$r = \frac{\alpha_1}{1 + \epsilon_1 \cos(\theta + \omega_\theta t)} \tag{7.31}$$

in which the time is defined by:

$$t = \int \left(\frac{2}{m} (H - U) - \frac{L_1^2}{m^2 r^2} \right)^{-1/2} dr. \tag{7.32}$$

Eqs. (7.31) and (7.32) can be solved simultaneously by computer algebra to give r in terms of θ. As shown in Note 343(4):

$$\theta = \cos^{-1} \left(\frac{1}{\epsilon_1} \left(\frac{\alpha_1}{r} - 1 \right) \right) - \omega_\theta \int \left(\frac{2}{m} (H - U) - \frac{L_1^2}{m^2 r^2} \right)^{-1/2} dr \tag{7.33}$$

an equation that can be inverted numerically to give a plot of r against θ, the required orbit.

The orbit of de Sitter precession follows immediately as:

$$r = \frac{\alpha_1}{1 + \epsilon_1 \cos(x\theta_1)} \tag{7.34}$$

where it is known experimentally that:

$$x = 1 - \frac{3MG}{c^2 \alpha_1}. \tag{7.35}$$

The half right latitude of the rotating frame is:

$$\alpha_1 = \frac{L_1^2}{m^2 MG} \tag{7.36}$$

and the eccentricity in the rotating frame is:

$$\epsilon_1 = \left(1 + \frac{2H_1 L_1^2}{m^3 M^2 G^2} \right)^{1/2}. \tag{7.37}$$

The reason for Eq. (7.34) is that de Sitter or geodedic precession is defined by rotating the plane polar coordinates system in which the precession of the planar orbit is observed. The original method by Sitter was much more complicated and based on the incorrect Einstein field equation.

In contrast, Eq. (7.34) is rigorously correct and much simpler, and based on the theory of ECE 2 relativity.

The orbital velocity from Eq. (7.31) is:

$$v_{N1}^2 = \frac{L_1^2}{m^2 r^4} \left(r^2 + \left(\frac{dr}{d\theta} \right)^2 \right) \tag{7.38}$$

in which the relativistic velocity is:

$$v^2 = v_{N1}^2 \left(1 - \frac{v_{N1}^2}{c^2} \right)^{-1}. \tag{7.39}$$

The relativistic velocity is the one defined by Eq. (7.34):

$$v^2 = \frac{L^2}{m^2} \left(\frac{1}{r^2} + \frac{x^2 \epsilon^2}{\alpha^2} \sin^2(x\theta_1) \right). \tag{7.40}$$

It follows that:

$$\frac{L^2}{m^2}\left(\frac{1}{r^2}+\frac{x^2\epsilon^2}{\alpha^2}\sin^2(x\theta_1)\right)=\frac{L_1^2\left(\frac{1}{r^2}+\frac{\epsilon_1^2}{\alpha_1^2}\sin^2\theta_1\right)}{1-\left(\frac{L_1}{mrc}\right)^2\left(\frac{1}{r^2}+\frac{\epsilon_1^2}{\alpha_1^2}\sin^2\theta_1\right)} \tag{7.41}$$

in which both L and L_1 are constants of motion. Here θ_1 is defined by:

$$\theta_1=\theta+\omega_\theta t. \tag{7.42}$$

The velocity of the Thomas precession is: the relativistic velocity:

$$v_T^2=\frac{L_1^2\left(\frac{1}{r^2}+\frac{\epsilon_1^2}{\alpha_1^2}\sin^2\theta_1\right)}{1-\left(\frac{L_1}{mrc}\right)^2\left(\frac{1}{r^2}+\frac{\epsilon_1^2}{\alpha_1^2}\sin^2\theta_1\right)} \tag{7.43}$$

and the Thomas angular velocity (the relativistic angular velocity) is:

$$\Omega_T=\frac{v_T}{r}. \tag{7.44}$$

This was used in UFT 110 to define the Thomas phase shift.

In the numerical analysis and graphics of UFT 343 it is shown that the Thomas precession produces a precessing orbit, which is therefore produced by rotating the plane polar coordinate system.

Planetary precession can also be thought of as a Larmor precession as described in UFT 344, it is the Larmor precession produced by the torque between the gravitomagnetic field of the sun and the gravitomagnetic dipole moment of the planet. In general any astronomical precession can be be explained with the ECE 2 gravitational field equations. This goes beyond what the obsolete Einstein theory was capable of. In UFT 318 the ECE 2 gravitational field equations were derived in a space in which equation are Lorentz covariant, and in which the torsion and curvature are both non zero. This is known as ECE 2 covariance. In UFT 117 and UFT 119 the gravitomagnetic Ampère law was used to describe the earth's gravitomagnetic precession and the precession of the equinox.

Consider the magnetic dipole moment of electromagnetism:

$$\mathbf{m}=-\frac{e}{2m}\mathbf{L} \tag{7.45}$$

where $-e$ is the charge on the electron, m its mass and $\mathbf{L}$ its orbital angular momentum. The following torque:

$$\mathbf{Tq}=\mathbf{m}\times\mathbf{B} \tag{7.46}$$

is produced between $\mathbf{m}$ and a magnetic flux density $\mathbf{B}$. Such a torque is animated by the well known Evans Pelkie animation on `www.aias.us` and youtube. The Larmor pecessional frequency due to the torque is:

$$\omega_L=\frac{eg}{2m}B \tag{7.47}$$

where g is the Landé factor described in previous chapters.

This well known theory can be adapted for planetary precession by calculating the gravitomagnetic dipole moment and using the orbital angular momentum of a planet. The charge $-e$ on the electron is replaced by the orbiting mass m, so the gravitomagnetic dipole moment is:

$$\mathbf{m}_g = \frac{m}{2m}\mathbf{L} = \frac{1}{2}\mathbf{L} \tag{7.48}$$

and is a constant of motion. The orbital angular momentum is defined by:

$$\mathbf{L} = \mathbf{r} \times \mathbf{p} = m\mathbf{r} \times \mathbf{v} \tag{7.49}$$

where $\mathbf{v}$ is the orbital velocity of m and where $\mathbf{r}$ is the distance between m and M. Therefore:

$$\mathbf{m}_g = \frac{m}{2}\mathbf{r} \times \mathbf{v}. \tag{7.50}$$

In general this theory is valid for any type of orbit, but for a planar orbit:

$$\mathbf{L} = mrv\mathbf{k}. \tag{7.51}$$

A torque is formed between $\mathbf{m}_g$ and the gravitomagnetic field $\mathbf{\Omega}$ of ECE 2 general relativity:

$$\mathbf{Tq} = \mathbf{m}_g \times \mathbf{\Omega} \tag{7.52}$$

resulting in the gravitomagnetic Larmor precession frequency:

$$\omega_g = \frac{1}{2}g_r\Omega \tag{7.53}$$

where g_r is the gravitomagnetic Landé factor. The precession frequency of a planet in this theory is the gravitomagnetic Larmor precession frequency. For example consider the sun to be a rotating sphere. It rotates every 27 days or so around an axis tilted to the axis of rotation of the earth, so $\mathbf{L}_{\text{earth}}$ is not parallel to $\mathbf{L}_{\text{sun}}$ and there is a non zero torque. The gravitomagnetic field of this rotating sphere in the dipole approximation is:

$$\mathbf{\Omega}_{\text{sun}} = \frac{2G}{c^2r^3}\left(\mathbf{L}_{\text{sun}} - 3\left(\mathbf{L}_{sun} \cdot \frac{\mathbf{r}}{r}\right)\frac{\mathbf{r}}{r}\right) \tag{7.54}$$

Here $\mathbf{r}$ is the distance from the sun to the earth. The rotation axis of the sun is tilted by 7.25° to the axis of the earth's orbit, so to a good approximation:

$$\mathbf{L}_{\text{sun}} \cdot \mathbf{r} \sim 0 \tag{7.55}$$

and in this approximation:

$$\mathbf{\Omega}_{\text{sun}} = \frac{2G}{c^2r^3}\mathbf{L}_{\text{sun}}. \tag{7.56}$$

The torque is therefore:

$$\mathbf{Tq} = \frac{G}{c^2 r^3}\mathbf{L}_{\text{earth}} \times \mathbf{L}_{\text{sun}} \tag{7.57}$$

and is non zero if and only if $\mathbf{L}_{\text{sun}}$ and $\mathbf{L}_{\text{earth}}$ are not parallel, where $\mathbf{L}_{\text{earth}}$ is the angular momentum of the earth's spin and $\mathbf{L}_{\text{sun}}$ is that of the sun's spin. The angle subtended by $\mathbf{L}_{\text{earth}}$ and $\mathbf{L}_{\text{sun}}$ is approximately $7.25°$.

The magnitude of the angular momentum of the sun can be modelled in the first approximation by that of a spinning sphere:

$$L = \omega I = \frac{2}{5}MR^2 \tag{7.58}$$

where I is the moment of inertia and $\mathbf{R}$ the radius of the sun. Therefore the magnitude of the gravitomagnetic field of the sun is:

$$\Omega_{\text{sun}} = \frac{MG\omega}{5c^2 R} \tag{7.59}$$

where ω is its angular velocity. After a rotation of 2π radians:

$$\omega = \frac{2\pi}{T} \tag{7.60}$$

where T is about 27 days. Therefore:

$$\Omega_{\text{sun}} = \frac{\pi}{5}\frac{r_0}{R}\frac{1}{T} \tag{7.61}$$

where:

$$r_0 = \frac{2MG}{c^2} = 2.95 \times 10^3\,\text{m} \tag{7.62}$$

and where the radius of the sun is:

$$R = 6.957 \times 10^9\,\text{m}. \tag{7.63}$$

In one earth year (365.25 days):

$$\Omega_{\text{sun}} = 365.25 \times 24 \times 3600\,\frac{\pi}{5}\frac{r_0}{R}\frac{1}{T} \tag{7.64}$$

in radians per year.

The Larmor precession frequency at the distance R is:

$$\omega_L = 1.802 \times 10^{-6}\,g_{\text{eff}}\,\text{rad}\,\text{s}^{-1} \tag{7.65}$$

where g_{eff} is the gravitomagnetic Landé factor. The observed perihelion precession of the earth at the earth sun distance is:

$$\omega(\text{perihelion}) = 5.741 \times 10^{-21}\,\text{rad}\,\text{s}^{-1}. \tag{7.66}$$

Therefore the earth's gravitomagnetic Landé factor is:

$$g_{\text{eff}}(\text{earth}) = 2\frac{\omega_g}{\Omega}. \tag{7.67}$$

Each planet has its characteristic g_{eff} and in general every object m in orbit around an object M has its own g_{eff}. This theory is rigorously correct and is again much simpler than the incorrect Einstein theory. In general, perihelion precession is a Larmor precession frequency:

$$\omega_L = g_{\text{eff}}\,\frac{\pi}{10}\left(\frac{r_0}{R}\right)\frac{1}{T}. \tag{7.68}$$

In one earth year, or revolution through 2π radians, the precession frequency at the point R is:

$$\omega_L = 365.25 \times 3600 \times 24\, g_{\text{eff}}\,\frac{\pi}{10}\left(\frac{r_0}{R}\right)\frac{1}{T}. \tag{7.69}$$

The experimentally observed precession of the perihelion is:

$$\omega_L = \frac{6\pi GM}{ac^2\left(1-\epsilon^2\right)}. \tag{7.70}$$

Later in this chapter this theory is developed numerically and graphically using spherical polar coordinates.

The well known geodetic and Lense Thirring precessions can be calculated straightforwardly in ECE 2 theory as in UFT 345. Consider the gravitomagnetic field of the earth in the dipole approximation [2]- [13], first used in UFT 117:

$$\boldsymbol{\Omega} = \frac{2}{5}\frac{MGR^2}{c^2r^3}\left(\boldsymbol{\omega} - 3\mathbf{n}\left(\boldsymbol{\omega}\cdot\mathbf{n}\right)\right) \tag{7.71}$$

where the earth is considered to be a spinning sphere. In Eq. (7.71), M is the mass of the earth, R is the radius of the earth, r is the distance from the centre of the earth to a satellite such as Gravity Probe B, $\boldsymbol{\omega}$ is the angular velocity vector of the earth and $\mathbf{n}$ is the unit vector defined by:

$$\mathbf{n} = \frac{\mathbf{r}}{r}. \tag{7.72}$$

Gravity Probe B was in polar orbit, orbiting in a plane perpendicular to the equator in a geocentric orbit. The angular velocity vector of the spinning earth is:

$$\boldsymbol{\omega} = \omega\mathbf{k} \tag{7.73}$$

because the earth spins around the k axis perpendicular to the equator. The distance between the centre of the earth and Gravity Probe B is defined in the plane perpendicular to $\mathbf{k}$:

$$\mathbf{r} = Y\mathbf{j} + Z\mathbf{k} \tag{7.74}$$

so:

$$\boldsymbol{\omega} - 3\mathbf{n}\left(\boldsymbol{\omega}\cdot\mathbf{n}\right) = \omega\left(\left(1-\frac{3Z^2}{r^2}\right)\mathbf{k} - \frac{3YZ}{r^2}\mathbf{j}\right). \tag{7.75}$$

The experimental inclination of Gravity Probe B was almost exactly 90°.

Therefore in the dipole approximation, as in UFT 117:

$$\boldsymbol{\Omega} = \frac{2}{5}\frac{MGR^2}{c^2r^3}\omega\left(\left(1-\frac{3Z^2}{r^2}\right)\mathbf{k} - \frac{3YZ}{r^2}\mathbf{j}\right). \tag{7.76}$$

The Gravity Probe B spacecraft carried precision gyroscopes which are currents of mass and which are therefore gravitomagnetic dipole moments ($\mathbf{m}$). The torque between the earth and the spacecraft is:

$$\mathbf{Tq} = \mathbf{m}\times\boldsymbol{\Omega} \tag{7.77}$$

and produces the Larmor precession frequency:

$$\Omega_{\mathrm{LT}} = \frac{1}{2}|\boldsymbol{\Omega}|. \tag{7.78}$$

This is known in the standard literature as Lense Thirring precession. The relevant data are as follows:

$$\begin{aligned} M &= 5.98\times10^{24}\,\mathrm{kg}\\ R &= 6.37\times10^{6}\,\mathrm{m}\\ r &= 7.02\times10^{6}\,\mathrm{m}\\ c &= 2.998\times10^{8}\,\mathrm{ms}^{-1}\\ G &= 6.67\times10^{-11}\,\mathrm{m}^3\mathrm{kg}^{-1}\mathrm{s}^{-2}\\ \omega &= 7.292\times10^{-5}\,\mathrm{rad\,s}^{-1}. \end{aligned} \tag{7.79}$$

At the equator:

$$\boldsymbol{\omega}\cdot\mathbf{n} = 0 \tag{7.80}$$

and the magnitude of the gravitomagnetic field of the earth from Eq. (7.76) is:

$$\Omega = 1.52\times10^{-14}\,\mathrm{rad\,s}^{-1} \tag{7.81}$$

compared with the experimental value from UFT 117 of:

$$\Omega(\mathrm{exp}) = 1.26\times10^{-14}\,\mathrm{rad\,s}^{-1}. \tag{7.82}$$

More generally:

$$\boldsymbol{\omega}\cdot\mathbf{n} = \frac{Z}{r}\omega\mathbf{k} \tag{7.83}$$

and:

$$3\mathbf{n}\left(\boldsymbol{\omega}\cdot\mathbf{n}\right)=\frac{3Z\omega}{r^2}\left(Y\mathbf{j}+Z\mathbf{k}\right). \tag{7.84}$$

It follows that:

$$\boldsymbol{\omega}-3\mathbf{n}\left(\boldsymbol{\omega}\cdot\mathbf{n}\right)=\omega\mathbf{k}-\frac{3\omega Z}{r}\left(\frac{Y}{r}\mathbf{j}+\frac{Z}{r}\mathbf{k}\right). \tag{7.85}$$

Defining:

$$\sin\theta=\frac{Z}{r},\ \cos\theta=\frac{Y}{r} \tag{7.86}$$

then:

$$\boldsymbol{\omega}-3\mathbf{n}\left(\boldsymbol{\omega}\cdot\mathbf{n}\right)=\omega\left(-3\sin^2\theta\,\mathbf{k}-3\sin\theta\cos\theta\,\mathbf{j}\right). \tag{7.87}$$

Therefore the Lense Thirring precession is:

$$\Omega_{\mathrm{LT}}=\frac{MGR^2\omega}{5c^2r^3}\left|\left(1-3\sin^2\theta\right)\mathbf{k}-3\sin\theta\cos\theta\,\mathbf{j}\right|. \tag{7.88}$$

Later in this chapter an average value of the precession is worked out and the latitude identified for precise agreement with Gravity Probe B. In general the Lense Thirring precession depends on latitude, so it is assumed that the experimental result is an average. It is not clear from the literature how the Lense Thirring effect is isolated experimentally from the geodetic precession. For the sake of argument we accept the experimental claims.

The analogue of Eq. (7.71) in magnetostatics is:

$$\mathbf{B}=\frac{\mu_0}{4\pi r^3}\left(\mathbf{m}-3\mathbf{n}\left(\mathbf{m}\cdot\mathbf{n}\right)\right) \tag{7.89}$$

where μ_0 is the magnetic permeability in vacuo. In Eq. (7.89) $\mathbf{m}$ is the magnetic dipole moment:

$$\mathbf{m}=-\frac{e}{2m}\mathbf{L}. \tag{7.90}$$

The gravitomagnetic vacuum permeability of the ECE 2 field equations is:

$$\mu_{0G}=\frac{4\pi G}{c^2} \tag{7.91}$$

so:

$$\boldsymbol{\Omega}=\frac{G}{c^2r^3}\left(\mathbf{m}_g-3\mathbf{n}\left(\mathbf{m}_g\cdot\mathbf{n}\right)\right) \tag{7.92}$$

where the gravitomagnetic dipole moment $\mathbf{m}_g$ is defined in analogy to Eq. (7.90) by

$$\mathbf{m}_g=\frac{1}{2}\mathbf{L}. \tag{7.93}$$

The angular momentum of the spinning spherical earth is:

$$\mathbf{L} = \frac{2}{5} MR^2 \boldsymbol{\omega} \tag{7.94}$$

so:

$$\Omega = \frac{MGR^2\omega}{5c^2r^3} = 49.4 \text{ millarcsec per year.} \tag{7.95}$$

The geodetic precession is is calculated from the same starting equation as the Lense Thirring precession:

$$\Omega = \frac{MG}{2c^2r} \left| \boldsymbol{\omega} - 3\mathbf{n} \left(\boldsymbol{\omega} \cdot \mathbf{n} \right) \right| . \tag{7.96}$$

The vector $\mathbf{r}$ is defined by Eq. (7.74) because Gravity Probe B was in polar orbit once every 90 minutes, giving an angular velocity of:

$$\omega = \frac{2\pi}{90 \times 60} = 1.164 \times 10^{-3} \, \mathrm{rad\, s^{-1}}. \tag{7.97}$$

As seen from a frame of reference fixed on Gravity Probe B, the earth rotates at a given angular velocity, generating the angular momentum:

$$\mathbf{L} = Mr\boldsymbol{\omega} \tag{7.98}$$

for an assumed circular orbit, a good approximation to the orbit of Gravity Probe B. If it is assumed that:

$$\boldsymbol{\omega} = \omega_X \mathbf{i} \tag{7.99}$$

perpendicular to the polar orbit, then:

$$\Omega = \frac{MG\omega}{2c^2r}. \tag{7.100}$$

For the earth:

$$\frac{MG}{2c^2} = 2.12175 \times 10^{-3} \, \mathrm{m}. \tag{7.101}$$

If it is assumed that r is the distance from the centre of the earth to Gravity Probe B then:

$$r = 7.02 \times 10^6 \, \mathrm{m} \tag{7.102}$$

giving:

$$\Omega = 3.677 \times 10^{-13} \, \mathrm{rad\, s^{-1}}. \tag{7.103}$$

The experimental claim is:

$$\Omega(\mathrm{exp}) = 1.016 \times 10^{-12} \, \mathrm{rad\, s^{-1}}. \tag{7.104}$$

The theory is in good agreement with the experimental claim. It has been assumed that the angular momentum needed for Eq. (7.96) is generated by a static earth in a rotating frame. This is the passive rotation equivalent to the active rotation of Gravity Probe B around the centre of the earth in a polar orbit once every ninety minutes. Exact agreement with the experimental data can be obtained by assuming an effective gravitomagnetic Landé factor, or by assuming that the rotation is described more generally by:

$$\boldsymbol{\omega} = \omega_X \mathbf{i} + \omega_Y \mathbf{j} \tag{7.105}$$

and

$$\mathbf{r} = Y\mathbf{j} + Z\mathbf{k}. \tag{7.106}$$

Later on in this chapter, computer algebra and graphics are used to evaluate the magnitude:

$$x = |\boldsymbol{\omega} - 3\mathbf{n}\,(\boldsymbol{\omega} \cdot \mathbf{n})| \tag{7.107}$$

from Eqs. (7.105) and (7.106). Therefore exact agreement with Gravity Probe B can be obtained from the gravitational field equations of ECE 2.

These field equations can be used to explain any astronomical precession in terms of magnitude of vorticity and the result can be expressed in terms of the tetrad and spin connection of Cartan geometry. This theory can be applied to the Lense Thirring, geodetic and perihelion precessions to give exact agreement in each case in terms of the vorticity of the underlying mathematical space of the ECE 2 theory. The perihelion precession in this type of theory is developed in terms of the orbital angular momentum of the sun as seen from the earth. In general any precession can be developed in terms of the magnitude of the vorticity spacetime, which can be expressed in terms of a well defined combination of tetrad and spin connection. This combination appears in the ECE 2 gravitational field equations.

As shown in Notes 346(1) to 346(3) any precession can be described in the dipole approximation in terms of angular momentum $\mathbf{L}$:

$$\Omega = \frac{G}{2c^2}\left|\boldsymbol{\nabla} \times \left(\frac{\mathbf{L} \times \mathbf{r}}{r^3}\right)\right| = \frac{G}{2c^2 r^3}\left|\frac{3\mathbf{r}}{r}\left(\frac{\mathbf{r}}{r} \cdot \mathbf{L}\right) - \mathbf{L}\right|. \tag{7.108}$$

When this equation is applied to perihelion precession of the earth about the sun, $\mathbf{r}$ is the distance from the earth to the sun. If the sun is considered to rotate about an axis $\mathbf{k}$, the plane of the earth's orbit is inclined to the plane perpendicular to $\mathbf{k}$ at an angle of 7.25°. So as in Note 346(3):

$$\mathbf{r} = \mathbf{i}X\cos\theta + \mathbf{k}X\sin\theta + Y\mathbf{j}. \tag{7.109}$$

The observed precession of the earth's perihelion is:

$$\Omega = (0.05 \pm 0.012)'' \text{ a year } = 7.681 \times 10^{-15}\,\text{rad}\,\text{s}^{-1}. \tag{7.110}$$

From the earth, the sun appears to be orbiting with an angular momentum:

$$\mathbf{L} = Mr^2\boldsymbol{\omega} \tag{7.111}$$

where M is the mass of the sun, and where $\boldsymbol{\omega}$ is the angular frequency of the orbit. The earth rotates around the sun once every year, or 3.156×10^7 sec, so:

$$\omega = \frac{2\pi}{3.156 \times 10^7} \,\mathrm{rad\,s^{-1}} \tag{7.112}$$

Using:

$$r = 1.4958 \times 10^{11} \,\mathrm{m} \tag{7.113}$$

$$\frac{MG}{c^2} = 1.475 \times 10^3 \,\mathrm{m} \tag{7.114}$$

the perihelion precession is found to be:

$$\Omega = 0.981 \times 10^{-15} \,\mathrm{rad\,s^{-1}}. \tag{7.115}$$

The experimental result is:

$$\Omega(\mathrm{exp}) = 7.681 \times 10^{-15} \,\mathrm{rad\,s^{-1}}. \tag{7.116}$$

Exact agreement can be found by using an effective angular momentum L. The above theory has used a circular orbit in the first approximation.

The fundamental assumption is that the orbit of the earth about the sun produces a torque:

$$\mathbf{Tq} = \mathbf{m}_g \times \boldsymbol{\Omega} \tag{7.117}$$

where $\mathbf{m}_g$ is the gravitomagnetic dipole moment:

$$\mathbf{m}_g = \frac{1}{2}\mathbf{L} \tag{7.118}$$

and where $\boldsymbol{\Omega}$ is the gravitomagnetic field. Here $\mathbf{L}$ is the orbital angular momentum. The gravitomagnetic field is the curl of the gravitomagnetic vector potential:

$$\boldsymbol{\Omega} = \boldsymbol{\nabla} \times \mathbf{W}_g \tag{7.119}$$

so:

$$\mathbf{W}_g = \frac{G}{2c^2 r^3}\mathbf{L} \times \mathbf{r}. \tag{7.120}$$

In direct analogy, the Lense Thirring precession of the earth with respect to the sun is due to to the latter's spin angular momentum about its own axis. The sun spins once every 27 days about its axis, so the relevant angular momentum in this case is the spin angular momentum of the sun:

$$\mathbf{L}_{\mathrm{sun}} = \frac{2}{5}MR^2\boldsymbol{\omega} = I\boldsymbol{\omega}. \tag{7.121}$$

Similarly the Lense Thirring precession of Gravity Probe B is due to the spin of the earth every 24 hours. This spin produces a mass current and a gravitomagnetic dipole moment:

$$\mathbf{m}_g(\text{spin}) = \frac{1}{2}\mathbf{L}_s \tag{7.122}$$

due to spin angular momentum.

The perihelion precession of the earth is a geodetic precession caused by an orbital angular momentum, the orbital angular momentum of the sun, which is observed in a frame of reference fixed on the earth.

As in previous chapters the magnetic flux density $\mathbf{B}$ of ECE 2 theory can be defined by curvature through the $\mathbf{W}$ potential:

$$\mathbf{B} = \boldsymbol{\nabla} \times \mathbf{W} = \boldsymbol{\nabla} \times \mathbf{A} + 2\boldsymbol{\omega}_s \times \mathbf{A}. \tag{7.123}$$

The $\mathbf{A}$ potential is defined by torsion, and $\boldsymbol{\omega}_s$ is the spin connection vector. In precise analogy the gravitomagnetic field is defined by:

$$\boldsymbol{\Omega} = \boldsymbol{\nabla} \times \mathbf{W}_g = \boldsymbol{\nabla} \times \mathbf{A}_g + 2\boldsymbol{\omega}_s \times \mathbf{A}_g. \tag{7.124}$$

where:

$$\mathbf{A}_g^{\mu} = (\Phi_g, c\mathbf{A}_g) \tag{7.125}$$

and where Φ_g is the scalar potential of gravitation. Note that $\mathbf{W}_g$ has the units of linear velocity, so:

$$\boldsymbol{\Omega} = \boldsymbol{\nabla} \times \mathbf{v}_g \tag{7.126}$$

which defines the gravitomagnetic field as a vorticity in analogy with fluid dynamics. This analogy is developed later in this book in chapters eight and nine. The vorticity is that of spacetime, or the aether or vacuum.

It follows that any precession can be defined precisely as follows:

$$\Omega = \frac{1}{2}|\boldsymbol{\Omega}| = \frac{1}{2}\left|\boldsymbol{\nabla} \times \mathbf{v}_g\right| \tag{7.127}$$

so all precessions of the universe are due to the vorticities of ECE 2 spacetime, vacuum or aether. If it is assumed that:

$$\boldsymbol{\nabla} \cdot \mathbf{v}_g = 0 \tag{7.128}$$

then the spacetime is inviscid, and in chapters 8 and 9 it is shown that spacetime is in general a fluid. The field equations of fluid dynamics can be unified with those of electrodynamics and gravitation.

The equations of gravitomagnetostatics are:

$$\boldsymbol{\nabla} \times \boldsymbol{\Omega} = \boldsymbol{\kappa} \times \boldsymbol{\Omega} = \frac{4\pi G}{c^2}\mathbf{J}_m \tag{7.129}$$

where:

$$\boldsymbol{\kappa} = \frac{1}{r^{(0)}}\mathbf{q} - \boldsymbol{\omega}_s. \tag{7.130}$$

Here $\mathbf{J}_m$ is the current density of mass, $\mathbf{q}$ is the tetrad vector, $\boldsymbol{\omega}_s$ is the spin connection vector, and $r^{(0)}$ is a scalar with units of metres. It follows from Eq. (7.129) that

$$\boldsymbol{\nabla} \cdot \boldsymbol{\nabla} \times \boldsymbol{\Omega} = \boldsymbol{\nabla} \cdot \boldsymbol{\kappa} \times \boldsymbol{\Omega} = 0. \tag{7.131}$$

Now use:

$$\boldsymbol{\nabla} \cdot (\boldsymbol{\kappa} \times \boldsymbol{\Omega}) = \boldsymbol{\Omega} \cdot (\boldsymbol{\nabla} \times \boldsymbol{\kappa}) - \boldsymbol{\kappa} \cdot (\boldsymbol{\nabla} \times \boldsymbol{\Omega}) = 0 \tag{7.132}$$

so:

$$\boldsymbol{\Omega} \cdot (\boldsymbol{\nabla} \times \boldsymbol{\kappa}) = \boldsymbol{\kappa} \cdot \boldsymbol{\nabla} \times \boldsymbol{\Omega}. \tag{7.133}$$

One possible solution is:

$$\boldsymbol{\Omega} = v_g \boldsymbol{\kappa} \tag{7.134}$$

where:

$$v_g = |\mathbf{v}_g|. \tag{7.135}$$

Therefore the ECE 2 equation of any precession is:

$$\boldsymbol{\Omega} = \boldsymbol{\nabla} \times \mathbf{v}_g = v_g \boldsymbol{\kappa} \tag{7.136}$$

where:

$$\Omega = \frac{1}{2} |\boldsymbol{\nabla} \times \mathbf{v}_g| = \frac{1}{2} v_g \left(\frac{q}{r^{(0)}} - \omega_s \right). \tag{7.137}$$

These are generally valid equations without any approximation, and are based on Cartan geometry.

In the dipole approximation:

$$\boldsymbol{\Omega} = \frac{G}{2c^2} \boldsymbol{\nabla} \times \left(\frac{\mathbf{L} \times \mathbf{r}}{r^3} \right) \tag{7.138}$$

and comparing Eqs. (7.136) and (7.138):

$$\mathbf{v}_g = \frac{G}{2c^2 r^3} \mathbf{L} \times \mathbf{r}. \tag{7.139}$$

This is also an expression for the $\mathbf{W}_g$ potential. Finally:

$$\boldsymbol{\kappa} = \frac{G}{2c^2 v_g} \boldsymbol{\nabla} \times \left(\frac{\mathbf{L} \times \mathbf{r}}{r^3} \right) = r^3 \boldsymbol{\nabla} \times \left(\frac{\mathbf{L} \times \mathbf{r}}{r^3 |\mathbf{L} \times \mathbf{r}|} \right) \tag{7.140}$$

which shows that any precession is due to Cartan geometry, Q. E. D.

Later in this chapter a numerical analysis with graphics is given using computer algebra to check the above calculations.

Using ECE 2 relativity and the minimal prescription the hamiltonian for a particle in the presence of a gravitomagnetic potential can be defined. The

lagrangian can be calculated from the hamiltonian using the canonical momentum and the relevant Euler Lagrange equations used to derive the gravitomagnetic Lorentz force equation. In the absence of gravitomagnetism this equation reduces to the Newton equation. The precession frequency of the Lorentz force equation is an orbital precession frequency of any kind. This method gives a simple general theory of precession in ECE 2 relativity.

Consider the gravitomagnetic minimal prescription:

$$\mathbf{p} \rightarrow \mathbf{p} + m\mathbf{v}_g \tag{7.141}$$

in which the linear momentum of a particle of mass m is incremented by the gravitomagnetic vector potential:

$$\mathbf{W}_g = \mathbf{v}_g. \tag{7.142}$$

The free particle hamiltonian becomes:

$$H = \frac{1}{2m}\left(\mathbf{p} + m\mathbf{v}_g\right) \cdot \left(\mathbf{p} + m\mathbf{v}_g\right) = \frac{p^2}{2m} + \frac{1}{2}m\mathbf{v}_g^2 + \frac{1}{2}\mathbf{L} \cdot \mathbf{\Omega}_g \tag{7.143}$$

where the orbital angular momentum is:

$$\mathbf{L} = \mathbf{p} \times \mathbf{r} \tag{7.144}$$

and the gravitomagnetic field is the vorticity:

$$\mathbf{\Omega} = \boldsymbol{\nabla} \times \mathbf{v}_g. \tag{7.145}$$

Any orbital precession frequency is defined, as we have argued earlier in this chapter, by:

$$\Omega = \frac{1}{2}|\mathbf{\Omega}|. \tag{7.146}$$

Consider an object of mass m in orbit around a mass M. The central gravitational potential is:

$$U(r) = -\frac{mMG}{r} \tag{7.147}$$

and the hamiltonian is:

$$H = \frac{1}{2m}\left(\mathbf{p} + m\mathbf{v}_g\right) \cdot \left(\mathbf{p} + m\mathbf{v}_g\right) + U(r). \tag{7.148}$$

This reduces to the Newtonian hamiltonian:

$$H = \frac{p^2}{2m} + U(r) \tag{7.149}$$

in the absence of a gravitomagnetic field. The Newtonian hamiltonian produces the conic section orbit:

$$r = \frac{\alpha}{1 + \epsilon\cos\theta}. \tag{7.150}$$

The hamiltonian (7.148) can be developed as:

$$H = \frac{p^2}{2m} + \frac{1}{2}mv_g^2 + \frac{1}{2}\mathbf{L}\cdot\boldsymbol{\Omega}_g + U(r) \tag{7.151}$$

as shown in all detail in the Notes accompanying UFT 347 on `www.aias.us`.

The lagrangian is calculated from the hamiltonian using the methods of classical dynamics and the canonical momentum:

$$p_q = \frac{\partial \mathscr{L}}{\partial \dot{q}} \tag{7.152}$$

where q is a generalized coordinate. Denote:

$$\dot{\mathbf{r}} = \frac{1}{m}\left(\mathbf{p} + m\mathbf{v}_g\right) \tag{7.153}$$

then:

$$H = \mathbf{p}\cdot\dot{\mathbf{r}} - \mathscr{L}. \tag{7.154}$$

The lagrangian is therefore:

$$\mathscr{L} = \frac{1}{2}m\left(\mathbf{p} + m\mathbf{v}_g\right)\cdot\left(\mathbf{p} + m\mathbf{v}_g\right) - U(r) - m\dot{\mathbf{r}}\cdot\mathbf{v}_g. \tag{7.155}$$

The relevant Euler Lagrange equation is:

$$\boldsymbol{\nabla}\mathscr{L} = \frac{d}{dt}\left(\frac{\partial \mathscr{L}}{\partial \dot{\mathbf{r}}}\right). \tag{7.156}$$

The left hand side of this equation is:

$$\boldsymbol{\nabla}\mathscr{L} = \boldsymbol{\nabla}\left(\frac{1}{2}m\dot{\mathbf{r}}\cdot\dot{\mathbf{r}} - U(r)\right) - m\boldsymbol{\nabla}\left(\dot{\mathbf{r}}\cdot\mathbf{v}_g\right). \tag{7.157}$$

In general:

$$\boldsymbol{\nabla}\left(\dot{\mathbf{r}}\cdot\mathbf{v}_g\right) = \left(\dot{\mathbf{r}}\cdot\boldsymbol{\nabla}\right)\mathbf{v}_g + \left(\mathbf{v}_g\cdot\boldsymbol{\nabla}\right)\dot{\mathbf{r}} + \dot{\mathbf{r}}\times\left(\boldsymbol{\nabla}\times\mathbf{v}_g\right) + \mathbf{v}_g\times\left(\boldsymbol{\nabla}\times\dot{\mathbf{r}}\right) \tag{7.158}$$

and reduces to

$$\boldsymbol{\nabla}\left(\dot{\mathbf{r}}\cdot\mathbf{v}_g\right) = \left(\dot{\mathbf{r}}\cdot\boldsymbol{\nabla}\right)\mathbf{v}_g + \dot{\mathbf{r}}\times\left(\boldsymbol{\nabla}\times\mathbf{v}_g\right) \tag{7.159}$$

if it is assumed that:

$$\left(\mathbf{v}_g\cdot\boldsymbol{\nabla}\right)\dot{\mathbf{r}} = \mathbf{0} \tag{7.160}$$

and

$$\boldsymbol{\nabla}\times\dot{\mathbf{r}} = \mathbf{0}. \tag{7.161}$$

So:

$$\boldsymbol{\nabla}\mathscr{L} = -\boldsymbol{\nabla}U(r) - m\left(\left(\dot{\mathbf{r}}\cdot\boldsymbol{\nabla}\right)\mathbf{v}_g + \dot{\mathbf{r}}\times\left(\boldsymbol{\nabla}\times\mathbf{v}_g\right)\right). \tag{7.162}$$

The right hand side of Eq. (7.156) is:

$$\frac{d}{dt}\left(\frac{\partial \mathscr{L}}{\partial \dot{\mathbf{r}}}\right) = \frac{d}{dt}\left(m\dot{\mathbf{r}} - m\mathbf{v}_g\right). \tag{7.163}$$

The total or Lagrange derivative must be used as follows:

$$\frac{dv_{gX}}{dt} = \frac{\partial v_{gX}}{\partial t} + \left(\frac{\partial X}{\partial t}\right)\left(\frac{\partial v_{gX}}{\partial X}\right) + \cdots \tag{7.164}$$

Therefore:

$$\frac{d\mathbf{v}_g}{dt} = \frac{\partial \mathbf{v}_g}{\partial t} + \left(\dot{\mathbf{r}} \cdot \boldsymbol{\nabla}\right)\mathbf{v}_g \tag{7.165}$$

and

$$\frac{d}{dt}\left(\frac{\partial \mathscr{L}}{\partial \dot{\mathbf{r}}}\right) = m\ddot{\mathbf{r}} - m\left(\frac{\partial \mathbf{v}_g}{\partial t} + \left(\dot{\mathbf{r}} \cdot \boldsymbol{\nabla}\right)\mathbf{v}_g\right). \tag{7.166}$$

The Euler Lagrange equation is therefore:

$$\frac{d}{dt}\left(\frac{\partial \mathscr{L}}{\partial \dot{\mathbf{r}}}\right) = m\ddot{\mathbf{r}} - m\left(\frac{\partial \mathbf{v}_g}{\partial t} + \left(\dot{\mathbf{r}} \cdot \boldsymbol{\nabla}\right)\mathbf{v}_g\right) \tag{7.167}$$

i. e.:

$$m\ddot{\mathbf{r}} = -\boldsymbol{\nabla}U(r) + m\frac{\partial \mathbf{v}_g}{\partial t} - m\dot{\mathbf{r}} \times \left(\boldsymbol{\nabla} \times \mathbf{v}_g\right). \tag{7.168}$$

Now define:

$$m\phi_g = -U(r) \tag{7.169}$$

and:

$$\boldsymbol{\Omega} = \boldsymbol{\nabla} \times \mathbf{v}_g \tag{7.170}$$

to find the gravitomagnetic Lorentz force equation:

$$\mathbf{F} = m\ddot{\mathbf{r}} = -m\left(\mathbf{E}_g + \dot{\mathbf{r}} \times \boldsymbol{\Omega}\right) \tag{7.171}$$

where:

$$\mathbf{E}_g = -\boldsymbol{\nabla}\phi_g - \frac{\partial \mathbf{v}_g}{\partial t} \tag{7.172}$$

is the gravitomagnetic analogue of the acceleration due to gravity in ECE 2 relativity.

The precession of any orbit is therefore governed by the gravitomagnetic force law (7.171) with precession frequency (7.146).

From Eqs. (7.169) and (7.147):

$$\phi_g = \frac{MG}{r} \tag{7.173}$$

and it follows that:

$$\boldsymbol{\nabla}\phi_g = -\frac{MG}{r^2}\mathbf{e}_r \tag{7.174}$$

so:

$$\mathbf{E}_g = \frac{MG}{r^2}\mathbf{e}_r - \frac{\partial \mathbf{v}_g}{\partial t}. \tag{7.175}$$

The gravitomagnetic Lorentz force is therefore:

$$\mathbf{F} = m\ddot{\mathbf{r}} = -\frac{mMG}{r^2}\mathbf{e}_r + m\frac{\partial \mathbf{v}_g}{\partial t} - m\dot{\mathbf{r}} \times \boldsymbol{\Omega} \tag{7.176}$$

where:

$$\dot{\mathbf{r}} = \frac{1}{m}\left(\mathbf{p} + m\mathbf{v}_g\right). \tag{7.177}$$

In the absence of a gravitomagnetic field Eq. (7.176) reduces to the Newtonian:

$$\mathbf{F} = m\ddot{\mathbf{r}} = -\frac{mMG}{r^2}\mathbf{e}_r. \tag{7.178}$$

For a planar orbit it is well known that:

$$\mathbf{v} = \dot{\mathbf{r}} = \frac{d\mathbf{r}}{dt} = \frac{d}{dt}\left(r\mathbf{e}_r\right) = \dot{r}\mathbf{e}_r + r\dot{\theta}\mathbf{e}_\theta \tag{7.179}$$

in the absence of a gravitomagnetic field. The acceleration in the absence of a gravitomagnetic field is:

$$\mathbf{a} = \ddot{\mathbf{r}} = \frac{d\mathbf{v}}{dt} = \frac{d}{dt}\left(\dot{r}\mathbf{e}_r + r\dot{\theta}\mathbf{e}_\theta\right) \tag{7.180}$$

an expression which gives rise to the well known centrifugal and Coriolis forces. So the gravitomagnetic force terms occur in addition to these well known forces, and result in precession, whereas the centrifugal and Coriolis terms do not result in a precessing orbit as is well known.

The gravitomagnetic field $\boldsymbol{\Omega}$ is governed by the gravitational equivalent of the Ampère Law [2]- [13]:

$$\boldsymbol{\nabla} \times \boldsymbol{\Omega} = \frac{4\pi G}{c^2}\mathbf{J}_g \tag{7.181}$$

where $\mathbf{J}_g$ is the localized current density of mass, analogous to electric current density in electrodynamics. The gravitomagnetic vacuum permeability is:

$$\mu_{0g} = \frac{4\pi G}{c^2} \tag{7.182}$$

and the gravitomagnetic four potential is:

$$W_g^\mu = \left(\phi_g, c\mathbf{W}_g\right). \tag{7.183}$$

In UFT 328 it was shown that simultaneous solution of the hamiltonian and lagrangian leads to orbital precession. The above analysis confirms that finding.

It can be shown as follows that a new type of precessing ellipse emerges from the hamiltonian (7.148), so this is the simplest way of describing any precession. The precessing ellipse obtained in this way is a rigorous and accurate description of the experimentally observed orbit because the observed precession frequency is used in the equations. The calculated precessing ellipse is similar in structure to:

$$r = \frac{\alpha}{1 + \epsilon \cos(x\theta)} \tag{7.184}$$

but in this new theory x is no longer a constant. For a uniform gravitomagnetic field the Lorentz force equation reduces to a precessional Binet equation. The orbit calculated from the hamiltonian can be used in this precessional Binet equation to give the force law. Later on in this chapter a description is given with graphics of the methods used to produce the precessing orbit.

For a uniform gravitomagnetic field:

$$v_g^2 = \Omega^2 r^2 \tag{7.185}$$

where Ω is the observed precessional frequency. As in the Notes for UFT 347 on `www.aias.us` the hamiltonian (7.148) may be developed as:

$$H = \frac{1}{2} m \left(v^2 + v_g^2 \right) + \Omega L + U(r) \tag{7.186}$$

where L is the constant magnitude of the angular momentum:

$$\mathbf{L} = \mathbf{r} \times \mathbf{p} \tag{7.187}$$

and where Ω is the observed precession frequency, considered to be a Larmor precession frequency. Eqs. (7.185) and (7.186) give

$$H = \frac{1}{2} m \left(v^2 + \Omega^2 r^2 \right) + \Omega L + U(r) \tag{7.188}$$

where:

$$v^2 = \left(\frac{dr}{dt} \right)^2 + r^2 \left(\frac{d\theta}{dt} \right)^2 . \tag{7.189}$$

Therefore the hamiltonian is:

$$H = \frac{1}{2} m \left(\left(\frac{dr}{dt} \right)^2 + r^2 \left(\frac{d\theta}{dt} \right)^2 + \Omega^2 \right) + \Omega L + U(r) \tag{7.190}$$

or:

$$H_1 = H - \Omega L = \frac{1}{2} m \left(\left(\frac{dr}{dt} \right)^2 + r^2 \left(\frac{d\theta_1}{dt} \right)^2 \right) + U(r) \tag{7.191}$$

where

$$\left(\frac{d\theta_1}{dt}\right)^2 = \left(\frac{d\theta}{dt}\right)^2 + \Omega^2. \tag{7.192}$$

A hamiltonian of type (7.191) leads to a conic section orbit:

$$r = \frac{\alpha}{1 + \epsilon \cos\theta_1}. \tag{7.193}$$

Denote:

$$\omega_1 = \frac{d\theta_1}{dt},\ \omega = \frac{d\theta}{dt} \tag{7.194}$$

to find that:

$$\omega_1^2 = \omega^2 + \Omega^2. \tag{7.195}$$

If

$$\Omega \ll \omega \tag{7.196}$$

then to an excellent approximation:

$$\frac{d\theta_1}{dt} = \left(1 + \frac{1}{2}\left(\frac{\Omega}{\omega}\right)^2\right)\frac{d\theta}{dt} \tag{7.197}$$

i. e.:

$$\omega_1 \sim \omega\left(1 + \frac{1}{2}\left(\frac{\Omega}{\omega}\right)^2\right) \tag{7.198}$$

so:

$$d\theta_1 = \left(1 + \frac{1}{2}\left(\frac{\Omega}{\omega}\right)^2\right)d\theta \tag{7.199}$$

and

$$\theta_1 = \int\left(1 + \frac{1}{2}\left(\frac{\Omega}{\omega}\right)^2\right)d\theta. \tag{7.200}$$

In Eq. (7.200) ω is the angular frequency corresponding to the hamiltonian:

$$H_0 = \frac{p_0^2}{2m} + U(r) \tag{7.201}$$

and is defined by:

$$\omega = \frac{L_0}{mr^2}. \tag{7.202}$$

In Eq. (7.202):

$$r = \frac{\alpha_0}{1 + \epsilon_0 \cos\theta} \tag{7.203}$$

therefore:

$$\frac{1}{\omega^2} = \frac{m^2 r^4}{L_0^2} = \frac{m^2 \alpha_0^4}{L_0^2 \left(1 + \epsilon_0 \cos\theta\right)^4} \tag{7.204}$$

and

$$\theta_1 = \int \left(1 + \frac{m^2 \alpha_0^4 \Omega^2}{2 \left(1 + \epsilon_0 \cos\theta\right)^4 L_0^2} \right) d\theta. \tag{7.205}$$

This integral is evaluated numerically later in this chapter. The orbit is:

$$r = \frac{\alpha}{1 + \epsilon \cos\theta_1} \tag{7.206}$$

and it is demonstrated numerically that this is a precessing orbit, Q. E. D.

Therefore the minimal prescription (7.141) is enough to produce a precessing orbit.

In the x theory of previous UFT papers it was assumed that:

$$\theta_1 = x\theta. \tag{7.207}$$

In this more accurate theory it is seen that x depends on θ. The most accurate theory of precession in ECE 2 is UFT 328, which is rigorously relativistic and which solves the relativistic hamiltonian and lagrangian simultaneously. However UFT 328 uses a scatter plot method and does not give a known analytical solution. The method described above gives an analytical solution in the non relativistic limit. In the above theory the constant angular momenta are:

$$L = mr^2 \frac{d\theta_1}{dt}, \; L_0 = mr^2 \frac{d\theta}{dt}, \tag{7.208}$$

the half right latitudes are:

$$\alpha = \frac{L^2}{m^2 MG}, \; \alpha_0 = \frac{L_0^2}{m^2 MG} \tag{7.209}$$

and the eccentricities are:

$$\epsilon^2 = 1 + \frac{2H_1 L^2}{m^3 M^2 G^2} \tag{7.210}$$

and

$$\epsilon_0^2 = 1 + \frac{2H L_0^2}{m^3 M^2 G^2}. \tag{7.211}$$

In general:

$$\theta_1 = \theta + \frac{m^2 \alpha_0^4 \Omega^2}{2L_0^2} \int \frac{d\theta}{\left(1 + \epsilon_0 \cos\theta\right)^4} \tag{7.212}$$

and this integral can be valuated analytically as shown later in this chapter. If it is assumed that:

$$\theta_1 = x\theta \tag{7.213}$$

then:

$$x = 1 + \frac{1}{2}\left(\frac{m\alpha_0^2\Omega}{L_0}\right)^2 \int \frac{d\theta}{(1+\epsilon_0\cos\theta)^4} \tag{7.214}$$

and the orbit can be put into the form of an orbit of x theory [2]- [13]:

$$r = \frac{\alpha}{1+\epsilon\cos(x\theta)}. \tag{7.215}$$

The orbit (7.206) is graphed later in this chapter and is shown to precess, Q. E. D. It is generated by the orbital Lorentz force equation:

$$\mathbf{F} = m\ddot{\mathbf{r}} = -\frac{mMG}{r^2}\mathbf{e}_r + m\frac{\partial \mathbf{v}_g}{\partial t} - m\dot{\mathbf{r}} \times \mathbf{\Omega} \tag{7.216}$$

in which the canonical momentum is:

$$m\dot{\mathbf{r}} = \mathbf{p} + m\mathbf{v}_g. \tag{7.217}$$

In the absence of a gravitomagnetic vector potential $\mathbf{v}_g$ Eq. (7.216) reduces to the Leibniz force equation:

$$\mathbf{F} = m\left(\ddot{r} - r\dot{\theta}^2\right)\mathbf{e}_r = -\frac{mMG}{r^2}\mathbf{e}_r \tag{7.218}$$

in which:

$$\ddot{\mathbf{r}} = \frac{d\dot{\mathbf{r}}}{dt} = \frac{d\mathbf{v}}{dt}. \tag{7.219}$$

Therefore the Leibniz equation is:

$$\ddot{r} - r\dot{\theta}^2 = F(r) \tag{7.220}$$

and can be transformed to the Binet equation:

$$\frac{d^2}{d\theta^2}\left(\frac{1}{r}\right) + \frac{1}{r} = -\frac{mr^2}{L^2}F(r). \tag{7.221}$$

The Leibniz equation gives the non precessing conic section:

$$r = \frac{\alpha}{1+\epsilon\cos\theta} \tag{7.222}$$

Eqs. (7.216) and (7.217) give:

$$\mathbf{F} = m\ddot{\mathbf{r}} = m\left(\frac{d\mathbf{v}}{dt} + \frac{d\mathbf{v}_g}{dt}\right) = -\frac{mMG}{r^2}\mathbf{e}_r + m\frac{\partial \mathbf{v}_g}{\partial t} - m\dot{\mathbf{r}} \times \mathbf{\Omega}_g. \tag{7.223}$$

To develop this equation consider the Lagrange derivative:

$$\frac{dv_X}{dt} = \frac{\partial v_X}{\partial t} + \frac{\partial X}{\partial t}\frac{\partial v_X}{\partial X} + \cdots \tag{7.224}$$

then to first order:

$$\frac{d\mathbf{v}}{dt} = \frac{\partial \mathbf{v}}{\partial t} + \left(\dot{\mathbf{R}} \cdot \boldsymbol{\nabla}\right)\mathbf{v} \tag{7.225}$$

where

$$\dot{\mathbf{R}} = \frac{\partial X}{\partial t}\mathbf{i} + \frac{\partial Y}{\partial t}\mathbf{j} + \frac{\partial Z}{\partial t}\mathbf{k}. \tag{7.226}$$

It follows that:

$$\frac{d\mathbf{v}}{dt} - \frac{\partial \mathbf{v}}{\partial t} = \left(\dot{\mathbf{R}} \cdot \boldsymbol{\nabla}\right)\mathbf{v} \tag{7.227}$$

so Eq. (7.223) becomes:

$$\begin{aligned} \mathbf{F} = m\frac{d\mathbf{v}}{dt} &= -\frac{mMG}{r^2}\mathbf{e}_r - \left(\dot{\mathbf{R}} \cdot \mathbf{v}\right)\mathbf{v}_g - m\dot{\mathbf{r}} \times \boldsymbol{\Omega}_g \\ &= m\left(\ddot{\mathbf{R}} - r\dot{\theta}^2\right)\mathbf{e}_r. \end{aligned} \tag{7.228}$$

Here:

$$\mathbf{R} = X\mathbf{i} + Y\mathbf{j} + Z\mathbf{k} = R\mathbf{e}_r \tag{7.229}$$

and

$$\mathbf{v} = \frac{d\mathbf{R}}{dt} = \dot{R}\mathbf{e}_r + R\dot{\theta}\mathbf{e}_\theta = \dot{\mathbf{R}} \tag{7.230}$$

and:

$$\ddot{\mathbf{R}} = \left(\ddot{R} - R\dot{\theta}^2\right)\mathbf{e}_r \tag{7.231}$$

for a planar orbit. Therefore the orbital Lorentz force equation becomes:

$$\mathbf{F} = m\left(\ddot{R} - R\dot{\theta}^2\right)\mathbf{e}_r = -\frac{mMG}{r^2}\mathbf{e}_r - \left(\dot{\mathbf{R}} \cdot \boldsymbol{\nabla}\right)\mathbf{v}_g - m\dot{\mathbf{r}} \times \boldsymbol{\Omega} \tag{7.232}$$

in which the canonical momentum is:

$$m\dot{\mathbf{r}} = m\left(\mathbf{v} + \mathbf{v}_g\right) = m\left(\dot{\mathbf{R}} + \mathbf{v}_g\right). \tag{7.233}$$

The lagrangian corresponding to this general equation is developed in Note 348(3).

The hamiltonian (7.188) and the orbit (7.206) are based on the assumption of a uniform gravitomagnetic field defined by:

$$\boldsymbol{\Omega} = \boldsymbol{\nabla} \times \mathbf{v}_g \tag{7.234}$$

and:

$$\mathbf{v}_g = \frac{1}{2}\boldsymbol{\Omega} \times \mathbf{r}. \tag{7.235}$$

As in Note 347(2):

$$v_g^2 = \frac{1}{4}\boldsymbol{\Omega} \times \mathbf{r} \cdot \boldsymbol{\Omega} \times \mathbf{r} = \frac{1}{4}\left(\Omega^2 r^2 - (\boldsymbol{\Omega} \cdot \mathbf{r})(\boldsymbol{\Omega} \cdot \mathbf{r})\right) \tag{7.236}$$

and if the gravitomagnetic field is perpendicular to the plane of the orbit:

$$v_g^2 = \frac{1}{4}|\boldsymbol{\Omega}|^2 r^2 = \Omega^2 r^2 \tag{7.237}$$

which is Eq. (7.185). In general the lagrangian is:

$$\mathscr{L} = \frac{1}{2m}(\mathbf{p} + m\mathbf{v}_g) \cdot (\mathbf{p} + m\mathbf{v}_g) - (\mathbf{p} + m\mathbf{v}_g) \cdot \mathbf{v}_g - U(r) \tag{7.238}$$

which can be written as:

$$\mathscr{L} = \frac{1}{2}m\left(v^2 - v_g^2\right) - U(r). \tag{7.239}$$

From Eqs. (7.237) and (7.239) the lagrangian becomes:

$$\mathscr{L} = \frac{1}{2}m\left(\dot{r}^2 + r^2\dot{\theta}^2 - \Omega^2 r^2\right) - U(r). \tag{7.240}$$

The rotational Euler Lagrange equation is:

$$\frac{\partial \mathscr{L}}{\partial \theta} = 0 = \frac{d}{dt}\frac{\partial \mathscr{L}}{\partial \dot{\theta}} \tag{7.241}$$

in which the conserved angular momentum is:

$$L = mr^2\dot{\theta}. \tag{7.242}$$

The other Euler Lagrange equation is:

$$\frac{\partial \mathscr{L}}{\partial r} = \frac{d}{dt}\frac{\partial \mathscr{L}}{\partial \dot{r}} \tag{7.243}$$

which gives the force equation:

$$F(r) = -\frac{\partial U}{\partial r} = m\left(\ddot{r} - r\left(\dot{\theta}^2 - \Omega^2\right)\right) \tag{7.244}$$

in which:

$$U = -\frac{mMG}{r},\ F = -\frac{mMG}{r^2}. \tag{7.245}$$

This is the Lorentz force equation of the precessing orbit (7.206), and as in Note 348(5) can be transformed to the precessional Binet equation:

$$F(r) = -\frac{L^2}{mr^2}\left(\frac{d^2}{d\theta^2}\left(\frac{1}{r}\right) + \frac{1}{r}\right) - m\Omega^2 r. \tag{7.246}$$

7.2 Numerical Analysis and Graphics

7.2.1 Vector Potential and Torque of a Dipole Field

A gravitomagnetic field in dipole approximation has already been analysed numerically and graphed in chapter 4, section 4.2.1. A scalar potential was used to construct a dipole field as described there. In this section we compute the dipole field

$$\mathbf{\Omega}_g = \boldsymbol{\nabla} \times \mathbf{W}_g \tag{7.247}$$

directly from the gravitomagnetic vector potential according to

$$\mathbf{W}_g = \frac{G}{c^2 r^3} \mathbf{m}_g \times \mathbf{r} \tag{7.248}$$

where $\mathbf{m}_g$ is a gravitational dipole moment. For a given $\mathbf{m}_g$ the vector potential and gravitomagnetic field can be computed in three dimensions by computer algebra. (The equations are quite complicated and not shown.) Positioning the dipole in the Z direction:

$$\mathbf{m}_g = \begin{bmatrix} 0 \\ 0 \\ 1 \end{bmatrix} \tag{7.249}$$

leads to a rotationally symmetric vector potential in the XY plane which is graphed in Fig. 7.1. The lines of constant values are circles. There are no Z components of $\mathbf{W}_g$. This can be seen in the 3D vector plot of Fig. 7.2. The vector potential is a type of spherical vortex, being strongest in the centre. The vector potential has units of a velocity vector whose vorticity is the gravitomagnetic field. Therefore the arrows in Fig. 7.2 can be interpreted as velocities directly, showing a hydrodynamical vortex.

An interesting question is what the torque

$$\mathbf{T}_q = \mathbf{m}_g \times \mathbf{\Omega}_g \tag{7.250}$$

looks like. This has been graphed in Fig. 7.3. It has a shape similar to the vector potential but with an essential difference: the torque is zero in the equatorial plane $Z = 0$ because it changes sign from below to above and vice versa. This can be seen when comparing the arrows in Fig. 7.3 with those of Fig. 7.2. If a planet moves on a non-equatorial orbit around the centre, there is a torque which takes both directions for one revolution cycle. If the orbit is a circle, the effects will cancel out but there are changes of velocity of both signs during one revolution.

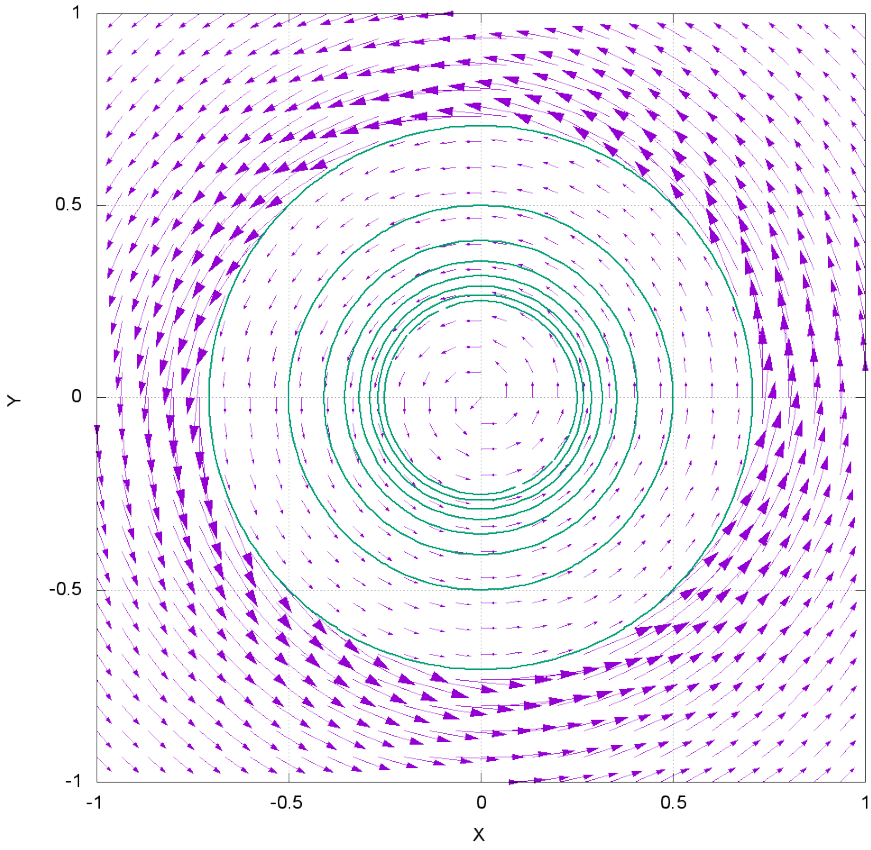

Figure 7.1: Dipole vector potential $\mathbf{W}_g$ in XY plane, only directional vectors shown within lines of constant absolute value.

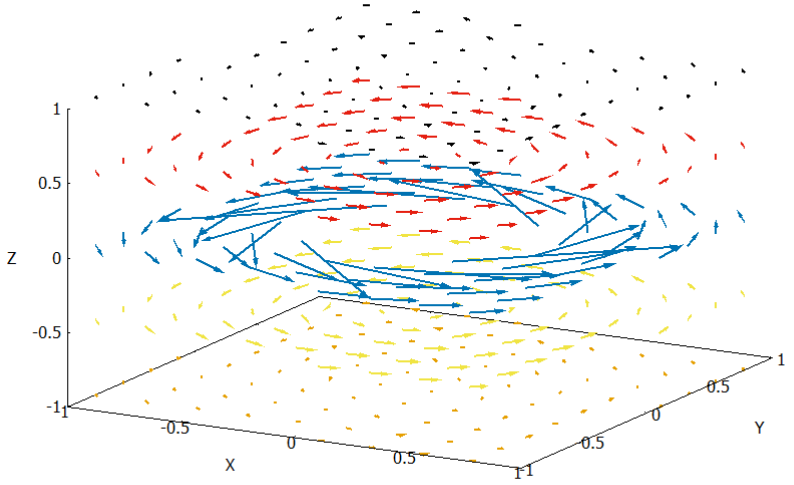

Figure 7.2: 3D view of dipole vector potential $\mathbf{W}_g$.

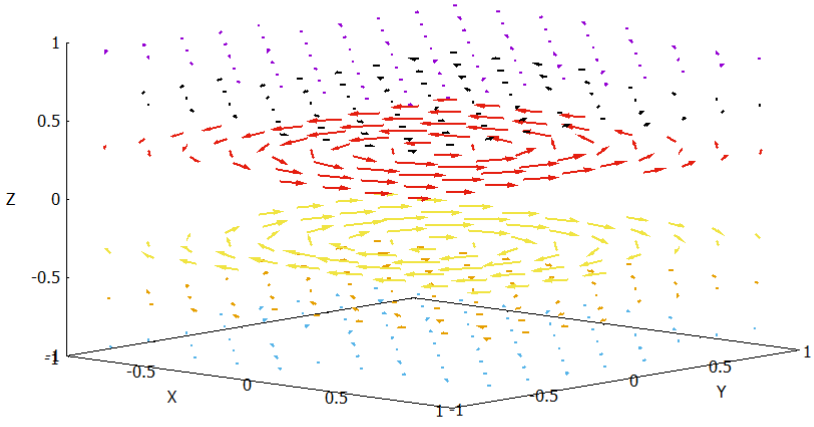

Figure 7.3: 3D view of dipole torque field $\mathbf{T}_q$.

7.2.2 The Gravitomagnetic Field in Spherical Symmetry

The gravitomagnetic field is given by Eq. (7.92):

$$\mathbf{\Omega} = \frac{G}{c^2 r^3} \left(\mathbf{m}_g - 3\mathbf{n} \left(\mathbf{m}_g \cdot \mathbf{n} \right) \right) \tag{7.251}$$

with gravitational dipole moment and angular momentum

$$\mathbf{m}_g = \frac{1}{2}\mathbf{L}. \tag{7.252}$$

It depends on space coordinates, X, Y, Z in a cartesian frame. In order to get an impression on its behaviour in a spherical symmetry we transform it to spherical coordinates (r, θ, ϕ), according to the transformation equations

$$X = r \sin\theta \cos\phi \tag{7.253}$$

$$Y = r \sin\theta \sin\phi \tag{7.254}$$

$$Z = r \cos\theta \tag{7.255}$$

with radius r, polar angle θ and azimutal angle ϕ. Applying an analogous transformation for the angular momentum, we obtain an expression for $\mathbf{\Omega}(r, \theta, \phi)$. Using the choice

$$\mathbf{L} = \begin{bmatrix} 0 \\ 0 \\ 1 \end{bmatrix} \tag{7.256}$$

(in arbitrary units) and restricting Ω to the XZ plane ($\phi = 0$), we obtain (with constants and radius set to unity):

$$\mathbf{\Omega} = 2 \begin{bmatrix} -3\cos\theta \sin\theta \\ 0 \\ 1 - 3\cos\theta^2 \end{bmatrix}. \tag{7.257}$$

The components of this vector have been graphed as a function of θ in Fig. 7.4. The Y component vanishes as expected, the X and Z components are phase shifted. At the equator ($\theta = \pi/2$) and at the poles there is only a Z component.

The structure of the gravitomagnetic field in dipole approximation (7.251) can further be demonstrated by computing two-dimensional hypersurfaces. These will be shown for the cartesian components $\Omega_{X,Y,Z}$. First we have to evaluate the full angular dependence in Eq. (7.251) which gives quite complicated expressions. Then we define a constant value $\Omega_{X,Y,Z} = \Omega_0$ for each of the components. This gives equations which can be resolved for the radial coordinate r, defining a hypersurface in 3D. We choose $\mathbf{L}$ again to lie in the Z axis as in Eq. (7.256). Then the equations for the hypersurfaces take the form

$$r = A_1 (\cos\phi \cos\theta \sin\theta)^{1/3} \tag{7.258}$$

$$r = A_1 (\sin\phi \cos\theta \sin\theta)^{1/3} \tag{7.259}$$

$$r = A_2 (2 - 3(\sin\theta)^2)^{1/3} \tag{7.260}$$

with constants A_1 and A_2. The first hypersurface (for the X component of $\mathbf{\Omega}$) has been graphed in Fig. 7.5. The surface for the Y component looks the same but is rotated by 90° around the Z axis. These have a shape of atomic p orbitals. The Z component (Fig. 7.6) has a different form, being reminiscent of an atomic d orbital. If the axis of angular momentum is rotated, the hypersurfaces change to a form similar as (but not identical to) a rotated Ω_Z. As an example we have plotted Ω_Z for an angular momentum

$$\mathbf{L} = \begin{bmatrix} 1 \\ 0 \\ 1 \end{bmatrix} \tag{7.261}$$

in Fig. 7.7. This effect will occur qualitatively in the solar system where the sun's rotation axis is tilted by about 7.25° from the axis of the earth's orbit.

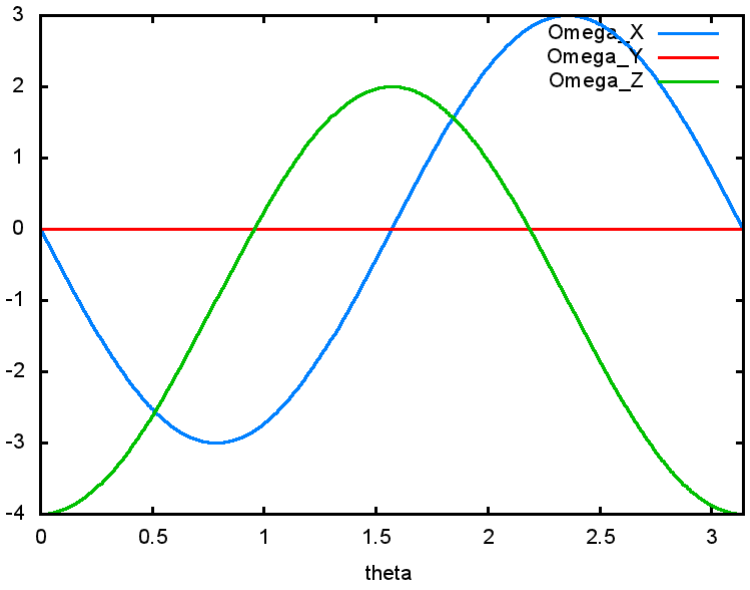

Figure 7.4: Components of $\mathbf{\Omega}$ according to Eq. (7.257).

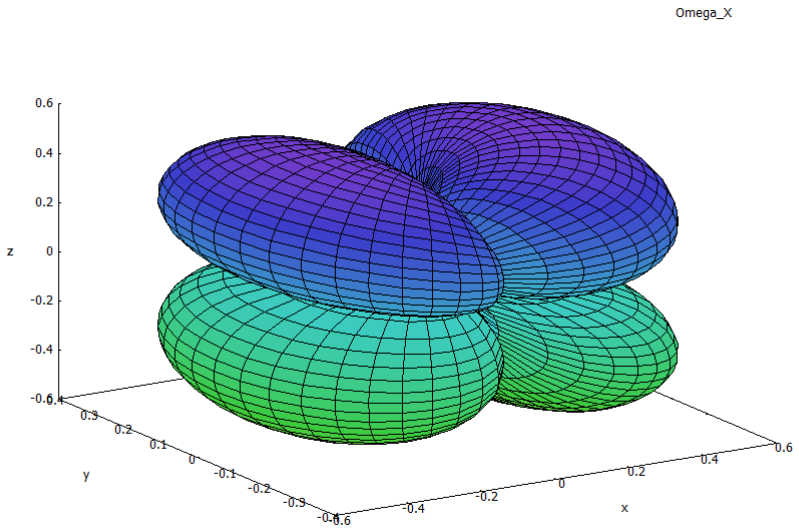

Figure 7.5: Hypersurface of Ω_X, identical to that of Ω_Y except a 90° rotation.

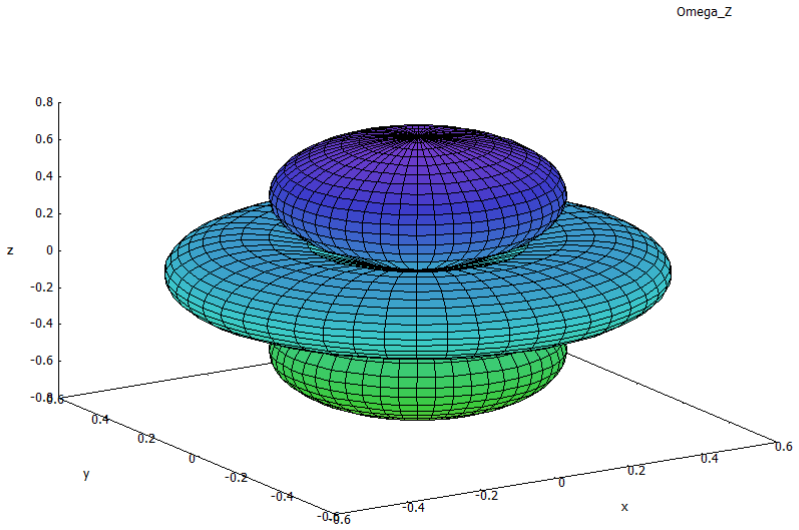

Figure 7.6: Hypersurface of Ω_Z.

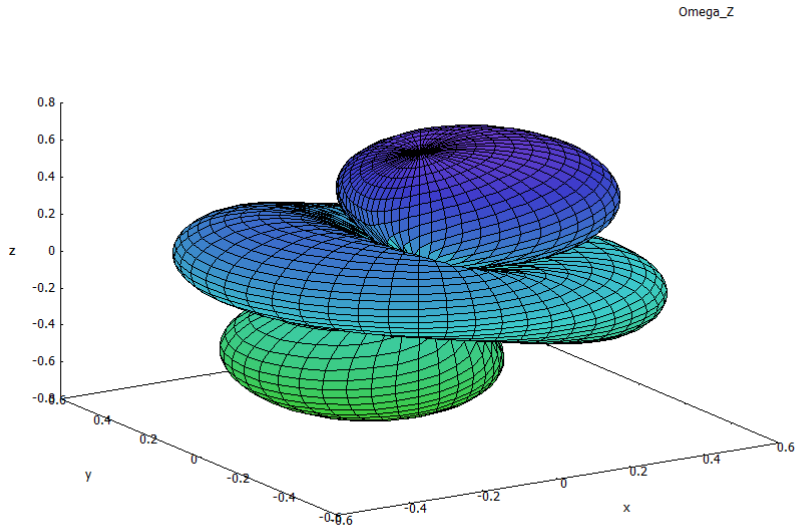

Figure 7.7: Hypersurface of Ω_Z for a tilted angular momentum $\mathbf{L} = [1, 0, 1]$.

7.2.3 Orbits of Thomas and de Sitter Precession

The orbits for Thomas and de Sitter precession will be analysed. The equations (7.31) and (7.32) have to be solved simultaneously for r and t. Eq.(7.33) can be used to obtain θ if the orbit r is known. For a Newtonian frame (r, θ_1) in which the ellipse is stationary, it is

$$\theta_1 = \theta + \omega_\theta \, t \tag{7.262}$$

and the radius function is

$$r = \frac{\alpha_1}{1 + \epsilon_1 \cos(x\theta_1)} \tag{7.263}$$

where we have Thomas precession for $x = 1$ and de Sitter precession (with additional rotation of the elliptic axes) for $x \neq 1$. Computation of the time dependence of θ could be done by solving the integral in (7.32) either analytically or numerically, but we use a simpler method derived in UFT 238, Eqs. (148/203):

$$t = \frac{2\alpha_1^2 m}{x\, L_1} \left(\frac{\operatorname{atan}\left(\frac{(2\,\epsilon_1 - 2)\sin(\theta_1\, x)}{2\sqrt{1-{\epsilon_1}^2}\,(\cos(\theta_1\, x)+1)} \right)}{\sqrt{1-{\epsilon_1}^2}\,({\epsilon_1}^2 - 1)} \right. \tag{7.264}$$

$$\left. - \frac{\epsilon_1 \sin(\theta_1\, x)}{(\cos(\theta_1\, x)+1)\left(\frac{({\epsilon_1}^3 - {\epsilon_1}^2 - \epsilon_1 + 1)\sin(\theta_1\, x)^2}{(\cos(\theta_1\, x)+1)^2} - {\epsilon_1}^3 - {\epsilon_1}^2 + \epsilon_1 + 1 \right)} \right).$$

We want to show how the ellipse rotates in a fixed frame with coordinates r, θ and t. The time t relates to the motion in the Newtonian frame as well as to the rotating frame. A complication is introduced by the fact that via (7.262) the angle θ_1 depends additionally on time, when considered from the fixed lab frame. Consequently, θ_1 is not an independent variable. An iterative solution procedure has been designed as follows. We define a grid of one-dimensional angular values θ_n etc. and compute the sequence

$$\theta_n = \theta_{n-1} + \Delta\theta \tag{7.265}$$

$$\theta_{1,n} = \theta_n + \omega_\theta \, t_{n-1} \tag{7.266}$$

$$t_n = t(\theta_{1,n}) \tag{7.267}$$

$$r_n = r(\theta_{1,n}) \tag{7.268}$$

with a fixed increment $\Delta\theta$. This allows for a numerical evaluation of the functions $r(\theta)$ and $t(\theta)$ which are graphed in Fig. 7.8 with numerical parameters $G = M = m = \alpha_1 = 1,\ L_1 = 5,\ H = -0.5,\ \epsilon_1 = 0.3$. We first study the effect of ω_θ. For a static ellipse we have $\omega_\theta = 0$. The time function as well as the radius function are scaled horizontally when switching to $\omega_\theta = 0.5$. The radius function is graphed in Fig. 7.9 as a polar diagram for both ω_θ values. There is a clear precession if $\omega_\theta > 0$. The reverse precession occurs if $\omega_\theta < 0$ (not shown). This is an example for orbital or Thomas precession. A de Sitter precession can be added by setting $x \neq 1$, for example $x = 0.95$ as done for Fig. 7.10. Now the original ellipse (for $\omega_\theta = 0$) precesses. When orbital precession is added (by $\omega_\theta > 0$, see Fig. 7.10), the orbital precession is compensated in part by the de Sitter precession. Both types of precession can give an increase or decrease of total precession, depending on the sign of ω_θ and the condition $x > 1$ or $x < 1$.

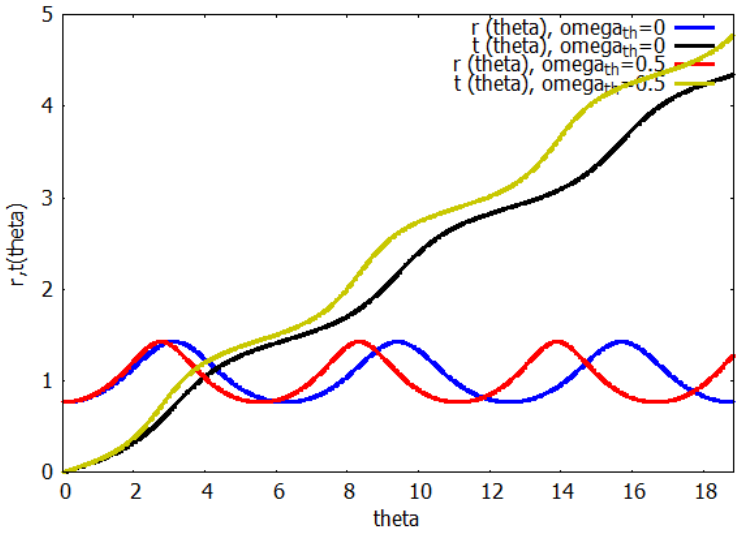

Figure 7.8: Orbit $r(\theta)$ and time $t(\theta)$ for a static ellipse ($\omega_\theta = 0$) and Thomas precession ($\omega_\theta > 0$).

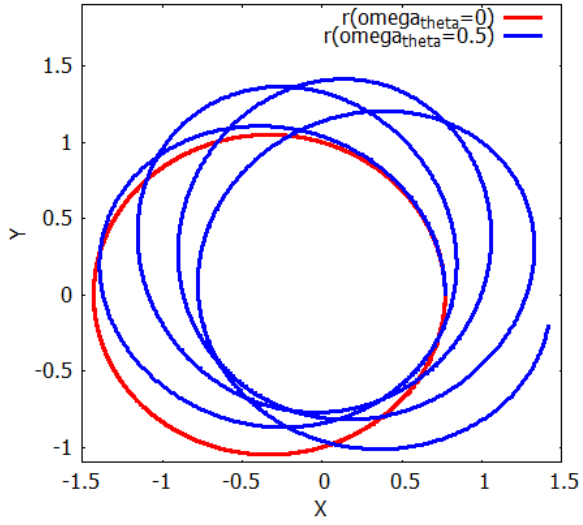

Figure 7.9: Polar plot of orbit $r(\theta)$ for a static ellipse (red) and Thomas precession (blue).

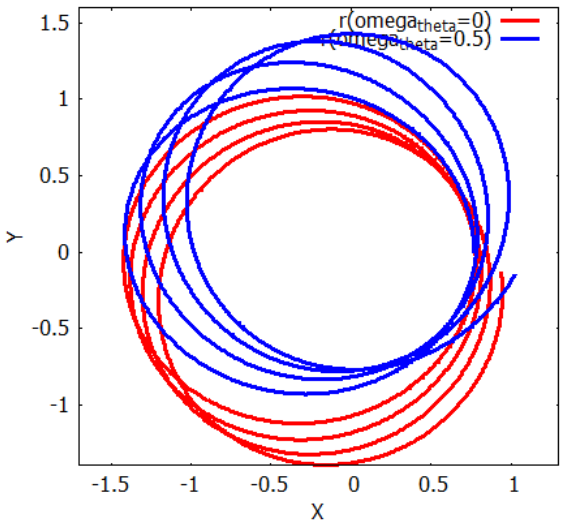

Figure 7.10: Polar plot of orbit $r(\theta)$, $x = 0.95$, for de Sitter precession (red) and de Sitter plus Thomas precession (blue).

7.2.4 Lense Thirring and Geodetic Precession

Lense Thirring Effect

For the Lense Thirring effect the gravitomagnetic field in dipole approximation is calculated from Eq. (7.71) which can be written

$$\mathbf{\Omega} = \frac{2}{5}\frac{MGR^2}{c^2 r^3}\omega\mathbf{x} \tag{7.269}$$

with the angular vectorial factor

$$\mathbf{x} = \boldsymbol{\omega}_n - 3\mathbf{n}(\boldsymbol{\omega}_n \cdot \mathbf{n}) \tag{7.270}$$

containing the unit vector of angular momentum $\boldsymbol{\omega}_n$. If $\boldsymbol{\omega}_n$ is perpendicular to the radius unit vector $\mathbf{n}$, it is

$$|\mathbf{x}| = 1 \tag{7.271}$$

while for $\boldsymbol{\omega}_n$ being parallel to $\mathbf{n}$, we have

$$|\mathbf{x}| = 2 \tag{7.272}$$

so the modulus of $\mathbf{x}$ varies between 1 and 2. It is assumed that the experimental value of $\mathbf{\Omega}$ is an angular averaged value. We can determine this average value as follows. For the special geometry of $\boldsymbol{\omega}$ in direction of the Z axis and $\mathbf{n}$ in the Y-Z plane, we have according to Eqs. (7.73-7.76):

$$\mathbf{x} = \begin{bmatrix} 0 \\ -3\sin\theta\cos\theta \\ 1 - 3\sin^2\theta \end{bmatrix} \tag{7.273}$$

and

$$x^2 = 9\sin^2\theta\cos^2\theta + \left(1 - 3\sin^2\theta)^2\right)^2 \tag{7.274}$$
$$= 4 - 3\cos^2\theta.$$

The angular dependencies of x^2 and x are graphed in Fig. 7.11, showing how x varies between 1 and 2. In addition, the Y and Z component of the angular vector $\mathbf{x}$ are shown. They are both crossing zero but at different angles θ, therefore the modulus of $\mathbf{x}$ is always greater than unity.

Taking the average of x^2:

$$\left\langle x^2 \right\rangle = \frac{1}{\pi/2}\int_0^{\pi/2} (4 - 3\cos^2\theta)\, d\theta \tag{7.275}$$

gives the result 5/2. Assuming

$$\left\langle x^2 \right\rangle = \langle x \rangle^2 \tag{7.276}$$

then we obtain

$$\langle x \rangle = \sqrt{\langle x^2 \rangle} = \sqrt{\frac{5}{2}} = 1.5811. \tag{7.277}$$

Multiplying the theoretical result of $\Omega = 1.52 \cdot 10^{-14}\,\mathrm{rad/s}$ obtained from Eq. (7.81) by this value gives

$$\Omega = 2.40 \cdot 10^{-14}\,\mathrm{rad/s} \tag{7.278}$$

and, using Eq. (7.82), a ratio

$$\frac{\Omega_{\mathrm{theory}}}{\Omega_{\mathrm{exp}}} = 1.91. \tag{7.279}$$

This could correspond to an effective gravitomagnetic g factor of the Larmor frequency:

$$g = 2 \cdot 1.91 = 3.82. \tag{7.280}$$

Another – perhaps more realistic – explanation of the deviation would be that the momentum of inertia for the earth was calculated assuming a homogeneous sphere, but the earth core has a much higher mass density than the earth mantle so the angular momentum is smaller than that of a homogeneous sphere of equal mass. The radius of the core and the average outer radius are

$$R_{\mathrm{core}} = 3.485 \cdot 10^6\mathrm{m}, \tag{7.281}$$
$$R_{\mathrm{earth}} = 6.371009 \cdot 10^6\mathrm{m}. \tag{7.282}$$

About 35% of the earth mass is concentrated in the core, therefore the masses of the core and the outer spherical shell (the earth mantle) are

$$M_{\mathrm{core}} = 0.35 \cdot 5.97219 \cdot 10^{24}\mathrm{kg} = 2.090 \cdot 10^{24}\mathrm{kg}, \tag{7.283}$$
$$M_{\mathrm{mantle}} = 0.65 \cdot 5.97219 \cdot 10^{24}\mathrm{kg} = 3.882 \cdot 10^{24}\mathrm{kg}. \tag{7.284}$$

The moments of inertia of earth core and mantle (a sphere and a spherical shell) are

$$I_{\text{core}} = \frac{2}{5} M_{\text{core}} R_{\text{core}}^2 = 1.015 \cdot 10^{37} \text{kg m}^2, \tag{7.285}$$

$$I_{\text{mantle}} = \frac{2}{5} M_{\text{mantle}} \frac{R_{\text{earth}}^5 - R_{\text{core}}^5}{R_{\text{earth}}^3 - R_{\text{core}}^3} = 7.167 \cdot 10^{37} \text{kg m}^2. \tag{7.286}$$

The sum is smaller than the moment of inertia taken simply by the earth mass and earth radius:

$$I_{\text{earth}} = \frac{2}{5} M_{\text{earth}} R_{\text{earth}}^2 = 9.696 \cdot 10^{37} \text{kg m}^2 \tag{7.287}$$

so that the ratio of both models is

$$\frac{I_{\text{core}} + I_{\text{mantle}}}{I_{\text{earth}}} = 0.8439\,. \tag{7.288}$$

So we have to multiply the results obtained for the gravitomagnetic field by this value. From the second line in Table 7.1, where the results are listed, we see that the minimal theoretical value (Lense-Thirring effect at the equator) coincides very well with the experimental value within 1.6%.

Geodetic Precession

The same calculation for the angular average as above can be done for the geodetic effect, described by Eq. (7.71) too. The angular factor is the same as for the Lense Thirring effect so the angular average is identical to Eq. (7.277). The theoretical value of geodetic precession ($3.675 \cdot 10^{-13}$ rad/s, Eq. (7.103)) here is lower than the experimental value ($1.016 \cdot 10^{-12}$ rad/s, Eq. (7.104)), therefore applying the average x factor leads to

$$\Omega = 5.811 \cdot 10^{-13} \text{ rad/s} \tag{7.289}$$

which is nearer to, but still below the experimental value. The averaging method has been repeated with a more general position of the angular momentum axis:

$$\boldsymbol{\omega} = \omega_X \mathbf{i} + \omega_Y \mathbf{j} \tag{7.290}$$

i.e. the position has been tilted from the X axis. The highest value of angular average x is obtained for a 45 degree's tilting (i.e. $\omega_X = \omega_Y$):

$$\langle x \rangle = 1.8587 \tag{7.291}$$

corresponding to

$$\Omega = 6.831 \cdot 10^{-13} \text{ rad/s}. \tag{7.292}$$

Even for the maximum value $x = 2$ the result remains below the experimental value. Translating $x = 1.5811$ into a geodetic gravitomagnetic g factor gives

$$g = \frac{\Omega_{\text{theory}}}{\Omega_{\text{exp}}} = 1.49 \tag{7.293}$$

	Theory min.	Theory max.	Theory av.	Exp.
Lense-Thirring effect, std. I	$1.52 \cdot 10^{-14}$	$3.04 \cdot 10^{-14}$	$2.40 \cdot 10^{-14}$	$1.26 \cdot 10^{-14}$
Lense-Thirring effect, improved I	$1.28 \cdot 10^{-14}$	$2.56 \cdot 10^{-14}$	$2.02 \cdot 10^{-14}$	
geodetic effect	$3.677 \cdot 10^{-13}$	$7.354 \cdot 10^{-13}$	$5.811 \cdot 10^{-13}$	$1.016 \cdot 10^{-12}$
geodetic effect, modified $\boldsymbol{\omega}$			$6.831 \cdot 10^{-13}$	

Table 7.1: Theoretical and experimental values of gravitomagnetic field in units of rad/s. I is moment of inertia, see text.

and could be an explanation of the deviation. We conclude that all theoretical results are close to the experimental findings. The numbers are comprehensively listed in Table 7.1. A final assessment can only be done after all details of the experiments have been understood.

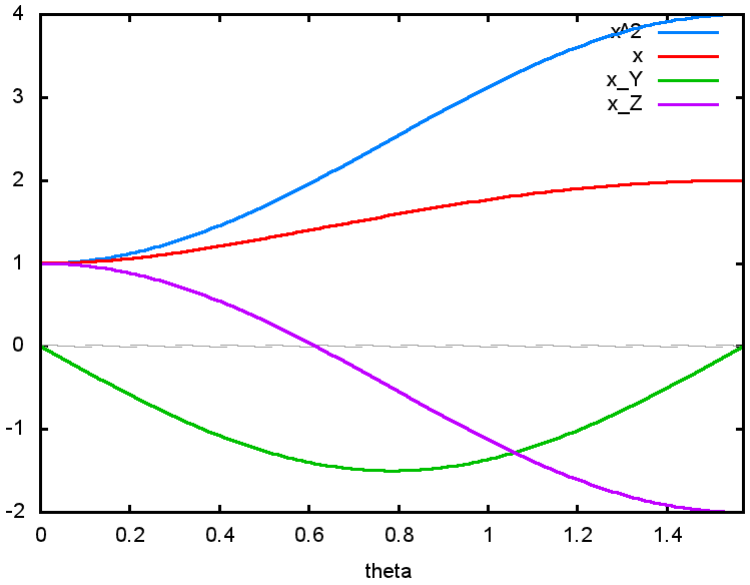

Figure 7.11: Angular factors x and x^2, and Y and Z components of vector $\mathbf{x}$.

7.2.5 Precession from Orbital Lorentz Force

It was shown earlier in this chapter that a uniform gravitomagnetic field gives precessional orbits. First we study the precession in terms of x theory, then we investigate some alternative methods of integrating the gravitomagnetic field into the lagrangian.

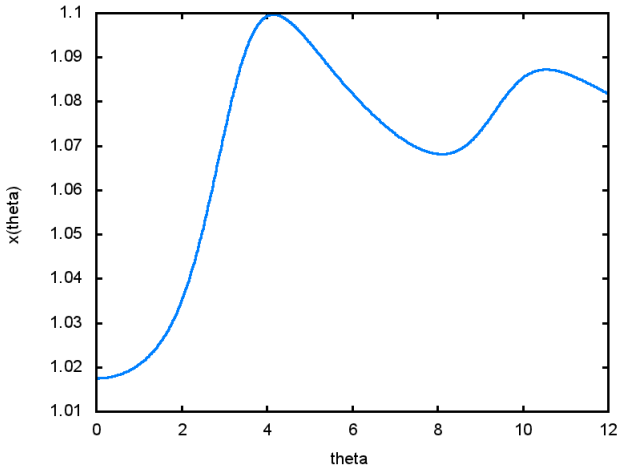

Figure 7.12: Angular dependence of x factor.

The precession factor x, defined by Eq. (7.214), is not constant and dependent on the angle θ. The integral can be solved analytically, yielding a lot of terms, whose leading term is a periodic arcustangens function:

$$\begin{aligned} x &= 1 + \frac{A}{\theta} \int \frac{d\theta}{(1+\epsilon_0 \cos\theta)^4} \\ &= 1 + a\frac{A}{\theta}\ \mathrm{atan}\left(\frac{(\epsilon_0 - 1)\ \sin\theta}{\sqrt{1-\epsilon_0^2}\ (\cos\theta + 1)} \right) + \dots \end{aligned} \tag{7.294}$$

with constants A and a. This function $x(\theta)$ is graphed in Fig. 7.12. It scales to be slightly larger than unity. The periodicity of 2π is visible but not exact because (7.214) is an approximation. The factor of $1/2\theta$ in (7.214) obviously outperforms the integral. The orbit (7.215) is shown in Fig. 7.13 for $x = 1$ and $x(\theta)$ given by Eq. (7.294). This results in a precessing ellipse as can clearly be seen.

Some variants of the Lagrangian for the Lorentz force equation are investigated in the following. First we consider a direct method where Lagrangian and Hamiltonian are given by

$$\mathscr{L} = T - U \tag{7.295}$$

$$H = T + U \tag{7.296}$$

with kinetic energy T and potential energy U. Replacing $\mathbf{p}$ by the canonical momentum

$$\mathbf{p} = m\mathbf{v} \to \mathbf{p} + m\mathbf{v}_g \tag{7.297}$$

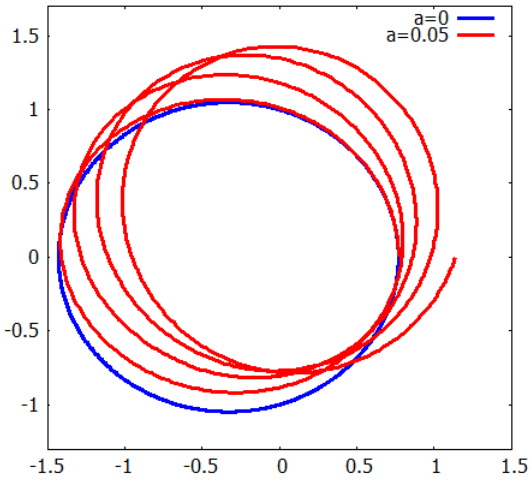

Figure 7.13: Elliptic orbitals for $a = 0$ and $a = 0.05$ (with precession).

then leads to

$$\mathscr{L}_1 = \frac{1}{2m}(\mathbf{p} + m\mathbf{v}_g)^2 - U(r), \tag{7.298}$$

$$H_1 = \frac{1}{2m}(\mathbf{p} + m\mathbf{v}_g)^2 + U(r). \tag{7.299}$$

(See Eq. (7.235) for definition of $\mathbf{v}_g$.) In a more general case, however, we can use the relation between Hamiltonian and Lagrangian known from Hamilton's equations. Then:

$$H = \sum_j p_j \dot{q}_j - \mathscr{L} \tag{7.300}$$

where q_j are the generalized coordinates and p_j the generalized momenta. In our case we only have one generalized momentum (7.297) – in vector form – which is obtained by the minimal prescription. Since q is the space position vector $\mathbf{r}$, its time derivative is the velocity $\mathbf{v}$. Evaluating (7.300) has to give the Hamiltonian (7.299). To achieve this result, the Lagrangian has to be defined as

$$\mathscr{L}_2 = \frac{1}{2m}(\mathbf{p} + m\mathbf{v}_g)^2 - (\mathbf{p} + m\mathbf{v}_g)\mathbf{v}_g - U(r) \tag{7.301}$$

so that we obtain again:

$$H_2 = H_1 = \frac{1}{2m}(\mathbf{p} + m\mathbf{v}_g)^2 + U(r). \tag{7.302}$$

For an example we will use plane polar coordinates (r, θ) in which the linear

$\mathscr{L}$	$\mathbf{v}_g$	$\mathscr{L}$
$\mathscr{L}_1$	$\mathbf{v}_{g1}$	$\frac{m}{2}\left(\left(r\,\dot\theta + r_g\,\dot\theta\right)^2 + (\dot r_g + \dot r)^2\right) - U(r)$
	$\mathbf{v}_{g2}$	$\frac{m}{2}\left(\left(r\,\dot\theta + r_g\,\dot\theta_g\right)^2 + (\dot r_g + \dot r)^2\right) - U(r)$
$\mathscr{L}_2$	$\mathbf{v}_{g1}$	$\frac{m}{2}\left(\dot r^2 + \left(r^2 - r_g^2\right)\dot\theta^2 - \dot r_g^2\right) - U(r)$
	$\mathbf{v}_{g2}$	$\frac{m}{2}\left(\dot r^2 + r^2\dot\theta^2 - \dot r_g^2 - r_g^2\dot\theta_g^2\right) - U(r)$

Table 7.2: Lagrangians for different $\mathbf{v}_g$ models.

velocity is given by

$$\mathbf{v} = \begin{bmatrix} \dot r \\ r\dot\theta \end{bmatrix}. \tag{7.303}$$

For the extra velocity derived from the gravitomagnetic field we use two variants. First we use

$$\mathbf{v}_{g1} = \begin{bmatrix} \dot r_g \\ r_g\dot\theta \end{bmatrix} \tag{7.304}$$

where the angular coordinate is the same as for the orbit, i.e. the particle m and velocity $\mathbf{v}_g$ rotate in the same frame. In the second case we use a completely independent $\mathbf{v}_g$ with both coordinates independent from the orbital motion:

$$\mathbf{v}_{g2} = \begin{bmatrix} \dot r_g \\ r_g\dot\theta_g \end{bmatrix}. \tag{7.305}$$

The Lagrangians of all four combinations $\mathscr{L}_{1,2}, \mathbf{v}_{g1,2}$ are listed in Table 7.2. For $\mathscr{L}_1$, mixed terms in $r\cdot r_g$ appear. This leads to corresponding combinations in the constants of motion (angular momentum) shown in Table 7.3. These have been calculated by the Lagrangian method, Eq. (7.241). A similar result appears in the third line of Table 7.3. However in the fourth line the angular momentum of a particle without precession appears. This astonishing result means that the angular motion is not impacted by the precessional velocity $\mathbf{v}_{g2}$. The reason is that in the Lagrangian the term $\dot\theta^2$ appears without a coupling factor to r_g so this result is plausible. The Hamiltonians (Table 7.4) are equal for $\mathscr{L}_1$ and $\mathscr{L}_2$ as expected. They only differ in the appearance of $\dot\theta_g$ by the different definitions of $\mathbf{v}_{g1}$ and $\mathbf{v}_{g2}$.

$\mathscr{L}$	$\mathbf{v}_g$	L
$\mathscr{L}_1$	$\mathbf{v}_{g1}$	$m(r+r_g)^2\,\dot{\theta}$
	$\mathbf{v}_{g2}$	$m\,r\,(r\,\dot{\theta}+r_g\,\dot{\theta}_g)$
$\mathscr{L}_2$	$\mathbf{v}_{g1}$	$m(r+r_g)(r-r_g)\,\dot{\theta}$
	$\mathbf{v}_{g2}$	$m\,r^2\,\dot{\theta}$

Table 7.3: Constants of motion L for different Lagrangians and $\mathbf{v}_g$ models.

$\mathscr{L}$	$\mathbf{v}_g$	H
$\mathscr{L}_1$	$\mathbf{v}_{g1}$	$\frac{m}{2}\left(\dot{r}^2+r^2\dot{\theta}^2+\dot{r}_g^2+r_g^2\dot{\theta}^2\right)+U(r)$
	$\mathbf{v}_{g2}$	$\frac{m}{2}\left(\dot{r}^2+r^2\dot{\theta}^2+\dot{r}_g^2+r_g^2\dot{\theta}_g^2\right)+U(r)$
$\mathscr{L}_2$	$\mathbf{v}_{g1}$	$\frac{m}{2}\left(\dot{r}^2+r^2\dot{\theta}^2+\dot{r}_g^2+r_g^2\dot{\theta}^2\right)+U(r)$
	$\mathbf{v}_{g2}$	$\frac{m}{2}\left(\dot{r}^2+r^2\dot{\theta}^2+\dot{r}_g^2+r_g^2\dot{\theta}_g^2\right)+U(r)$

Table 7.4: Hamiltonians H for different Lagrangians and $\mathbf{v}_g$ models.

Chapter 8

Triple Unification: Fluid Electrodynamics

8.1 General Theory

The field equations of fluid dynamics, electrodynamics and gravitation can be unified using ECE 2 theory, providing the opportunity for many fundamental developments. Spacetime, (or the aether or vacuum) can be developed with the concepts of fluid dynamics, and in theory can become turbulent. This turbulence can be observed with the circuit of UFT 311 on `www.aias.us`. Concepts can be transferred between one subject area and the other, for example Ohm's Law and the Lorentz force law have their equivalents in both fluid dynamics and gravitation and are intrinsic parts of the geometrical structure of ECE 2.

In a development of work by Kambe [26]- [27] Note 349(1) gives the following ECE 2 equations of fluid dynamics:

$$\boldsymbol{\nabla} \cdot \mathbf{B}_F = 0 \tag{8.1}$$

$$\boldsymbol{\nabla} \cdot \mathbf{E}_F = q_F \tag{8.2}$$

$$\boldsymbol{\nabla} \times \mathbf{E}_F + \frac{\partial B_F}{\partial t} = \mathbf{0} \tag{8.3}$$

$$\boldsymbol{\nabla} \times \mathbf{B}_F - \frac{1}{a_0^2} \frac{\partial \mathbf{E}_F}{\partial t} = \mu_{0F} \mathbf{J}_F \tag{8.4}$$

which are identical in structure with field equations of electrodynamics and gravitation developed earlier in this book. All three sets of equations are based on the same geometrical structure so this theory is a powerful unification of fluid dynamical gravitational theory, classical dynamics and electrodynamics. In Eq. (8.1), $\mathbf{B}_F$ is the fluid magnetic flux density:

$$\mathbf{B}_F = \boldsymbol{\nabla} \times \mathbf{v} \tag{8.5}$$

and also the vorticity, where $\mathbf{v}$ is the fluid velocity field [2]- [13]. The fluid

electric field strength is:

$$\mathbf{E}_F = -\frac{\partial \mathbf{v}}{\partial t} - \boldsymbol{\nabla} h \tag{8.6}$$

where h is the enthalpy per unit mass in joules per kilogram. The four potential of ECE 2 fluid dynamics is:

$$\phi_F^{\mu} = \left(\frac{h}{a_0}, \mathbf{v} \right) \tag{8.7}$$

where a_0 is the speed of sound and the d'Alembertian of fluid dynamics is:

$$\Box = \frac{1}{a_0^2} \frac{\partial^2}{\partial t^2} - \nabla^2. \tag{8.8}$$

The fluid dynamical four potential is directly analogous with the four potential of ECE 2 electrodynamics defined earlier in this book and in UFT 318 on `www.aias.us`:

$$W^{\mu} = \left(\frac{\phi_W}{c}, \mathbf{W} \right) = W^{(0)} \omega^{\mu} \tag{8.9}$$

where ω^{μ} is the spin connection four vector. Kambe derives the Lorenz condition of fluid dynamics:

$$\partial_{\mu} \phi_F^{\mu} = 0 \tag{8.10}$$

where:

$$\partial^{\mu} = \left(\frac{1}{a_0} \frac{\partial}{\partial t}, \boldsymbol{\nabla} \right). \tag{8.11}$$

In vector notation:

$$\frac{1}{c^2} \frac{\partial \phi_W}{\partial t} + \boldsymbol{\nabla} \cdot \mathbf{W} = 0. \tag{8.12}$$

In ECE 2 electrodynamics the Lorenz condition is:

$$\partial_{\mu} J^{\mu} = \frac{\partial \rho}{\partial t} + \boldsymbol{\nabla} \cdot \mathbf{J} = 0 \tag{8.13}$$

where:

$$J^{\mu} = (c\rho, \mathbf{J}). \tag{8.14}$$

In vector notation:

$$\partial_{\mu} \phi_F^{\mu} = \frac{1}{a_0^2} \frac{\partial h}{\partial t} + \boldsymbol{\nabla} \cdot \mathbf{v} = 0. \tag{8.15}$$

The continuity equation of ECE 2 fluid dynamics is:

$$\frac{\partial q_F}{\partial t} + \boldsymbol{\nabla} \cdot \mathbf{J}_F = 0 \tag{8.16}$$

where the charge and current densities of fluid dynamics are:

$$q_F = \boldsymbol{\nabla} \cdot ((\mathbf{v} \cdot \boldsymbol{\nabla})\, \mathbf{v}) \tag{8.17}$$

and

$$\mathbf{J}_F = \frac{\partial^2 \mathbf{v}}{\partial t^2} + \boldsymbol{\nabla} \frac{\partial h}{\partial t} + a_0^2 \boldsymbol{\nabla} \times (\boldsymbol{\nabla} \times \mathbf{v}) \tag{8.18}$$

respectively. In direct analogy the continuity equation of ECE 2 electrodynamics is:

$$\partial_\mu J^\mu = \frac{\partial \rho}{\partial t} + \boldsymbol{\nabla} \cdot \mathbf{J} = 0 \tag{8.19}$$

where the electromagnetic charge current density is:

$$J^\mu = (c\rho, \mathbf{J})\,. \tag{8.20}$$

It can be shown that transition to turbulence in fluid dynamics can be developed in terms of Ohm's law of electrodynamics in the presence of a magnetic flux density [28]:

$$\mathbf{J} = \sigma\,(\mathbf{E} + \mathbf{v} \times \mathbf{B}) \tag{8.21}$$

where σ is the conductivity in units of $\mathrm{C^2 J^{-1} m^{-1} s^{-1}}$. In the non relativistic limit the Lorentz force equation of ECE 2 electrodynamics was developed earlier in this book and can be extended to force density as follows:

$$\mathbf{F}_0 = \rho\,(\mathbf{E} + \mathbf{v} \times \mathbf{B}) \tag{8.22}$$

where $\mathbf{F}_0$ is the force density. The force is:

$$\mathbf{F} = \int \mathbf{F}_0\, dV. \tag{8.23}$$

Therefore:

$$F_0 = \frac{\rho}{\sigma} J. \tag{8.24}$$

With these definitions it can be shown that the structure of the ECE 2 field equations of electromagnetism, developed earlier in this book and in UFT 317 and UFT 318 contain Ohm's Law and the Lorentz force equation. This is an important advance because the Maxwell Heaviside (MH) field equations do not contain Ohm's law nor do they contain the Lorentz force equation.

The complete ECE 2 field equations of electrodynamics are:

$$\boldsymbol{\nabla} \cdot \mathbf{B} = \boldsymbol{\kappa} \cdot \mathbf{B} \tag{8.25}$$

$$\boldsymbol{\nabla} \cdot \mathbf{E} = \boldsymbol{\kappa} \cdot \mathbf{E} \tag{8.26}$$

$$\frac{\partial \mathbf{B}}{\partial t} + \boldsymbol{\nabla} \times \mathbf{E} = -\left(\kappa_0 c \mathbf{B} + \boldsymbol{\kappa} \times \mathbf{E}\right) \tag{8.27}$$

$$\boldsymbol{\nabla} \times \mathbf{B} - \frac{1}{c^2} \frac{\partial \mathbf{E}}{\partial t} = \frac{\kappa_0}{c} \mathbf{E} + \boldsymbol{\kappa} \times \mathbf{B} \tag{8.28}$$

$$\kappa_0 = 2\left(\frac{q_0}{r^{(0)}} - \omega_0\right) \tag{8.29}$$

$$\boldsymbol{\kappa} = 2\left(\frac{1}{r^{(0)}} \mathbf{q} - \boldsymbol{\omega}\right). \tag{8.30}$$

The spin connection four vector is:

$$\omega^{\mu} = (\omega_0, \boldsymbol{\omega}) \tag{8.31}$$

and the tetrad four vector is:

$$q^{\mu} = (q_0, \mathbf{q}) \tag{8.32}$$

where $r^{(0)}$ has the units of metres. The charge current density is:

$$J^{\mu} = (c\rho, \mathbf{J}) \tag{8.33}$$

and the A^{μ} and W^{μ} four potentials are:

$$A^{\mu} = \left(\frac{\phi}{c}, \mathbf{A}\right) \tag{8.34}$$

and:

$$W^{\mu} = \left(\frac{\phi_W}{c}, \mathbf{W}\right). \tag{8.35}$$

The field potential equations are:

$$\mathbf{E} = -\boldsymbol{\nabla}\phi_W - \frac{\partial \mathbf{W}}{\partial t} \tag{8.36}$$

and:

$$\mathbf{B} = \boldsymbol{\nabla} \times \mathbf{W} \tag{8.37}$$

with:

$$\phi_W = W^{(0)}\omega_0 = cW_0, \ \mathbf{W} = W^{(0)}\boldsymbol{\omega}. \tag{8.38}$$

In general:

$$\rho = \epsilon_0 \boldsymbol{\kappa} \cdot \mathbf{E} \tag{8.39}$$

and:

$$\mathbf{J} = \frac{1}{\mu_0}\left(\frac{\kappa_0}{c}\mathbf{E} + \boldsymbol{\kappa} \times \mathbf{B}\right). \tag{8.40}$$

It follows immediately that the Lorentz force density equation has a geometrical structure:

$$\mathbf{F}_0 = \frac{\rho}{\mu_0 \sigma}\left(\frac{\kappa_0}{c}\mathbf{E} + \boldsymbol{\kappa} \times \mathbf{B}\right) = \frac{\rho}{\mu_0 \sigma}\left(\boldsymbol{\nabla} \times \mathbf{B} - \frac{1}{c^2}\frac{\partial \mathbf{E}}{\partial t}\right). \tag{8.41}$$

The MH field equations are:

$$\boldsymbol{\nabla} \cdot \mathbf{B} = 0 \tag{8.42}$$

$$\boldsymbol{\nabla} \cdot \mathbf{E} = \frac{\rho}{\epsilon_0} \tag{8.43}$$

$$\frac{\partial \mathbf{B}}{\partial t} + \boldsymbol{\nabla} \times \mathbf{E} = \mathbf{0} \tag{8.44}$$

$$\boldsymbol{\nabla} \times \mathbf{B} - \frac{1}{c^2}\frac{\partial \mathbf{E}}{\partial t} = \mu_0 \mathbf{J} \tag{8.45}$$

and do not contain Ohm's Law or the Lorentz force equation. The MH equations use zero torsion and curvature, which is incorrect geometry. The ECE 2 field equations are based on Cartan geometry [2]- [13] in which both torsion and curvature are identically non zero.

In the presence of material polarization $\mathbf{P}$ and magnetization $\mathbf{H}$:

$$\mathbf{D} = \epsilon_0 \mathbf{E} + \mathbf{P},\ \mathbf{B} = \mu_0 \left(\mathbf{H} + \mathbf{M} \right) \tag{8.46}$$

where ϵ_0 and μ_0 are the permittivity and permeability in vacuo and where $\mathbf{D}$ is the electric displacement and $\mathbf{H}$ the magnetic field strength, and the MH equations become the homogeneous:

$$\boldsymbol{\nabla} \cdot \mathbf{B} = 0 \tag{8.47}$$

$$\boldsymbol{\nabla} \times \mathbf{E} + \frac{\partial \mathbf{B}}{\partial t} = \mathbf{0} \tag{8.48}$$

and the inhomogeneous:

$$\boldsymbol{\nabla} \cdot \mathbf{D} = \rho \tag{8.49}$$

$$\boldsymbol{\nabla} \times \mathbf{H} - \frac{\partial \mathbf{D}}{\partial t} = \mathbf{J}. \tag{8.50}$$

In ECE 2 electrodynamics the homogeneous field equations are (8.25) and (8.27) and the inhomogeneous equations are:

$$\boldsymbol{\nabla} \cdot \mathbf{D} = \boldsymbol{\kappa} \cdot \mathbf{D} \tag{8.51}$$

$$\boldsymbol{\nabla} \times \mathbf{H} - \frac{\partial \mathbf{D}}{\partial t} = \frac{\kappa_0}{c} \mathbf{D} + \boldsymbol{\kappa} \times \mathbf{H} = \mathbf{J}. \tag{8.52}$$

Therefore in presence of polarization and magnetization:

$$\mathbf{F}_0 = \frac{\rho}{\sigma} \left(\frac{\kappa_0}{c} \mathbf{D} + \boldsymbol{\kappa} \times \mathbf{H} \right) = \frac{\rho}{\sigma} \left(\boldsymbol{\nabla} \times \mathbf{H} - \frac{\partial \mathbf{D}}{\partial t} \right). \tag{8.53}$$

If it is assumed that magnetic charge/current density is zero, then:

$$\boldsymbol{\kappa} \cdot \mathbf{B} = 0 \tag{8.54}$$

$$\kappa_0 c \mathbf{B} + \boldsymbol{\kappa} \times \mathbf{E} = \mathbf{0}. \tag{8.55}$$

Eq. (8.55) implies Eq. (8.54) because from Eq. (8.55):

$$\mathbf{B} = -\frac{1}{\kappa_0 c} \boldsymbol{\kappa} \times \mathbf{E} \tag{8.56}$$

and:

$$\boldsymbol{\kappa} \cdot \boldsymbol{\kappa} \times \mathbf{E} = \mathbf{E} \cdot \boldsymbol{\kappa} \times \boldsymbol{\kappa} = \mathbf{0} \tag{8.57}$$

giving Eq. (8.54). By definition:

$$\mathbf{B} = \boldsymbol{\nabla} \times \mathbf{W} \tag{8.58}$$

and if there is no magnetic monopole (i. e. magnetic charge density):

$$\boldsymbol{\kappa} \cdot \boldsymbol{\nabla} \times \mathbf{W} = 0. \tag{8.59}$$

Using the vector identity:

$$\boldsymbol{\kappa} \cdot \boldsymbol{\nabla} \times \mathbf{W} = \mathbf{W} \cdot \boldsymbol{\nabla} \times \boldsymbol{\kappa} - \boldsymbol{\nabla} \cdot \boldsymbol{\kappa} \times \mathbf{W} \tag{8.60}$$

it follows that the absence of a magnetic monopole requires:

$$\mathbf{W} \cdot \boldsymbol{\nabla} \times \boldsymbol{\kappa} = \boldsymbol{\nabla} \cdot \boldsymbol{\kappa} \times \mathbf{W} \tag{8.61}$$

where:

$$\mathbf{W} = W^{(0)} \boldsymbol{\omega} \tag{8.62}$$

and:

$$\boldsymbol{\kappa} = 2 \left(\frac{1}{r^{(0)}} \mathbf{q} - \boldsymbol{\omega} \right). \tag{8.63}$$

The geometrical condition for the absence of a magnetic monopole is:

$$r^{(0)} \boldsymbol{\omega} \cdot \boldsymbol{\nabla} \times \boldsymbol{\omega} = \boldsymbol{\omega} \cdot \boldsymbol{\nabla} \times \mathbf{q} - \boldsymbol{\nabla} \cdot \mathbf{q} \times \boldsymbol{\omega}. \tag{8.64}$$

Now consider the Cartan identity in vector notation: (UFT 350, chapter three) and earlier in this book:

$$\boldsymbol{\nabla} \cdot \boldsymbol{\omega}^{a}{}_{b} \times \mathbf{q}^{b} = \mathbf{q}^{b} \cdot \boldsymbol{\nabla} \times \boldsymbol{\omega}^{a}{}_{c} - \boldsymbol{\omega}^{a}{}_{b} \cdot \boldsymbol{\nabla} \cdot \mathbf{q}^{b}. \tag{8.65}$$

The procedure of removing internal indices that produces ECE 2 theory leads to:

$$\boldsymbol{\nabla} \cdot \boldsymbol{\omega} \times \mathbf{q} = \mathbf{q} \cdot \boldsymbol{\nabla} \times \boldsymbol{\omega} - \boldsymbol{\omega} \cdot \boldsymbol{\nabla} \times \mathbf{q}. \tag{8.66}$$

which is a well known vector identity. The derivation of this identity confirms the procedures that lead to the ECE 2 field equations.

From Eqs (8.64) and (8.66), the geometrical condition for the absence of magnetic charge density and magnetic current density is:

$$\boldsymbol{\nabla} \cdot \mathbf{q} \times \boldsymbol{\omega} = r^{(0)} \boldsymbol{\omega} \cdot \boldsymbol{\nabla} \times \boldsymbol{\omega}. \tag{8.67}$$

This geometry is transformed into electromagnetism using the definitions:

$$\mathbf{A} = A^{(0)} \mathbf{q} \tag{8.68}$$

$$\mathbf{W} = W^{(0)} \boldsymbol{\omega}. \tag{8.69}$$

For the absence of magnetic charge current density:

$$r^{(0)} \boldsymbol{\nabla} \cdot \mathbf{A} \times \mathbf{W} = \mathbf{W} \cdot \boldsymbol{\nabla} \times \mathbf{W} \tag{8.70}$$

an equation which implies

$$\boldsymbol{\nabla} \cdot \mathbf{B} = 0 \tag{8.71}$$

which in turn implies the Beltrami structure:

$$\boldsymbol{\nabla} \times \mathbf{B} = k\mathbf{B} \tag{8.72}$$

so:

$$\boldsymbol{\nabla} \times (\boldsymbol{\nabla} \times \mathbf{W}) = k\boldsymbol{\nabla} \times \mathbf{W}. \tag{8.73}$$

If it is assumed that $\mathbf{W}$ is a Beltrami potential then:

$$\boldsymbol{\nabla} \times \mathbf{W} = k\mathbf{W}. \tag{8.74}$$

and the condition for the absence of a magnetic monopole reduces to

$$\boldsymbol{\nabla} \cdot \mathbf{A} \times \mathbf{W} = \frac{k}{r^{(0)}} \mathbf{W} \cdot \mathbf{W} = x. \tag{8.75}$$

The integral form of this equation is found from the divergence theorem:

$$\int_V \boldsymbol{\nabla} \cdot \mathbf{A} \times \mathbf{W}\, dV = \oint_S \mathbf{A} \times \mathbf{W} \cdot \mathbf{n}\, dA = \int x\, dV. \tag{8.76}$$

Later on in this chapter a numerical and graphical analysis of these results is given, based on Section 3 of UFT 349 and using graphical analysis of flow.

Using these ideas the field equations of "fluid electrodynamics", a new subject area of physics, can be developed as follows. The Reynolds number can be incorporated, allowing transition to turbulence. Electric power from spacetime is a direct consequence of fluid electrodynamics. The Stokes and convective derivatives of fluid electrodynamics are examples of the Cartan covariant derivative, whose spin connection is a foundational property both of fluid electrodynamics and of electrodynamics. Numerical solutions of the key equations illustrate the fluid flows of spacetime (or aether or vacuum).

The main field equations of fluid dynamics can be established as follows. The minimal prescription shows that the velocity $\mathbf{v}$ and ECE 2 vector potential $\mathbf{W}$ of a single particle are related by:

$$\mathbf{v} = \frac{e}{m}\mathbf{A} \tag{8.77}$$

where e and m are the charge and mass of the particle. For the continuum fluid:

$$\mathbf{v} = \frac{\rho}{\rho_m}\mathbf{A} \tag{8.78}$$

where ρ is the charge density and ρ_m is the mass density. The basic S. I. Units

are as follows:

$$\begin{aligned}
[\mathbf{E}] &= \text{volt}\,\text{m}^{-1} = \text{JC}^{-1}\text{m}^{-1} \\
[\mathbf{W}] &= \text{JsC}^{-1}\text{m}^{-1} \\
[\phi_W] &= \text{JC}^{-1} = \text{volt} \\
[\mathbf{B}] &= \text{JsC}^{-1}\text{m}^{-2} = \text{tesla} \\
[\rho] &= \text{Cm}^{-3} \\
[\mathbf{J}] &= \text{Cm}^{-2}\text{s}^{-1} \\
[\epsilon_0] &= \text{J}^{-1}\text{C}^2\text{m}^{-1} \\
[\mu_0] &= \text{Js}^2\text{C}^{-2}\text{m}^{-1}
\end{aligned} \tag{8.79}$$

The Kambe field equations of fluid dynamics are converted into the equations of fluid electrodynamics as follows:

Kambe's "fluid electric field" is:

$$\mathbf{E}_F = -\frac{\partial \mathbf{v}}{\partial t} - \boldsymbol{\nabla} h = (\mathbf{v} \cdot \boldsymbol{\nabla})\,\mathbf{v} \tag{8.80}$$

where the velocity field is the following function of Cartesian coordinates X, Y, Z and time:

$$\mathbf{v} = \mathbf{v}\,(X(t), Y(t), Z(t), t) \tag{8.81}$$

and where the following definition is used of enthalpy per unit mass h:

$$\boldsymbol{\nabla} h = \frac{1}{\rho_m} \boldsymbol{\nabla} P. \tag{8.82}$$

Here P denotes pressure, defined in non standard units. In ECE 2 electrodynamics, the electric field strength is:

$$\mathbf{E} = -\boldsymbol{\nabla}\phi_W - \frac{\partial \mathbf{W}}{\partial t}. \tag{8.83}$$

From Eqs. (8.80) and (8.83);

$$\mathbf{W} = \frac{\rho_m}{\rho}\mathbf{v} \tag{8.84}$$

and it follows that:

$$\phi_W = \frac{\rho_m}{\rho} h \tag{8.85}$$

in units of joules per coulomb.

Kambe's "fluid magnetic field" is defined to be the vorticity:

$$\mathbf{B}_F = \mathbf{w} = \boldsymbol{\nabla} \times \mathbf{v} \tag{8.86}$$

and it follows that:

$$\boldsymbol{\nabla} \cdot \mathbf{B}_F = \boldsymbol{\nabla} \cdot \mathbf{w} = 0. \tag{8.87}$$

Kambe's "fluid charge" and "fluid current" are respectively:

$$q_F = \boldsymbol{\nabla} \cdot \mathbf{E}_F = \boldsymbol{\nabla} \cdot ((\mathbf{v} \cdot \boldsymbol{\nabla})\, \mathbf{v}) \tag{8.88}$$

and

$$\mathbf{J}_F = \frac{\partial^2 \mathbf{v}}{\partial t^2} + \boldsymbol{\nabla} \frac{\partial h}{\partial t} + a_0^2\, \boldsymbol{\nabla} \times (\boldsymbol{\nabla} \times \mathbf{v})\,. \tag{8.89}$$

It follows that the charge density ρ and the current density $\mathbf{J}$ of fluid electrodynamics are:

$$\rho = \epsilon_0 \frac{\rho_m}{\rho} q_F \tag{8.90}$$

and

$$\mathbf{J} = \epsilon_0 \frac{\rho_m}{\rho} \mathbf{J}_F. \tag{8.91}$$

Therefore the Colomb Law of fluid electrodynamics is

$$\boldsymbol{\nabla} \cdot \left(\frac{\rho}{\rho_m} \mathbf{E} \right) = \frac{\rho}{\rho_m} \boldsymbol{\nabla} \cdot \mathbf{E} + \mathbf{E} \cdot \boldsymbol{\nabla} \left(\frac{\rho}{\rho_m} \right) = \frac{1}{\epsilon_0} \frac{\rho^2}{\rho_m} \tag{8.92}$$

and contains more information than the Coulomb law of electrodynamics. The former reduces to the latter if:

$$\boldsymbol{\nabla} \cdot \left(\frac{\rho}{\rho_m} \right) = \mathbf{0}. \tag{8.93}$$

The inhomogeneous field equation of Kambe is:

$$a_0^2\, \boldsymbol{\nabla} \times \mathbf{B}_F - \frac{\partial \mathbf{E}_F}{\partial t} = \mathbf{J}_F \tag{8.94}$$

where a_0 is the constant speed of sound. It follows that the Ampère Maxwell Law of fluid electrodynamics is:

$$a_0^2\, \boldsymbol{\nabla} \times \left(\frac{\rho}{\rho_m} \mathbf{B} \right) - \frac{\partial}{\partial t} \left(\frac{\rho}{\rho_m} \mathbf{E} \right) = \frac{1}{\epsilon_0} \frac{\rho}{\rho_m} \mathbf{J} \tag{8.95}$$

in which:

$$\boldsymbol{\nabla} \times \left(\frac{\rho}{\rho_m} \mathbf{B} \right) = \frac{\rho}{\rho_m} \boldsymbol{\nabla} \times \mathbf{B} + \left(\boldsymbol{\nabla} \frac{\rho}{\rho_m} \right) \times \mathbf{B} \tag{8.96}$$

and:

$$\frac{\partial}{\partial t} \left(\frac{\rho}{\rho_m} \mathbf{E} \right) = \frac{\rho}{\rho_m} \frac{\partial \mathbf{E}}{\partial t} + \mathbf{E} \frac{\partial}{\partial t} \left(\frac{\rho}{\rho_m} \right). \tag{8.97}$$

Eq. (8.95) becomes the Ampère Maxwell law of electrodynamics if:

$$\frac{\partial}{\partial t} \left(\frac{\rho}{\rho_m} \right) = 0,\ \boldsymbol{\nabla} \left(\frac{\rho}{\rho_m} \right) = \mathbf{0},\ a_0 \to c \tag{8.98}$$

in which case:

$$\boldsymbol{\nabla} \times \mathbf{B} - \frac{1}{c^2}\frac{\partial \mathbf{E}}{\partial t} = \mu_0 \mathbf{J}. \tag{8.99}$$

Eq. (8.95) can be written as:

$$\boldsymbol{\nabla} \times \mathbf{B} - \frac{1}{a_0^2}\frac{\partial \mathbf{E}}{\partial t} = \mu \mathbf{J} \tag{8.100}$$

if

$$\frac{\partial}{\partial t}\left(\frac{\rho}{\rho_m}\right) = 0, \ \boldsymbol{\nabla}\left(\frac{\rho}{\rho_m}\right) = \mathbf{0} \tag{8.101}$$

where the fluid permeability is defined as:

$$\mu = \frac{1}{\epsilon_0 a_0^2}. \tag{8.102}$$

Using Eqs. (8.88), (8.90) and (8.94), the sound equation of fluid electrodynamics is:

$$\frac{\partial^2}{\partial t^2}\left(\frac{\rho}{\rho_m}\mathbf{E}\right) + a_0^2 \boldsymbol{\nabla} \times \left(\boldsymbol{\nabla} \times \left(\frac{\rho}{\rho_m}\mathbf{E}\right)\right) = -\frac{1}{\epsilon_0}\frac{\partial}{\partial t}\left(\frac{\rho}{\rho_m}\mathbf{J}\right) \tag{8.103}$$

and under conditions (8.93) and (8.98) this becomes:

$$\frac{\partial^2 \mathbf{E}}{\partial t^2} + a_0^2 \boldsymbol{\nabla} \times (\boldsymbol{\nabla} \times \mathbf{E}) = -\frac{1}{\epsilon_0}\frac{\partial \mathbf{J}}{\partial t}. \tag{8.104}$$

In conventional electrodynamics the vacuum is defined by:

$$\rho = 0, \ \mathbf{J} = \mathbf{0} \tag{8.105}$$

but in fluid electrodynamics the vacuum is a richly structured fluid that can create electric and magnetic fields in a circuit as in the Ide circuit of UFT 311.

Therefore to translate the Kambe equations into fluid electrodynamics use:

$$\mathbf{v} = \left(\frac{\rho}{\rho_m}\right)\mathbf{W} \tag{8.106}$$

$$h = \left(\frac{\rho}{\rho_m}\right)\phi_W \tag{8.107}$$

$$\mathbf{B}_F = \left(\frac{\rho}{\rho_m}\right)\mathbf{B} \tag{8.108}$$

$$\mathbf{E}_F = \left(\frac{\rho}{\rho_m}\right)\mathbf{E} \tag{8.109}$$

$$q_F = \frac{1}{\epsilon_0}\frac{\rho^2}{\rho_m}. \tag{8.110}$$

The S. I. Units of the quantities used by Kambe are:

$$q_F = \mathrm{s}^{-2},\ \mathbf{E}_F = \mathrm{ms}^{-2},\ \mathbf{J}_F = \mathrm{ms}^{-3},\ \mathbf{B}_F = \mathrm{s}^{-1}. \tag{8.111}$$

The continuity equation of fluid electrodynamics is:

$$\frac{\partial \rho_m}{\partial t} + \boldsymbol{\nabla} \cdot \mathbf{J}_m = 0 \tag{8.112}$$

where ρ_m is mass density and $\mathbf{J}_m$ the current of mass density defined by:

$$\mathbf{J}_m = \rho_m \cdot \mathbf{v}. \tag{8.113}$$

Therefore:

$$\frac{\partial \rho_m}{\partial t} + \rho_m \boldsymbol{\nabla} \cdot \mathbf{v} + \mathbf{v} \cdot \boldsymbol{\nabla} \rho_m = 0. \tag{8.114}$$

Kambe transforms Eq. (8.112) into:

$$\frac{\partial q_F}{\partial t} + \boldsymbol{\nabla} \cdot \mathbf{J}_F = 0. \tag{8.115}$$

The continuity equation of ECE electrodynamics is:

$$\frac{\partial \rho}{\partial t} + \boldsymbol{\nabla} \cdot \mathbf{J} = 0 \tag{8.116}$$

where ρ is electric charge density and $\mathbf{J}$ is electric current density. It follows that the charge density of fluid electrodynamics is:

$$\rho = \epsilon_0 \frac{\rho_m}{\rho} q_F \tag{8.117}$$

and is a property of the velocity field of the fluid being considered. This can be matter or the vacuum, depending on context.

The continuity equation in fluid dynamics is the conservation of matter, which can be neither created nor destroyed in a conservative, classical system. The other fundamental equations of fluid dynamics are conservation of fluid linear momentum (the Euler and Navier Stokes equations); conservation of fluid energy; and conservation of fluid angular momentum (the vorticity equation). The Euler equation given by Kambe is:

$$\frac{D\mathbf{v}}{Dt} = \frac{\partial \mathbf{v}}{\partial t} + (\mathbf{v} \cdot \boldsymbol{\nabla})\,\mathbf{v} = \frac{1}{\rho} \boldsymbol{\nabla} P \tag{8.118}$$

and can be developed into the Navier Stokes equation by adding terms on the right hand side. The convective derivative is defined by:

$$\frac{D\mathbf{v}}{Dt} = \frac{\partial \mathbf{v}}{\partial t} + (\mathbf{v} \cdot \boldsymbol{\nabla})\,\mathbf{v} \tag{8.119}$$

and the Stokes derivative is:

$$\frac{D\rho}{\partial t} = \frac{\partial \rho}{\partial t} + \mathbf{v} \cdot \boldsymbol{\nabla} \rho. \tag{8.120}$$

Conservation of fluid energy is defined by Kambe through conservation of entropy per unit mass:

$$\frac{DS}{Dt} = \frac{\partial S}{\partial t} + \mathbf{v} \cdot \boldsymbol{\nabla} S. \tag{8.121}$$

Conservation of fluid angular momentum is expressed by Kambe as the vorticity equation:

$$\frac{\partial \mathbf{w}}{\partial t} + \boldsymbol{\nabla} \times (\mathbf{w} \times \mathbf{v}) = \mathbf{0}. \tag{8.122}$$

More generally Eq. (8.122) is developed as in Note 351(1) on `www.aias.us` for the Reynolds number R:

$$\frac{\partial \mathbf{w}}{\partial t} + \boldsymbol{\nabla} \times (\mathbf{w} \times \mathbf{v}) = \frac{1}{R} \nabla^2 \mathbf{w}. \tag{8.123}$$

The Reynolds number produces turbulence and shearing. In general the Kambe equations apply to compressible fluids with finite viscosity. In inviscid fluids:

$$\boldsymbol{\nabla} \cdot \mathbf{v} = 0. \tag{8.124}$$

The Kambe field equations are the result of rearranging these fundamental conservation equations. The rearrangement results in field equations whose structure is shown in this chapter to be that of Cartan geometry itself. This is the same structure as the ECE 2 electrodynamics and gravitation. This is referred to as "triple unification". The Stokes derivative is:

$$\frac{D\rho}{Dt} = \frac{\partial \rho}{\partial t} + \boldsymbol{\nabla} \rho \cdot \mathbf{v} = \frac{\partial \rho}{\partial t} + \frac{\partial \rho}{\partial X}\frac{dX}{dt} + \frac{\partial \rho}{\partial Y}\frac{dY}{dt} + \frac{\partial \rho}{\partial Z}\frac{dZ}{dt} \tag{8.125}$$

where the fluid mass density is the function:

$$\rho = \rho\left(X(t), Y(t), Z(t), t\right). \tag{8.126}$$

The covariant derivative of Cartan geometry is:

$$\frac{DV^a}{Dx^\mu} = \frac{\partial V^a}{\partial x^\mu} + \omega^a{}_{\mu b} V^b \tag{8.127}$$

where the general vector field V^a is defined in a tangent space at point P of the base manifold. The general spin connection is $\omega^a{}_{\mu b}$. Define the four vector:

$$V^\mu = (c\rho, \mathbf{v}\rho) \tag{8.128}$$

and consider the indices:

$$\mu = 0, \ a = 0. \tag{8.129}$$

It follows that:

$$\frac{D\rho}{Dt} = \frac{\partial \rho}{\partial t} + \omega^0{}_{01}\rho\frac{dX}{dt} + \omega^0{}_{02}\rho\frac{dY}{dt} + \omega^0{}_{03}\rho\frac{dZ}{dt}. \tag{8.130}$$

This is the Stokes derivative, Q. E. D., provided that:

$$\omega^0{}_{01}\rho = \frac{\partial\rho}{\partial X},\ \omega^0{}_{02}\rho = \frac{\partial\rho}{\partial Y},\ \omega^0{}_{03}\rho = \frac{\partial\rho}{\partial Z} \tag{8.131}$$

i. e.

$$\boldsymbol{\nabla}\rho = \boldsymbol{\omega}\rho \tag{8.132}$$

where the spin connection vector is:

$$\boldsymbol{\omega} = \omega^0{}_{01}\mathbf{i} + \omega^0{}_{02}\mathbf{j} + \omega^0{}_{03}\mathbf{k}. \tag{8.133}$$

Similarly the convective or material derivative is:

$$\frac{D\mathbf{v}}{Dt} = \frac{\partial\mathbf{v}}{\partial t} + (\mathbf{v}\cdot\boldsymbol{\nabla})\,\mathbf{v} \tag{8.134}$$

where the fluid velocity field is:

$$\mathbf{v} = \mathbf{v}\left(X(t), Y(t), Z(t), t\right). \tag{8.135}$$

The convective derivative is therefore:

$$\frac{D\mathbf{v}}{Dt} = \frac{\partial\mathbf{v}}{\partial t} + \left(v_X\frac{\partial}{\partial X} + v_Y\frac{\partial}{\partial Y} + v_Z\frac{\partial}{\partial Z}\right)\mathbf{v}. \tag{8.136}$$

The X component for example is:

$$\frac{Dv_X}{Dt} = \frac{\partial v_X}{\partial t} + v_X\frac{\partial v_X}{\partial t} + v_Y\frac{\partial v_X}{\partial Y} + v_Z\frac{\partial v_X}{\partial Z} = \frac{\partial v_X}{\partial t} + \mathbf{v}\cdot\boldsymbol{\nabla}\,v_X. \tag{8.137}$$

Considering the index:

$$\mu = 0 \tag{8.138}$$

in Eq. (8.127) implies that:

$$\omega^1{}_{01} = \frac{\partial v_X}{\partial X},\ \omega^1{}_{02} = \frac{\partial v_X}{\partial Y},\ \omega^1{}_{03} = \frac{\partial v_X}{\partial Z} \tag{8.139}$$

and in general the spin connection of the convective derivative is:

$$\omega^a{}_{0b} = \frac{\partial v^a}{\partial x^b} \tag{8.140}$$

Q. E. D. So all the equations of fluid dynamics originate in the spin connection of Cartan geometry, which also describes the field equations of fluid dynamics.

Kambe's "fluid magnetic field" is the vorticity:

$$\mathbf{B}_F = \mathbf{w} = \boldsymbol{\nabla}\times\mathbf{v} \tag{8.141}$$

so:

$$\boldsymbol{\nabla}\cdot\mathbf{B}_F = \boldsymbol{\nabla}\cdot\mathbf{w} = 0. \tag{8.142}$$

The homogeneous field equation of Kambe is:

$$\boldsymbol{\nabla} \times \mathbf{E}_F + \frac{\partial \mathbf{B}_F}{\partial t} = \mathbf{0} \tag{8.143}$$

where:

$$\mathbf{B}_F = \mathbf{w} \tag{8.144}$$

and the vorticity equation used by Kambe is:

$$\frac{\partial \mathbf{w}}{\partial t} + \boldsymbol{\nabla} \times (\mathbf{w} \times \mathbf{v}) = \mathbf{0}. \tag{8.145}$$

Therefore Kambe's convective derivative is:

$$\frac{D\mathbf{v}}{Dt} = \frac{\partial \mathbf{v}}{\partial t} + \mathbf{E}_F. \tag{8.146}$$

From Eqs. (8.143) and (8.145),

$$\mathbf{E}_F = \mathbf{v} \times \mathbf{w} = (\mathbf{v} \cdot \boldsymbol{\nabla})\, \mathbf{v}. \tag{8.147}$$

In the particular case of Beltrami flow:

$$\boldsymbol{\nabla} \times \mathbf{v} = k\mathbf{v} \tag{8.148}$$

and:

$$(\mathbf{v} \cdot \boldsymbol{\nabla})\, \mathbf{v} = \mathbf{0}. \tag{8.149}$$

For a general flow, Eq. (8.147) must be solved numerically for $\mathbf{v}$:

$$\mathbf{v} \times (\boldsymbol{\nabla} \times \mathbf{v}) = (\mathbf{v} \cdot \boldsymbol{\nabla})\, \mathbf{v}. \tag{8.150}$$

The Reynolds number R responsible for turbulent flow enters into the analysis using:

$$\frac{\partial \mathbf{w}}{\partial t} + \boldsymbol{\nabla} \times (\mathbf{w} \times \mathbf{v}) = \frac{1}{R} \nabla^2 \mathbf{w} \tag{8.151}$$

so:

$$\boldsymbol{\nabla} \times \mathbf{E}_F = \frac{1}{R} \nabla^2 \mathbf{w} - \boldsymbol{\nabla} \times (\mathbf{w} \times \mathbf{v})\,. \tag{8.152}$$

Now use:

$$\boldsymbol{\nabla} \times (\boldsymbol{\nabla} \times \mathbf{w}) = \boldsymbol{\nabla}\, (\boldsymbol{\nabla} \cdot \mathbf{w}) - \nabla^2 \mathbf{w} \tag{8.153}$$

and

$$\boldsymbol{\nabla} \cdot \mathbf{w} = 0 \tag{8.154}$$

to find that:

$$\nabla^2 \mathbf{w} = -\boldsymbol{\nabla} \times (\boldsymbol{\nabla} \times \mathbf{w}) . \tag{8.155}$$

It follows from Eqs. (8.152) and (8.155) that:

$$\mathbf{E}_F = (\mathbf{v} \cdot \boldsymbol{\nabla}) \mathbf{v} = \mathbf{v} \times \mathbf{w} - \frac{1}{R} \boldsymbol{\nabla} \times \mathbf{w}. \tag{8.156}$$

Therefore transition to turbulence is governed in general using:

$$\boldsymbol{\nabla} \times \mathbf{w} = -R \left((\mathbf{v} \cdot \boldsymbol{\nabla}) \mathbf{v} - \mathbf{v} \times \mathbf{w} \right) . \tag{8.157}$$

Turbulence in Beltrami flow is defined by:

$$\boldsymbol{\nabla} \times \mathbf{w} = -R (\mathbf{v} \cdot \boldsymbol{\nabla}) \mathbf{v}. \tag{8.158}$$

Here:

$$\boldsymbol{\nabla} \times \mathbf{w} = \boldsymbol{\nabla} \times (\boldsymbol{\nabla} \times \mathbf{v}) = \mathbf{v} (\boldsymbol{\nabla} \cdot \mathbf{v}) - \nabla^2 \mathbf{v} \tag{8.159}$$

so from Eqs. (8.158) and (8.159) turbulence in Beltrami flow is governed by:

$$\nabla^2 \mathbf{v} = R (\mathbf{v} \cdot \boldsymbol{\nabla}) \mathbf{v} + \boldsymbol{\nabla} (\boldsymbol{\nabla} \cdot \mathbf{v}) \tag{8.160}$$

which can be solved numerically.

Examples of numerical solutions from flow algorithms are given later in this chapter.

The Kambe equations can be developed to include the viscous force and other terms in the most general Navier Stokes and vorticity equations. The general Navier Stokes equation is:

$$\frac{D\mathbf{v}}{Dt} = \frac{\partial \mathbf{v}}{\partial t} + (\mathbf{v} \cdot \boldsymbol{\nabla}) \mathbf{v} = -\boldsymbol{\nabla} h - \boldsymbol{\nabla} \phi + \mathbf{f}_{\text{visc}} \tag{8.161}$$

where $\mathbf{f}_{\text{visc}}$ is the viscous force and ϕ is a potential such as the gravitational potential. Kambe used the equation:

$$\frac{D\mathbf{v}}{Dt} = \frac{\partial \mathbf{v}}{\partial t} + (\mathbf{v} \cdot \boldsymbol{\nabla}) \mathbf{v} = -\boldsymbol{\nabla} h \tag{8.162}$$

so omitted two terms. The more general definition of Kambe's "fluid electric field" is:

$$\mathbf{E}_F = -\boldsymbol{\nabla} h - \boldsymbol{\nabla} \phi + \mathbf{f}_{\text{visc}} - \frac{\partial \mathbf{v}}{\partial t}. \tag{8.163}$$

The viscous force is defined most generally [2]- [13] by:

$$\mathbf{f}_{\text{visc}} = \mu \nabla^2 \mathbf{v} + (\mu + \mu') \boldsymbol{\nabla} (\boldsymbol{\nabla} \cdot \mathbf{v}) \tag{8.164}$$

and it follows that:

$$\Phi = h + \phi - (\mu + \mu') \boldsymbol{\nabla} \cdot \mathbf{v} - \phi_1 \tag{8.165}$$

where μ and μ' are coefficients to be determined. Here:

$$\mathbf{E}_F = -\boldsymbol{\nabla}\Phi - \frac{\partial \mathbf{v}}{\partial t} \tag{8.166}$$

$$\boldsymbol{\nabla}\phi_1 = \mu\nabla^2\mathbf{v}. \tag{8.167}$$

With this definition of the scalar potential Φ, the Kambe field equations follow:

$$\boldsymbol{\nabla}\cdot\mathbf{B}_F = \boldsymbol{\nabla}\cdot\mathbf{w} = \boldsymbol{\nabla}\cdot\boldsymbol{\nabla}\times\mathbf{v} = \mathbf{0} \tag{8.168}$$

$$\boldsymbol{\nabla}\times\mathbf{E}_F + \frac{\partial \mathbf{B}_F}{\partial t} = \mathbf{0} \tag{8.169}$$

$$\boldsymbol{\nabla}\cdot\mathbf{E}_F = q_F \tag{8.170}$$

$$a_0^2\,\boldsymbol{\nabla}\times\mathbf{B}_F - \frac{\partial \mathbf{E}_F}{\partial t} = \mathbf{J}_F. \tag{8.171}$$

It has been shown that the most general form of fluid dynamics can be expressed as ECE 2 covariant field equations, Q. E. D. Here a_0 is the assumed constant speed of sound as used by Kambe. In general a_0 is not constant.

The most general vorticity equation is:

$$\frac{\partial \mathbf{w}}{\partial t} + \boldsymbol{\nabla}\times(\boldsymbol{\nabla}\times\mathbf{w}) = \frac{1}{\rho^2}\boldsymbol{\nabla}\rho\times\boldsymbol{\nabla}P + \frac{\mu}{\rho}\nabla^2\mathbf{w}. \tag{8.172}$$

Kambe omitted the second and third terms on the right hand side of Eq. (8.172), the baroclinic and Reynolds number terms.

In the field equations (8.168) to (8.171) the fluid charge is defined by:

$$q_F = \boldsymbol{\nabla}\cdot\mathbf{E}_F = \boldsymbol{\nabla}\cdot((\mathbf{v}\cdot\boldsymbol{\nabla})\,\mathbf{v}) \tag{8.173}$$

and the fluid current by:

$$\mathbf{J}_F = a_0^2\,\boldsymbol{\nabla}\times(\boldsymbol{\nabla}\times\mathbf{v}) - \frac{\partial}{\partial t}\left((\mathbf{v}\cdot\boldsymbol{\nabla})\,\mathbf{v}\right). \tag{8.174}$$

As in Note 353(5) it follows that:

$$\nabla^2\Phi + \frac{\partial}{\partial t}\left(\boldsymbol{\nabla}\cdot\mathbf{v}\right) = -q_F \tag{8.175}$$

and:

$$\Box\,\mathbf{v} + \boldsymbol{\nabla}\left(\boldsymbol{\nabla}\cdot\mathbf{v} + \frac{1}{a_0^2}\frac{\partial\Phi}{\partial t}\right) = \frac{1}{a_0^2}\mathbf{J}_F \tag{8.176}$$

where the d'Alembertian operator is defined by:

$$\Box := \frac{1}{a_0^2}\frac{\partial^2}{\partial t^2} - \nabla^2. \tag{8.177}$$

These equations can be simplified using the continuity equation:

$$\frac{\partial q_F}{\partial t} + \boldsymbol{\nabla}\cdot\mathbf{J}_F = 0. \tag{8.178}$$

As shown in detail in Note 353(6), this is an exact consequence of the definitions (8.173) and (8.174). With the definitions:

$$J_F^\mu = (a_0 q_F, \mathbf{J}_F) \tag{8.179}$$

$$\partial_\mu = \left(\frac{1}{a_0} \frac{\partial}{\partial t}, \boldsymbol{\nabla} \right) \tag{8.180}$$

and (8.178), the continuity equation can be written as:

$$\partial_\mu J_F^\mu = 0. \tag{8.181}$$

Now define the velocity four vector:

$$v^\mu = \left(\frac{\Phi}{a_0}, \mathbf{v} \right) \tag{8.182}$$

and assume:

$$\partial_\mu v^\mu = \frac{1}{a_0^2} \frac{\partial \Phi}{\partial t} + \boldsymbol{\nabla} \cdot \mathbf{v} = 0. \tag{8.183}$$

This is the Lorenz gauge assumption of fluid electrodynamics. With the assumption (8.183), Eqs. (8.175) and (8.176) reduce to:

$$\Box \, \Phi = q_F \tag{8.184}$$

and:

$$\Box \, \mathbf{v} = \frac{1}{a_0^2} \mathbf{J}_F \tag{8.185}$$

which can be combined in to the single wave equation:

$$\Box \, v^\mu = \frac{1}{a_0^2} J_F^\mu \tag{8.186}$$

Q. E. D.

The relevant S. I. Units are as follows:

$$\Box = \mathrm{m}^{-2}, \ \Phi = \mathrm{m}^2 \mathrm{s}^{-2}, \ q_F = \mathrm{s}^{-2}, \ \mathbf{J}_F = \mathrm{ms}^{-3}, \ a_0 = \mathrm{ms}^{-1}. \tag{8.187}$$

From Eqs. (8.178), (8.184) and (8.185):

$$\frac{1}{a_0^2} \frac{\partial}{\partial t} (\Box \, \Phi) + \boldsymbol{\nabla} \cdot \Box \, \mathbf{v} = 0 \tag{8.188}$$

and by commutativity of differential operators:

$$\Box \left(\frac{1}{a_0^2} \frac{\partial \Phi}{\partial t} + \boldsymbol{\nabla} \cdot \mathbf{v} \right) = 0. \tag{8.189}$$

The Lorenz condition (8.183) is a possible solution of Eq. (8.189), Q. E. D. So the analysis is rigorously self consistent. It has been shown that the entire

subject of fluid dynamics can be reduced to a single wave equation, which like all wave equations of physics, is an example of the ECE wave equation

$$(\square + R)\, v^{\mu} = 0 \tag{8.190}$$

of Cartan geometry [2]- [13], provided that the scalar curvature is defined by:

$$Rv^{\mu} := -\frac{1}{a_0^2} J_F^{\mu}. \tag{8.191}$$

Later in this chapter these results are analysed with graphics and animations, using advanced flow dynamics algorithms. The animations are archived on `www.aias.us`.

Using these results, simple equations can be developed to describe the transfer of energy and power from a fluid vacuum or aether or spacetime to a circuit. The process rigorously conserves total energy momentum and total charge current density.

The electric field ($\mathbf{E}_F$) of ECE 2 fluid dynamics is defined by the Kambe equation:

$$\boldsymbol{\nabla} \cdot \mathbf{E}_F(\text{circuit}) = q_F(\text{spacetime}) \tag{8.192}$$

where the Kambe charge is:

$$q_F(\text{spacetime}) = \boldsymbol{\nabla} \cdot ((\mathbf{v} \cdot \boldsymbol{\nabla})\, \mathbf{v}) \tag{8.193}$$

so:

$$\mathbf{E}_F(\text{circuit}) = (\mathbf{v} \cdot \boldsymbol{\nabla})\, \mathbf{v}. \tag{8.194}$$

The electric field strength in volts per metre induced in the circuit is:

$$\mathbf{E}(\text{circuit}) = \left(\frac{\rho_m}{\rho}\right)(\text{circuit})\, \mathbf{E}_F(\text{circuit}) \tag{8.195}$$

in the notation of this chapter. Not carefully that the ratio of mass density to charge density is that in the circuit, while $\mathbf{v}$ is the velocity field of the fluid vacuum. So $\mathbf{E}$ of the circuit is calculated directly from $\mathbf{v}$ of the vacuum (or spacetime or aether). The latter is computed numerically from the vacuum vorticity equation:

$$\frac{D\mathbf{v}}{Dt} = \frac{\partial \mathbf{v}}{\partial t} + (\mathbf{v} \cdot \boldsymbol{\nabla})\, \mathbf{v} = \frac{1}{2} \boldsymbol{\nabla} v^2 - \frac{1}{R} \left(\boldsymbol{\nabla} (\boldsymbol{\nabla} \cdot \mathbf{v}) + \nabla^2 \mathbf{v} \right) \tag{8.196}$$

where R is the vacuum Reynolds number. The boundary conditions of Eq. (8.196) are determined by the design of the circuit in contact with the ubiquitous vacuum.

Having found $\mathbf{v}$ from Eq. (8.196) the Kambe current of the fluid vacuum can be found from:

$$\mathbf{J}_F = a_0^2\, \boldsymbol{\nabla} \times (\boldsymbol{\nabla} \times \mathbf{v}) - \frac{\partial}{\partial t} ((\mathbf{v} \cdot \boldsymbol{\nabla})\, \mathbf{v}). \tag{8.197}$$

The Kambe magnetic field induced in the circuit by the fluid vacuum is:

$$\mathbf{B}_F = \mathbf{w} = \boldsymbol{\nabla} \times \mathbf{v} \tag{8.198}$$

so the magnetic field strength in tesla induced in the circuit by the vacuum is:

$$\mathbf{B}(\text{circuit}) = \frac{\rho_m}{\rho}(\text{circuit})\, \boldsymbol{\nabla} \times \mathbf{v}. \tag{8.199}$$

Eqs. (8.195) and (8.199) are simple expressions for $\mathbf{E}$ and $\mathbf{B}$ induced in a circuit such as that of UFT 311 on `www.aias.us`. Conversely, $\mathbf{E}$ and $\mathbf{B}$ of any circuit produce patterns of flow in the vacuum. The great advantage of this method is its simplicity, and the fact that knowledge is required only of ρ_m/ρ in the circuit. The electric field strength in volts per metre induced in the circuit can be expressed as:

$$\begin{aligned} \mathbf{E}(\text{circuit}) &= \left(\frac{\rho_m}{\rho}\right)(\text{circuit})\left((\mathbf{v}\cdot\boldsymbol{\nabla})\,\mathbf{v}\right)(\text{spacetime}) \\ &= \left(\frac{\rho_m}{\rho}\right)(\text{circuit})\left(-\boldsymbol{\nabla}\Phi - \frac{\partial \mathbf{v}}{\partial t}\right)(\text{spacetime}) \end{aligned} \tag{8.200}$$

where Φ is the general potential of fluid dynamics defined earlier in this chapter. Using the spacetime Lorenz condition defined earlier in this chapter:

$$\frac{1}{a_0^2}\frac{\partial \Phi}{\partial t} + \boldsymbol{\nabla}\cdot\mathbf{v} = 0 \tag{8.201}$$

the potential can be defined by:

$$\Phi = -a_0^2 \int \boldsymbol{\nabla}\cdot\mathbf{v}\, dt. \tag{8.202}$$

As in Note 355(5) on `www.aias.us` it can be used to define a simplified Navier Stokes equation:

$$\frac{D\mathbf{v}}{Dt} = \frac{\partial \mathbf{v}}{\partial t} + (\mathbf{v}\cdot\boldsymbol{\nabla})\,\mathbf{v} = a_0^2\,\boldsymbol{\nabla}\left(\int \boldsymbol{\nabla}\cdot\mathbf{v}\, dt\right) \tag{8.203}$$

from which $\mathbf{v}$ may be computed numerically. Eq. (8.203) may be more amenable to numerical solution than:

$$\frac{\partial \mathbf{v}}{\partial t} = \mathbf{v}\times(\boldsymbol{\nabla}\times\mathbf{v}) - \frac{1}{R}\boldsymbol{\nabla}\times(\boldsymbol{\nabla}\times\mathbf{v}). \tag{8.204}$$

As in Note 355(2) the Lorenz condition (8.201) corresponds to the wave equation of fluid electrodynamics:

$$\Box\, W^{\mu}(\text{circuit}) = \mu_0 J^{\mu}(\text{spacetime}) \tag{8.205}$$

where:

$$W^{\mu}(\text{circuit}) = \left(\frac{\phi_W}{c}, \mathbf{W}\right)(\text{circuit}). \tag{8.206}$$

The four current of fluid spacetime is defined by:

$$J_F^{\mu}(\text{spacetime}) = (a_0 q_F, \mathbf{J}_F)\,. \tag{8.207}$$

Defining the velocity four vector:

$$v^{\mu} = \left(\frac{\Phi_0}{a_0}, \mathbf{v}\right). \tag{8.208}$$

it follows that:

$$\Box\, v^{\mu}(\text{circuit}) = \frac{1}{a_0^2} J_F^{\mu}(\text{spacetime}). \tag{8.209}$$

This equation is equivalent to:

$$\Box\, \Phi(\text{circuit}) = q_F(\text{spacetime}) \tag{8.210}$$

$$\Box\, \mathbf{v}(\text{circuit}) = \frac{1}{a_0^2} \mathbf{J}_F(\text{spacetime}) \tag{8.211}$$

and to:

$$\Box\, W^{\mu}(\text{circuit}) = \frac{1}{c^2} \left(\frac{\rho_m}{\rho}\right)(\text{circuit})\, J_F^{\mu}(\text{spacetime}). \tag{8.212}$$

It follows that the wave equation defining transfer of energy/momentum from spacetime is:

$$\Box\, W^{\mu}(\text{circuit}) = \left(\frac{a_0}{c}\right)^2 \left(\frac{\rho_m}{\rho}\right)(\text{circuit})\, \Box\, v^{\mu}(\text{circuit}). \tag{8.213}$$

The converse of this theory shows that material or circuit potentials and electric and magnetic fields induce a rich structure in the fluid vacuum.

Consider the velocity field $\mathbf{v}_F$ of any fluid. The fluid magnetic and electric fields are defined by:

$$\mathbf{B}_F = \mathbf{w}_F = \boldsymbol{\nabla} \times \mathbf{v}_F \tag{8.214}$$

and:

$$\mathbf{E}_F = (\mathbf{v}_F \cdot \boldsymbol{\nabla})\, \mathbf{v}_F. \tag{8.215}$$

The fluid velocity field itself is the fluid vector potential:

$$\mathbf{W}_F = \mathbf{v}_F. \tag{8.216}$$

Define:

$$x = \left(\frac{\rho_m}{\rho}\right)(\text{material}) \tag{8.217}$$

in the notation of this chapter. It follows that the vector potential $\mathbf{W}$, the electric field strength $\mathbf{E}$ and the magnetic flux density $\mathbf{B}$ of a material or circuit in contact with the vacuum are:

$$\mathbf{W} = x\mathbf{W}_F,\ \mathbf{E} = x\mathbf{E}_F,\ \mathbf{B} = x\mathbf{B}_F. \tag{8.218}$$

For example consider a static electric field strength in volts per metre in a spherical polar coordinate system:

$$\mathbf{E} = -\frac{e}{4\pi\epsilon_0 r^2}\mathbf{e}_r = x\left(\mathbf{v}_F \cdot \boldsymbol{\nabla}\right)\mathbf{v}_F \tag{8.219}$$

where $-e$ is the charge on the electron, $\mathbf{e}_r$ is the radial unit vector, $\mathbf{r}$ the distance between two charges and ϵ_0 the S. I. permittivity in vacuo. Eq. (8.219) is a non-linear partial differential equation in the velocity field $\mathbf{v}_F$. For a static electric field strength in volts per metre of a material or circuit:

$$\mathbf{E}_r = -\frac{e}{4\pi\epsilon_0 r^2} = x\left(\mathbf{v}_F \cdot \boldsymbol{\nabla}\right)v_{rF} \tag{8.220}$$

$$\mathbf{E}_\phi = 0 = x\left(\mathbf{v}_F \cdot \boldsymbol{\nabla}\right)v_{\phi F} \tag{8.221}$$

$$\mathbf{E}_\theta = 0 = x\left(\mathbf{v}_F \cdot \boldsymbol{\nabla}\right)v_{\theta F} \tag{8.222}$$

and may be solved using Maxima to give:

$$v_{rF} = \frac{\left(-\frac{er^3}{\epsilon_0 x} - \frac{12\pi C}{x}\right)^{1/2}}{(6\pi)^{1/2}\, r^2} \tag{8.223}$$

where C is a constant of integration. This solution is graphed later in this chapter. The same type of solution applies to a gravitational field:

$$\mathbf{g} = -\frac{MG}{r^2}\mathbf{e}_r \tag{8.224}$$

and the subject of fluid gravitation emerges. It is developed in chapter nine.

In Cartesian coordinates:

$$\mathbf{E} = -\frac{e}{4\pi\epsilon_0 Z^2}\mathbf{k} = x\left(\mathbf{v}_F \cdot \boldsymbol{\nabla}\right)\mathbf{v}_F \tag{8.225}$$

for a static electric field aligned in the Z axis. The system to be solved is:

$$E_Z = x\left(v_{FX}\frac{\partial}{\partial X} + v_{FY}\frac{\partial}{\partial Y} + v_{FZ}\frac{\partial}{\partial Z}\right)v_{FZ} = -\frac{e}{4\pi\epsilon_0 Z^2} \tag{8.226}$$

$$E_Y = x\left(v_{FX}\frac{\partial}{\partial X} + v_{FY}\frac{\partial}{\partial Y} + v_{FZ}\frac{\partial}{\partial Z}\right)v_{FY} = 0 \tag{8.227}$$

$$E_Z = x\left(v_{FX}\frac{\partial}{\partial X} + v_{FY}\frac{\partial}{\partial Y} + v_{FZ}\frac{\partial}{\partial Z}\right)v_{FZ} = 0 \tag{8.228}$$

which is comprised of three linear differential equations in three unknowns, and can be solved given a set of boundary conditions.

The above equations are augmented by Eq. (8.218), which calculates the vacuum velocity field directly from the material's $\mathbf{W}$ potential. Knowing $\mathbf{v}_F$, the electric and magnetic fields of the vacuum can be calculated without the need to solve differential equations. The $\mathbf{B}_F$ and $\mathbf{E}_F$ of the vacuum induce material electric and magnetic properties as follows:

$$\mathbf{E} = x\mathbf{E}_F,\ \mathbf{B} = x\mathbf{B}_F \tag{8.229}$$

and this is energy from spacetime (ES) currently the subject of a House of Lords Committee on new sources of energy. Various types of vector potential are listed in Note 356(7), and each type can be used to compute vacuum properties as reported late in this chapter.

Having computed $\mathbf{v}_F$ induced in the vacuum, the following vacuum properties can also be computed.

1) The induced vacuum acceleration field:

$$\mathbf{a}_F = \frac{\partial \mathbf{v}_F}{\partial t} + (\mathbf{v}_F \cdot \boldsymbol{\nabla})\,\mathbf{v}_F \tag{8.230}$$

where:

$$(\mathbf{v}_F \cdot \boldsymbol{\nabla})\,\mathbf{v}_F = \frac{1}{2}\boldsymbol{\nabla}\mathbf{v}_F^2 - \mathbf{v}_F \times (\boldsymbol{\nabla} \times \mathbf{v}_F)\,. \tag{8.231}$$

2) The induced electric charge of the fluid vacuum:

$$q_F = \boldsymbol{\nabla} \cdot \mathbf{E}_F. \tag{8.232}$$

3) The induced electric current of the fluid vacuum:

$$\mathbf{J}_F = a_0^2\,\boldsymbol{\nabla} \times (\boldsymbol{\nabla} \times \mathbf{v}_F) - \frac{\partial \mathbf{E}_F}{\partial t}. \tag{8.233}$$

4) The induced scalar potential Φ_F using the vacuum Lorenz condition:

$$\frac{\partial \Phi_F}{\partial t} + a_0^2\,\boldsymbol{\nabla} \cdot \mathbf{v}_F = 0. \tag{8.234}$$

5) The induced magnetic field of the fluid vacuum:

$$\mathbf{B}_F = \mathbf{w}_F = \boldsymbol{\nabla} \times \mathbf{v}_F. \tag{8.235}$$

6) The induced electric field of the fluid vacuum:

$$\begin{aligned}\mathbf{E}_F &= (\mathbf{v}_F \cdot \boldsymbol{\nabla})\,\mathbf{v}_F = \frac{1}{2}\boldsymbol{\nabla}v_F^2 - \mathbf{v}_F \times (\boldsymbol{\nabla} \times \mathbf{v}_F) \\ &= -\boldsymbol{\nabla}\Phi_F - \frac{\partial \mathbf{v}_F}{\partial t}.\end{aligned} \tag{8.236}$$

7) The induced vacuum scalar potential from the vacuum wave equation:

$$\Box\,\Phi_F = q_F. \tag{8.237}$$

8) The induced vacuum current $\mathbf{J}_F$ using:

$$\Box \mathbf{v}_F = \frac{1}{a_0^2}\mathbf{J}_F. \tag{8.238}$$

9) The induced enthalpy gradient of the vacuum:

$$\boldsymbol{\nabla} h_F = \frac{1}{\rho_F}\boldsymbol{\nabla} P_F = -\frac{\partial \mathbf{v}_F}{\partial t} - \mathbf{E}_F. \tag{8.239}$$

10) The induced baroclinic torque of the vacuum:

$$\frac{1}{\rho_F^2}\boldsymbol{\nabla}\rho_F \times \boldsymbol{\nabla} P_F = \frac{\partial w_F}{\partial t} + \boldsymbol{\nabla} \times (\mathbf{W}_F \times \mathbf{v}_F) - \frac{1}{R_F}\nabla^2 \mathbf{w}_F \tag{8.240}$$

where R_F is the vacuum Reynolds number.

11) The induced vacuum Reynolds number for vanishing baroclinic torque:

$$\frac{\partial \mathbf{w}_F}{\partial t} + \boldsymbol{\nabla} \times (\mathbf{w}_F \times \mathbf{v}_F) = \frac{1}{R_F}\nabla^2 \mathbf{w}_F. \tag{8.241}$$

Later on in this chapter these quantities are computed and graphed.

Finally in this chapter it is shown that fluid electrodynamics gives an explanation to any precision of the well known radiative corrections, exemplified by the anomalous g factor of the electron and the Lamb shift. The former is due to the vacuum vorticity induced by a material flux density in tesla, and the latter by the existence of the vacuum potential.

Consider the well known Dirac hamiltonian defined by the interaction of a magnetic flux density $\mathbf{B}$ and and an electron of charge modulus e and mass m:

$$H = -\frac{e}{2m}(\mathbf{L} + 2\mathbf{S}) \cdot \mathbf{B}. \tag{8.242}$$

Here $\mathbf{L}$ is the orbital angular momentum and $\mathbf{S}$ is the spin angular momentum of the electron. The factor of two that premultiplies $\mathbf{S}$ is the g factor of the Dirac electron. However the experimental g factor to nine decimal places is:

$$g = 2.002319314. \tag{8.243}$$

The experimental result (8.243) has long been considered to be due to the vacuum, a radiative correction. It is a well established proof of energy from spacetime (or vacuum or aether). The explanation of the anomalous g of the electron rests on the existence of the vacuum potential $\mathbf{W}(\text{vac})$ induced by the material magnetic flux density. In ECE 2 fluid electrodynamics:

$$\mathbf{w} = \frac{1}{2}\mathbf{B} \times \mathbf{r} \tag{8.244}$$

where $\mathbf{v}(\text{vac})$ is the velocity field induced in the vacuum by $\mathbf{B}$. The induced vacuum potential in turn induces a potential:

$$\mathbf{W}_1 = \frac{m}{e}\mathbf{v}(\text{vac}) \tag{8.245}$$

in the electron. So the relevant minimal prescription is:

$$\mathbf{p} \to \mathbf{p} - e\mathbf{W} - m\mathbf{W}_1 = \mathbf{p} - e\left(\mathbf{W} + \mathbf{W}_2\right). \tag{8.246}$$

Assume that:

$$\mathbf{W}_2 = x\mathbf{W} \tag{8.247}$$

then as shown in Note 357(2) the interaction hamiltonian (8.242) is changed to:

$$H_1 = -\frac{e}{2m}\left(\left(1 + x\right)\left(2\mathbf{S} \cdot \mathbf{B}\right) + \mathbf{L}\right) \tag{8.248}$$

giving the anomalous g factor of the electron:

$$g = 2\left(1 + x\right). \tag{8.249}$$

Therefore to nine decimal places:

$$x = 0.002319314. \tag{8.250}$$

The additional magnetic flux density induced in the electron by fluid spacetime is:

$$\mathbf{B}_1 = \frac{m}{e}\boldsymbol{\nabla} \times \mathbf{v}(\text{vac}) = x\mathbf{B} \tag{8.251}$$

where the spacetime vorticity is:

$$\mathbf{w}(\text{vac}) = \boldsymbol{\nabla} \times \mathbf{v}(\text{vac}). \tag{8.252}$$

Finally assume that:

$$\mathbf{B} = B_Z\mathbf{k} \tag{8.253}$$

to find that:

$$x = \frac{m}{e}\frac{w_Z(\text{vac})}{B_Z} = 0.002319314. \tag{8.254}$$

For a magnetic flux density of one tesla the vacuum vorticity needed to produce the observed g factor of the electron is:

$$w_Z(\text{vac}) = -4.07923 \times 10^8\,\text{s}^{-1}. \tag{8.255}$$

In general:

$$w_Z(\text{vac}) = 0.002319314\,\frac{e}{m}B_Z \tag{8.256}$$

which is the equation defining the vacuum vorticity induced by a static magnetic flux density.

In the Dirac theory of Note (357(3)) the following energy levels of the H atom are degenerate:

$$2S_{1/2}\,(n=2,\,l=0,\,j=1/2) \tag{8.257}$$

$$2P_{1/2}\,(n=2,\,l=1,\,j=1/2)\,. \tag{8.258}$$

However it is observed experimentally that $2S_{1/2}$ is higher in frequency by:

$$\omega = 6.64675\times 10^{9}\,\mathrm{rad\,s^{-1}}. \tag{8.259}$$

This is known as the Lamb shift, also a radiative correction that indicates directly that energy is transferred from the vacuum to the H atom. It was first explained by Bethe using a fluctuating Coulomb potential:

$$U = U\,(\mathbf{r}+\delta\mathbf{r}) \tag{8.260}$$

so:

$$\Delta U = U\,(\mathbf{r}+\delta\mathbf{r}) - U(\mathbf{r}). \tag{8.261}$$

For the $2S_{1/2}$ orbital of the H atom:

$$\begin{aligned}\langle\Delta U\rangle &= \frac{1}{6}\left\langle(\delta\mathbf{r})^2\right\rangle\langle\nabla^2 U\rangle \\ &= \frac{1}{6}\left\langle(\delta\mathbf{r})^2\right\rangle\int\psi^*\nabla^2\left(\frac{-e^2}{4\pi\epsilon_0 r}\right)\psi\,d\tau \\ &= \frac{e^2}{48\pi\epsilon_0 r_B^3}\left\langle(\delta\mathbf{r})^2\right\rangle\end{aligned} \tag{8.262}$$

where r_B is the Bohr radius. Therefore the additional potential energy induced in the ${}^2S_{1/2}$ orbital by the vacuum is:

$$U_W = e\Phi_W = m\Phi = \frac{e^2}{48\pi\epsilon_0 r_B^3}\left\langle(\delta r)^2\right\rangle. \tag{8.263}$$

In fluid electrodynamics this additional energy is explained by the scalar potential Φ of the fluid vacuum. This induces the potential energy:

$$\Phi_W = \frac{m}{e}\Phi \tag{8.264}$$

in the ${}^2S_{1/2}$ orbital of the H atom in such a way that:

$$U_W = e\Phi_W = m\Phi. \tag{8.265}$$

The vacuum potential needed to explain the Lamb shift is:

$$\Phi = \frac{e^2}{48\pi\epsilon_0 m r_B^3}\left\langle(\delta\mathbf{r})^2\right\rangle \tag{8.266}$$

and is non zero if the expectation value of $\nabla^2 U$ is non zero. It is non zero in the ${}^2S_{1/2}$ orbital of the H atom, but zero in the ${}^2P_{1/2}$ orbital of the H atom. The potential energy may be expressed as:

$$U_W = m\Phi = \hbar\omega. \tag{8.267}$$

so can be calculated from the observed Lamb shift. It is:

$$\Phi = 7.6947924 \times 10^5 \,\mathrm{m^2 s^{-2}} \tag{8.268}$$

and from this value, the Bethe radius is:

$$\left(\left\langle \Delta \mathbf{r}^2 \right\rangle\right)^{1/2} = 7.35 \times 10^{-14}\,\mathrm{m}. \tag{8.269}$$

The free electron radius is

$$r_e = 2.8 \times 10^{-15}\,\mathrm{m} \tag{8.270}$$

and the Bohr radius is:

$$r_B = 5.29 \times 10^{-11}\,\mathrm{m}. \tag{8.271}$$

Fluid electrodynamics is therefore much simpler and more powerful than quantum electrodynamics.

8.2 Technical Appendix: Scheme for Computation and Animation

This appendix is based on UFT 352, and describes a scheme for the computation and animation of the electric field strength and magnetic flux density induced in a circuit by the vacuum. The scheme starts with the vorticity equation of fluid dynamics, in which the Reynolds number appears. All relevant quantities are computed and animated in terms of the velocity field of the vacuum, which becomes turbulent at a given Reynolds number. The animations are archived on `www.aias.us`.

The first step is to calculate and animate the vacuum velocity field from the simplified vorticity equation:

$$\frac{\partial \mathbf{v}}{\partial t} + \mathbf{w} \times \mathbf{v} = -\frac{1}{R} \boldsymbol{\nabla} \times \mathbf{w} \tag{8.272}$$

where the vorticity is:

$$\mathbf{w} = \boldsymbol{\nabla} \times \mathbf{v} \tag{8.273}$$

Subsequent steps compute the vacuum current:

$$\mathbf{J}_F = -\frac{\partial}{\partial t} \left((\mathbf{v} \cdot \boldsymbol{\nabla}) \, \mathbf{v} \right) + a_0^2 \, \boldsymbol{\nabla} \times (\boldsymbol{\nabla} \times \mathbf{v}) \tag{8.274}$$

and vacuum electric field:

$$\mathbf{E}_F = (\mathbf{v} \cdot \boldsymbol{\nabla})\,\mathbf{v}. \tag{8.275}$$

The vacuum charge density and current density are then calculated using:

$$\rho(\text{vac}) = \epsilon_0 \frac{\rho_m}{\rho} q_F \tag{8.276}$$

$$\mathbf{J}(\text{vac}) = \epsilon_0 \frac{\rho_m}{\rho} \mathbf{J}_F \tag{8.277}$$

and these induce the electric field strength $\mathbf{E}$ in volts per meter and the magnetic flux density $\mathbf{B}$ in tesla using:

$$\boldsymbol{\nabla} \cdot \left(\left(\frac{\rho}{\rho_m} \right)_{\text{circuit}} \mathbf{E} \right) = \frac{1}{\epsilon_0} \frac{\rho^2}{\rho_m} (\text{vacuum}) \tag{8.278}$$

and

$$\begin{aligned} a_0^2\, \boldsymbol{\nabla} \times \left(\left(\frac{\rho}{\rho_m} \right)_{\text{circuit}} \mathbf{B} \right) - \frac{\partial}{\partial t} \left(\left(\frac{\rho}{\rho_m} \right)_{\text{circuit}} \mathbf{E} \right) \\ = \frac{1}{\epsilon_0} \left(\frac{\rho}{\rho_m} \mathbf{J} \right) (\text{vacuum}). \end{aligned} \tag{8.279}$$

The four potential in the circuit can be computed from

$$\Box\, W^\mu(\text{circuit}) = \mu_0 J^\mu(\text{vacuum}). \tag{8.280}$$

The results of this appendix are discussed later in this chapter.

8.3 Numerical Analysis and Graphics

8.3.1 Examples of Kambe Fields

Dynamic Charge Distribution

We investigate the dynamic charge density q derived from the velocity field $\mathbf{v}$ by Kambe (Eq. 8.17):

$$q = \boldsymbol{\nabla} \cdot (\mathbf{v} \cdot \boldsymbol{\nabla})\,\mathbf{v}. \tag{8.281}$$

For an incompressible fluid it is required that the velocity field is divergence-free:

$$\boldsymbol{\nabla} \cdot \mathbf{v} = 0. \tag{8.282}$$

We will inspect some velocity models by specifying $\mathbf{v}$ analytically. We use plane polar coordinates that are identical with cylindrical coordinates with $Z =$

0. Therefore we can use the differential operators of cylindrical coordinates (r, θ, Z). Then we have

$$\boldsymbol{\nabla}\psi = \begin{bmatrix} \frac{\partial\psi}{\partial r} \\ \frac{1}{r}\frac{\partial\psi}{\partial\theta} \\ \frac{\partial\psi}{\partial Z} \end{bmatrix} \tag{8.283}$$

and

$$\boldsymbol{\nabla}\cdot\mathbf{v} = \frac{1}{r}\frac{\partial(r\,v_r)}{\partial r} + \frac{1}{r}\frac{\partial v_\theta}{\partial\theta} + \frac{\partial v_Z}{\partial Z}, \tag{8.284}$$

$$\boldsymbol{\nabla}\times\mathbf{v} = \begin{bmatrix} \frac{1}{r}\frac{\partial v_Z}{\partial\theta} - \frac{\partial v_\theta}{\partial Z} \\ \frac{\partial v_r}{\partial Z} - \frac{\partial v_Z}{\partial r} \\ \frac{1}{r}\frac{\partial(r\,v_\theta)}{\partial r} - \frac{1}{r}\frac{\partial v_r}{\partial\theta} \end{bmatrix} \tag{8.285}$$

for a scalar function ψ and vector $\mathbf{v}$.

A first simple case is

$$\mathbf{v}_1 = \begin{bmatrix} \frac{a}{r} \\ b \\ 0 \end{bmatrix} \tag{8.286}$$

with constants a and b from which follows

$$\boldsymbol{\nabla}\cdot\mathbf{v}_1 = 0 \tag{8.287}$$

and

$$(\mathbf{v}_1\cdot\boldsymbol{\nabla})\,\mathbf{v}_1 = \begin{bmatrix} -\frac{a^2}{r^3} \\ 0 \\ 0 \end{bmatrix}, \tag{8.288}$$

$$\boldsymbol{\nabla}\times\mathbf{v}_1 = \begin{bmatrix} 0 \\ 0 \\ \frac{b}{r} \end{bmatrix}. \tag{8.289}$$

The result (8.288), representing the electric field, does not depend on b, and so does not the charge distribution:

$$q_1 = \frac{2a^2}{r^4}. \tag{8.290}$$

All results were obtained by computer algebra. Tests showed that a radial component dependent on r is necessary to give a vanishing divergence of $\mathbf{v}$. The velocity field $\mathbf{v}_1$ has been graphed in Fig. 8.1. This is a vortex around the coordinate origin where the angle of velocity is a tangent to a circle in the far field but not in the near field. This is the impact of $1/r$. The first component of (8.288) and the charge distribution (8.290) look similar as $\mathbf{v}_1$ but have higher exponents of r in the denominator. q_1 is graphed in Fig. 8.2 in a contour plot, showing the steep rise of charge density.

The next example is non-trivial. It was chosen so that the divergence vanishes, although this is not obvious from the velocity field:

$$\mathbf{v}_2 = \begin{bmatrix} \frac{a\cos\theta}{r^2} \\ \frac{a\sin\theta}{r^2} + b \\ 0 \end{bmatrix} \tag{8.291}$$

with constants a and b. Computer algebra gives the results:

$$\boldsymbol{\nabla} \cdot \mathbf{v}_2 = 0, \tag{8.292}$$

$$(\mathbf{v}_2 \cdot \boldsymbol{\nabla})\, \mathbf{v}_2 = -\frac{a}{r^5} \begin{bmatrix} a\sin^2\theta + b\, r^2 \sin\theta + 2\, a\cos^2\theta \\ \cos\theta \left(a\sin\theta - b\, r^2 \right) \\ 0 \end{bmatrix}, \tag{8.293}$$

$$\boldsymbol{\nabla} \times \mathbf{v}_2 = \begin{bmatrix} 0 \\ 0 \\ \frac{b}{r} \end{bmatrix}, \tag{8.294}$$

$$q_2 = \frac{a}{r^6} \left(5\, a\sin^2\theta + b\, r^2 \sin\theta + 7\, a\cos^2\theta \right). \tag{8.295}$$

The vector field (8.291) is shown in Fig. 8.3. There is a centre of rotation below the coordinate centre. The velocities are much higher above the centre than below. This leads to partially asymmetric electric field components E_r and E_θ, Eq. (8.293), which are graphed in Figs. 8.4 and 8.5. There are sharp peaks for E_θ at four sides. The E field has been converted to vector form in the XY plane and its (normalized) directional vectors are graphed in Fig. 8.6. The lower centre in Fig. 8.3 can be identified to produce a kind of "hole" in the electric field. There is a kind of flow along the Y axis which would not be expected from the form of the velocity field in Fig. 8.3. Despite these asymmetries, the charge distribution of this model velocity is mainly centrally symmetric as can be seen from Fig. 8.7. This result was not obvious from the formulas.

A more general example can be constructed by

$$\mathbf{v}_3 = \begin{bmatrix} \frac{a}{r^n} \\ f(r,\theta) \\ 0 \end{bmatrix} \tag{8.296}$$

with a general function $f(r,\theta)$. Then it follows

$$\boldsymbol{\nabla} \cdot \mathbf{v}_3 = r^{-n-1} \left(r^n\, \frac{d}{d\,\theta}\, \mathrm{f}\,(r,\theta) - a\, n + a \right), \tag{8.297}$$

$$(\mathbf{v}_3 \cdot \boldsymbol{\nabla})\, \mathbf{v}_3 = \begin{bmatrix} -a^2\, n\, r^{-2\,n-1} \\ r^{-n-1} \left(r^n\, \mathrm{f}\,(r,\theta)\ \frac{d}{d\,\theta}\, \mathrm{f}\,(r,\theta) + a\, r\, \frac{d}{d\,r}\, \mathrm{f}\,(r,\theta) \right) \\ 0 \end{bmatrix}, \tag{8.298}$$

$$\boldsymbol{\nabla} \times \mathbf{v}_3 = \begin{bmatrix} 0 \\ 0 \\ \frac{d}{d\,r}\mathrm{f}\,(r,\theta) + \frac{1}{r}\mathrm{f}\,(r,\theta) \end{bmatrix} \tag{8.299}$$

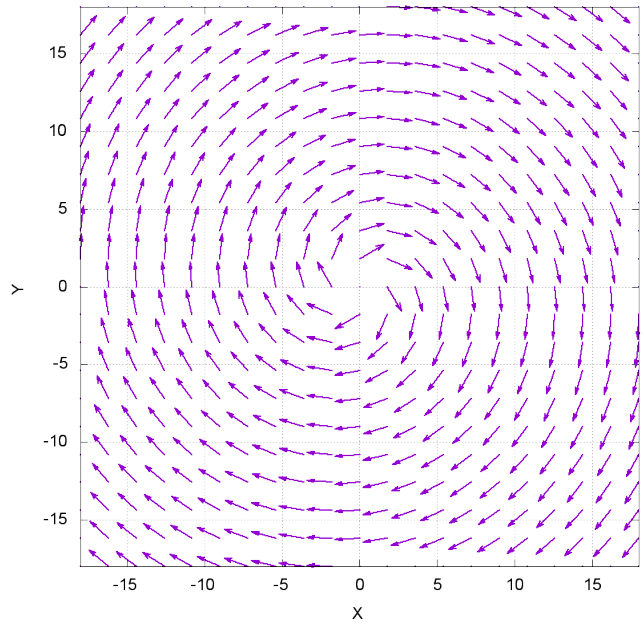

Figure 8.1: Velocity model $\mathbf{v}_1$.

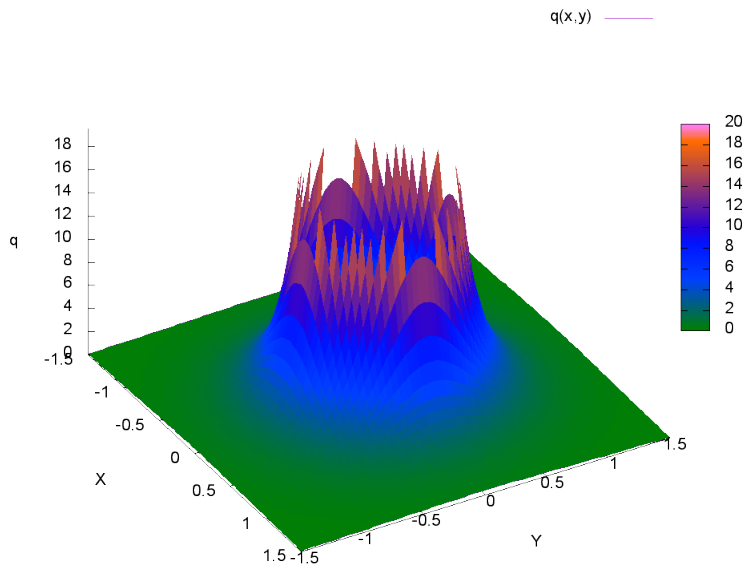

Figure 8.2: Velocity model $\mathbf{v}_1$, charge distribution q_1.

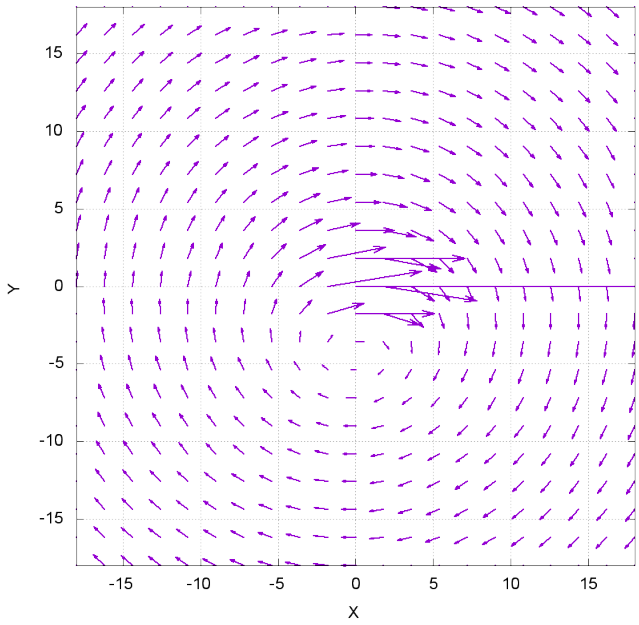

Figure 8.3: Velocity model $\mathbf{v}_2$.

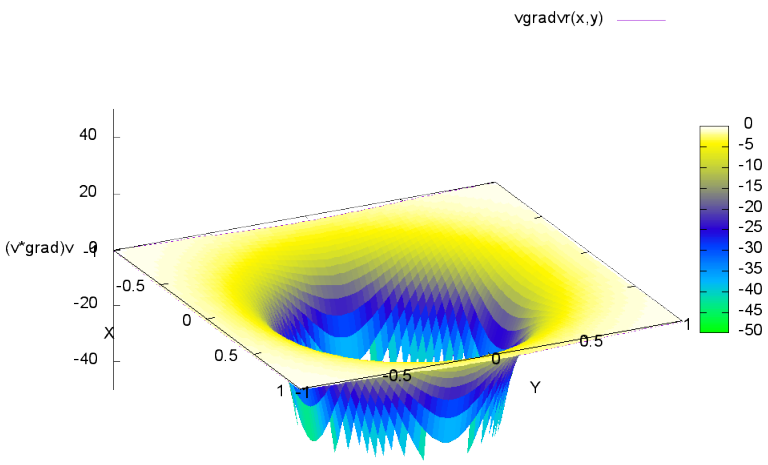

Figure 8.4: Velocity model $\mathbf{v}_2$, first component (E_r) of Eq. (8.293).

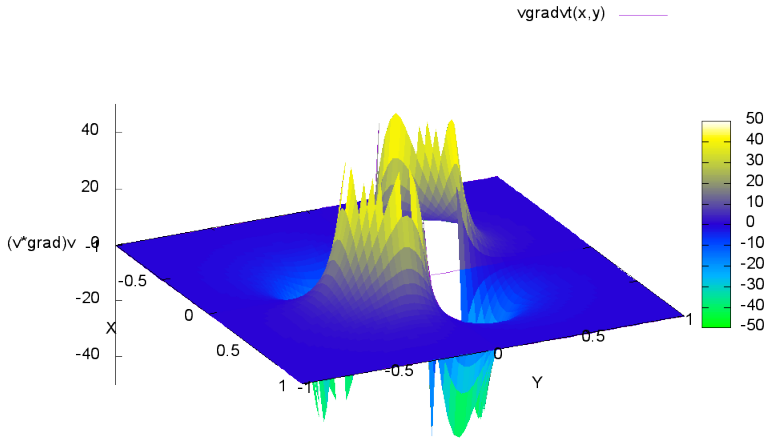

Figure 8.5: Velocity model $\mathbf{v}_2$, second component (E_θ) of Eq. (8.293).

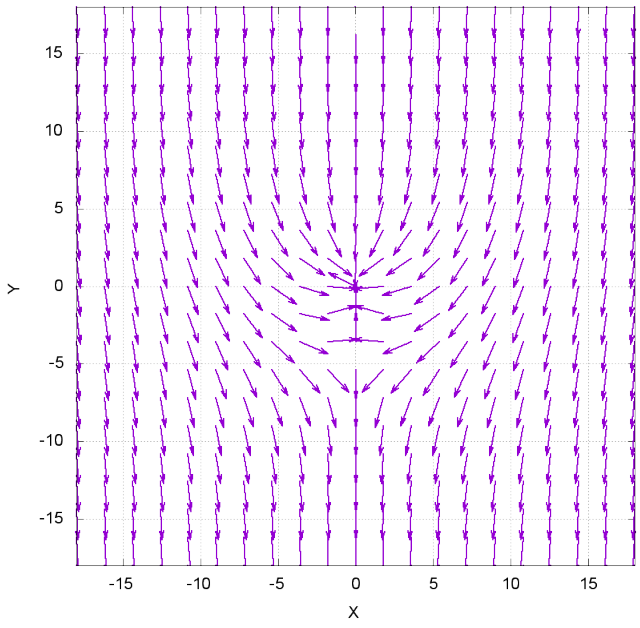

Figure 8.6: Velocity model $\mathbf{v}_2$, directional vectors of $\mathbf{E}$ field.

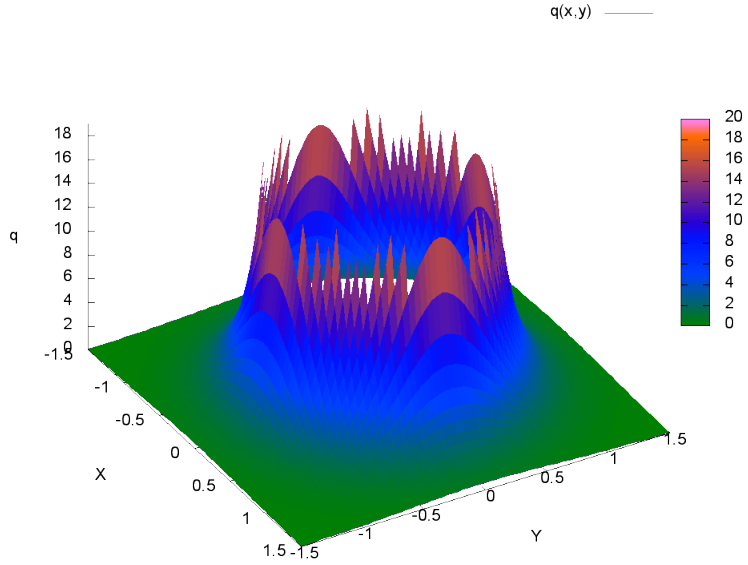

Figure 8.7: Velocity model $\mathbf{v}_2$, charge distribution q_2.

and the charge distribution takes the form

$$q_3 = r^{-2\,n-2}\left(r^{2\,n}\,\mathrm{f}\,(r,\theta)\,\frac{d^2}{d\,\theta^2}\,\mathrm{f}\,(r,\theta)\right. \tag{8.300}$$
$$\left. + r^{2\,n}\left(\frac{d}{d\,\theta}\,\mathrm{f}\,(r,\theta)\right)^2 + a\,r^{n+1}\frac{d^2}{d\,r\,d\,\theta}\,\mathrm{f}\,(r,\theta) + 2\,a^2\,n^2\right).$$

The divergence of this velocity model vanishes if

$$r^{-n-1}\left(r^n\left(\frac{d}{d\,\theta}\,\mathrm{f}\,(r,\theta)\right) - a\,n + a\right) = 0, \tag{8.301}$$

which is a differential equation for $f(r,\theta)$ with the solution

$$\mathrm{f}\,(r,\theta) = \frac{a\,(n-1)\;\theta}{r^n} + c. \tag{8.302}$$

For $n = 1$ we obtain the model for $\mathbf{v}_1$ discussed above.

Solution of Ampère-Maxwell Law

The complete Ampère-Maxwell law of ECE 2 reads in the electrodynamic case:

$$\boldsymbol{\nabla} \times \mathbf{B} - \frac{1}{c^2}\frac{\partial \mathbf{E}}{\partial t} = \mu_0 \mathbf{J} \tag{8.303}$$

with current density (Eq.(8.40)):

$$\mathbf{J} = \frac{1}{\mu_0}\left(\frac{\kappa_0}{c}\mathbf{E} + \boldsymbol{\kappa} \times \mathbf{B}\right) \tag{8.304}$$

which in in non-relativistic approximation is:

$$\mathbf{J} = \sigma\left(\mathbf{E} + \mathbf{v} \times \mathbf{B}\right). \tag{8.305}$$

Here $\mathbf{v}$ is the velocity of charge carriers moving in a medium with conductivity σ. In the static case the law simplifies to

$$\boldsymbol{\nabla} \times \mathbf{B} = \frac{\kappa_0}{c}\mathbf{E} + \boldsymbol{\kappa} \times \mathbf{B} = \sigma\left(\mathbf{E} + \mathbf{v} \times \mathbf{B}\right), \tag{8.306}$$

which is a destination equation for the magnetic field if all other quantities are given. In the absence of an electric field the equation

$$\boldsymbol{\nabla} \times \mathbf{B} = \boldsymbol{\kappa} \times \mathbf{B} \tag{8.307}$$

has to be solved. In the case of a constant $\boldsymbol{\kappa}$, this gives three differential equations for the three components of the $\mathbf{B}$ field, but computer algebra shows that these equations are under-determined. For example making an approach with oscillatory functions:

$$\mathbf{B} = \mathbf{A}\exp(-i\ (x\,\kappa_x + y\,\kappa_y + z\,\kappa_z)) \tag{8.308}$$

leads to a solution for the (complex-valued) vectorial amplitude

$$\mathbf{A} = \begin{bmatrix} \alpha^2/\kappa_y \\ i\ \alpha/\kappa_y \\ \alpha \end{bmatrix} \tag{8.309}$$

with an arbitrary constant α. If an electric field is included as in Eq.(8.306), there is no solution to that equation with the approach (8.308).

The situation changes if we assume a Beltrami solution for $\mathbf{B}$. Then we have

$$\boldsymbol{\nabla} \times \mathbf{B} = \kappa\mathbf{B} \tag{8.310}$$

with a constant κ, and for the pure magnetic case without electric field (non-relativistically):

$$\kappa\mathbf{B} = \mu_0\mathbf{J} = \mu_0\sigma\mathbf{v} \times \mathbf{B}. \tag{8.311}$$

However, for a fixed $\mathbf{v}$, there is no solution of this equation for $\mathbf{B}$. This is an important result, showing that not all equations being derivable from simplifications of ECE 2 theory are deployable for solving real world problems. This situation changes as soon as the electric field is included in the Beltrami structure for $\mathbf{B}$:

$$\kappa\mathbf{B} = \mu_0\sigma\left(\mathbf{E} + \mathbf{v} \times \mathbf{B}\right). \tag{8.312}$$

This gives an inhomogeneous linear equation system for the components of $\mathbf{B}$, in contrast to Eq. (8.311), which is a homogeneous system. Defining a velocity constant

$$w = \frac{\mu_0 \sigma}{\kappa}, \tag{8.313}$$

the general solution is

$$\mathbf{B} = \frac{1}{w(w^2+v^2)} \begin{bmatrix} (v_x\, v_z + w\, v_y)\; E_z - w\, E_y\, v_z + v_x\, v_y\, E_y + \left(v_x^2 + w^2\right)\; E_x \\ (v_y\, v_z - w\, v_x)\; E_z + w\, E_x\, v_z + \left(v_y^2 + w^2\right)\; E_y + v_x\, E_x\, v_y \\ \left(v_z^2 + w^2\right)\; E_z + (v_y\, E_y + v_x\, E_x)\; v_z + w\, v_x\, E_y - w\, E_x\, v_y \end{bmatrix}. \tag{8.314}$$

Trivially, Eq. (8.312) can also be resolved for $\mathbf{E}$, giving

$$\mathbf{E} = \begin{bmatrix} -v_y\, B_z + B_y\, v_z + w\, B_x \\ v_x\, B_z - B_x\, v_z + w\, B_y \\ w\, B_z - v_x\, B_y + B_x\, v_y. \end{bmatrix}. \tag{8.315}$$

It is important to note that the same equation is not a valid equation for $\mathbf{v}$, there is no solution. Therefore it is not possible to specify $\mathbf{E}$ and $\mathbf{B}$ a priori and find a suitable charge carrier velocity $\mathbf{v}$.

Finally we give a numerical example for the Beltrami solution (8.314). Setting

$$w = 1, \quad \mathbf{v} = \begin{bmatrix} 1 \\ 0 \\ 0 \end{bmatrix}, \quad \mathbf{E} = \begin{bmatrix} 0 \\ 0 \\ 1 \end{bmatrix} \tag{8.316}$$

results to

$$\mathbf{B} = \begin{bmatrix} 0 \\ -1/2 \\ 1/2 \end{bmatrix}. \tag{8.317}$$

Defining this a little bit more general:

$$w = 1, \quad \mathbf{v} = \begin{bmatrix} v_x \\ 0 \\ 0 \end{bmatrix}, \quad \mathbf{E} = \begin{bmatrix} 0 \\ 0 \\ E_z \end{bmatrix} \tag{8.318}$$

this leads to

$$\mathbf{B} = \begin{bmatrix} 0 \\ -\frac{v_x E_z}{v_x^2+1} \\ \frac{E_z}{v_x^2+1} \end{bmatrix}. \tag{8.319}$$

For a better understanding, a vector map $(v_x, E_z) \to (B_y, B_z)$ has been constructed in Fig. 8.8 to show the resulting magnetic field in the YZ plane. There is a zero field for $E_z = 0$. Directions of the $\mathbf{B}$ field are maintained by crossing this line but the signs differ.

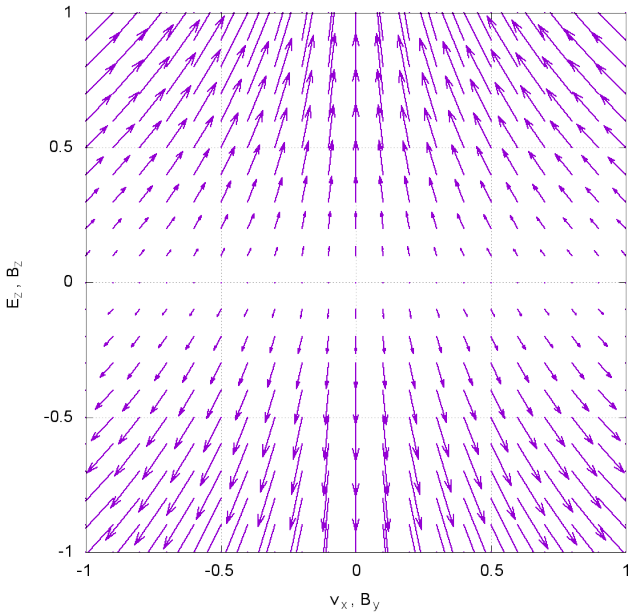

Figure 8.8: Vector map $(v_x, E_z) \to (B_y, B_z)$ for model of Eq. (8.318).

8.3.2 Solutions of Fluid Dynamics Equations

The equations (8.155), (8.157) and (8.160) have been solved numerically by the finite element program FlexPDE. The 3D volume was chosen as for typical Navier-Stokes applications: a plenum box with a circular inlet at the bottom and an offset circular outlet at the top, see Fig. 8.9. The boundary conditions were set to $\mathbf{v} = \mathbf{0}$ at the borders of the box and a directional derivative perpendicular to the openings area was assumed. This allows for a free floating solution of the velocity field. As a test, a solution for the Navier-Stokes equation

$$(\mathbf{v} \cdot \boldsymbol{\nabla})\, \mathbf{v} + \boldsymbol{\nabla} p - \eta\, \nabla^2 \mathbf{v} = \mathbf{0}. \tag{8.320}$$

was computed, with η being a viscosity. The pressure term was added because the equation is otherwise homogeneous which means that there is no source term, leading to a solution which does not guarantee conservation of mass. The divergence of the pressure gradient is assumed to be in proportion to the divergence of the velocity field:

$$\boldsymbol{\nabla} \cdot \boldsymbol{\nabla} p = P\, \boldsymbol{\nabla} \cdot \mathbf{v} \tag{8.321}$$

with a constant P for "penalty pressure". This represents an additional equation for determining the pressure. The result for the velocity is graphed in Fig. 8.10, showing a straight flow through the box which is perpendicular to the inlet and outlet surfaces as requested by boundary conditions.

Next the vorticity equation (8.155) was solved, again with the pressure term to guarantee solutions:

$$\nabla^2 \mathbf{w} + \boldsymbol{\nabla} \times (\boldsymbol{\nabla} \times \mathbf{w}) + \boldsymbol{\nabla} p = \mathbf{0}. \tag{8.322}$$

It is difficult to define meaningful boundary conditions because this is a pure flow equation for the vorticity $\mathbf{w}$. We used the same as for the Navier-Stokes equations. The result is graphed in Fig. 8.11. There is a flow-like structure with a divergence at the left, the flow is not symmetric. By definition, there should not be a divergence because of Eq. (8.154). We assume that the boundary conditions are not adequate for this type of equation.

The situation is more meaningful for Eq. (8.157) which we solved as

$$\boldsymbol{\nabla} \times \mathbf{w} + R\left((\mathbf{v} \cdot \boldsymbol{\nabla})\,\mathbf{v} - \mathbf{v} \times \mathbf{w}\right) + \boldsymbol{\nabla} p = \mathbf{0}. \tag{8.323}$$

The solution for $R = 1$ gives an inclined input and output flow (Fig. 8.12). In the middle hight of the box the flow is more over the sides, therefore the intensity of velocity is low in the middle plane shown. The divergence (not shown) is practically zero in this region. Fig. 8.13 shows a divergent and convergent flow in the XY plane, the flow goes over the full width of the box. Results for higher Reynolds numbers reveal no significant difference.

Finally we solved Eq. (8.160) which holds for a Beltrami flow:

$$\nabla^2 \mathbf{v} - R\,(\mathbf{v} \cdot \boldsymbol{\nabla})\,\mathbf{v} - \boldsymbol{\nabla}\,(\boldsymbol{\nabla} \cdot \mathbf{v}) + \boldsymbol{\nabla} p = \mathbf{0}. \tag{8.324}$$

Here the flow is strongly enhanced in the middle region (Fig. 8.14). In the perpendicular plane a similar effect can be seen (Fig. 8.15). The field is not divergence-free there. For a Beltrami field we should have

$$\mathbf{w} \times \mathbf{v} = k\mathbf{v} \times \mathbf{v} = \mathbf{0}. \tag{8.325}$$

The vorticity $\mathbf{w}$ corresponding to Fig. 8.15 has been graphed in Fig. 8.16. There are indeed large regions where both $\mathbf{w}$ and $\mathbf{v}$ are parallel or antiparallel. The factor k seems to be location dependent, we did not constrain the Beltrami property by further means. Therefore the result is satisfactory. For larger R values the results remain similar again.

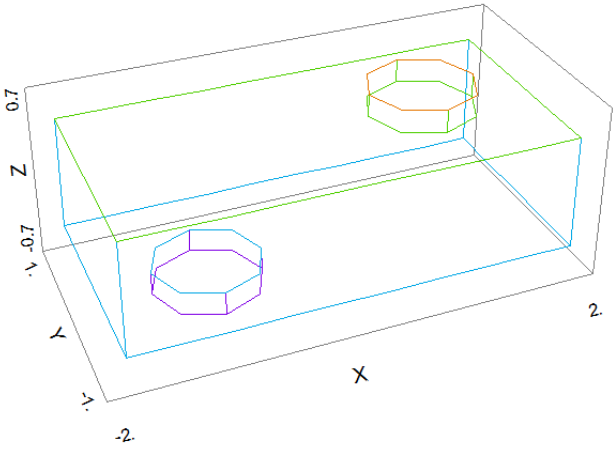

Figure 8.9: Geometry of FEM calculations.

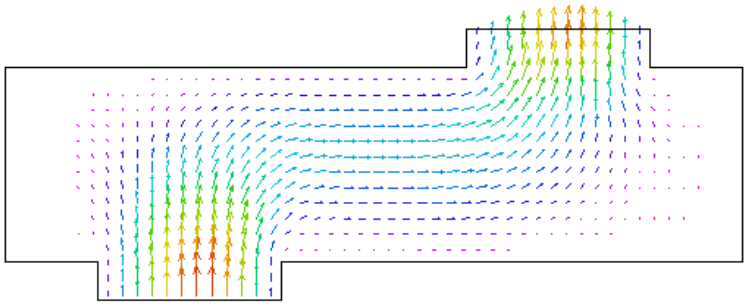

Figure 8.10: Velocity solution for Navier-Stokes Equation (8.320).

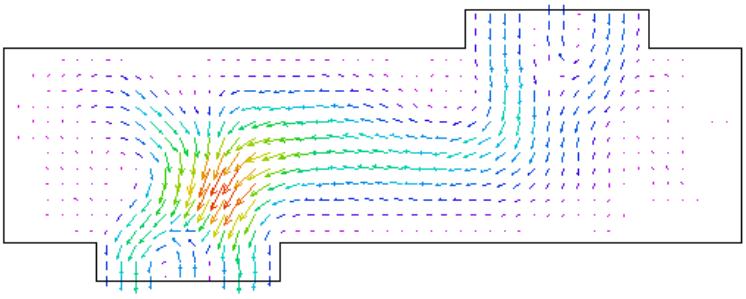

Figure 8.11: Vorticity solution for Eq. (8.322).

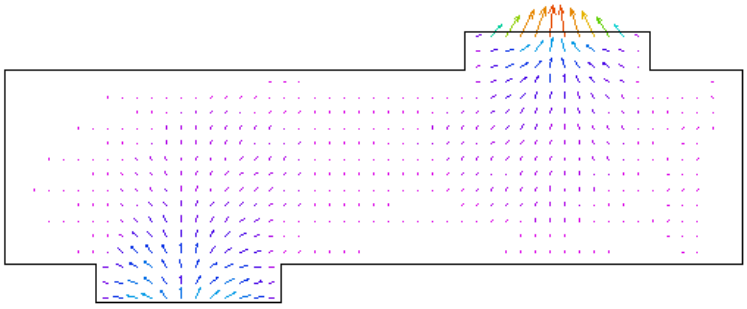

Figure 8.12: Velocity solution of Eq. (8.323) for $R = 1$, plane $Y = 0$.

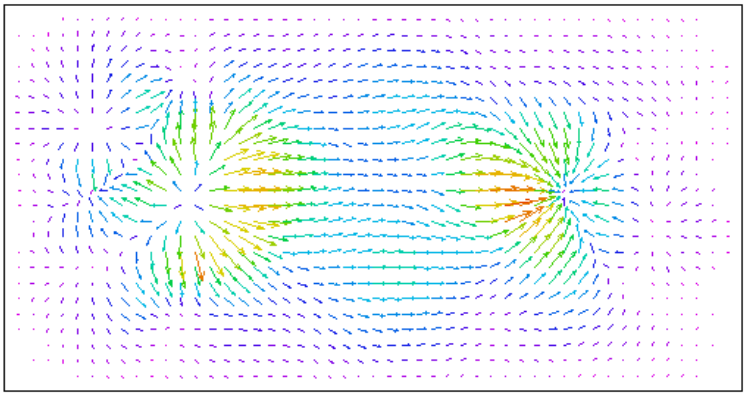

Figure 8.13: Velocity solution of Eq. (8.323) for $R = 1$, plane $Z = 0$.

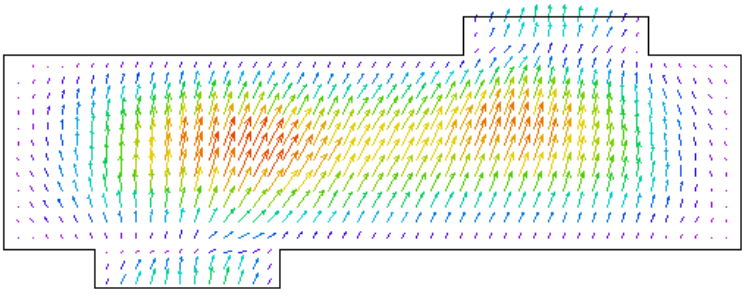

Figure 8.14: Beltrami solution of Eq. (8.324) for $R = 1$, plane $Y = 0$.

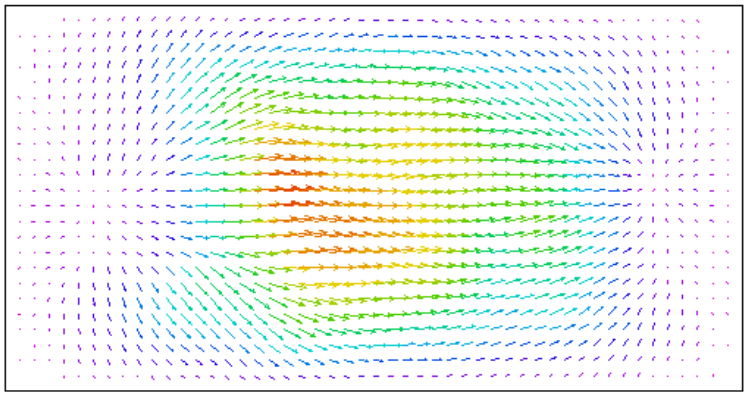

Figure 8.15: Beltrami solution of Eq. (8.324) for $R = 1$, plane $Z = 0$.

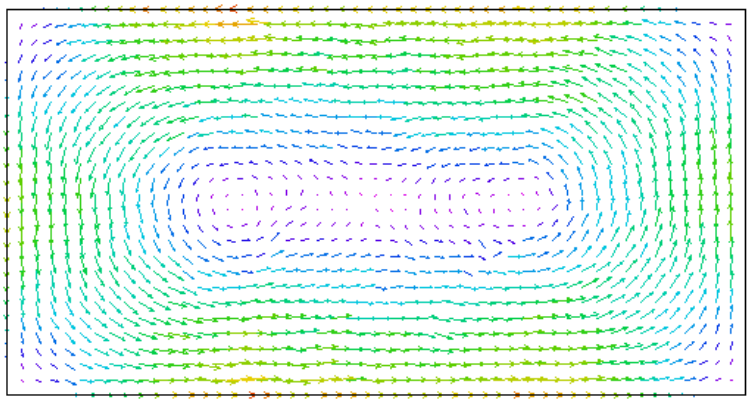

Figure 8.16: Vorticity of solution for Eq. (8.324) for $R = 1$, plane $Z = 0$.

8.3.3 Wave Equations of Fluid Electrodynamics

In this section the wave equations of fluid electrodynamics have been developed. In case of an external current density $\mathbf{J}$ the wave equation (8.185) of standard electrodynamics reads

$$\frac{1}{a_0^2}\frac{\partial^2 \mathbf{v}}{\partial t^2} - \nabla^2 \mathbf{v} = \frac{1}{a_0^2}\mathbf{J}. \tag{8.326}$$

Assuming a harmonic time dependence, we define

$$\mathbf{v}(\mathbf{r}, t) = \mathbf{v}_S(\mathbf{r}) \exp(i\omega t) \tag{8.327}$$

and

$$\mathbf{J}(\mathbf{r}, t) = \mathbf{J}_S(\mathbf{r}) \exp(i\omega t) \tag{8.328}$$

with a time frequency ω and only space-dependent velocities $\mathbf{v}_S$ and current densities $\mathbf{J}_S$. Then Eq. (8.326) reads

$$-\frac{\omega^2}{a_0^2}\mathbf{v}_S - \nabla^2\mathbf{v}_S = \frac{1}{a_0^2}\mathbf{J}_S \tag{8.329}$$

which is an eigenvalue equation. For vanishing current density it can be written in the standard form

$$\nabla^2\mathbf{v}_S + \lambda\mathbf{v}_S = \mathbf{0} \tag{8.330}$$

with positive eigenvalues

$$\lambda := \frac{\omega^2}{a_0^2} \tag{8.331}$$

which correspond to acoustic eigen frequencies for example. This equation can be solved numerically by the finite element method. In our example we readopt the 3D flow box of the preceding section with corresponding boundary conditions, irrespective of further utility considerations. The first six eigenvalues (in arbitrary units) are listed in Table 8.1. There is a degeneracy between the first and second eigenvalue and between the fifth and sixth eigenvalue. This is due to internal symmetry of the flow box. The values are lying near to each other. The modulus of the first and sixth velocity eigen state has been graphed in Figs. 8.17-8.20 for two planes of symmetry ($Z = 0$ and $Y = 0$). The sixth eigen state has a node in the middle plane of symmetry. This symmetry is also present in the vorticity vectors, see Figs. 8.21-8.22. The divergence of velocity has been graphed in Figs. 8.23 and 8.24. The divergence is not restricted to the boundary regions and is more pronounced for the higher eigen state.

For a correct treatment of the wave equation within fluid electrodynamics, we have to include the current density (8.174):

$$\mathbf{J}_F = a_0^2\boldsymbol{\nabla}\times(\boldsymbol{\nabla}\times\mathbf{v}) - \frac{\partial}{\partial t}\left((\mathbf{v}\cdot\boldsymbol{\nabla})\mathbf{v}\right). \tag{8.332}$$

The second term is not linear in $\mathbf{v}$ so the time-harmonic approach is only possible for the first term. From (8.329) this gives the more general eigenvalue equation

$$\nabla^2\mathbf{v}_S + \boldsymbol{\nabla}\times(\boldsymbol{\nabla}\times\mathbf{v}_S) + \lambda\mathbf{v}_S = \mathbf{0}. \tag{8.333}$$

As a result, the eigenvalues are very small, compared to Eq. (8.330), and there are a lot more turbulences. The numerical calculation takes half an hour on a standard PC but converges. The numerical precision, however, is not satisfactory, therefore these result can only show a tendency. The first six eigenvalues are listed in Table 8.2. There is no degeneration any more. In Figs. 8.25-8.30 the vorticity in the plane $Y = 0$ has been graphed, this can be compared with Figs. 8.21 and 8.22. Obviously Eq. (8.333) incurs a lot more of turbulence structures. One can see that eigen state n possesses $n + 1$ vortices. This seems to be a particularity of Eq. (8.333).

A time-dependent calculation has been tried by assuming that the second-order time derivative can be neglected against the first-order time derivative in the current density:

$$\nabla^2 \mathbf{v}_S = -\boldsymbol{\nabla} \times (\boldsymbol{\nabla} \times \mathbf{v}) + \frac{\partial}{\partial t} \left((\mathbf{v} \cdot \boldsymbol{\nabla}) \mathbf{v} \right). \tag{8.334}$$

Adding a pressure term $\boldsymbol{\nabla} p$ as described in the previous section gives a non-singular equation but no time solution. Obviously the nonlinearity prevents a solution – at least for this special problem of boundary values considered.

Coming back to the solution of Eq. (8.333), this seems to be the first time that an ECE 2 wave equation of type

$$(\Box + R)\mathbf{v} = \mathbf{0} \tag{8.335}$$

(see Eq. (8.190)) has been solved for a curvature R which in turn depends on the variable $\mathbf{v}$. This is certainly a step beyond contemporary standard equations of physics, e.g. the Dirac equation, where always a constant curvature has been assumed. The numerical problems, however, are enormous and a lot of work will be required to develop this field of ECE 2 physics.

No.	Eigenvalue
1	12.1031274
2	12.1031274
3	12.1919561
4	13.2402655
5	13.3685992
6	13.3685992

Table 8.1: Eigenvalues of Eq. (8.330).

No.	Eigenvalue
1	2.56351677e-3
2	2.68244759e-3
3	4.08141046e-3
4	6.27378404e-3
5	7.79542935e-3
6	8.34876355e-3

Table 8.2: Eigenvalues of Eq. (8.333).

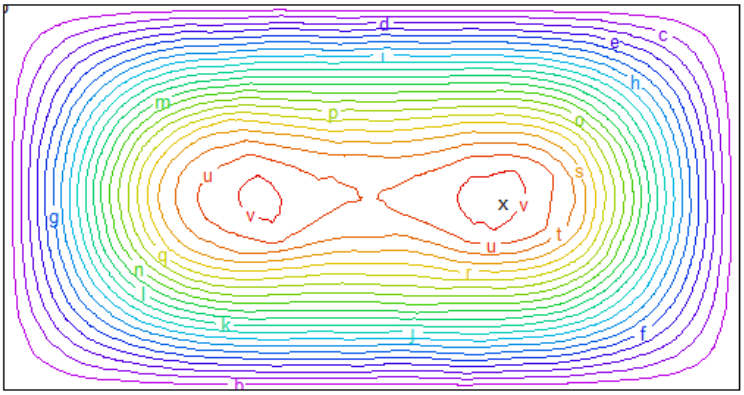

Figure 8.17: Velocity modulus of Eq. (8.330) on Z=0, eigen state 1.

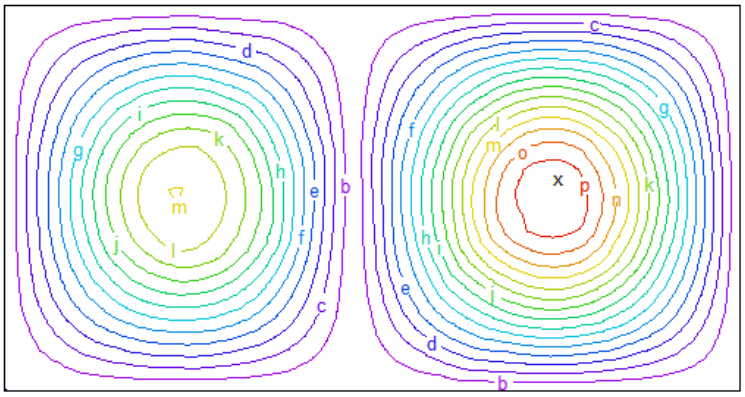

Figure 8.18: Velocity modulus of Eq. (8.330) on Z=0, eigen state 6.

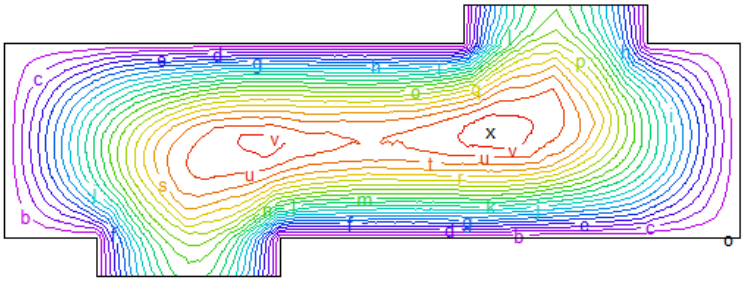

Figure 8.19: Velocity modulus of Eq. (8.330) on Y=0, eigen state 1.

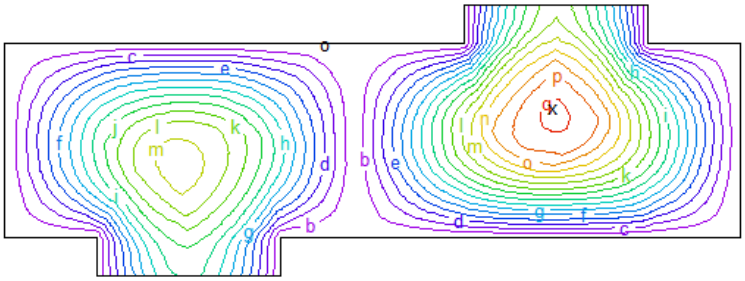

Figure 8.20: Velocity modulus of Eq. (8.330) on Y=0, eigen state 6.

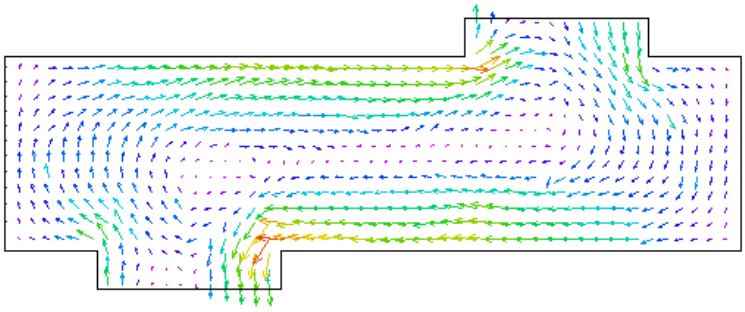

Figure 8.21: Vorticity of Eq. (8.330) on Y=0, eigen state 1.

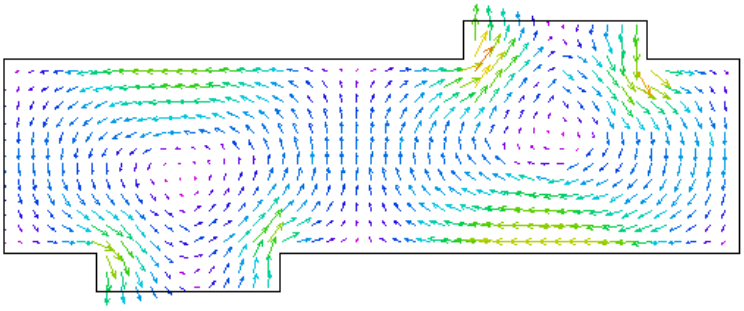

Figure 8.22: Vorticity of Eq. (8.330) on Y=0, eigen state 6.

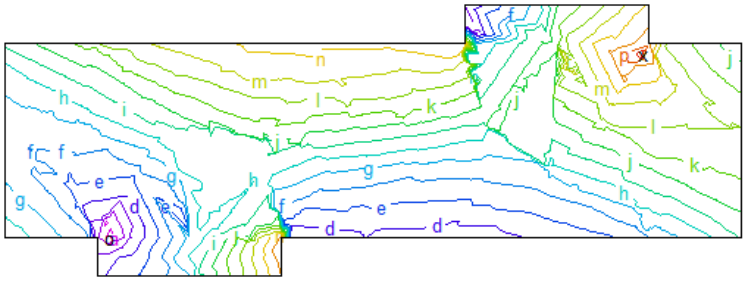

Figure 8.23: Divergence of velocity of Eq. (8.330) on Y=0, eigen state 1.

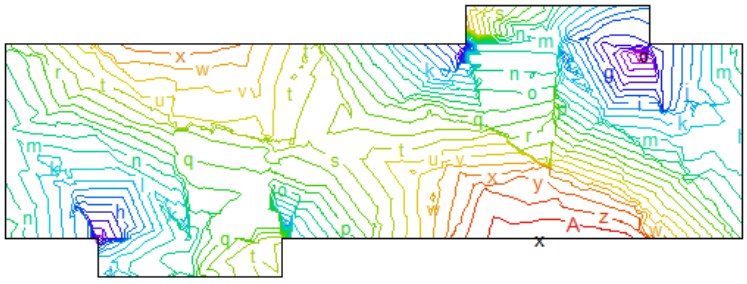

Figure 8.24: Divergence of velocity of Eq. (8.330) on Y=0, eigen state 6.

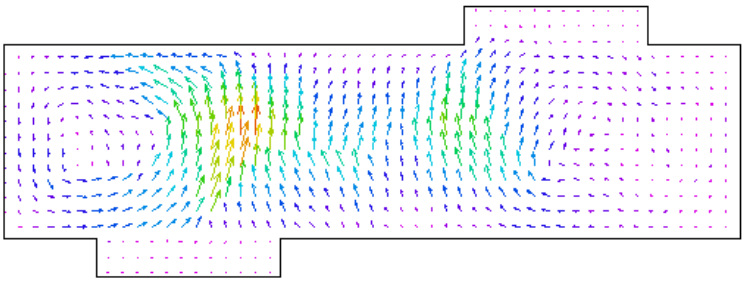

Figure 8.25: Vorticity of Eq. (8.333) on Y=0, eigen state 1.

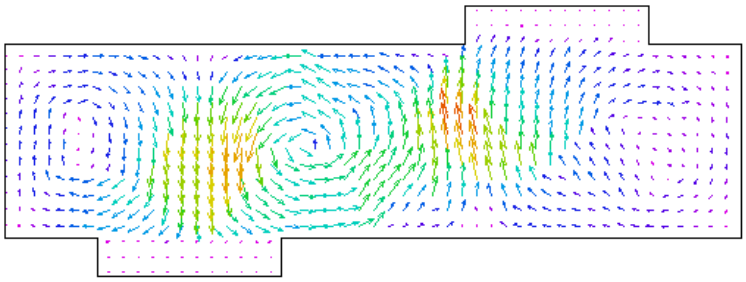

Figure 8.26: Vorticity of Eq. (8.333) on Y=0, eigen state 2.

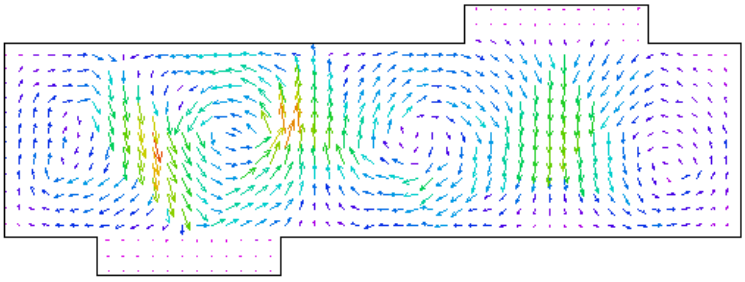

Figure 8.27: Vorticity of Eq. (8.333) on Y=0, eigen state 3.

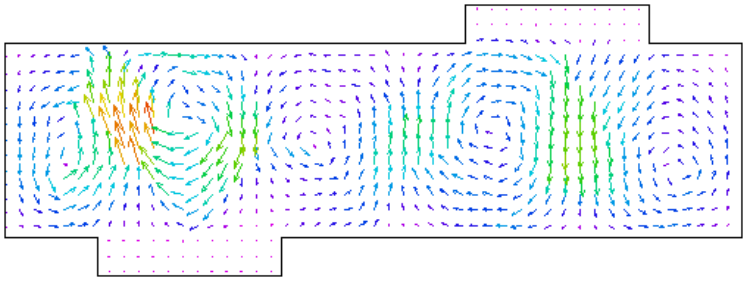

Figure 8.28: Vorticity of Eq. (8.333) on Y=0, eigen state 4.

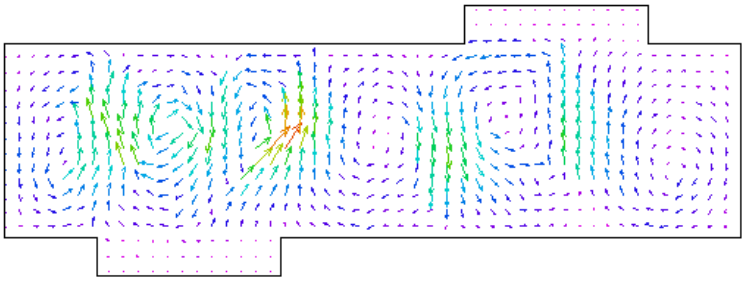

Figure 8.29: Vorticity of Eq. (8.333) on Y=0, eigen state 5.

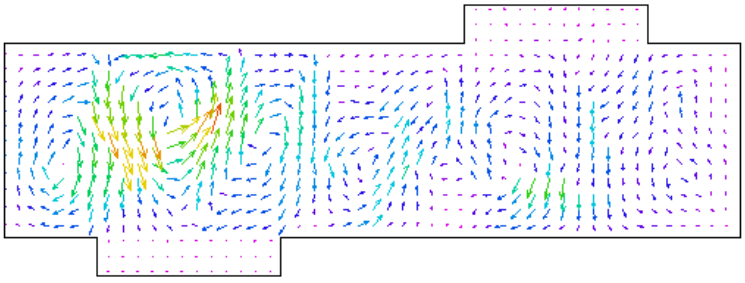

Figure 8.30: Vorticity of Eq. (8.333) on Y=0, eigen state 6.

8.3.4 Examples for Applications of Fluid Electrodynamics

We start with the operator $(\mathbf{v}\cdot\boldsymbol{\nabla})\mathbf{v}$. This is part of the total derivative of variables, sometimes named the convective derivative or material derivative, see Eq. (8.134) and also Eqs. (8.194, 8.200). In the examples of this section, the operator has to be expressed in spherical coordinates. In detail, this operator in cartesian, cylindrical and spherical coordinates is defined for arbitrary vector functions $\mathbf{a}$ and $\mathbf{b}$ [29] as follows:

$$(\mathbf{a}_{\rm cart}\cdot\boldsymbol{\nabla})\mathbf{b}_{\rm cart} = \begin{bmatrix} a_X\frac{\partial b_X}{\partial X} + a_Y\frac{\partial b_X}{\partial Y} + a_Z\frac{\partial b_X}{\partial Z} \\ a_X\frac{\partial b_Y}{\partial X} + a_Y\frac{\partial b_Y}{\partial Y} + a_Z\frac{\partial b_Y}{\partial Z} \\ a_X\frac{\partial b_Z}{\partial X} + a_Y\frac{\partial b_Z}{\partial Y} + a_Z\frac{\partial b_Z}{\partial Z} \end{bmatrix}, \tag{8.336}$$

$$(\mathbf{a}_{\rm cyl}\cdot\boldsymbol{\nabla})\mathbf{b}_{\rm cyl} = \begin{bmatrix} a_r\frac{\partial b_r}{\partial r} + \frac{a_\theta}{r}\frac{\partial b_r}{\partial\theta} + a_Z\frac{\partial b_r}{\partial Z} - \frac{a_\theta b_\theta}{r} \\ a_r\frac{\partial b_\theta}{\partial r} + \frac{a_\theta}{r}\frac{\partial b_\theta}{\partial\theta} + a_Z\frac{\partial b_\theta}{\partial Z} + \frac{a_\theta b_r}{r} \\ a_r\frac{\partial b_Z}{\partial r} + \frac{a_\theta}{r}\frac{\partial b_Z}{\partial\theta} + a_Z\frac{\partial b_Z}{\partial Z} \end{bmatrix}, \tag{8.337}$$

$$(\mathbf{a}_{\rm sph}\cdot\boldsymbol{\nabla})\mathbf{b}_{\rm sph} = \begin{bmatrix} a_r\frac{\partial b_r}{\partial r} + \frac{a_\theta}{r}\frac{\partial b_r}{\partial\theta} + \frac{a_\phi}{r\sin\theta}\frac{\partial b_r}{\partial\phi} - \frac{a_\theta b_\theta + a_\phi b_\phi}{r} \\ a_r\frac{\partial b_\theta}{\partial r} + \frac{a_\theta}{r}\frac{\partial b_\theta}{\partial\theta} + \frac{a_\phi}{r\sin\theta}\frac{\partial b_\theta}{\partial\phi} + \frac{a_\theta b_r}{r} - \frac{a_\phi b_\phi\cot\theta}{r} \\ a_r\frac{\partial b_\phi}{\partial r} + \frac{a_\theta}{r}\frac{\partial b_\phi}{\partial\theta} + \frac{a_\phi}{r\sin\theta}\frac{\partial b_\phi}{\partial\phi} + \frac{a_\phi b_r}{r} + \frac{a_\phi b_\theta\cot\theta}{r} \end{bmatrix}. \tag{8.338}$$

The operator (8.338) for spherial coordinates has to be used in Eq. (8.219), leading to the solution for the radial velocity component

$$v_r = \pm \frac{e}{\sqrt{2\pi\epsilon_0 x}} \sqrt{\frac{1}{r} - c} \tag{8.339}$$

with an integration constant c. This is a function of type $1/\sqrt{r}$ and has been graphed in Fig. 8.31 for three values of c. Setting $c > 0$ gives imaginary solutions, and $c < 0$ gives asymptotes different from zero for $r \to \infty$, therefore $c = 0$ seems to be the physically best choice.

In the following we will consider examples for vector potentials of given material fields. These give rise to spacetime fluid effects as described by Eqs. (8.192-8.219). We will present selected cases with graphics.

Simple rotating field

The first example is a magnetic vector potential

$$\mathbf{W} = \frac{B^{(0)}}{2} \begin{bmatrix} Y \\ -X \\ 0 \end{bmatrix}. \tag{8.340}$$

This gives a spacetime velocity field

$$\mathbf{v}_F = \frac{\rho}{\rho_m} \mathbf{W} = \frac{B^{(0)} \rho}{2\rho_m} \begin{bmatrix} Y \\ -X \\ 0 \end{bmatrix} \tag{8.341}$$

and the resulting vacuum electric field

$$\mathbf{E}_F = (\mathbf{v}_F \cdot \boldsymbol{\nabla}) \mathbf{v}_F = \frac{(B^{(0)})^2 \rho^2}{4\rho_m^2} \begin{bmatrix} -X \\ -Y \\ 0 \end{bmatrix}. \tag{8.342}$$

Eq. (8.341) describes a rigid mechanical rotation since the rotation velocity rises linearly with radius, see Fig. 8.32. The total derivative operator transforms this into a central electric field, also increasing linearly with radial distance (Fig. 8.33). The velocity field is that of a rigid body but there is no classical counterpart for the induced electric field. The spacetime velocity further induces a magnetic field

$$\mathbf{B}_F = \boldsymbol{\nabla} \times \mathbf{v}_F = \frac{B^{(0)} \rho}{\rho_m} \begin{bmatrix} 0 \\ 0 \\ -1 \end{bmatrix} \tag{8.343}$$

which is constant everywhere, and a constant Kambe charge density

$$q_F = \boldsymbol{\nabla} \cdot \mathbf{E}_F = -\frac{(B^{(0)})^2 \rho^2}{2\rho_m^2}. \tag{8.344}$$

The stationary part of the fluid electric current vanishes:

$$\mathbf{J}_F = a_0^2 \boldsymbol{\nabla} \times (\boldsymbol{\nabla} \times \mathbf{v}_F) = 0. \tag{8.345}$$

Plane Wave Potential

A potential for plane waves in the circular cartesian basis is given by

$$\mathbf{W} = \frac{W^{(0)}}{\sqrt{2}} \exp(i\omega t - \kappa_Z Z) \begin{bmatrix} 1 \\ -i \\ 0 \end{bmatrix} \tag{8.346}$$

where ω is the time frequency and κ_Z the wave vector component in Z direction. The derived spacetime quantities are

$$\mathbf{v}_F = \frac{W^{(0)}}{\sqrt{2}} \frac{\rho}{\rho_m} \exp(i\omega t - \kappa_Z Z) \begin{bmatrix} 1 \\ -i \\ 0 \end{bmatrix}, \tag{8.347}$$

$$\mathbf{E}_F = 0, \tag{8.348}$$

$$\mathbf{B}_F = \kappa_Z \frac{W^{(0)}}{\sqrt{2}} \frac{\rho}{\rho_m} \exp(i\omega t - \kappa_Z Z) \begin{bmatrix} 1 \\ -i \\ 0 \end{bmatrix}, \tag{8.349}$$

$$q_F = 0, \tag{8.350}$$

$$\mathbf{J}_F = a_0^2 \kappa_Z^2 \frac{W^{(0)}}{\sqrt{2}} \frac{\rho}{\rho_m} \exp(i\omega t - \kappa_Z Z) \begin{bmatrix} 1 \\ -i \\ 0 \end{bmatrix}. \tag{8.351}$$

In contrast to the simple rotating field, the derived fluid electric field and charge density disappear. Velocity, magnetic field and current density are all in parallel, having no Z component. The real part is schematically plotted in Fig. 8.34 for an instant of time t. The tops of the vector arrows describe a helix in space.

Magnetostatic Current Loop

The field of a circular current loop is best described in spherical polar coordinates (r, θ, ϕ). The vector potential of a loop with radius a and current I has only a ϕ component given by

$$\mathbf{W} = \begin{bmatrix} 0 \\ 0 \\ \frac{\mu_0 \, a^2 \, r \sin(\theta) \, I \left(\frac{15 \, a^2 \, r^2 \sin(\theta)^2}{8 \left(r^2 + a^2\right)^2} + 1 \right)}{4 \left(r^2 + a^2\right)^{\frac{3}{2}}} \end{bmatrix}. \tag{8.352}$$

This gives the velocity field

$$\mathbf{v}_F = \frac{\rho}{\rho_m} \mathbf{W} \neq 0 \tag{8.353}$$

and an electric field perpendicular to $\mathbf{v}_F$ in the (r, θ) plane:

$$\mathbf{E}_F = \frac{\mu_0^2 \, a^4 \, r \, \rho^2 \, I^2 \left(\frac{15 \, a^2 \, r^2 \sin(\theta)^2}{8 \left(r^2 + a^2\right)^2} + 1 \right)^2}{16 \, \rho_m^2 \left(r^2 + a^2\right)^3} \begin{bmatrix} -\sin(\theta)^2 \\ -\cot(\theta) \sin(\theta)^2 \\ 0 \end{bmatrix}. \tag{8.354}$$

The other fields $\mathbf{B}_F, q_F, \mathbf{J}_F$ are also different from zero but highly complicated. $\mathbf{B}_F$ has components in r and θ direction and $\mathbf{J}_F$ in ϕ direction.

The dependence of the component v_ϕ is graphed in Fig. 8.35 for $a = 1$. this is largest in the XY plane ($\theta = \pi/2$) and vanishes at the poles. The absolute strength decreases with distance from $r = a$ as expected. The angular distribution of electric field components E_r, E_θ is shown in Fig. 8.36.

Centre Fed Linear Antenna

Next we consider a linear antenna with length d and sinusoidal current density in the wire. The cartesian Z component of the vector potential is given [30] by

$$W_Z = \frac{\mu_0\, e^{i\,k\,r}\, \left(\cos\left(\frac{d\,k\cos(\theta)}{2}\right) - \cos\left(\frac{d\,k}{2}\right)\right) I}{2\,\pi\,k\,r\sin\left(\theta\right)^2} \tag{8.355}$$

where $k = \omega/c$ is the wave number of the sinusoidal current with angular frequency ω. Since W_Z is given in dependence of the spherical polar angle θ, we first transform this expression to spherical coordinates:

$$\begin{aligned}\mathbf{W} &= \begin{bmatrix} \cos\left(\phi\right)\sin\left(\theta\right) & \sin\left(\phi\right)\sin\left(\theta\right) & \cos\left(\theta\right) \\ \cos\left(\phi\right)\cos\left(\theta\right) & \sin\left(\phi\right)\cos\left(\theta\right) & -\sin\left(\theta\right) \\ -\sin\left(\phi\right) & \cos\left(\phi\right) & 0 \end{bmatrix} \begin{bmatrix} 0 \\ 0 \\ W_Z \end{bmatrix} \\ &= W_Z \begin{bmatrix} \cos(\theta) \\ -\sin(\theta) \\ 0 \end{bmatrix}.\end{aligned} \tag{8.356}$$

There is no ϕ component because the vector potential is symmetric in azimutal direction (see graph in Fig. 8.37). The resulting electric field has components in r and θ coordinates as well as the current density. The magnetic field goes only in ϕ direction, this is similar as a magnetic field of a linear current wire. There is also a non-vanishing spacetime charge density. Both q_F and B_ϕ have been graphed in Fig. 8.38. B_ϕ is largest in the XY plane similar to the velocity in Fig. 8.35. The Kambe charge density is highest at the poles, i.e. in Z direction.

Nuclear Dipole Potential

Dipole fields were already investigated in previous sections. Here we start directly from a dipole vector potential in cartesian coordinates:

$$\mathbf{m}_D = \frac{\mu_0}{4\,\pi\left(X^2+Y^2+Z^2\right)^{\frac{3}{2}}} \begin{bmatrix} m_Y Z - m_Z Y \\ m_Z X - m_X Z \\ m_X Y - m_Y X \end{bmatrix}. \tag{8.357}$$

This field is plotted for

$$\mathbf{m} = \begin{bmatrix} 0 \\ 0 \\ 1 \end{bmatrix} \tag{8.358}$$

in Fig. 8.39 in the XY plane. It leads to an electric spacetime field similar to Fig. 8.33 but with increasing ampliudes for the radius going to zero according to r^{-3}. All spacetime fields do not vanish. The shapes of B_Z and q are presented in Fig. 8.40 along the X axis. There is a a divergence of both at the centre where the source dipole is located.

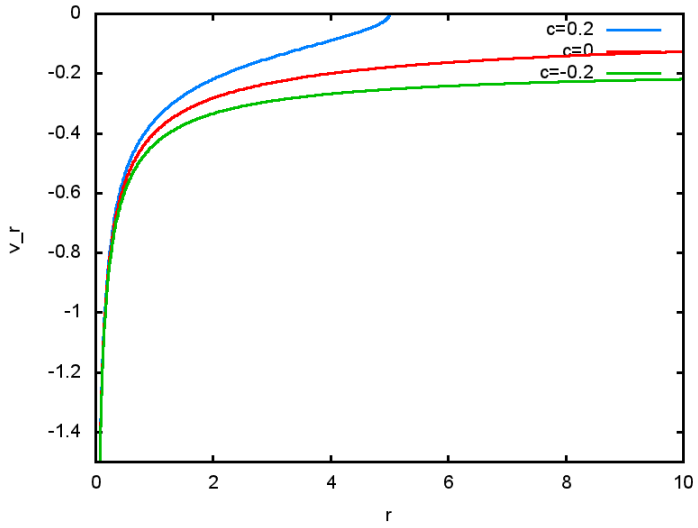

Figure 8.31: Radial velocity component (8.339) of solution for Eq. (8.219).

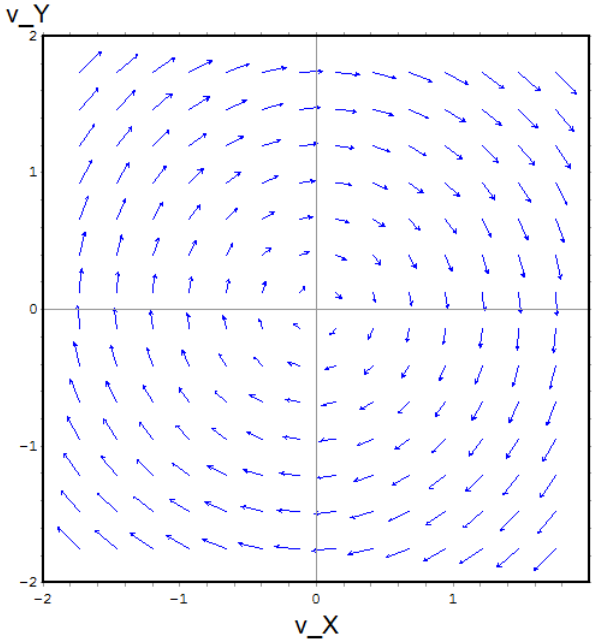

Figure 8.32: Simple velocity field (8.341).

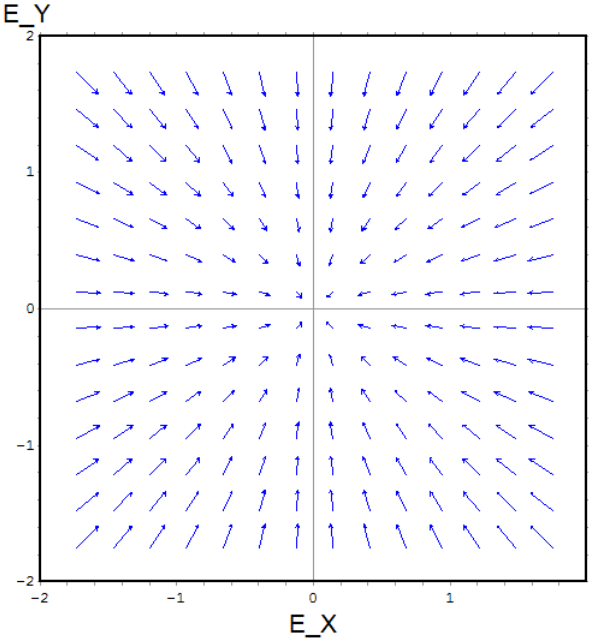

Figure 8.33: Central electric field (8.342) derived from (8.341).

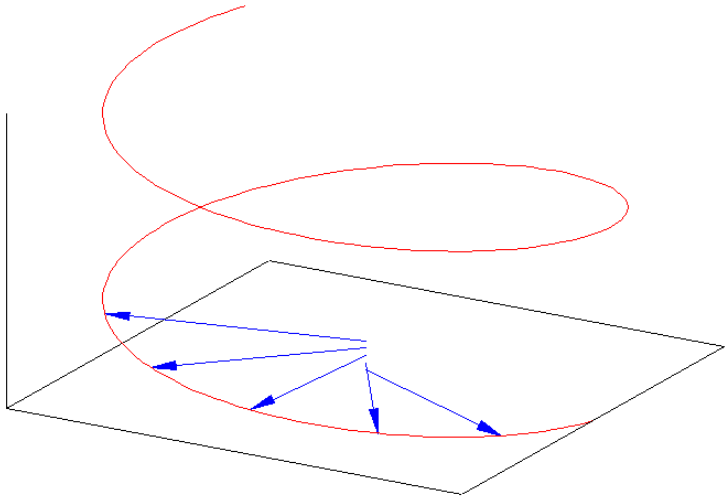

Figure 8.34: Vectors $\mathbf{v}_F$, $\mathbf{B}_F$, and $\mathbf{J}_F$ of the plane wave potential.

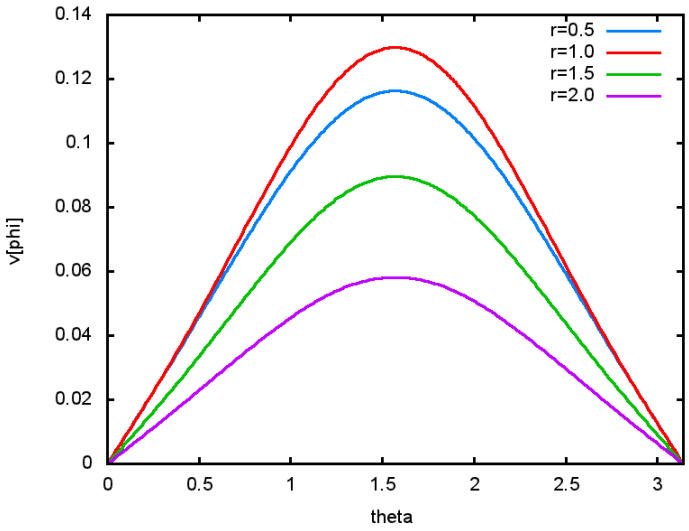

Figure 8.35: Velocity component v_ϕ of the magnetostatic current loop.

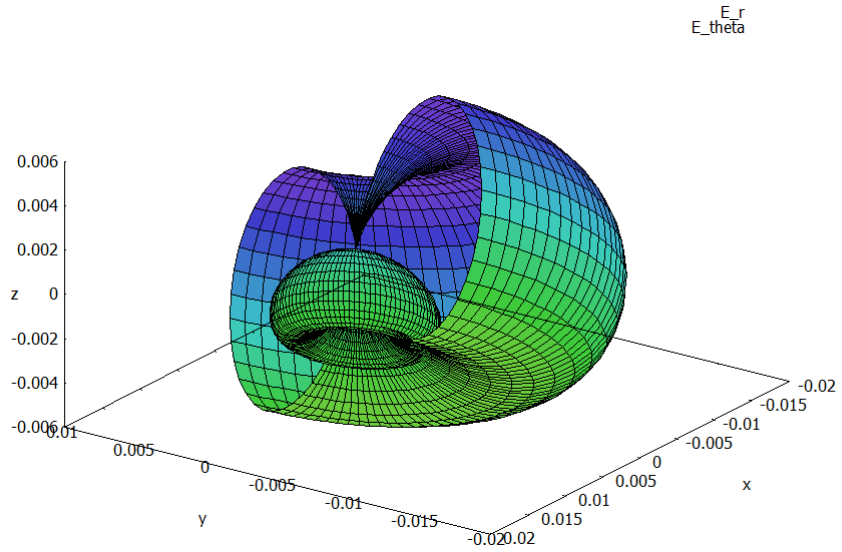

Figure 8.36: Components E_r (outer) and E_θ (inner) of electric field for the magnetostatic current loop, spherical distribution.

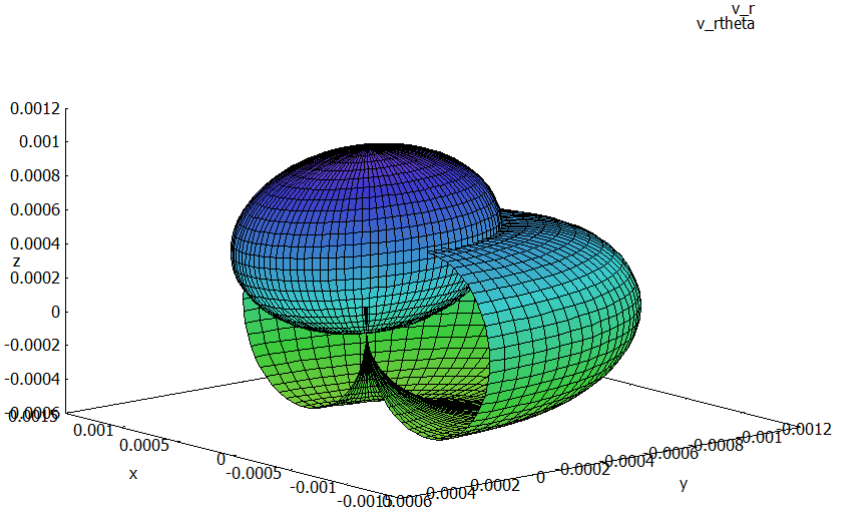

Figure 8.37: Components v_r (ellipsoid) and v_θ (torus) of velocity field for the center-fed antenna, spherical distribution.

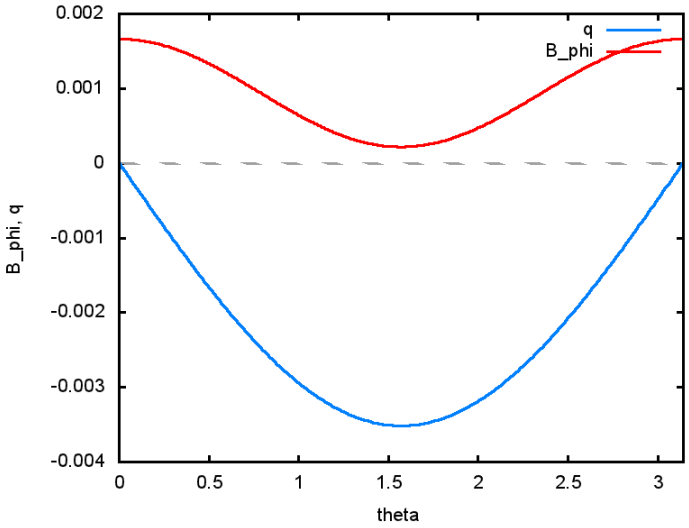

Figure 8.38: Component B_ϕ and q_F for the center-fed antenna.

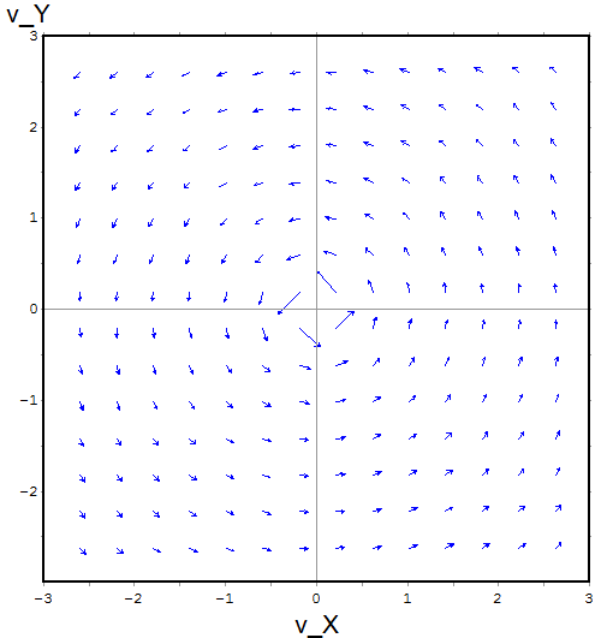

Figure 8.39: Velocity field (v_X, v_Y) in the plane $Z = 0$ for a nuclear dipole potential.

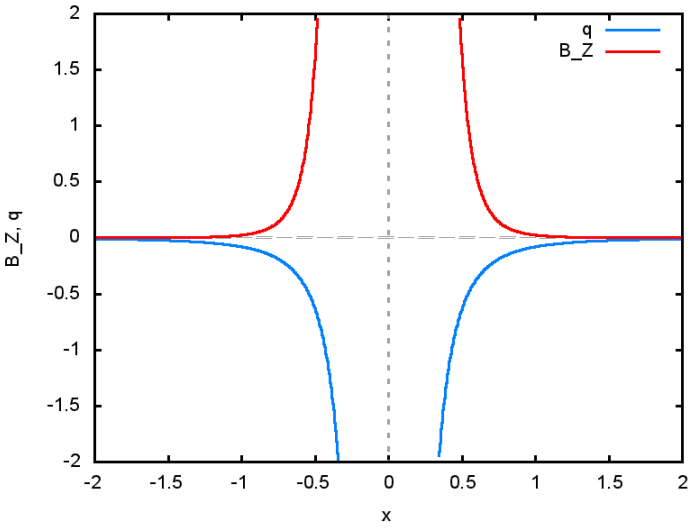

Figure 8.40: Component B_Z and q_F at $Y = 0$, $Z = 0$ for the nuclear dipole potential.

Chapter 9

Triple Unification: Fluid Gravitation

9.1 General Theory

In this chapter the ECE 2 theory is used to unify the field equations of fluid dynamics and gravitation to produce the subject of fluid dynamics, which can be described as the effect of the fluid vacuum or aether on gravitational theory. To start the chapter it is shown that fluid dynamics can describe all the main features of a whirlpool galaxy, so is preferred both to the Newton theory and the Einstein theory.

In fluid gravitation the acceleration due to gravity is defined as:

$$\mathbf{g}(\text{matter}) = \mathbf{E}_F(\text{vacuum}) \tag{9.1}$$

where $\mathbf{E}_F$ is the Kambe electric field of fluid dynamics, used in chapter eight:

$$\mathbf{E}_F = (\mathbf{v}_F \cdot \boldsymbol{\nabla})\,\mathbf{v}_F = -\boldsymbol{\nabla} h_F - \frac{\partial \mathbf{v}_F}{\partial t} \tag{9.2}$$

where $\mathbf{v}_F$ is the velocity field of the spacetime, aether or vacuum, h_F is the enthalpy per unit mass, and Φ_F is the scalar potential defined by:

$$\Phi_F = h_F. \tag{9.3}$$

The vacuum magnetic field is the vorticity:

$$\mathbf{B}_F = \mathbf{w}_F = \boldsymbol{\nabla} \times \mathbf{v}_F \tag{9.4}$$

and the vacuum law:

$$\boldsymbol{\nabla} \times \mathbf{E}_F + \frac{\partial \mathbf{B}_F}{\partial t} = \mathbf{0} \tag{9.5}$$

follows from Eqs. (9.2) to (9.4). This is equivalent to the Faraday law of induction of electrodynamics.

The Newtonian acceleration due to gravity is defined by:

$$\mathbf{g} = -\frac{MG}{r^2}\mathbf{e}_r = (\mathbf{v}_F \cdot \boldsymbol{\nabla})\,\mathbf{v}_F \tag{9.6}$$

where M is a gravitating mass, G is Newton's constant and $\mathbf{r}$ the distance between M and an orbiting mass m. The acceleration due to gravity $\mathbf{g}$ induces $\mathbf{E}_F$ in the vacuum, and conversely the vacuum velocity field induces $\mathbf{g}$ in matter.

There is an exact analogy between the ECE 2 gravitational field equations:

$$\boldsymbol{\nabla} \cdot \boldsymbol{\Omega} = 0 \tag{9.7}$$

$$\boldsymbol{\nabla} \times \mathbf{g} + \frac{\partial \boldsymbol{\Omega}}{\partial t} = \mathbf{0} \tag{9.8}$$

$$\boldsymbol{\nabla} \cdot \mathbf{g} = 4\pi G\rho_m = \boldsymbol{\kappa} \cdot \mathbf{g} \tag{9.9}$$

$$\boldsymbol{\nabla} \times \boldsymbol{\Omega} - \frac{1}{c^2}\frac{\partial \mathbf{g}}{\partial t} = \frac{4\pi G}{c^2}\mathbf{J}_m = \boldsymbol{\kappa} \times \boldsymbol{\Omega} \tag{9.10}$$

$$\mathbf{g} = -\boldsymbol{\nabla}\phi_g - \frac{\partial \mathbf{v}_g}{\partial t} \tag{9.11}$$

$$\boldsymbol{\Omega} = \boldsymbol{\nabla} \times \mathbf{v}_g \tag{9.12}$$

and the ECE 2 field equations of fluid dynamics:

$$\boldsymbol{\nabla} \cdot \mathbf{B}_F = 0 \tag{9.13}$$

$$\boldsymbol{\nabla} \times \mathbf{E}_F + \frac{\partial \mathbf{B}_F}{\partial t} = \mathbf{0} \tag{9.14}$$

$$\boldsymbol{\nabla} \cdot \mathbf{E}_F = q_F \tag{9.15}$$

$$\boldsymbol{\nabla} \times \mathbf{B}_F - \frac{1}{a_0^2}\frac{\partial \mathbf{E}_F}{\partial t} = \frac{1}{a_0^2}\mathbf{J}_F. \tag{9.16}$$

Both sets of equations are ECE 2 covariant. Here $\boldsymbol{\Omega}$ is the gravitomagnetic field, $\mathbf{g}$ is the gravitational field, ρ_m is the mass density, $\boldsymbol{\kappa}$ is defined in terms of the spin connection, $\mathbf{J}_m$ is the current of mass density, ϕ_g is the scalar potential of ECE 2 gravitation, and $\mathbf{v}_g$ is the vector potential of ECE 2 gravitation. In the ECE 2 equations of fluid dynamics, $\mathbf{E}_F$ is the fluid electric field, $\mathbf{B}_F$ is the fluid magnetic field, q_F is the fluid charge, $\mathbf{J}_F$ is the fluid current, and a_0 the assumed constant speed of sound.

It follows that:

$$\boldsymbol{\Omega}(\text{matter}) = \boldsymbol{\nabla} \times \mathbf{v}_F = \mathbf{w}_F \tag{9.17}$$

and

$$\begin{aligned} \mathbf{g}(\text{matter}) &= \left(-\boldsymbol{\nabla}\phi_g - \frac{\partial \mathbf{v}_g}{\partial t}\right)(\text{matter}) \\ &= \left(-\boldsymbol{\nabla}\Phi_F - \frac{\partial \mathbf{v}_F}{\partial t}\right)(\text{vacuum}) \end{aligned} \tag{9.18}$$

and that:

$$\boldsymbol{\Omega}(\text{matter}) = (\boldsymbol{\nabla} \times \mathbf{W})\,(\text{matter}) = (\boldsymbol{\nabla} \times \mathbf{v}_F)\,(\text{vacuum}). \tag{9.19}$$

From the gravitational field equation:

$$\boldsymbol{\nabla} \cdot \mathbf{g}(\text{matter}) = 4\pi G \rho_m(\text{matter}) = (\boldsymbol{\kappa} \cdot \mathbf{g})\,(\text{matter}) \tag{9.20}$$

it follows that:

$$\boldsymbol{\nabla} \cdot \mathbf{g}(\text{matter}) = 4\pi G \rho_m(\text{matter}) = q_F(\text{vacuum}) \tag{9.21}$$

so material mass density is:

$$\rho_m(\text{matter}) = \frac{q_F(\text{vacuum})}{4\pi G} \tag{9.22}$$

and originates in the vacuum charge:

$$q_F(\text{vacuum}) = (\boldsymbol{\nabla} \cdot \mathbf{E}_F)\,(\text{vacuum}). \tag{9.23}$$

In general:

$$(\boldsymbol{\nabla} \cdot ((\mathbf{v}_F \cdot \boldsymbol{\nabla})\,\mathbf{v}_F))\,(\text{vacuum}) = 4\pi G \rho_m(\text{matter}) \tag{9.24}$$

so any spacetime velocity field gives rise to material mass density. Conversely any mass density induces a spacetime velocity field.

The vacuum wave equation of chapter eight and UFT 349 ff. is:

$$\Box\, \Phi_F = q_F \tag{9.25}$$

given the vacuum Lorenz condition:

$$\frac{\partial \Phi_F}{\partial t} + a_0^2\, \boldsymbol{\nabla} \cdot \mathbf{v}_F = 0 \tag{9.26}$$

which is a particular solution of vacuum continuity equation:

$$\frac{\partial q_F}{\partial t} + a_0^2\, \boldsymbol{\nabla} \cdot \mathbf{v}_F = 0 \tag{9.27}$$

in which the vacuum current is:

$$\mathbf{J}_F = a_0^2\, \boldsymbol{\nabla} \times (\boldsymbol{\nabla} \times \mathbf{v}_F) - \frac{\partial}{\partial t} \left((\mathbf{v}_F \cdot \boldsymbol{\nabla})\,\mathbf{v}_F\right). \tag{9.28}$$

The d'Alembertian in Eq. (9.25) is:

$$\Box = \frac{1}{a_0^2} \frac{\partial^2}{\partial t^2} - \nabla^2. \tag{9.29}$$

The Newtonian solution is:

$$((\mathbf{v}_F \cdot \boldsymbol{\nabla})\,\mathbf{v}_F)\,(\text{vacuum}) = -\left(\frac{MG}{r^2}\mathbf{e}_r\right)(\text{matter}) \tag{9.30}$$

as in Note 358(3). This equation is formally identical to (8.219) and its solution has already been discussed numerically and graphically at the beginning of

section 8.2.4. To exemplify the elegance of fluid gravitation consider as in Note 358(4) on `www.aias.us` the constant vacuum angular momentum:

$$\mathbf{L}_F = m_r \mathbf{r}_F \times \mathbf{v}_F \tag{9.31}$$

which can be defined for any central force between m and M. Here $\mathbf{r}_F$ is the position vector and $\mathbf{v}_F$ the velocity field. The reduced mass is defined by:

$$m_r = \frac{mM}{m+M} \tag{9.32}$$

of m orbiting M. The subscript F for any quantity denotes the fluid vacuum. For a planar orbit:

$$\begin{aligned} \mathbf{r}_F \times \mathbf{L}_F &= m_r \mathbf{r}_F \times (\mathbf{r}_F \times \mathbf{v}_F) \\ &= m_r \left(\mathbf{r}_F \left(\mathbf{r}_F \cdot \mathbf{v}_F \right) - \mathbf{v}_F \left(\mathbf{r}_F \cdot \mathbf{r}_F \right) \right) \end{aligned} \tag{9.33}$$

and:

$$\mathbf{r}_F \cdot \mathbf{v}_F = 0 \tag{9.34}$$

so the vacuum velocity field is:

$$\mathbf{v}_F = -\frac{1}{m_r r_F^2} \mathbf{L}_F \times \mathbf{r}_F \tag{9.35}$$

where:

$$\mathbf{L}_F = L_{FZ} \mathbf{k} \tag{9.36}$$

and:

$$\mathbf{v}_F = \frac{L_{FZ}}{m_r r_F^2} \left(-Y_F \mathbf{i} + X_F \mathbf{j} \right). \tag{9.37}$$

This is a divergenceless velocity field:

$$\boldsymbol{\nabla} \cdot \mathbf{v}_F = 0. \tag{9.38}$$

The material gravitomagnetic field is then:

$$\boldsymbol{\Omega}(\text{matter}) = \frac{2}{m r_F^2} \mathbf{L}_F \tag{9.39}$$

and is perpendicular to the plane of the orbit. In a whirlpool galaxy for example the gravitomagnetic field is perpendicular to the plane of the galaxy and the gravitational field between a star of mass m of the whirlpool galaxy and its central mass M is:

$$\mathbf{g}(\text{matter}) = \left(\mathbf{v}_F \cdot \boldsymbol{\nabla} \right) \mathbf{v}_F. \tag{9.40}$$

In Cartesian coordinates:

$$\mathbf{v}_F \cdot \boldsymbol{\nabla} = \frac{L_{FZ}}{m_r r_F^2} \left(-Y_F \frac{\partial}{\partial X_F} + X_F \frac{\partial}{\partial Y_F} \right) \tag{9.41}$$

so:

$$\mathbf{g}(\text{matter}) = \frac{L_{FZ}^2}{m_r^2 r_F^4}\left(\left(Y_F\frac{\partial Y_F}{\partial X_F} - X_F\right)\mathbf{i} + \left(X_F\frac{\partial X_F}{\partial Y_F} - Y_F\right)\mathbf{j}\right). \quad (9.42)$$

Now assume that

$$\frac{\partial Y_F}{\partial X_F} = \frac{\partial X_F}{\partial Y_F} = 0 \quad (9.43)$$

and it follows that:

$$\mathbf{g}(\text{matter}) = -\frac{L_{FZ}^2}{m_r^2 r_F^4}\mathbf{r}_F \quad (9.44)$$

where:

$$\mathbf{r}_F = X_F\mathbf{i} + Y_F\mathbf{j}. \quad (9.45)$$

Finally use:

$$\mathbf{r}_F = r_F\mathbf{e}_r \quad (9.46)$$

to find an inverse cube law between m and M:

$$\mathbf{g}(\text{matter}) = -\frac{L_{FZ}^2}{m_r^2 r_F^3}\mathbf{e}_r \quad (9.47)$$

the force being:

$$\mathbf{F} = m_r\mathbf{g}(\text{matter}). \quad (9.48)$$

From the vacuum Binet equation:

$$\mathbf{F} = -\frac{L_F^2}{m_r r_F^2}\left(\frac{1}{r_F} + \frac{d^2}{d\theta^2}\left(\frac{1}{r_F}\right)\right) \quad (9.49)$$

the orbit of m around M is the hyperbolic spiral:

$$\frac{1}{r_F} = \frac{\theta}{r_{0F}}. \quad (9.50)$$

In plane polar coordinates (r, θ) the velocity of a star in the whirlpool galaxy is:

$$v^2 = \left(\frac{dr}{dt}\right)^2 + r^2\left(\frac{d\theta}{dt}\right)^2 = \left(\frac{d\theta}{dt}\right)^2\left(r^2 + \left(\frac{dr}{d\theta}\right)^2\right). \quad (9.51)$$

From lagrangian theory:

$$\frac{d\theta}{dt} = \frac{L}{m_r r^2} \quad (9.52)$$

so the velocity of the star is:

$$v^2 = \frac{L^2}{m^2}\left(\frac{1}{r^2} + \frac{1}{r_0^2}\right) \xrightarrow[r\to\infty]{} \left(\frac{L}{mr_0^2}\right)^2 = \text{constant}. \tag{9.53}$$

From Eqs. (9.26) and (9.38) it follows that:

$$\frac{\partial \Phi_F}{\partial t} = \frac{\partial h_F}{\partial t} = 0 \tag{9.54}$$

so the vacuum potential is constant:

$$\Phi_F = h_F = \text{constant} \tag{9.55}$$

in a whirlpool galaxy. It follows from the wave equation (9.25) that:

$$\nabla^2 \Phi_F = -4\pi G \rho_m(\text{matter}). \tag{9.56}$$

The vacuum charge of the whirlpool galaxy is:

$$q_F = (\boldsymbol{\nabla} \cdot \mathbf{g})\,(\text{matter}) = \left(\frac{L_{FZ}}{m_r r_F^2}\right) \tag{9.57}$$

so from Eq. (9.24):

$$\rho_m(\text{matter}) = \frac{1}{4\pi G}\left(\frac{L_{FZ}}{m_r r_F^2}\right)^2 \xrightarrow[r\to 0]{} \infty \tag{9.58}$$

and there is a very large mass at the centre of the galaxy, as observed.

The spacetime current (9.28) that gives rise to a whirlpool galaxy is:

$$\mathbf{J}_F = a_0^2\, \boldsymbol{\nabla} \times (\boldsymbol{\nabla} \times \mathbf{v}_F) \tag{9.59}$$

if $\mathbf{E}_F$ is time independent. Therefore with this assumption:

$$\mathbf{J}_F = \frac{4a_0^2}{r_F^2}\mathbf{v}_F \tag{9.60}$$

and $\mathbf{J}_F$ is proportional to $\mathbf{v}_F$.

Numerical and graphical analysis of these characteristics are developed later in this chapter.

In the subject of fluid gravitation. Newtonian gravitation produces a rich structure in the fluid vacuum, a structure which can be illustrated with the velocity field, vorticity, charge and static current using Gnuplot graphics. A new law of planar orbital theory can be inferred and the Newtonian acceleration due to gravity becomes the convective derivative of the orbital linear velocity.

The velocity field $\mathbf{v}_F$ induced by the Newtonian acceleration due to gravity $\mathbf{g}$ is defined by:

$$\mathbf{g} = -\frac{MG}{r^2}\mathbf{e}_r = (\mathbf{v}_F \cdot \boldsymbol{\nabla})\,\mathbf{v}_F \tag{9.61}$$

where:

$$\mathbf{r} = r\mathbf{e}_r. \tag{9.62}$$

Similarly, the static electric field strength in volts per metre induces vacuum structure in an exactly analogous manner:

$$\mathbf{E} = -\frac{e}{4\pi\epsilon_0 r^2}\mathbf{e}_r = x\left(\mathbf{v}_F \cdot \boldsymbol{\nabla}\right)\mathbf{v}_F. \tag{9.63}$$

In general there are many solutions of Eq. (9.61), one of which is developed as follows from Note 359(6) on `www.aias.us`:

$$\mathbf{v}_F = \mathbf{v}_{F1} + \mathbf{v}_{F2} + \mathbf{v}_{F3} \tag{9.64}$$

where:

$$\mathbf{v}_{F1} = \frac{\sqrt{2}\left(MG\right)^{1/2}}{\left(X^2+Y^2+Z^2\right)^{3/4}}\left(-Y\mathbf{i} + X\mathbf{j}\right) \tag{9.65}$$

$$\mathbf{v}_{F2} = \frac{\sqrt{2}\left(MG\right)^{1/2}}{\left(X^2+Y^2+Z^2\right)^{3/4}}\left(-Z\mathbf{i} + X\mathbf{k}\right) \tag{9.66}$$

$$\mathbf{v}_{F3} = \frac{\sqrt{2}\left(MG\right)^{1/2}}{\left(X^2+Y^2+Z^2\right)^{3/4}}\left(-Z\mathbf{j} + Y\mathbf{k}\right). \tag{9.67}$$

These components are graphed later on in this chapter using Gnuplot, and are richly structured. The above velocity field gives:

$$\mathbf{g} = -\frac{MG}{r^2}\mathbf{e}_r \tag{9.68}$$

where:

$$r^2 = X^2 + Y^2 + Z^2. \tag{9.69}$$

The three vacuum charges are:

$$q_{F1} = \boldsymbol{\nabla}\cdot\mathbf{g}_{F1} = -\frac{MG}{2}\left(\frac{2Z^2 - Y^2 - X^2}{\left(X^2+Y^2+Z^2\right)^{5/2}}\right) \tag{9.70}$$

$$q_{F2} = \boldsymbol{\nabla}\cdot\mathbf{g}_{F2} = \frac{MG}{2}\left(\frac{Z^2 - 2Y^2 + X^2}{\left(X^2+Y^2+Z^2\right)^{5/2}}\right) \tag{9.71}$$

$$q_{F3} = \boldsymbol{\nabla}\cdot\mathbf{g}_{F3} = \frac{MG}{2}\left(\frac{Z^2 + Y^2 - 2X^2}{\left(X^2+Y^2+Z^2\right)^{5/2}}\right) \tag{9.72}$$

and sum to zero in this solution:

$$q_{F1} + q_{F2} + q_{F3} = 0. \tag{9.73}$$

The vacuum charges exhibit a swirling motion as shown by Gnuplot later on in this chapter. The vacuum vorticities are:

$$\begin{aligned}\mathbf{w}_{F1} &= \boldsymbol{\nabla} \times \mathbf{v}_{F1} \\ &= \frac{(MG)^{1/2}}{2^{3/2}\left(X^2+Y^2+Z^2\right)^{7/4}}\left(3XZ\mathbf{i}+3YZ\mathbf{j}+\left(4Z^2+Y^2+X^2\right)\mathbf{k}\right)\end{aligned} \tag{9.74}$$

$$\begin{aligned}\mathbf{w}_{F2} &= \boldsymbol{\nabla} \times \mathbf{v}_{F2} \\ &= \frac{(MG)^{1/2}}{2^{3/2}\left(X^2+Y^2+Z^2\right)^{7/4}}\left(-3XY\mathbf{i}-\left(Z^2+4Y^2+X^2\right)\mathbf{j}-3YZ\mathbf{k}\right)\end{aligned} \tag{9.75}$$

$$\begin{aligned}\mathbf{w}_{F3} &= \boldsymbol{\nabla} \times \mathbf{v}_{F3} \\ &= \frac{(MG)^{1/2}}{2^{3/2}\left(X^2+Y^2+Z^2\right)^{7/4}}\left(\left(Z^2+Y^2+4X^2\right)\mathbf{i}+3XY\mathbf{j}+3XZ\mathbf{j}\right)\end{aligned} \tag{9.76}$$

and self consistently obey the equations:

$$\boldsymbol{\nabla} \cdot \mathbf{w}_{F1} = \boldsymbol{\nabla} \cdot \mathbf{w}_{F2} = \boldsymbol{\nabla} \cdot \mathbf{w}_{F3} = 0. \tag{9.77}$$

These are also graphed later in this chapter using Gnuplot, and also exhibit a swirling motion.

We therefore arrive at a new law of orbits where the Newtonian acceleration due to gravity between m and M is the convective derivative of the orbital linear velocity.

By definition:

$$\boldsymbol{\nabla} \cdot \mathbf{w}_F = 0, \tag{9.78}$$

$$\boldsymbol{\nabla} \times \mathbf{g}_F + \frac{\partial \mathbf{w}_F}{\partial t} = \mathbf{0}. \tag{9.79}$$

In ECE 2 electromagnetism they become the homogeneous field equations:

$$\boldsymbol{\nabla} \cdot \mathbf{B} = 0 \tag{9.80}$$

$$\boldsymbol{\nabla} \times \mathbf{E} + \frac{\partial \mathbf{B}}{\partial t} = \mathbf{0}. \tag{9.81}$$

The vacuum current is defined by:

$$\mathbf{J}_F = a_0^2 \boldsymbol{\nabla} \times (\boldsymbol{\nabla} \times \mathbf{v}_F) - \frac{\partial}{\partial t}\left((\mathbf{v}_F \cdot \boldsymbol{\nabla})\mathbf{v}_F\right) \tag{9.82}$$

where a_0 is the assumed constant speed of sound. Therefore the inhomogeneous field equations of the vacuum are:

$$\boldsymbol{\nabla} \cdot \mathbf{v}_F = q_F \tag{9.83}$$

and

$$\boldsymbol{\nabla} \times \mathbf{w}_F - \frac{1}{a_0^2} \frac{\partial \mathbf{g}_F}{\partial t} = \frac{1}{a_0^2} \mathbf{J}_F. \tag{9.84}$$

If it is assumed that:

$$\frac{\partial \mathbf{g}_F}{\partial t} = \mathbf{0} \tag{9.85}$$

then:

$$\mathbf{J}_F = a_0^2 \, \boldsymbol{\nabla} \times (\boldsymbol{\nabla} \times \mathbf{v}_F) \tag{9.86}$$

and using Eq. (9.61):

$$\mathbf{J}_{F1} = \frac{9a_0^2}{2^{5/2} \left(X^2 + Y^2 + Z^2\right)^{7/4}} \left(-Y\mathbf{i} + X\mathbf{j}\right) \tag{9.87}$$

$$\mathbf{J}_{F2} = \frac{9a_0^2}{2^{5/2} \left(X^2 + Y^2 + Z^2\right)^{7/4}} \left(-Z\mathbf{i} + X\mathbf{k}\right) \tag{9.88}$$

$$\mathbf{J}_{F3} = \frac{9a_0^2}{2^{5/2} \left(X^2 + Y^2 + Z^2\right)^{7/4}} \left(-Z\mathbf{i} + Y\mathbf{k}\right) \tag{9.89}$$

which again exhibit a swirling motion.

The fundamental philosophy of fluid gravitation is:

$$\mathbf{g}(\text{matter}) = \mathbf{g}_F(\text{vacuum}) \tag{9.90}$$

so the familiar Newtonian $\mathbf{g}$(matter) induces $\mathbf{v}_{F1}$, $\mathbf{v}_{F2}$, $\mathbf{v}_{F3}$, $\mathbf{g}_{F1}$, $\mathbf{g}_{F2}$, $\mathbf{g}_{F3}$, q_{F1}, q_{F2}, q_{F3}, $\mathbf{w}_{F1}$, $\mathbf{w}_{F2}$, $\mathbf{w}_{F3}$, $\mathbf{J}_{F1}$, $\mathbf{J}_{F2}$, $\mathbf{J}_{F3}$ in the vacuum. The converse is also true as developed in chapter eight.

In order to apply fluid gravitation to planar orbits consider the linear velocity in plane polar coordinates:

$$\mathbf{v} = \dot{r}\mathbf{e}_r + r\dot{\theta}\mathbf{e}_\theta \tag{9.91}$$

where the unit vectors are:

$$\mathbf{e}_r = \mathbf{i}\cos\theta + \mathbf{j}\sin\theta \tag{9.92}$$

and

$$\mathbf{e}_\theta = -\mathbf{i}\sin\theta + \mathbf{j}\cos\theta. \tag{9.93}$$

In fluid gravitation there is a new and general relation between the orbital velocity $\mathbf{v}$ and the Newtonian acceleration $\mathbf{g}$:

$$\mathbf{g} = (\mathbf{v} \cdot \boldsymbol{\nabla})\, \mathbf{v}. \tag{9.94}$$

From Eqs. (9.65) and (9.91) it follows that:

$$v^2 = \dot{r}^2 + r^2\dot{\theta}^2 = \frac{MG}{\left(X^2 + Y^2\right)^{1/2}} \tag{9.95}$$

and

$$(MG)^{1/2} X \left(X^2 + Y^2\right)^{-3/4} = \dot{r} \sin\theta + r\dot{\theta} \cos\theta \tag{9.96}$$

$$(MG)^{1/2} Y \left(X^2 + Y^2\right)^{-3/4} = r\dot{\theta} \sin\theta - \dot{r} \cos\theta. \tag{9.97}$$

From Eqs. (9.96) and (9.97) it follows that:

$$v^2 = \frac{MG}{(X^2 + Y^2)^{1/2}} \tag{9.98}$$

therefore for any planar orbit:

$$X = \frac{MG}{v^3} \left(\dot{r} \sin\theta + r\dot{\theta} \cos\theta\right) \tag{9.99}$$

and

$$Y = \frac{MG}{v^3} \left(r\dot{\theta} \sin\theta - \dot{r} \cos\theta\right). \tag{9.100}$$

For an elliptical planar orbit for example:

$$v^2 = \dot{r}^2 + r^2\dot{\theta}^2 = MG \left(\frac{2}{r} - \frac{1}{a}\right) \tag{9.101}$$

and:

$$\frac{1}{(X^2 + Y^2)^{1/2}} = \frac{2}{r} - \frac{1}{a} \tag{9.102}$$

where:

$$a = \frac{\alpha}{1 - \epsilon^2} \tag{9.103}$$

is the semi major axis, α the half right latitude and ϵ the eccentricity. In plane polar coordinates:

$$r = \frac{\alpha}{1 + \epsilon \cos\theta} \tag{9.104}$$

and in Cartesian coordinates:

$$\frac{X^2}{a^2} + \frac{Y^2}{b^2} = 1 \tag{9.105}$$

where the semi minor axis is:

$$b = \frac{\alpha}{(1 - \epsilon^2)^{1/2}}. \tag{9.106}$$

In the case of the ellipse:

$$\frac{dr}{d\theta} = \frac{\epsilon r^2}{\alpha} \sin\theta \tag{9.107}$$

and:

$$\frac{d\theta}{dt} = \frac{L}{mr^2}, \tag{9.108}$$

$$L^2 = m^2 MG\alpha. \tag{9.109}$$

It follows that for the planar elliptical orbit:

$$X = \alpha^{1/2}\left(\frac{\epsilon}{\alpha}\sin^2\theta + \frac{1}{r}\cos\theta\right)\left(\frac{2}{r} - \frac{1}{a}\right)^{-3/2} \tag{9.110}$$

and:

$$Y = \alpha^{1/2}\left(\frac{1}{r}\sin\theta - \frac{\epsilon}{\alpha}\sin\theta\cos\theta\right)\left(\frac{2}{r} - \frac{1}{a}\right)^{-3/2}. \tag{9.111}$$

These properties are graphed and analyzed later in this section.

For circular orbits:

$$\epsilon = 0,\ \frac{2}{a} - \frac{1}{r} = \frac{1}{r},\ r = \alpha \tag{9.112}$$

so:

$$X = r\cos\theta \tag{9.113}$$

$$Y = r\sin\theta \tag{9.114}$$

Therefore a new and general theory of orbits has been inferred.

Using fluid gravitation it can be shown as follows that all observable orbits can be expressed as a generally covariant inverse square law:

$$\mathbf{g} = -\frac{MG}{r^2}\mathbf{e}_r = (\mathbf{v}\cdot\boldsymbol{\nabla})\,\mathbf{v}. \tag{9.115}$$

Therefore $\mathbf{g}$ is the convective derivative of $\mathbf{v}$. For planar orbits, the inverse square law is:

$$\mathbf{g} = -\frac{MG}{X^2 + Y^2}\mathbf{e}_r \tag{9.116}$$

and from Eq. (9.115) the orbital velocity is:

$$\mathbf{v} = (MG)^{1/2}\,\frac{(-X\mathbf{i} + Y\mathbf{j})}{(X^2 + Y^2)^{3/4}}. \tag{9.117}$$

In plane polar coordinates:

$$v^2 = \frac{MG}{(X^2 + Y^2)^{1/2}} = \dot{r}^2 + r^2\dot{\theta}^2 \tag{9.118}$$

and for elliptical orbits:

$$v^2 = MG\left(\frac{2}{r} - \frac{1}{a}\right) \tag{9.119}$$

so for the elliptical orbit:

$$\frac{1}{(X^2+Y^2)^{1/2}} = \frac{2}{r} - \frac{1}{a} = \frac{1}{MG}\left(\dot{r}^2 + r^2\dot{\theta}^2\right) \tag{9.120}$$

and the acceleration due to gravity is:

$$\begin{aligned}\mathbf{g} &= -\frac{MG}{X^2+Y^2}\mathbf{e}_r = -MG\left(\frac{2}{r} - \frac{1}{a}\right)^2\mathbf{e}_r \\ &= -\frac{1}{MG}\left(\dot{r}^2 + r^2\dot{\theta}^2\right)^2\mathbf{e}_r.\end{aligned} \tag{9.121}$$

Eq. (9.120) shows that the acceleration due to gravity can be expressed as:

$$\mathbf{g} = -\frac{v^4}{MG}\mathbf{e}_r. \tag{9.122}$$

For all planar orbits:

$$X = MG\left(\dot{r}\sin\theta + r\dot{\theta}\cos\theta\right)\left(\dot{r}^2 + r^2\dot{\theta}^2\right)^{-3/2} \tag{9.123}$$

and

$$Y = MG\left(r\dot{\theta}\sin\theta - \dot{r}\cos\theta\right)\left(\dot{r}^2 + r^2\dot{\theta}^2\right)^{-3/2}. \tag{9.124}$$

In the case of the whirlpool galaxy:

$$r = \frac{r_0}{\theta} \tag{9.125}$$

and it follows that:

$$\dot{r}^2 + r^2\dot{\theta}^2 = \frac{L^2}{m^2}\left(\frac{1}{r^2} + \frac{1}{r_0^2}\right) \tag{9.126}$$

where the angular momentum L is a constant of motion. It follows as in Note 360(3) that:

$$X = MG\left(\frac{L}{mr}\cos\left(\frac{r_0}{r}\right) - \frac{L}{mr_0}\sin\left(\frac{r_0}{r}\right)\right)\left(\frac{L^2}{m^2}\left(\frac{1}{r^2} + \frac{1}{r_0^2}\right)\right)^{-3/2} \tag{9.127}$$

and

$$Y = MG\frac{L}{m}\left(\frac{1}{r}\sin\left(\frac{r_0}{r}\right) - \frac{1}{r_0}\cos\left(\frac{r_0}{r}\right)\right)\left(\frac{L^2}{m^2}\left(\frac{1}{r^2} + \frac{1}{r_0^2}\right)\right)^{-3/2}. \tag{9.128}$$

For the precessing orbit in a plane in a simple model:

$$r = \frac{\alpha}{1 + \epsilon\cos(x\theta)} \tag{9.129}$$

where:

$$x = 1 + \frac{3MG}{c^2\alpha}. \tag{9.130}$$

It follows as in Note 360(4) that:

$$\dot{r} = \frac{dr}{dt} = \frac{x\epsilon L}{m\alpha}\left(1 + \frac{1}{\epsilon^2}\left(\frac{\alpha}{r} - 1\right)^2\right)^{1/2} \tag{9.131}$$

and

$$\dot{\theta} = \frac{L}{mr^2} \tag{9.132}$$

so X and Y can be graphed. They are illustrated later on in this chapter.

As shown in Note 360(5):

$$\mathbf{g} = -\frac{v^4}{MG}\mathbf{e}_r \tag{9.133}$$

so for the precessing orbit:

$$\mathbf{g} = -\frac{L^4}{m^4 MG}\left(\frac{x^2\epsilon^2}{\alpha^2}\left(1 - \frac{1}{\epsilon^2}\left(\frac{\alpha}{r} - 1\right)^2\right) + \frac{1}{r^2}\right)^2. \tag{9.134}$$

ECE 2 dynamics with the convective derivative can be developed as in UFT 361 by expressing the velocity field as:

$$\mathbf{v} = \mathbf{v}\left(r(t), \theta(t), Z(t), t\right) \tag{9.135}$$

where cylindrical polar coordinates have been used. In classical dynamics:

$$\mathbf{v} = \mathbf{v}(t). \tag{9.136}$$

The material derivative is:

$$\begin{aligned}
\frac{D\mathbf{v}}{Dt} &= \frac{\partial \mathbf{v}}{\partial t} + (\mathbf{v}\cdot\boldsymbol{\nabla})\,\mathbf{v} \\
&= \frac{\partial \mathbf{v}}{\partial t} + \left(v_r\frac{\partial}{\partial r} + \frac{v_\theta}{r}\frac{\partial}{\partial\theta} + v_Z\frac{\partial}{\partial Z}\right)(v_r\mathbf{e}_r + v_\theta\mathbf{e}_\theta + v_Z\mathbf{k}) \\
&= \frac{\partial \mathbf{v}}{\partial t} + v_r\frac{\partial}{\partial r}(v_r\mathbf{e}_r) + \frac{v_\theta}{r}\frac{\partial}{\partial\theta}(v_r\mathbf{e}_r) + v_Z\frac{\partial}{\partial Z}(v_r\mathbf{e}_r) \\
&\quad + v_r\frac{\partial}{\partial r}(v_\theta\mathbf{e}_\theta) + \frac{v_\theta}{r}\frac{\partial}{\partial\theta}(v_\theta\mathbf{e}_\theta) + v_Z\frac{\partial}{\partial Z}(v_\theta\mathbf{e}_\theta) \\
&\quad + v_r\frac{\partial}{\partial r}(v_Z\mathbf{k}) + \frac{v_\theta}{r}\frac{\partial}{\partial\theta}(v_Z\mathbf{k}) + v_Z\frac{\partial}{\partial Z}(v_Z\mathbf{k})
\end{aligned} \tag{9.137}$$

in which:

$$\frac{\partial \mathbf{e}_r}{\partial r} = \frac{\partial \mathbf{e}_r}{\partial\theta} = \frac{\partial \mathbf{e}_r}{\partial Z} = \frac{\partial \mathbf{e}_\theta}{\partial Z} = \frac{\partial \mathbf{k}}{\partial r} = \frac{\partial \mathbf{k}}{\partial\theta} = \frac{\partial \mathbf{k}}{\partial Z} = \mathbf{0} \tag{9.138}$$

and:

$$\frac{\partial r}{\partial \theta} = 0 \tag{9.139}$$

is a property of the coordinate system. By construction:

$$\frac{\partial \mathbf{e}_r}{\partial \theta} = \mathbf{e}_\theta, \ \frac{\partial \mathbf{e}_\theta}{\partial \theta} = -\mathbf{e}_r \tag{9.140}$$

so it follows that:

$$\begin{aligned}\frac{D\mathbf{v}}{Dt} &= \frac{\partial \mathbf{v}}{\partial t} + \left(v_r \frac{\partial v_r}{\partial r} + \frac{v_\theta}{r}\frac{\partial v_r}{\partial \theta} + v_Z \frac{\partial v_r}{\partial Z} \right) \mathbf{e}_r + \frac{v_\theta v_r}{r}\frac{\partial \mathbf{e}_r}{\partial \theta} \\ &\quad + \left(v_r \frac{\partial v_\theta}{\partial r} + \frac{v_\theta}{r}\frac{\partial v_\theta}{\partial \theta} + v_Z \frac{\partial v_\theta}{\partial Z} \right) \mathbf{e}_\theta - \frac{v_\theta^2}{r}\frac{\partial \mathbf{e}_\theta}{\partial r} \\ &\quad + \left(v_r \frac{\partial v_Z}{\partial r} + \frac{v_\theta}{r}\frac{\partial v_Z}{\partial \theta} + v_Z \frac{\partial v_Z}{\partial Z} \right) \mathbf{k} \\ &= \frac{\partial}{\partial t}\begin{bmatrix} v_r \\ v_\theta \\ v_Z \end{bmatrix} + \left(\begin{bmatrix} \frac{\partial v_r}{\partial r} & \frac{1}{r}\frac{\partial v_r}{\partial \theta} & \frac{\partial v_r}{\partial Z} \\ \frac{\partial v_\theta}{\partial r} & \frac{1}{r}\frac{\partial v_\theta}{\partial \theta} & \frac{\partial v_\theta}{\partial Z} \\ \frac{\partial v_Z}{\partial r} & \frac{\partial v_Z}{\partial \theta} & \frac{\partial v_Z}{\partial Z} \end{bmatrix} + \begin{bmatrix} 0 & -\frac{v_\theta}{r} & 0 \\ \frac{v_\theta}{r} & 0 & 0 \\ 0 & 0 & 0 \end{bmatrix} \right) \begin{bmatrix} v_r \\ v_\theta \\ v_Z \end{bmatrix}.\end{aligned} \tag{9.141}$$

The second matrix has the antisymmetric structure of a rotation generator. The derivative (9.141) is a special case of the Cartan derivative:

$$\frac{Dv^a}{Dt} = \frac{\partial v^a}{\partial t} + \omega^a{}_{0b} v^b \tag{9.142}$$

in which the spin connection in plane polar coordinates is:

$$\omega^a{}_{0b} = \begin{bmatrix} \frac{\partial v_r}{\partial r} & \frac{1}{r}\frac{\partial v_r}{\partial \theta} \\ \frac{\partial v_\theta}{\partial r} & \frac{1}{r}\frac{\partial v_\theta}{\partial \theta} \end{bmatrix} + \begin{bmatrix} 0 & -\frac{v_\theta}{r} \\ \frac{v_\theta}{r} & 0 \end{bmatrix}. \tag{9.143}$$

Therefore:

$$\frac{D}{Dt}\begin{bmatrix} v_r \\ v_\theta \end{bmatrix} = \frac{\partial}{\partial t}\begin{bmatrix} v_r \\ v_\theta \end{bmatrix} + \left(\begin{bmatrix} \frac{\partial v_r}{\partial r} & \frac{1}{r}\frac{\partial v_r}{\partial \theta} \\ \frac{\partial v_\theta}{\partial r} & \frac{1}{r}\frac{\partial v_\theta}{\partial \theta} \end{bmatrix} + \begin{bmatrix} 0 & -\frac{v_\theta}{r} \\ \frac{v_\theta}{r} & 0 \end{bmatrix} \right) \begin{bmatrix} v_r \\ v_\theta \end{bmatrix}. \tag{9.144}$$

The velocity vector in plane polar coordinates is:

$$\mathbf{v} = \dot{r}\mathbf{e}_r + r\dot{\theta}\mathbf{e}_\theta \tag{9.145}$$

so:

$$v_r = \dot{r}, \ v_\theta = r\dot{\theta} \tag{9.146}$$

and:

$$\begin{bmatrix} 0 & -\frac{v_\theta}{r} \\ \frac{v_\theta}{r} & 0 \end{bmatrix} = \begin{bmatrix} 0 & -\dot{\theta} \\ \dot{\theta} & 0 \end{bmatrix} \tag{9.147}$$

where the angular velocity of the rotating frame is:

$$\omega = \dot{\theta} = \frac{d\theta}{dt}. \tag{9.148}$$

Therefore the spin connection components are:

$$\omega^1{}_{01} = \frac{\partial \dot{r}}{\partial r} \tag{9.149}$$

$$\omega^1{}_{02} = \frac{1}{r}\frac{\partial \dot{r}}{\partial \theta} - \dot{\theta} \tag{9.150}$$

$$\omega^2{}_{01} = \frac{\partial\left(r\dot{\theta}\right)}{\partial r} + \dot{\theta} \tag{9.151}$$

$$\omega^2{}_{02} = \frac{1}{r}\frac{\partial\left(r\dot{\theta}\right)}{\partial \theta} \tag{9.152}$$

and in terms of unit vectors:

$$\begin{aligned}\frac{D\mathbf{v}}{Dt} = \frac{\partial v_r}{\partial t}\mathbf{e}_r + \frac{\partial v_\theta}{\partial t}\mathbf{e}_\theta + \left(v_r\frac{\partial v_r}{\partial r} + \frac{v_\theta}{r}\frac{\partial v_r}{\partial \theta} - \frac{v_\theta^2}{r}\right)\mathbf{e}_r \\ + \left(v_r\frac{\partial v_\theta}{\partial r} + \frac{v_\theta}{r}\frac{\partial v_\theta}{\partial \theta} + \frac{v_\theta v_r}{r}\right)\mathbf{e}_\theta.\end{aligned} \tag{9.153}$$

Eq. (9.153) is the following covariant derivative of Cartan geometry:

$$\mathbf{a} = \frac{D\mathbf{v}}{Dt} = \frac{Dv_r}{Dt}\mathbf{e}_r + \frac{Dv_\theta}{Dt}\mathbf{e}_\theta. \tag{9.154}$$

So for any acceleration:

$$\mathbf{a} = \frac{\partial \mathbf{v}}{\partial t} + (\mathbf{v}\cdot\boldsymbol{\nabla})\,\mathbf{v} = \frac{Dv_r}{Dt}\mathbf{e}_r + \frac{Dv_\theta}{Dt}\mathbf{e}_\theta. \tag{9.155}$$

The individual covariant derivatives are:

$$\frac{Dv_r}{Dt} = \frac{\partial v_r}{\partial r} + \dot{r}\frac{\partial \dot{r}}{\partial r} + \dot{\theta}\frac{\partial \dot{r}}{\partial \theta} - r\dot{\theta}^2 \tag{9.156}$$

and

$$\frac{Dv_\theta}{Dt} = \frac{\partial v_\theta}{\partial t} + r\ddot{\theta} + 2\dot{r}\dot{\theta} + r\dot{r}\frac{\partial \dot{\theta}}{\partial r} + \dot{\theta}^2\frac{\partial r}{\partial \theta}. \tag{9.157}$$

Therefore:

$$v_r\frac{\partial v_r}{\partial r} + \frac{v_\theta}{r}\frac{\partial v_r}{\partial \theta} - \frac{v_\theta^2}{r} = \left(\begin{bmatrix}\frac{\partial v_r}{\partial r} & \frac{1}{r}\frac{\partial v_r}{\partial \theta} \\ 0 & 0\end{bmatrix} + \begin{bmatrix}0 & -\dot{\theta} \\ 0 & 0\end{bmatrix}\right)\begin{bmatrix}v_r \\ v_\theta\end{bmatrix} \tag{9.158}$$

and:

$$\begin{aligned}v_r\frac{\partial v_\theta}{\partial r} + \frac{v_\theta}{r}\frac{\partial v_\theta}{\partial \theta} + \frac{v_\theta v_r}{r} &= r\ddot{\theta} + 2\dot{r}\dot{\theta} + r\dot{r}\frac{\partial \dot{\theta}}{\partial r} + \dot{\theta}^2\frac{\partial r}{\partial \theta} \\ &= \begin{bmatrix}0 & 0 \\ \frac{\partial v_\theta}{\partial r} & \frac{1}{r}\frac{\partial v_\theta}{\partial \theta}\end{bmatrix}\begin{bmatrix}v_r \\ v_\theta\end{bmatrix} + \begin{bmatrix}0 & 0 \\ \dot{\theta} & 0\end{bmatrix}\begin{bmatrix}v_r \\ v_\theta\end{bmatrix}.\end{aligned} \tag{9.159}$$

There are new accelerations:

$$\mathbf{a}_1 = \left(\dot{r} \frac{\partial \dot{r}}{\partial r} + \dot{\theta} \frac{\partial \dot{r}}{\partial \theta} \right) \mathbf{e}_r + \left(r\dot{r} \frac{\partial \dot{\theta}}{\partial r} + \dot{\theta}^2 \frac{\partial r}{\partial \theta} \right) \mathbf{e}_\theta \tag{9.160}$$

which are absent from classical dynamics, in which:

$$\begin{aligned} \mathbf{a} = \frac{d\mathbf{v}}{dt} &= \frac{d}{dt}\left(v_r \mathbf{e}_r\right) + \frac{d}{dt}\left(r\dot{\theta}\mathbf{e}_\theta\right) \\ &= \left(\ddot{r} - r\dot{\theta}^2\right)\mathbf{e}_r + \left(r\ddot{\theta} + 2\dot{r}\dot{\theta}\right)\mathbf{e}_\theta. \end{aligned} \tag{9.161}$$

On the right hand side of Eq. (9.161) appear the Newtonian acceleration:

$$\mathbf{a}_N = \ddot{r}\mathbf{e}_r \tag{9.162}$$

the centrifugal acceleration:

$$\mathbf{a}_{\text{cent}} = -r\dot{\theta}^2 \mathbf{e}_r \tag{9.163}$$

and the Coriolis accelerations:

$$\mathbf{a}_{\text{Coriolis}} = \left(r\ddot{\theta} + 2\dot{r}\dot{\theta}\right)\mathbf{e}_\theta. \tag{9.164}$$

The use of the convective derivative leads to the accelerations (9.160) which occur in addition to the fundamental accelerations of classical dynamics. They are the result of replacing $\mathbf{v}(t)$ of classical dynamics by the velocity field:

$$\mathbf{v} = \mathbf{v}\left(r(t), \theta(t), t\right). \tag{9.165}$$

These new accelerations are interpreted later on in this chapter and developed numerically.

These concepts can be used as in UFT 362 to investigate the effect of the vacuum on orbital theory. In classical dynamics there is no such effect. Consider the convective derivative of any vector field:

$$\frac{D\mathbf{F}}{Dt} = \frac{\partial \mathbf{F}}{\partial t} + \left(\mathbf{v} \cdot \boldsymbol{\nabla}\right)\mathbf{F} \tag{9.166}$$

in plane polar coordinates. In Eq. (9.166) the velocity field is:

$$\mathbf{v} = \mathbf{v}\left(r(t), \theta(t), t\right). \tag{9.167}$$

In plane polar coordinates Eq. (9.166) becomes:

$$\begin{aligned} \frac{D\mathbf{F}}{Dt} &= \frac{\partial \mathbf{F}}{\partial t} + \left(v_r \frac{\partial}{\partial r} + \frac{v_\theta}{r}\frac{\partial}{\partial \theta}\right)\left(F_r \mathbf{e}_r + F_\theta \mathbf{e}_\theta\right) \\ &= \frac{\partial \mathbf{F}}{\partial t} + v_r\left(\frac{\partial F_r}{\partial r}\mathbf{e}_r + F_r \frac{\partial \mathbf{e}_r}{\partial r} + \frac{\partial F_\theta}{\partial r}\mathbf{e}_\theta + F_\theta \frac{\partial \mathbf{e}_\theta}{\partial r}\right) \\ &\quad + \frac{v_\theta}{r}\left(\frac{\partial F_r}{\partial \theta}\mathbf{e}_r + F_r \frac{\partial \mathbf{e}_r}{\partial \theta} + \frac{\partial F_\theta}{\partial \theta}\mathbf{e}_\theta + F_\theta \frac{\partial \mathbf{e}_\theta}{\partial \theta}\right) \end{aligned} \tag{9.168}$$

where the Leibniz Theorem has been used. For plane polar coordinates [2]-[13]:

$$\frac{\partial \mathbf{e}_r}{\partial r} = \frac{\partial \mathbf{e}_\theta}{\partial r} = 0, \ \frac{\partial \mathbf{e}_r}{\partial \theta} = \mathbf{e}_\theta, \ \frac{\partial \mathbf{e}_\theta}{\partial \theta} = -\mathbf{e}_r \tag{9.169}$$

so the convective derivative (9.168) is

$$\begin{aligned} \frac{D\mathbf{F}}{Dt} = \frac{\partial \mathbf{F}}{\partial t} &+ \left(v_r \frac{\partial F_r}{\partial r} + \frac{v_\theta}{r} \frac{\partial F_r}{\partial \theta} - \frac{v_\theta}{r} F_\theta \right) \mathbf{e}_r \\ &+ \left(v_r \frac{\partial F_\theta}{\partial r} + \frac{v_\theta}{r} \frac{\partial F_\theta}{\partial \theta} + \frac{v_\theta}{r} F_r \right) \mathbf{e}_\theta \end{aligned} \tag{9.170}$$

where:

$$\frac{v_\theta}{r} = \dot{\theta} = \frac{d\theta}{dt} = \omega. \tag{9.171}$$

In component format:

$$\frac{D}{Dt} \begin{bmatrix} F_r \\ F_\theta \end{bmatrix} = \frac{\partial}{\partial t} \begin{bmatrix} F_r \\ F_\theta \end{bmatrix} + \begin{bmatrix} \frac{\partial F_r}{\partial r} & \frac{1}{r} \frac{\partial F_r}{\partial \theta} \\ \frac{\partial F_\theta}{\partial r} & \frac{1}{r} \frac{\partial F_\theta}{\partial \theta} \end{bmatrix} \begin{bmatrix} v_r \\ v_\theta \end{bmatrix} + \begin{bmatrix} 0 & -\dot{\theta} \\ \dot{\theta} & 0 \end{bmatrix} \begin{bmatrix} F_r \\ F_\theta \end{bmatrix} \tag{9.172}$$

so:

$$\mathbf{F} = F_r \left(r(t), \theta(t), t \right) \mathbf{e}_r + F_\theta \left(r(t), \theta(t), t \right) \mathbf{e}_\theta. \tag{9.173}$$

In classical dynamics:

$$\mathbf{F} = \mathbf{F}(t) \tag{9.174}$$

and there is no functional dependence of $\mathbf{F}$ on $r(t)$ and $\theta(t)$. In classical dynamics therefore:

$$\frac{D}{Dt} \begin{bmatrix} F_r \\ F_\theta \end{bmatrix} = \frac{\partial}{\partial t} \begin{bmatrix} F_r \\ F_\theta \end{bmatrix} + \begin{bmatrix} 0 & -\dot{\theta} \\ \dot{\theta} & 0 \end{bmatrix} \begin{bmatrix} F_r \\ F_\theta \end{bmatrix} \tag{9.175}$$

and this result is assumed implicitly in classical orbital theory and cosmology.

The assumption (9.174) simplifies Eq. (9.170) to:

$$\frac{D\mathbf{F}}{Dt} = \frac{\partial \mathbf{F}}{\partial t} - \dot{\theta} F_\theta \mathbf{e}_r + \dot{\theta} F_r \mathbf{e}_\theta \tag{9.176}$$

which is the ECE 2 Cartan derivative with spin connection:

$$\omega^a{}_{0b} = \begin{bmatrix} 0 & -\dot{\theta} \\ \dot{\theta} & 0 \end{bmatrix} \tag{9.177}$$

which is the rotation generator of the axes of the plane polar system. In classical dynamics, if $\mathbf{F}(t)$ represents the position vector $\mathbf{r}(t)$, then the orbital velocity is given by the Cartan derivative:

$$\frac{D}{Dt} \begin{bmatrix} r \\ 0 \end{bmatrix} = \frac{\partial}{\partial t} \begin{bmatrix} r \\ 0 \end{bmatrix} + \begin{bmatrix} 0 & -\dot{\theta} \\ \dot{\theta} & 0 \end{bmatrix} \begin{bmatrix} r \\ 0 \end{bmatrix}. \tag{9.178}$$

In vector notation the orbital velocity is:

$$\mathbf{v} = v_r \mathbf{e}_r + v_\theta \mathbf{e}_\theta = \dot{r}\mathbf{e}_r + r\dot{\theta}\mathbf{e}_\theta. \tag{9.179}$$

If $\mathbf{F}(t)$ represents the time dependent velocity vector $\mathbf{v}(t)$ of classical dynamics then the orbital acceleration is given by:

$$\frac{D}{Dt}\begin{bmatrix} \dot{r} \\ r\dot{\theta} \end{bmatrix} = \frac{\partial}{\partial t}\begin{bmatrix} \dot{r} \\ r\dot{\theta} \end{bmatrix} + \begin{bmatrix} 0 & -\dot{\theta} \\ \dot{\theta} & 0 \end{bmatrix}\begin{bmatrix} \dot{r} \\ r\dot{\theta} \end{bmatrix}. \tag{9.180}$$

In vector notation:

$$\mathbf{a} = a_r \mathbf{e}_r + a_\theta \mathbf{e}_\theta = \left(\ddot{r} - r\dot{\theta}^2\right)\mathbf{e}_r + \left(r\ddot{\theta} + 2\dot{r}\dot{\theta}\right)\mathbf{e}_\theta. \tag{9.181}$$

In the UFT papers on `www.aias.us` it has been shown that the Coriolis accelerations vanish for any planar orbit:

$$r\ddot{\theta} + 2\dot{r}\dot{\theta} = 0 \tag{9.182}$$

so the Leibniz equation:

$$\mathbf{F} = m\mathbf{a} = m\left(\ddot{r} - \omega^2 r\right)\mathbf{e}_r = -\frac{mMG}{r^2}\mathbf{e}_r \tag{9.183}$$

is inferred for any planar orbit.

In classical dynamics the vacuum is a "nothingness", but in fluid gravitation it is richly structured as argued earlier in this chapter. It follows that the velocity (9.178) is generalized to:

$$\frac{D}{Dt}\begin{bmatrix} r \\ 0 \end{bmatrix} = \frac{\partial}{\partial t}\begin{bmatrix} r \\ 0 \end{bmatrix} + \begin{bmatrix} 0 & -\dot{\theta} \\ \dot{\theta} & 0 \end{bmatrix}\begin{bmatrix} r \\ 0 \end{bmatrix} + \begin{bmatrix} \Omega^1{}_{01r} & \Omega^1{}_{02r} \\ \Omega^2{}_{01r} & \Omega^2{}_{02r} \end{bmatrix}\begin{bmatrix} \dot{r} \\ r\dot{\theta} \end{bmatrix} \tag{9.184}$$

and that the acceleration (9.180) is generalized to:

$$\frac{D}{Dt}\begin{bmatrix} \dot{r} \\ r\dot{\theta} \end{bmatrix} = \frac{\partial}{\partial t}\begin{bmatrix} \dot{r} \\ r\dot{\theta} \end{bmatrix} + \begin{bmatrix} 0 & -\dot{\theta} \\ \dot{\theta} & 0 \end{bmatrix}\begin{bmatrix} \dot{r} \\ r\dot{\theta} \end{bmatrix} + \begin{bmatrix} \Omega^1{}_{01v} & \Omega^1{}_{02v} \\ \Omega^2{}_{01v} & \Omega^2{}_{02v} \end{bmatrix}\begin{bmatrix} \dot{r} \\ r\dot{\theta} \end{bmatrix} \tag{9.185}$$

in an orbit influenced by the vacuum. Different types of spin connection components appear in Eqs. (9.184) and (9.185). In Eq. (9.184):

$$\begin{bmatrix} \Omega^1{}_{01r} & \Omega^1{}_{02r} \\ \Omega^2{}_{01r} & \Omega^2{}_{02r} \end{bmatrix} = \begin{bmatrix} \frac{\partial R_r}{\partial r} & \frac{1}{r}\frac{\partial R_r}{\partial \theta} \\ \frac{\partial R_\theta}{\partial r} & \frac{1}{r}\frac{\partial R_\theta}{\partial \theta} \end{bmatrix} \tag{9.186}$$

and in Eq. (9.185):

$$\begin{bmatrix} \Omega^1{}_{01v} & \Omega^1{}_{02v} \\ \Omega^2{}_{01v} & \Omega^2{}_{02v} \end{bmatrix} = \begin{bmatrix} \frac{\partial v_r}{\partial r} & \frac{1}{r}\frac{\partial v_r}{\partial \theta} \\ \frac{\partial v_\theta}{\partial r} & \frac{1}{r}\frac{\partial v_\theta}{\partial \theta} \end{bmatrix} \tag{9.187}$$

For example the orbital velocity components of classical dynamics are generalized to:

$$v_r = \left(1 + \Omega^1{}_{01r}\right)\dot{r} + \Omega^1{}_{02r}\omega r \tag{9.188}$$

and:

$$v_\theta = \left(1 + \Omega^2{}_{01r}\right) \omega r + \Omega^2{}_{01r} \dot{r} \tag{9.189}$$

so that the velocity vector becomes:

$$\mathbf{v} = v_r \mathbf{e}_r + v_\theta \mathbf{e}_\theta \tag{9.190}$$

and its square becomes:

$$v^2 = v_r^2 + v_\theta^2. \tag{9.191}$$

Orbital precession can be explained straightforwardly as an effect of the fluid vacuum.

Consider the position vector $\mathbf{R}$ of an element of a fluid:

$$\mathbf{R} = \mathbf{R}\left(\mathbf{r}, t\right) \tag{9.192}$$

it follows that the velocity field of the fluid is:

$$\mathbf{v}\left(\mathbf{r}, t\right) = \frac{D\mathbf{R}}{Dt} = \frac{\partial \mathbf{R}}{\partial t} + \left(\mathbf{v} \cdot \boldsymbol{\nabla}\right) \mathbf{R} \tag{9.193}$$

and in component format:

$$\frac{D}{Dt} \begin{bmatrix} R_r \\ R_\theta \end{bmatrix} = \frac{\partial}{\partial t} \begin{bmatrix} R_r \\ R_\theta \end{bmatrix} + \begin{bmatrix} 0 & -\dot{\theta} \\ \dot{\theta} & 0 \end{bmatrix} \begin{bmatrix} R_r \\ R_\theta \end{bmatrix} + \begin{bmatrix} \frac{\partial R_r}{\partial r} & \frac{1}{r}\frac{\partial R_r}{\partial \theta} \\ \frac{\partial R_\theta}{\partial r} & \frac{1}{r}\frac{\partial R_\theta}{\partial \theta} \end{bmatrix} \begin{bmatrix} v_r \\ v_\theta \end{bmatrix}. \tag{9.194}$$

In plane polar coordinates:

$$\mathbf{R} = R\mathbf{e}_r \tag{9.195}$$

so:

$$R_r = R, \; R_\theta = 0. \tag{9.196}$$

The relevant spin connection matrix is therefore:

$$\begin{bmatrix} \Omega^1{}_{01r} & \Omega^1{}_{02r} \\ \Omega^2{}_{01r} & \Omega^2{}_{02r} \end{bmatrix} = \begin{bmatrix} \frac{\partial R_r}{\partial r} & \frac{1}{r}\frac{\partial R_r}{\partial \theta} \\ 0 & 0 \end{bmatrix} \tag{9.197}$$

with components:

$$\begin{aligned} &\Omega^1{}_{01r} = \frac{\partial R_r}{\partial r}, \quad \Omega^1{}_{02r} = \frac{1}{r}\frac{\partial R_r}{\partial \theta}, \\ &\Omega^2{}_{01r} = 0, \qquad \Omega^2{}_{02r} = 0. \end{aligned} \tag{9.198}$$

The velocity field components are therefore:

$$v_r = \left(1 + \Omega^1{}_{01r}\right) \dot{r} + \Omega^1{}_{02r} \omega r \tag{9.199}$$

and:

$$v_\theta = \dot{\theta} r = \omega r. \tag{9.200}$$

The hamiltonian and lagrangian are therefore:

$$H = \frac{1}{2}m\left(v_r^2 + v_\theta^2\right) + U \tag{9.201}$$

and:

$$\mathscr{L} = \frac{1}{2}m\left(v_r^2 + v_\theta^2\right) - U \tag{9.202}$$

where U is the potential energy. It is known in the solar system that precession is a very tiny effect, so:

$$\Omega^1{}_{01r} \sim \Omega^1{}_{02r} \ll 1. \tag{9.203}$$

In contrast to the above analysis, classical dynamics is defined by:

$$\mathbf{v}(t) = \frac{D\mathbf{r}(t)}{Dt} = \frac{\partial \mathbf{r}(t)}{\partial t} + (\mathbf{v}\cdot\boldsymbol{\nabla})\,\mathbf{r}(t) \tag{9.204}$$

i. e. by the convective derivative of the position $\mathbf{r}(t)$ of a particle rather than the position $\mathbf{R}(\mathbf{r}, t)$ of a fluid element. So in classical dynamics:

$$\begin{bmatrix} v_r \\ v_\theta \end{bmatrix} = \frac{\partial}{\partial t}\begin{bmatrix} r(t) \\ 0 \end{bmatrix} + \begin{bmatrix} 0 & -\dot{\theta} \\ \dot{\theta} & 0 \end{bmatrix}\begin{bmatrix} r(t) \\ 0 \end{bmatrix}. \tag{9.205}$$

In component format Eq. (9.205) is:

$$v_r = \frac{\partial r(t)}{\partial t} \tag{9.206}$$

$$v_\theta = \dot{\theta}\, r(t) \tag{9.207}$$

which gives the pendant to the Coriolis velocity:

$$\mathbf{v} = \dot{r}\mathbf{e}_r + r\dot{\theta}\mathbf{e}_\theta \tag{9.208}$$

Q. E. D.

The Euler Lagrange equations of the system are:

$$\frac{\partial \mathscr{L}}{\partial r} = \frac{d}{dt}\frac{\partial \mathscr{L}}{\partial \dot{r}} \tag{9.209}$$

and:

$$\frac{\partial \mathscr{L}}{\partial \theta} = \frac{d}{dt}\frac{\partial \mathscr{L}}{\partial \dot{\theta}}. \tag{9.210}$$

From Eq. (9.209) a new force law can be found using the lagrangian:

$$\begin{aligned}\mathscr{L} = \frac{1}{2}m\Big(&\left(1 + \Omega^1{}_{01r}\right)^2\dot{r}^2 + \Omega^1{}_{02r}{}^2 r^2\dot{\theta}^2 \\ &+2\Omega^1{}_{02r}\left(1 + \Omega^1{}_{01r}\right)\dot{r}\dot{\theta}r + \dot{\theta}^2 r^2\Big) - U\end{aligned} \tag{9.211}$$

and is:

$$F = m\left(\left(1+{\Omega^1}_{01r}\right)^2\ddot{r} + {\Omega^1}_{02r}\left(1+{\Omega^1}_{01r}\right)\left(r\ddot{\theta}+\dot{\theta}\dot{r}\right) - \left(1+{\Omega^1}_{02r}{}^2\right)r\dot{\theta}^2 - {\Omega^1}_{02r}\left(1+{\Omega^1}_{01r}\right)\dot{r}\dot{\theta}\right). \tag{9.212}$$

In comparison, the force law of a conic section orbit is:

$$F = m\left(\ddot{r} - r\dot{\theta}^2\right) \tag{9.213}$$

so the orbit is changed by ${\Omega^1}_{01r}$ and ${\Omega^1}_{02r}$.

Assume for the sake of analytical tractability that:

$${\Omega^1}_{02r} = \frac{1}{r}\frac{\partial R_r}{\partial\theta} \sim 0 \tag{9.214}$$

and the lagrangian simplifies to:

$$\mathscr{L} = \frac{1}{2}m\left(\left(1+{\Omega^1}_{01r}\right)^2\dot{r}^2 + \dot{\theta}^2r^2\right) - U. \tag{9.215}$$

The constant angular momentum can be found from the Euler Lagrange equation (9.210):

$$L = \frac{\partial\mathscr{L}}{\partial\theta} = mr^2\dot{\theta} \tag{9.216}$$

and is a constant of motion:

$$\frac{dL}{dt} = 0. \tag{9.217}$$

In the approximation (9.214) the force law (9.212) becomes:

$$F = m\left(\left(1+{\Omega^1}_{01r}\right)^2\ddot{r} - r\dot{\theta}^2\right). \tag{9.218}$$

Using the Binet variable:

$$u = \frac{1}{r} \tag{9.219}$$

it follows that:

$$\left(1+{\Omega^1}_{01r}\right)^2\frac{d^2}{d\theta^2}\left(\frac{1}{r}\right) + \frac{1}{r} = -\frac{mr^2}{L^2}F(r) \tag{9.220}$$

and can be interpreted as the Binet equation of an orbit in a fluid aether or vacuum. It reduces to the Binet equation of classical dynamics when:

$${\Omega^1}_{01r} \to 0. \tag{9.221}$$

If the orbit is a conic section:

$$r = \frac{\alpha}{1+\epsilon\cos\theta} \tag{9.222}$$

it follows from Eq. (9.220) that its force law is:

$$F(r) = -\frac{L^2}{mr^2}\left(\frac{1-y}{\alpha} + \frac{y}{r}\right) \tag{9.223}$$

where:

$$y = 1 - \left(1 + \Omega^1{}_{01r}\right)^2. \tag{9.224}$$

It is known from UFT 193 that the force law of a precessing ellipse modelled by

$$r = \frac{\alpha}{1 + \epsilon\cos(x\theta)} \tag{9.225}$$

is:

$$F(r) = -\frac{L^2}{mr^2}\left(\frac{x^2}{\alpha} + \frac{1}{r}\left(1 - x^2\right)\right) \tag{9.226}$$

from the Binet equation of classical dynamics

$$\frac{d^2}{d\theta^2}\left(\frac{1}{r}\right) + \frac{1}{r} = -\frac{mr^2}{L^2}F(r). \tag{9.227}$$

Therefore:

$$y = 1 - x^2 \tag{9.228}$$

and

$$x = 1 + \Omega^1{}_{01r}. \tag{9.229}$$

To contemporary precision in astronomy:

$$x = 1 + \frac{3MG}{\alpha c^2} \tag{9.230}$$

so:

$$\Omega^1{}_{01r} = \frac{\partial R_r}{\partial r} = \frac{3MG}{\alpha c^2}. \tag{9.231}$$

Therefore orbital precession is due to the effect of the fluid dynamic function $\partial R_r/\partial r$, which is the rate of displacement of a position element $\mathbf{R}(\mathbf{r}, t)$ of a fluid dynamic background, or vacuum. The spin connection makes the orbit precess. The conic section orbit (9.222) used in the Binet equation of fluid dynamics (9.220) is exactly equivalent to the use of the precessing orbit (9.225) in the Binet equation of classical dynamics. In both cases the law of attraction is the sum of terms inverse squared and inverse cubed in r. The obsolete Einstein theory incorrectly claims to give a precessing orbit with a sum of inverse squared and inverse fourth power terms.

9.2 Numerical Analysis and Graphics

9.2.1 Examples for Fluid Spacetime Fields

The Newtonian acceleration, Eq. (9.61), leads to several fields of fluid spacetime as described by Eqs. (9.63-9.89). These fields have been analyzed graphically, using unity constants (except $\epsilon = 0.3$). The mapping of equations to the graphs is compiled in Table 9.1. The velocity fields $\mathbf{v}_{F1}$-$\mathbf{v}_{F3}$ are parallel to the planes spanned by the three cartesian axes. The total field $\mathbf{v}_F$ is a vortex with angular momentum axis in [1,-1,1] direction. This axis can be altered by using different signs for the velocity components. This shows that different solutions for the velocity field are possible. The gravitational field $\mathbf{g}_F$ is a central field as expected. The vorticity $\mathbf{w}_F$ looks complicated. An analysis by computer algebra shows that $\mathbf{w}_F$ is always perpendicular to $\mathbf{v}_F$. The current $\mathbf{J}_F$ is parallel to the velocitiy field as expected. The three components of the Kambe charge density q_F look different but their sum vanishes, indicating a new kind of symmetry not yet investigated.

The concept of fluid gravitation has been applied to planar orbits, starting with Eq. (9.91). The lines for Figs. 9.11 and 9.12 of Table 9.1 describe the cartesian elliptical orbit components $X(\theta)$ and $Y(\theta)$ for an orbit $r(\theta)$, according to definitions of Eqs. (9.99-9.104). Their graph shows an oscillating behaviour. When, in addition, the radius is taken as a parameter, There are surfaces $X(r,\theta)$ and $Y(r,\theta)$ whose intersections represent the behaviour of orbits with a fixed $r(\theta)$ relation.

Finally the line for Fig. 9.13 in Table 9.1 relates to a hyperbolic spiral. Their components $X(r)$, $Y(r)$ have been plotted on a logarithmic scale.

Figure no.	graphed Quantity	Equations
9.1	$\mathbf{v}_{F1}$	(9.65)
9.2	$\mathbf{v}_{F2}$	(9.66)
9.3	$\mathbf{v}_{F3}$	(9.67)
9.4	$\mathbf{v}_F$	(9.64)
9.5	$\mathbf{g}_F$	(9.61)
9.6	$\mathbf{w}_F$	(9.74-9.76)
9.7	$\mathbf{J}_F$	(9.86)
9.8	q_{F1}	(9.70)
9.9	q_{F2}	(9.71)
9.10	q_{F3}	(9.72)
9.11	$X(\theta), Y(\theta)$	(9.104, 9.110-9.111)
9.12	$X(r,\theta), Y(r,\theta)$	(9.110-9.111)
9.13	$X(r), Y(r)$	(9.127-9.128)

Table 9.1: Mapping of figures to equations.

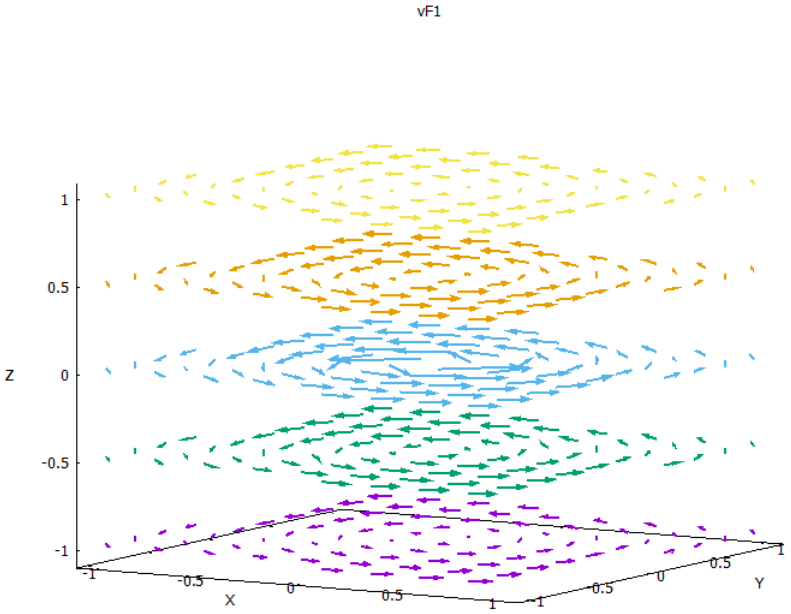

Figure 9.1: Component $\mathbf{v}_{F1}$ of velocity field.

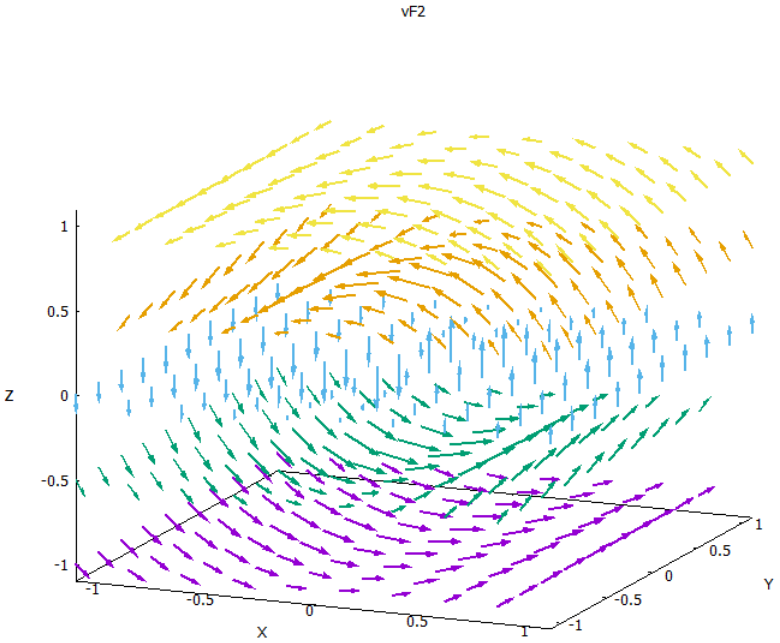

Figure 9.2: Component $\mathbf{v}_{F2}$ of velocity field.

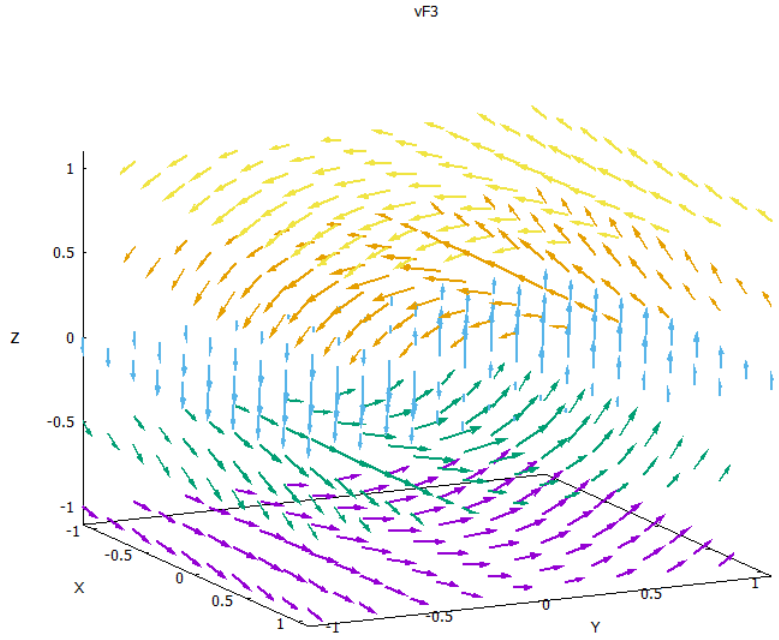

Figure 9.3: Component $\mathbf{v}_{F3}$ of velocity field.

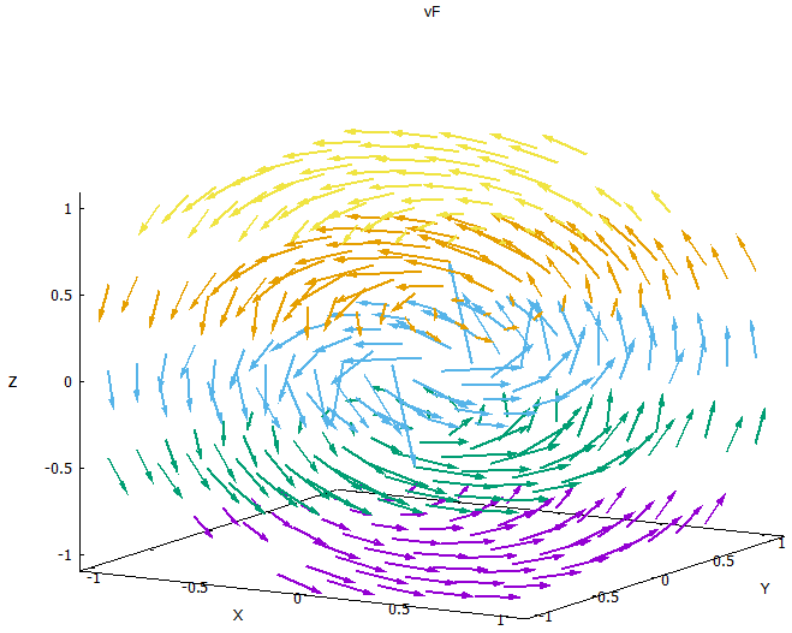

Figure 9.4: Velocity field $\mathbf{v}_F$.

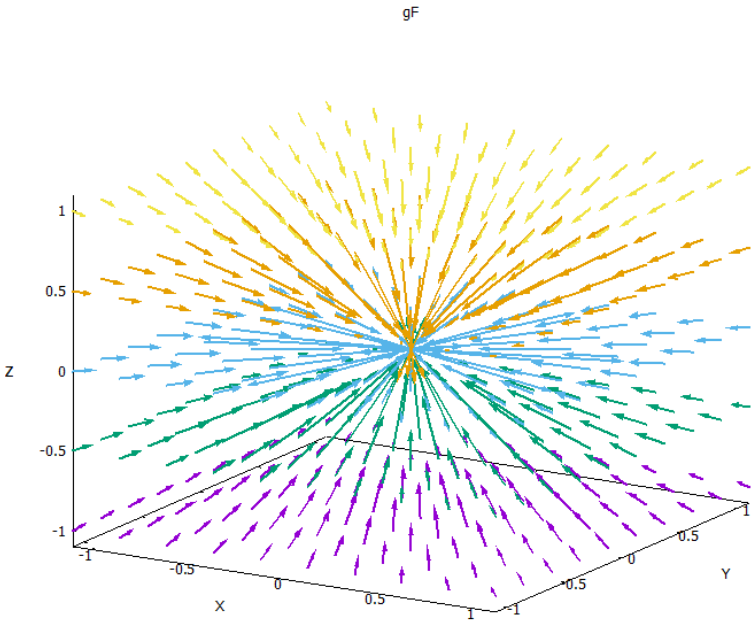

Figure 9.5: Gravitational field $\mathbf{g}_F$.

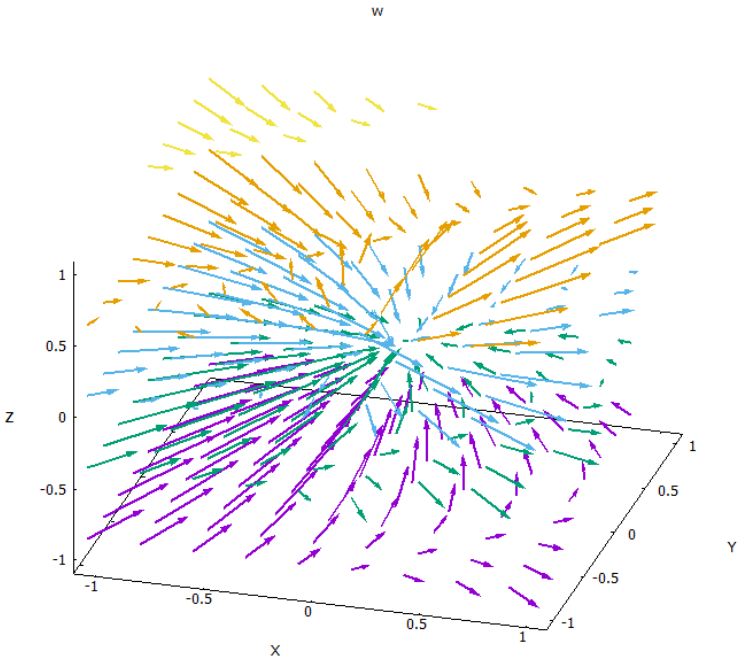

Figure 9.6: Vorticity field $\mathbf{w}_F$.

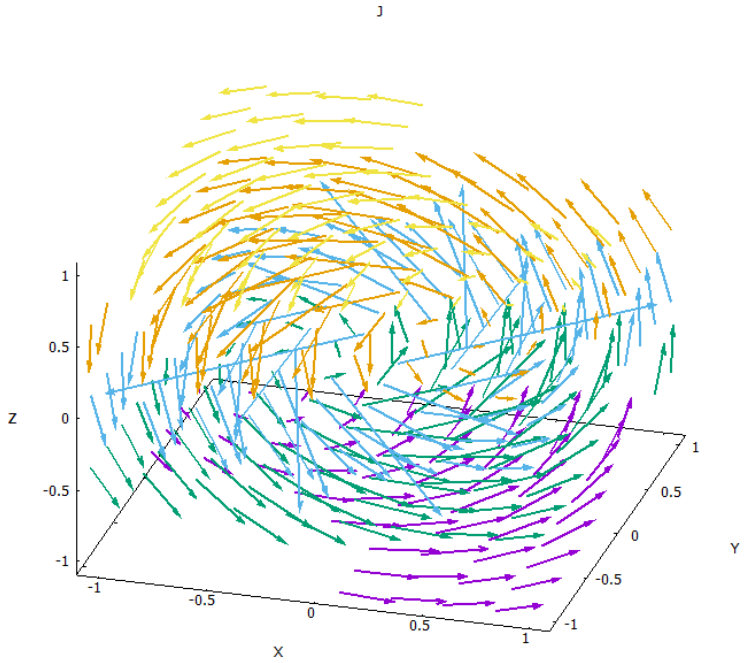

Figure 9.7: Static current density $\mathbf{J}_F$.

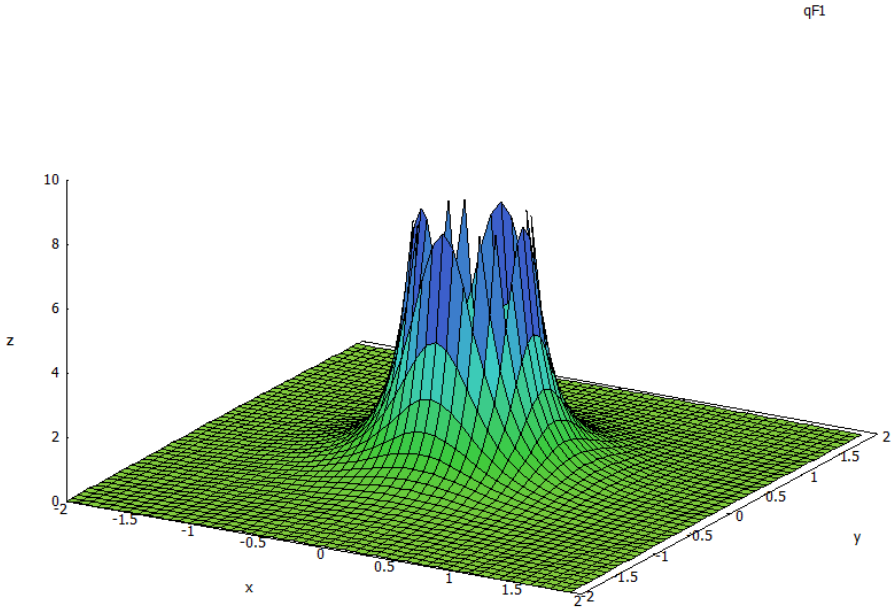

Figure 9.8: Kambe charge density q_{F1} for $Z = 0$.

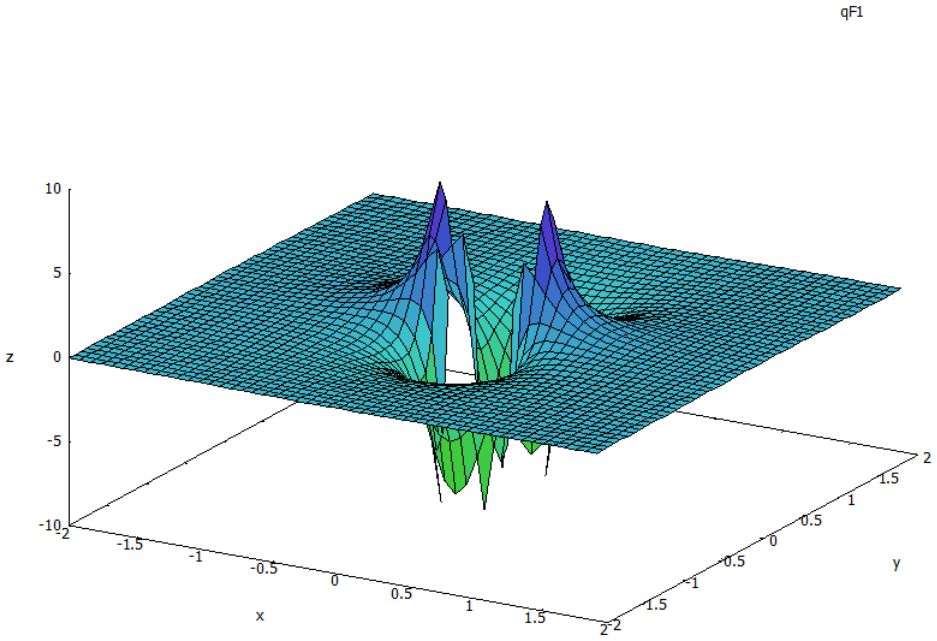

Figure 9.9: Kambe charge density q_{F2} for $Z = 0$.

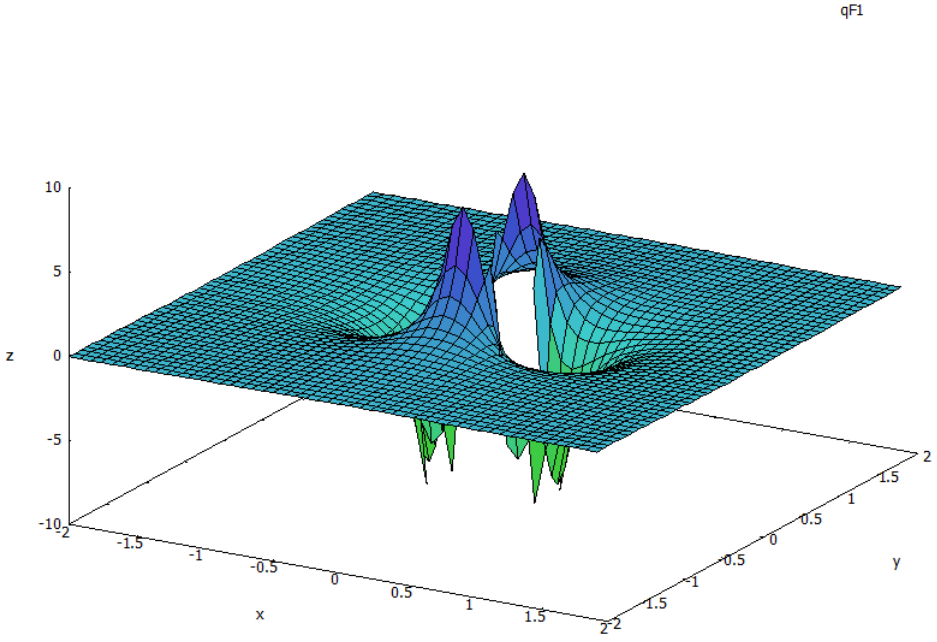

Figure 9.10: Kambe charge density q_{F3} for $Z = 0$.

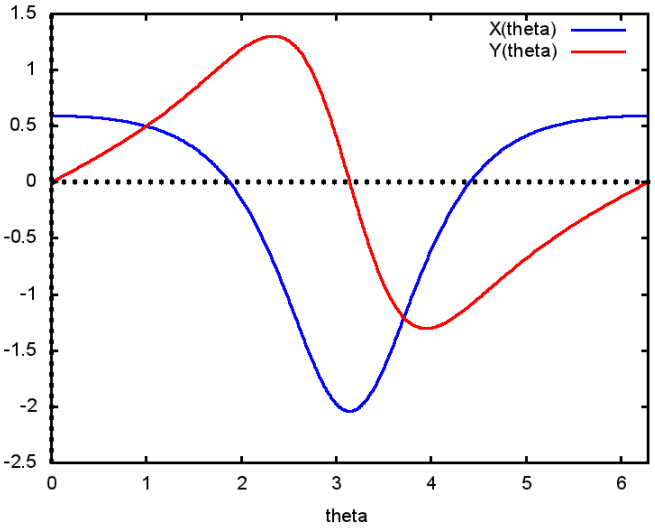

Figure 9.11: Elliptical orbit components $X(\theta)$ and $Y(\theta)$.

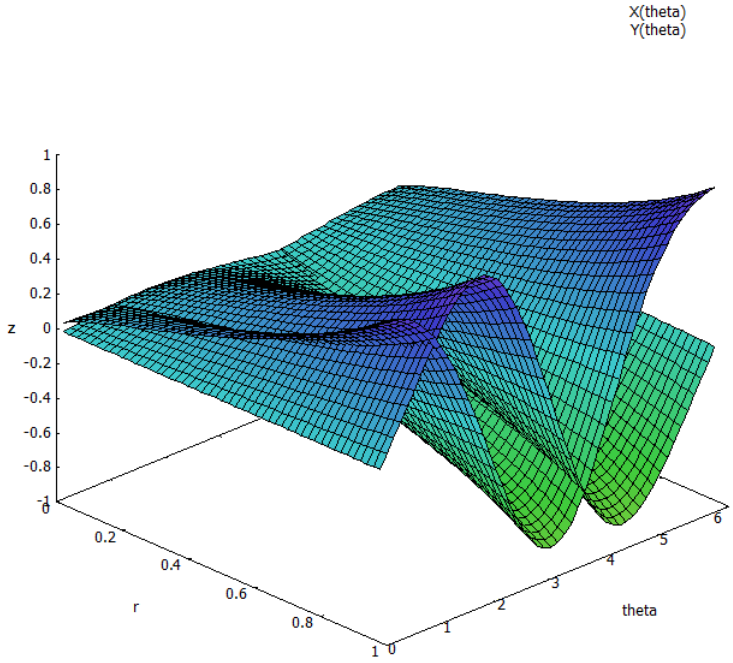

Figure 9.12: Elliptical orbit components $X(r,\theta)$ and $Y(r,\theta)$ in the (r,θ) plane.

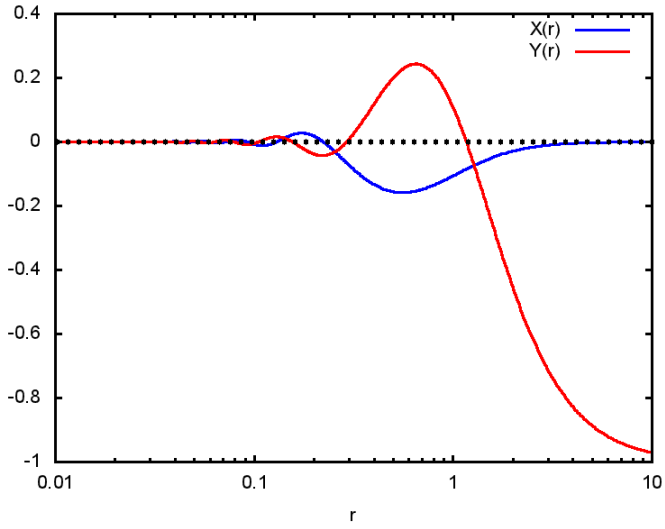

Figure 9.13: Orbit coordinates $X(r)$ and $Y(r)$ for a hyperbolic spiral.

9.2.2 Non-classical Acceleration

First we do some calculations on the accelerations in ECE 2 fluid dynamics. The Newtonian acceleration (9.161) in plane polar coordinates is

$$\mathbf{a} = (\ddot{r} - r\dot{\theta}^2)\mathbf{e}_r + (r\ddot{\theta} + 2\dot{r}\dot{\theta})\mathbf{e}_\theta, \tag{9.232}$$

and there is an extra acceleration due to fluid spacetime (9.160):

$$\mathbf{a}_1 = \left(\dot{r}\frac{\partial \dot{r}}{\partial r} + \dot{\theta}\frac{\partial \dot{r}}{\partial \theta}\right)\mathbf{e}_r + \left(r\dot{r}\frac{\partial \dot{\theta}}{\partial r} + \dot{\theta}^2\frac{\partial r}{\partial \theta}\right)\mathbf{e}_\theta. \tag{9.233}$$

Now use

$$\frac{\partial \dot{\theta}}{\partial \theta} = \frac{\partial \dot{\theta}}{\partial t}\frac{dt}{d\theta} = \frac{\ddot{\theta}}{\dot{\theta}}, \tag{9.234}$$

and similarly

$$\frac{\partial \dot{\theta}}{\partial r} = \frac{\ddot{\theta}}{\dot{r}}, \qquad \frac{\partial \dot{r}}{\partial \theta} = \frac{\ddot{r}}{\dot{\theta}}, \tag{9.235}$$

$$\frac{\partial \dot{r}}{\partial r} = \frac{\ddot{r}}{\dot{r}}, \qquad \frac{\partial r}{\partial \theta} = \frac{\dot{r}}{\dot{\theta}}\ . \tag{9.236}$$

Inserting this into (9.233) gives

$$\mathbf{a}_1 = 2\ \ddot{r}\ \mathbf{e}_r + \left(r\ddot{\theta} + \dot{r}\dot{\theta}\right)\mathbf{e}_\theta. \tag{9.237}$$

In total, the acceleration now is

$$\mathbf{a}_{\rm tot} = \mathbf{a} + \mathbf{a}_1 = (3\ddot{r} - r\dot{\theta}^2)\mathbf{e}_r + (2r\ddot{\theta} + 3\dot{r}\dot{\theta})\mathbf{e}_\theta. \tag{9.238}$$

This is a massive modification of (9.232). The latter is valid for mass point dynamics only with $\mathbf{v} = \mathbf{v}(t)$.

For evaluation of examples, the time dependence shall be eliminated. From conservation of angular momentum L_0 in Z direction follows

$$\dot{\theta} = \frac{L_0}{mr^2} \tag{9.239}$$

and

$$\ddot{\theta} = \frac{d\dot{\theta}}{dt} = \frac{dr}{dt}\frac{\partial}{\partial r}\left(\frac{L_0}{mr^2}\right) = -2\,\dot{r}\frac{L_0}{mr^3}. \tag{9.240}$$

Similarly:

$$\dot{r} = \frac{\partial r}{\partial\theta}\dot{\theta}, \tag{9.241}$$

$$\ddot{r} = \frac{d}{dt}\left(\frac{\partial r}{\partial\theta}\dot{\theta}\right) = \frac{d}{dt}\left(\frac{\partial r}{\partial\theta}\right)\dot{\theta} + \frac{\partial r}{\partial\theta}\ddot{\theta} = \frac{d\theta}{dt}\frac{\partial}{\partial\theta}\left(\frac{\partial r}{\partial\theta}\right)\dot{\theta} + \frac{\partial r}{\partial\theta}\ddot{\theta} \tag{9.242}$$

$$= \frac{\partial^2 r}{\partial\theta^2}\dot{\theta}^2 + \frac{\partial r}{\partial\theta}\ddot{\theta}.$$

By inserting (9.239, 9.240), all quantities depend on θ and r only. For cylindrical coordinates it follows correspondingly:

$$\dot{Z} = \frac{\partial Z}{\partial\theta}\dot{\theta}, \tag{9.243}$$

$$\ddot{Z} = \frac{\partial^2 Z}{\partial\theta^2}\dot{\theta}^2 + \frac{\partial Z}{\partial\theta}\ddot{\theta}, \tag{9.244}$$

$$\frac{\partial\dot{Z}}{\partial\theta} = \frac{\partial^2 Z}{\partial\theta^2}\dot{\theta}. \tag{9.245}$$

All time derivatives have been brought into a form depending on θ and $\dot{\theta}$ which is given by (9.239).

As a non-trivial example we consider a three-dimensional vortex field called Torkado [31], see Fig. 9.14. This could also be a description for the dynamics of the plasma model of galaxies. We concentrate on a streamline in the middle of the structure which may be described by the analytical approach in cylindrical coordinates (r, θ, Z):

$$r(\theta) = 0.05 + \cos\left(\frac{\theta}{10}\right)^2, \tag{9.246}$$

$$Z(\theta) = 2\sin\left(\frac{\theta}{5}\right), \tag{9.247}$$

For a plot in cartesian coordinates, the plane polar part is to be transformed by

$$X = r\cos(\theta), \tag{9.248}$$
$$Y = r\sin(\theta). \tag{9.249}$$

In order to make the analysis not too complicated, we restrict it to the plane polar parts of the acceleration as given in Eqs. (9.232, 9.233, 9.238). The orbital quantities $r(\theta)$, $Z(\theta)$, $\partial r/\partial\theta$ and $\partial Z/\partial\theta$ are graphed in Fig. 9.15 in dependence of θ. These are oscillatory as to be expected from (9.246, 9.247). The time derivatives of r, θ and Z, calculated with aid of (9.240-9.245), are essential where r is small due to conservation of angular momentum (Fig. 9.16). The radial acceleration parts a_r, a_{1r} and its sum $a_r + a_{1r}$ are presented in Fig. 9.17, showing that the signs of a_r and a_{1r} are different, leading to zero crossings in the sum of both. The angular part of $\mathbf{a}_1$ reflects the well known fact that for a plane polar system $a_\theta = 0$, i.e. there is no angular force component. This does not hold for $a_{1\theta}$.

The correct handling requires use of Eq. (8.337) of the preceding chapter for describing the acceleration in 3D cylindrical coordinates. The result from computer algebra is:

$$\frac{D\mathbf{v}}{Dt} = \frac{\partial\mathbf{v}}{\partial t} + (\mathbf{v}\cdot\boldsymbol{\nabla})\,\mathbf{v} = \begin{bmatrix} \ddot{r} - r\dot{\theta}^2 + \frac{\partial\dot{r}}{\partial\theta}\dot{\theta} \\ r\ddot{\theta} + (r\frac{\partial\dot{\theta}}{\partial\theta} + \frac{\partial r}{\partial\theta}\dot{\theta})\dot{\theta} + 3\dot{r}\dot{\theta} \\ \ddot{Z} + \frac{\partial\dot{Z}}{\partial\theta}\dot{\theta} \end{bmatrix}. \tag{9.250}$$

This can be re-expressed by

$$\begin{aligned} \frac{D\mathbf{v}}{Dt} &= \begin{bmatrix} \ddot{r} - r\dot{\theta}^2 + \frac{\ddot{r}}{\dot{\theta}}\dot{\theta} \\ r\ddot{\theta} + (r\frac{\ddot{\theta}}{\dot{\theta}} + \frac{\partial r}{\partial\theta}\dot{\theta})\dot{\theta} + 3\dot{r}\dot{\theta} \\ \frac{\partial^2 Z}{\partial\theta^2}\dot{\theta}^2 + \frac{\partial Z}{\partial\theta}\ddot{\theta} + \frac{\partial^2 Z}{\partial\theta^2}\ddot{\theta} \end{bmatrix} \\ &= \begin{bmatrix} 2\ddot{r} - r\dot{\theta}^2 \\ 2r\ddot{\theta} + 4\dot{r}\dot{\theta} \\ \frac{\partial^2 Z}{\partial\theta^2}\dot{\theta}^2 + (\frac{\partial Z}{\partial\theta} + \frac{\partial^2 Z}{\partial\theta^2})\ddot{\theta} \end{bmatrix} \end{aligned} \tag{9.251}$$

where the derivatives of Z can be calculated from (9.247). This result is different from the plane polar case as expected. The three components are graphed in Fig. 9.18. There is qualitative similarity to Figs. 9.17 for the radial component, it reflects both extremal points. The θ component surprisingly vanishes again as for the plane polar system. Obviously there is no coupling to the Z component that would prevent this. The Z component is antisymmetric to the two radial peaks, indicating the lower and upper turning points of the orbit.

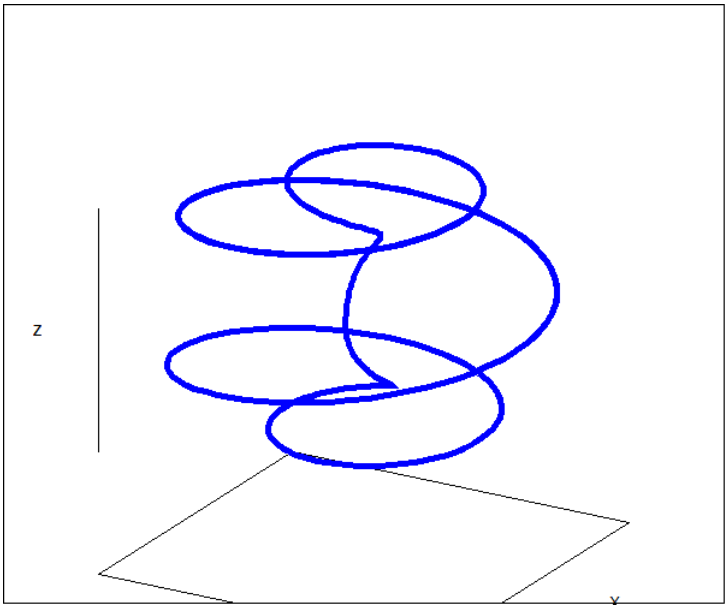

Figure 9.14: Structure of Torkado 3D orbit (vortex) after [31].

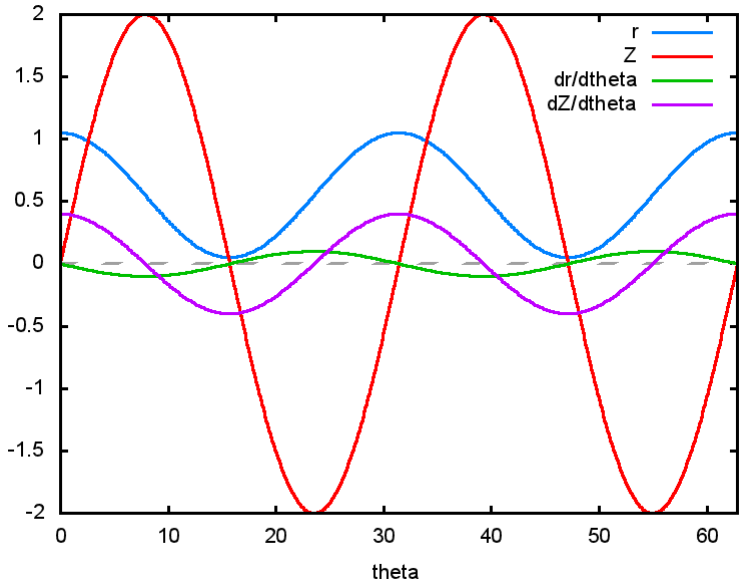

Figure 9.15: Angular dependence of $r, Z, \partial r/\partial\theta, \partial r/\partial Z$.

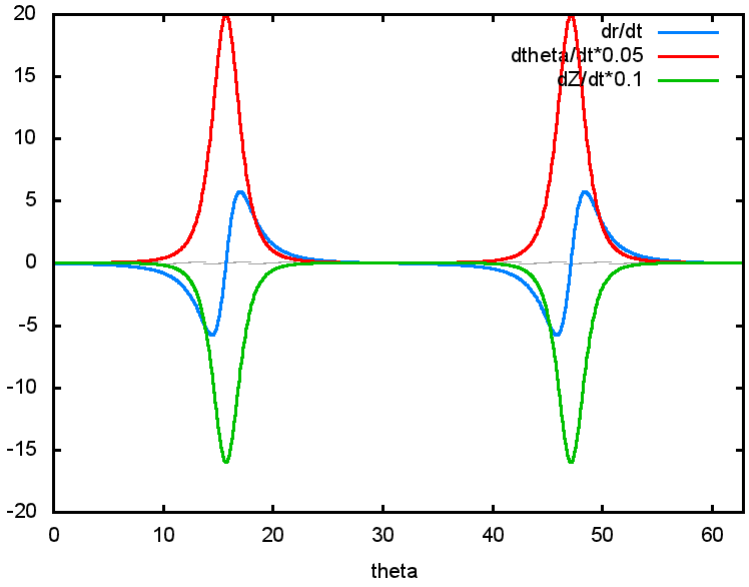

Figure 9.16: Scaled angular dependence of $dr/dt, d\theta/dt, dZ/dt$.

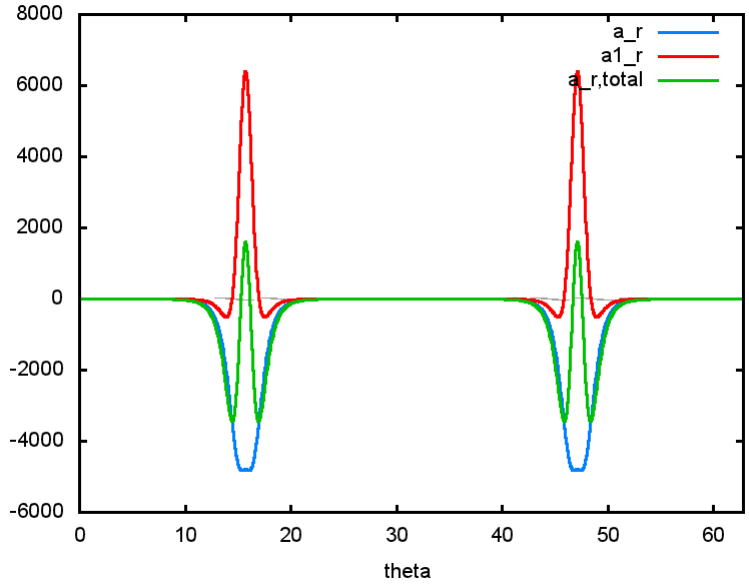

Figure 9.17: Angular dependence of radial accelerations.

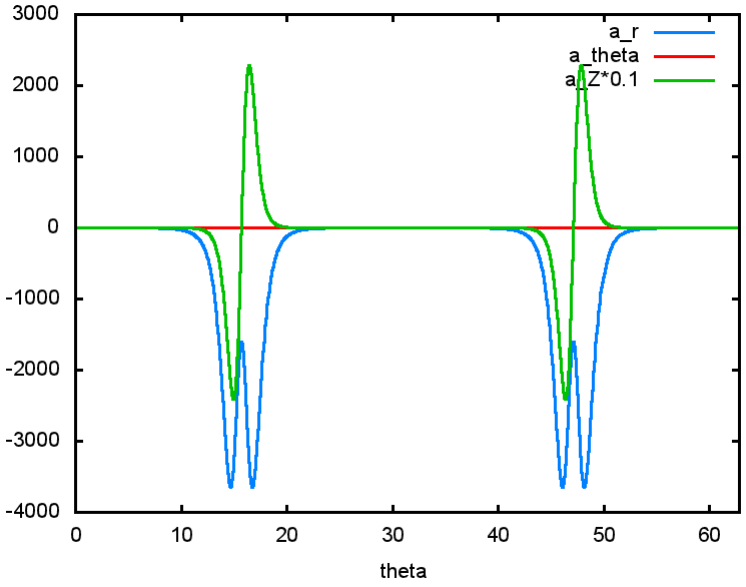

Figure 9.18: Angular dependence of acceleration components for full cylindrical coordinates.

9.2.3 New Force Law and Precession

An orbit in fluid dynamics spacetime is influenced by the vacuum according to the spin connection terms introduced in Eqs. (9.184-9.187). In general the acceleration $\mathbf{a} = \mathbf{F}/m$ has a radial and an angular component which in the case of a fluid dynamics spacetime is expressed by

$$\mathbf{a} = \left(-\frac{MG}{r^2} + \Omega^1{}_{01} \frac{L}{mr^2} \frac{dr}{d\theta} + \Omega^1{}_{02} \frac{L}{mr} \right) \mathbf{e}_r + \left(\Omega^2{}_{01} \frac{L}{mr^2} \frac{dr}{d\theta} + \Omega^2{}_{02} \frac{L}{mr} \right) \mathbf{e}_\theta \tag{9.252}$$

(see note 363(3)). Here we are using the classical limits

$$r = \frac{\alpha}{1 + \epsilon \cos(\theta)}, \tag{9.253}$$

$$\frac{dr}{d\theta} = \frac{\epsilon r^2}{\alpha} \sin(\theta), \tag{9.254}$$

$$\omega = \dot{\theta} = \frac{L}{mr^2}. \tag{9.255}$$

In the following we present graphical examples for the acceleration (or force) components. Using the classical limits, the components of (9.252) can be

expressed either as a function of r or a function of θ. We present both possibilities in Figs. 9.19 and 9.20, blue and green lines. The Newtonian form can be obtained by setting all spin connection components to zero. According to Newtonian theory, then there is no angular component of acceleration as can be seen from from both figures.

For the non-Newtonian case, we use the full form (9.252) for acceleration with choice of spin connections:

$$\Omega^1{}_{01} = 0.2, \tag{9.256}$$

$$\Omega^1{}_{02} = -0.2, \tag{9.257}$$

$$\Omega^2{}_{01} = 0.2, \tag{9.258}$$

$$\Omega^2{}_{02} = -0.2. \tag{9.259}$$

In this case, both acceleration components are different from zero, denoted by "P" in Figs. 9.19 and 9.20 (red and purple lines). These components are now defined only in the range of the elliptic orbit and a bit more negative than in the Newtonian case denote by "N". The angular component varies with angle θ as can seen from Fig. 9.20. The acceleration components are periodic in 2π as required.

So far we have assumed an elliptic orbit even for the non-Newtonian case. Actually it is a precessing ellipse as we have found from the solution of the Lagrange equations obtained from the Lagrangian (9.211). We have assumed that only $\Omega^1{}_{01}$ is significantly different from zero as in (9.215). Then we obtain the equations of motion

$$\ddot{\theta} = -\frac{2\dot{r}\,\dot{\theta}}{r}, \tag{9.260}$$

$$\ddot{r} = \frac{r^3\,\dot{\theta}^2 - GM}{\left(\Omega^1{}_{01} + 1\right)^2\, r^2}, \tag{9.261}$$

which differ from the Newtonian form by the spin connection in the denominator of the second equation. These equations have been solved numerically by using initial conditions of bound orbits. This gives the trajectories $\theta(t)$ and $r(t)$ as graphed in Fig. 9.21. The three-dimensional orbit plot shows that the orbit is not closed but a precessing ellipse in the plane $Z = 0$, see Fig. 9.22. Obviously the existence of one fluid dynamic spin connection term suffices to result in non-Newtonian orbits. Alternatively, such precessing ellipses were obtained in UFT 328 by relativistic effects. This was already discussed in section 4.2.3 of this book.

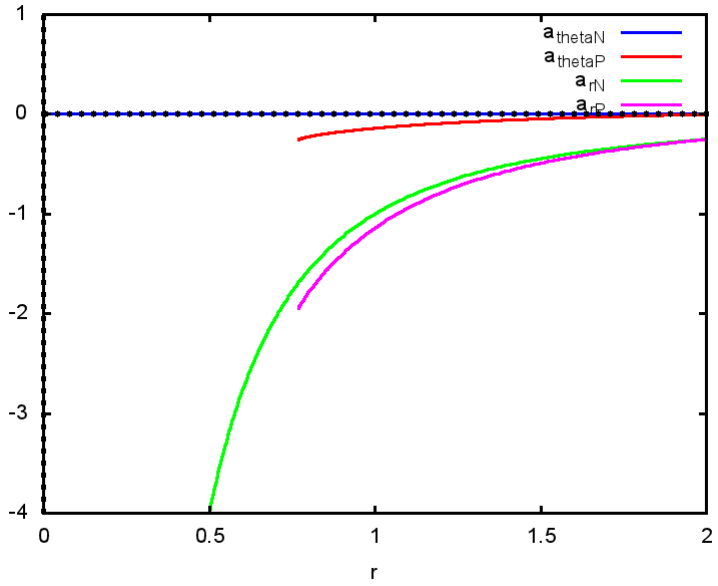

Figure 9.19: Acceleration components (Newtonian N and non-Newtonian P) in dependence of r.

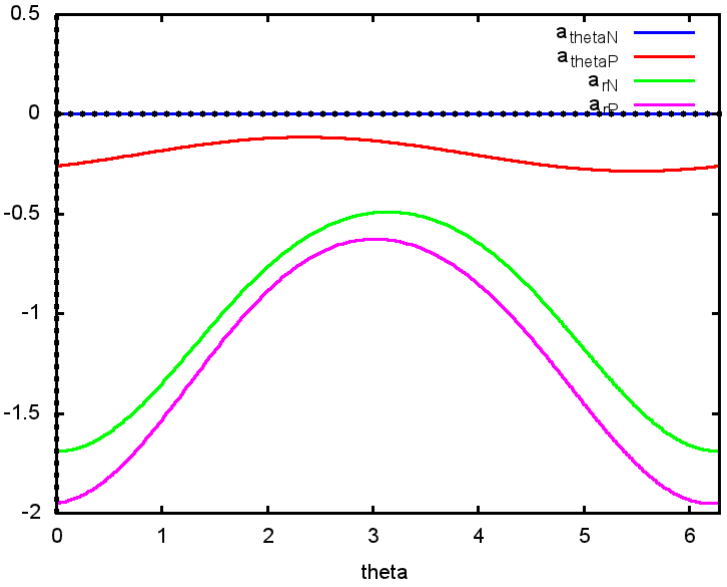

Figure 9.20: Acceleration components (Newtonian N and non-Newtonian P) in dependence of θ.

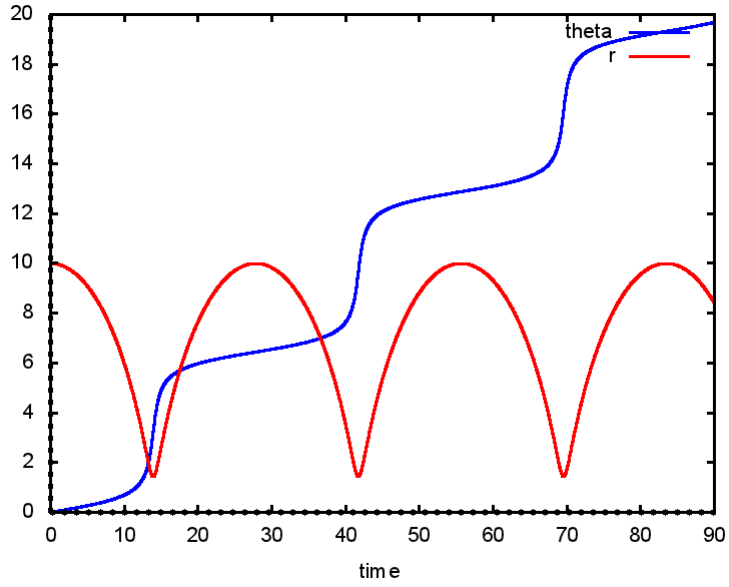

Figure 9.21: Trajectories $\theta(t)$ and $r(t)$.

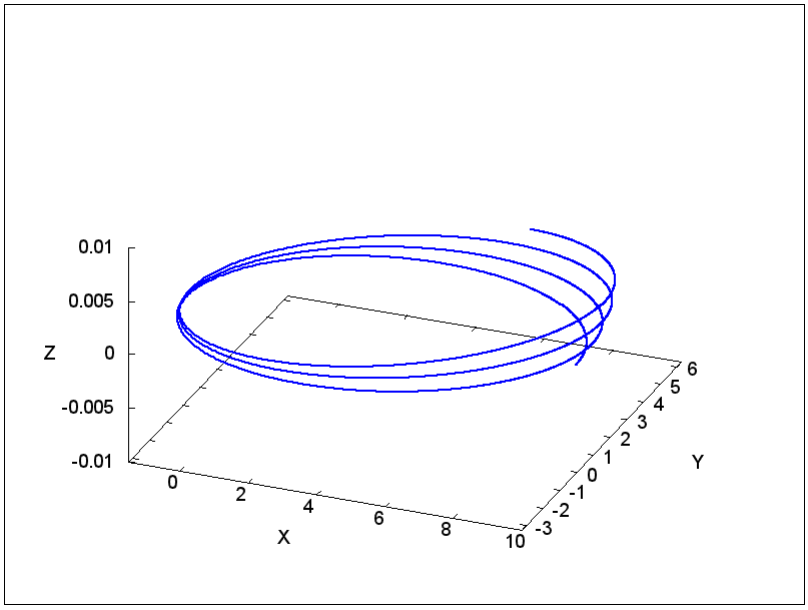

Figure 9.22: Precessing elliptic orbit due to fluid dynamics effects.

Chapter 10

Unified Field Theory of the Rainich Space: Determining Properties of Elementary Particles

10.1 Introduction

The well known numerical method of approximating differential quotients by quotients of differences is used in a novel context. This method is commonly underestimated, wrongly. The method is explained by an ordinary differential equation first. Then it is demonstrated how this simple method proves successful for non-linear field equations with chaotic behaviour. Using certain discrete values of their integration constants, a behaviour comparable with MANDELBROT sets is obtained. Instead of solving the differential equations directly, their convergence behaviour is analyzed. As an example the EINSTEIN-MAXWELL equations are investigated, where discrete particle quantities are obtained from a continuous theory, which is possible only by this method. The special set of integration constants contains values identical with particle characteristics. Known particle values are confirmed, and unknown values can be predicted. In this paper, supposed neutrino masses are presented.

In preceding work of RAINICH [32, 33] and, later, BRUCHHOLZ [34, 35] the geometry of electromagnetism has been determined by unifying electrodynamics with EINSTEIN's theory of general relativity [36]. The RICCI tensor [37] is constructed from the electromagnetic field in tensor representation. This geometry is conterminous with the geometry of the V4 of signature 2 in general. The singularity problem arising from the equations of this geometry is solved geometrically. The geometric equations are formulated numerically, i.e. as difference equations. The integration constants are parameters in corresponding recursion formulae, and take on discrete values. Variation of the parameters

leads to a characteristic convergence behaviour of the numerical equations. There are points in the parameter space leading to minimal divergence that are taken as their physically relevant values. – The physical significance of these insights and results is obvious.

In section 10.2, the theory of the unified field is explained. In the third section, the numerical method is described. This is applied in sections 10.5 and 10.6 with the parameters determined in section 10.4. The algorithms are discussed in the sixth section, and some computational results are given in section 10.7, in particular for the neutrino masses which have not been determined by any other theoretical method to date. Section 10.8 draws some conclusions.

10.2 The Equations

The theory is based on the relativistic tensor equations [34] of RIEMANNian (non-EUCLIDean) geometry (quoted from [38]):

$$R_{ik} = \kappa \, (\frac{1}{4} \, g_{ik} F_{ab} F^{ab} - F_{ia} F_k{}^a) \quad , \tag{10.1}$$

$$F_{ij,k} + F_{jk,i} + F_{ki,j} = 0 \quad , \tag{10.2}$$

$$F^{ia}{}_{;a} = 0 \quad , \tag{10.3}$$

in which g_{ik} are the components of metrics, R_{ik} those of the RICCI tensor and F_{ik} those of the electromagnetic field tensor. κ is EINSTEIN's gravitation constant. The partial derivative is denoted by a comma, the covariant derivative by a semicolon. If we express the field tensor by a vector potential $\mathbf{A}$ with

$$F_{ik} = A_{i,k} - A_{k,i} \quad , \tag{10.4}$$

equation (10.2) is identically fulfilled. Thus, we can base the calculations on quantities having the character of potentials that are metrics and the electromagnetic vector potential.

These equations are known as EINSTEIN-MAXWELL equations. The energy-momentum tensor of electrodynamics is equated to the energy-momentum tensor of EINSTEIN's theory [36]. In detail, the *homogeneous* MAXWELL equations are used. Only these fulfill force equilibrium and conservation of energy and momentum (mathematically expressed by the BIANCHI identities, see also appendix). These equations describe physically the electrovacuum around a particle and involve geometry described by the EINSTEIN part (equation (10.1)) of the equations. It is the geometry of the V4 of signature 2, also called space-time, as long as we do not consider constant curvature (see [37]), which is linearly superimposed with the fields.

These equations and the involved geometry were found by RAINICH already in the year 1924 [32,33]. Therefore, we will call the space-time RAINICH space. BRUCHHOLZ [34] derived this geometry independently of RAINICH in a different way traced out by EISENHART [37], with the same result.

The geometric equations yield only 10 independent equations for 14 components g_{ik}, A_i, what means that the geometry respectively the field is not completely determined. As well, it will be demonstrated that the omnipresent quantization in physics has nothing to do with this indeterminacy. The quantization is the consequence from chaotic behaviour of the geometric equations, even also if we override the indeterminacy with additional conditions.

10.3 Explanation of the Numerical Method

For completeness of arguments we repeat in this section what was already worked out in [38].

In direct numerical solutions of differential equations the differential quotient is replaced by a quotient of finite differences. This leads to recursion rules on the calculational grid. In the following we will derive a scheme of differences which is suitable for the type of problems we will solve in section 10.6. We consider a differential equation of the form

$$f''(x, c_\nu) + F(x, f'(x), c_\nu) = 0 \tag{10.5}$$

where F is a function of the derivative of the function $f(x)$ to be found. F and f depend on a set of constants c_ν. With difference quotients

$$\frac{\partial f}{\partial x}\Big|_{x_n} = \frac{f_{n+1} - f_{n-1}}{2\ \Delta x} \tag{10.6}$$

and for the second derivative

$$\frac{\partial^2 f}{\partial x^2}\Big|_{x_n} = \frac{f_{n+2} - 2f_n + f_{n-2}}{(2\ \Delta x)^2} \tag{10.7}$$

we obtain a recursion formula for the discrete function value of f at x_{n+2}:

$$f_{n+2} = 2f_n - f_{n-2} - (2\ \Delta x)^2 F_n(c_\nu) \tag{10.8}$$

or, rewritten,

$$f(x+2\ \Delta x) = 2f(x) - f(x-2\ \Delta x) - (2\ \Delta x)^2 F(x-\Delta x, x, x+\Delta x, c_\nu)\ . \tag{10.9}$$

We have chosen a difference of two grid points for the second derivative in order to obtain a simple recursion formula. The parameters c_ν denote the integration constants of the differential equations and are part of the initial conditions. The latter are obtained from appropriate approximations of f in the initial range of x. For real-valued x and c_ν this iteration formula is able to behave in a chaotic manner, in dependence of the parameters c_ν. These results can be generalized for systems of partial differential equations with many variables. In definition regions where the functions have diverging solutions, we obtain a map of the "degree of divergence" which can be graphed in a plane if we have two parameters c_1 and c_2 for example. All this is in analogy to the well known MANDELBROT sets familiar from chaos theory [39, 40].

We shall see from the EINSTEIN-MAXWELL equations that different values of the integration constants (as parameters) lead to a varying divergence behaviour. While f immediately diverges in most cases, there are discrete values of the parameters c where f diverges at a relatively sharply defined x value which stands for the radius here. (Further details are given in section 10.6.) These special values of the parameters perform a special set leading to a kind of "semi-stable" solutions of f. – In practice, this behaviour will be smeared over due to rounding errors. (Otherwise, we would not find the relevant discrete values.)

10.4 Determination of the Parameters

Differential equations of the discussed type result with first approximation in wave equations

$$\Box f = 0 \quad . \tag{10.10}$$

The integration constants from the wave equations are the parameters of the corresponding recursion formulae, named in section 10.3. It is detailedly explained in [35] how to compare the wave equations with corresponding POISSON equations, which have an additional source term. The integration constants of the wave equations then replace the sources of the POISSON equations. Concrete terms for the EINSTEIN-MAXWELL equations can be seen in section 10.6.

10.5 The Singularity Problem and its Solution

According to a theorem of EINSTEIN and PAULI [41], analytic solutions of equations (10.1,10.3,10.4) lead commonly to singularities. There are two types of singularities. The first type is a singularity inferred by assuming for example point masses and point charges in order to simplify the equations so that analytical solutions are feasible. This is often considered as a deficit when comparing a calculation with the situation in reality. However, in our calculations, these formal singularities are placed into the inner of the particle (according to observer's coordinates) which is not subject of calculation. The reason is as follows:
The observer uses coordinates in a tangent (asymptotic) space around the particle (with the singularity). The coordinates of the observer are projected onto the RAINICH space around the particle. We have a physically irrelevant region where this projection is not possible. The physically irrelevant regions are "behind" a geometric limit, which is the limit for this projection. Geometric limit means, at least one physical metrical component (explained in section 10.6) takes on an absolute value of 1. With spherical coordinates, the formal singularity is at the centre.

The basic idea of calculation is as follows. The equations (10.1,10.3,10.4) are evaluated on a radial grid from outer to inner and so one approaches the unknown inner area successively. At a certain radius, the calculation starts to diverge because the central singularity becomes predominant. It is important

to notice that this radius of divergence is clearly separated from the central singularity so a second type of singularity here appears. ECKARDT called the second type a "numerical singularity" [38]. SCHMUTZER told that the (formal) singularity is displaced due to the chaos in the recursion formulae [1]. However, also the numerical singularity is always "behind" the geometric limit and, therefore, in the physically irrelevant region. – So neither the numerical singularity nor the formal singularity are a problem for geometric equations. The geometric limit will be revealed to be a boundary at the conjectural particle radius with numerical simulations according to the EINSTEIN-MAXWELL equations.

The geometric limit is the mathematical reason for the existence of discrete "semi-stable" (explained in section 10.3) solutions. Here a mix from chaos (see [35] and previous sections) and marginal-problems is acting. – These discrete solutions involve discrete values of the integration constants, which are also called eigenvalues in context with the marginal-problems. We shall see that the RAINICH space is able to produce such eigenvalues, and that the eigenvalues represent a set identical with the entirety of the particle characteristics.

10.6 Numerical Simulations

In order to gain eigenvalues, one has to do lots of tests, because the particle quantities are integration constants and have to be inserted into the initial conditions (for more details see [35]), which are defined for the electrovacuum around the particle.

As already mentioned, the basis for computations are equations (10.1,10.3,10.4). For the sake of simplicity, we restrict equations (10.1,10.3,10.4) to time independence and rotational symmetry. That results, with spherical coordinates

$$x^1 = r \ , \ x^2 = \vartheta \ , \ x^3 = \varphi \ , \ x^4 = \mathrm{j}ct \ ,$$

in 6 independent equations for 8 components with character of a potential, $A_3, A_4,\ g_{11}, g_{12}, g_{22}, g_{33}, g_{34}, g_{44}$, the other vanish. In order to override the indeterminacy by the two missing equations, we define

$$g_{12} = 0 \qquad \text{(and, consequently, } g^{12} = 0) \tag{10.11}$$

and

$$g = \det|g_{ik}| = r^4 \sin^2\vartheta \quad . \tag{10.12}$$

These conditions are arbitrary, in which the second is taken from the free-field MINKOWSKI metric. They are in combination leading to reasonable results. Important to notice: The integration constants do not change with arbitrary conditions like equations (10.11), (10.12).

The integration constants from equations (10.1,10.3,10.4) result from a series expansion. The first coefficients of expansion are the input for the simulations and are inserted into the initial conditions [35]. The output is the number

[1] private information by Ernst Schmutzer, formerly Univ. Jena

of grid points along the radius until divergence occurs, which is a measure for the stability of the solution.

The first coefficients (integration constants) are

$$c_1 = -\frac{\kappa\, m}{4\pi} \Longrightarrow \frac{\kappa\, m}{4\pi} \tag{10.13}$$

(mass),

$$c_2 = \mathrm{j}\,\frac{\kappa\, s}{4\pi c} \Longrightarrow \frac{\kappa\, s}{4\pi c} \tag{10.14}$$

(spin),

$$c_3 = -\mathrm{j}\,\frac{\mu_\circ{}^{\frac{1}{2}}\, Q}{4\pi} \Longrightarrow \frac{\kappa^{\frac{1}{2}}\, \mu_\circ{}^{\frac{1}{2}}\, Q}{4\pi} \tag{10.15}$$

(charge), and

$$c_4 = -\frac{\varepsilon_\circ{}^{\frac{1}{2}}\, M}{4\pi} \Longrightarrow \frac{\kappa^{\frac{1}{2}}\, \varepsilon_\circ{}^{\frac{1}{2}}\, M}{4\pi} \tag{10.16}$$

(magnetic moment).

As explained, these follow from a comparison of series expansion from the Einstein-Maxwell equations (homogeneous Maxwell equations) with the solutions of corresponding inhomogeneous equations, see [35]. The dimensionless terms after the arrow are taken for computation, and have positive values. The imaginary unit has been eliminated. The unit radius ($r = 1$) corresponds to 10^{-15}m. By this, the initial conditions become, using $T = \frac{\pi}{2} - \vartheta$,

$$g_{11} = 1 + \frac{c_1}{r} - \frac{1}{2}(\frac{c_3}{r})^2 + \frac{(\frac{c_4}{r^2})^2(1+\cos^2 T)}{10}, \tag{10.17}$$

$$g_{22} = r^2\{1 + (\frac{c_4}{r^2})^2(\frac{1}{3}\cos^2 T - \frac{3}{10})\}\ , \tag{10.18}$$

$$g_{33} = r^2\cos^2 T\{1 + (\frac{c_4}{r^2})^2(\frac{\cos^2 T}{15} - \frac{3}{10})\}\ , \tag{10.19}$$

$$g_{44} = 1 - \frac{c_1}{r} + \frac{1}{2}\{(\frac{c_3}{r})^2 + (\frac{c_4}{r^2})^2\sin^2 T\}\ , \tag{10.20}$$

$$g_{34} = r\cos^2 T\ (\frac{c_2}{r^2} - \frac{1}{2}\frac{c_3 c_4}{r^3})\ , \tag{10.21}$$

$$A_3 = r\cos^2 T\ \frac{c_4}{r^2}\ , \tag{10.22}$$

$$A_4 = \frac{c_3}{r}\ . \tag{10.23}$$

The physically relevant parts of the metrical components are called physical metric components. These are the complement to unity in equations (10.17-10.20). Denoting the complements by $g_{(11)}$ etc. the above equations read

$$g_{11} = 1 + g_{(11)}\ , \tag{10.24}$$

$$g_{22} = r^2\,(1 + g_{(22)})\ , \tag{10.25}$$

$$g_{33} = r^2\sin^2\vartheta\,(1 + g_{(33)})\ , \tag{10.26}$$

$$g_{44} = 1 + g_{(44)}\ . \tag{10.27}$$

The physical metric components have a magnitude of ca 10^{-40} or smaller at the unit radius. Since several components contain unities, the physical components would have no effect due to lack of numerical precision during computation. Therefore, the actual computation is done with quantities performed from these physical components, with the consequence that the unity summands in the equations are eliminated.

We have to insert the values of the integration constants into the modified initial conditions (with physical components), see program in the data package (available at the author's website[2]). The conversion of physical into normalized (dimensionless) values and vice versa is described in detail in [35]. Table 10.1 shows some values with radius unit of 10^{-15}m. These examples allow for convenient conversion.

	physical value	norm. value
proton mass	1.672×10^{-24}g	2.48×10^{-39}
electr. mass	0.911×10^{-27}g	1.35×10^{-42}
$\hbar$	1.054×10^{-27}cm^{2}g/s	5.20×10^{-40}
elem. charge	1.602×10^{-19}As	1.95×10^{-21}
μ_B	1.165×10^{-27}Vs cm	3.70×10^{-19}

Table 10.1: Physical and normalized values for conversion.

Higher moments are missing in the equations because of lack of knowledge, their influence is estimated to be rather small. In the results section we will insert known values and values deviating from them, and compare the results.

The algorithm for evaluating the equations requires numerical differentiation. We do this by separating the quantity with highest radius index at the left-hand side as described in section 10.3. All previously evaluated quantities are at the right-hand side. These quantities come from equations (10.1) and (10.3) using (10.4). For example when we calculate spherical shells from outside to inside, the new quantity is $f_{m+2,n}$. In the following difference equations f stands for *any* potential-like quantity:

$$\left.\frac{\partial f}{\partial r}\right|_{r_m,T_n} = \frac{f_{m-1,n} - f_{m+1,n}}{2\ \Delta r}\ , \tag{10.28}$$

$$\left.\frac{\partial^2 f}{\partial r^2}\right|_{r_m,T_n} = \frac{f_{m+2,n} - 2f_{m,n} + f_{m-2,n}}{(2\ \Delta r)^2}\ , \tag{10.29}$$

$$\left.\frac{\partial f}{\partial T}\right|_{r_m,T_n} = \frac{f_{m,n+1} - f_{m,n-1}}{2\ \Delta T}\ , \tag{10.30}$$

$$\left.\frac{\partial^2 f}{\partial T^2}\right|_{r_m,T_n} = \frac{f_{m,n+1} - 2f_{m,n} + f_{m,n-1}}{\Delta T^2}\ . \tag{10.31}$$

[2] http://www.bruchholz-acoustics.de/physics/neutrino_data.tar.gz

¿From equation (10.29), and secondarily from equations (10.28), (10.30), (10.31), we obtain recursion formulae of the kind

$$f_{m+2,n} = 2f_{m,n} - f_{m-2,n} - (2\ \Delta r)^2 F_{m,n}(c_\nu)\ , \tag{10.32}$$

see also section 10.3. The $F_{m,n}$ are very complex, and contain the non-linearities of the EINSTEIN-MAXWELL equations. Detailed formulae are available in the Pascal code (see author's web site above). This method is made possible by the fact that 2nd derivatives in the tensor equations appear always linearly. Therefore the doubled difference in equation (10.29) was introduced.

When the program runs, the values of the several components are successively quantified in one spherical shell after the other. The computation is done for all components along the inclination (ϑ values) at a given radius, and along the radius (with all inclination values) from outside to inside step by step until geometric limits are reached. After starting the procedure, we get the values as expected from the initial conditions. Suddenly, the values grow over all limits. At this point geometric limits are reached and the calculation is stopped.

The step count (number of iterations) up to the first geometric limit of a metrical component (where the absolute value of the "physical" component becomes unity) depends on the inserted values of the integration constants. A relatively coarse grid reflects strong dependencies, however, the referring values of the integration constants are imprecise. Computations with finer grid lead to smaller contrast of the step counts, but the values are more precise.

The resulting eigenvalues of the integration constants are obtained where the step count until divergence is at maximum. Round-off errors have to be respected because these can be in the order of step count differences for the formulae.

In order to see the eigenvalues, lots of tests were run with parameters more and less deviating from reference values. The output parameter (used for the plots discussed in the results section) is the mentioned step count. In order to make visible the differences, the step count above a "threshold" is depicted in resulting figures by a more or less fat "point".

Though neutrinos are uncharged, one has to use always the full EINSTEIN-MAXWELL equations (with zero charge and magnetic moments) to account for the inherent non-linearity. Because the information is in the entire field outside the geometric boundary, one has to do so even if charge and magnetic moment are zero. Higher moments exist anyway and are included in the calculation. Only in the (outer) initial conditions (when starting the calculations) they are neglected.

10.7 Computational Results

10.7.1 Spins, Electric Charges, Magnetic Moments

Tests including parameters different from mass had to be run with an initial radius close to the conjectural particle radius. Here, the influences of the four

relevant parameters onto the metric (about 10^{-40}) are comparable.

The best result has been achieved with the free electron, see [35]. The magnetic moment of the electron arises specially sharply, due to the dominant influence.

Unfortunately, the mass gets lost in the "noise" from rounding errors. Only cases with charge and mass together can be made visible in exceptional cases, see for example [35, 42].

10.7.2 Masses

Masses of nuclei

The influence of mass on metrics prevails in a certain distance from the conjectural particle or nucleus radius, respectively. It proves being possible to set the remaining parameters to zero. Figs. 10.1 and 10.2 show related tests, with possible assignment of maxima in the figures to nuclei [42].

It was necessary in the tests according to Figs. 10.1, 10.2 to "pile up" the data. For this purpose, several test series with *slightly* different parameters (mostly initial radius) have been run, and the related step counts (the output) have been added. So the "noise" from rounding errors is successively suppressed. With 80 bit floating point registers, the rounding error is in the 20th decimal. As well, the relative deviation of difference quotients from related differential quotients *in the first step* is roughly 10^{-20} – that is the limit, where the onset of chaotic behaviour can be seen. Consequently, simulations with only 64 bit (double) lead to no meaningful results.

One can see certain patterns in the figures, which could arise from errors by neglecting other parameters.

Masses of leptons

It is principally possible to deduce the masses of all free particles, if they are stable to some extent. Since the electron mass is relatively small, one needs an initial radius of about 4×10^{-13} m in order to be able to neglect the influence of spin, charge, magnetic moment to some extent, see Fig. 10.3 [38]. One step count maximum (piled) appears fairly correctly at the experimental value, flanked by adjoining maxima, possibly caused by the neglected parameters.

The success in detecting known masses gives us confidence for trying a prediction of neutrino masses. That implies that neutrinos are stationary particles, i.e. have rest mass at all. Then they can never reach light speed.

The Particle Data Group [43] commented in the year 2002:
There is now compelling evidence that neutrinos have nonzero mass from the observation of neutrino flavor change, both from the study of atmospheric neutrino fluxes by SuperKamiokande, and from the combined study of solar neutrino cross sections by SNO (charged and neutral currents) and SuperKamiokande (elastic scattering).

The neutrino has the advantage of being electromagnetically neutral. As well, the spin does not perceptibly influence other components of metrics than those for the spin itself. So we can unscrupulously neglect the spin, and search for quite tiny masses.

Quoting the Particle Data Group (in 2002) again [43]:
Mass[3] $m < 3\,\mathrm{eV}$.
Interpretation of tritium beta decay experiments is complicated by anomalies near the endpoint, and the limits are not without ambiguity.
Newer experiments re-verify this ambiguity, just providing multiple mass bounds.

Ten plausible maxima have been found in our calculations for the electron neutrino, see Figs. 10.4, 10.5, 10.6, 10.7, 10.8, (quoted from [38]) and the supplementary data. Obtained values are 0.068 eV, 0.095 eV, 0.155 eV, 0.25 eV, 0.31 eV, 0.39 eV, 0.56 eV, 1.63 eV, 2.88 eV, 5.7 eV. Smaller values are less convincing.

The mentioned ambiguity gets along with the fact that multiple mass values have been detected. It could be possible that the set of values is reduced by computation with spin. The precision with 80 bit registers is not sufficient for such calculations. However, it could well be possible interpreting some values as composites from smaller values. Here we could have comparable circumstances like in nuclei so that there is no reason for the assumption that only one value can exist. This conclusion is supported by multiple experimental mass bound values.

Many mass values are integer multiples of $\sim 0.08\,\mathrm{eV}$, within the tolerances of the method. At the place of this value there is a hole in the figure, flanked by maxima at 0.068 eV and 0.095 eV. This could be:
1) a methodical error, or an effect of overdriving, known from electrical engineering,
2) both values are a kind of basic values, where the other values are composites from.
Other interpretations cannot be precluded.

10.8 Conclusion

It has been shown in this paper that the singularity problem is irrelevant for geometric equations, just for those of the Rainich space, the known Einstein-Maxwell equations. So these equations can be numerically solved. Even more, the discrete values of particle quantities, for example neutrino masses, can be predicted by numerical calculations based on Einstein-Maxwell theory. Starting from a finite difference scheme for differential equations, chaos properties of these equations were investigated in dependence of parameters being integration constants of the theory.

The resulting masses for supposed electron neutrinos come out to lie in the range being known by experiments. This is probably the first time that neutrino masses are predicted by a theory based on first principles.

Acknowledgement:
We express our thank to Bernhard Foltz who suggested searching for neutrino

[3] of electron neutrino

masses according to the described numerical method. Also, he reported the state of experimental neutrino research.

Appendix: Basic Formulae of General Relativity

The tensor calculus is a lot more clear than conventional vector analysis so that the formalism of the general theory of relativity [36] is reduced to few formulae:
The BIANCHI identities [37]

$$(R_i^k - \frac{1}{2}R\delta_i^k)_{;k} = 0$$

are always fulfilled by

$$R_{ik} = 0 \quad .$$

Therefore, only 6 independent equations exist for 10 components g_{ik}. If we set (EINSTEIN and GROSSMANN [36])

$$R_{ik} - \frac{1}{2}Rg_{ik} = -\kappa T_{ik} \quad ,$$

the divergences of the energy tensor must vanish

$$T_i^k{}_{;k} = 0 \quad ,$$

as dictated by nature. For the variables in the energy tensor, separate conditions follow, which do not take the place of the lacking conditions in metrics.

The divergences of the energy tensor of distributed mass

$$T^{ik} = \sigma \frac{\mathsf{d}x^i}{\mathsf{d}s}\frac{\mathsf{d}x^k}{\mathsf{d}s}$$

with the mass density σ are

$$T^{ik}_{;k} = \sigma k^i$$

with the (space-like) curvature vector $\mathbf{k}$. One can see the equivalence principle [36] in the curvature vector, because the curvature vector consists of accelerated motion and the gravitational field. - Since the curvature vector of any time-like curve in space-time is different from zero in general, σ must be zero everywhere. Distributed mass does not exist.

There is an exception when we start from discrete masses (which can only be integration constants). The force onto a body with the mass m then were

$$K^i = mk^i \quad .$$

For force equilibrium it must be $k^i = 0$. That results in four equations of motion. The curve described by the body in space-time is a geodesic.

The electromagnetic energy tensor (LORENTZ, see EINSTEIN [36])

$$T_{ik} = F_{ia}F_k{}^a - \frac{1}{4}g_{ik}F_{ab}F^{ab}$$

would result in a force density (LORENTZ force)

$$T^{ik}_{;k} = F^i{}_a S^a \quad ,$$

i. e. **S** must be zero. That means, there are no distributed charges and currents. Discrete charges are analogous to discrete masses. Equations of motions result together with the mass (the curves are no geodesics then).

From this we see:
1) Complete determinacy is not given.
2) There are no distributed charges and masses (sources).
3) Only the electromagnetic energy tensor is applicable in EINSTEIN's gravitational equation.
4) In order to calculate fields (gravitational and electromagnetic), we have to deal with integration constants instead of sources.

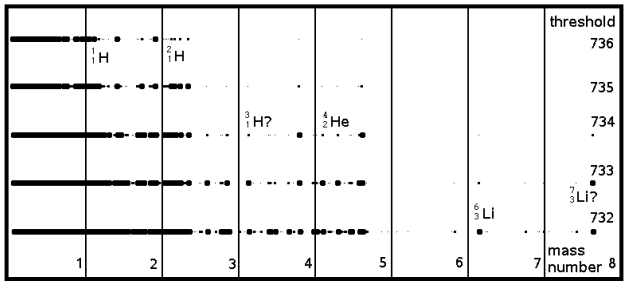

Figure 10.1: Tests for nuclei with mass numbers up to 8. Initial radius 4, 400 values, 4 times piled (1600 tests).

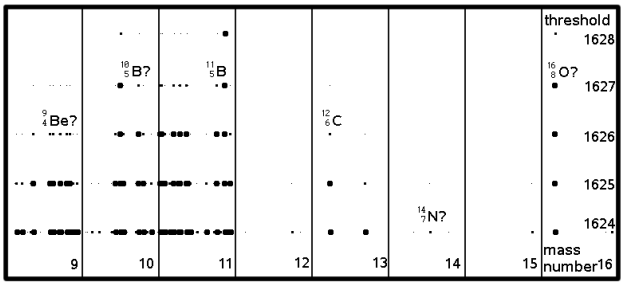

Figure 10.2: Tests for nuclei with mass numbers from 8 to 16. Initial radius 5, 400 values, 5 times piled (2000 tests).

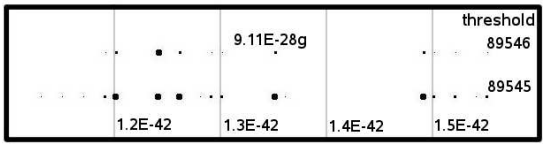

Figure 10.3: Tests for the free electron. Initial radius 400, 51 values, 9 times piled (459 tests).

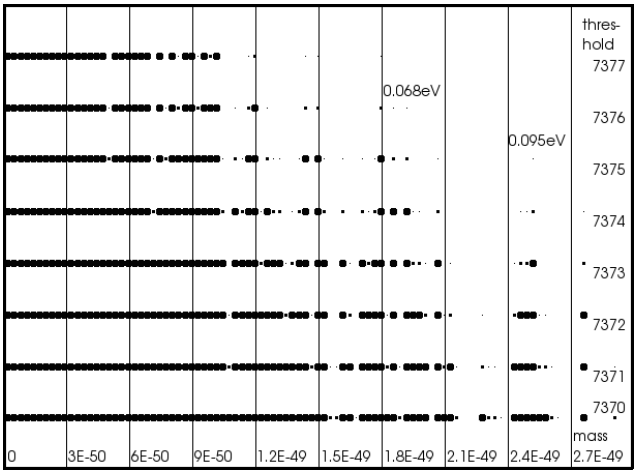

Figure 10.4: Tests for the electron neutrino, masses $< 0.11\,\mathrm{eV}$. Initial radius 5, 100 values, 9 times piled (900 tests).

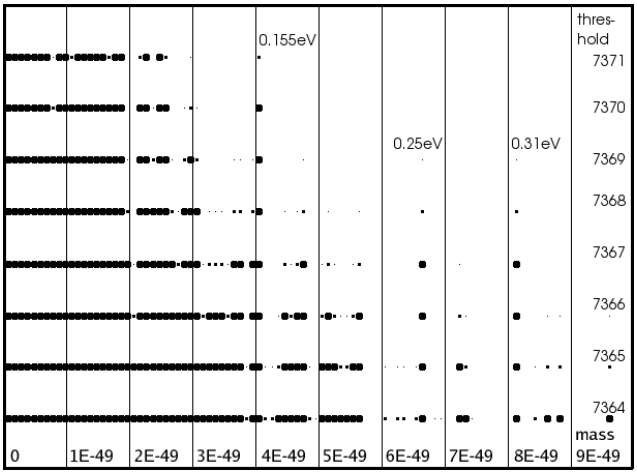

Figure 10.5: Tests for the electron neutrino, masses $< 0.4\,\mathrm{eV}$. Initial radius 5, 100 values, 9 times piled (900 tests).

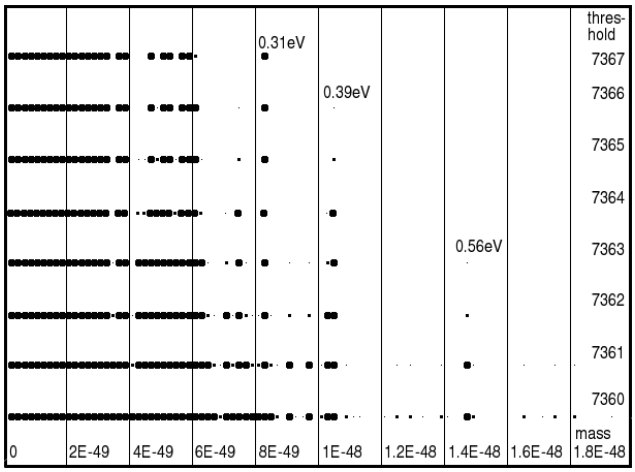

Figure 10.6: Tests for the electron neutrino, masses $< 1\,\mathrm{eV}$. Initial radius 5, 99 values, 9 times piled (891 tests).

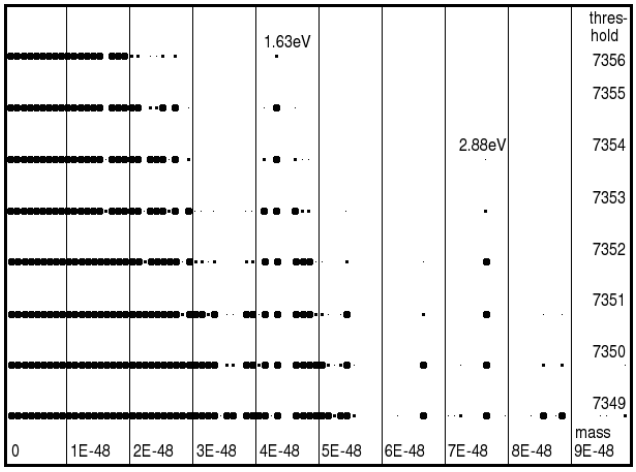

Figure 10.7: Tests for the electron neutrino, masses $< 4\,\mathrm{eV}$. Initial radius 5, 99 values, 9 times piled (891 tests).

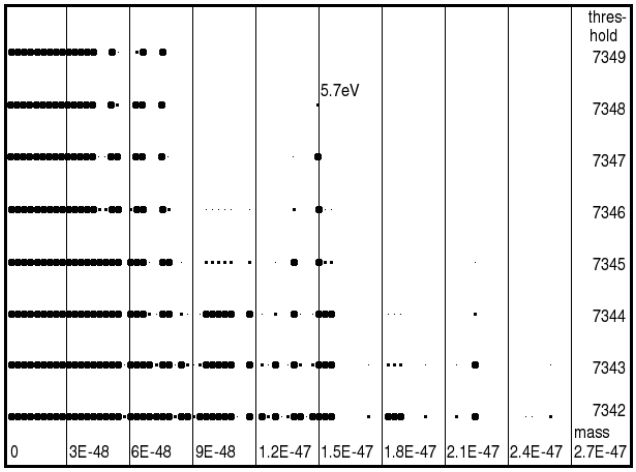

Figure 10.8: Tests for the electron neutrino, masses $< 11\,\mathrm{eV}$. Initial radius 5, 100 values, 9 times piled (900 tests).

Chapter 11

Kirchhoff's Law of Thermal Emission and its Consequences for Astronomy, Astrophysics and Cosmology

11.1 Introduction

Kirchhoff's Law of Thermal Emission is a pillar of modern physics. In assuming its validity Max Planck went on to obtain his famous equation for thermal spectra, wherein he introduced the quantum of action. Quantum mechanics was then born, and the theoretical physics of thermal emission and beyond, fixed to universality of Planck's equation. By this universality, Planck's equation has been widely applied in physics and astronomy. Astronomers report the temperature of the Sun's photosphere at ≈5,800 K by means of Planck's equation. Cosmologists insist that there is an isotropic Cosmic Microwave Background Radiation pervading the universe, left over from a big bang creation event, having a blackbody spectrum (i.e. a planckian distribution of frequencies) at a temperature of ≈2.725 K. Astronomy and astrophysics apply universality of Planck's equation everywhere.

Planck's equation is his answer to the riddle of 'blackbody radiation', because it was upon black materials such as lampblack (i.e. soot) that Kirchhoff constructed his Law. Nonetheless, Kirchhoff permitted his Law to encompass not just black materials such as soot, but any opaque solid material. Planck's equation similarly came to hold within its ambit a vast array of solid materials other than carbon, gases, gaseous plasmas, quark-gluon plasmas, and various clouds of exotic particles that existed, according to big bang cosmology, in the first 400,000 years of the big bang universe, which created itself from noth-

ing [44]. According to this theory, time, being a component of the Universe, did not exist before the big bang, because nothing existed before the big bang. The big bang delivered existence itself. Cosmology therefore 'counts time' from zero at the big bang.

Yet Planck's equation remains without a firm connexion to physical processes, for its ætiology is largely unknown. As Robitaille [45] has emphasised,

> "*In processes where light is emitted, there are five aspects to consider: 1) the physical setting, 2) separate energy levels created in this setting, 3) a transition species which will make use of these energy levels, 4) the production of a photon, and 5) an equation. For instance, for Lyman-α radiation these correspond to 1) the hydrogen atom, 2) the two electronic orbitals involved in the transition, principle quantum numbers N=2 and N=1, 3) the electron as the transition species, 4) the Lyman-α emission at 1216Å, and 5) the Rydberg formula. Alternatively, in speaking of the proton nuclear magnetic resonance line from water, these correspond to 1) the hydrogen atoms of the water molecules placed in a magnetic field, 2) the hydrogen nuclear spin up or spin down states, 3) the hydrogen nuclear spin as a transition species, 4) the hydrogen line at 4.85 ppm, and 5) the Larmor equation. Analogous entries can be made for any spectroscopic process in physics, with the exception of blackbody radiation. In that case, only the 4th and 5th entries are known: 4) the nature of the light and 5) Planck's equation.*"

The fundamental physics of thermal emission was established by the Scottish experimental physicist Balfour Stewart, who, in 1858, published the Law of Equivalence (i.e. Stewart's Law), which states that at thermal equilibrium radiative emission equals radiative absorption:

> "*The absorption of a plate equals its radiation, and that for every description of heat.*" [46, §19]

> "*That the absorption of a particle is equal to its radiation, and that for every description of heat.*" [46, §33]

Thus, at thermal equilibrium, the thermal energy absorbed by a material is equal to the thermal energy it emits.

In 1859, Kirchhoff [47] published his Law of Thermal Emission, which incorporated Stewart's Law. Although Kirchhoff was well aware of Stewart's work and publications, he did not cite him. This led to some acrimony between the two scientists. Moreover, Kirchhoff, using theory alone, went well beyond experimental findings, for Kirchhoff attributed to all opaque solids the universal property of 'blackbody radiation'; the radiation being dependent only upon the emitter's temperature, at thermal equilibrium. Kirchhoff thereby made all opaque solid materials blackbodies. It is this property that Planck embraced and which became a canon of theoretical physics, in the form of his equation for thermal spectra. Astronomy and cosmology subsequently did away with opaque solids and enclosures in order to admit free and bound gases and

clouds of exotic particles into the blackbody fold, and finally became lax with the requirement of thermal equilibrium. In these ways cosmology has built its theoretical basis, not just upon Einstein's General Theory of Relativity, but even more so upon thermal emission. Without Kirchhoff's Law of Thermal Emission and universality of Planck's equation cosmology and astronomy are without firm foundations. It is therefore essential to ensure that the physics of thermal emission is correctly employed. Unfortunately, cosmology and astronomy have failed to do so, violating the physics of thermal emission at every turn, invoking *ad hoc* unrealistic processes and a swag of new particles *ad arbitrium* in their endeavours to shore up a theory that has become another canon to be maintained despite the evidence.

11.2 Kirchhoff's Law of Thermal Emission (Blackbody Radiation)

One is hard-pressed to find the correct statement of Kirchhoff's Law of Thermal Emission in textbooks and scientific papers. The best source of Kirchhoff's Law of Thermal Emission is Kirchhoff himself [48, §16]:

> "*If a space be entirely surrounded by bodies of the same temperature, so that no rays can penetrate through them, every pencil in the interior of the space must be so constituted, in regard to its quality and intensity, as if it had proceeded from a perfectly black body of the same temperature, and must therefore be independent of the form and nature of the bodies, being determined by the temperature alone ... In the interior therefore of an opake red-hot body of any temperature, the illumination is always the same, whatever be the constitution of the body in other respects.*"

Fig. 11.1 depicts three hollow enclosures: a box made of granite, a sphere made of carbon, and a pyramid made of highly polished silver. If a small hole be made in each so that the radiation within can be sampled from outside when all three cavities are at the same temperature, according to Kirchhoff, the radiation is the same from all three cavities, as if they were all made of carbon or lined with soot, since the nature and form of the cavity walls is irrelevant to the radiation field within them.

The setting of Kirchhoff's Law of Thermal Emission is an opaque solid cavity at thermal equilibrium. Planck's equation for thermal spectra was forged upon this setting. For Kirchhoff and Planck the nature and form of an arbitrary cavity at thermal equilibrium is irrelevant to the radiation it contains. Their cavities all behave as if they were lined with lampblack at the same temperature. Thus, all thermally equilibrated cavity radiation is black, even the theoretical cavity made from a perfect reflector. This is the essential feature of Kirchhoff's Law and the basis for universality of Planck's equation. The only restriction on cavity form is that it must be large enough so that the effects of diffraction are unimportant. In addition, when conduction or convection are

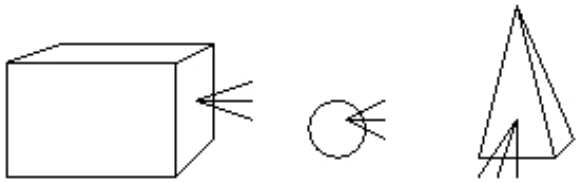

Figure 11.1: Hollow objects: a granite box, a carbon sphere, and a highly polished silver pyramid. By Kirchhoff's Law of Thermal Emission, when all three cavities are at the same temperature, the radiation field within them is always the same: that of blackbody radiation: irrespective of the nature and form of the cavity, as if all were made of carbon.

present, materials responding under their influence cannot ever be blackbodies [49, 50]. A blackbody can maintain thermal equilibrium only by radiative means.

> "*For the heat of the body depends only on heat radiation, since, on account of the uniformity in temperature, no conduction of heat takes place.*" [50]

To these cavities arcanum Kirchhoff attached what he thought to be a profound physical property: that the (black) radiation therein is a function of only temperature and frequency. This relation subsumes Stewart's Law of Equivalence.

> "*The ratio between the emissive power and the absorptive power is the same for all bodies at the same temperature . . .*" [48, §3]

Kirchhoff rendered this relation mathematically as,

$$\frac{E}{A} = e, \tag{1}$$

where he called E 'emissive power', A 'absorptive power', and e is an unknown universal function of only temperature T and frequency ν, for all cavities constucted from opaque solid materials, irrespective of their nature and form. Finally he set $A = 1$ so that $E = e$ acquires the mysterious property of universality, because neither E nor e are unity. The elucidation of the universal function e Kirchhoff believed to be of great scientific importance. It was Planck who finally gave e a definite form. However, when $A = 0$ Kirchhoff's universal function is undefined, and his terminology is otherwise confounding. In modern notation Kirchhoff's 'universal function' is given by,

$$\frac{E_\nu}{\alpha_\nu} = f\left(T, \nu\right), \tag{2}$$

where E_ν is emissive power, α_ν is the unitless absorptivity, and $e = f\left(T, \nu\right)$ [49].

In 1901 Max Planck [53] adduced his equation for blackbody radiation. He elaborated on it in his book in 1914 [50]. The spectral density u of radiation is given by [50]:

$$u = \frac{8\pi h\nu^3}{c^3} \frac{1}{e^{h\nu/kT} - 1}, \tag{3}$$

where c is the speed of light, T the temperature, ν the frequency, h Planck's constant, and k Boltzmann's constant; all being quantities independent of the nature and form of the cavity.

Furthermore, Planck [50, §10], contrary to Kirchhoff's thesis and the experimental facts, permitted even transmissive solids to be blackbodies, by means of their 'thickness':

> "*... the blackbody must have a certain minimum thickness depending on its absorbing power, in order to insure that the rays after passing into the body shall not be able to leave it again at a different point of the surface. The more absorbing a body is, the smaller the value of this minimum thickness, while in the case of bodies with vanishingly small absorbing power only a layer of infinite thickness may be regarded as black.*"

Yet the absorptivity of any material is not a function of thickness. Kirchhoff [48, §2] argued that only the surfaces of materials absorb and emit radiation:

> "*This investigation will be much simplified if we imagine the enclosure to be composed, wholly or in great part, of bodies which, for infinitely small thickness, completely absorb all rays which fall upon them.*"

Physically speaking, there can be no narrower layer of a material than an atomic layer. In pure geometry a surface has no thickness at all because a geometric surface is 2-dimensional. Purely geometric surfaces cannot absorb or emit radiation, because they are not physical. Moreover, real materials are not all black, not because they are not sufficiently thick, but because they possess reflection, which occurs at their surfaces. This includes the 'perfect reflector', which can only reflect, as its absorbing and emitting powers are naught. The perfect absorber (i.e. a blackbody) is opaque and absorbs all incident radiation at its surface because its reflective power is naught.

There has never been a theoretical or experimental proof of Kirchhoff's Law of Thermal Emission. Kirchhoff formulated his Law from theorising alone. Planck's theoretical proof of Kirchhoff's Law does not hold because, ironically, he violated the physics of thermal emission and of optics [49]. Moreover, there has always been ample experimental evidence that Kirchhoff's Law is false, since if it was true, then resonant cavities would not exist because all cavities at thermal equilibrium would be blackbodies, incapable of producing standing waves. Conversely, if standing waves are present within a cavity, the radiation is not black. Resonant devices and associated microwave technologies attest to the falsity of Kirchhoff's Law.

Although the details of the mechanism of thermal emission are unknown, as already pointed out in §1 above, it is known that thermal emission requires

a lattice [54]. Only condensed matter possesses a lattice. Gases do not have a lattice structure. Consequently, gases do not emit a planckian spectrum. Gases emit generally in narrow bands, as shown for hydrogen gas in Fig. 11.2.

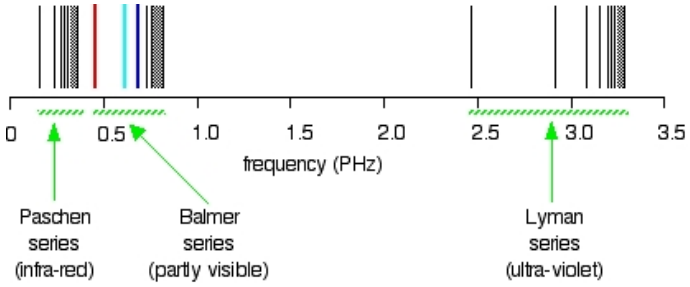

Figure 11.2: The spectrum of hydrogen gas is not continuous. Gases do not possess a lattice.

The blackbody spectrum is a continuous spectrum. Astronomy and cosmology nonetheless invoke blackbody spectra for the Sun and stars modelled as balls of hot gaseous plasma, and for the so-called 'Cosmic Microwave Background' (CMB). Statistical mechanics treats a 'photon gas' within a thermally equilibrated cavity as a blackbody spectrum, by assuming *a priori* that the material nature of the enclosure is irrelevant [55, §9.2]. This necessarily leads to universality of Planck's equation by the logical fallacy of *petitio principii*. A general equation for thermal spectra must account for the material nature of the enclosure. Physics has not ascertained such an equation. Planck's equation strictly pertains only to a blackbody in the setting of thermally equilibrated cavities. Otherwise, any temperature obtained from Planck's equation is, in general, uncertain.

When investigating cavity radiation Kirchhoff and Planck permitted all the energy in the walls thereof to be available to thermal emission. Pumping heat into these walls causes them to increase their temperature and this heat Kirchhoff and Planck made immediately available to exchange with the cavity radiation. In doing so they instantly made all cavities black because soot essentially has this property. Moreover, this is the reason why their cavities are independent of the nature of the walls. At thermal equilibrium the radiation density of any cavity is the same as if the cavity was made of or lined with carbon. The only difference between the views of Kirchhoff and Planck is that the latter permitted cavities made from transmissive solids, subject to 'thickness', whereas the former maintained that only the surface of an opaque solid emits and absorbs thermal radiation; a physical 'surface' being very thin. Planck's 'thickness' argument has no basis in physical reality, as the experiments of Stewart and Kirchhoff himself attest. Indeed, to this day there is no evidence whatsoever for Planck's 'thickness' hypothesis. Transmissive materials are not black, not because they are not very thick, or 'infinitely thick', but because they have low emissivity. In the case of the perfect reflector, it cannot produce blackbody cavity radiation because it has an emissivity of zero - it cannot emit any thermal radiation within a cavity of otherwise. Radiation from a perfect

reflector is entirely reflected radiation. In relation to the 'Cosmic Microwave Background Radiation' which he calls "*a diffuse background of radio static left over from near the beginning of the universe*", Weinberg [56] repeats the fundamental error in the usual fashion:

> "*Inside a box with opaque walls, the intensity of the radio noise at any given wavelength depends only on the temperature of the walls - the higher the temperature, the more intense the static.*"

Real materials possess reflectivity. By failing to understand reflectivity, thereby neglecting it entirely, Kirchhoff and Planck incorrectly made all cavities black. If ρ is reflectivity and ϵ is emissivity, then for opaque materials $\epsilon + \rho = 1$: the total thermal energy issuing from a material surface is a combination of that which is emitted and that which is reflected. A receiver of this radiation cannot discern which part is due to emission and which due to reflection, without knowing beforehand the nature of the material involved. In the case of a blackbody, $\rho = 0$, so its emissivity is 1. In the case of a perfect reflector, $\rho = 1$, so its emissivity is 0. All other opaque materials lie within the given range subject to the constraint $\epsilon + \rho = 1$. When heat is injected into the walls of an arbitrary cavity, the temperature of the walls rises, but not all of this energy is convertible to the thermal radiation field. In general, there is always energy within the walls of a thermally equilibrated cavity that is not available to exchange with the emission field inside the cavity. Energetic degrees of freedom exist within the walls which are not coupled to one another. Consequently, the radiation field within an arbitrary thermally equilibrated cavity does not report the true temperature of the cavity walls; only an apparent temperature. Nuclear Magnetic Resonance (NMR) and Magnetic Resonance Imaging (MRI) are thermal processes. For this very reason Felix Bloch called T1 the 'thermal relaxation constant'. Nonetheless, physics since Bloch has forgotten this, and astronomy and cosmology have never realised this. Robitaille [57] has made the fact stark - if Kirchhoff's Law of Thermal Emission is true, then MRI would be impossible. But MRI exists and is used in medicine every day. NMR and MRI are facilitated by means of spin-lattice relaxation, from which it follows that there is energy within the walls of an arbitrary cavity that is not available to thermal emission. The clinical existence of MRI is proof alone that Kirchhoff's Law of Thermal Emission has always been false. Consequently, Planck's equation is not universal. But without Kirchhoff's 'Law', and hence the universality of Planck's equation, big bang cosmology is invalidated in one stroke, without any need to consider the mathematical obfuscations of Einstein's General Theory of Relativity. Big bang cosmology is a product entire of General Relativity. It follows that Einstein's is a theory built upon sand. The properties of energy are the downfall of the General Theory of Relativity, for not only does it, in one way or another, invoke violations of the physics of thermal emission, it also violates the usual conservation of energy and momentum for a closed system [58–60]; thereby in conflict with a vast array of experiments. Moreover, Robitaille [61, 62] has proven by means of a simple experiment that Kirchhoff's Law of Thermal Emission is certainly false.

Thermal spectra do not in general reveal the temperature of the emitter [49]. Only in the case of a known black solid, such as soot or graphite, at thermal equilibrium within a cavity, is the temperature certain. All other temperatures extracted from thermal spectra are uncertain - they are only apparent temperatures. The Sun is a case in point. Solar scientists report that the photosphere has a temperature of about 5,800 K [63], from the Sun's 'blackbody spectrum'. But the Sun is not within an enclosure and is not in thermal equilibrium with an enclosure. Although the solar spectrum has a planckian distribution, it is not a blackbody spectrum. The temperature extracted from the solar spectrum is therefore only apparent. To appear to have a temperature of 5,800 K, the photosphere must be hotter than 5,800 K because it must have a temperature high enough to look like a true blackbody at 5,800 K. Only if the photosphere is composed of a solid black material, such as graphite, is a temperature of 5,800 K absolute. Since the photosphere is not graphite, it is not at 5,800 K. Moreover, according to the standard solar model, the Sun is a ball of hot gaseous plasma, in which case it does not have a lattice structure and is therefore unable to emit a planckian spectrum. Yet the solar spectrum is continuous, mimicking a blackbody at 5,800 K. The sprectra for several stars are illustrated in Fig. 11.3.

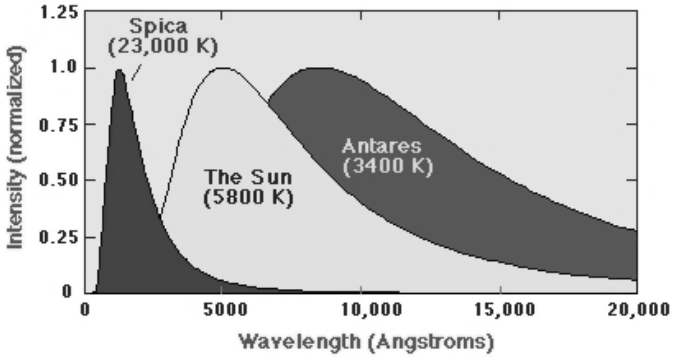

Figure 11.3: The spectra of three stars. Note that they are continuous and follow a planckian distribution. The temperatures are not real, only apparent, because stars are not blackbodies and are not at thermal equilibrium within an enclosure.

The conclusion is that the Sun is not gaseous - it must be condensed matter. The gaseous model of the Sun is an example of the misapplication of Kirchhoff's Law of Thermal Emission, even if the Law be true, and misinterpretation of its thermal spectrum, by the incorrect assumption of universality of Planck's equation. To mimic a blackbody at 5,800 K the Sun must have an emission mechanism similar to graphite - at the very least it must possess a lattice structure. Only condensed matter possesses a lattice. Matter that is not condensed cannot emit a planckian spectrum. Robitaille [45, 51, 52] has argued cogently that the Sun is condensed matter, mostly likely liquid metallic hydrogen. Liquid metallic hydrogen has a hexagonal-planar structure similar to graphite. This structure accounts very well for the observational evidence

from the Sun. Different star types have different lattice structures.

By means of microwave ovens in the home and submarine radio communications it is well known that water is a good absorber of microwaves. It is also well known from the laboratory that a good absorber is a good emitter, and at the same frequencies. Thus, water is a good emitter of microwaves. Approximately 70% of the Earth's surface is covered by water. This water is not microwave silent. It is in steady state with the atmosphere. Microwave emissions from the oceans are scattered by the atmosphere, producing an isotropic microwave bath therein. It therefore does not matter from which direction or at what time of day or of season, when sampled from the ground, this microwave signal is present and robust. Water is condensed matter. As with all liquids, it has a fleeting lattice. In the case of water there are two bonds: (1) the hydroxyl bond, (2) the hydrogen bond. The strengths of these two bonds are not the same. The hydrogen bond has a force constant that is ≈100 times weaker than the hydroxyl bond. Fig. 11.4 depicts the fleeting lattice of water. Each water molecule forms four hydrogen bonds with surrounding water molecules, in the essentially linear subunits, O-H$\cdots$O, schematically depicted in Fig. 11.4.

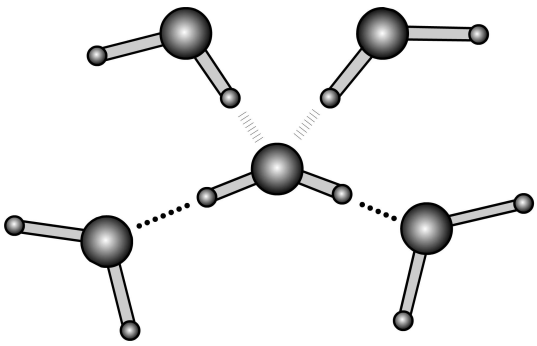

Figure 11.4: The water lattice. Each water molecule acts to accept and donate four hydrogen bonds. The subunit O-H$\cdots$O is essentially linear. Reproduced from Robitaille [75], with permission.

The energy in the hydroxyl bond is not available to microwave emission, whereas the hydrogen bond, acting as an oscillator, is responsible for microwave emissions from water [75, 76]. The water dimer is depicted in Fig. 11.5.

Water is an example of energetic degrees of freedom being uncoupled. Since the hydrogen bonds form a lattice, water emits microwaves in a planckian distribution. From this spectrum a Wein's temperature can be mathematically extracted. However, most of the water's energy is contained in the microwave inaccessible hydroxyl bond. If E_1 is the energy in the hydroxyl bond, E_2 the energy in the hydrogen bond, k_1 and k_2 the respective bond force constants, then the ratio of the energies, and hence of the temperatures, is equal to the

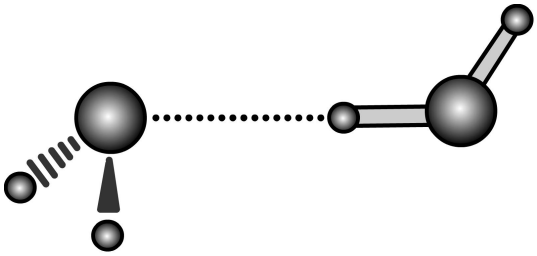

Figure 11.5: Schematic representation of the trans-linear water dimer. The subunit O-H$\cdots$O is essentially linear. Reproduced from Robitaille [75], with permission.

ratio of the force constants [75, 76]:

$$\frac{E_1}{E_2} = \frac{T_1}{T_2} = \frac{k_1}{k_2}. \tag{4}$$

Since it is known that $k_1/k_2 = 100$ [75], and if the mean temperature of the oceans is ≈300 K, then,

$$T_2 \approx \frac{300K}{100} \approx 3K.$$

> "*Consequently, a mechanism for creating isotropy from an anisotropic ocean signal is indeed present for the oceanic ≈3 K Earth Microwave Background.*" [75]

Hence, the spectrum from the hydrogen bond does not report the temperature of the body of water emitting microwaves. This temperature is only an apparent temperature - it is not the temperature of anything; illustrating the fact that Planck's equation is not universal. The consequences of this for cosmology are dire, for it was from the ground, in 1964, that Penzias and Wilson [77] detected what has since been dubbed the Cosmic Microwave Background (CMB) radiation. They assigned an absolute temperature of 3.5 ± 1 K to their residual signal. In assigning an absolute temperature they violated the physics of thermal emission because they knew nothing of the source of the signal. Only from a known black solid at thermal equilibrium can an absolute temperature be assigned with certainty. Temperatures extracted from spectra of unknown sources are uncertain, since the source might not be black, near black, or in thermal equilibrium.

11.3 The 'Cosmic Microwave Background'

Cosmology asserts that there is an isotropic cosmic microwave signal (CMB) pervading the Universe and that it has the profile of a blackbody spectrum at an absolute temperature of ≈2.725 K, produced by a big bang creation event:

> "*According to the big bang theory, the universe was in thermal equilibrium during its early stages. A searing light pervaded all locations and traveled in all directions, with the characteristics of a blackbody at very high temperature.*" [64]

It is said to be the thermal remnant of a big bang creation event, "*the fading archive of the Universe's fiery beginning billions of years ago*" [63], "*an all-pervasive hum of radiation with a temperature equivalent of a little more than 3 degrees Kelvin (three degrees above absolute zero) ... a faded snapshot of the universe as it was some three hundred thousand years after the big bang*" [64]. Cosmology claims to be able to reconstruct its big bang universe right back to the tender age of 10^{-43} seconds [63]. Between this 'time' and some 380,000 years after *creation ex nihilo*, the big bang universe was occupied only by particle-exotica such as neutrinos, quarks, gluons, leptons, atomic nuclei, and photons (i.e. electromagnetic radiation) [56, 63, 65]. To invoke the thermal equilibrium requirement of Kirchhoff's Law of Thermal Emission and Planck's equation, it is merely claimed that these primæval particles were in thermal equilibrium: "*According to big bang theory, the universe was in thermal equilibrium during its early stages.*" [64]. No explanation is given as to how thermal equilibrium was achieved, bearing in mind that cosmology also asserts that "*At the big bang itself, the universe is thought to have had zero size, and so to have been infinitely hot*" [66]. Since temperature is a manifestation of the kinetic energy, and hence the speed, of particles other than photons (i.e. particles that, according to cosmologists, have 'rest mass'), one can only wonder how fast these particles must have been moving in order to be 'infinitely hot', all the while occupying and speeding through zero volume, at thermal equilibrium! That which has zero size has no volume and hence cannot contain mass or have a temperature. According to the physicists and the chemists, temperature is the motion of atoms or molecules. The more energy imparted to the atoms or molecules the faster they move about and so the higher the temperature. In the case of a solid the atoms or molecules vibrate about their equilibrium positions in a lattice structure and this vibration increases with increased temperature. Pauling [67] conveys this:

> "*As the temperature rises, the molecules become more and more agitated; each one bounds back and forth more and more vigorously in the little space left for it by its neighbours, and each one strikes its neighbours more and more strongly as it rebounds from them.*"

Increased energy causes atoms or molecules of a solid to break down the long range order of its lattice structure to form a liquid or gas. Liquids have short range order, or long range disorder. Gases have a great molecular or atomic disorder. In the case of an ideal gas its temperature is proportional to the mean kinetic energy of its molecules [55, 68, 69]:

$$\frac{3}{2}kT = \frac{1}{2}m\left\langle v^2\right\rangle,$$

where $\left\langle v^2\right\rangle$ is the mean squared molecular speed, m the molecular mass, and k is Boltzmann's constant. But that which has zero size has no space for atoms or molecules to exist in or for them to move about in. And just how fast must atoms and molecules be moving about to be infinitely hot? Nothing can have zero size and infinite hotness. Nonetheless, according to Misner, Thorne and Wheeler [70],

> "*One crucial assumption underlies the standard hot big-bang model: that the universe 'began' in a state of rapid expansion from a very nearly homogeneous, isotropic condition of infinite (or near infinite) density and pressure.*"

Just how close to infinite must one get to be "*near infinite*"? Infinite and 'near infinite' density and pressure are no more meaningful than infinite hotness of zero size.

At the age of ≈380,000 years, called the 'time of decoupling' or the 'time of recombination', the supposed expanding universe became transparent to radiation, thereby setting free the CMB. Continued expansion of the 'spacetime' of this universe effectively stretched the wavelength of its CMB, reducing its 'temperature':

> "*. . . the 'hot big bang model.' This assumes that the universe is described by a Friedmann model, right back to the big bang. In such models one finds that as the universe expands, any matter or radiation in it gets cooler.*" [66]

However, since thermal spectra can only be produced by condensed matter, it is impossible for a blackbody spectrum to be produced by the exotic non-condensed matter of which the Universe was then only supposedly comprised. Cosmology however, to bring matter that is not condensed into the fold of blackbody radiation, simply and incorrectly asserts that "*Blackbody radiation arises whenever particles collide with each other very rapidly in thermal equilibrium*" [64]. Weinberg [56] asserts that "*Any sort of body at any temperature above absolute zero will always emit radio noise, produced by the thermal motion of electrons within the body*". Soot and graphite are blackbodies. Anything that produces a blackbody spectrum must have a structure similar to that of soot or graphite. Particle collisions do not fall within the necessary structural character. Anything that produces a planckian spectrum must possess a lattice [54]. Free particles do not have lattice structure, neither do thermal electrons. Particles colliding "*with each other very rapidly in thermal equilibrium*" do not produce a continuous spectrum, let alone a planckian one.

Penzias and Wilson [77] discovered that the residual signal in their antenna did not vary with the time of day, the direction of their antenna, or with the seasons. In the same issue of the journal that published their findings, in the pages immediately before their paper, the theoretical cosmologists Dicke, Peebles, Roll and Wilkinson [78], assigned the signal to the Cosmos, as the remnant of a big bang creation event, to accord with the Friedmann-Robertson-Walker metric obtained as a cosmological solution to a certain set of Einstein's General Theory of Relativity field equations. They too insisted that the spectrum is that of a blackbody, so that the temperature extracted from it is absolute. But Earth takes its atmosphere and its oceans with it as it orbits the Sun and rotates on its axis. From the ground, the microwave emissions from the oceans, scattered to isotropy in the atmosphere by the atmosphere [82, 83] are independent of time of day, of seasons, and of antenna direction, just as Penzias and Wilson reported. Shown in Fig. 11.6 is Earth.

Approximately 70% of the surface of Earth is covered by water. The oceans are not microwave silent.

Figure 11.6: Approximately 70% of the surface of Earth is covered by water. This water is not microwave silent. That COBE did not report any microwave interference from Earth is precisely because Earth is the source of the signal, from its oceans.

Penzias and Wilson in fact sampled the microwave emissions of the oceans, present isotropically in the atmosphere due to atmospheric scattering, but eventually came to believe that this signal has a cosmic origin, because they did not realise that the source of their signal was proximal. The signal is not of cosmic origin. Subsequent detection of the 'CMB' monopole signal by the Earth orbiting COBE satellite, at an altitude of ≈900 km, reaffirmed that the signal is the oceanic microwave emission profile, even though the COBE Team also assigned it to the Cosmos, on the basis of big bang predilection and concomitant oversight of the nature of oceanic water. The immediate consequence of this is that big bang cosmology is again invalidated.

The CMB is mathematically modelled by means of an infinite series of spherical harmonics. The first term in the series is the monopole signal, the second is the dipole signal, after which come the quadrupole, the hexadecapole, and so on in the multipoles. This mathematical model, *ipso facto*, does not fix the same physical causation to each component of the infinite series. The existence of the dipole signal does not mean that the 'CMB' monopole signal detected by COBE-FIRAS must exist throughout the Universe. The dipole signal is, according to cosmology, on its assumptions for the CMB monopole, due to a Doppler effect associated with motion of the local galactic group through the CMB.

> "*If the Earth is moving, however, there is a smooth variation in temperature across the sky, because of the Doppler effect. In the direction in which the Earth is moving, the cosmic background*

looks warmer; in the direction of recession, cooler. ... The amount of warming and cooling is proportional to the speed of motion compared to the speed of light, and the direction of the dipole lines up with the direction of motion. ... the sky was warmest in the direction of Leo and coolest in the direction of Aquarius, which means that the Earth was moving toward the former and away from the latter. That is not the direction in which the Galaxy rotates. ... Not only is the entire Galaxy rotating, as it should be, but, unexpectedly, it is also moving through space. And it is moving very fast - six hundred kilometers a second, or more than a million miles an hour. ... while Earth and the Solar System are moving toward Leo at about 350 kilometers per second - more than ten times the velocity of the Earth going around the Sun - the Milky Way galaxy is traveling about 600 kilometers per second. ... And the Mily Way is not alone in its extreme velocity. About a dozen neighboring galaxies - the Local Group - are also moving presumably under the influence of the distant unseen structure." [64]

The dipole signal is not isotropic, and had been detected by instruments aboard balloons, planes and rockets, before COBE. The Soviet Relikt-1 satellite, for instance, detected the dipole signal [79]; COBE confirmed the finding, and from its measurements its 'temperature' at 3.353 ± 0.024 mK in the direction $(l, b) = (264.26^{\circ} \pm 0.33^{\circ}, 48.22^{\circ} \pm 0.13^{\circ})$ galactic longitude and latitude. Since Earth is in fact the source of the strong monopole signal detected by COBE-FIRAS, cosmology's mathematical model of the CMB bears no relation to reality, despite the existence of the dipole signal. The cause of the dipole signal must lie elsewhere [84]. Merely aligning it to a component of the mathematical model does not make its ultimate ætiology the same, explicitly or implicitly, as the strong monopole detected very near Earth. Cosmology's mathematical model simply reflects the assumptions by which it was constructed. Nothing in the mathematical model compels the assumptions for it to be true.

11.4 The Cosmic Background Explorer satellite

On November 18, 1989, the Cosmic Background Explorer satellite (COBE) was launched, commissioned to survey cosmic microwaves and infrared signals at an altitude of ≈900 km above Earth. It carried two instruments for microwave purpose; (1) the Far Infrared Absolute Spectrophotometer (FIRAS), (2) the Differential Microwave Radiometers (DMR). FIRAS was to sample the CMB monopole signal and DMR primordial anisotropies in the CMB. Both instruments returned data for the dipole signal. Fig. 11.7 is a schematic of COBE-FIRAS.

"*FIRAS was designed to function as a differential radiometer, wherein the sky signal could be nulled by the reference horn Ical.*"

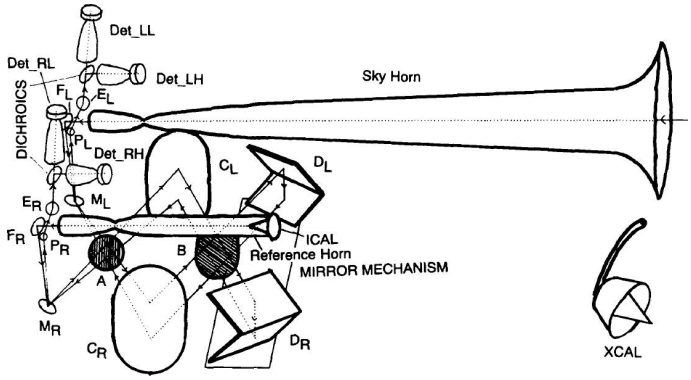

Figure 11.7: Salient components of FIRAS: Sky horn, reference horn, Ical (2 thermometers), and Xcal (3 thermometers) (Ical = Internal calibrator, Xcal = External calibrator). From [81], courtesy of NASA and the COBE Science Working Group. Accessed online 16$^{\text{th}}$ August 2017, https://lambda.gsfc.nasa.gov/product/cobe/firas_exsupv4.cfm

[82]

The CMB monopole temperature was reported by FIRAS as 2.725±0.001 K [80] over a blackbody spectrum. The signal to noise for the monopole was so great that the error bars on the graph of the spectrum are some 400 times smaller than the width of the line used to draw the graph, shown in Fig. 11.8.

The COBE Team reported that the satellite's shield covered the frequency range 30 GHz to 3,000 GHz, although FIRAS sampled principally in the 30-600 GHz range. This is a 100-fold shield frequency range. But no such broadband shield exists. Moreover, a shield to intercept extraneous microwaves must be specially designed. Examination of the COBE shield design [88] reveals that no measures were specially taken for microwaves. COBE's shield was not able to prevent microwave diffraction over its shield. Indeed, the COBE-FIRAS Team reported that they detected unexpectedly higher intensity at the lower frequencies and unexpectedly lower intensity at the higher frequencies [80]. This is precisely the effect expected however due to microwave diffraction over the shield.

The COBE Team did not report any microwave interference from Earth. This attests to the Earth being the actual source of the signal [82, 83].

Since the COBE shield was helpless before microwave diffraction over its perimeter, microwave emission originating from the oceans below it, scattered to isotropy by Earth's atmosphere, were able to freely diffract over the shield and into the FIRAS horn. Bearing in mind that the signal to noise for FIRAS was enormous, the source of the signal must be proximal. Since the ≈2.725 K monopole signal is so powerful, any satellite located anywhere should, with a suitable detector, find no less signal to noise power. Yet no cosmological satellite far beyond the confines of Earth reported detection of the ≈2.725 K CMB monopole signal. Without the CMB monople signal beyond the confines of Earth, all arguments for its existence and its supposed anisotropies have no

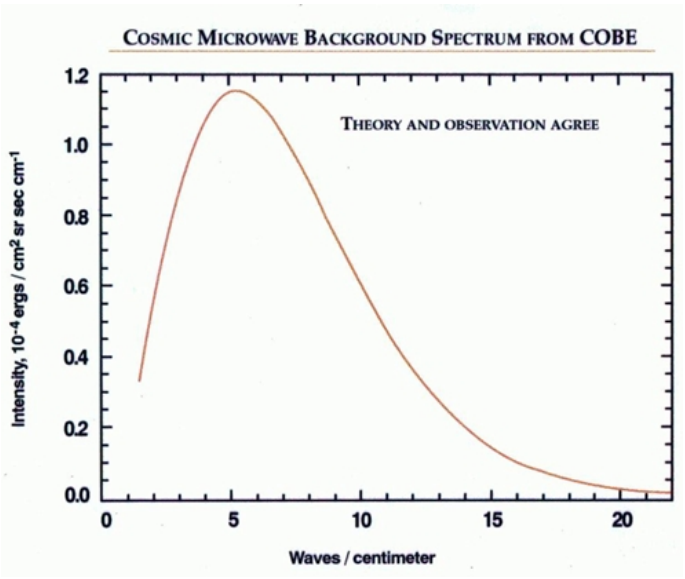

Figure 11.8: The planckian spectrum of the CMB monopole signal reported by COBE-FIRAS. FIRAS was sensitive not directly to the sky but to the difference between the sky and the FIRAS external calibrator, *xcal*. Hence, this spectrum is that of the external calibrator, matched to the sky. Although data was initially reported by the FIRAS Team for $< 2\text{cm}^{-1}$, this data was subsequently dropped from the plot, without explanation, and the frequency axis was offset to the left. Figure courtesy of NASA and the COBE Science Working Group. Accessed online 11$^{\text{th}}$ August 2017, https://lambda.gsfc.nasa.gov/product/cobe/cobe_image_table.cfm

scientific merit. There can be no doubt that the ≈2.725 K monopole signal has its origin on Earth [82].

The COBE-FIRAS Team reported a set of three interferograms, obtained in-flight, in a single image (Fig. 11.9). The top trace had the Internal Calibrator (ICAL) set at 2.759 K and compared to the sky. The trace seems to contain only small deviations from the horizontal and is reported as "*near null*". The second trace has ICAL set at 2.771 K and compared to the sky. It contains significant vertical displacement and is reported as "*off null*". The third and final trace has ICAL set at 2.759 K and the External Calibrator (XCAL) set at 2.750 K and contains a significant vertical displacement. Despite reporting a "*near null*" at 2.759 K the FIRAS team ultimately reported a 'CMB' temperature of 2.725 K. However, Robitaille [82] has pointed out that the top and bottom traces are not drawn to the same scale. This is evident from the noise power in the traces. The noise power should be the same for all three traces. It is most clearly evident in the middle trace as it is the jitter in the baseline of the trace. For the top and bottom traces to appear on the same scale as the middle trace, so that the jitter is of the same amplitude, they must be amplified by a factor between 3 and 5. The result is that the "*near null*" report is far from near null. The top and bottom traces have

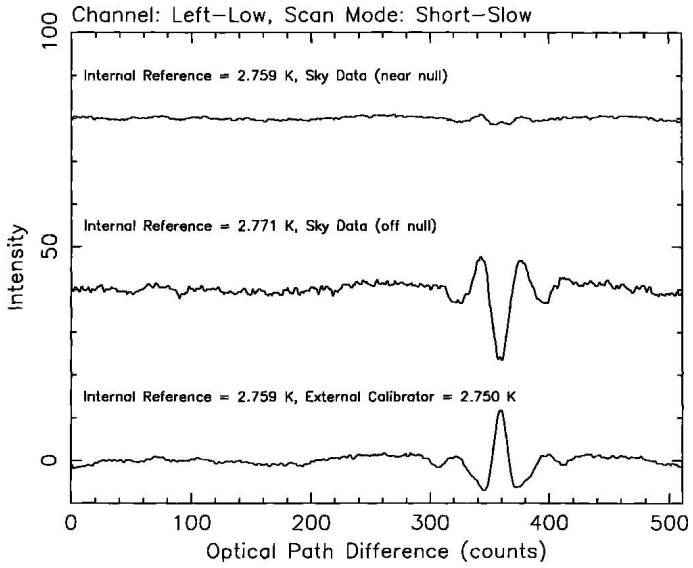

Figure 11.9: Interferograms obtained in flight with FIRAS. The top and bottom traces are not on the same scale as the middle trace. The traces are deceptive. From Mather et al. (1990) [87], courtesy of NASA and the COBE Science Working Group. Accessed online 16$^{\text{th}}$ August 2017, https://lambda.gsfc.nasa.gov/product/cobe/firas_exsupv4.cfm

had their amplitudes suppressed, apparently to give the false impression that a 'near null' was obtained. These traces are deceptive [85]. Moreover, the spectral precision reported by the FIRAS Team is well beyond the capacity of the instrumentation that was on COBE:

> "*Finally, in 2002, Fixsen and Mather advance that 'the measured deviation from this spectrum are 50 parts per million (PPM, rms) of the peak brightness of the CMBR spectrum, within the uncertainty of the measurement'. Using technology established in the 1970's, the FIRAS team reported a spectral precision well beyond that commonly achievable today in the best radiometry laboratories of the world.*" [82]

The reported a null at 2.759 K is 34 mK above the reported sky temperature, 2.725 ± 0.001 K. Null should ideally occur at the sky temperature. Owing to 18 mK error in the thermometers, ≈3 mK temperature drift, 5 mK error in the sky horn Xcal, and 4 mK error in *Ical*, Robitaille determines an overall error bar of ≈64 mK in the microwave background. Yet the FIRAS team reported only ≈1 mK. Errors were evidently dumped into the calibration files. And as Robitaille [82] observes, "*a 1 mK error does not properly reflect the experimental state of the spectrometer*". Moreover, the FIRAS team's calibration procedures produced calculated *Ical* emissivities great than 1.3 at the higher frequencies; but the theoretical maximum for emissivity is exactly 1 by definition.

FIRAS was unable to obtain proper nulls, despite the FIRAS team's reports that they obtained "*the most perfect blackbody spectrum ever measured*" [89]:

> "*It is sometimes stated that this is the most perfect blackbody spectrum ever measured, but the measurement is actually the difference between the sky and the calibrator.*" [89]

Robitaille [82] expresses the relationship thus:

$$\text{(Sky - Ical) - (Xcal - Ical) = (Sky - Xcal).}$$

It is clear from this relation that the effects of *Ical* and instrumental factors should be negligible: but that is not what the FIRAS team found. It is also clear that if *Xcal* matches the sky a null will result. *Xcal* is assumed an ideal blackbody spectrum and so the sky would also be an ideal blackbody spectrum in the event of a null. The FIRAS team assumed from the outset that the sky is as an ideal blackbody. Note that if the calibration obtained with *Xcal* in place is dominated by leakage of sky signal into the horn then a perfect blackbody spectrum would result because the sky would then be compared with itself. Robitaille [82] has shown that there was significant sky leakage into the horn during calibration with *Xcal*.

Unable to obtain a proper null, the FIRAS team blamed instrument problems and the calibrations, but never entertained the possibility that the sky, owing to emissions originating from the Earth diffracting over the RF shield, was not behaving as a blackbody, as they assumed. Fixen et al [81] remarked: "*However, the measured emission is higher than predicted, particularly at the lowest frequencies*; at the very frequencies at which diffraction of photons from Earth would be a maximum over the RF shield. In addition, all data when the Earth illuminated the instrument were rejected outright, thereby removing any effect of earthshine that might well assign the microwave background to the oceans.

> "*In the end, the FIRAS team transfers the error from the spectrum of interest into the calibration file ... Using this approach it would be possible, in principle, to attain no deviations whatever from the perfect theoretical blackbody. Given enough degrees of freedom and computing power, errors begin to lose physical meaning. The calibration file became a repository for everything that did not work for FIRAS*" [82]

To extract the cosmic microwave anisotropies thought by cosmology to be lurking beneath the CMB monopole signal, COBE-DMR had to contend with the presence of the microwave monopole, the dipole, and the galactic foreground which is ≈1000 times stronger than the signal sought (the galactic contaminaiton is in mK). This is a dynamic range problem, similar to water suppression in biological proton Nuclear Magnetic Resonance (NMR). For instance, a biochemical compound of interest is often dissolved in water, in the aqueous cytosol of a cell. Water is ≈110 molar in protons. A compound of interest might be ≈1 - 100 millimolar. A best case scenario is then an ≈1,000

fold required water signal removal. In biological proton NMR, water suppression can be 100,000 or more. To achieve suppression of water resonances that swamp the resonance of the dissolved compound of interest, various techniques have been developed, either physically, as in specialised spin excitation, or biochemically through substitution. One example of how this is achieved is sufficient to make the point: Biochemical substitution involves removal of most of the water protons by substituting deuterium oxide (D_2O) using a process called lyopholisation, where the sample is repeatedly frozen then sublimated under vacuum. The water solvent is then replaced by D_2O, which has a nuclear magnetic resonance far from water, thereby revealing the resonance of the compound of interest at the relevant frequency. This is an example of modification of the sample in order to secure the signal of a compound that has a resonance that lies below that of the aqueous solvent. An example of this process is depicted in Fig. 11.10.

The cosmological satellites attempting to extract anisotropies from the CMB are even worse off than the example of Fig. 11.9, because the hypothesised anisotropies are, analogously, located directly beneath the water resonance. Thus, as Robitaille [90] has emphasised, laboratory experience attests that it is impossible to extract a signal ≈1000 times weaker than the enveloping noise without being able to manipulate the source of the signal or without *a priori* knowledge of the nature of the signal source; neither of which were available to COBE-DMR. George Smoot, the principal investigator for COBE-DMR, related that to extract the weak multipoles, which he called "*wrinkles in the fabric of time*" [64], by computer data-processing, required first the removal of the 2.725 K monopole, the dipole, the galactic foreground, and then the quadrupole. He puzzled over why the multipoles did not appear until the quadrupole was finally removed by computer data-processing methods, since the raw data contained no systematic signal variations:

> "*We were confident that the quadrupole was a real cosmic signal. ... By late January and early February, the results were beginning to gel, but they still did not quite make sense. I tried all kinds of different approaches, plotting data in every format I could think of, including upside down and backwards, just to try a new perspective and hoping for a breakthrough. Then I thought, why not throw out the quadrupole - the thing I'd been searching for all those years - and see if nature had put anything else there. ... Why, I puzzled, did I have to remove the quadrupole to see the wrinkles?*" [64].

Robitaille's [82] answer is simple:

> "*However, when Smoot and his colleagues imposed a systematic removal of signal, they produced a systematic remnant. In essence, the act of removing the quadrupole created the multipoles and the associated systematic anisotropies. ... these findings have no relevance to cosmology and are purely an artifact of signal processing.*"

Smoot's "*wrinkles in the fabric of time*" are nothing more than consistent residual ghost signals produced by his computer data-processing. The

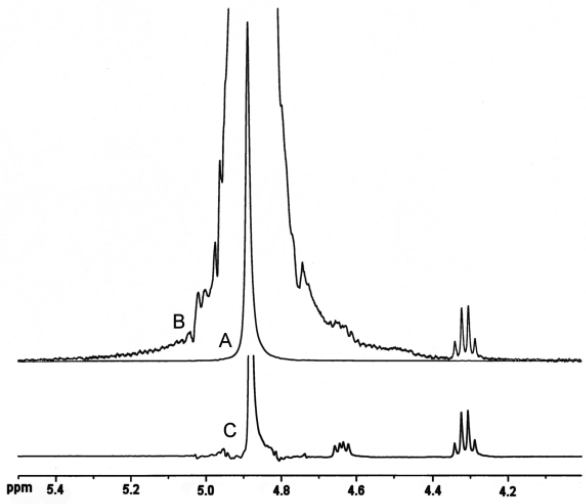

Figure 11.10: Proton nuclear magnetic resonance (NMR) spectra acquired from a 0.1 M solution of 0.1 M N-benzoyl-L-arginine ethyl ester hydrochloride in water (A, B). The spectrum is shown in full scale (A). In (B) the vertical axis has been expanded by a factor of 100, such that the resonance lines from the N-benzoyl-L-arginine ethyl ester can be visualized. A 1H-NMR spectrum acquired from 0.1 M N-benzoyl-L-arginine ethyl ester hydrochloride in deuterium oxide (D_2O) is also displayed (C). Spectra display only the central region of interest (4.0-5.5 ppm). Acquisition parameters are as follows: frequency of observation 400.1324008 MHz, sweep width 32,768 Hz, receiver gain 20, and repetition time 5 seconds. The sample dissolved in D_2O (C) was acquired first using a single acquisition and a 90 degree nutation. A field lock was obtained on the solvent. This was used in adjusting the feld homogeneity for both samples. For (A) and (B), 20 acquisitions were utilized to enable phase cycling of the transmitter and receiver. In this case, the nutation angle had to be much less than 90 degrees in order not to destroy the preamplifer. A field lock could not be achieved since D_2O was not present in the sample. These slight differences in acquisition parameters and experimental conditions make no difference to the discussion in the text relative to problems of dynamic range. Figure and caption reproduced from [90] with permission.

appearance of such systematic ghost signals throughout an image when computer data-processing large contaminating signals is very well known in medical imaging, an example of which is Fig. 11.11.

"*Apparent anisotropy must not be generated by processing*" [82,90]. This is not to say that the sky is not anisotropic, since the microwave contamination is anisotropic, but that the anisotropies reported by COBE-DMR are not present in the sky, rather only as self-induced artifacts of computer data-processing, mistaken for signal.

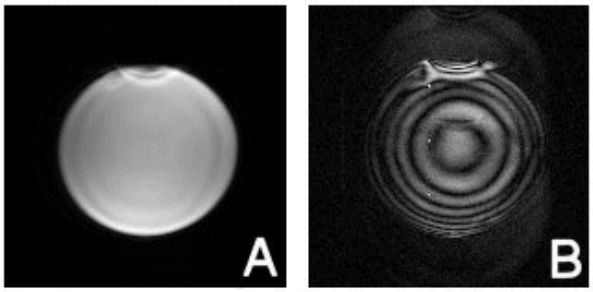

Figure 11.11: Ultra High Field 8 Tesla MRI image of an 18 cm ball of mineral oil acquired using a 3-dimentional acquisition. A) Axial slice representing a region contained within the physical space occupied by the 18 cm mineral oil ball. (B) Axial slice through a region located outside the physical space occupied by the ball. Note that the image displayed in (B) should be entirely devoid of signal. The severe image processing artifacts contained in (B) are a manifestation that the processing of powerful signals can result in the generation of weak spurious ghost signals. Figure and caption reproduced from [90] with permission.

11.5 The Wilkinson Microwave Anisotropy Probe satellite

The Wilkinson Microwave Anisotropy Probe (WMAP) sampled the sky from the 2$^{\text{nd}}$ Lagrange Point (L2), 1.5 million kilometres from Earth, depicted in Fig. 11.12.

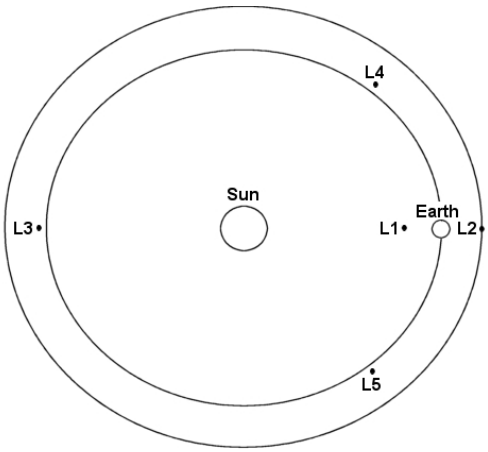

Figure 11.12: The Lagrange points and the location of WMAP at L2. Reproduced from [84] with permission.

WMAP did not measure absolute intensity of any microwave signal because it was strictly a differential instrument: It operated by measuring the signal

difference between input antennae. All data was therefore 'difference data'. Signal from the sky was sampled by two receivers and the difference continually monitored. The pseudo-correlation radiometers of WMAP are shown schematically in Fig. 11.13. Signal from different parts of the sky enter the two sky horns. These signals are subtracted by the instrument so that any signal that is common to each sky horn vanishes in the output data. What is left is difference data. Any differences that persist represent anisotropies. Thus, if the CMB monopole signal is present at L2, it is subtracted out immediately by the instrument. WMAP, by its differential operation, was totally blind at L2 to the presence or absence of the strong monopole signal detected by COBE-FIRAS near Earth. In the case of the dipole signal, since it is anisotropic, it appears in the difference data of WMAP. The WMAP Team reported detection of the dipole signal at L2. Because the dipole signal is noise in relation to the sought after anisotropies of the assumed CMB, it had to be removed. Removal of the dipole signal was done by computer data-processing because it cannot be subtracted out instrumentally. In addition to the dipole, anisotropic signals from the galactic foreground, and numerous points sources of microwaves, both galactic and extragalactic, also had to be removed by computer data-processing. Thus, everything depended on computer data-processing after differencing of the sky horns, whether or not the CMB monopole signal even existed at L2.

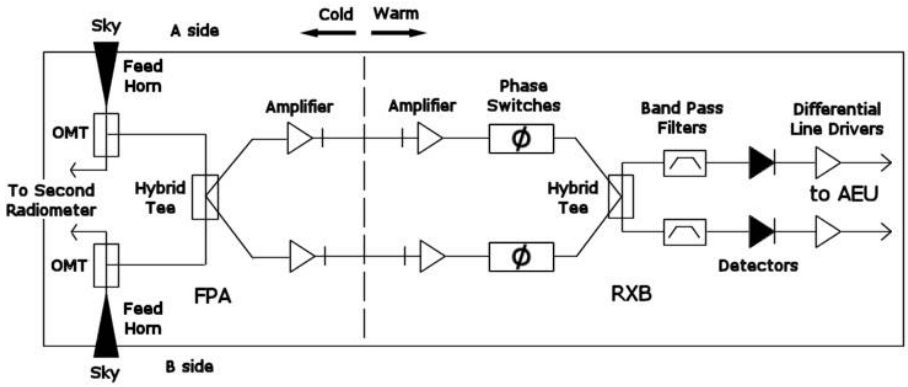

Figure 11.13: Partial schematic representation of the WMAP pseudo-correlation differential radiometers [91]. The signal from each horn first travels to an orthomode transducer (OMT) wherein two orthogonal outputs are produced, one for each radiometer. One output from the OMT travels to the 180^{o} hybrid tee before entering the phase-matched leg of the radiometer. The signal from each horn was compared directly to its paired counterpart. The satellite did not make use of internal reference loads and could not operate in absolute mode. (Reproduced from [84] with permission.)

WMAP sampled at five frequencies: K $\equiv$ 23GHz, Ka $\equiv$ 33GHz, Q $\equiv$ 41GHz, V $\equiv$ 61GHz, W $\equiv$ 94GHz, shown in Fig. 11.14. The red-coloured irregular horizontal band dominating each of the images is due to the galactic

foreground, which constitutes noise that must be removed, by computer data-processing.

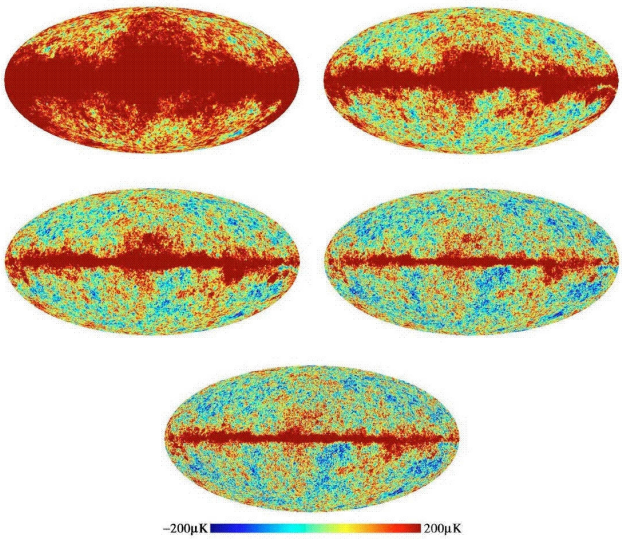

Figure 11.14: The five frequency bands observed by the WMAP satellite. Images correspond to 23 GHz (K band, upper left), 33 GHz (Ka band, upper right), 41 GHz (Q band, middle left), 61 GHz (V band, middle right), and 94 GHz (W band, bottom). Reprinted portion of Fig. 2 from [92] with permission from Tegmark, M., de Oliveira-Costa, A., Hamilton, A.J.S. Copyright (2003) by the American Physical Society.

WMAP essentially had to look through the galactic noise (peer through the galaxy), which is all over the sky, with the highest intensity in the galactic plane as revealed in Fig. 11.13. This is the very same dynamic range problem that COBE-DMR had to contend with. Like Smoot's DMR Team, the WMAP Team had no means to physically or chemically manipulate any microwave anisotropy source and no *a priori* knowledge of the nature of such sources it sought to identify. Consequently, the WMAP Team also could not zero the galactic foreground.

Notwithstanding the impossibility to do so, the WMAP Team, just as the COBE-DMR Team, claimed to have successfully removed the galactic foreground noise from its all-sky anisotropy map. In its attempt to do so the WMAP Team took each all-sky image it had obtained for each of the five frequencies sampled (Fig. 11.14) and divided them into the same twelve sections, shown in Fig. 11.15.

Each region was then processed by a linear combination of each frequency image obtained for that same region. For instance, region 0 was fully constructed by a linear combination of region 0 from each frequency image, by means of assigning a weighting to region 0 in each frequency image; and so on for all regions. The Integrated Linear Combination (ILC) coefficients and

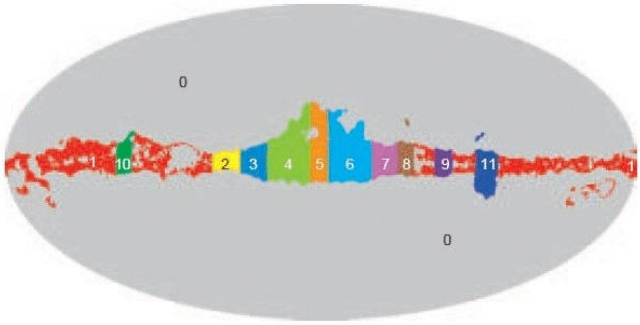

Figure 11.15: The 12 regions used to generate the ILC maps for year 3 average data; from Hinshaw et. al. [96]. Reproduced with permission of D. Spergel.

weightings are listed in Table 11.1.

Region	K-band	Ka-band	Q-band	V-band	W-band
0	0.1559	-0.8880	0.0297	2.0446	-0.3423
1	-0.0862	-0.4737	0.7809	0.7631	0.0159
2	0.0385	-0.4543	-0.1173	1.7245	-0.1887
3	-0.0807	0.0230	-0.3483	1.3943	0.0118
4	-0.0781	0.0816	-0.3991	0.9667	0.4289
5	0.1839	-0.7466	-0.3923	2.4184	-0.4635
6	-0.0910	0.1644	-0.4983	0.9821	0.4428
7	0.0718	-0.4792	-0.2503	1.9406	-0.2829
8	0.1829	-0.5618	-0.8002	2.8462	-0.6674
9	-0.0250	-0.3195	-0.0728	1.4570	-0.0397
10	0.1740	-0.9532	0.0073	2.7037	-0.9318
11	0.2412	-1.0328	-0.2142	2.5579	-0.5521

Table 11.1: ILC weights by regions. ILC coefficients used in the analysis of 3-year data by the WMAP team. This table corresponds to Table 5 in Hinshaw et. al. [96].

Note that the V-band in Table 11.1 was given a favoured weighting. There is no scientific basis for this. Weighting of the V-band was entirely arbitrary. Any band can be favoured *ad arbitrium*. Moreover, claiming that the large galactic foreground signal can be removed, despite absence of access to signal source or *a priori* knowledge of it, the WMAP Team produced Integrated Linear Combination (ILC) images, effectively assuming, without any scientific basis, that the galactic foreground signal is frequency dependent and the sought after underlying anisotropies frequency independent.

Numerical coefficients used by the WMAP team to process each section of their final image, vary by more than 100%.

"*The WMAP team invokes completely different linear combinations of data to process adjacent regions of the galactic plane.*

> *... The coefficients for section 4, correspond to* -0.0781*,* 0.0816*,* -0.3991*,* 0.9667*, and* 0.4289 *for K, Ka, Q, V, and W bands, respectively. In sharp contrast, the coefficients for section 5 correspond to* 0.1839*,* -0.7466*,* -0.3923*,* 2.4184*, and* -0.4635*, for these bands. The WMAP team alters the ILC weights by regions, used in galactic signal removal, by more than 100% for the fourth coefficient, despite the adjacent locations of these sections.*" [84]

The ILC coefficients were nothing more than a means to add and subtract data in order to obtain a desired result. "*The sole driving force for altering the weight of these coefficients lies in the need to zero the foreground. The selection of individual coefficients is without scientific basis, with the only apparent goal being the attainment of a null point*" [84]. To any favoured frequency band there corresponds a particular set of ILC maps, and so different sets of cosmological constants would result depending upon the band emphasised; as products of data processing. Clearly, "*The requirement that the signals of interest are frequency independent cannot be met, and has certainly never been proven*" [84], and "*There is no single map of the anisotropy, since all maps are equally valid, provided coefficients sum to 1*" [84], which is precisely the condition set by the WMAP Team. Consequently: "*There is no unique solution and therefore each map is indistinguishable from noise. There are no findings relative to anisotropy, since there are no features in the maps which could guide astrophysics relative to the true solution*" [84]. Since there is no unique map, none of the maps have any real meaning. Any number of different anisotropy maps can be generated by simply altering the ILC coefficients *ad libitum*. WMAP has no unique all-sky anisotropy map. Indeed, Tegmark et. al. [92] generated a different all-sky anisotropy map from the WMAP database by allowing the coefficient weightings to depend upon angular scale and on distance to the galactic plane. Consequently, the all-sky anisotropy maps presented by the WMAP Team and Tegmark et. al. have no scientific merit.

The galactic foreground is of the order of mK, whereas the desired anisotropies are of the order of μK. Note in Table 11.1 that many of the ILC coefficients were assigned negative values. Physically this corresponds to negative temperatures for the galactic foreground, thereby making the sought after CMB anisotropies hotter than the galactic foreground, when the supposed anisotropies are colder than the galactic foreground, requiring therefore that the galactic foreground contamination be removed in the first place.

The most important determinant of image quality is signal to noise. High signal to noise can permit some signal sacrifice to enhance contrast and resolution. Without high signal to noise, contrast and resolution will always be poor. Medicine is the most exacting field of imaging science and technology. An example from medicine illustrates the utmost importance of signal to noise for image quality. Fig. 11.15 is an image of a sagittal section of a human brain using a 1.5 Tesla MRI scanner, operating at the uppermost limit of its capacity. "*The resolution is high (matrix size = 512 × 512) and the slice thickness is thin (2 mm). At the same time, the nutation angle, echo times, and repetition times are all suboptimal. As a result, this image is of extremely poor clinical*

quality. The contrast between grey and white matter has disappeared and the signal to noise is ≈5" [84].

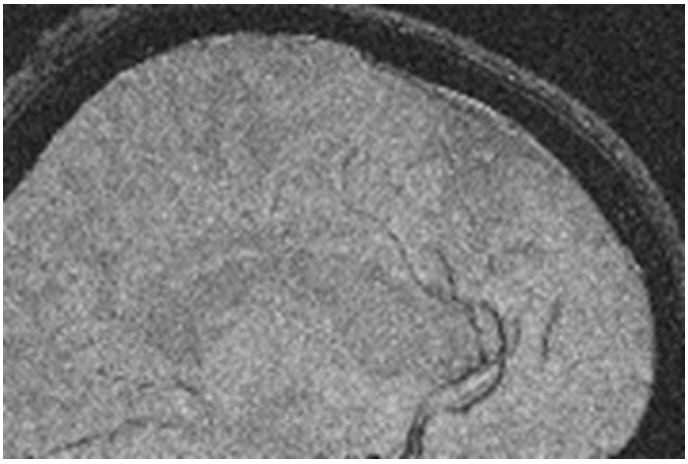

Figure 11.16: Section (490 × 327) of a high resolution sagittal image of the human head acquired at 1.5 Tesla. Acquisition parameters are as follows: acquisition sequence = gradient recalled echo, matrix size = 512 × 512, slice thickness = 2 mm, feld of view 20 cm × 20 cm, repetition time = 750 msec, echo time = 17 msec, and nutation angle = 45 degrees. Figure and caption reproduced from [93] with permission.

Compare Fig. 11.16 with Fig. 11.17. Fig. 11.17 was acquired with the first Ultra-High Field MRI scanner [93–95], operating at a field strength of 8 Tesla. The image in Fig. 11.16 has phenomenal contrast; the delineation of grey and white matter and the appearance of vasculature is spectacular. This image was acquired with a much larger image resolution (matrix size = 2,000 × 2,000) while maintaining nearly the same parameters as for Fig. 11.16. Despite its higher resolution, the image in Fig. 11.17 has a signal to noise of ≈20. Although it took longer to acquire, due to increased phase encoding steps, the time per pixel is less than that for Fig. 11.16. "*Clearly, signal to noise can purchase both contrast and resolution*" [84].

WMAP images however have a maximum signal to noise that barely exceeds 1. Consequently, "*WMAP is unable to confirm that the 'anisotropic signal' observed at any given point is not noise. The act of attributing signal characteristics to noise does not in itself create signal. ... WMAP images do not meet accepted standards in medical imaging research*" [84].

In the absence of high signal to noise, the only indicative feature of images is reproducibility. However, WMAP images cannot evidently be reproduced, since the WMAP team not only selectively weighted the V-band, but varied all ILC coefficients from year to year, for the central region of its images, and also averaged images for a 3-year data image which differs significantly from the first year image. There was no stability on a year-to-year basis let alone on cosmological time scales (which can never be realised). Moreover, the WMAP team's difference images are between year 1 and the averaged 3 year,

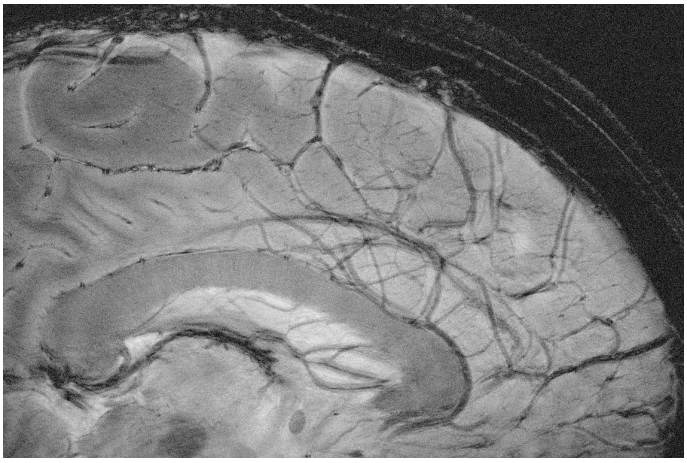

Figure 11.17: Section (1139 × 758) of a high resolution sagittal image of the human head acquired at 8 Tesla. Acquisition parameters are as follows: acquisition sequence = gradient recalled echo, matrix size = 2,000 × 2,000, slice thickness = 2 mm, feld of view 20 cm 4 × 4 20 cm, repetition time = 750 msec, echo time = 17 msec, and nutation angle = 17 degrees. This image corresponds to Figure 3A in Robitaille P.M.L., Abduljalil A.M., Kangarlu A., Ultra high resolution imaging of the human head at 8 Tesla: 2K×2K for Y2K. *J Comp. Assist. Tomogr.*, 2000, v. 24, 2-7. Caption reproduced from [84], with permissions. Pressaging danger to science, Wolters Kluwer, the publisher of *J Comp. Assist. Tomogr.*, charged $130.40 AUD for permission to reproduce this image.

the latter containing the year 1 image itself, not between images year to year. Fig. 11.18 depicts comparative images; "*the difference images are shown with reduced resolution contrary to established practices in imaging science*" [84].

WMAP has no unique map. The final all-sky map presented by the WMAP Team is entirely arbitrary. Merely by adjusting the ILC coefficients entirely different WMAP maps can be produced. Any number of such different maps can be produced in this way. That Tegmark et al. [92] produced a different map from WMAP 'data', reinforces the fact that none of these anisotropy maps are distinguishable from noise.

Attempts to establish stablity in the all-sky anisotropy maps are futile because they must be stable on cosmological time scales, not merely on an *averaged* 3-year basis. Cosmological time scales are not available to cosmologists, and so claims of image stability are meaningless. Even so, WMAP images are not even stable on a yearly basis. The galactic foreground and the point sources are inherently unstable. This is clearly demonstrated in the year 1 and year 3 WMAP all-sky images [83, 90]. The 3-year average constitutes an inappropriate attempt to smooth the image. The 'cleaning' of the maps is *ad hoc* because the WMAP team cannot know the extent to which galactic signals must be removed from each channel. It is simply impossible for the active and unstable galactic foreground to be zeroed. As stated above, the 3-year average ILC image differs significantly from the first-year ILC image,

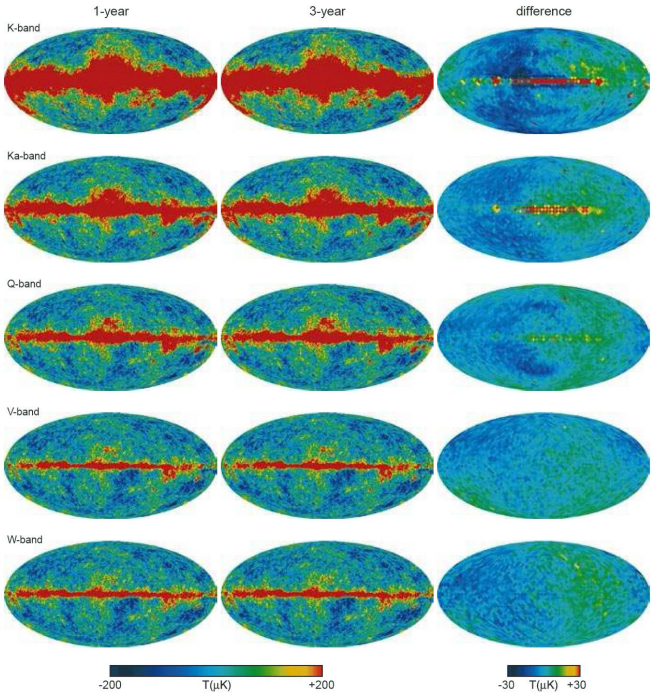

Figure 11.18: Comparison of 3-year average data with year-1 data through difference for the K, Ka, Q, V, and W bands of the WMAP satellite. The WMAP Team presents the difference images with reduced resolution contrary to established practices in imaging science. From [96] (Fig. 3) with permission from D. Spergel.

shown in Fig. 11.19.

Note that the difference images in Figs. 11.18 and 11.19 are presented by the WMAP Team at lower resolution than the 1-year map and the 3-year average map, contrary to standards and practice in imaging science. The lower resolution of the difference maps hides differences in the two maps that were differenced. Moreover, the WMAP Team varied the ILC coefficients from year to year. For example, in the 1-year map the region 0 was given the ILC coefficients K = 0.109, Ka = -0.684, Q = -0.096, V = 1.921, W = -0.250, whilst the 3-year average map was assigned the corresponding values (0.1559, -0.8880, 0.0297, 2.0446, -0.3423), as shown in Table 11.1, also bearing in mind that the 1-year map is itself a component of the 3-year average map. Note that the K-band was changed by nearly 50% and that the Q-band changed sign and decreased in magnitude by a factor of 3.

The vagarious methods employed by the WMAP Team to produce all-sky[1] anisotropy maps attest that there are in fact no CMB anisotropies anywhere. The notion that the ≈2.725 K monopole pervades the Universe as a thermal remnant of a big bang creation *ex nihilo*, is due to theory that violates of the

[1] 'All-sky' means that the entire galactic plane is included.

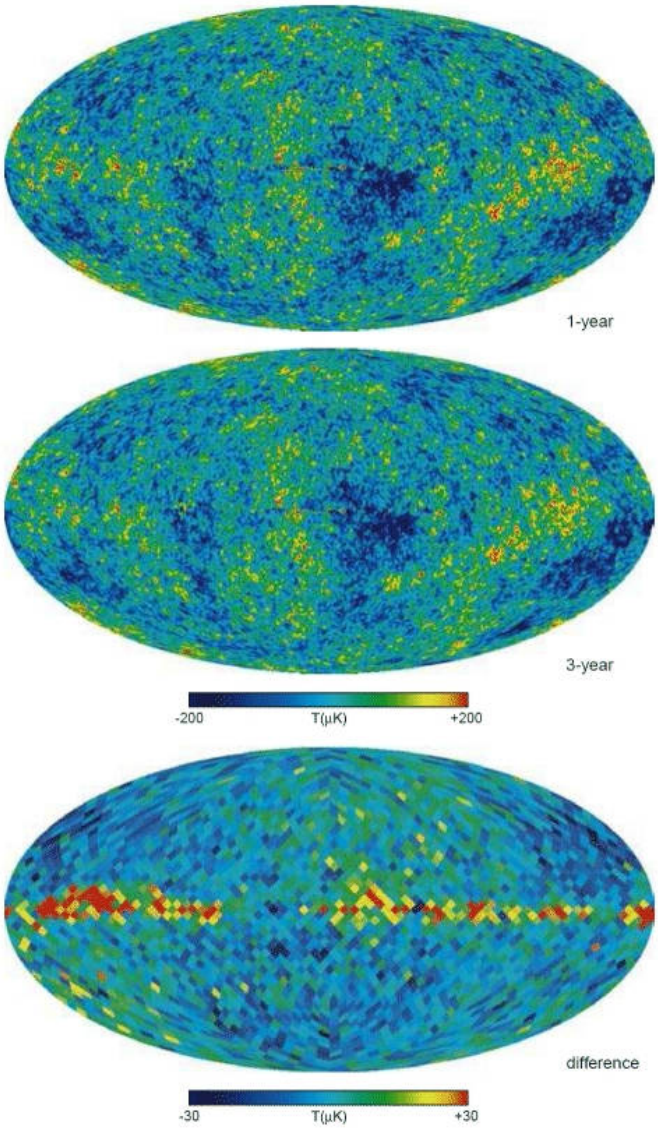

Figure 11.19: Comparison of the 3-year average ILC map with the year-1 ILC map. Note that the difference images are shown at reduced resolution contrary to established practices in imaging science. This figure corresponds to Fig. 9 in Hinshaw et. al. [96]. Reproduced with permission of D. Spergel.

physics of thermal emission and thermodynamics. Kirchhoff's Law of Thermal Emission is false and Planck's equation for thermal spectra is not universal. One cannot assign an absolute temperature to the microwave signals detected from the ground by Penzias and Wilson and by COBE-FIRAS in Earth orbit.

In any event the ≈2.725 K monopole signal has its source in the oceans of Earth and does not reach to L2.

11.6 The *Planck* Satellite

The European Space Agency's *Planck* satellite, as with NASA's WMAP, was located at L2. It carried two instuments for determination of CMB anisotropies; the Low Frequency Instrument (LFI) and the High Frequency Instrument (HFI). The HFI was limited to anisotropy survey as it was not capable of detection of a CMB monopole:

> "*Planck cannot measure accurately the monopole (uniform part of the emission) because many sources contribute (telescope, horns, filters, ...*" [97]

Since COBE-FIRAS reported an enormous signal to noise, *Planck* HFI would have experienced the same, so the impact of spurious signals from telescope, horns, filters, etc. on *Planck* would be of little concern.

The LFI however was able to operate in both differential and absolute mode because it carried two onboard 4 K blackbody reference loads. In this regard it was similar to COBE-FIRAS which carried a blackbody calibrator. In differential mode the LFI functioned like WMAP and COBE-DMR, in order to survey anisotropies. Fig. 11.20 is a schematic of the *Planck* LFI differential radiometers.

In absolute mode the LFI could compare the sky directly with its reference loads and thereby ascertain the presence of an ≈2.725 K monople signal L2. But the *Planck* Team has never reported detection of the CMB monopole signal at L2. In fact, the *Planck* Team utilised the COBE-FIRAS strong monopole signal as its reference base:

> "*The CMB is given by a perfect blackbody with only a single spectral parameter, namely the CMB temperature. We adopt a mean value of* T_{cmb} *= 2:7255 ±0:0006K (Fixsen 2009), and note that the uncertainty in this value is sufficiently small to justify its use as a delta function prior.*"

The temperature reported in this passage from the *Planck* Team is that detected by COBE-FIRAS ≈900 km from Earth. It is a scientific fact that the ≈2.725 K monopole signal has never been detected beyond ≈900 km of Earth. Without this monopole signal beyond Earth, all claims for the 'CMB' and its anisotropies have no scientific merit: just wishful thinking.

The reference loads of the LFI had to be kept at the temperature 4 K. There was no direct means on the LFI to do so. The shield of the HFI however was cooled cryogenically to 4 K. To ensure operational temperature of the reference loads of the LFI, the *Planck* Team attached the them directly to the HFI shield by means of steel screws and washers:

> "*stainless steel (AISI304) thermal washers, ... interposed between the loads and the interface points to the HFI. ... These are*

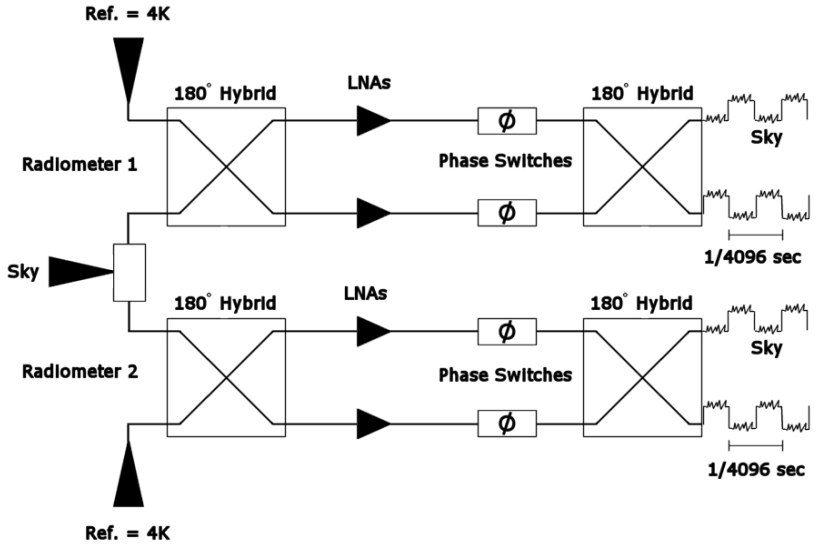

Figure 11.20: Partial schematic representation of the PLANCK LFI pseudo-correlation differential radiometers. Prior to entering each radiometer, the signal from each sky horn travels to an orthomode transducer (OMT) where two orthogonal linearly polarized signals are produced. Each of these signals is then compared directly to a reference load maintained at 4 K. Unlike WMAP, PLANCK can operate both in absolute and differential mode. In absolute mode, PLANCK will be able to directly compare the amplitude signal observed from the sky with that produced by the reference loads. Importantly, in order to maintain a minimal knee frequency PLANCK assumes that the differences between the sky and reference signals will be small. Figure and caption reproduced from [84] with permission.

> *small cylinders (typically 5 mm long, 1 mm wall thickness) whose dimensions are optimized to dump temperature fluctuations in order to meet requirements, ... screws (mounted on the HFI), ... The optimization of the thermal washers allowed to increase the damping factor, ... Cases, supported by an Al structure, are mounted on the HFI using Stainless Steel thermal decouplers (washers), which allows to carefully control the thermal behavior,... Thermal interface is dominated by conduction through thermal washers,... Metal parts are assembled using Stainless Steel screws at high torque, to make thermal contact as close as possible to an ideal value.*" [98,99]

Although this method ensured that the reference loads maintained a temperature of ≈4 K, they did so by conduction, not by thermal emission and absorption. The conduction paths introduced by the steel attachments between the reference loads and the HFI shield ensured that the reference loads could never be blackbodies. The error permitted heat to be shunted directly from the reference loads to the HFI shield by conduction so that the reference

loads emitted few or no photons to the reference horns, making the reference loads appear to the reference horns to have a temperature of ≈ 0 K. In attaching the reference loads to the HFI shield by steel screws and washers the *Planck* Team overlooked the basic physics of thermal emission and heat transfer relating to blackbodies. It thereby became impossible for the LFI to work even before it left the launching pad. Fig. 11.21 is a schematic of the 4 K reference loads and their attachment to the HFI shield.

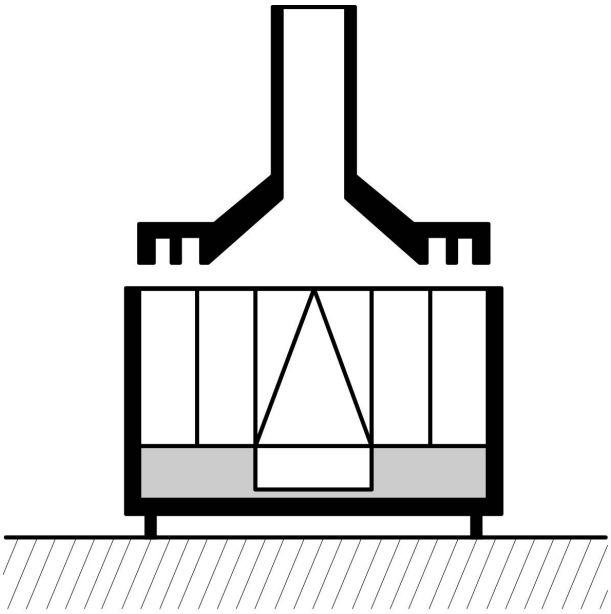

Figure 11.21: Schematic representation of a *Planck* LFI reference load. Each load is comprised of a reference horn (upper section) and a target (middle section) separated by a 1.5 mm gap. The targets are constructed from molded Eccosorb (CR-110 or 117) absorber, surrounded by an aluminum casing which acts to preserve thermodynamic steady state within each unit, using conduction. Heat is allowed to flow out of the target casing through a conductive path directly into the 4 K shield of the HFI (represented by the hatched area in the lower section). This path is provided by stainless steel cylindrical washers and screws. By providing a conductive path out of the target, the Planck LFI team created a situation wherein a Type-8 error is introduced [100]. By itself, the design ensured that the targets could not operate as $\approx$4 K blackbody reference loads. Figure reproduced from [99] with permission.

The *Planck* Team reported testing of the 4 K reference loads before launch. The reference loads produced internal standing waves, as the *Planck* LFI return-loss traces prove (Fig. 11.21). In other words the reference loads responded as resonant cavities, not as blackbodies. Standing waves are not thermal processes. Thus, once again, the 4 K loads were never blackbodies. Blackbodies do not produce standing waves. Consequently, a blackbody reference load must not produce standing waves. The presence of standing waves is proof sufficient that the *Planck* LFI reference loads were never able to func-

tion as blackbodies even if they were not attached by conduction paths to the HFI shield. Note the significant resonances in Fig. 11.22, as low as -50dB at some frequencies. If the target was black, these resonances would not have appeared.

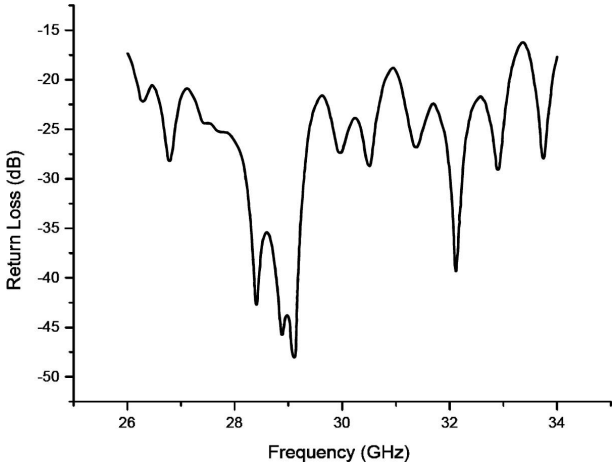

Figure 11.22: A network analyzer tracing for a 30 GHz reference target system, as provided by the *Planck* LFI team [98]. This particular tracing was extracted from Fig. 26 in [98] in order to better visualize its features. Note the presence of significant resonances on this tracing, indicating the existence of standing waves within the horn-target system. It is well known, based on elementary considerations in electromagnetics [74], that cavities, waveguides, and enclosures, at microwave frequencies, can sustain standing waves in a manner depending on their size and geometry (see [74] and references therein). This problem is particularly important when the dimensions of the target approach the wavelengths of interest. In this case, 30 GHz corresponds to a wavelength of ≈1 cm in vacuum. The target casings are 3:3 × 3:3 × (≈ 2) cm (see Table 1 and Fig. 12 in [98]). The presence of such resonances in the ≈4 K reference loads, demonstrates unambiguously that the targets are not black. In fact, the targets are still acting as resonant devices [74]. For a blackbody to exist, all such resonances must be suppressed (i.e. as ideally seen by a constant -50 dB tracing across the spectral range). In this case however, and when combined with the data in Fig. 11.22, it appears that approximately -15 to -20 dB of return loss can be accounted for by leakage from the 1.5 mm gap. Then, between -20 to -25 dB of return loss can be attributed, at certain frequencies, to the existence of resonance features. Note that 29 GHz gives a wavelength of ≈1.03 cm in vacuum, and perhaps a little more in Eccosorb (see [100] and references therein). As such, the resonances at 28.5-29.2 GHz correspond almost exactly to 3 wavelengths in a square 3.3 cm enclosure. Figure reproduced from [98] with permission of the IOP and L. Valenziano on behalf of the authors and the *Planck* LFI consortium. Caption reproduced from [99] with permission.

The *Planck* Team's own computational analyses of the 4 K reference loads revealed that microwave radiation could not be contained within the reference load casing. Microwave radiation leaked out everywhere. The computational analysis reported by the *Planck* Team, of field distributions both inside and

around the targets, during testing with microwave radiation, clearly reveals microwave flowing freely throughout the space in front and around the target. This is particularly evident in the left frame of Fig. 11.23. The computational

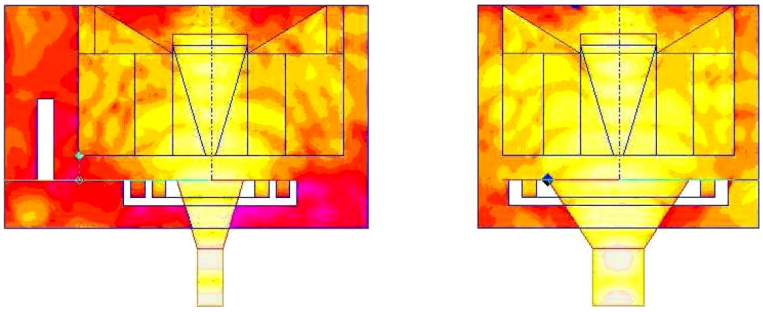

Figure 11.23: Computational determination of the E-field distribution at 70 GHz for a horn-target assembly as reproduced from Fig. 10 in [98]. White areas represent perfect conductors, whereas regions of increased brightness depict more intense fields [98]. The left panel corresponds to PHI = 90 while the right panel to PHI = 0. Further details are available in [98]. Note how the target is unable to localize microwave energy. Leakage of radiation beyond the 1.5 mm gap separating the horn and the target is evident, especially in the right panel. If leakage appears to be less intense in the left panel (examine the left edge of the casing), it is because the horn dimension in this cut is substantially smaller than the target. Nonetheless, some restriction of radiation is visible on the left edge of the casing in the left panel. This acts to confirm that none of the other edges are able to confine the radiation. Note also that the section of CR-117 absorber below the pyramid is actually acting to reflect rather than absorb the radiation. This is especially evident in the left panel (note red area beneath the central pyramid (see [98] for more detail). From these calculations, it is apparent that the Planck LFI targets at 70 GHz are not black, enabling dissipation of energy well beyond the horn-target assembly. Unfortunately, the Planck team does not display corresponding results at 30 and 44 GHz. Reproduced from [98] with permission of the IOP and L.Valenziano on behalf of the authors and the Planck LFI consortium. Caption reproduced from [99] with permission.

analyses provide unambiguous evidence that the return-loss measurements far overstate the performance of the reference loads when attempting to evaluate emissivity. The LFI Team did not correctly evaluate the emissivity of the 4 K reference loads.

> "*Indeed, Valenziano et al. [98] do not even provide the estimated emissivity of their targets. By itself, this constitutes an implicit indication that these values cannot be properly determined, with such methods, as I previously stated.*" [99]

Nothwithstanding, the *Planck* Team assumed that in making their return-loss measurements, no leakage into the gap could take place, even though such leakage is evident in their own calculations, as shown in Fig. 11.23. They further assumed, contrary to their own return-loss measurements, as shown in Fig. 11.22, that the reference load casings could not support any standing waves.

The LFI consortium has demonstrated a major deficiency in knowledge of, and violation of, even the fundamental principles of thermodynamics by permitting the 4 K reference loads to be perfect conductors:

> "*the 70 GHz loads are assumed to be perfect thermal conductors, due to their small thickness and mass.*" [98]

This issue has been examined in fine detail in [100].

It is curious that the *Planck* Team maintains that one can take the 70 GHz map from the LFI and compare it to the 100 GHz map from the HFI, two completely different instruments, and see at high galactic latitude the same anisotropies, bearing in mind that the LFI did not even work. It is also interesting to note that the *Planck* Team reported better than expected performance from the LFI. The reason for this unexpected better performance is that the 4 K reference loads appeared as $\approx$ O K reference loads because their emission profiles were drastically compromised by conduction to the HFI shield. Table 11.2 summarises the logical possibilities.

Expected performance of the *Planck* LFI receivers		
	Sky Temperature $\approx$3 K	Sky Temperature $\approx$0 K
Reference $\approx$4 K	As expected	Poor
Reference $\approx$0 K	Poor	Better than expected

Table 11.2: All logical possibilities for performance of the LFI. Adapted from [99].

In any event, the fatal flaws in the design of the *Planck* instruments do not circumvent the fact that the strong monopole signal detected by COBE-FIRAS does not exist at L2. The evidence that the strong monopole signal detected by COBE-FIRAS is overwhelming [75, 76, 82, 83, 90]. Ironically, the failure of the LFI produced certain evidence that the strong monopole detected by COBE-FIRAS does not exist at L2.

Planck is but one of three satellites that have allegedly detected 'CMB' anisotropies. All these satellites must agree, if their anisotropies are real. They do not agree. The alleged anisotropies are not stable. This has been proven by WMAP. WMAP has no unique map. The final all-sky map presented by the WMAP Team is entirely arbitrary. Tegmark produced a different map from the WMAP 'data', reinforcing the fact that none of these maps are anything but noise. WMAP ILC coefficients vary from year to year, by as much as 100%, and in adjacent sections of the images. Since there is no unique anisotropy map, and no means to assign meaning to any particular such map, the maps are indistinguishable from noise. Consequently the alleged 'CMB' anisotropies have no meaning. COBE-DMR did not detect 'CMB' anisotropies either. Arbitrarily removing the quadrupole from nothing but noise certainly produces data-processing artifacts. Changing instrument from COBE to WMAP to *Planck* does not make the galactic foreground, point sources, or the alleged 'CMB' anisotropies, become stable. It is the galactic foreground and the point sources that are inherently unstable. This is clearly demonstrated in the year 1 and year 3 WMAP all-sky images, and another reason why there is no

unique map. Moreover, COBE, WMAP and *Planck* suffer from the same insurmountable problem - they must peer through the galactic foreground in order to find their alleged anisotropies. However, galactic foreground is noise as far as the 'anisotropies' are concerned, and must be removed, by data-processing. Similarly, the dipole signal must be removed, again by data-processing. The best radiometric laboratories on Earth today cannot achieve what the 'CMB' anisotropy satellites claim to have achieved in space, because it is known to be impossible under the conditions experienced by the CMB satellites. Moreover, stability must be determined on a cosmological time scale. None of the CMB satellites have any possibility of determining anisotropy on a cosmological time scale.

Ultimately, the assignment of an absolute temperature to the strong monopole signal from Earth is a violation of the laws of thermal emission, even if Kirchhoff's Law of Thermal Emission was true. The strong monopole signal from Earth is not the temperature of anything: it is an apparent temperature, due to the oceans on Earth. There can be no CMB without Kirchhoff's Law of Thermal Emission and universality of Planck's equation for thermal spectra. However, Kirchhoff's Law is certainly false; hence Planck's equation for thermal spectra is not universal. Consequently, big bang cosmology and its fiery CMB have no scientific basis.

Bibliography

Chapter 1 and General References

[1] M. W. Evans, H. Eckardt, D. W. Lindstrom, S. J. Crothers, "Principles of ECE Theory: A New Paradigm of Physics", New Generation Publishing and ePubli (2016).

[2] M. W. Evans, "Generally Covariant Unified Field Theory: the Geometrization of Physics" (Abramis Academic, 2005 to present), vols. 1 to 4, vol. 5 in prep. (Papers 71 to 93 on www.aias.us).

[3] L. Felker, "The Evans Equations of Unified Field Theory" (Abramis Academic, 2007).

[4] K. Pendergast, "Crystal Spheres" (preprint on www.aias.us, Abramis to be published).

[5] Omnia Opera Section of www.aias.us.

[6] H. Eckardt, "ECE Engineering Model", http://www.aias.us/documents/miscellaneous/ECE-Eng-Model.pdf.

[7] M. W. Evans, (ed.), "Modern Non-linear Optics", a special topical issue of I. Prigogine and S. A. Rice, "Advances in Chemical Physics" (Wiley Interscience, New York, 2001, second edition), vols. 119(1) to 119(3).

[8] M. W. Evans and S. Kielich (eds.), ibid., first edition (Wiley Interscience, New York, 1992, 1993, 1997), vols. 85(1) to 85(3).

[9] M. W. Evans and L. D. Crowell, "Classical and Quantum Electrodynamics and the B(3) Field" (World Scientific, 2001).

[10] M. W. Evans and J.-P. Vigier, "The Enigmatic Photon" (Kluwer, 1994 to 2002), in five volumes.

[11] M. W. Evans and A. A. Hasanein, "The Photomagneton in Quantum Field Theory" (World Scientific, 1994).

[12] M. W. Evans, "The Photon's Magnetic Field, Optical NMR" (World Scientific, 1992).

[13] M. W. Evans, Physica B, **182**, 227 and 237 (1992).

[14] S. P. Carroll, "Spacetime and Geometry, an Introduction to General Relativity" (Addison Wesley, New York, 2004), chapter three.

[15] J. B. Marion and S. T. Thornton, "Classical Dynamics of Particles and Systems" (Harcourt Brace College Publishers, 1988, third edition).

[16] S. Crothers, papers and references therein on the www.aias.us site and papers 93 of the ECE UFT series on www.aias.us.

[17] P. W. Atkins, "Molecular Quantum Mechanics" (Oxford University Press, 1983, 2nd edition and subsequent editions).

[18] J. R. Croca, "Towards a Non-linear Quantum Physics" (World Scientific, 2001).

[19] E. G. Milewski (Chief Editor), "The Vector Analysis Problem Solver" (Research and Education Association, New York, 1987, revised printing).

[20] J. D. Jackson, "Classical Electrodynamics" (Wiley, New York, 1999, third edition).

[21] M. W. Evans, Acta Phys. Polonica, **38**, 2211 (2007).

[22] M. W. Evans and H. Eckardt, Physica B, **400**, 175 (2007).

[23] M. W. Evans, Physica B, **403**, 517 (2008).

[24] Michael Krause (Director), "All About Tesla" (a film available on DVD that premiered in 2007).

Chapter 2

[25] S. Jensen, "General Relativity with Torsion: Extending Wald's Chapter on Curvature", http://www.slimy.com/~steuard/teaching/tutorials/GRtorsion.pdf.

Chapter 8

[26] T. Kambe, "On Fluid Maxwell Equations‘", http://www.epitropakisg.gr/grigorise/T.Kambe.pdf.

[27] T. Kambe, "On Fluid Maxwell Equations" in: Sidharth B., Michelini M., Santi L. (eds) Frontiers of Fundamental Physics and Physics Education Research. Springer Proceedings in Physics, vol 145 (2014). Springer, Cham.

[28] A. Thess et al., "Sensitivity analysis of a Lorentz force flowmeter for laminar and turbulent flows in a circular pipe", Center for Turbulence Research Proceedings of the Summer Program 2006, Stanford (2006).

[29] http://mathworld.wolfram.com/ConvectiveOperator.html

[30] John David Jackson, Classical Electrodynamics, 3rd edition, Wiley 1998, p. 416.

Chapter 9

[31] Gabriele Müller, Viva Vortex, ISBN 9783741287213, 2016, and http://www.viva-vortex.de/.

Chapter 10

[32] G. Y. Rainich, Electrodynamics in the General Relativity Theory. *Proc. N.A.S.*, **10** (1924), 124-127.

[33] G. Y. Rainich, Second Note Electrodynamics in the General Relativity Theory. *Proc. N.A.S.*, **10** (1924), 294-298.

[34] U. E. Bruchholz, Geometry of Space-Time, *Progress in Physics*, **5** (4) (2009), 65-66.
http://www.ptep-online.com/index_files/2009/PP-19-06.PDF

[35] U. E. Bruchholz, Key Notes on a Geometric Theory of Fields, *Progress in Physics*, **5** (2) (2009), 107-113.
http://www.ptep-online.com/index_files/2009/PP-17-17.PDF

[36] A. Einstein, *Grundzüge der Relativitätstheorie*. A back-translation from the Four Lectures on Theory of Relativity. Akademie-Verlag Berlin, Pergamon Press Oxford, Friedrich Vieweg & Sohn Braunschweig (1969).

[37] L. P. Eisenhart, *Riemannian Geometry*, Princeton university press (1949).

[38] U. E. Bruchholz and H. Eckardt, A Numerical Method for Prediction of Masses of Real Particles, e.g. Neutrinos, *Theoretical Mathematics & Applications*, **6**, no. 4 (2016), 53-69.
http://www.scienpress.com/

[39] J. Gleick, *Chaos, die Ordnung des Universums. Vorstoß in Grenzbereiche der modernen Physik.* (Engl. orig.: Chaos. Making a new science.) Droemer Knaur München (1990) ISBN 3-426-04078-6.

[40] G. Küppers (Ed.), *Chaos und Ordnung.* Formen der Selbstorganisation in Natur und Gesellschaft. Reclam Ditzingen (1996) ISBN 3-15-009434-8.

[41] A. Einstein and W. Pauli, On the non-existence of regular stationary solutions of relativistic field equations, *Ann. of Math.*, **44** (2) (1943), 131.

[42] U. E. Bruchholz, Masses of Nuclei Constituted from a Geometric Theory of Fields, *Adv. Studies Theor. Phys.*, **7** no.19 (2013), 901-906. http://dx.doi.org/10.12988/astp.2013.3885

[43] K. Hagiwara et al. (Particle Data Group), *Phys. Rev.* D 66, 010001 (2002) (URL: http://pdg.lbl.gov)

Chapter 11

[44] Krauss, L.M., A Universe from Nothing: Why There Is Something Rather than Nothing, Free Press, New York, 2012.

[45] Robitaille, P.-M., Forty Lines of Evidence for Condensed Matter - The Sun on Trial: Liquid Metallic Hydrogen as a Solar Building Block, *Progress in Physics*, Special Report, v.4, pp.90-142, 2013, http://vixra.org/abs/1310.0110

[46] Stewart, B., An account of some experiments on radiant heat, involving an extension of Prévost's theory of exchanges. *Trans. Royal Soc. Edinburgh*, 1858, v. 22, no. 1, 1-20.

[47] Kirchhoff, G.R., Über den Zusammenhang zwischen Emission und Absorption von Licht und. Ẅarme. *Monatsberichte der Akademie der Wissenschaftenzu Berlin*, sessions of Dec. 1859, 1860, 783-787.

[48] Kirchhoff, G.R., Überber das Verhältnis zwischen dem Emissionsvermögen und dem Absorptionsvermogen. der Körper fur Wärme und Licht. *Poggendorfs Annalen der Physik und Chemie*, 1860, v. 109, 275-301. (English translation by F. Guthrie: Kirchhoff G. On the relation between the radiating and the absorbing powers of different bodies for light and heat. *Phil. Mag.*, 1860, ser. 4, v.20, 1-21).

[49] Robitaille, P.-M., Crothers, S.J., "The Theory of Heat Radiation" Revisited: A Commentary on the Validity of Kirchhoff's Law of Thermal Emission and Max Planck's Claim of Universality, *Progress in Physics*, v.11, pp.120-132, 2015, http://vixra.org/pdf/1502.0007v2.pdf

[50] Planck, M., The theory of heat radiation, P. Blakiston's Son & Co., Philadelphia, PA, 1914, http://gutenberg.org/ebooks/40030

[51] Robitaille, P.-M., The Life Cycle of the Stars, https://www.youtube.com/watch?v=FDn_0hwLsKM

[52] Robitaille, P.-M., Sky Scholar series on the Sun and stars, https://www.youtube.com/channel/UCL7QIOZteWPpBWBOl8i0e-g

[53] Planck, M., Über das Gesetz der Energieverteilung im Normalspektrum. *Annalen der Physik*, 1901, v.4, 553-563.

[54] Robitaille, P.-M., On the validity of Kirchhoff's law of thermal emission, *IEEE Trans. Plasma Sci.*, v.31(6), pp.1263-1267, 2003.

[55] Zemansky, M.W., and Dittman, R.H., Heat and Thermodynamics, McGraw-Hill Book Company, 1981.

[56] Weinberg, S., The First Three Minutes, Basic Books, 2nd Ed., 1988.

[57] Robitaille, P.-M., Kirchhoff's Law and Magnetic Resonance Imaging: Do Arbitrary Cavities Always Contain Black Radiation?, Abstract: D4.00002, Bulletin of the American Physical Society, 2016 Annual Spring Meeting of the APS Ohio-Region Section Friday-Saturday, April 8-9, 2016; Dayton, Ohio, http://meetings.aps.org/Meeting/OSS16/Session/D4

[58] Crothers, S.J., A Critical Analysis of LIGO's Recent Detection of Gravitational Waves Caused by Merging Black Holes, *Hadronic Journal*, Vol. 39, 2016, http://vixra.org/pdf/1603.0127v4.pdf

[59] Evans, M.W., Eckardt, H., Lindstrom, D.W., Crothers, S.J., Principles of ECE Theory, A New Paradigm of Physics, Chpt. 9, 2016, http://vixra.org/pdf/1611.0296v1.pdf

[60] Levi-Civita, T., Mechanics - On the Analytical Expression that Must be Given to the Gravitational Tensor in Einstein's Theory, *Rendiconti della Reale Accadmeia dei Lincei*, 26: 381, 1917.

[61] Robitaille, P.-M., Robitaille, L., Kirchhoff's Law of Thermal Emission: What Happens When a Law of Physics Fails an Experimental Test? http://vixra.org/pdf/1708.0053v1.pdf

[62] Robitaille, P.-M., Is Kirchhoff's Law True? The Experiment! https://www.youtube.com/watch?v=YQnTPRDT03U

[63] Gaensler, B., Extreme Cosmos, Penguin, New York, 2011.

[64] Smoot, G., Wrinkles in Time, Little, Brown and Company, Great Britain, 1993.

[65] Weinberg, S., Gravitation and Cosmology: Principles and Applications of the General Theory of Relativity, John Wiley & Sons, Inc., New York, 1972.

[66] Hawking, S.W., A Brief History of Time, Bantam Press, 1988.

[67] Pauling, L., General chemistry: an Introduction to Descriptive Chemistry and Modern Chemical Theory, 2nd Ed., W. H. Freeman and Company, San Francisco, 1953.

[68] Sears, F. W., An Introduction to Thermodynamics, The Kinetic Theory of Gases, and Statistical Mechanics, Addison-Wesley Publishing Company. Inc., Cambridge, Massachusetts, 1955.

[69] Beiser, A., Concepts of Modern Physics (International Edition), McGraw-Hill Book Company, 1987.

[70] Misner, C.W., Thorne, K.S., Wheeler, J.A., Gravitation, W. H. Freeman and Company, New York, 1973.

[71] Robitaille, P.-M., An analysis of universality in blackbody radiation, *Prog. in Phys.*, v.2, pp.22-23, 2006, arXiv: physics/0507007

[72] Robitaille, P.-M., Blackbody Radiation and the Carbon Particle, *Prog. in Phys.*, v.3, pp.36-55, 2008, http://www.ptep-online.com/index_files/2008/PP-14-07.PDF

[73] Robitaille, P.-M., A Critical Analysis of Universality and Kirchhoff's Law: A Return to Stewart's Law of Thermal Emission, http://www.ptep-online.com/index_files/2008/PP-14-06.PDF

[74] Robitaille, P.-M., Kirchhoff's Law of Thermal Emission: 150 Years, *Prog. in Phys.*, v.4, pp.3-13, 2009, http://www.ptep-online.com/index_files/2009/PP-19-01.PDF

[75] Robitaille, P.-M., Water, Hydrogen Bonding, and the Microwave Background, *Lettrs. to Prog. in Phys.*, v.2, pp.L5-L8, 2009, http://vixra.org/pdf/1310.0129v1.pdf

[76] Robitaille, P.-M., The Structure of Liquid Water, https://www.youtube.com/watch?v=w3uZjdyrYeU

[77] Penzias, A.A., and Wilson, R.W., A measurement of excess antenna temperature at 4080 Mc/s, *Astrophys. J.*, v.1, pp.419-421, 1965.

[78] Dicke, R.H., Peebles, P.J.E., Roll, P.G., Wilkinson, D.T., Cosmic blackbody radiation, *Astrophys. J.*, v.1, pp.414-419, 1965.

[79] Kylpin, A.A., Strukov, I.A., Skulachev, D.P., The Relikt missions: results and prospects for detection of the Microwave Background Anisotropy, *Mon. Not. Astr. Soc.*, v.258, pp.71-81, 1992.

[80] Fixen, D.L., et al, The Cosmic Microwave Background spectrum from the full COBE FIRAS data set, *Astrophys. Jr.*, v.473, pp.576-587, 1996.

[81] Fixen D.J., Cheng E.S., et al., Calibration of the COBE FIRAS instrument, *Astrophys. J.*, v.420, pp.457-473, 1994.

[82] Robitaille, P.-M., COBE: A Radiological Analysis, *Prog. in Phys.*, v.4, pp.17-42, 2009, http://vixra.org/pdf/1310.0125v1.pdf

[83] Robitaille, P.-M., The Cosmic Microwave Background, https://www.youtube.com/watch?v=i8ijbu3bSqI

[84] Robitaille, P.-M., On the Nature of the Microwave Background at the Lagrange 2 Point. Part I., *Prog. in Phys.*, v.4, pp.74-83, 2007, http://www.ptep-online.com/index_files/2007/PP-11-11.PDF

[85] Crothers, S.J., COBE and WMAP: Signal Analysis by Fact or Fiction?, *Electronics World*, pp.26-31, March 2010, http://vixra.org/pdf/1101.0009v1.pdf
http://viewer.zmags.com/htmlCat/index.php?mid=rpdgfh&pageid=25

[86] Fixen, D.J., Cheng, E.S., Gales, J.M., Mather, J.C., Shafer, R.A., Wright, E.L., The cosmic microwave background spectrum from the full COBE FIRAS data set, *Astrophys. J.*, v.473, pp.576-587, 1996.

[87] Mather, J.C., Cheng E.S., et al., A preliminary measurement of the cosmic microwave background spectrum by the cosmic background explorer (COBE) satellite, *Astrophys. J.*, v.354, L37-L40, 1990.

[88] Stewart, A.C., (NASA-TM-104959) COBE ON-ORBIT ENGINEERING PERFORMANCE, v.1, (NASA) 321 PCSLC 22B, COBE/DELTA THERMAL/RF SHIELD ON-ORBIT ENGINEERING PERFORMANCE, pp.214-230, March 1990, http://ntrs.nasa.gov/archive/nasa/casi.ntrs.nasa.gov/19920008877.pdf

[89] Fixen, D.J., Mather, J.C., The spectral results of the far infrared absolute spectrophotometer instrument on COBE, *Astrophys. J.*, v.581, pp.817-822, 2002.

[90] Robitaille, P.-M., WMAP: A Radiological Analysis, *Prog. in Phys.*, v.1, pp.3-18, 2007, http://www.ptep-online.com/index_files/2007/PP-08-01.PDF

[91] Jarosik, N., Bennett, C.L., Halpern, M., Hinshaw, G., Kogut, A., Limon, M., Meyer, S.S., Page, L., Pospieszalski, M., Spergel, D.N., Tucker, G.S., Wilkinson, D.T., Wollack, E., Wright, E.L., and Zhang, Z., Design, implementation and testing of the MAP radiometers. *Astrophys. J. Suppl.*, v.145, pp.413-436, 2003.

[92] Tegmark, M., de Oliveira-Costa, A., Hamilton A.J.S., A high resolution foreground cleaned CMB map from WMAP, *Phys. Rev. D*, v.68(12), 123523, 2003, http://link.aps.org/abstract/PRD/v68/e123523. Copyright (2003) by the American Physical Society.

[93] Robitaille, P.-M.L., Berliner, L.J. (eds). Biological magnetic resonance: ultra high feld magnetic resonance imaging. Springer, New York, 2006.

[94] Robitaille, P.M.L., Abduljalil, A.M., Kangarlu, A., Zhang X., Yu Y., Burgess R., Bair S., Noa P., Yang L., Zhu H., Palmer B., Jiang Z., Chakeres D.M., Spigos D., Human magnetic resonance imaging at eight Tesla. *NMR Biomed.*, v.11, 263-265, 1998.

[95] Robitaille, P.M.L., Abduljalil A.M., Kangarlu A. Ultra high resolution imaging of the human head at 8 Tesla: 2K × 2K for Y2K. J Comp. Assist. Tomogr., 2000, v. 24, 2-7. 42. Robitaille, P.M.L., Berliner L.J. (eds). Biological magnetic resonance: ultra high feld magnetic resonance imaging. Springer, New York, 2006.

[96] Hinshaw G., Nolta M.R., Bennett C.L., Bean R., Dore O., Greason M.R., Halpern M., Hill R.S., Jarosik N., Kogut A., Komatsu E., Limon M., Odegard N., Meyer S.S., Page L., Peiris H.V., Spergel D.N., Tucker G.S., Verde L., Weiland J.L., Wollack E., Wright E.L. Three-year Wilkinson Microwave Anisotropy Probe (WMAP) observations: temperature analysis. *Astrophys. J.*, 2006.

[97] Lamarre, et al., http://herschel.esac.esa.int/Hcal/documents/Lamarre.pdf

[98] Valenziarno, et al, Planck-LFI: design and performance of the 4 Kelvin Reference Load Unit. *JINST*, 2009, v. 4, T12006.

[99] Robitaille, P.-M., The Planck Satellite LFI and the Microwave Background: Importance of the 4K Reference Targets, Progress in Physics, v.3, pp.11-18, 2010, http://vixra.org/pdf/1310.0123v1.pdf

[100] Robitaille, P.-M., Calibration of microwave reference blackbodies and targets for use in satellite observations: An analysis of errors in theoretical outlooks and testing procedures, *Prog. Phys.*, v. 3, pp.3-10, 2010, http://www.ptep-online.com/index_files/2010/PP-22-01.PDF